ESA PSS-01-609 Issue 1
(May 1993)

THE RADIATION DESIGN HANDBOOK

Prepared by:
Product Assurance & Safety Department and
Automation & Informatics Department
European Space Research and Technology Centre
Noordwijk, The Netherlands

Approved by:
The Inspector General, ESA

european space agency / agence spatiale européenne
8-10, rue Mario-Nikis, 75738 PARIS CEDEX, France

Published by ESA Publications Division,
ESTEC, Noordwijk, The Netherlands

Printed in the Netherlands.

ESA Price Code: E4

ISSN 0379-4059

ABSTRACT

This handbook addresses the engineering problem of radiation effects in spacecraft and some of its management aspects. Summary graphs, tables and flow charts are compiled from a wide range of sources. The environment, the penetration and the effects of the space radiation environment are detailed. Assessment methods are also discussed.

The text and charts are to help spacecraft and instrument designers to gauge the significance of the space radiation problem from the project point of view, to communicate this problem to management and to implement engineering solutions.

DOCUMENT CHANGE RECORD

Issue number and date	Sections affected	Remarks

TABLE OF CONTENTS

SECTION 1. SCOPE

This handbook provides general engineering guidelines suitable for project groups engaged in the design of spacecraft required to operate in regions of space where they will be exposed to significant doses of radiation. The radiation environment is very variable in time and position. The natural level of radiation can be high and cause malfunctions in components. The levels can also be perturbed by man, especially by the use of nuclear or beam weapons. It is necessary for the spacecraft designer to give proper consideration to the radiation environment and its impact on design. This impact may be severe and strong guidelines on radiation effects should be followed, even in the earliest stages of system engineering.

This document brings together much of the information necessary for guidelines. However, because the different circumstances of each project give rise to very different guidelines, no attempt is made here to specify procedures except in the field of effects prediction and radiation testing. It will be up to Project Management, advised by Systems Engineering, Product Assurance and other groups, to develop the guidelines appropriate to a project.

The scope includes detailed discussion of the charged particle environment in geomagnetospheric space, the physics of radiation effects on solid-state devices and materials (including ionisation effects, single-event upsets and bulk displacement damage) in all the designs of devices likely to be used in spacecraft. Methods of assessing the impact of these effects are given, including procedures for calculating the orbital radiation environment, dose-depth curves within electronic enclosures and the end-of-life degradation of devices and circuits.

While no rigid procedures for handling these problems can be set out, special attention is given to methods of alleviating the problems presented. These methods cover trade-off studies of orbit versus shield weight, layout rules for spacecraft, the use of redundancy and housekeeping dosimetry, device selection, device verification and the design of radiation-tolerant circuits.

PAGE LEFT INTENTIONALLY BLANK

SECTION 2. INTRODUCTION

This Radiation Design Handbook is intended to serve as a tool for designers of satellite equipment and scientific instruments to improve chances of survival in the space radiation environment.

The objective of this handbook is to provide an overview of spacecraft design requirements arising from the radiation environments which may be encountered in space. The aim is to discuss and explain the various likely radiation effects, their impact, and the variety of design and operational solutions which are available. Particular emphasis is placed on known areas of concern such as semiconductor technology and optics, and critical subsystems such as automated mechanisms and imagers.

A major administrative aim is to ensure that a better flow of information on radiation effects reaches the design teams working with the European Space Agency. This document is intended to increase the general understanding of technical and management staff, to improve mutual understanding on important radiation related design problems and to achieve uniform radiation tolerance in space systems, with less redundancy of effort than at present. These objectives are not easily attained because the technical problems are intricate and novel.

Consequently, this document contains complex information, sometimes accompanied by detailed discussion and explanatory diagrams. It is intended that technical personnel utilise it to evolve appropriate techniques and to recommend appropriate management policies.

PAGE LEFT INTENTIONALLY BLANK

SECTION 3. THE RADIATION ENVIRONMENT

3.1. THE EARTH'S MAGNETIC FIELD

3.1.1. The magnetosphere

The morphology, or spatial distribution, of the radiation environment experienced by Earth-orbiting spacecraft is largely a manifestation of the interaction of charged particles with the Earth's magnetic field. To a first approximation, this field is that of a magnetic dipole and, in those regions where the field lines are "closed", charged particles become trapped in the magnetosphere (see Section 3.2).

The field is not geographically symmetrical, however. Local distortions are caused by an offset and tilt of the magnetic axis with respect to the Earth's axis and by geological influences; one particularly marked feature is known as the "South Atlantic anomaly". This is important for low earth orbits. At high altitude, the effect of the solar wind is to distort the magnetosphere to a great degree. The resulting form of the field has characteristics comparable to the bow-wave and wake of a solid object moving through a fluid. This effect is well illustrated in Figure 3.1. The magnetosphere here is divided into regions of different trapping capability. The direction of the Sun is to the left of the figure.

The field is also not constant with time. Apart from short-term variations associated with storms, the strength of the field is decreasing with time at the rate of about 0.1% per year. The dipole moment, associated with the dipolar elements of the field currently has a value 0.304 gauss $(R_E)^3$, where R_E is the Earth's radius.

3.1.2. Co-ordinates

It is useful to consider the magnetosphere and its associated radiation structure as a simplified structure. An idealised form of the Earth's field is used to define a system of co-ordinates by means of which points in the magnetosphere may be defined. Each field line (the surface of revolution of which is a "magnetic shell" or "drift shell") is defined by a parameter L (Mc Ilwain, 1961).

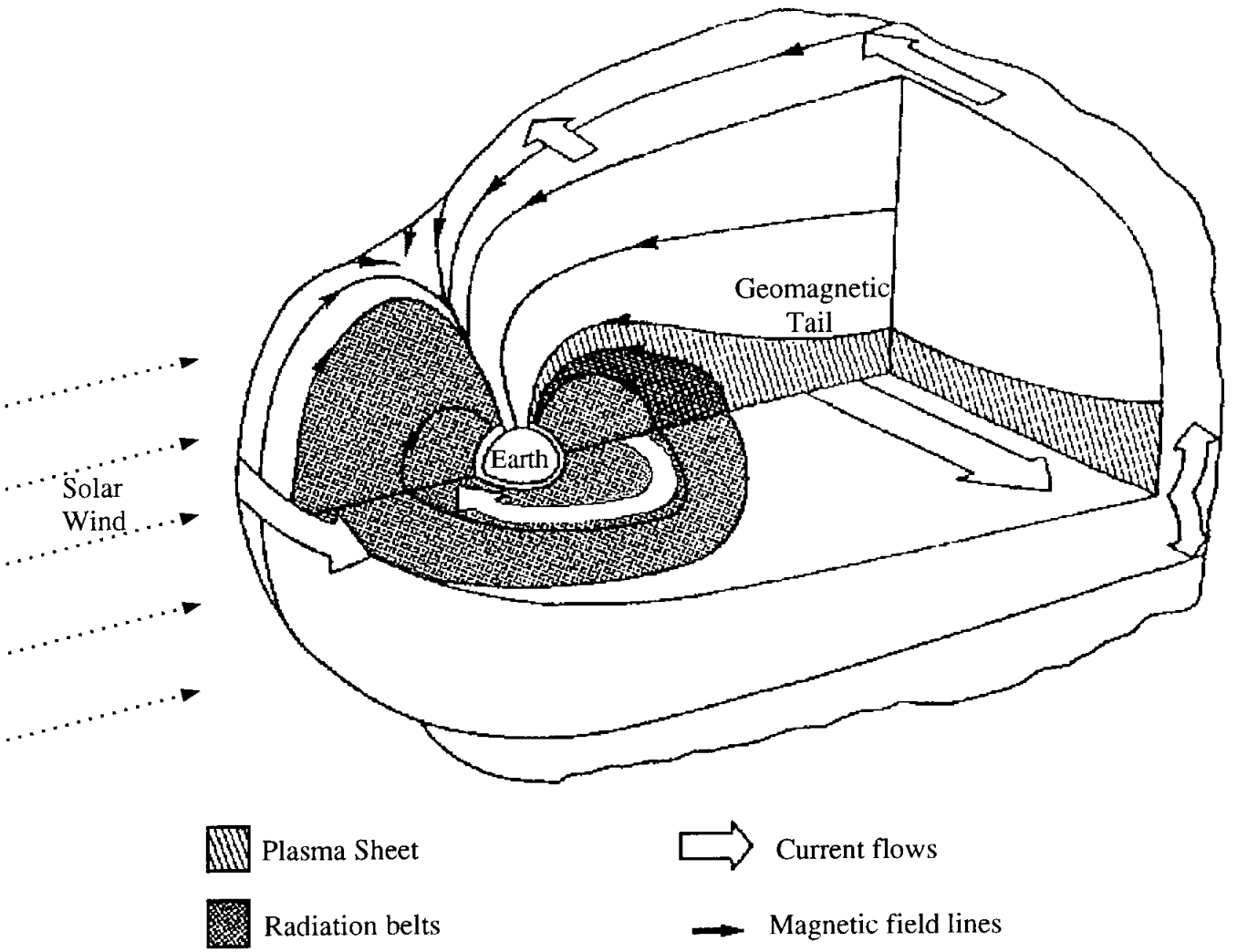

The Magnetosphere and Radiation Belts showing the distortion of the Earth's field which is approximately dipolar at low altitude and becomes strongly affected by the solar wind at high altitude. The Sun is to the left.

FIGURE 3.1 - THE MAGNETOSPHERE AND RADIATION BELTS

In an ideal dipole, this is equal to the geocentric radius at which the shell cuts the magnetic equator; it is measured in units of earth radii R_E and all points on that field line and drift shell have the same L value. The position of a point on a field line is defined by a parameter B which is the magnetic field strength. At constant L, the value of B varies from a minimum at the magnetic equator to a maximum where the field line cuts the Earth's surface: B-L space is a fixed ideal co-ordinate system and is not affected by the temporal and local variations in the magnetosphere referred to earlier.

As an alternative, points may be defined in R-λ space. This system does not refer to field lines or shells; R is the geocentric distance of the point and λ is the magnetic latitude. Either co-ordinate system may be used in the appropriate circumstances. In this section, reference will be frequently made to the parameter L.

Mc Ilwain (1961) described a method whereby locations in the Earth's true internally generated field could be transformed numerically into the B-L. co-ordinates of an "equivalent perfect dipole".

Numerous computer-based models of the Earth's internally generated magnetic field are available, including the International Geophysical Reference Field, IGRF, which describe the field's spatial and long-term temporal variations. The National Space Science Data Centre, NSSDC, at NASA-GSFC provides these and other field models, including some which model the external source field corrections to the internal source. For radiation environment computations, an internal source field model is normally used.

3.2. TRAPPED RADIATION

The trapping of charged particles, in particular electrons and protons, by the Earth's magnetic field, creates the toroidal radiation belts known as the "Van Allen" belts which encircle the Earth (see Figure 3.1.)

A trapped charged particle follows a path spiralling about a line of force; it has an angular motion about the field line and a linear motion along it. The linear velocity is greatest at the magnetic equator where the field is weakest. As it moves along a line towards the poles and into regions of higher field strength, the linear component is reduced until a "mirror point" is reached where the particle is reflected back towards the equator, unless it is lost to the upper atmosphere. If it survives, the particle continually retraces its path back and forth along a field line while also drifting around the Earth (Hess, 1968).

This state of affairs is not entirely static. Particles are continually being lost to the atmosphere or are gained from extraterrestrial

origins, from the solar wind or cosmic-ray-induced neutron decay (Schultz, 1982). Schultz (1982) also indicates that Jupiter may be supplying significant fluxes of energetic electrons to the Earth's outer magnetosphere. The environment varies over a number of time scales. An important variation is that linked to the solar activity cycle. This cycle with a duration of approximately 11 years reflects the changing frequency of sunspots and solar flares and changes in the steady efflux of charged particles and electromagnetic radiation from the Sun. The rate of injection of particles into the Earth's trapped radiation environment and the Earth's atmospheric density both change over the solar cycle, influencing creation and loss processes and causing changes in the equilibrium fluxes.

In the past, the equilibrium was affected artificially by the injection of particles resulting from the explosion of nuclear devices. The American "Starfish" explosion in 1962 caused very large changes in trapped electron distribution, an effect which was unexpectedly stable and persisted until at least 1965. Military spacecraft are designed to survive such intentional injections of energetic "fission-spectrum" electrons.

Since the morphology of the belts is governed by the distorted dipole field, the belts are subject to the same spatial and time-dependent distortions. As with the magnetic field itself, it is often convenient to consider the structure of the belts in a time-averaged form. This is reasonable when the total radiation exposure of most spacecraft will be accumulated over a large number of orbits and a large number of days. Problems arise when the mission duration is short or when the short-term variations influence operations; for example, the variation of particle fluxes on the orbit of an astronomy mission which leads to detector background.

Figures 3.2 and 3.3 illustrate the average structure of the trapped electron and proton belts. The contours join points of equal average particle flux and are derived from the AE8 and AP8 environment models corresponding to solar-minimum conditions. In fact these figures are plotted as if the Earth's field were dipolar.

The electron environment consists of particles of energies up to about 7 MeV, with the most energetic particles occurring in the "outer zone" described below. In contrast, proton energies of several hundred MeV are found, the most energetic protons being found at lower altitudes.

It will be observed that the electron environment is so structured that there are two flux maxima; it is conventional to refer to the inner and outer electron zones, each zone being associated with one of the flux maxima. It will also be seen that the outer zone envelops the inner zone, its contours extending towards the Earth in cusps of relatively high flux. These extensions of the outer zone approach the Earth at high magnetic latitudes (60°-70°), the regions

associated with auroral phenomena. A line passing through these earthward extensions of successive flux contours is a field line cutting the magnetic equator at a geocentric distance of approximately 4.5 earth radii. The parameter L = 4.5 may therefore be taken as the "centre" of the outer zone. Similarly, the field line passing through the less obvious cusps of the inner zone is close to L = 1.4, while the "boundary" between the zones is marked by the field line close to L = 2.3.

The region between the zones is often referred to as the "slot", possibly a consequence of the combination of radial diffusion and losses induced by wave particle interactions (Lyons and Williams, 1984). The increase in trapped electron population at times of high solar activity results in a pronounced "slot-filling" tendency. The same effect was observed after artificial increases in electron population following nuclear tests. The structure of the trapped proton environment is simpler. There is a single belt with a flux maximum in the region of L = 1.7; this is also commonly referred to as the inner zone.

The effect of the South Atlantic Anomaly, where, because of the offset and tilt of the geomagnetic field, field lines containing significant energetic-particle fluxes approach the Earth's surface, is shown in Figure 3.4. The resulting flux enhancement close to South America on low orbits is apparent. Also clearly shown are the high-latitude enhancements where the geomagnetic field brings energetic, trapped, outer-zone electrons to low altitudes.

For practical purposes, the particle fluxes are normally regarded as isotropic. This is a simplification, as fluxes do in fact show important "anisotropies" in some places.

At low altitudes, in the South Atlanctic Anomaly, particle velocities are almost completely perpendicular to the field lines. In addition, atmospheric absorption of the gyrating particles results in a higher flux of protons from the west. For energetic protons at low altitudes, the ratio of fluxes can exceed two orders of magnitude.

The outer-zone electron environment is very dynamic, exhibiting large variations over a number of time scales. A 27-day periodicity in relativistic electron fluxes indicates a close link with solar wind streams and possibly Jupiter (Baker et al, 1986).

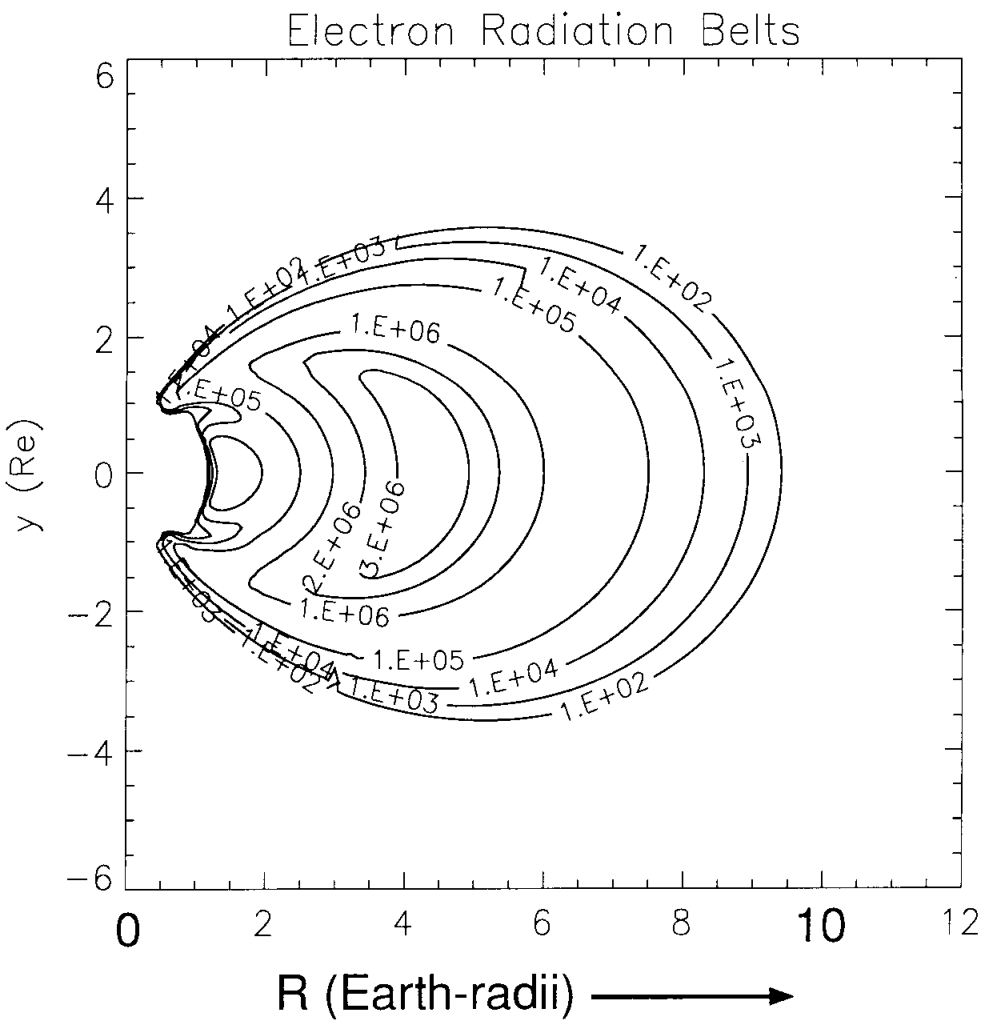

Radiation-belt electron model flux contours in "idealised dipole space". *z* is aligned with the dipole axis and *x* is a radial distance from the axis. Both are in units of earth radii.

FIGURE 3.2 - TRAPPED ELECTRON RADIATION BELTS

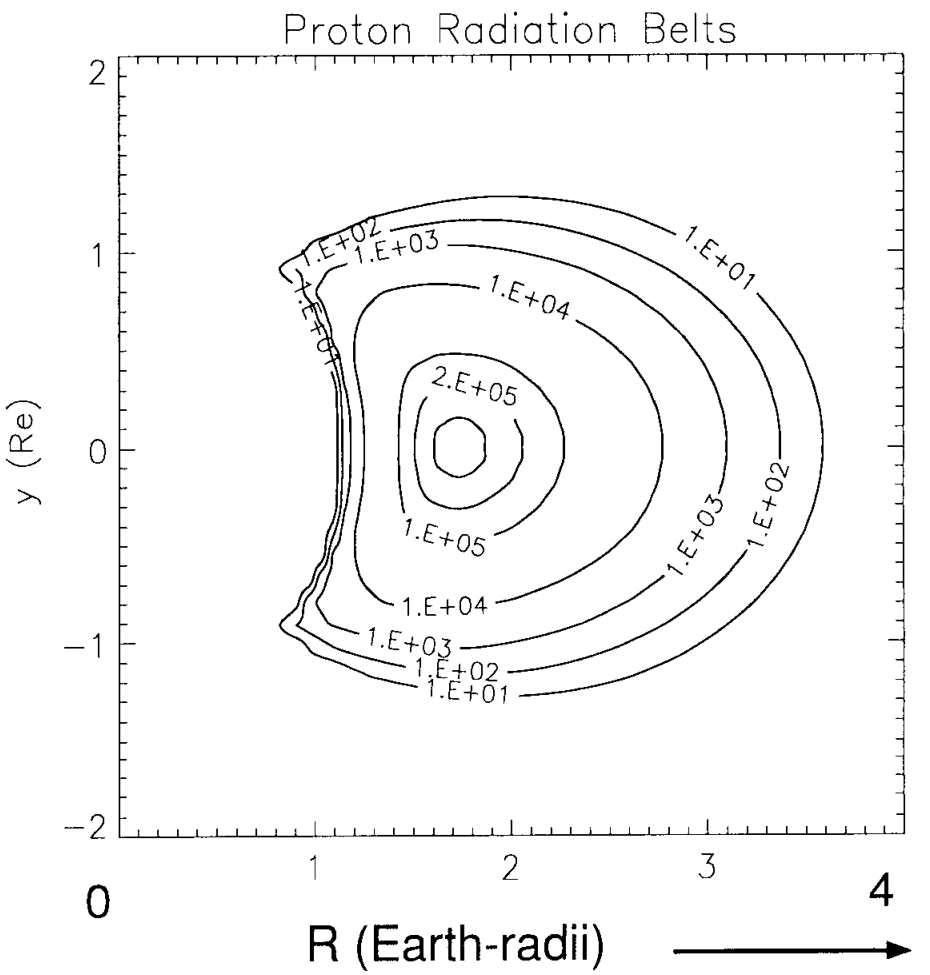

Radiation-belt proton model flux contours in "idealised dipole space".

FIGURE 3.3 - TRAPPED PROTON RADIATION BELTS

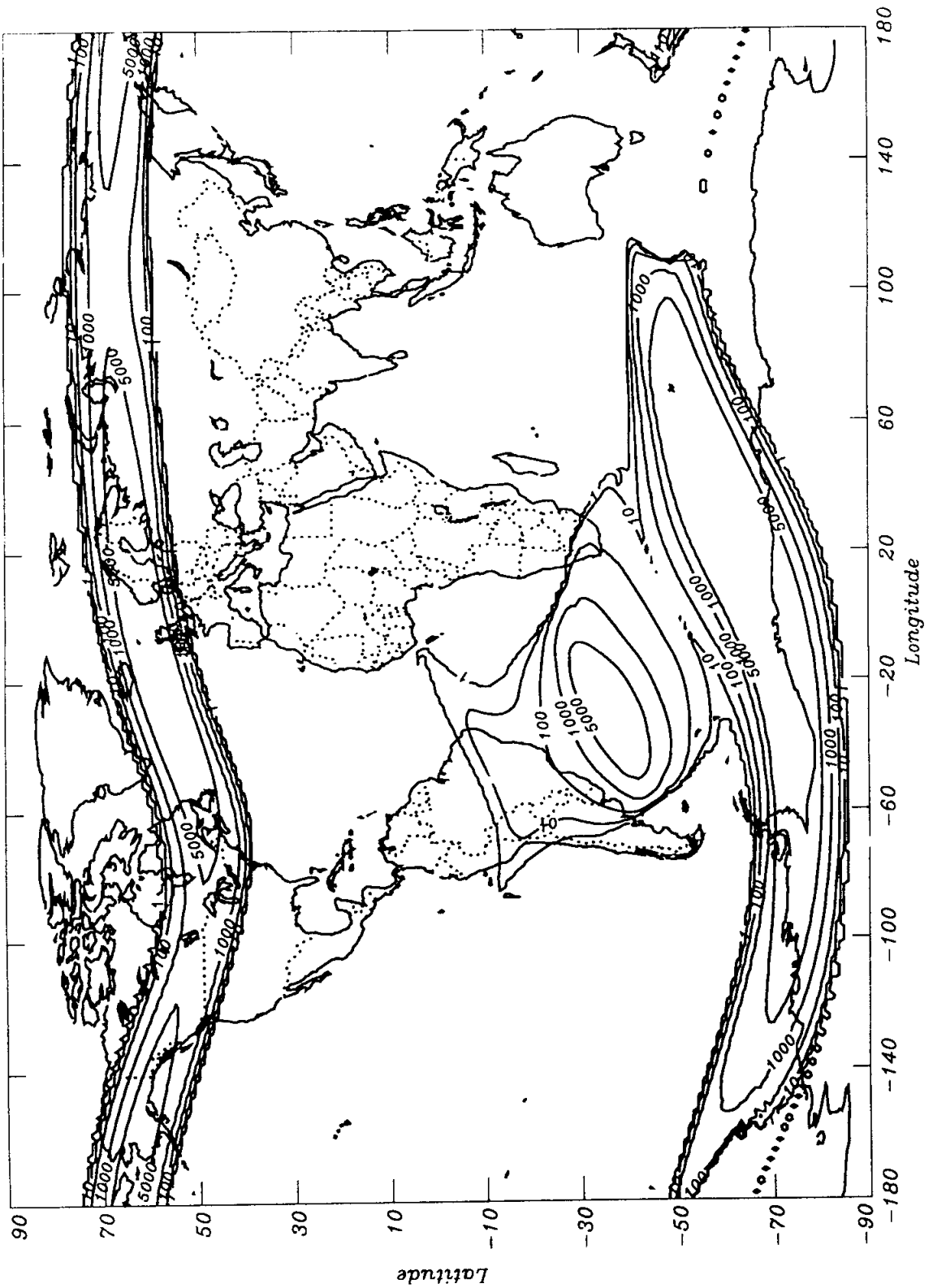

Contours of electron fluxes at > 1MeV showing the way in which the radiation belts, following the Earth's magnetic field come to low altitudes over the South Atlantic and at high latitudes

FIGURE 3.4 - THE SOUTH ATLANTIC ANOMALY AND OUTER ZONE FLUXES

3.3. SOLAR FLARES

In addition to exposure to the trapped radiation environment, a spacecraft is likely to encounter other transient radiation fluxes. The major effect to be considered is that due to solar flare protons. These particles, together with others such as electrons and alpha particles of a less significant nature, are emitted by the Sun in bursts during solar-flare activity ("solar storms") and their fluxes, besides being intermittent, vary overall with the solar cycle. The flux-energy spectra of solar protons are likely to be softer than those associated with trapped protons, but a spacecraft may nevertheless be exposed to considerable total fluence (time-integrated flux) levels. A single flare in August 1972 completely dominated the solar cycle number 20 (1964-1974) in terms of fluence and total dose. No flare as large was seen in cycle 21 (1974-1985), but Figure 3.5 (McGuire, 1983) shows that cycle 19 probably had a number of severe flares. The cycle in progress at the time of writing, cycle 22, contains a number of significant events. In particular, the October 1989 event was larger at low energies than that of August 1972 although it was still well below that event at E>10 MeV. Flare fluxes are about as predictable as most storms and are usually dealt with on a probability basis.

The degree of exposure to such effects is highly dependent upon orbital parameters. The Earth's magnetic field exhibits a shielding effect in equatorial regions, but allows the proton flux to be funnelled in towards the magnetic poles. (These protons produce the well-known polar absorption phenomenon in the ionosphere which has a strong disturbing effect on radio communications.) Thus, equatorial orbits will be shielded from solar-proton flux except at very high altitudes, whereas polar or highly inclined orbits may be greatly exposed even at low altitudes.

Geomatic shielding exhibits a significant east-west asymmetry, protons being able to penetrate to lower altitudes from the west than from the east. Disturbances in the magnetosphere also affect geomagnetic shielding. The shielding has been seen to weaken significantly in the wake of geomagnetic storms (Adams et al, 1981 and Daly, 1988).

3.4. COSMIC RAYS

3.4.1. Galactic cosmic rays

These are primary cosmic rays which originate outside the solar system but are associated with the galaxy. Cosmic rays are isotropic, highly energetic, charged particles, typically of 1 MeV to 1 GeV, although measurements have been made up to the 1 TeV range. They consist of electrons, protons and highly charged nuclei.

The most numerous particles are protons, with smaller populations of alpha particles, helium nuclei and decreasing numbers of the lighter nuclei. Beyond Z=30, the numbers of particles are very small. In addition, some Z>90 particles have been detected, but these are extremely rare.

Elemental abundances of galactic cosmic rays are shown in Figure 3.6 together with solar-system elemental abundances. For comparison, Figure 3.7 shows how the cosmic-ray abundances have been modified by fragmentation from their original source composition.

Variation of the overall galactic cosmic-ray flux is due to several effects. The most important effect is the intensity decrease during the solar maxima which occur in cycles of about 11 years (Figure 3.8). This flux decrease is thought to be due to the interaction of the galactic cosmic rays with the solar wind and so depends on the level of solar activity. Adams et al. (1981) chose a sine function as a means of predicting the modulation of their environment model:

$$M = A \sin \omega (t - t_0) + B \qquad \text{.....3(i)}$$

where: $\omega = 2\pi/10.9$ years^{-1} = 0.576 radians/year, t_0 = 1950.6 and A and B are constants chosen for the best fit to the data.

3.4.2. Solar cosmic rays

In addition to producing an intense burst of UV and X-rays, solar flares accelerate solar material to high velocities. Solar-flare protons were discussed earlier, but particles of higher Z are also produced in abundance. These solar particles are similar to galactic cosmic rays but, owing to their different origin, are not identical in composition (Chenette and Dietrich, 1984). During a flare, cosmic rays are dominated at low and medium energies by solar material of low atomic weight. In addition, the extragalactic overall cosmic radiation in an earth orbit may increase dramatically. This is because solar flares cause geomagnetic disturbances resulting in considerable lowering of the geomagnetic barrier. The

importance of "geomagnetic shielding" will be discussed later. See Adams et al (1981) for a fuller discussion.

3.4.3. Terrestrial cosmic rays

The primary cosmic radiation which penetrates the Earth's atmosphere is rapidly transformed by interactions which produce a cascade of secondary radiation. These cascades take place in the main body of the atmosphere and the secondary rays produced are the principal component of cosmic radiation at the Earth's surface. This process has been described at length by Rossi (1964) and also by Ziegler (1979) in relation to electronic devices on the earth's surface. Tsao et al (1984) have recently studied the atmospheric cosmic-ray environment at high altitude.

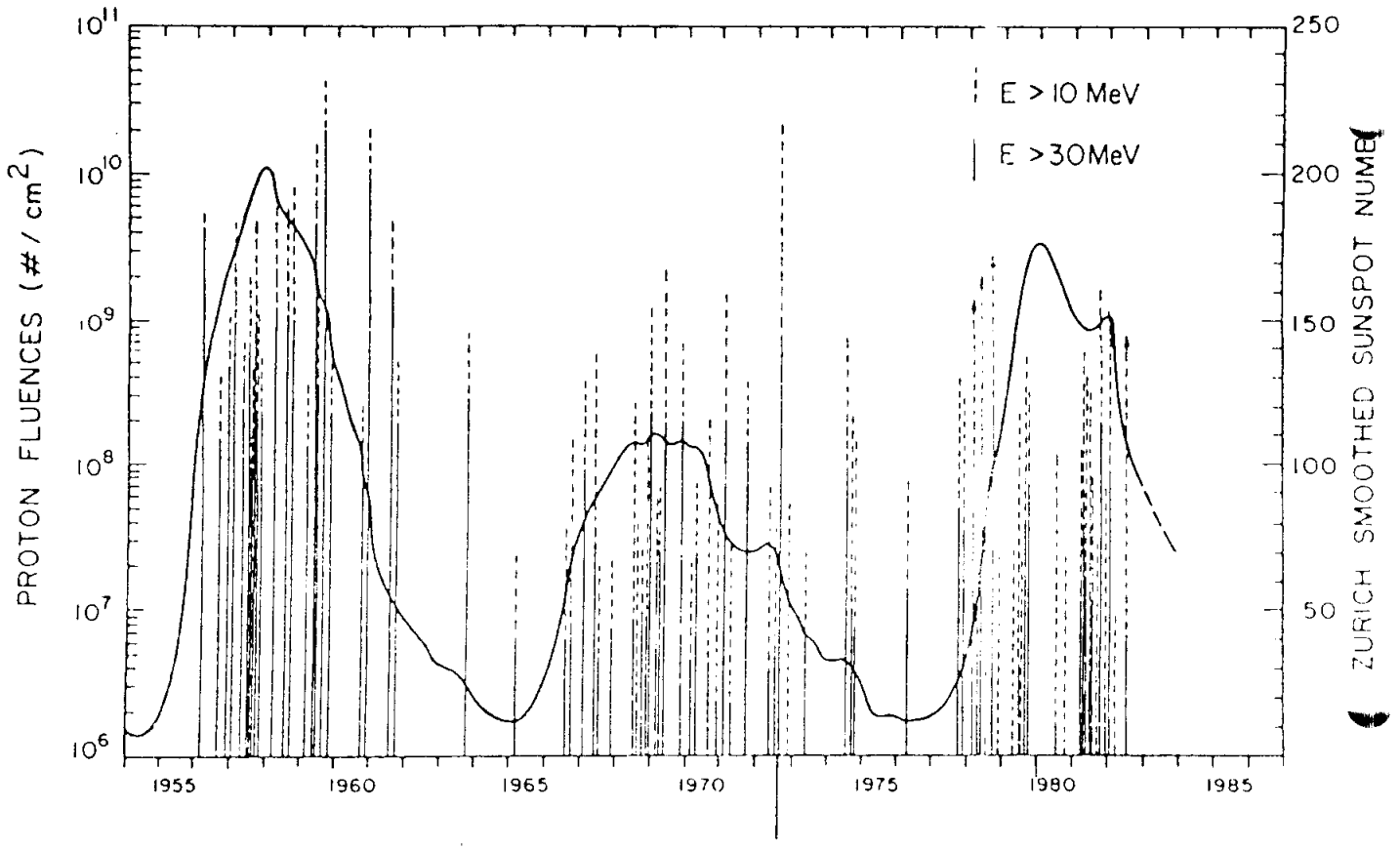

The occurrence of large solar-flare fluences (vertical lines) over the last three solar cycles superimposed on the sunspot number curve. The anomalous size of the August 1972 event is apparent.

FIGURE 3.5 - SOLAR FLARES

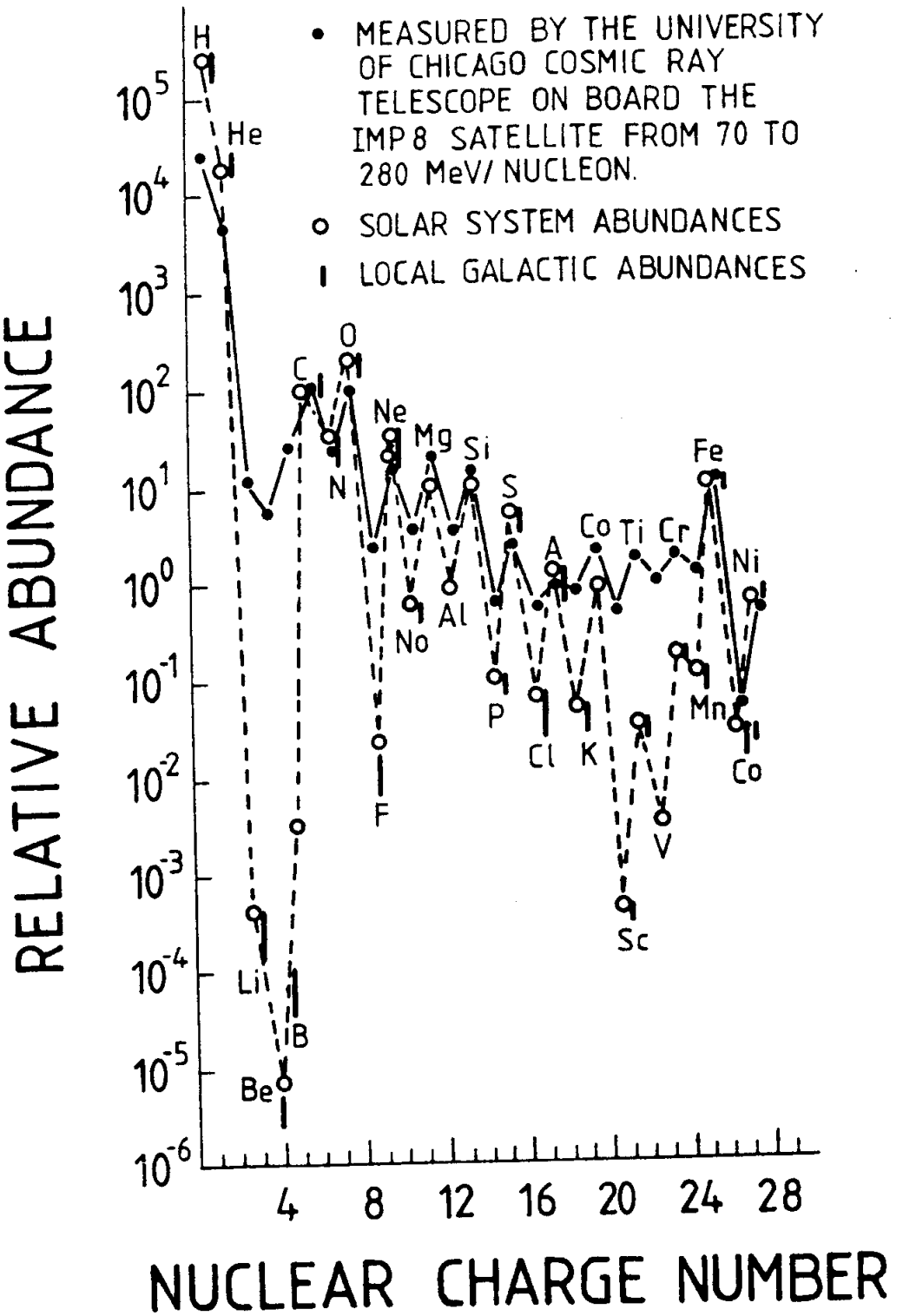

FIGURE 3.6 - ELEMENTAL ABUNDANCE OF GALACTIC COSMIC RAYS COMPARED WITH SOLAR SYSTEM ABUNDANCES

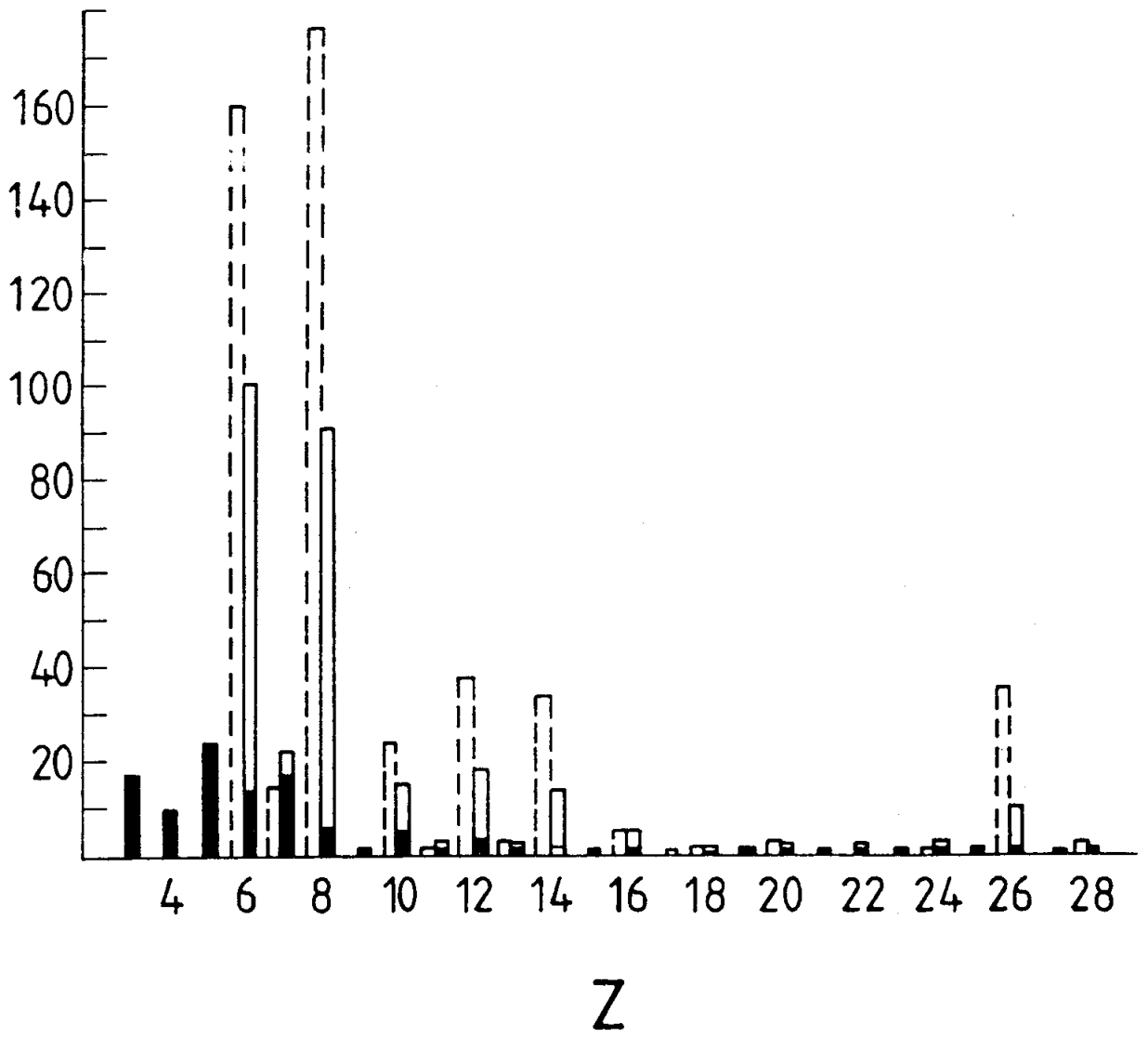

Dashed bars show source composition. Adjacent bars show arriving composition, the filled portion being nuclei produced by fragmentation and the open portion surviving primordial nuclei.

FIGURE 3.7 - COSMIC RAY FRAGMENTATION

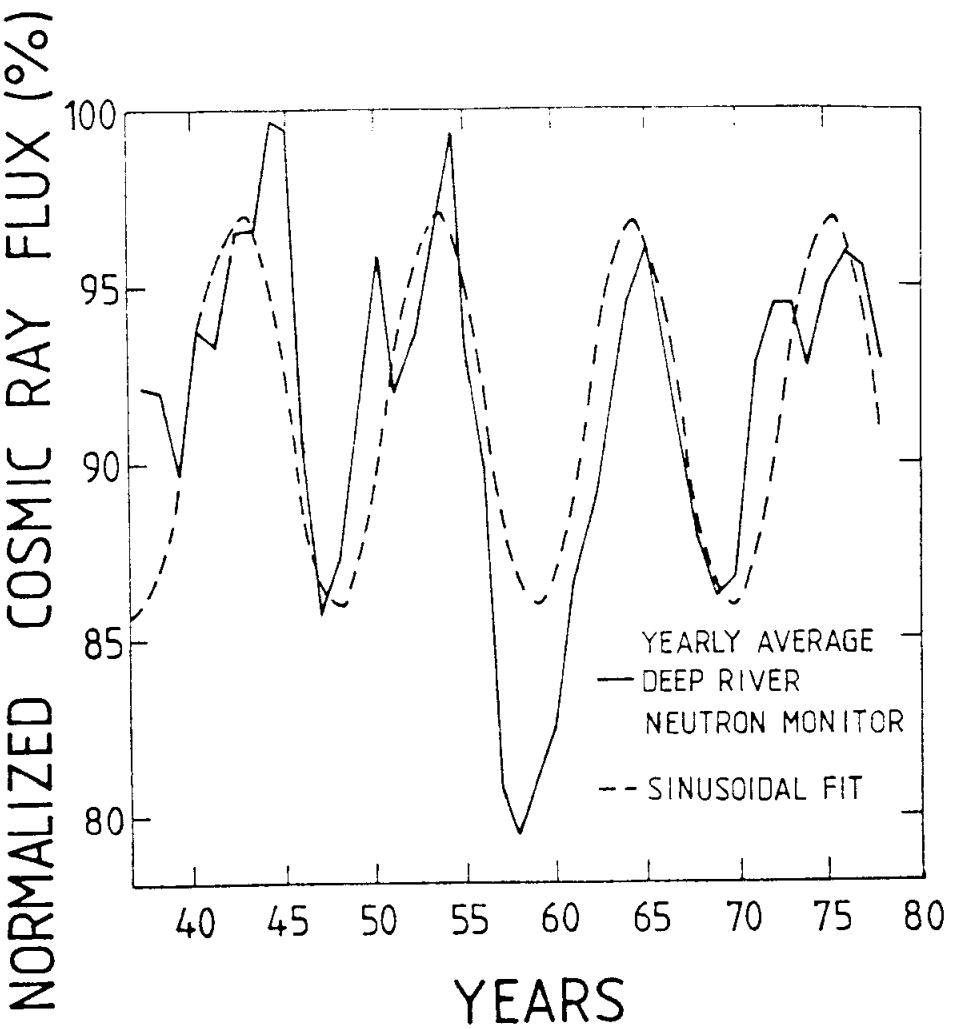

FIGURE 3.8 - THE 11-YEAR SOLAR CYCLE AS MEASURED BY THE GROUND - LEVEL COSMIC-RAY INTENSITY AT THE DEEP RIVER NEUTRON MONITOR (ONTARIO, CANADA)

3.4.4. Geomagnetic shielding

For cosmic rays to reach a spacecraft in earth orbit or the Earth's surface, they must penetrate the Earth's magnetic field. Since they are moving charged particles, they will tend to be deflected by the magnetic field. However, this tendency is opposed by the energy of the particles as they move at high velocity towards the Earth. A particle's penetrating ability is determined by its momentum divided by its charge and this quotient is referred to as its "magnetic rigidity".

So, for each point within the Earth's magnetic field, there is a minimum magnetic rigidity which a cosmic ray requires to reach that point. Particles below the minimum will be deflected and this minimum is called the geomagnetic cut-off value. As mentioned earlier, geomagnetic disturbances may affect the cut-off, lowering it. The cut-off value falls to zero at the edges of the magnetosphere and at the Earth's magnetic poles. Since the cosmic ray flux is highest at low energies, a satellite in earth orbit will be protected to some extent from cosmic rays by the magnetic field. The degree of protection will depend on the altitude and orientation of the orbit (Adams et al, 1983 and Adams, 1986). Geostationary orbits are afforded virtually no geomagnetic shielding against cosmic rays and polar orbits are also significantly exposed.

3.4.5. Other sources of cosmic rays

Adams (1981) referred to two other sources of energetic charged particles in the interplanetary medium. "Co-rotating events" give rise to infrequent modest increases in particle flux in the energy range up to 20 MeV. The particles are thought to be ejected from the high-energy tail of the solar wind and the streams are correlated with phenomena co-rotating with the Sun.

The "anomalous cosmic ray component" makes a more significant contribution but, near the Earth, appears infrequently at each solar minimum or at alternate ones. The anomalous spectra are observed for helium, nitrogen and oxygen and it is thought that the particles involved are singly charged. Their origin could be clouds of neutral interstellar gas entering the solar system. They become ionised as they approach the Sun and are then accelerated in collisions between fast and slow moving streams of solar wind. The energies of the nuclei are mainly in the range 1 to 30 MeV. An important point is that, if the anomalous component is only singly charged, the particles will penetrate deeper into the magnetosphere than cosmic rays of similar mass and energy.

3.5. LOW-ENERGY PARTICLES AND PLASMA

At the other end of the energy spectrum, protons and electrons in the energy range up to about 100 KeV are encountered throughout

the space environment. Within the trapped radiation belts, these particles merely represent the low-energy extremes of the trapped electron and proton populations.

Since these particles will be stopped effectively by minute thicknesses of material, only the most exposed surfaces are expected to be vulnerable. Thermal-control surfaces of spacecraft will be affected. These particles can penetrate sensors on some astrophysics satellites and produce a "background" signal.

Of course, the plasma environment at geostationary altitudes is well known for its ability to induce high levels of electrostatic charging on spacecraft. Energetic particles are also known to cause charging of internal spacecraft dielectrics such as those found on cabling, etc.

3.6. OTHER PLANETS

This subject is of special importance at the present time when long-term missions to remote parts of the solar system are under way or being planned. The giant planets have trapped radiation belts similar to, but more intense than, Earth's. Measurements of Jupiter's environment have been made by the Pioneer 10 and Voyager spacecraft and, more recently, by Ulysses, and a great deal of work has been carried out to prepare spacecraft electronics for survival in that environment. There are reports suggesting that Jupiter's electrons are occasionally transported to the Earth's magnetosphere (Baker et al, 1986). Saturn is also known to have an energetic radiation environment.

3.7. SECONDARY RADIATION

When real spacecraft are considered, the natural radiation environment is complicated by the secondary effect of "Bremsstrahlung" (brake-radiation) X-rays. This type of radiation is caused when electrons are slowed down in any way, e.g. by their interaction with the spacecraft material. Megavolt Bremsstrahlung will penetrate about one centimetre of aluminium with only 10% loss of intensity. It can sometimes therefore be considered as having an irreducible effect on unmanned spacecraft which are rarely constructed of aluminium thicker than 3 to 8 mm.

Secondary protons and neutrons are generated by high-energy protons in space. Radioactivity induced by high-energy nuclei in spacecraft is at a level too low to produce component degradation, but can interfere with instrument operation.

The products of proton-induced nuclear interactions can cause component upset (see below).

3.8. PREDICTION OF RADIATION LEVELS - ENVIRONMENTAL MODELS

3.8.1. General

The foregoing sections make it clear that, owing to the highly structured nature of the trapped radiation environment, the flux received at the surface of Earth-orbiting spacecraft varies considerably with orbital altitude and inclination. Figure 3.2 shows for example that a polar orbit will pass four times through the cusps of the outer zone even though an equatorial orbit at the same altitude may be well inside the inner zone. Other effects arise from geomagnetic anomalies. Figure 3.4 shows that low-altitude circular orbits will continually pass through the South Atlantic anomaly, giving rise to a highly variable flux exposure. Geostationary satellites, with a fixed geographic latitude, will vary in geomagnetic latitude depending on their longitude, because of the tilted field axis, and will thus experience different fluxes. Furthermore, as described earlier, the effect of the solar wind is to distort the Earth's field, and hence the radiation belts, into a highly asymmetric shape, so that a spacecraft - even if describing a circular equatorial orbit - will be subject to a diurnally (day-night) varying flux of particles. It will be clear also that time factors such as the solar activity cycle are influential.

In response to the obvious need for quantitative prediction of radiation levels likely to be encountered during space missions, models of trapped radiation environment have been constructed. These present data in graphical and numerical form and allow either manual calculation or computer handling. The models were derived from measurements by particle detector equipment aboard a large number of spacecraft. The standard models were produced by the National Space Science Data Center (NSSDC at NASA Goddard SFC).

Since the radiation environment is in a continual state of change, either rapid or slow, no published model is ever completely up-to-date. Successive versions reflected these changes together with improvements in particle measurement and data handling techniques and new data from scientific probes in orbit. However, the most recent models are based on satellite data acquired before 1971. The reader is referred to Holmes-Siedle et al. (1985), McCormack (1986), Gussenhoven et al. (1987) and Gussenhoven et al. (1991) for reports of comparisons between flight experience and model predictions.

It is useful to note various terms and conventions before describing the models in more detail:

(i) Particle fluxes, usually described as "omnidirectional", are often considered as isotropic from all directions. In fact, omnidirectional really means treating fluxes from all directions equally. It is a subtle difference, but the variation of omnidirectional flux along a field line can be used to derive the directional distribution at any point (Hess, 1968).

(ii) "Orbital integrations" are presented for various altitudes and inclinations. The fluxes quoted are averages around an orbit, thus allowing for the passage of an orbit through different radiation zones.

(iii) "Integral flux" is the total flux ($cm^{-2}\ s^{-1}$) at all energies above a quoted threshold energy. "Differential flux" is the rate of change of flux with energy at a specific energy ($cm^{-2}\ s^{-1}\ MeV^{-1}$).

(vi) Models are ascribed to particular epochs and versions relate specifically to either solar minimum or solar maximum conditions.

The latest NSSDC models are described below. They are distributed as hard copy, microfiche and in computer-readable form. The models are described by FORTRAN BLOCK DATA subprograms in the format originated by Kluge and Lenhart (1971). Here, the equatorial $\log_{10}$ fluxes at discrete energy (E) and L values are stored and the B variation described by tabulating at each (E, L) point the changes in B/B_0 required for constant $\log_{10}$ flux decreases. B_0 is the field strength at the geomagnetic equator where the field is a minimum. So, as normally distributed, these models provide integral omnidirectional fluxes as functions of E, L and B/B_0.

There are other features of the radiation environment which may be important in some situations such as flux anisotropy (Watts et al. 1989), diurnal (day-night) variations described above and short-term (e.g. magnetic storm) effects. The NSSDC documentation for earlier models (e.g. Teague and Vette, 1972, Singley and Vette, 1972) describe forms of those models which included pitch-angle distributions, local-time dependence and a statistical model. The condensed-format convention for the new models does not include these features (although pitch-angle distributions can be derived from the B variation as mentioned above).

McCormack (1986) reported on the importance of the choice of geomagnetic field epoch used when accessing the NSSDC

environment models. Before the fluxes are computed from the models, it is necessary to compute the geomagnetic B-L co-ordinates of the point of interest by using a geomagnetic field model. Problems arise from the fact that the geomagnetic field is varying slowly. As pointed out above, the environment data were acquired in the 1960s. Since then the field has decayed and shifted somewhat and predictions of further "secular" variations to the 1990s or beyond yield a significantly modified field. The data were obviously organised according to the 1960 field. Using updated or extrapolated field epochs implies that, because the field has shifted, corresponding field lines are closer to the Earth and the radiation belts have come down to lower altitude giving higher exposure in low-Earth orbit. The fact is that the radiation environment is not permanently frozen on a field line, but is the result of an equilibrium between continual creation and loss processes (Daly, 1989). The observed environment has in fact varied less in spatial terms than if it were tied so closely to the varying geomagnetic field. The initial recommendation of the NSSDC was that geomagnetic model epochs should not be extrapolated beyond the 60's in using these models. Lemaire et al. (1990) point out that no extrapolation should be performed.

3.8.2. Trapped electrons - AE8

AE8 is a model for the electron environment for energies of 40keV to 7MeV and L values of 1.2 to 11 R_E. It is available in two versions, AE8MAX and AE8MIN for solar maximum and solar minimum periods respectively. These models have only recently been documented (Vette, 1991). Figure 3.9 shows the radial variation of the model omnidirectional fluxes at the geomagnetic equator for three energy thresholds. The models replace previous models for inner-zone electrons and models for outer-zone electrons whose documentation is still of some relevance to the AE8 model (Teague and Vette, 1974 and Teague et al., 1976).

At low energy and equatorially, the AE8 model looks much like the previous models. At high energy in the outer zone, the fluxes are generally below those of its predecessor, the AEI7 model. The location along the field line of the atmospheric cutoff of fluxes has also been revised, leading again to a lowering of fluxes. Figure 3.10 shows a comparison of AE8 equatorial radial flux variations at E > 4MeV and those for the AEI7 models. Figure 3.11 shows a comparison between the flux variations along the field lines at E > 2MeV and L=3 and 5. An example of the electron spectrum derived from the AE8MAX model when an average is performed over a geostationary orbit (see Section 18, "Computer Methods") is given in Figure 3.12.

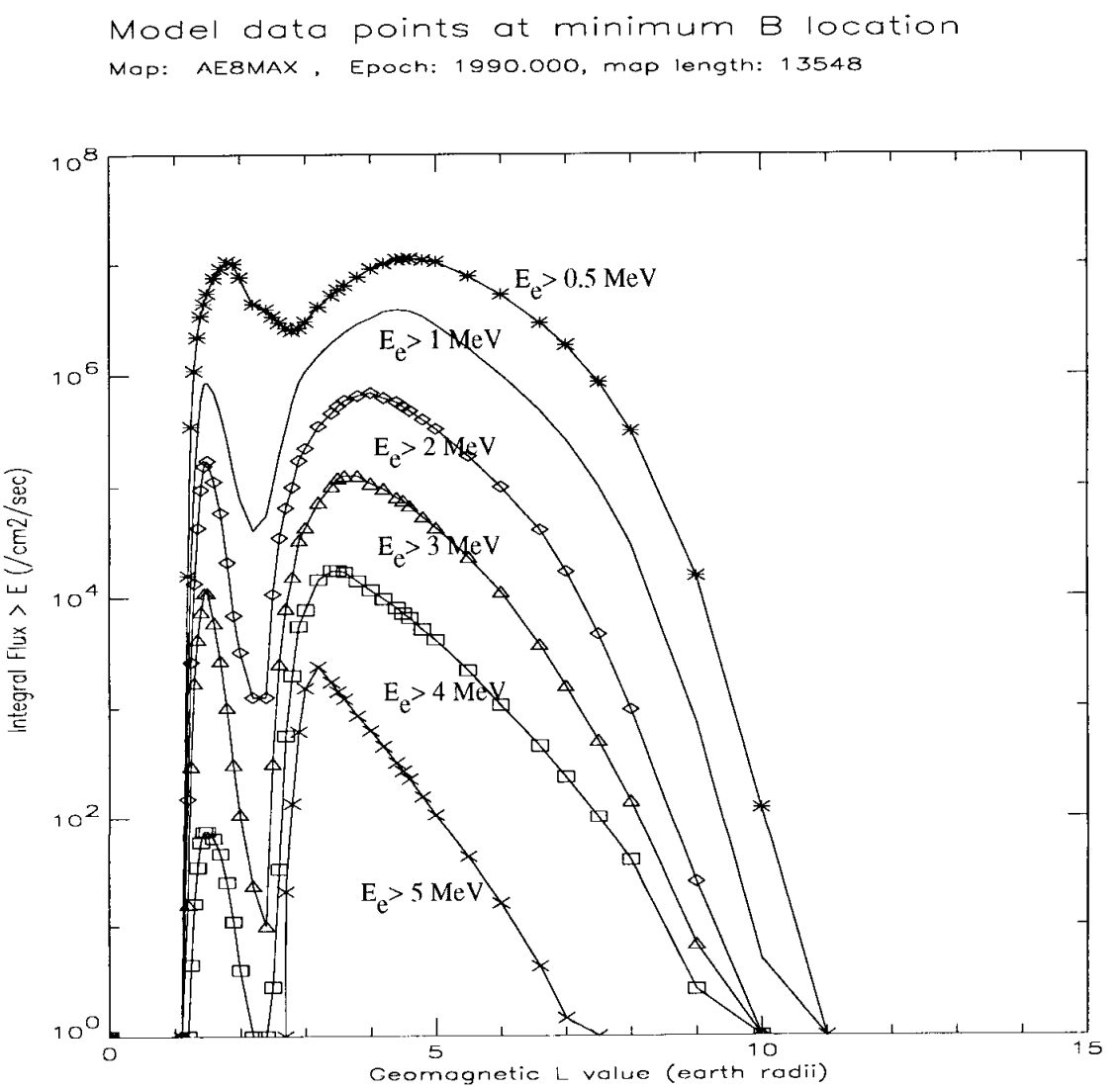

Radial variation of AE8 model omnidirectional fluxes at the geomagnetic equator for three energy thresholds.

FIGURE 3.9 - RADIAL ELECTRON FLUX VARIATIONS

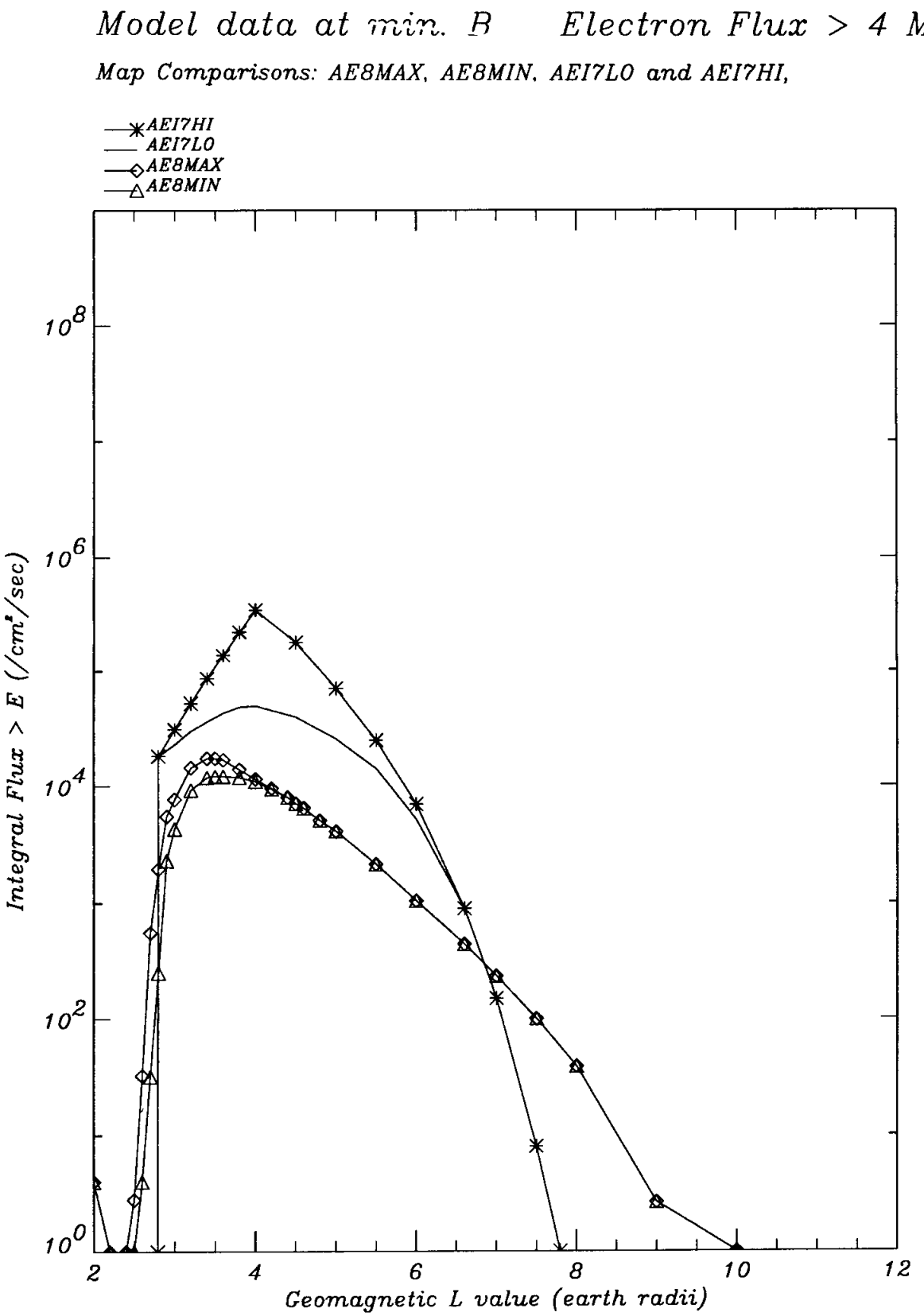

A comparison of equatorial radial variations of AE8 model omnidirectional fluxes at E > 4 MeV with those for the AEI7 models.

FIGURE 3.10 - COMPARISON OF ELECTRON MODELS AE8 AND AEI7

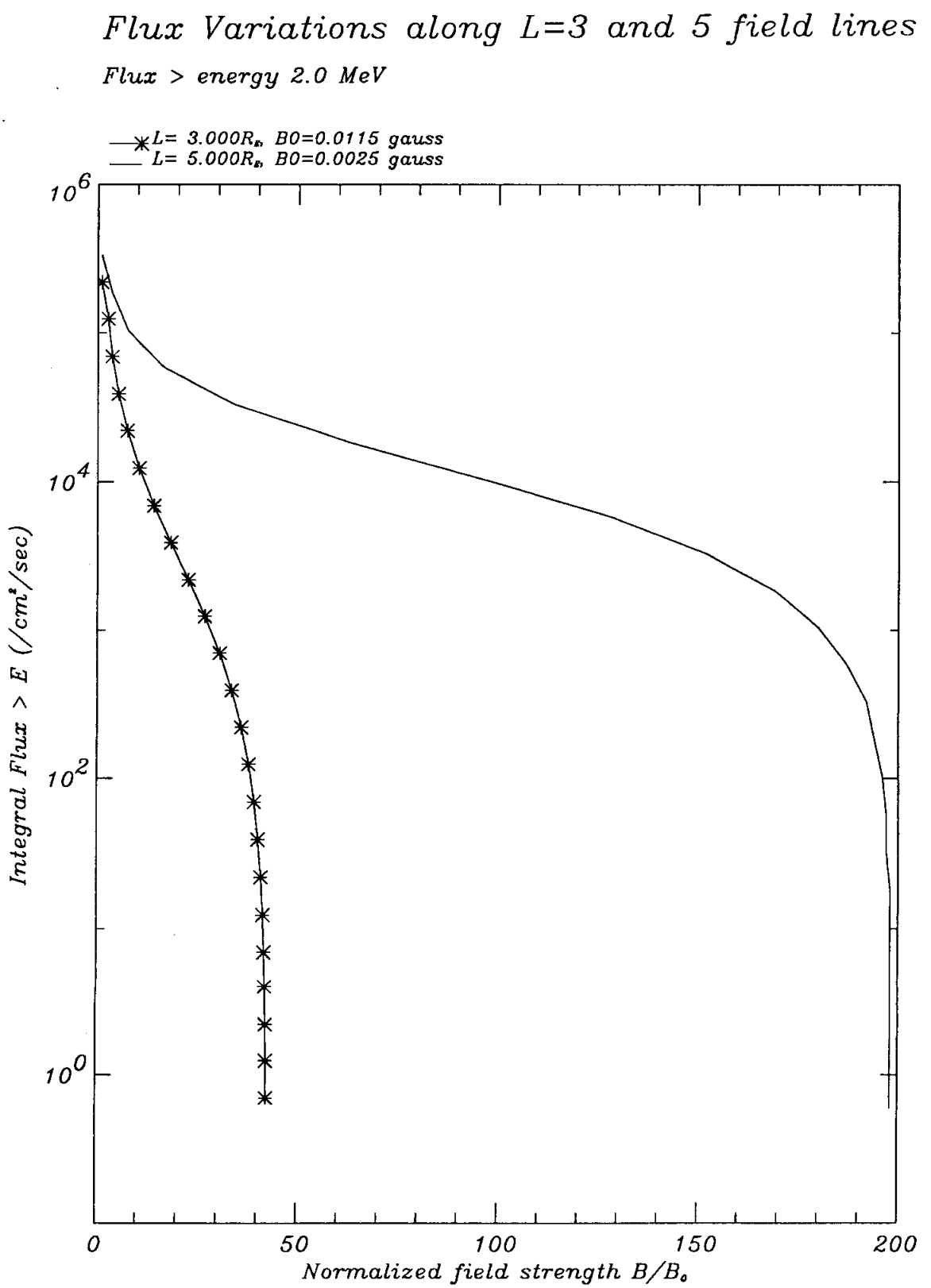

A comparison between the electron flux variations along the field lines at E > 2 MeV and L=3 and 5.

FIGURE 3.11 - AE8 FLUX VS. B VARIATIONS

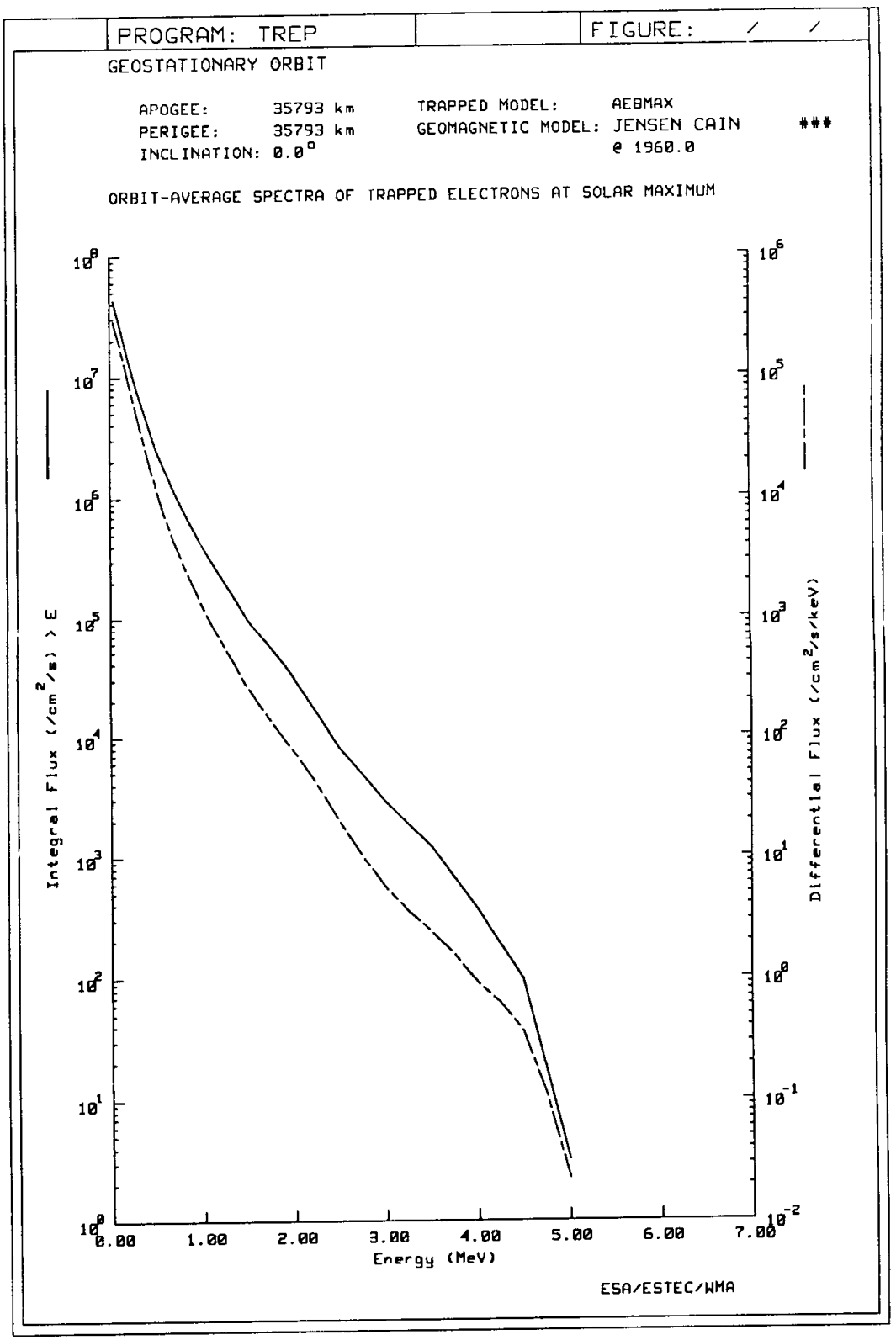

Example of electron spectrum derived from the AE8MAX model when an average is performed over a geostationary orbit.

FIGURE 3.12 - EXAMPLE ELECTRON SPECTRUM

3.8.3. Trapped protons - AP8

The AP8 model (Sawyer and Vette, 1976) is the latest model of the trapped proton environment for energies of 100 keV to 400 MeV and L values of 1.15 to 6.6 R_E. Again, it contains solar maximum and solar minimum versions, AP8MAX and AP8MIN respectively, which are distributed as FORTRAN BLOCK DATA subprograms in the format of Kluge and Lenhart, providing average omnidirectional fluxes as functions of E, L and B.

Figure 3.13 shows plots of AP8 equatorial radial flux variations at a number of energy thresholds. Figure 3.14 shows the flux variations along the field lines at E > 20 MeV and the L=1.5, 2 and 3. An example of the proton spectrum derived from the AP8MIN model when an average is performed over a circular low Earth orbit (500 km, 28°) is given in Figure 3.15.

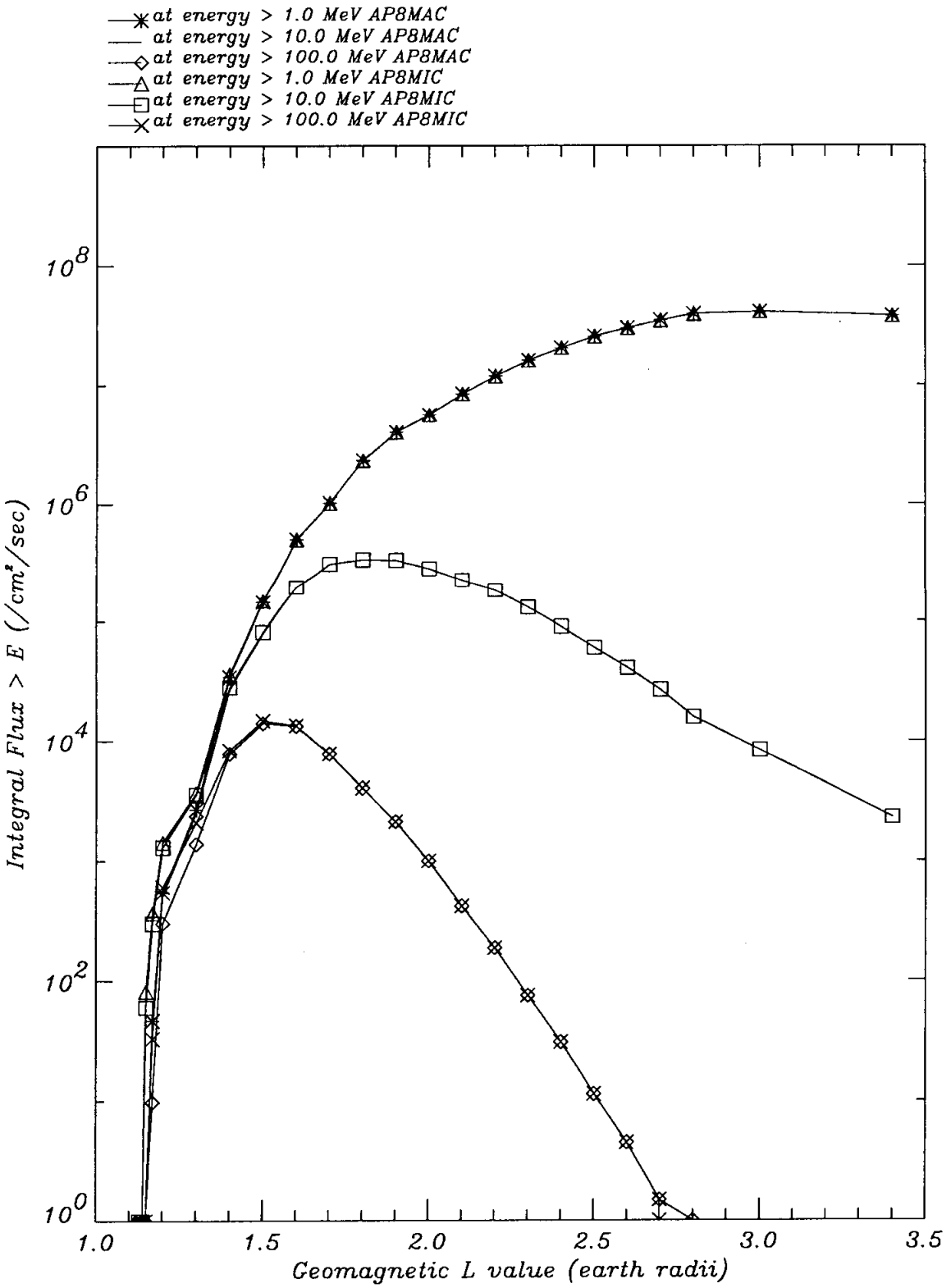

Plots of AP8 model equatorial flux radial variations at a number of energy thresholds.

FIGURE 3.13 - RADIAL PROTON FLUX VARIATIONS

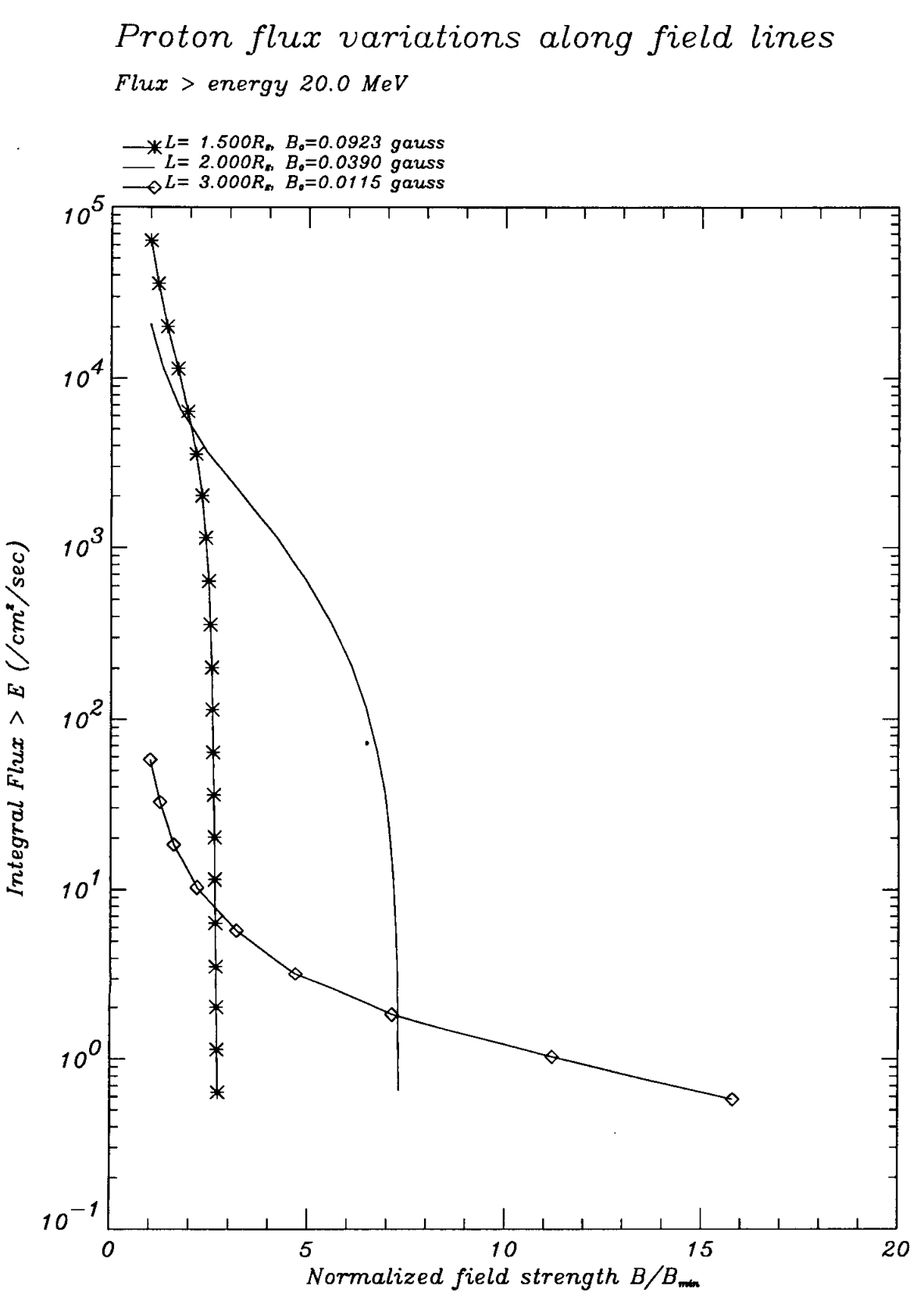

The figure shows the proton flux variations along the field lines at E > 20 MeV and L=1.5, 2 and 3.

FIGURE 3.14 - PROTON FLUX VARIATIONS WITH B.

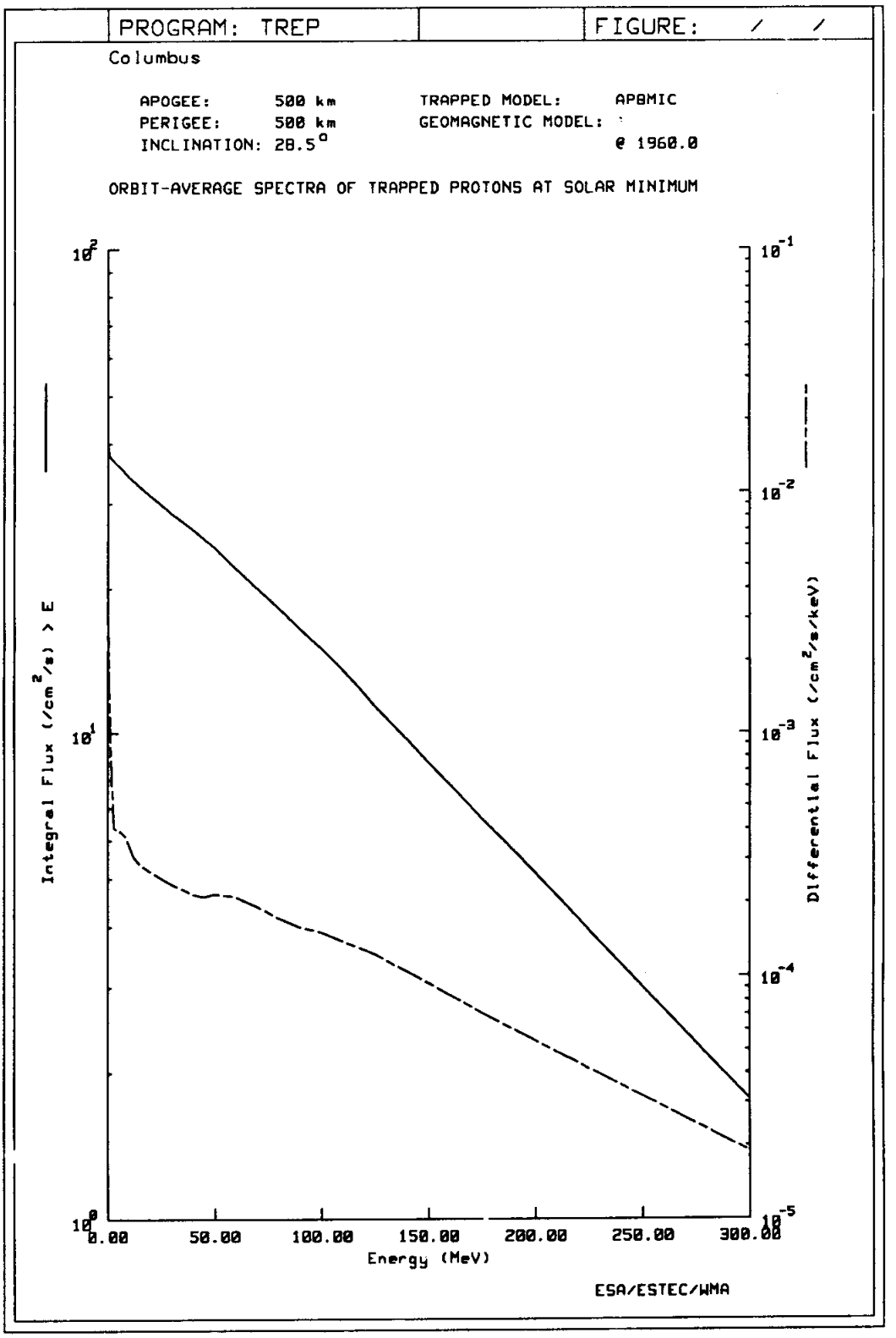

Example of Proton Spectrum derived from the AP8MIN model when an average is performed over a circular low earth orbit (500 km, 28°).

FIGURE 3.15 - EXAMPLE OF PROTON SPECTRUM

3.8.4. Solar flare protons

Predicting solar-proton fluxes and constructing a model on which to base calculations is an entirely different matter from that associated with trapped radiation. The problem has been tackled by NASA and predictions for solar cycle 21 (1974 - 1985) have resulted from the work of King (1984) and Stassinopoulos and King (1984). King's work was essentially based on one solar cycle's worth of data. Recently, Feynman et al. (1990) evaluated three cycles and produced a new statistical model and the models were compared with each other and the event record by Tranquille and Daly (1992).

For prediction purposes, it has been found most reasonable to regard the solar cycle as consisting of seven active years, in which significant solar-proton flux may be expected, and four quiet years during which only minor events occur.

The history of recent cycles is shown in Figure 3.16 from Tranquille and Daly (1992), while Figure 3.17 gives the integral flux predicted by the King model on the above simple model for three energy thresholds over the seven active years. The actual annual fluence for cycle 20 at the 10 MeV threshold is also shown. A flux versus energy spectrum based upon this model is included in Figure 3.18. The difficulty in making such a prediction is illustrated by the fact that in the very active year of 1972 almost all this year's fluence was received during one August week; in fact, the contribution from this one week represents 67% of the total fluence for the entire seven years.

Flares are assessed on a statistical basis. The King model is based on the observation of one anomalously large (AL) flare of the August 1972 type in a 7 year period. A worst-case assessment is normally made, yielding a number of flare events with a high probability (90% or even 95%) that the number of flares will not be exceeded. This modified Poisson statistic is due to Burrell and is described by King (1974). The table below shows the probability of occurrence of flares in a seven-year period given that one was observed in a previous seven-year period.

Number of Events n	Probability of n
0	25%
1	25%
2	19%
3	12% –> 81% confidence of no more
4	8% –> 89% confidence of no more
5	5% –> 94% confidence of no more
6	3% –> 97% confidence of no more

In the model of Feynman et al., no distinction is made between ordinary and anomalously large events since all are found to lie on a log-normal fluence distribution, as shown in Figure 3.19. The Feynman model is now recommended as the standard. A detailed comparison between the models of King and Feynman et al. was performed by Tranquille and Daly (1992). This showed, for example, that the worst one-year period in the solar event record corresponds to a confidence level in the Feynman et al. model for more than 96%, indicating that high confidence levels are not unduly pessimistic. They also make comparisons between the models and more recent data. Figure 3.20, from their work, shows comparisons between King and Feynman et al. model spectra for various periods.

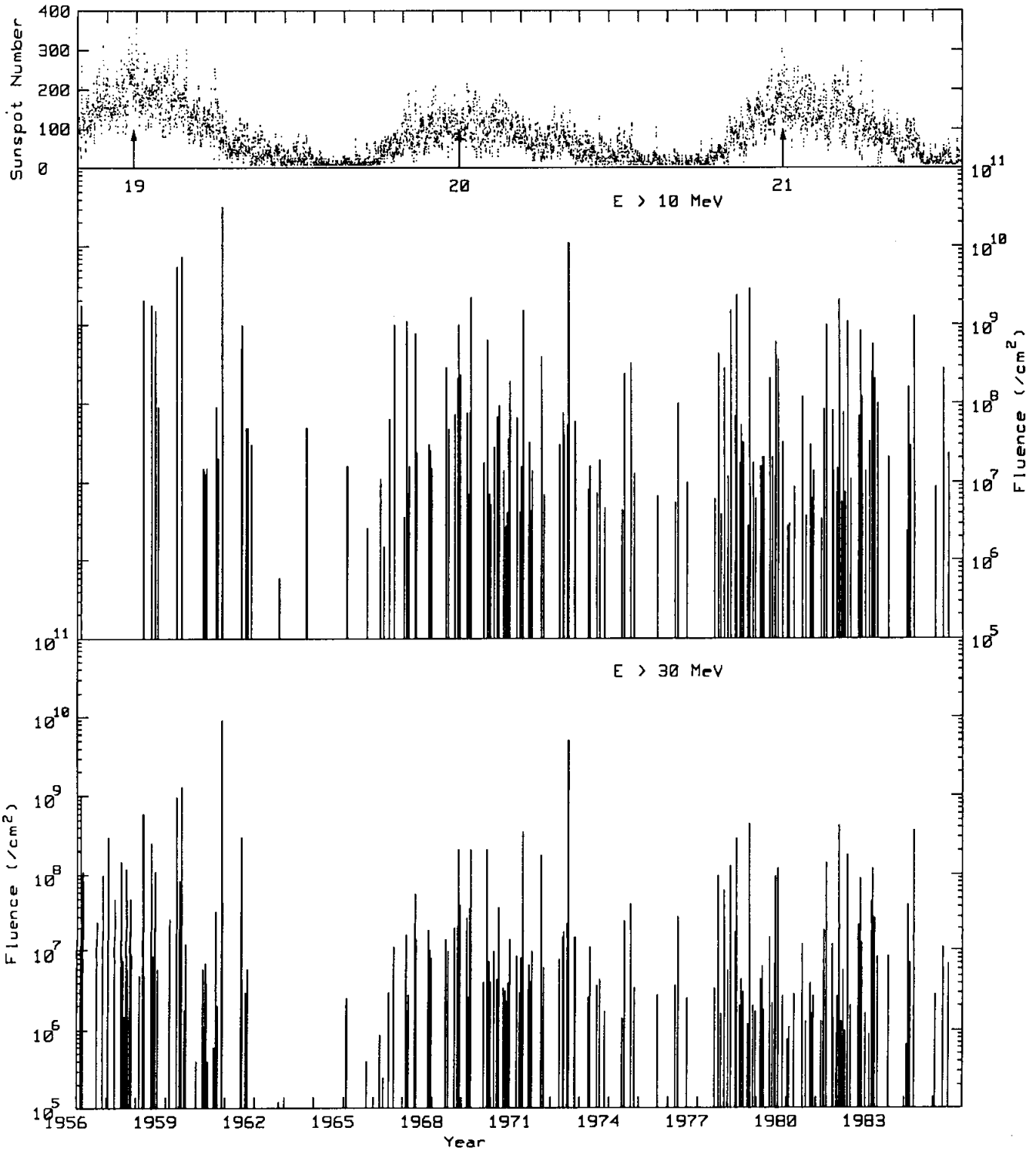

Solar activity cycles 19, 20 and 21. This shows the periodicity of sunspot maxima and minima and the way particle events are linked to this periodicity. Event-integrated proton fluences are shown for two energy thresholds (Tranquille and Daly 1992).

FIGURE 3.16 - SOLAR ACTIVITY OVER 3 SOLAR CYCLES

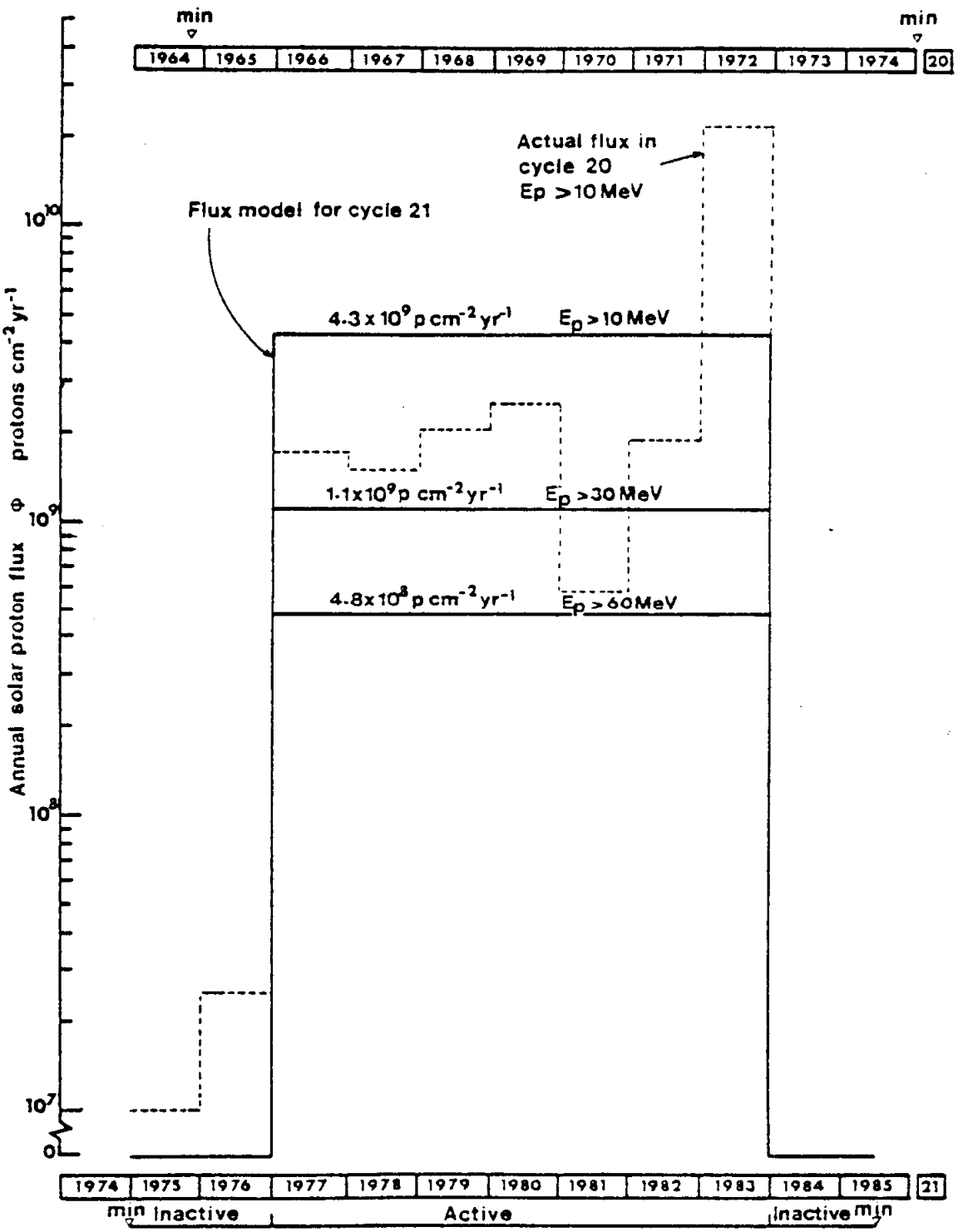

Predicted model for solar-flare proton integral flux in free space at Earth's orbit, for solar cycle 21.

FIGURE 3.17 - SOLAR PROTON MODEL

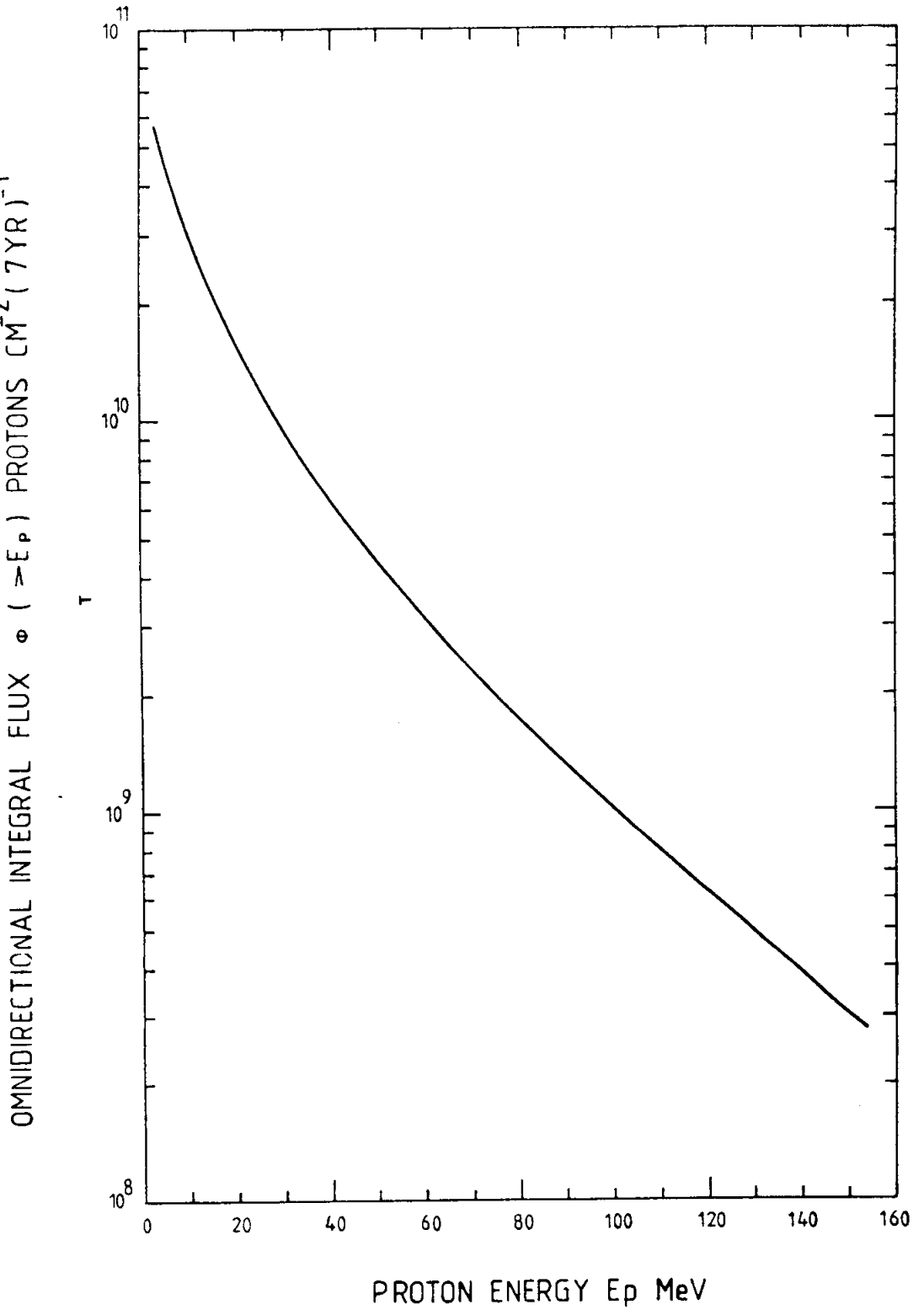

Integral flux spectrum derived from the model for solar cycle 21. Seven active years.

FIGURE 3.18 - SOLAR PROTON SPECTRUM

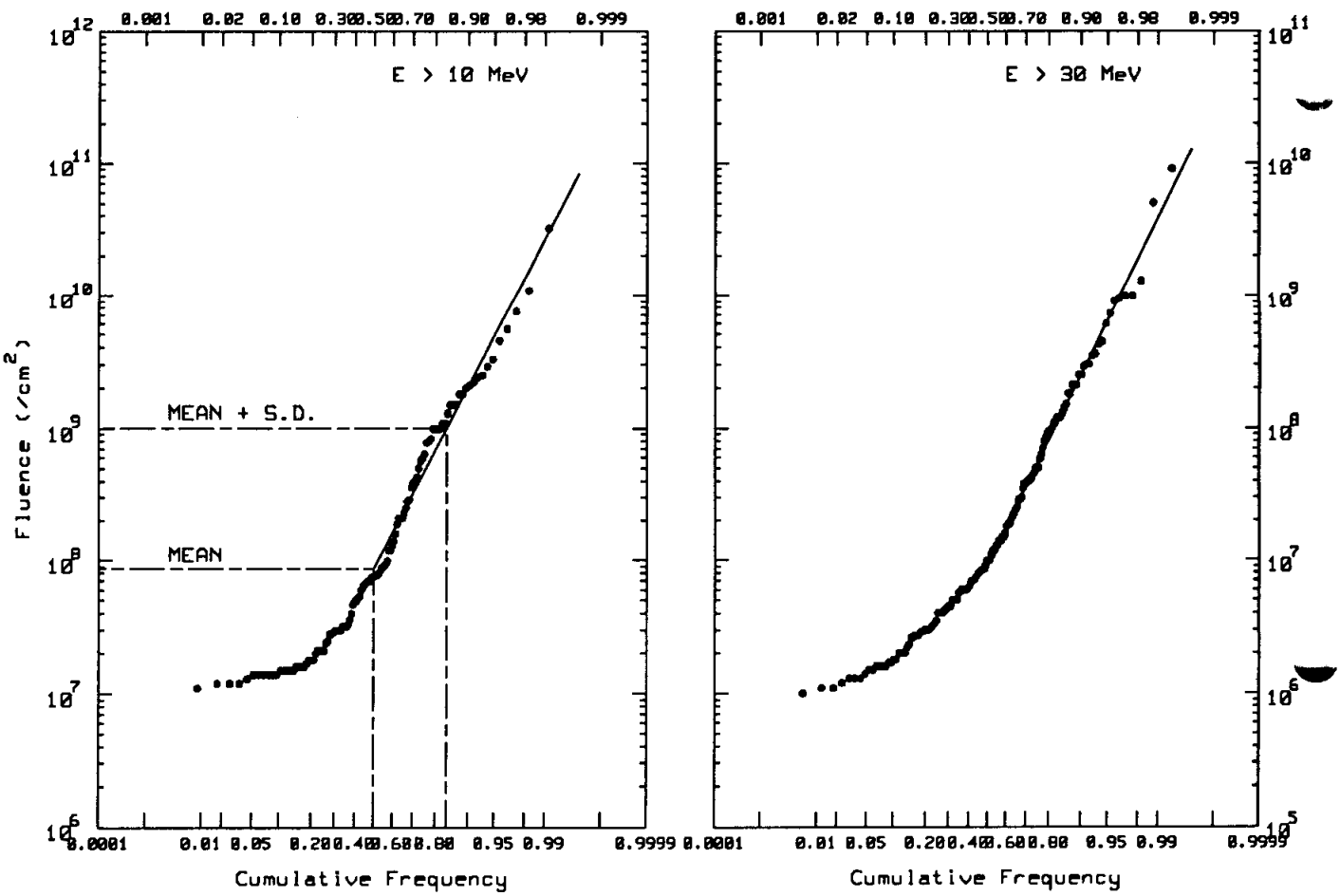

The Cumulative Event Fluence Distribution use for the statistical event model of Feynman et al. This shows that even large events follow a log-normal distribution. (From Tranquille and Daly, 1992).

FIGURE 3.19 - THE CUMULATIVE EVENT FLUENCE DISTRIBUTION

The models are based upon conditions of free space (outside the Earth's magnetic field) at the Earth's orbital distance from the sun. However, we have already mentioned in Section 3.4.4. that geomagnetic shielding keeps some particles from reaching certain locations. Stassinopoulos and King also consider the likelihood of the solar protons penetrating the Earth's field. It is assumed that protons in the energy range 10-100 MeV can be expected to penetrate to magnetic shell L = 5 approximately. Thus, a satellite in geostationary orbit may be considered to be completely exposed, while one in an equatorial orbit at 18 530 km altitude L = 3.9) is to be considered to be completely shielded by the Earth's field. In polar or highly inclined orbits, of course, spacecraft may pass back and forth between regions of high L (high exposure) and low L (effective shielding). "Percentage exposure" maps, relating solar proton exposure to orbital altitude and inclination, are provided by Stassinopoulos and King (1984).

The direction of arrival at a point in the Earth's field also plays a role in geomagnetic shielding. It can be shown (e.g. Daly, 1988) that cosmic rays penetrate the geomagnetic field more easily from the west than from the east. Computing the geomagnetic cut-off for vertically arriving protons shows that the Stassinopoulos and King model corresponds to excluding protons of E < 200 MeV from arriving vertically al L < 5 in a quiet magnetosphere. Figure 3.20 (from Daly, 1988) however, shows that protons of lower energy can penetrate below L=5 with other arrival directions, especially in a disturbed magnetosphere where the geomagnetic shielding is weakened. For westward arrival at the L=5 geomagnetic equator in a disturbed magnetosphere, the energy cut-off could be as low as 30 MeV. An arrival-direction-dependent model for flare-proton cut-offs throughout B, L space can be used by the ESA UNIRAD system (see Section 18 "Computer methods"). Recently, Gussenhoven and Muller (1992) have reported that during the March 1991 solar-proton event, the CRRES satellite observed abnormally deep penetration of solar protons into the inner magnetosphere.

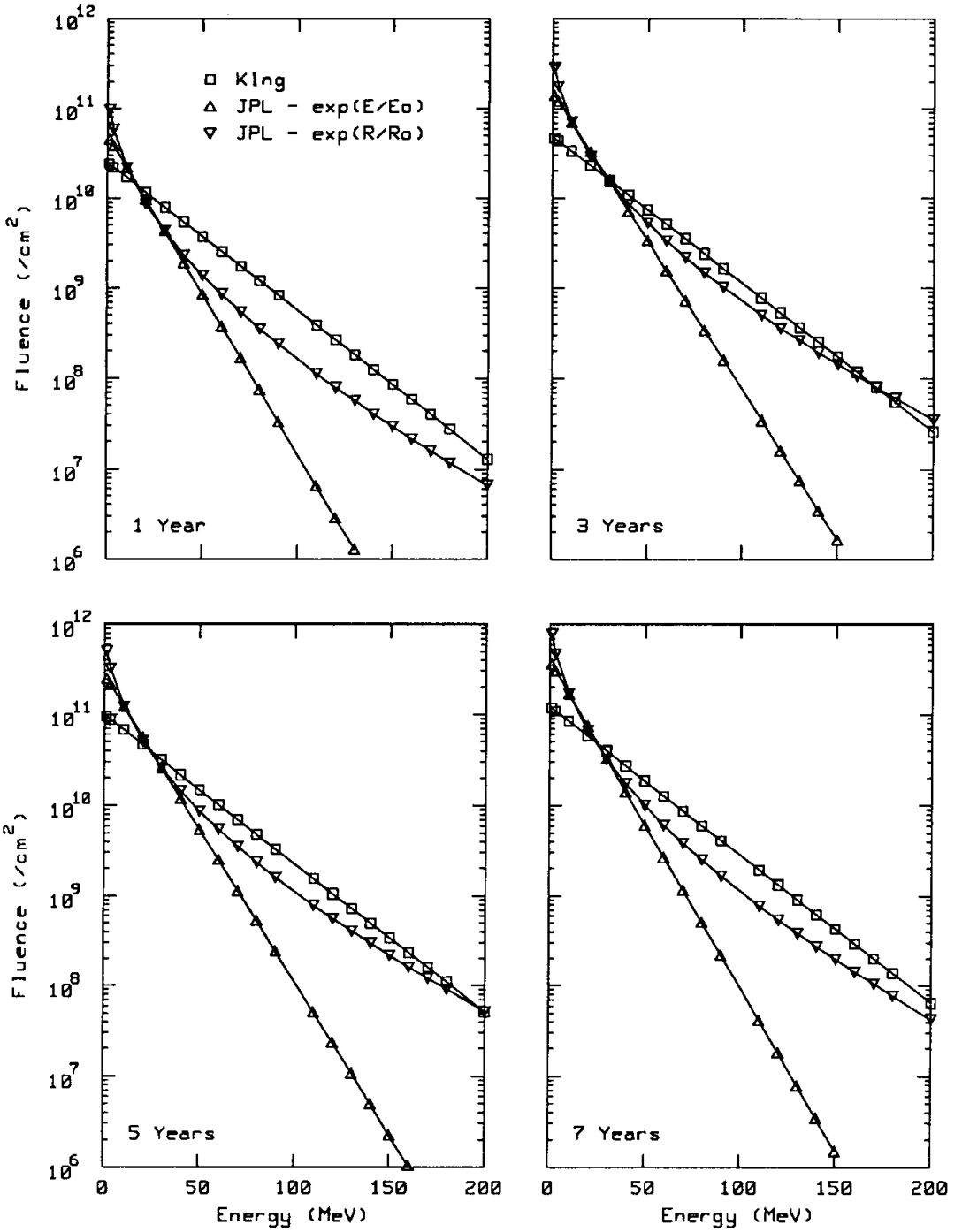

FIGURE 3.20 - COMPARISONS BETWEEN SOLAR PROTON SPECTRA FROM MODELS OF KING AND OF FEYNMAN ET AL.

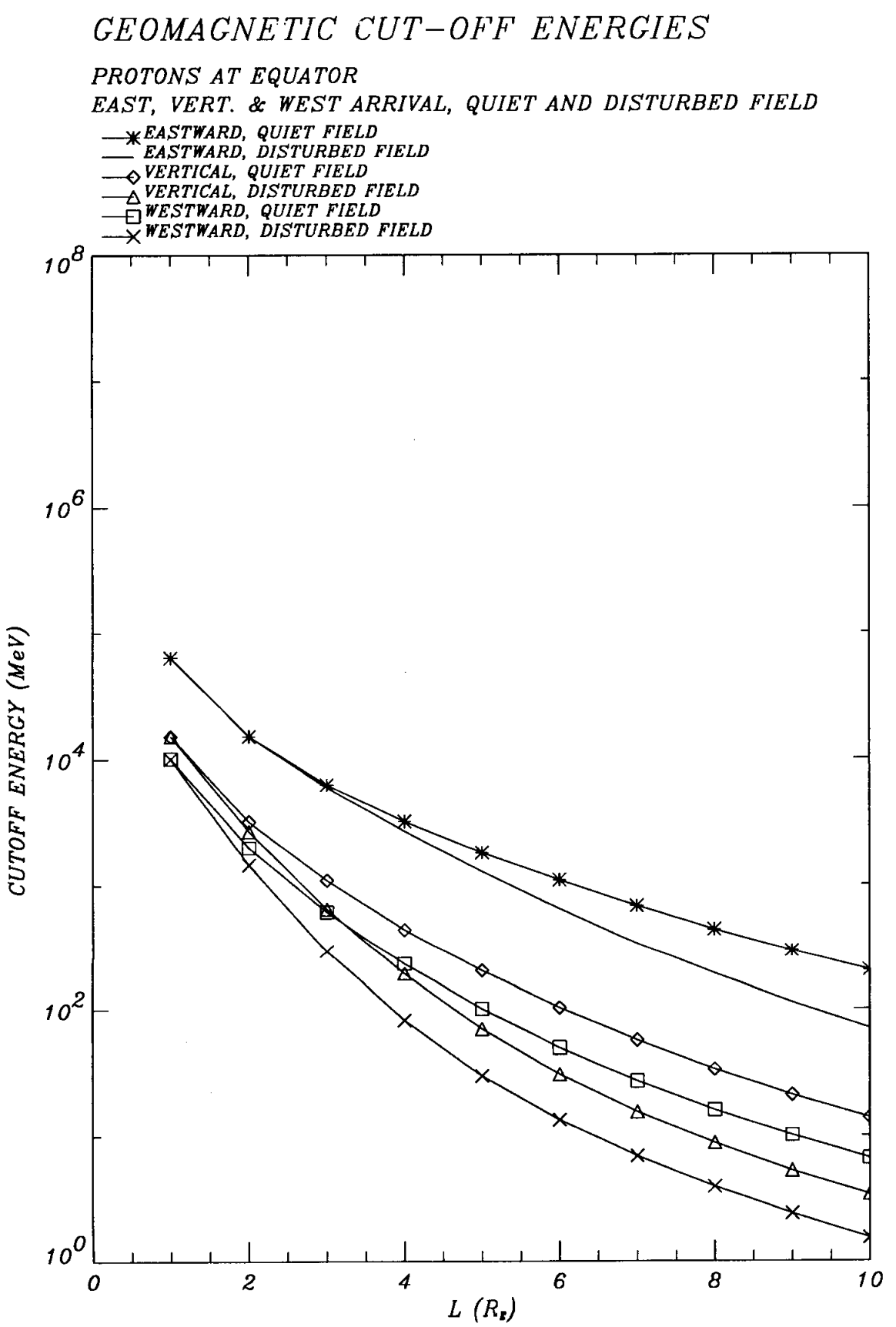

FIGURE 3.21- PROTON CUT-OFF ENERGIES

3.8.5. Environments for specific orbits

To estimate radiation levels likely to be encountered in specific missions, data from the appropriate environment models must be processed in such a way as to provide orbit-integrated particle flux spectra for specific orbital parameters. This is particularly relevant to other than simple circular orbits. Computer programs for the provision of orbital environments for a range of missions are used widely throughout the US and Europe. Software for the purpose is readily available (see Section 18 "Computer Methods").

3.8.6. Conclusions

The radiation environment models described represent the best estimates upon which predictions of exposure may be made. Models are undergoing continual re-appraisal and totally new models will be produced as a result of the high-quality data acquired by the CRRES mission. Initial results indicate important shortcomings in the models. However, it may be some time before new models are available.

A useful comparison between fluxes of the various types of natural radiation is made in Figure 3.21.

Successive sections of this document will discuss the effect of this radiation upon the performance of spacecraft components and describe the methods used to convert the environment data into estimates of radiation dose received by the components within the spacecraft structure.

3.8.7. Recommendations

It is recommended that:

- AE8 and AP8 be used as models for the trapped radiation environment, accessed using the Jensen and Cain model geomagnetic field with epoch 1960 for the solar minimum versions and GSFC 1966 with extrapolation to 1970 for solar maximum;
- the solar proton model of Feynman et al (1990) be used as the model for solar protons;
- the CREME models be used for heavy ions.

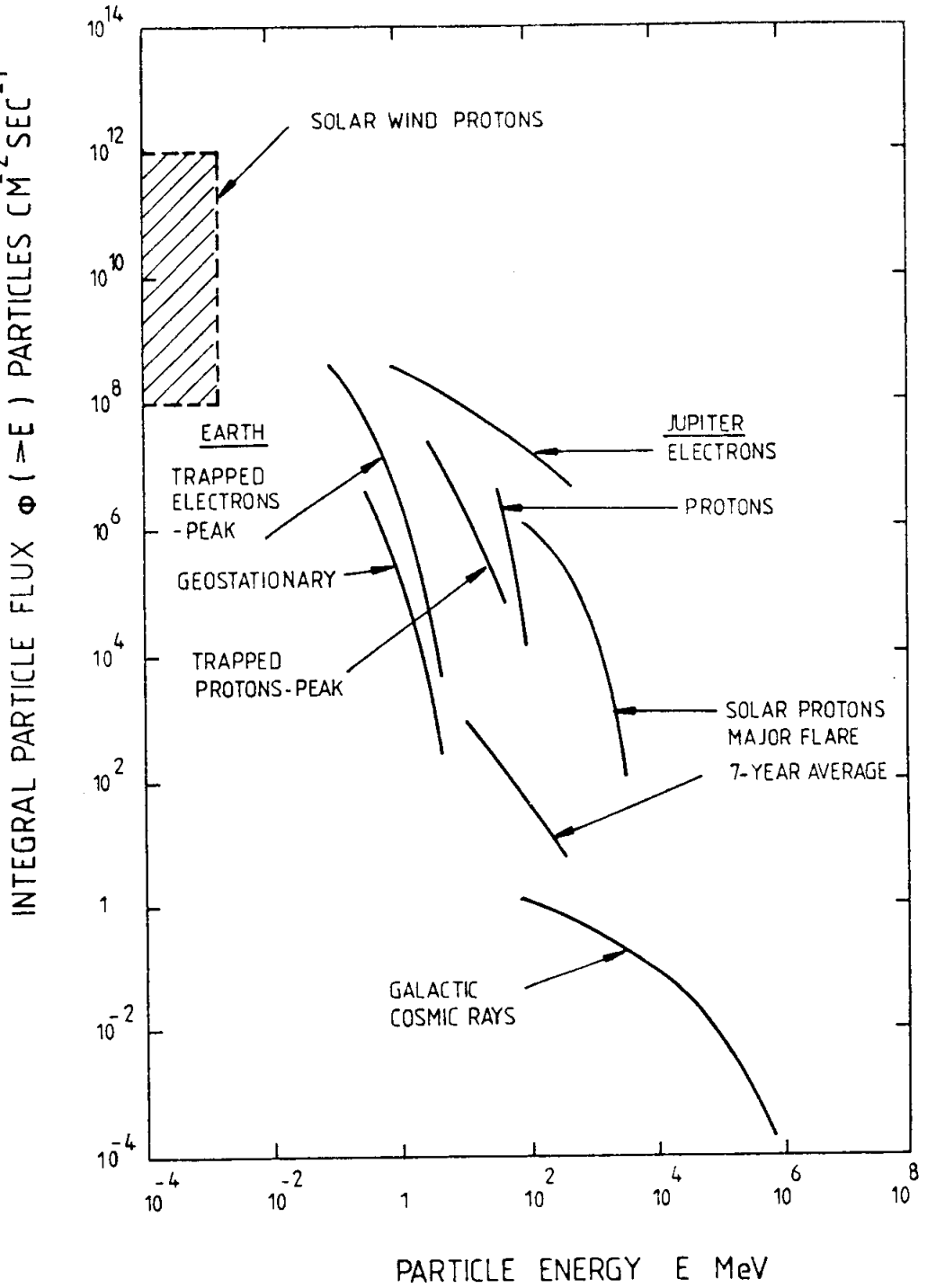

Integral spectra for the various components of the Earth's natural radiation environment. Jovian fluxes are shown for comparison.

FIGURE 3.22 - SUMMARY OF RADIATION SPECTRA

REFERENCES

Adams J.H., Letaw J.F. and Smart D.F., "Cosmic Ray Effects on Microelectronics Part I: The Near-Earth Particle Environment" NRL Memorandum Report 4506 1981.

Adams J.H., Letaw J.F. and Smart D.F., "Cosmic Ray Effects on Microelectronics Part II: The Geomagnetic Cutoff Effects", NRL Memorandum Report 5099 1983.

Adams J.H., "Cosmic Ray Effects on Microelectronics Part IV", NRL Memorandum Report 5901 1986.

Chenette D.L. and Dietrich W.F., "The Solar Flare Heavy Ion Environment for Single-Event"
Upsets: A Summary of Observations Over the Last Solar Cycle, 1973-1983", IEEE Trans. Nucl. Sci. NS-31, p. 1217, December 1984.

Daly E.J., "Models of the Earth's Radiation Environment", Estec Working Paper, 1987.

Daly E.J., "The Evaluation of Space Radiation Environments for ESA Projects", ESA Journal 12, 229 (1988).

Daly E.J., "Effects of Geomagnetic Field Evolution on Predictions of the Radiation Environment at Low Altitudes", ESTEC Working Paper 1531, January 1989.

Feynman J., Armstrong T.P., Dao-Gibner L. and Silverman S., "New Interplanetary Proton Fluence Model", J. Spacecraft and Rockets 27, 403,1990.

Goswami J.N., McGuire R.E., Reedy R.C., Lal D. and Jha R., "Solar Flare Protons and Alpha Particles During the Last Three Solar Cycles", J. Geophys. Res. 93, 7195 (1988).

Gussenhoven M.S., Mullen E.G., Filz R.C., Brautigam D.H. and Hanser F.A., "New Low-Altitude Dose Measurements", IEEE Trans. Nucl. Sci. NS-34, 676 (1987).

Gussenhoven M.S., Mullen E.G., Brautigam D.H., Holeman E., Jordan C., Hanser F. and Dichter B., "Preliminary Comparison of Dose Measurements on CRRES to NASA Model Predictions", IEEE Trans. Nucl. Sci. NS-38, 1655 (1991).

Gussenhoven M.S. and Mullen E.G., "Solar Particle Events as Seen on CRRES", Cospar paper F2.5-M.1.02, World Space Congress, Washington DC, September 1992.

Henley M.W., "Shielding Distribution for Anisotropic Radiation in Low Earth Orbit", J. Spacecraft and Rockets 23, p108, Jan 1986.

Hess W.N., "The Radiation Belt and the Magnetosphere", Blaisdell Publ. Co. (1968).

Holmes-Siedle A., Adams L., Marsden S. and Pauly B., "Calibration and Flight Testing of a Low-Field pMOS Dosimeter", IEEE Trans. Nucl. Sci. NS-32, p4425, December 1985.

King J.H., "Solar Proton Fluences for 1977-1983 Space Missions", J. Spacecraft and Rockets 11, p401, 1974.

Kluge G. and Lenhart K.G., "A Unified Computing Procedure for Trapped Radiation Models", ESRO/ESOC Internal Note 78, March 1971.

Konradi A., Hardy A.C. and Atwell W., "Radiation Environment Models and the Atmospheric Cut-off", J. Spacecraft 24, 284 (1987).

Lemaire J., Daly E.J., Vette J.I., McIlwain C.E. and McKenna-Lawlor S., "Secular Variations in the Geomagnetic Field and Calculations of Future Low Altitude Radiation Environments", Proc. ESA Space Environment Analysis Workshop, October 1990, ESA-WPP-23, in press. (Also Lemaire J. et al., ESA CR(P)-3126, September 1990.

Lyons L.R. and Williams D.J., "Quantative Aspects of Magnetospheric Physics", D. Reidel, Dordrecht, Holland, 1984.

McCormack P.D., "Radiation Dose and Shielding for the Space Station", paper IAF/IAA-86-380, 37th Congress of IAF, Innsbruck, Austria, October 1986.

McGuire R.E., Goswami J.N., Jha R., Lal D., Reedy R.C., "Solar Flare Particle Fluences During Solar Cycles 19, 20 and 21", 18th Int. Cosmic Ray Conference, Vol. 4, p66, Bangalore, India, 1983.

McIlwain C.E., "Coordinates for Mapping the Distribution of Magnetically Trapped Particles", J. Geophys. Res., 66, 3681, 1961.

Pruett R.G., "Comparison of DMSP and NTS-2 Dosimeter Measurements with Predictions", J. Spacecraft and Rockets 17, p270, 1980.

Teague M.J. and Vette J.I., "The Inner Zone Electron Model AE-5", NSSDC 72-10, November 1972.

Teague M.J. and Vette J.I., "A Model for the Trapped Electron Population for Solar Minimum", NSSDC 74-03, April 1974.

Teague M.J., Chan K.W. and Vette J.I., "AE 6: A Model Environment for Solar Maximum, NSSDC 76-04, May 1976.

Tranquille C. and Daly E.J., "An Evaluation of Solar Proton Event Models for ESA Missions", ESA Journal 16, 3, 275 (1992).

Tsao C.H., Silberberg R., Adams J.H. and Letars J.R., "Cosmic Rays Effects on Microelectronics, Part III": Propagations of Cosmic Rays in the Atmosphere, NRL Memorandum Report.

Sawyer D.M. and Vette J.I., "AP-8 Trapped Proton Environment for Solar Maximum and Solar Minimum",. NSSDC 76-06, December 1976.

Schultz M., "Earth's Radiation Belts", Review of Geopys. and Space Sci. 20, no.3, pp 613-621, August 1982.

Singley W. and Vette J.I., "The AE4 Model of the Outer Radiation Zone Electron Environment", NSSDC 72-06, August 1972.

Singley W. and Vette J.I., "A Model Environment for Outer Zone Electrons", NSSDC 72-13, December 1972.

Stassinopoulos E.G. and King J.H., "Empirical Solar Proton Model for Orbiting Spacecraft Applications", IEEE Trans. Aerosp. and Electr. Systems AES-10, p442, 1984.

Stassinopoulos E.G., "World Maps of Constant B, L and Flux Contours", NASA SP-3054, 1970.

Vette J.I. "The AE8 Trapped Electron Model Environment", NSSDC Report 91-24, NASA/GSFC November 1991.

Watts J.W., Parnell T.A. and Heckman H.H., "Approximate Angular Distribution and Spectra for Geomagnetically Trapped Protons in Low-Earth Orbit" in: High Energy Radiation Background in Space, Rester A.C. and Trombka J.I. (eds.), AIP (1989).

Ziegler J.F. and W.A. Landford, "The Effect of Sea Level Cosmic Rays on Electronic Devices", J. Appl. Physics 52 (6) June 1981.

SECTION 4. ARTIFICIAL RADIATION ENVIRONMENTS IN ORBIT

4.1. GENERAL

In the natural space environment, intense, transient pulses of ionising radiation do not occur except in the form of single-particle events. However, it is possible that even civil satellites may be exposed to the effects of distant nuclear weapons exploded in space, as happened in the 1962 "Starfish" nuclear test. In the future, exposure to pulsed beams of ionising radiation from spaceborne particle accelerators, X-ray generators or nuclear reactors is also possible. We will therefore give a brief account of "Transient Radiation Effects in Electronics" (TREE) and give references to the very extensive sources of information which have been generated mainly by defence agencies. An unclassified version of the yields from a nuclear event is given in Figure 4.1

4.2. WEAPON EFFECTS

A nuclear explosion generates a very short (20 ns) pulse of gamma rays from nuclear reactions, and X-ray, neutron and electromagnetic pulses which may last for milliseconds. Particle accelerators and X-ray machines can generate continuous beams, but are often operated in a series of pulses of microsecond duration. The exposure of a device to one of these sources will produce:

(a) dose-rate or "transient" effects (e.g. photocurrents),

(b) "total dose" or long-lived effects (e.g. charging or bulk damage).

There is likely to be "rapid annealing" of the material response during the first few seconds, then more gradual relaxations over many hours. In logic circuits, the transient photocurrents generate spurious signals and may produce "logic upset" or, at higher intensities, induce thermal destruction. In some semiconductor devices containing 4-layer junction structures, a low impedance condition, known as latchup may be triggered. Latchup leads to thermal destruction caused by the energy from the power supply.

"Logic upset" is fundamentally a transient effect, but - in some circuits - may have a permanent result. For example, while a simple NAND gate, set in the logic "1" state, may transiently indicate a "0" state during the burst, it will return to the "1" state within microseconds. A bistable circuit such as a memory cell may return to the original state or, instead, change to the opposite state. These two upset effects are called "temporary" and "permanent" respectively.

Brucker has tabulated some general values for the levels of pulsed radiation environment at which the above effects take place in certain CMOS and bipolar integrated circuits. These levels are given in Table 4(1). Only orders of magnitude are stated here, but the data still supply useful guidance for system engineers and circuit designers. Brucker notes that bulk CMOS logic gates can be used in a transient radiation environment (20 nanosecond pulse) if they are not required to operate during the radiation burst. Limiting resistors or SCR crow bars can be used on CMOS voltage supplies as protection against latchup. Bulk CMOS shift registers or memories are vulnerable if they are required to store data through a radiation burst without loss. These devices are subject to permanent upset or scrambling of stored data. SOS CMOS shift registers, memories or logic gates can be used in a transient environment without risk of latchup. Logic gates are still subject to temporary and permanent upsets, but the limiting dose rates of the SOS devices exceed those of the bulk devices by at least an order of magnitude.

Brucker comments further that upset and latchup rates are strongly dependent on the circuit design and that the reduction of operating voltage from 10 to 5 volts increases by at least a factor of two the dose rate threshold for latchup. In some circuits, latchup dose rates may be very high. For example, the CD4061 is very resistant to latchup. In a transient environment, the higher noise immunity of CMOS devices makes them preferable to TTL.

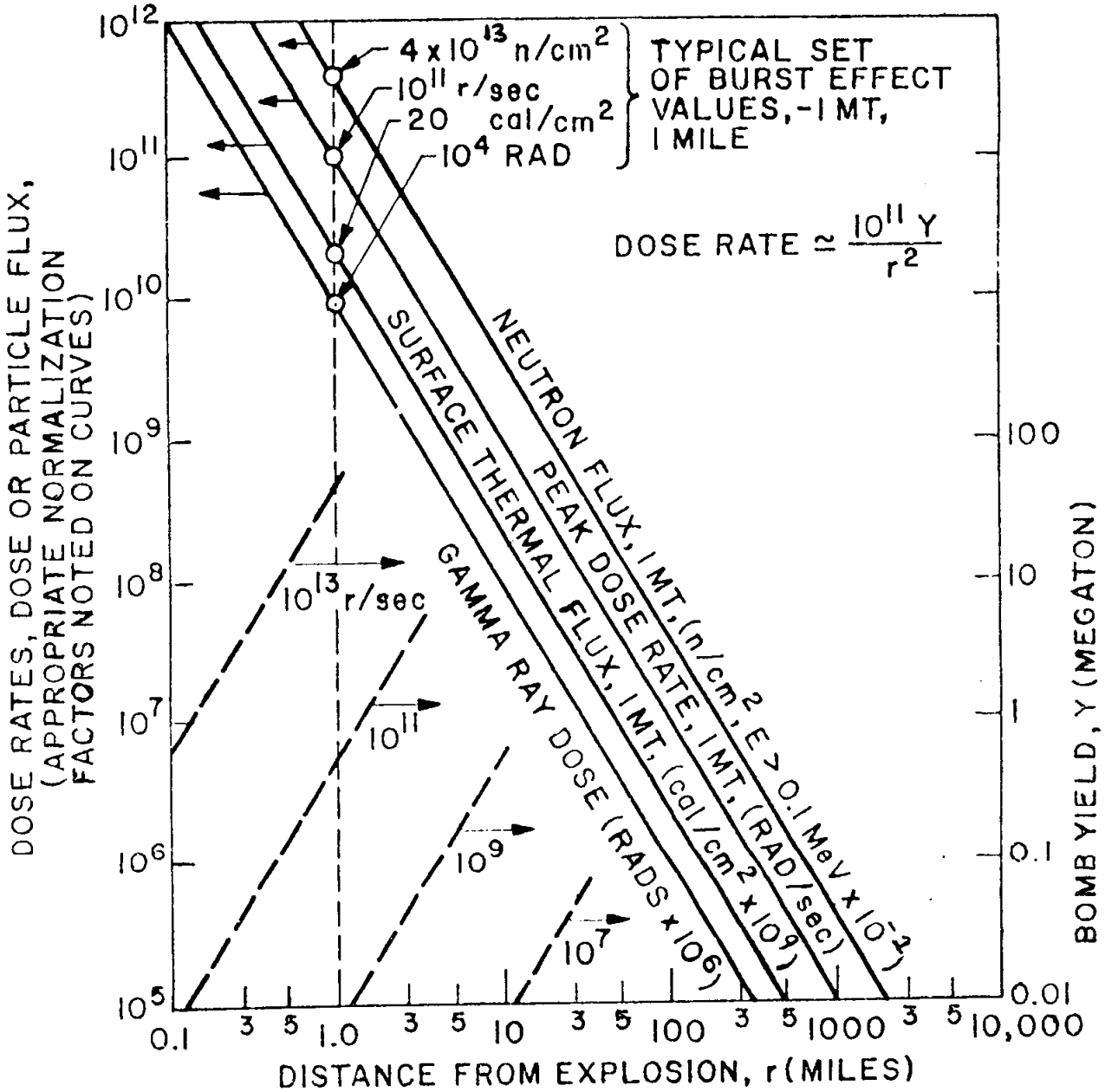

FIGURE 4.1 - NOMINAL RADIATION LEVELS FROM NUCLEAR EXPLOSIVES IN SPACE

TABLE 4.(1) - SOME UPSET LEVELS FOR CMOS CIRCUITS

	Effect	General range
CMOS/BULK LOGIC GATES		
	Temporary upset	10^8 - 10^9 rad/s
	Latchup	10^6 - $5x10^9$ rad/s
- Transient (20 ns pulse)	Survival	10^{12} - 10^{13} rad/s
- Long-lived	Total dose	10 - 1000 Krad
	Neutrons	10^{15} n/cm^2
CMOS/BULK SHIFT REGISTERS		
	Temporary upset	10^8 - 10^9 rad/s
	Permanent upset	$5x10^8$ - $5x10^9$ rad/s
- Transient	Latchup	10^8 - $5x10^9$ rad/s
- Long-lived	Survival	10^{12} - 12^{13} rad/s
	Total dose	10 - 1000 rad
CMOS/BULK MEMORIES		
	Temporary upset	10^7 - 10^8 rad/s
- Transient	Permanent upset	8 x 10^7 rad/s
	Latchup	8 x11 rad/s
	Survival	10^{11} rad/s
- Long-lived	Total dose	10 - 1000 Krad
	Neutrons	10^{15} n/cm^2
CMOS/SOS MEMORIES		
	Temporary upset	7 x 10^9 rad/s
- Transient	Permanent upset	10^{11} rad/s
	Latchup	Not possible
	Survival	10^{11} rad/s
- Long-lived	Total dose	6 Mrad
	Neutrons	10^{15} n/cm^2
CMOS/BULK MICROPROCESSORS		
	Permanent upset	10^8 rad/s
	Latchup	10^8 rad/s
	Survival	10^{11} - 10^{12} rad/s
	Total dose	10 Krad
	Neutrons	10^{15} n/cm^2

TABLE 4(1) - SOME UPSET LEVELS FOR CMOS CIRCUITS
(Continued)

	Effect	General range
TTL LOGIC, JUNCTION ISOLATED	Temporary upset Latchup	10^8 - 10^9 rad/s Very limited evidence of existence
- Transient - Long-lived	Survival Total dose Neutrons	10^{12} rad/s 10 Mrad 5×10^{13} n/cm^2
TTL DIELECTRIC-ISOLATED LOGIC	Temporary upset Latchup Survival Total dose Neutrons	10^9 - 10^{10} rad/s Not possible 10^{12} rad/s 10 Mrad 3×10^{14} n/cm^2
I^2L LOGIC	Temporary upset Latchup Survival Total dose Neutrons	2×10^9 rad/s Not possible 10^{12} rad/s 1 Mrad 10^{13} n/cm^2

PAGE INTENTIONALLY LEFT BLANK

SECTION 5. THE RESPONSE OF MATERIALS AND DEVICES TO RADIATION - OVERALL SURVEY

5.1. INTRODUCTION

5.1.1. General

The effect of irradiating an electronic material and the consequent degradation in performance of devices made from such material can follow a number of courses. The final result will depend upon the type of radiation, its mode and rate of interaction with the material, the type of material and its particular contribution to the device function and the physical principles upon which the function of the device is based. Table 5.1 gives an impression of the variety of effects which radiation can have on devices.

This section provides a general introduction to radiation effects on materials and devices, describing first the two main types of interaction of radiation with materials (atomic displacement and ionisation) and, second, the consequences in general of these interactions for the individual parts of a device. The description is extended to a classification of about 60 varieties of electronic media or devices. This classification is given in greater detail in Holmes-Siedle (1974).

A more detailed discussion of the effects of various types of radiation on particular devices is given in later sections.

5.1.2. Dose rates

It is often necessary to specify the dose rate at which radiation is delivered. For example, a spacecraft orbiting in the Van Allen belts is said to be exposed to a low dose rate and a sample close to a reactor core to a high dose rate. A nuclear weapon pulse delivers an even higher rate. We can specify this rate in terms of the average energy absorbed per unit mass and time (e.g. rads per second). This method of specifying rates is adequate for high-energy electrons and photons. However, local ionisation effects on very dense electronic components exposed to certain particles may lead to strong transient electrical response. Special questions of dose rate effects such as these will be dealt with as required.

5.2. DEGRADATION PROCESSES

Energetic particles or photons passing through matter lose energy through a variety of interactions and scattering mechanisms. It is not within the scope of this study to discuss these complex mechanisms in detail; it is sufficient to note that we are concerned primarily with the two major consequences of energy transfer from radiation to electronic materials, namely ionisation and atomic displacement.

5.2.1. Atomic displacement

A small but significant fraction of the energy of particles passing through an absorber is dissipated in the transfer of momentum to the atoms of the absorber. Provided an atom subject to such a collision receives sufficient kinetic energy (displacement energy E), it will be removed from its position in the lattice and leave a vacancy or defect. The removed atom may meet another such vacancy and "recombine" or lodge in an interstitial position in the lattice. Persisting vacancies may be mobile and either combine with impurity atoms or cluster with other vacancies. The resulting vacancy complexes are usually electronically active in semiconductors, but the interstitial atoms are less active. The consequences of displacement in a solid are clearly complex; in addition, the incident particle must have a certain threshold energy before displacement occurs. The process is conventionally termed "bulk damage".

The effect of displacement damage on the minority carrier lifetime of silicon, caused by 1 MeV electron irradiation, is shown in Figure 5.1 (after Wertheim (1957). It can be seen that, over a wide range of electron fluence (ϕ), lifetime varies with fluence as follows:

$$\frac{1}{\tau} - \frac{1}{\tau_o} = K_\tau \phi \quad \text{..... 5(i)}$$

where τ_o and τ are the values before and after irradiation. K_τ is known as the minority carrier lifetime damage constant; it expresses the "damage" (change in lifetime) per unit electron fluence.

TABLE 5(1) - RADIATION EFFECTS

A Summary of Radiation-induced Degradation Effects

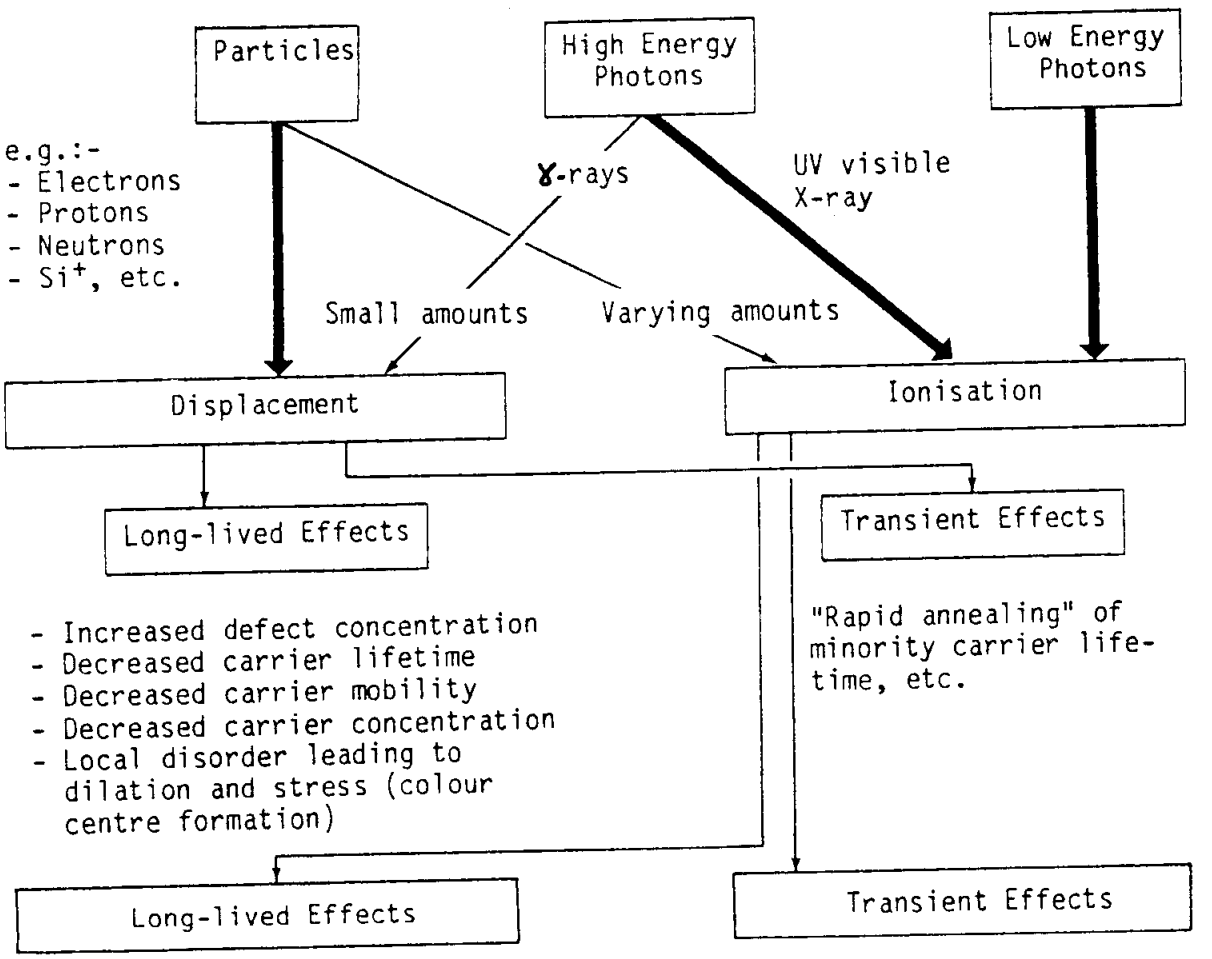

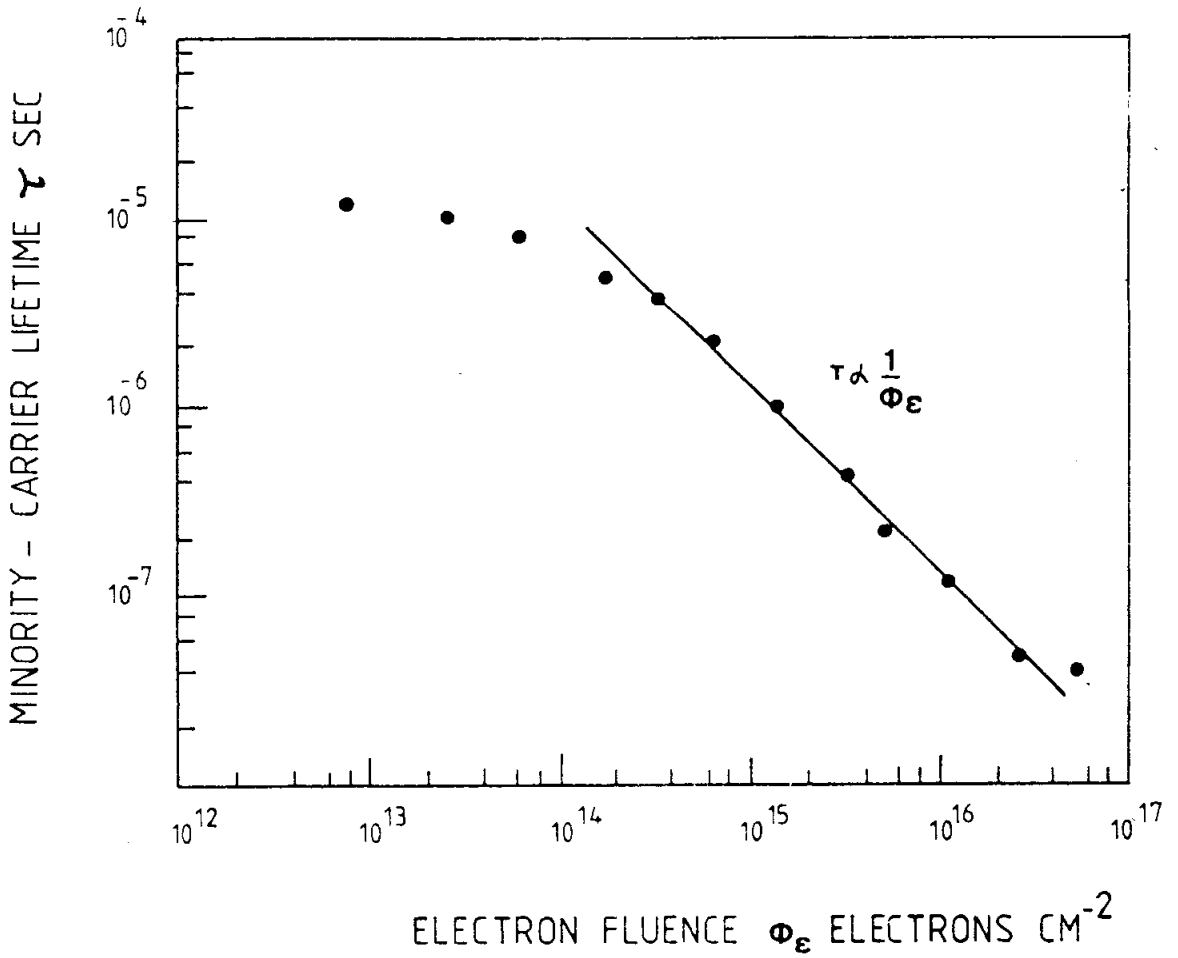

The effect of 1 MeV electron irradiation on the lifetime of holes in N-type silicon.

FIGURE 5.1 - ATOMIC DISPLACEMENT DAMAGE

The value of K_τ for 1 MeV electrons is often taken as the standard with which the effect of all other particles is compared. An electron of higher energy will displace more atoms per unit volume, whilst a proton of the same kinetic energy will displace over a thousand times more because it has far greater momentum and is more rapidly stopped.

As the damage caused - though not identical for all particles at all energies - is of the same general kind, it is possible to express the effect on silicon of all particles in terms of the damage equivalent fluence of a 1 MeV electron. This concept has been described by Brown, Gabbe and Rosenzweig (1963).

The question of damage equivalents extends into neutron damage physics (reactor and weapon effects), and Van Lint et al (1975) suggest 3 MeV electrons, 20 MeV protons and 1 MeV neutrons as standard particles for relating the effects of the three particle species.

Whilst developing design rules for the TELSTAR satellite, Brown, Gabbe and Rosenzweig expressed the variations of damage constants with electron and proton energy. Their sets of curves illustrating the relation between damage and particle energy and the effect of protective shielding are given later. The "no front shield" curve in these figures indicates the effect of omnidirectional particles on a bare "semi-infinite" silicon solar cell (i.e. with an infinite amount of absorber protecting the back of the wafer). This geometry is not representative of either internal electronics or the solar cell panels of today (which have limited absorber at the back), but the complex energy-dependence of proton damage and the threshold energy of electrons are suitably illustrated by these curves.

Van Lint et al reviewed minority carrier lifetime damage equivalents for electrons, protons and neutrons in silicon. Srour, Othmer and Chiu (1975) have also reported some improved measurements. In the light of this work, the figures produced by Brown and his colleagues - although calculated for silicon of relatively high resistivity (greater than 1 ohm/cm) and the solar cell mode of operation - would still seem to be generally correct.

For typical transistor designs, the damage constants are probably lower because lifetime is less affected when the concentration of injected minority carriers ("injection level") is high. However, the effect of the lower resistivity of the typical transistor base region may operate to counteract this reduction of the lifetime damage effect.

The possibility of damage caused by bremsstrahlung X-rays must also be considered. X-rays (or gamma rays of the same energy) are photons which possess negligibly small momentum. Therefore,

they themselves cannot interact with, and displace, an atom in a crystal. They may, however, generate an appreciable quantity of high-energy Compton electrons which, in turn, can produce damage (1 rad of ^{60}Co gamma rays produces about 107 Compton electrons cm^{-2} of energies up to about 1.3 MeV in the steel cap of a transistor). Thus, high doses of electromagnetic radiation may produce displacement damage, the amount depending upon details of the component's shielding configuration; however, the effect in space is usually negligible.

5.2.2. Ionisation

The primary interactions between energetic radiation and the electronic structure of atoms are more complex and varied than the simple transfer of momentum to nuclei of atoms described earlier. Despite the initial variety of interaction (see Johns and Cunningham (1971) for example), much of this loss of energy to the electrons in semiconductors and inorganic insulators is ultimately converted to the form of electron hole pairs. In this process, known as ionisation, the valence band electrons in the solid are excited to the conduction band and are highly mobile if an electric field is applied.

Any solid - even an insulator - thus conducts for a time at a level higher than is normal. The positively charged holes are also mobile, but to a different degree because their motion is effectively that of valence band electrons in the opposite direction.

The production and subsequent trapping of these positive holes in oxide films, which cause serious degradation in MOS and bipolar devices, are the main subjects of later sections of this document. In polymers, the main result of electronic excitation may be instead the breaking of chemical bonds and the creation of new ones. In this case, conduction may also result, but other forms of physical breakdown may be more apparent.

It is worth noting that the net energy required to create an electron hole pair is relatively small (e.g. 18eV in SiO_2). Therefore, since no momentum transfer to atoms is involved, the energy of the radiation causing ionisation is not so critically important as in atomic displacement (of course, the number of pairs created depends upon the particle or photon energy). Thus, ionisation effects as produced by megavolt particles in space may often be simulated by much lower energy X-rays, electron beams or even ultraviolet light. For displacement damage, freedom of choice of simulation methods is more limited.

The deposition of energy in a material by means of ionisation is conventionally termed "dose" and measured in rads or Grays. One rad is equivalent to the deposition of 100 ergs in one gram of material; the SI unit (the "Gray") is equivalent to the deposition of one joule in one kilogram and therefore equal to 100 rad.

5.3. THE CONSEQUENCES OF DEGRADATION

5.3.1. General

To consider the degrading effects of radiation on electronic devices requires their classification according to the following three points:

1. Degradation may be caused by either ionisation or atomic displacement;

2. The effect may be long-lived or transient;

3. Degradation may be associated with particular active "sub-elements" which can be classified as dielectric, semiconductor or conductor.

It can be seen that there is scope for an extremely complex interaction of processes to be involved in the loss of function of any particular device, integrated circuit or electronics module. Fortunately, the field is often considerably narrowed. For instance, degradation of an MOS device, especially in the relatively low dose rate environment in space, is almost entirely due to the long-lived effects of ionisation in the dielectric subelement, i.e. in the gate insulator.

Many modern semiconductor devices make use of electronic processes that are seriously affected by the alterations produced in materials by high-energy radiation. A prime example is the bipolar transistor. Like many (but not all) p-n junction devices, the "key material parameter" is the minority carrier lifetime. The production of gain relies on the efficient transport of minority carriers across several hundred nanometres of silicon.

Displacement of atoms and the subsequent formation of vacancy-impurity complexes provide centres for recombination of those carriers and, the more sophisticated the device structure, the greater the possibility of loss of other minority carriers, e.g. at interfaces. It is probably a fair generalisation to say that the more complex the geometry and operational principle of a solid-state device becomes, the more vulnerable it is to radiation-induced changes. Further, as we move from the purely electronic type of device to the type in which light is used to produce electronic effects in the solid, or which itself generates light by such effects, the

possibilities of interference or degradation of efficiency as a result of irradiation are even more varied.

The following pages describe the modes of degradation which are likely to be induced by ionisation and displacement of atoms in the various "subelement" materials. The types of device which are, in consequence, likely to be most affected are listed in Table 5(2) together with a summary of the more important effects.

The information in these tables has been derived from the results of a very large number of physical experiments and radiation tests performed on devices in the U.S. and Europe during the design of electronics for space vehicles, military equipment and reaction components. This concise summary is intended to introduce the reader to the range and variety of effects to be expected before the detailed discussion of particular cases in following paragraphs.

5.3.2. Degradation of conductors

Radiation effects on conductors in space applications are less important than on those in reactor technology. In some circumstances, the atomic displacement effect may cause changes in conductivity such as occur in carefully balanced resistive elements. Also, at extra high particle fluences, say, greater than 10^{20} neutrons.cm^{-2} (likely to be encountered, for example, in reactor cores), atom displacement may lead to serious changes in mechanical strength. Ionisation is not likely to create problems, except that photo-emission and charge-scattering may cause electrical currents that can affect sensitive circuits. No important example of degradation of a metal by radiation in space has yet been encountered.

5.3.3. Atomic displacement in semiconductors

Displacement effects in semiconductors are long-lived and usually result in the reduction of carrier mobility and lifetime or in the removal of carriers by trapping. We mentioned elsewhere the effects in bipolar transistors, where displacement-induced defects provide recombination centres. Besides bipolar transistors, the most sensitive devices in space technology are solar cells and silicon-controlled rectifiers, all of which require a high minority carrier lifetime for efficient operation. Field Effect Transistors (FETs) are less sensitive and would require particle fluences higher than normally experienced in a space mission before their performance was affected significantly.

A few types of devices are sensitive to the slow emptying of displacement-induced charge traps in the semiconductor sub-element. This effect may produce inconvenient "tails" on the otherwise sharply falling edge of electrical pulses (for example, this could increase the dark current of an imaging device). Only at higher fluences would "other properties" (e.g. the electro-mechanical constant of a transducer) be affected, but such effects are unlikely in the space environment. New high electron mobility transistors are sensitive to these effects.

5.3.4. Ionisation in semiconductors

In semiconductors, high-energy radiation produces electron hole pairs, leading to spurious photocurrents. The magnitude of this effect is clearly dependent upon dose rate rather than total dose and the photocurrents produced in the space environment will generally be insignificant. At worst, these currents may register as background "noise" in some extremely sensitive circuits. Galactic cosmic rays can produce local pulses of photocurrent and this is a problem in dense semiconductor devices using small geometries. Single-event upset and latchup due to cosmic rays are dealt with in detail in later sections. Logic upset and latchup in MOS and bipolar circuits require dose rates of at least 10^7 rad.s^{-1} of high-energy radiation, i.e. over a million times higher than those experienced by orbiting equipment.

5.3.5. Atomic displacement in dielectrics

This effect is well-known in optical materials and metal halide salts. The vacancies so produced are known as "colour centres". However, displacement defects in dielectrics rarely interfere with the function of electronic devices.

Dielectric materials do not require crystalline perfection in order to be good dielectrics. Many are glasses, with no crystalline structure at all. Consequently, the displacement of nuclei from their original sites has no significant effect on a dielectric material's dielectric properties. Thus, for example, capacitance and leakage currents are not sensitive to radiation-induced displacements in the dielectric of a capacitor, and the function of a stand-off insulator is not impaired by such displacement events.

The chief contribution of radiation-induced displacement events to radiation effects in modern electronic devices is through the ionisation which accompanies the displacement, generated by interactions between the electric field of the displaced nucleus with the electrons of other nuclei as it passes by on its way to its resting place. Such ionisation contributes to charge trapping, as discussed in Section 5.3.6.

Radiation-induced displacement in dielectrics is therefore rarely a functional problem. Moreover, dielectrics used in electronic devices are seldom required to have quite the same degree of purity as semiconductors, so that the creation of new defects has proportionately less effect. (By contrast, the action of existing defects in trapping charge generated by ionisation is the main cause of the radiation problem in MOS devices and glasses.) Possible exceptions to this are certain phosphors and photochromic materials in which the device principle involves the exchange of charge between a controlled number of defect levels. An example of such an exception is thermoluminescence in lithium fluoride dosimeters.

5.3.6. Ionisation in dielectrics

In space technology at the present time, the ionising effect of radiation on dielectric subelements is of particular significance. This is especially true in large- and medium-scale MOS integrated-circuit devices. The effect of ionisation in a dielectric will be the production and transport of charge in media which are specifically designed to be nonconducting. This motion will persist only while excitation continues. However, the permanent effects resulting from the motion of radiation-induced charge can be drastic, particularly the charge-trapping (space-charge buildup) in MOS gate oxides and bipolar transistor passivation layers. They may also be accompanied by rearrangement of atomic bonds in the dielectric semiconductor interface (interface state production) and, just possibly, by chemical decomposition (mainly in organic dielectrics under the most severe exposure). Much of the following paragraphs will be concerned with these permanent effects.

The potentially harmful effects of ionisation in dielectrics are diverse for a number of reasons. First, the variety of dielectrics employed is much greater than the variety of semiconductors. Second, the gap between valence and conduction bands of a dielectric is large; additionally, dielectrics are usually covalent compounds often involving several chemical elements. Thus, a large variety of trapping levels and excitations is possible, while polarisation effects may be long-lived. Third, impurity concentrations tend to be higher because, unlike semiconductors, processes analogous to "doping" are not commonly used; this being so, the need for rigorous preliminary refinement, as is essential for semiconductor materials, is removed.

Devices incorporating dielectrics will often be sensitive to the fields produced by charge-trapping since charge transport and trapping, sensed by its field effect, is sometimes used as a device principle (e.g. the NMOS device).

Table 5.(3) summarises the long-lived effects of ionisation in the dielectric subelements of a number of devices. The table is divided

according to whether the dielectric has an active or a passive electrical or optical function. The number of 'X' symbols gives a preliminary idea of the degree of sensitivity of a device to ionisation induced in its dielectric subelement and indicates the problems which may arise when the device is used in a severe radiation environment. However, the magnitude of the effect is not indicated. For example, it is possible that electroluminescent phosphors withstand larger doses than a photochromatic device which, though having 'X' symbols in the same three columns, is probably much sooner affected in memory storage capability than most phosphors in respect of luminescent efficiency.

5.3.7. Induced radioactivity

Any material exposed to the space environment becomes radioactive. Protons, neutrons, nuclei and pions are capable of transforming stable nuclei of any spacecraft material into radioactive nuclei by the removal of nucleons or, in the case of low-energy neutrons, by neutron capture. A wide range of radioactive nuclei is produced and these decay at a later time according to their characteristic half-lives. The majority decay by emitting a positron (beta+) or by capture of an orbital electron, often accompanied by gamma-ray emission while, in a few cases - such as neutron capture - emission of an electron (beta–) occurs. Such products have typical energies in the range 0.01 to 10 MeV. In space, primary protons are the most abundant particles producing radioactivity, while in thick materials activation by secondary protons, pions and especially neutrons becomes increasingly important. The total interaction cross-section for protons increases monotonically with energy, reaching a peak at 30 MeV, after which it falls slightly to a constant level for energies greater than 200 MeV. While total cross-sections are known to within 5%, the spallation cross-sections for production of particular radionuclides are mostly unknown, but can be estimated to within a factor of 2 by means of semi-empirical formulas. For high-Z target materials, some 200 radionuclides contribute significantly to the induced radioactivity.

In space, the most intense proton fluxes are to be found in the heart of the inner radiation belt where radioactivity is induced by the energetic proton component in the energy range 30 to 400 MeV. At altitudes below or above this trapped proton regime, the more energetic (GeV) cosmic rays dominate the induced radioactivity and the precise flux and level of induced activity varies with the geomagnetic latitude. At high altitudes (e.g. GEO or interplanetary space), solar flare protons can penetrate and will typically provide the major component of activation for some 20 days per year at solar maximum.

Doses due to induced radioactivity are small compared with the dose produced directly by the inducing radiation (Fishman, 1976). However, it is a major source of background in the performance of

highly sensitive X-ray and gamma-radiation astronomy and remote-sensing spectroscopy. Induced radioactivity was first observed directly in a scintillation spectrometer carried on board the OSO-1 spacecraft following passages through the trapped radiation belt in the South Atlantic Anomaly region (Peterson, 1965). More detailed observations of induced radioactivity resulting from trapped protons were made possible by spectrometers carried on OSO's 3, 5, 7 and 8, HEAO's 1 and 3, the Solar Maximum Mission and DOD spacecraft 1972-076B and P78-1. Activity dominated by cosmic rays has been observed on APOLLO's 15, 16 and 17 operating in interplanetary space and on APOLLO- SOYUZ operating in LEO below the trapped radiation belts (Dyer et al, 1980). Packages have been returned to earth in order to monitor the radioactivity from APOLLO 17, APOLLO-SOYUZ (Dyer et al, 1980) and SKYLAB (Fishman, 1976).

Calculations of induced radioactivity in thin homogeneous materials can be made with the aid of methods and formulas given by Dyer et al, 1980 and Barbier, 1969, and based either on semi-empirical cross-sections or on ground-based irradiations using representative particle beams. To a first approximation, 1 radioactive decay results from each proton interaction so that a saturated activity of some 4 to 6 decays per second per kilogram of material is attained in a cosmic-ray flux of 1 particle $cm^2.s.^{-1}$ Trapped protons can be stopped by ionisation without interacting and, in general, are at least a factor of 3 less efficient in inducing a decay even under minimal shielding. The detailed decay behaviour and spectrum of emissions is a complex superposition of many radionuclides and required methods such as those described by Dyer et al, 1980. For heavy spacecraft, activation by secondary neutrons becomes important and particle transport calculations must be performed. Activation by neutron capture is very dependent on the spectrum of neutrons and the detailed cross-section of the material of interest, the former varying considerably with location as evidenced by results (Fishman, 1976; Dyer et al, 1980). For heavy detector systems, activation by secondary neutrons generated within the detector volume may dominate (Dyer and Hammond, 1985).

5.4. CONCLUSIONS - AN OVERALL VIEW OF DEVICE DEGRADATION

The complex nature of degradation effects induced by radiation has been indicated. Table 5(3) will serve as a useful summary of physical, chemical and functional effects, both long-lived and transient, caused by atomic displacement and ionisation in electronic device materials.

The reader may also refer to Figure 5.2 to obtain an indication of the general dose range at which the effects that have been

described begin to degrade the function of various types of device and material. The information shown has been derived from tests in nuclear reactors on mass-produced devices and degradation results from neutron and gamma radiation. It is "general" in the sense that several mechanisms may combine to cause the general degradation of "utility" indicated by the bars. The fact that the bar indicating, say, "mild to moderate" degradation extends over perhaps six decades of radiation fluence is because one member of a class may degrade much more rapidly than another. For instance, a capacitor employing an organic dielectric (such as Mylar) may degrade more quickly than one employing an inorganic dielectric (such as mica). Even the mechanisms can be different and multiple; the Mylar device may develop leakage via the degraded dielectric, change capacitance owing to dimensional change, or rupture owing to gas release, while the mica would probably not suffer from any of these effects.

Two interesting points arise from the comparative data in Figure 5.2. First, the compilers found that, in general, the same positions of the bars resulted no matter whether reactor neutrons or 3 MeV electrons had been used for irradiation. This suggests that tests performed with one radiation environment in mind may also provide useful data for other environments (see Section 19 on radiation testing). Second, the radiation sensitivity of the semiconductor group is markedly apparent; few such devices survive far into the "high" range of radiation fluence.

Having provided a general review of the problem of radiation-induced degradation in devices and materials, this document will now concentrate on electronic components used in spacecraft technology.

TABLE 5(2) - ATOMIC DISPLACEMENT EFFECTS IN SEMICONDUCTOR DEVICES

XX - Primary failure mode
X - Secondary failure mode

Device	Carrier life-time reduction	Carrier removal by trap-ping	Carrier mobility decrease	Slow empty-ing of traps	Other
P-N JUNCTION DEVICES					
(a) Low reverse fields					
Bipolar transistor & SCRs	XX	X			
MIS (MOS) Field effect transist.		XX	X		
Variable-threshold MIS ,,	XX	X			
Junction FETs		XX	X		
Rectifying/blocking diodes	XX	X			
Tunnel diodes					X
Schottky barrier diodes	XX	X			
Junction photosensors	XX	X		X	
Opto-isolators	XX	X		X	
Junction electroluminescent diodes		X		XX	
MIS electroluminininescent diodes		X		XX	
Solar cells	XX	X			
(b) Avalanche devices					
Zener and IMPATT diodes	X	XX			
Surface-controlled Aval.diodes		XX			X
(c) Other					
Charge-coupled devices		XX		X	
Hall-effect devices		X	XX		
OTHER DEVICES					
Transferred electron devices		X		XX	
Photoconductive photosensors			X	X	
Storage photosensors			X	X	
Mechanical transducers		XX	X		
Ovonic threshold switches				X	XX
Ovonic memory cells				X	XX
Amorphous tunnel triodes				X	XX
Photostructural switches				X	XX
Cold cathode electron emitters	X	X	XX		

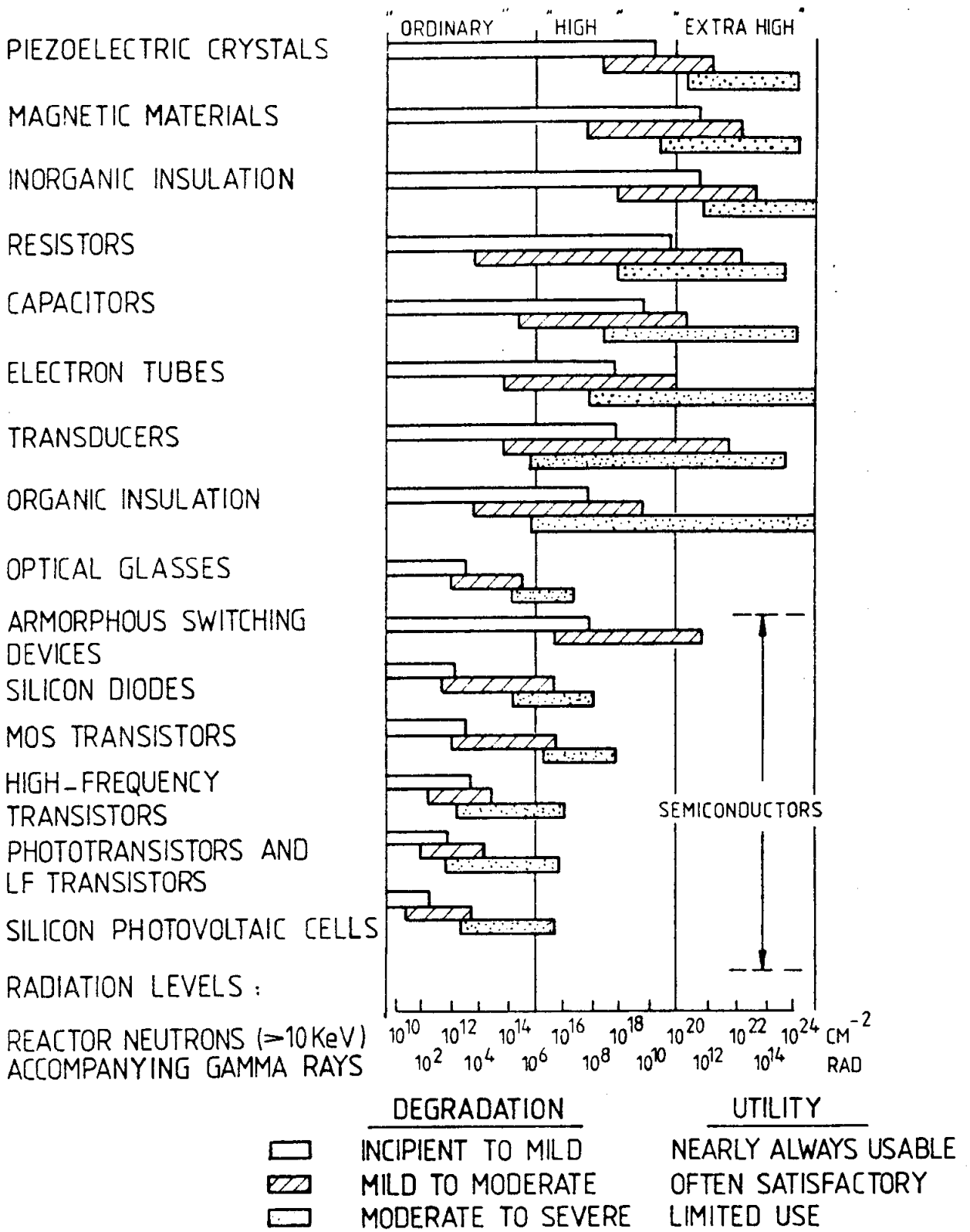

A comparison of the tolerance of various materials and devices to reactor irradiation.

FIGURE 5.2 - RADIATION EFFECTS

TABLE 5(3) - ORBITAL ENVIRONMENT

Typical ESA specification of Orbit-integrated trapped particle environments 2-year EXOSAT mission; Apogee: 200.000 km; Perigee: 200 km; Inclination: 80° (PT-PR-040 000, 1976)

Electrons		Protons	
Energy E MeV	Flux ϕ (E) cm^{-2} (2 yr) $^{-1}$	Energy Ep MeV	Flux ϕ (Ep) cm^{-2} (2 yr) $^{-1}$
0.1	0.782 E 14	0.1	0.112 E 15
0.125	0.434 E 14	0.5	0.394 E 14
0.25	0.149 E 14	1.0	0.133 E 14
0.375	0.912 E 13	2.0	0.245 E 13
0.5	0.775 E 13	3.0	0.762 E 12
0.625	0.544 E 14	4.0	0.355 E 12
0.75	0.393 E 13	5.0	0.219 E 12
1.0	0.220 E 13	6.0	0.138 E 12
1.25	0.137 E 13	7.0	0.867 E 11
1.5	0.861 E 12	8.0	0.549 E 11
1.75	0.550 E 12	9.0	0.436 E 11
2.0	0.353 E 12	10.0	0.346 E 11
2.5	0.143 E 12	11.0	0.275 E 11
3.0	0.525 E 11	12.0	0.219 E 11
3.125	0.375 E 11	13.0	0.175 E 11
3.25	0.268 E 11	14.0	0.139 E 11
3.375	0.192 E 11	15.0	0.111 E 11
3.5	0.138 E 11	16.0	0.890 E 10
3.625	0.788 E 10	18.0	0.729 E 10
3.75	0.450 E 10	20.0	0.600 E 10
3.875	0.258 E 10	25.0	0.374 E 10
4.0	0.148 E 10	30.0	0.238 E 10
4.125	0.665 E 9	35.0	0.156 E 10
4.25	0.264 E 9	40.0	0.104 E 10
4.375	0.984 E 8	45.0	0.717 E 9
4.5	0.317 E 8	50.0	0.507 E 9
4.625	0.126 E 8	55.0	0.473 E 9
4.74	0.398 E 7	60.0	0.444 E 9
4.875	0.102 E 7	80.0	0.346 E 9
5.0	0.233 E 6	100.0	0.272 E 9

TABLE 5(4) - IONISATION IN DIELECTRICS: LONG-LIVED EFFECTS CHARACTERISED

Device	Charge excitation		Structural change	
	Re-trapped locally	Charge transport	Bonding changes only	Decom-position
SUBELEMENT HAS ACTIVE ELECTRICAL FUNCTION				
Charge storage				
Variable threshold transistors	–	–	–	–
Storage photosensors	–	X	–	X
Special MIS systems (e.g. Everhart EB-addressed MOS arrays, MOS dosimeters, FAMOS memories)	–	X	–	–
Charge emission				
Photo-emitters/multipliers, photo-tubes/channes/multipliers, etc.	–	X	–	–
Charge transport				
Tunnel emission cathodes	–	–	–	–
Filamentary switches	–	–	X	–
Other transduction				
Pyroelectric detectors	–	–	–	X
Acoustic surface wave devices	–	–	–	–

TABLE 5(4) - IONISATION IN DIELECTRICS: LONG-LIVED EFFECTS CHARACTERISED (Continued)

Device	Charge excitation		Structural change	
	Re-trapped locally	Charge transport	Bonding changes only	Decom-position
PASSIVE ELECTRICAL FUNCTION				
Bipolar, MOS and CCD devices	–	X	–	–
Josephson devices	–	–	–	–
Spacers in IC's				
- Metallisation separators	–	X	X	–
- Surface encapsulation layers	–	X	X	–
- Dielectric substrates	–	X	–	–
Capacitor insulators	–	X	X	X
Stand-off insulators	X	X	–	X
ACTIVE OPTICAL FUNCTION				
Light-beam modulators	X	–	–	X
Light-beam deflectors	X	–	–	X
Storage medium				
Photostructural switches	–	–	X	–
Photochromic memories	X	X	X	–
Thermoplastic memories	–	–	X	X

TABLE 5(4) - IONISATION IN DIELECTRICS: LONG-LIVED EFFECTS CHARACTERISED (Continued)

Device	Charge excitation		Structural change	
	Re-trapped locally	Charge transport	Bonding changes only	Decom-position
Phosphors and display media				
Laser media	X	–	X	–
Cathodoluminescent phosphors	X	–	X	–
Electroluminescent phosphors	X	X	X	–
Thermoluminescent phosphors	X	X	–	–
Scintillator	X	–	X	X
Dark-field displays	X	–	X	–
PASSIVE OPTICAL FUNCTION				
Lenses and filters	X	–	X	–
Interference coatings	X	–	X	–
Light guides	X	–	X	X
Thermal-control coatings	X	–	X	X
Glass dosimeters	X	–	X	–
PASSIVE MECHANICAL OR THERMAL FUNCTION				
Corrosion-protection coatings	–	X	X	X
Refractory layers	–	–	X	X
Nuclear-fuel encapsulants	–		X	X
Thermal inlsulators	X	X	X	X
Solid-lubricant systems	–	–	X	X

REFERENCES

M. Barbier, "Induced Radioactivity", Amsterdam, London, North Holland Publ. Co. (1969).

W.L. Brown, J.D. Gabbe and W. Rosenzweig Bell System Technical Journal 42 (4) 1505-1559 (1963).

C.S. Dyer, J.I. Trombka, S.M. Seltzer, L.G. Evans, "Calculation of Radioactivity Induced Gamma Ray Spectrometers During Spaceflight", Nuclear Instruments and Methods, Vol. 173, p. 585 (1980).

C.S. Dyer and N.D.A. Hammond, "Neutron Capture Induced Radioactive Background in Spaceborne, Large Volume, NaI Gamma Ray Spectrometers", IEEE Trans. Nucl. Sci. NS-32 (6), p. 4421 (1985).

A.G. Holmes-Siedle, Reports on Progress in Physics, 37, pp. 699-769 (1974).

H.E. Johns and J.R. Cunningham, "The Physics of Radiology", C.C. Thomas, Illinois (1971).

L.E. Peterson, "Radioactivity Induced in Sodium Iodide by Trapped Protons", J. Geophys. Res., Vol. 70, p. 1762 (1965).

J.R. Srour, S. Othmer and K.Y. Chiu, ibid, pp. 2656-2662 (1975).

V.A.J. Van Lint, G. Gigas and J. Barengoltz, IEEE Trans. Nucl. Sci. NS-22 (6) 2663-2668 (Dec. 1975).

G.K. Wertheim, Phys. Rev. 105 1730 (1975).

SECTION 6. METAL-OXIDE SEMICONDUCTOR (MOS) DEVICES

6.1. INTRODUCTION

MOS integrated circuits, particularly those of the complementary form (CMOS), are extremely well adapted electrically for use in space. Power consumption is low and MOS devices employ voltage signals rather than current signals. These features are uniquely suitable for advanced data-handling and spacecraft-control systems. It is unfortunate therefore that many MOS devices show a strong, unpredictable and long-lived response to total-dose radiation. Not all regions of space present a serious problem, but those that are so affected include earth orbits heavily used for unmanned flight, including the geostationary orbits.

If degradation of MOS devices is to be avoided in these orbits, special attention will often have to be paid to both spacecraft design and device procurement. This section will discuss the problem and indicate the best approach to its management. The mechanisms which are the most important in device degradation are attributable to ionisation (hole-electron pair creation) within the silicon dioxide layers. This effect and the consequent effects upon function are described. Structural and operational factors - particularly the thickness of, and electrical stress in, the oxide - have an important influence upon device function in the presence of radiation and are described in detail, but the most important influence derives from the material parameters of the oxide which, in turn, are critically affected by the processing conditions during and after oxide growth.

The term "MOS" has been extended to the recently developed devices in which the metal gate is replaced by a polycrystalline silicon electrode. These are distinguished by the name "silicon-gate MOS devices". Reference is made in the following pages to both discrete MOS devices and integrated circuits, particularly the complementary MOS network (CMOS) which incorporates a number of p- and n-channel transistors on a single chip. Figure 6.1(a) shows an example of a CMOS circuit configuration (2 CMOS inverters in cascade) and a schematic representation of the device structure. The typical characteristics of the MOS structure can be seen. The source and drain regions are heavily doped, diffused "islands" in the substrate or body, and the channels are the surface regions lying between source and drain.

N-type material is typically produced by doping with phosphorus while P-type may be obtained by doping with boron. The gate oxide layer, thermally grown SiO_2, is typically 1000Å (0.1 nm) thick and the metal electrodes are termed "gates".

Figure 6.1(b) shows further details of a CMOS chip. The device shown is a large-scale integrated (LSI) circuit. Dimensions may be

as small as 1 micrometre, the gates are made of polycrystalline silicon and the gate oxide thickness may be as small as 0.03 nm. The thicker "field oxides" present additional radiation-effect problems.

One particular source of confusion in nomenclature should be noted here. The term "radiation-hardness" is often used to describe several different forms of tolerance to radiation in MOS and other devices. This term has a military connotation. Originally, "hard" meant "invulnerable to attack". Where possible, we will use the term "tolerance (or sensitivity) to radiation" instead of "hardness". However, the term "hardness assurance" is already widely used in the U.S. "Megarad-hard" is now used to signify "capable of withstanding one megarad of ionising radiation".

Confusion may arise on account of the military requirement to survive the transient effects of an intense burst of gamma rays and neutrons at a dose rate at least 10 billion times higher than that experienced in space. The long-lived effects or "total doses" received from this burst may be of the same order as that accumulated in a space mission, but neutron damage may be received from the military environment. From typical figures for the space and military environments, given in Table 6(1), it can be seen that transient effects, usually the dominant problem in military devices, will be negligible in the case of radiation belts. The space doses are for a typical internal location within a spacecraft structure.

Because of the "logic upset" produced in the military case, special device structures, which minimise the photocurrents produced, have been developed. These may not necessarily have good tolerance to total-dose effects. Thus, in the procurement of devices, the term "radiation-hardened" should be investigated and qualified before its relevance to space can be established. Similar distinctions should be drawn when considering testing methods.

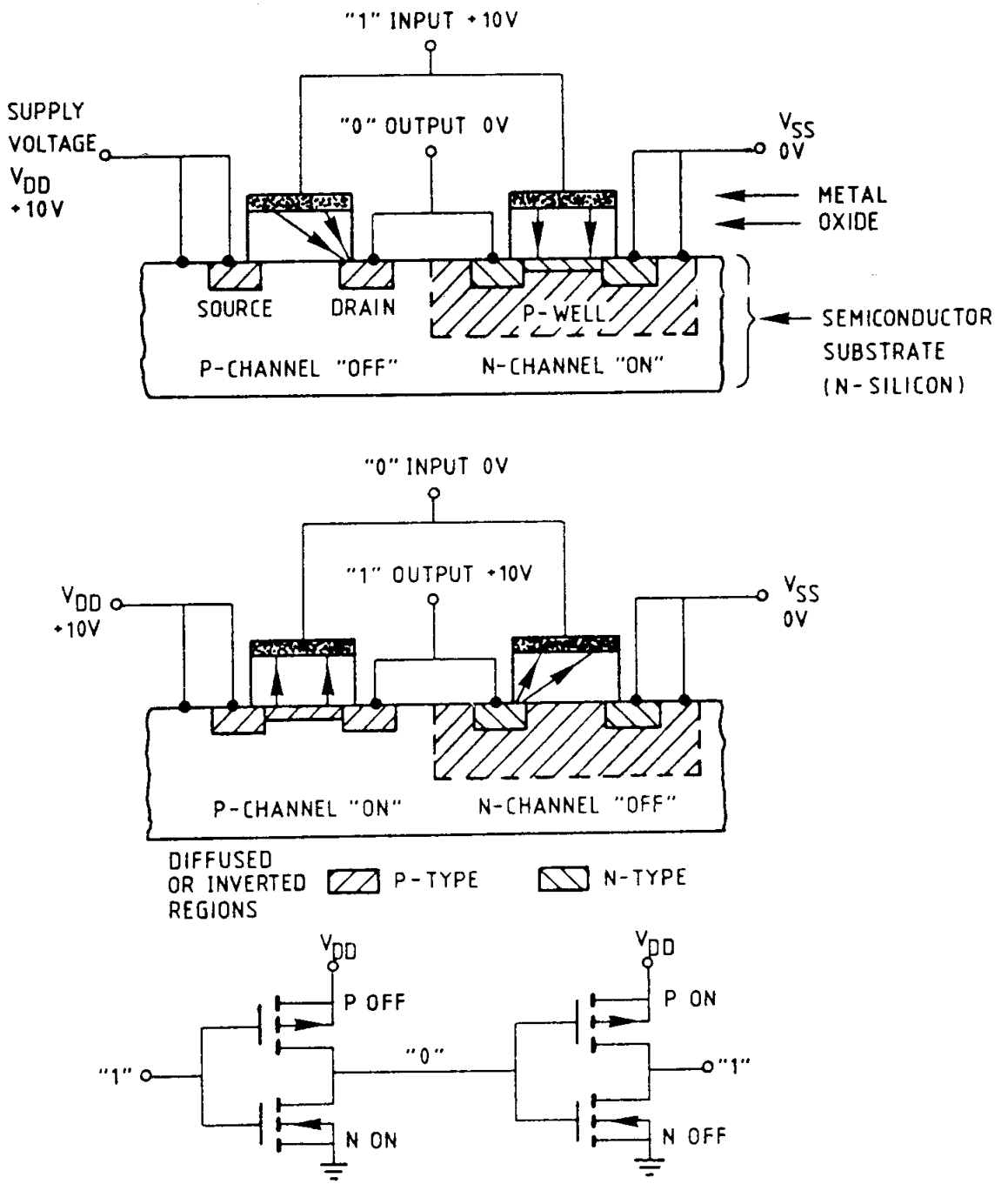

The structure of an integrated complementary-symmetry MOS (CMOS)inverter showing typical bias and logic levels. The lower figure shows two inverters in cascade.

FIGURE 6.1 (a) - THE TYPICAL MOS STRUCTURE

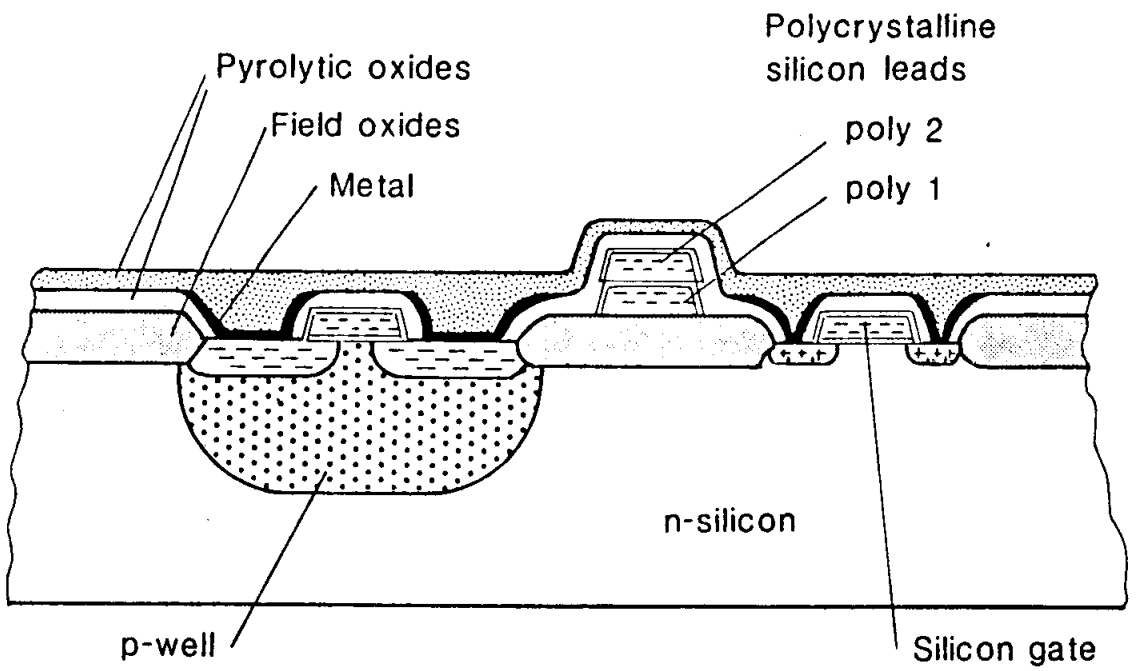

FIGURE 6.1 (b) - TYPICAL SILICON-GATE CMOS STRUCTURE OF 3 - MICROMETRE SCALE

TABLE 6(1) - COMPARISON BETWEEN TYPICAL RADIATION ENVIRONMENTS IN A MILITARY "WEAPON BURST" AND SPACE RADIATION BELTS

	Military	Space
DAMAGE : Neutron fluence (cm^{-2})	10^{14}	–
equiv. 1 MeV electron fluence (cm^{-2})	10^{17}	10^{12}
TOTAL DOSE : rad (Si)	10^{16}	10^{15}
DOSE RATE : rad (Si)	10^{11}	10^{-2}

6.2. EARLY INVESTIGATIONS

The effect of radiation on the performance of MOS devices was first noted in 1964 by Hughes and Giroux. This observation contradicted the earlier belief that because surface channel devices would not be affected by the production of minority-carrier recombination centres in silicon, they would not undergo strong changes as a result of irradiation. Even though radiation-induced charge-trapping had long been recognised as, for example, the source of colour-centre formation in bulk silica and other insulators, it was not appreciated that similar effects in the insulator layer of any MOS device would strongly influence performance.

At this time, unexpected surface degradation effects were also observed in planar bipolar transistors. It could be shown that these effects were not due solely to the well-known atomic displacement damage; charge-trapping in the passivating oxide layer was again believed to be the cause.

During 1965 and 1966, much experimental evidence was produced to support the theory that radiation-induced degradation in MOS devices was caused by the trapping of charge (holes) in the oxide layer and that the amount of charge trapped depended strongly upon the voltage across the oxide during irradiation. It was also concluded that a secondary effect, involving the rearrangement of atomic bonds at the oxide/silicon interface, was contributing to the degradation; this is the production of new "interface states".

Figure 6.2 illustrates the two effects mentioned above. Note that the term "irradiation bias" (V_I) is used to define specifically the gate voltage applied to a device during irradiation. This is commonly a steady voltage which induces the electric field in the oxide (it may however be variable during real device operation). The influence of this field is very important in determining the rate of device degradation in space. Atomic displacement damage in either the silicon or the insulator does not appear to play a significant role in these phenomena. The trapping mechanism appears to occur to

some extent in all insulator types. Preliminary attempts were made to discover the origin of the hole-trapping and to suppress it, but these did not meet with immediate practical success. Some users then settled down to try and understand, control and accommodate the large changes produced by radiation in commercial MOS devices.

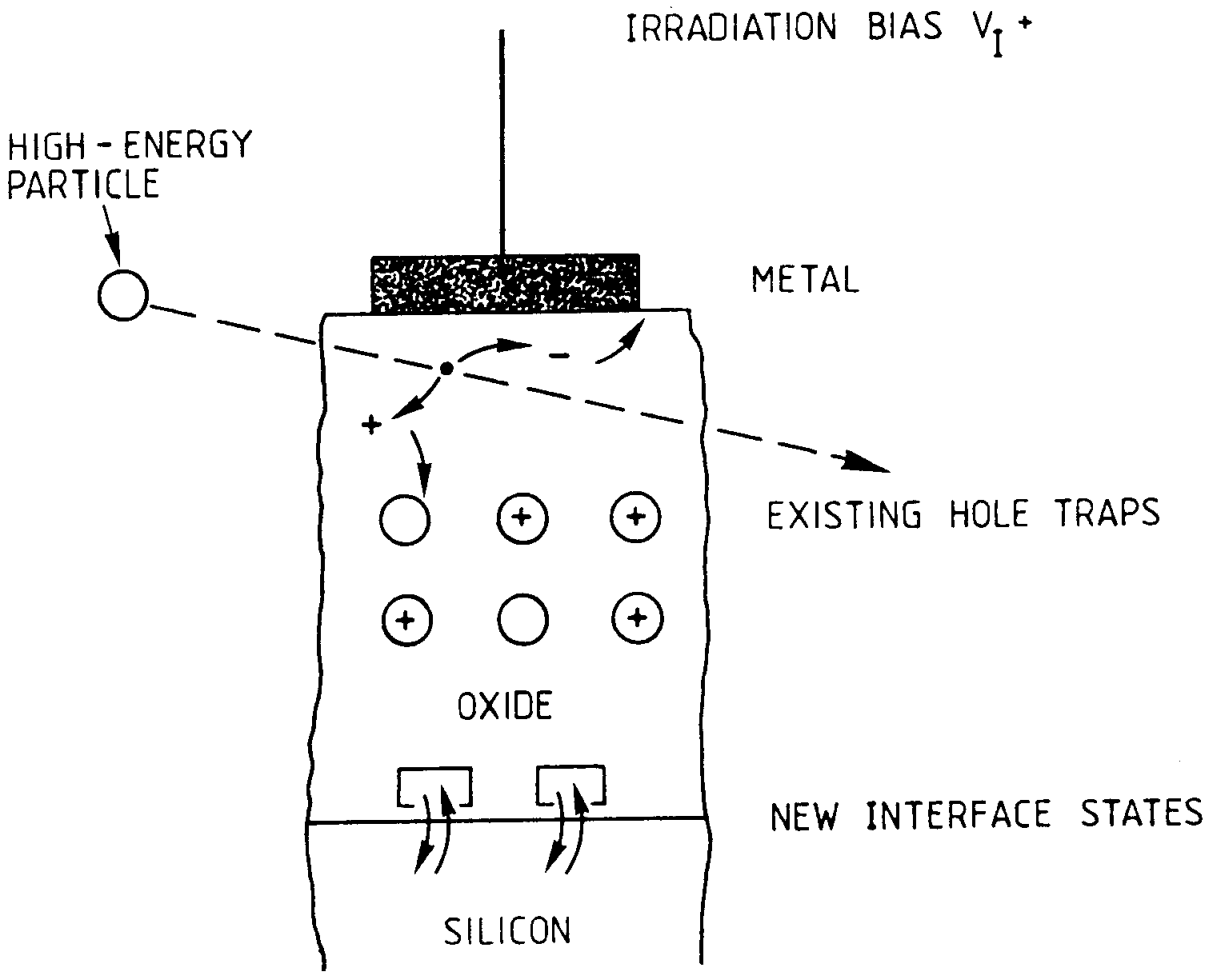

The ionisation, charge transport, hole-trapping and interface-state mechanisms in the gate insulator.

FIGURE 6.2 - MOS DEGRADATION

Research and development to produce a practical "Megarad-hard" CMOS technology was funded by the U.S. Government, through Naval Research Laboratories, NASA and other agencies. Semiconductor laboratories leading the effort included Sandia National Laboratory, RCA, National Semiconductor and Harris. European governments funded research at a lower level, for example in the 1970's at GEC Hirst Research Centre, Wembley; SGS, Milan and C.E.N., Grenoble. Progress reports of the above work can be found in the annual proceedings of the IEEE Nuclear and Space Radiation Effects Conference, published regularly as the December issue of the IEEE Transactions of Nuclear Science. More recently, Japanese contributions have been made, funded by the Future Electron Devices Programme of M.I.T.I.

6.2.1. MOS failure mechanisms

The electrical consequences of radiation-induced physical changes in MOS devices are the progressive loss of function and eventual "failure" of a MOS circuit. Figure 6.3(a) shows a series of parallel I_D-V_G curves for an n-channel device, resulting from successive increases in dose. Each of the curves corresponds to the onset of particular malfunction in, say, the CMOS logic gate shown in Figure 6.1. We can consider each type of malfunction as defining a "failure mode".

Table 6(2) lists the four major performance degradation effects which are likely to appear at the four dose levels indicated in Figure 6.3 (a). The table also gives an indication of the real dose and threshold shift associated with each failure mode in a typical CMOS circuit.

It is clear that if one were designing CMOS circuits specially, one could build in some tolerance to these effects. However, in commercial LSI circuits, the internal circuit design is predetermined and may have poor tolerance to one of the four effects noted above. Thus, "failure" cannot be defined at the level of the single device element, but is rather the point at which a particular network of devices no longer tolerates these effects. We can define a radiation dose limit or "Maximum Acceptable Dose", D_A(max), for any CMOS circuit based on the dose at which the significant failure mechanism appears for that circuit. In spacecraft applications, which are limited for power, this is usually the effect noted in Table 6(2) as "V_{TN} crossing zero (VTNZ)", which leads to large increases of quiescent current. The acceptable levels of current increase may be very low.

TABLE 6(2) - PROGRESSIVE NATURE OF CMOS FAILURE AS A FUNCTION OF RADIATION DOSE

Dose level in Fig. 6.3(a)	Failure mechanism number	Main degradation effect	Symbol	Typical values for CMOS LSI	
				Dose rad (Si)	$-\Delta V_T$ volts
1	1	Minor 'noise immunity reduction'; possibly minor loss in switching speed	NIR	8×10^2	0.2
2	2	Sharp quiescent current increase due to 'V_T of N-channel crossing zero	VTNZ	5×10^3	1
3	3	Switching speed reduction	SSR	1×10^4	2
4	4	Change of logic state impossible: 'Logic failure'	LF	3×10^4	4

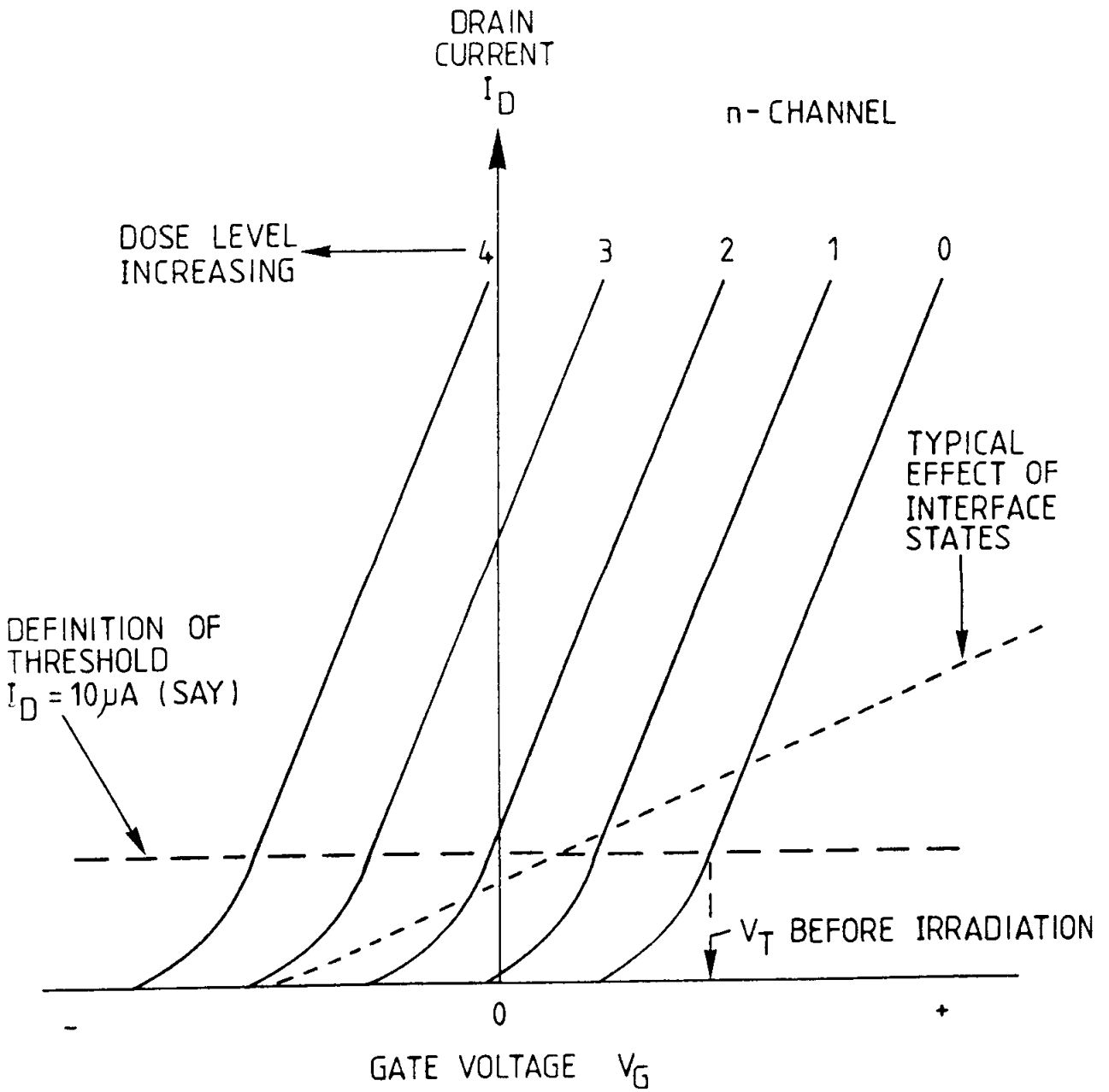

Typical drain-current/gate-voltage curves for an N-Channel MOS device, showing the progressive effect of increasing radiation dose. The dose levels shown (1 to 4) correspond to the "failure mechanism" described in Table 6(2). The solid curves show the ideal case, where positive charge only is introduced into existing traps; the effect of the production of interface states on the shape of the curves is shown by the broken line.

FIGURE 6.3(a) - CMOS DEGRADATION AND FAILURE

6.2.2. The VTNZ effect and its impact

The growth of leakage, or quiescent current (I_{SS}), in CMOS devices as a function of dose is illustrated in Figure 6.3(b). This important functional consequence of threshold shift is often the most easily monitored parameter in MSI or LSI circuits. In this case, the "Maximum Acceptable I_{SS} Value" has been arbitrarily set at 0.5 μA.

If leakage at the "maximum acceptable I_{SS} value" produces system failure, note that the maximum acceptable dose value can vary by over a hundredfold from type to type. At a constant daily dose rate, this means that the life of the system can vary by a hundredfold depending on the material parameters of the CMOS gate oxides. It is this uncertainty which makes extensive radiation testing necessary.

6.2.3. Other effects on logic operation

A CMOS gate may be regarded as a type of "potential divider" with the potential, V_{DD} , being dropped across various sections of the device according to its logic state. Clearly, a pronounced leakage current in a transistor which is meant to be "OFF" will reduce the potential difference across that channel. Thus, the difference in output voltage between the '0' and '1' states will be reduced, correspondingly degrading the input (gate) voltages to the next inverter pair. This is the Noise Immunity Reduction (NIR) noted in Table 6(2).

The effect of this is illustrated in Figure 6.4. The full curves show the voltage waveform associated with CMOS gate-switching before and after various doses of radiation. The broken curves show the relevant channel current which flows during the switching phase. In the experiment shown, V_{DD} was +10V and the irradiation bias was +10V for the n-channel and zero for the p-channel.

Note that, in LSI devices, leakage can occur under the field oxides and produce increases in the I_{SS} value even though the N-channel transistor itself has not crossed zero V_T.

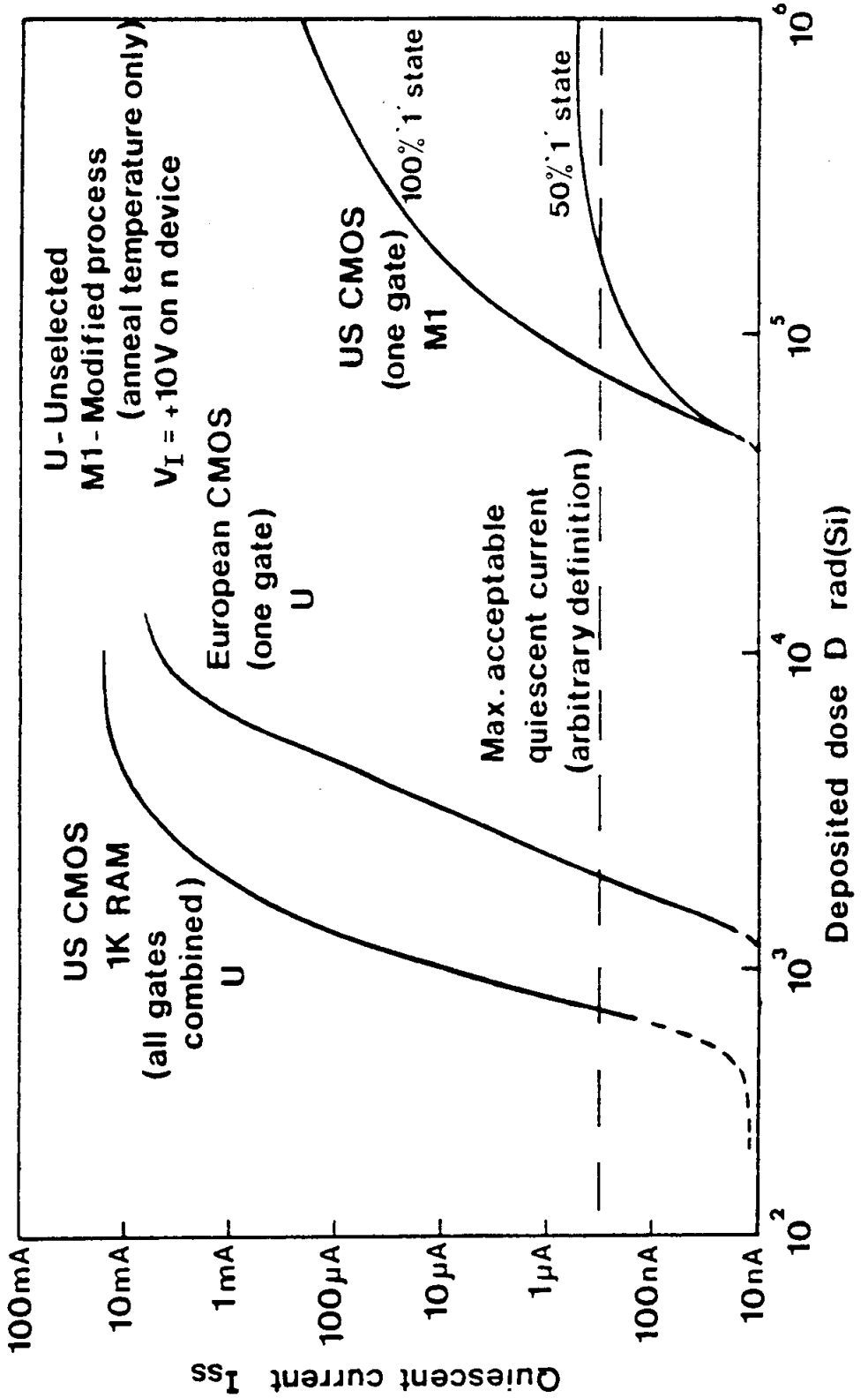

Quiescent current (supply current when the gates are not changing state) as a function of dose in typical CMOS integrated circuits. Growth of this current is one important functional effect of the shift of threshold voltage in the n-channel element (VTNZ effect).

FIGURE 6.3(b) - LEAKAGE CURRENT IN CMOS DEVICES

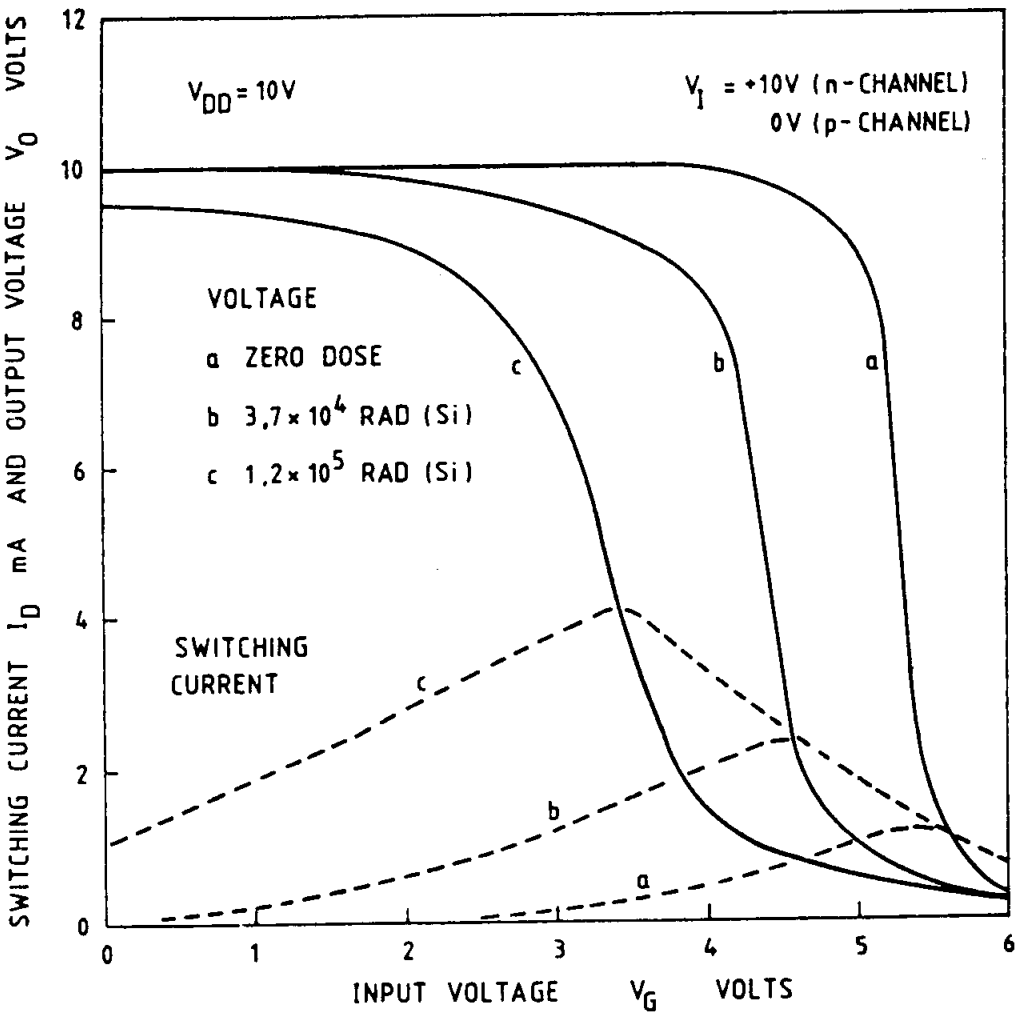

Radiation-induced changes in logic transfer characteristics of a CMOS inverter. Increasing dose causes progressive loss of a logic definition and decrease in height of the output voltage step, with corresponding increase in power consumption. The left-hand side of the switching-current waveform is controlled by the N-channel component (large shift observable) and the right-hand side by the p-channel (no shift).

FIGURE 6.4 - CMOS SWITCHING CHARACTERISTICS

6.2.4. The effect of interface states on logic operation

The qualitative effect of interface states (the complex rearrangements of atomic bonding in the SiO_2/silicon interface caused by ionisation) is to distort both the I_D-V_G and C-V characteristics. The common result is that the I_D-V_G curve is reduced in slope, as shown by the broken curve in Figure 6.4. In an n-channel device, this effect is to a degree beneficial in that the threshold shift is effectively reduced. A high degree of interface state production can decrease the I_D-V_G slope so much that the threshold voltage, V_{TN}, becomes even higher than its pre-irradiation value ("rebound"). The "transconductance" of the channel (the rate of change of I_D with V_G at given gate and supply voltages) is reduced and this may lead to further degradation of switching speed in a CMOS device.

6.3. LOSS OF FUNCTION IN MOS DEVICES

6.3.1. MOS transistor action

Figure 6.5 shows the electron energy levels of the conduction and valence bands at the interface between SiO_2 and a p-type silicon substrate (*). Note that the band-gap in silicon is 1.1 eV (the difference in energy between the conduction and valence bands) while that in the insulator, SiO_2, is about 9 eV. The Fermi level which, in an intrinsic semiconductor, is mid-way between the two bands, is nearer to the valence band in p-type silicon. If the system is in equilibrium (the gate and semiconductor are at the same potential), the Fermi level must remain constant throughout the two regions. As shown, the differences in work function between the semiconductor and the gate electrode must then be resolved across the interface through bending of the Si energy bands.

In simple terms, the downward bending of the silicon energy bands at the interface may be interpreted as having the effect of pushing the majority-carriers, holes in p-silicon, away from the interface, leaving a narrow "depletion" region of ionised immobile acceptor atoms (boron) in energy states just above the valence band.

Application of a low negative voltage to the gate (with respect to the substrate) will create an electric field across the insulator and, initially, have the effect of flattening the energy bands at the interface.

(*) For further details of the solid-state physics of MOS function, refer to textbooks by Grove and Sze.

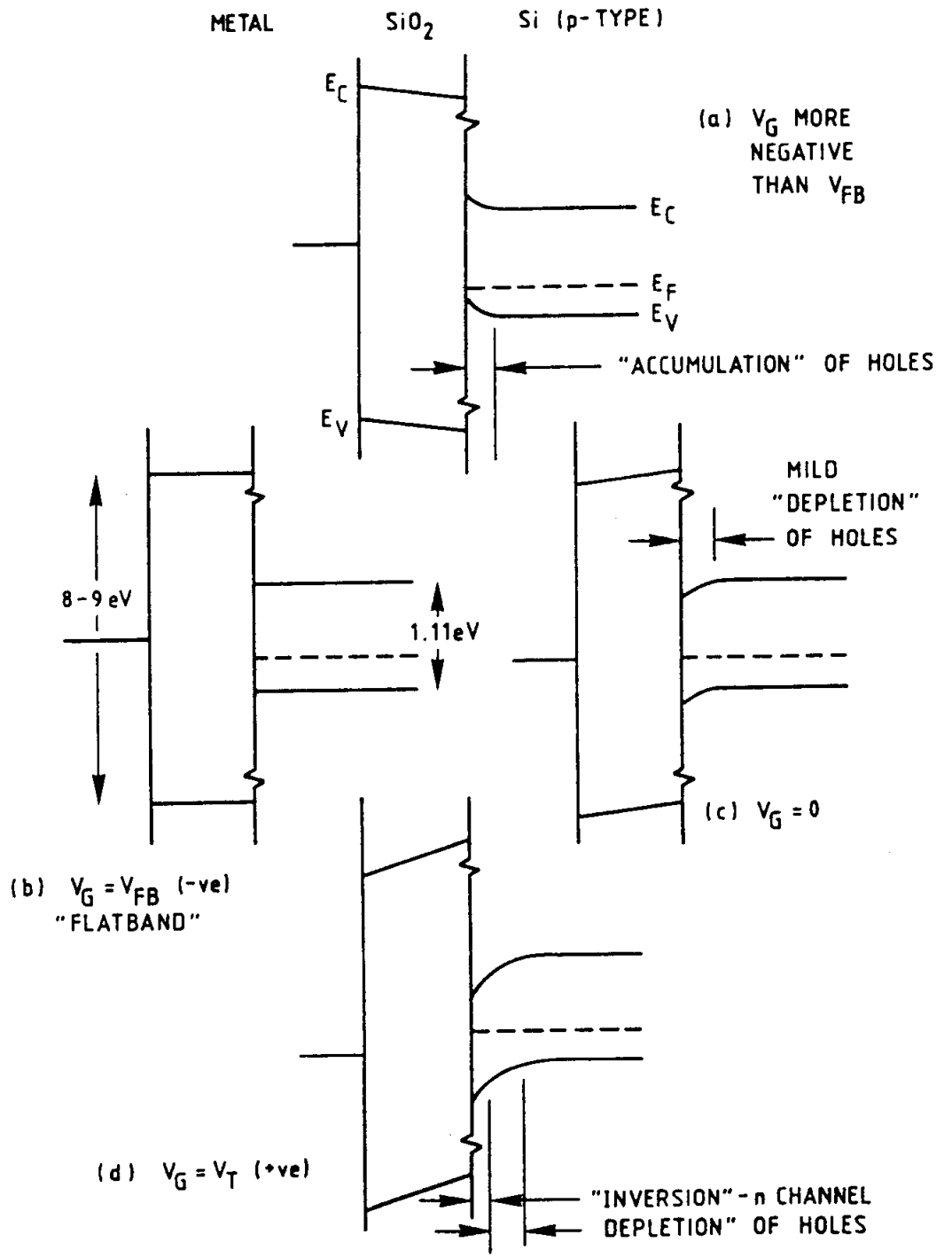

The electronic energy levels at the oxide/silicon interface showing band bending and the 'Flatband' condition. Band bending in the silicon at zero gate voltage will result from a difference in work function between the silicon and the gate electrode and from the presence of fixed oxide charge.

FIGURE 6.5 - ENERGY BANDS AT THE INTERFACE

The voltage at which the bands are perfectly flat is known as the "flatband voltage", V_{FB}. Further increase in negative voltage will cause the bands to bend upwards, creating an "accumulation" of majority carriers, holes in p-silicon, at the interface.

Application of a voltage between the source and drain junction of a MOS transistor in the "accumulation" condition will not cause a channel current to flow, owing to the conflicting rectifying actions of the two p-n junctions (source/substrate and substrate/drain).

Application of a positive gate voltage, on the other hand, will cause the energy bands to bend further downwards. This will have the initial effect of "pushing" more holes away from the interface, increasing the width of the depletion region. With increasing positive gate voltage, the depletion will reach a "limit" and "inversion" will occur. At this point, there is a rapid generation of conduction band electrons in the surface region. The conduction band at the surface will now be very close to the Fermi level and, in this respect, the silicon at the surface will resemble n-type material in its transport properties (hence the term "inversion"). A voltage between n-type source and drain, V_{DD}, will now cause conduction through this region, called the "channel". The gate voltage at which inversion is sufficiently established to cause a measurable channel current to flow (typically 10 μA) is defined as the "threshold voltage" (V_T).

The picture given above is simplified, but will perhaps assist in understanding the mode of operation of this device and the mechanism of radiation-induced degradation. There are of course no sharp divisions between accumulation, depletion and inversion.

6.3.2. Flatband and threshold shift

The threshold voltage of a MOS transistor is ascertained by measuring the channel current (usually termed "drain current)", I_D as a function of the gate voltage, V_G, at a constant supply voltage, V_{DD} (see Figure 6.3 (a)). The resulting characteristic curve for a p-substrate device is shown in Figure 6.6. Flat band voltage is usually estimated by plotting the small signal gate capacitance (C_g) versus the gate voltage of the device. The resulting "C-V curve" for a P-substrate device is of the form shown in Figure 6.6(a). The minimum in this curve reflects the transition from "depletion" to "inversion" conditions. Comparing Figures 6.6 (a), note how the value of V_T on the I-V characteristic is always aligned with a point near this minimum. The flatband condition is known to occur when the ratio C/C_o is approximately 0.8. Note that this measurement does not involve the measurement of channel current and, in fact, can be accomplished by means of an MOS capacitor with appropriately doped silicon substrate; source and drain diffusions are not

required. MOS capacitors are therefore a useful aid in the laboratory investigation of radiation effects.

Positive charge (trapped holes) induced by ionisation in the oxide layer of a MOS device will have the same qualitative effect on the potentials in the silicon as the application of a positive gate voltage, it will bend the energy bands further downwards and tend to induce inversion in a p-type substrate.

An alternative interpretation of this effect, without involving energy bands, is to say that the trapped positive charge induces negative image charge in both the gate and substrate; the charge in the substrate therefore increases the n-type conductivity in an n-channel device. Thus, a smaller threshold voltage will then be registered. Given sufficient trapped charge, inversion may be established by the charge alone and a "leakage current" will flow in the channel even in the absence of a gate voltage. This is the VTNZ effect in Table 6(2).

If V_T of the n-channel has passed zero, the device is "ON" when it should be "OFF". Similarly, the existence of trapped charge will mean that a greater negative gate voltage will be required to achieve the flatband condition. Thus, simple trapped-charge accumulation results in an essentially parallel shift of the C/V and I_D-V_G characteristics. Discussion of these shifts in threshold, V_T, and flatband, V_{FB}, voltages forms the major part of this section. If we ignore various distorting effects, V_T is equal to V_{FB}. As described, the degree of parallel shift observed in MOS devices varies very widely with the material parameters of the insulator layer.

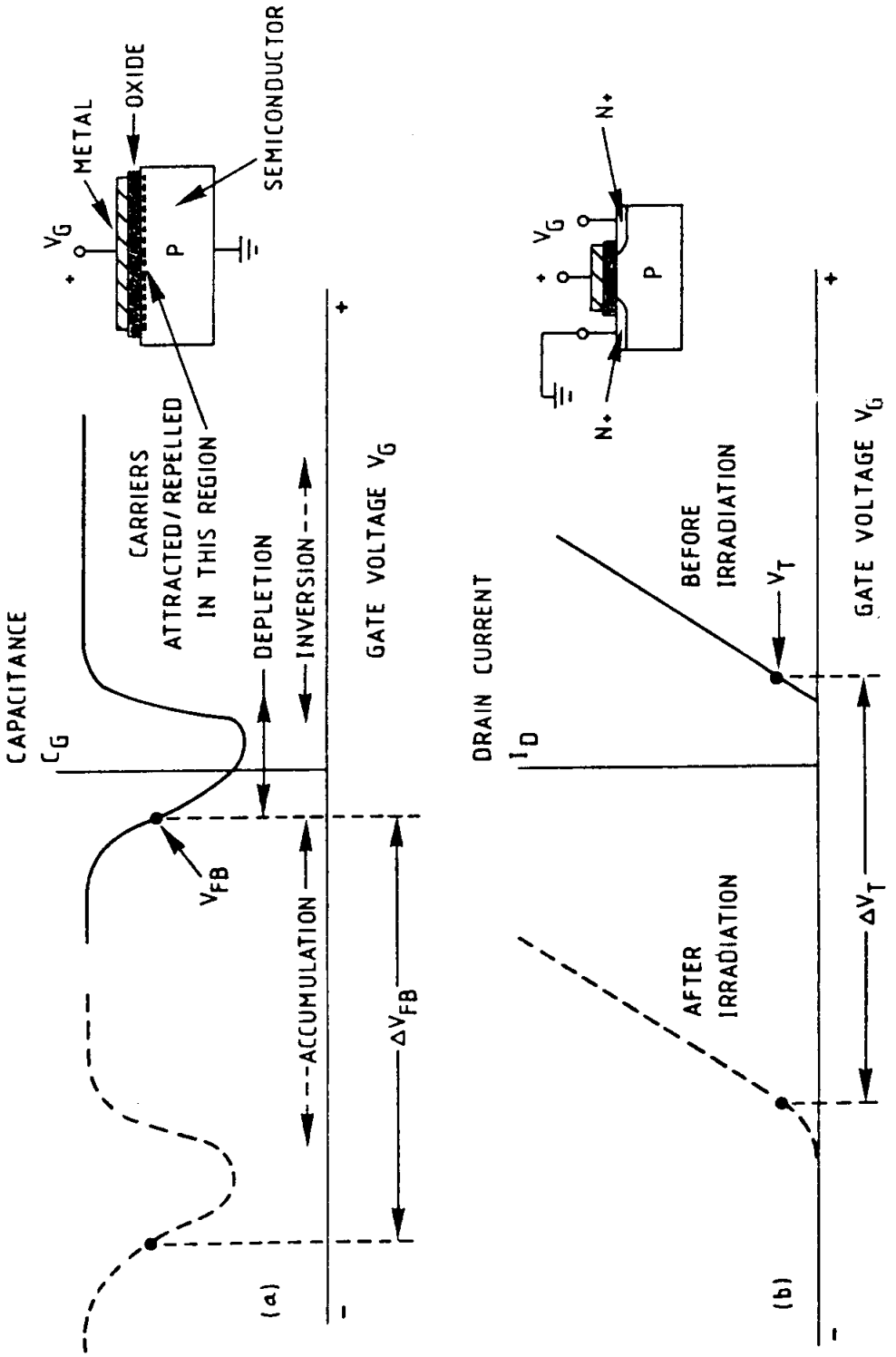

Typical variation of capacitance and drain current with gate voltage showing the shifts in flatband and threshold voltages due to trapped charge (no interface states)

FIGURE 6.6 - MOS CHARACTERISTICS

6.3.3. Equivalent effects in P-channel devices

While, in the absence of space charge build-up, an n-channel MOS requires a positive gate voltage to cause the channel to conduct, a p-channel devices requires a negative bias. As shown in Figure 6.7, the parallel shift in the I_D-V_G characteristic caused by trapped charge means that an increasing negative bias is required to operate the device. At high radiation doses, it may therefore become impossible to switch the device "ON". Additionally, the creation of interface states, resulting in a typical characteristic as shown by the dotted curve, must always - in contrast with n-channel devices - make matters worse.

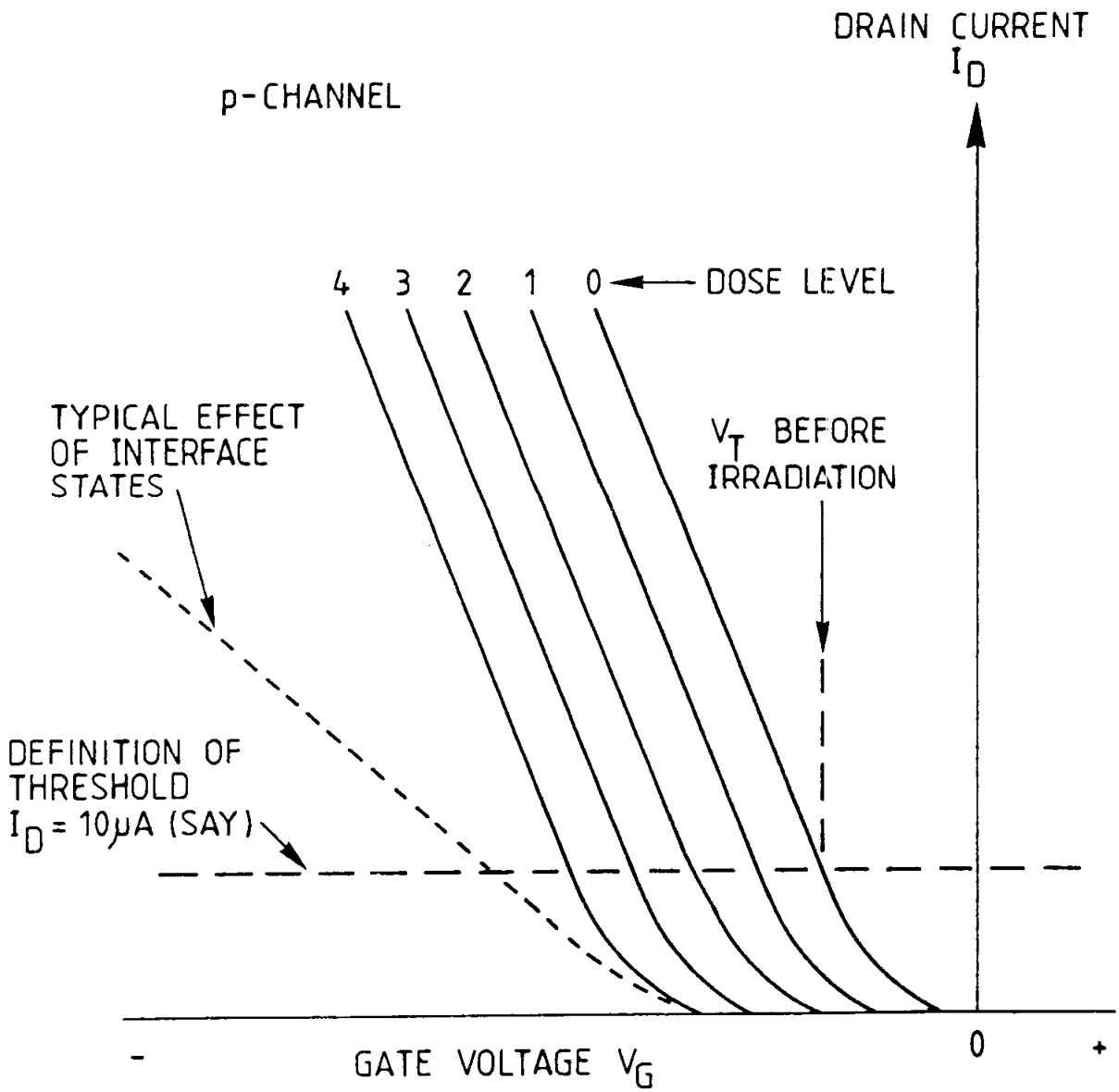

Typical radiation-induced shift in the drain-current/gate-voltage characteristic of a p-channel device. Leakage current will not be a problem in this case, but progressively higher gate voltages will be required to invert the channel region.

FIGURE 6.7 - DEGRADATION OF P-CHANNEL MOS

6.4. DEGRADATION MODELS OF MOS DEVICES

6.4.1. A simple analysis of radiation effects in MOS devices

As part of the "Fulmer Radiation Effects Engineering Handbook" project, simple prediction models were developed to deal with threshold voltage shift in MOS devices as a function of dose and electrical stress applied during irradiation. These were subsequently published (Freeman and Holmes-Siedle, 1978).

The physical model used is in accordance with current research, but uses simplified assumptions with respect to trap location in the oxide and yield of available charge. It employs a "worst-case" (linear dependence) of charge build-up on dose. The result is an analytical method suitable for characterising the behaviour of commercial MOS devices under laboratory radiation test and the subsequent extrapolation of the test data to degradation with time in space.

In the analysis, laboratory test data are used to characterise the gate oxide of an individual transistor by an A-value. This is a charge-trapping probability and the most sensitive devices have an A-value of 1.0. The threshold voltage shift in space, ΔV_T, is predicted with the aid of the formula:

$$\Delta V_T = R.A.D. \qquad .....6(i)$$

where R is calculated from oxide thickness and other parameters while D is the mission dose predicted for the device in a given position in a satellite. If the original V_T values cannot be measured in the laboratory, the manufacturer can supply the original value of V_T for the devices as used in integrated circuits. Given these data, we can calculate the earliest time at which the device may malfunction in space.

Refinements of the model can deal with electrical stress effects, interface effects and post-irradiation effects (Freeman and Holmes-Siedle, 1978; Holmes-Siedle and Adams, 1983; D.K. Nichols, 1983).

6.4.2. Importance of electrical conditions during irradiation

Radiation effects in MOS devices are unusual because these devices are extremely sensitive to the application of voltage, especially gate voltage, V_I, during irradiation. This arises directly from the physical mechanism which, as explained earlier, involves the transport of charge across the gate oxide. The yield of charge available for trapping is very sensitive to the value of the field in the oxide film when the charge pairs are being generated by the irradiation. This is dealt with in the simple analytical model, described earlier, by the use of a calculated charge yield, f(E).

While experimental results vary from this owing to interface effects, the use of the charge yield factor gives an acceptable "worst-case" model for powered devices. However, the prediction of "zero degradation" for unpowered devices is not correct and test data should be used to establish the effect of devices in a "resting condition".

The terminology adopted here for the gate bias values applied during irradiation is as follows:

V_I + : positive bias applied to gate during irradiation,
V_I – : negative bias applied to gate during irradiation,
V_I 0 : zero bias (gate shorted to body) during irradiation.

Thus, for example "irradiation at V_I + 5" would describe the application during irradiation of +5V to the gate relative to the silicon body or substrate of the device. The oxide field, E_I, created thereby in an oxide thickness of 0.1 μm would be 50V per micrometre. In a CMOS gate in the "1" condition with V_{DD} = 5V, the n-channel device is in the V_I + 5 condition, but the p-channel device is in a different condition, not unlike "V_I0".

6.4.3. Intermittent biasing

It has been known for some time that when the electric field across the oxide layer of a MOS device is released during irradiation, the trapped charge begins to decline. This is due to the neutralising effect of photoelectrons emitted into the oxide by the electrodes. This mechanism is effective even if the rate of cycling of the field were many times per second. Thus, for devices which are subject to cycling, the maximum acceptable dose is likely to be higher, typically by a factor of 5, than if the irradiation bias were constantly applied. Figure 6.8 shows the marked effect on the maximum acceptable dose of "50% cycling" (V_I applied for half the time). Use of a lower bias value not only increased the acceptable dose, but also enhanced the effect of cycling. It should be noted that the broken sections of the curves in this figure tend towards a very high dose value.

A further illustration of the effect of intermittent biasing is shown in Figure 6.9. Here, irradiation biases of zero and -9V are applied to a typical p-channel MOS device. If the cycling procedure is interrupted and the bias thereafter held constant, the resulting "growth curve" should gradually approach the upper and lower limit curves. There is scope for introducing a "resting" policy, either within the chip or over the whole subsystem. Such redundancy would significantly prolong the useful life of all MOS components in space. However, the build-up of interface states often continues during irradiation at zero bias; therefore, caution should be exercised in applying this technique. The best approach is to

simulate in the laboratory the type of cycling expected in use and operate the devices in this mode during laboratory irradiation tests.

6.4.4. Gate oxide thickness dependence

Experimental work on oxide thickness dependence, described by Derbenwick, Gregory and Fossum (1975), indicates that radiation-induced threshold shifts vary as the cube of the oxide thickness, d_{ox}^3, if the oxides are grown directly to a number of desired thickness values. Hughes and Powell (1976) disagree with the conclusions of Derbenwick and colleagues and show experimental evidence of a d_{ox}^2 dependence even for oxides grown to varying thicknesses. In the very simple model of derived threshold shift, described earlier in this report, threshold voltage shift is effectively dependent upon the square of the oxide thickness.

6.4.5. Simple engineering model of MOS degradation

The equations derived in the simple analytical model described above have been used to construct the set of curves shown in Figures 6.10 to 6.13. These figures show examples of a number of possible sets of curves which could be derived from the model. As shown in the insets, some typical values of oxide thickness and charge distribution have been selected. In modern technologies, the oxide thickness values may be lower than those shown.

Figures 6.12 and 6.13 show initial growth and both types of saturation for a range of 'A' values from 1.0 ("soft") to 0.01 ("hard") with V_I equal to 10V. Note that the case of the unpowered device ($V_I 0$ condition) is not covered here. Experimentally, a finite charge build-up is found for improved devices although the simple model predicts no change. Here, each case should be examined experimentally, although research is proceeding on models for the unpowered case (Hughes, 1985; Holmes-Siedle, Adams, Pauly & Marsden, 1985).

These curves may be combined by the engineer in a variety of ways. Figure 6.12 may be regenerated for V_I = +8V merely by displacing the whole set of curves by the same horizontal distance by which the 8V curve is displaced from the 10V curve in Figure 6.10.

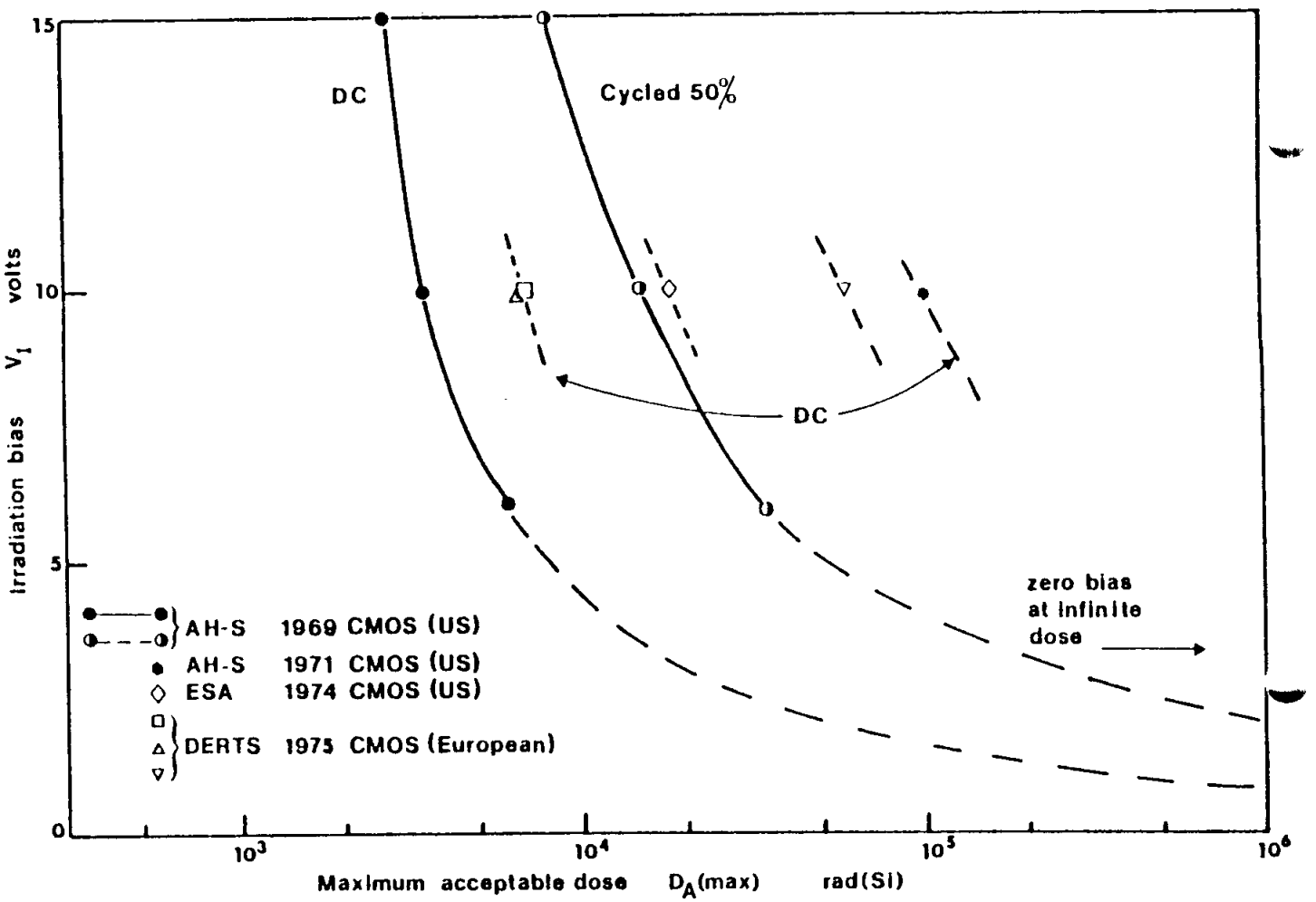

The "maximum acceptable dose" for some specific devices as a function of irradiation bias. The beneficial effect of "50% cycling" in the 1969 series is clear. Some later measurements of "maximum acceptable dose" at a single bias value are included for comparison; these were all obtained under conditions of continuous operation.

FIGURE 6.8 - THE EFFECT OF INTERMITTENT BIAS

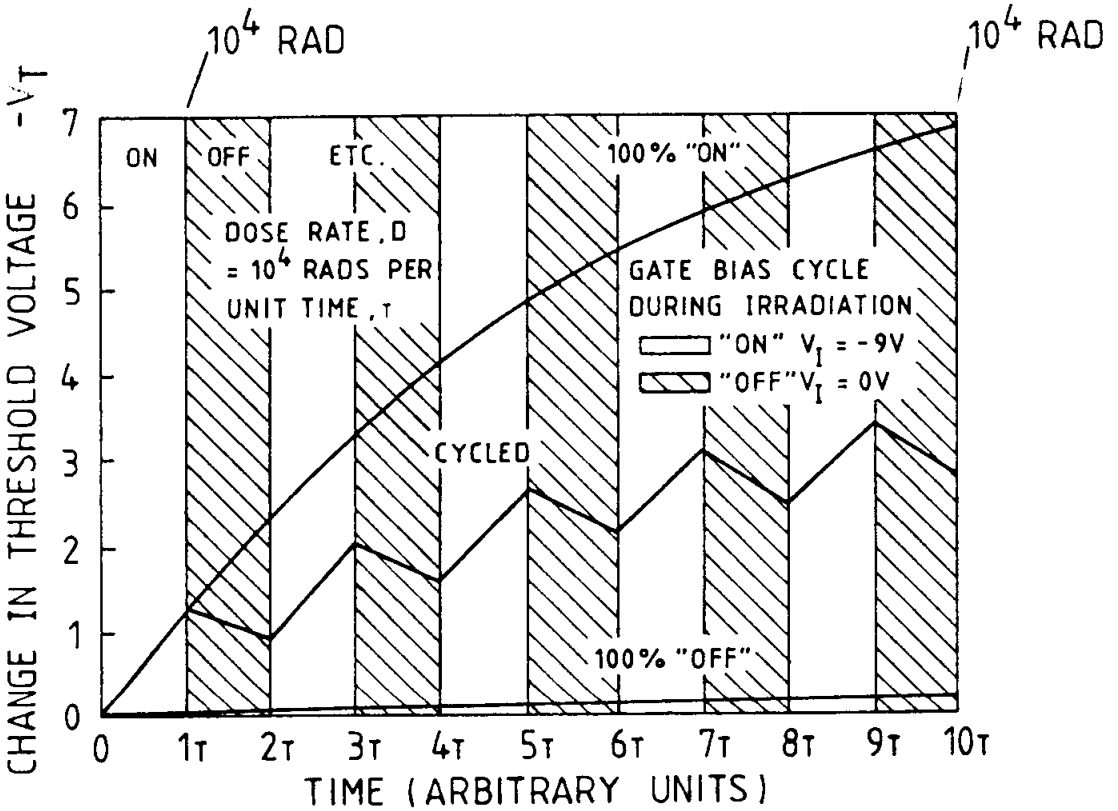

Threshold voltage shifts as a function of time (equivalent to dose) for a typical p-channel MOS device subject to zero bias, 50% cycling, or constant bias during irradiation.

FIGURE 6.9 - THE EFFECT OF INTERMITTENT BIAS

By comparing experimentally determined V_T growth curves with theoretical sets such as those illustrated, it should be possible to obtain a measure of radiation sensitivity of a MOS device in terms of the trap density and "trapping probability" ('A' value) of the oxide (*).

(*) Experimental data at low doses will indicate the 'A' value; those at very high doses the trap density.

6.4.6. Classification of "hard", "soft", and "medium"

Figure 6.14 shows a classification scheme based on the "growth curve" format presented earlier. The figure is for device irradiation under a positive gate bias of 10V. An oxide thickness of 0.1 nm is taken. The format is divided into three areas: "hard", "medium" and "soft". The position of a device test result in this framework is a useful indication of the suitability of that device for use in the space environment. Experimental results generally follow the "corridors" shown.

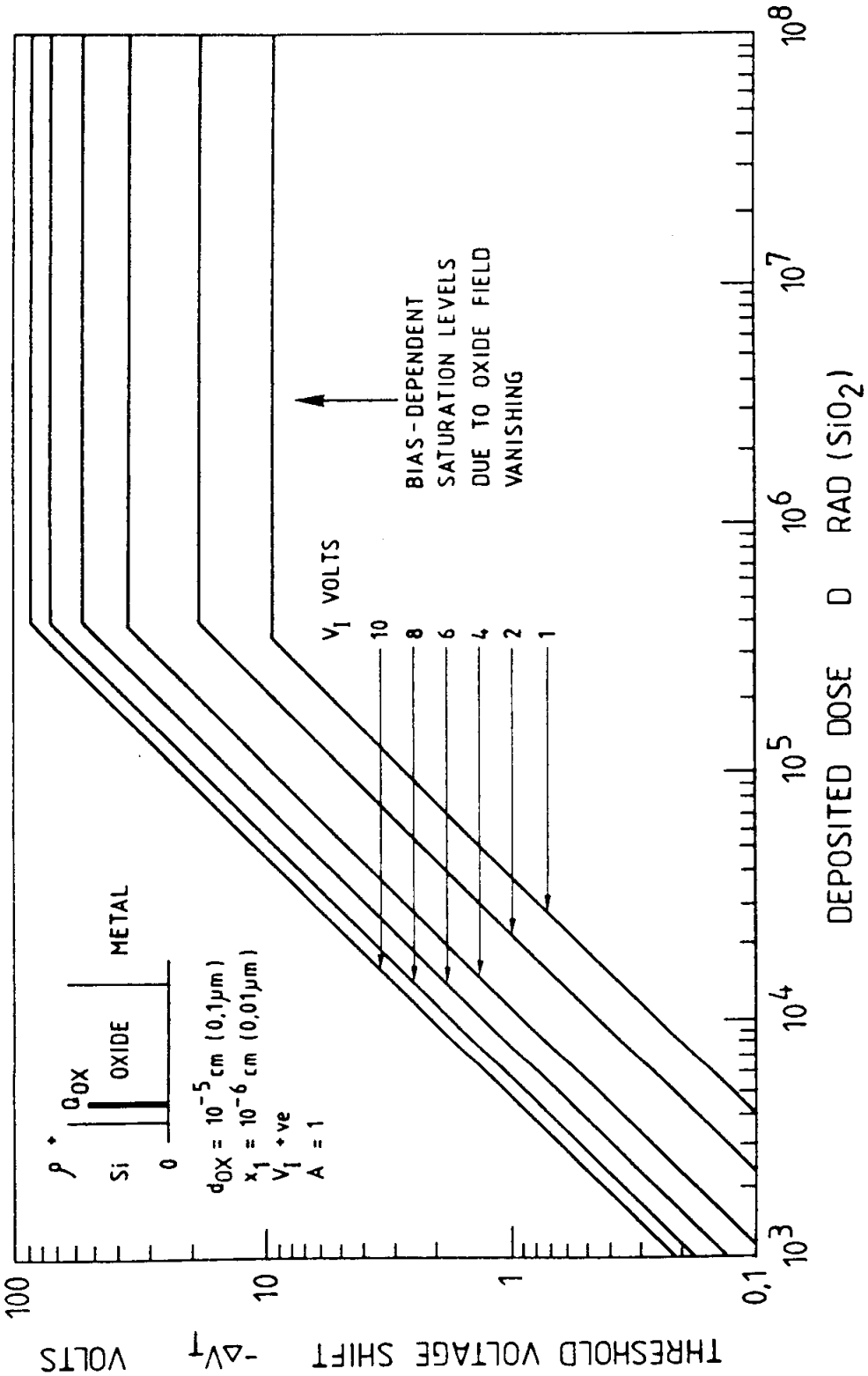

Simple model of threshold shift as a function of dose for several values of positive irradiation bias, with trapping probability equal to unity.

FIGURE 6.10 - ENGINEERING GROWTH CURVES

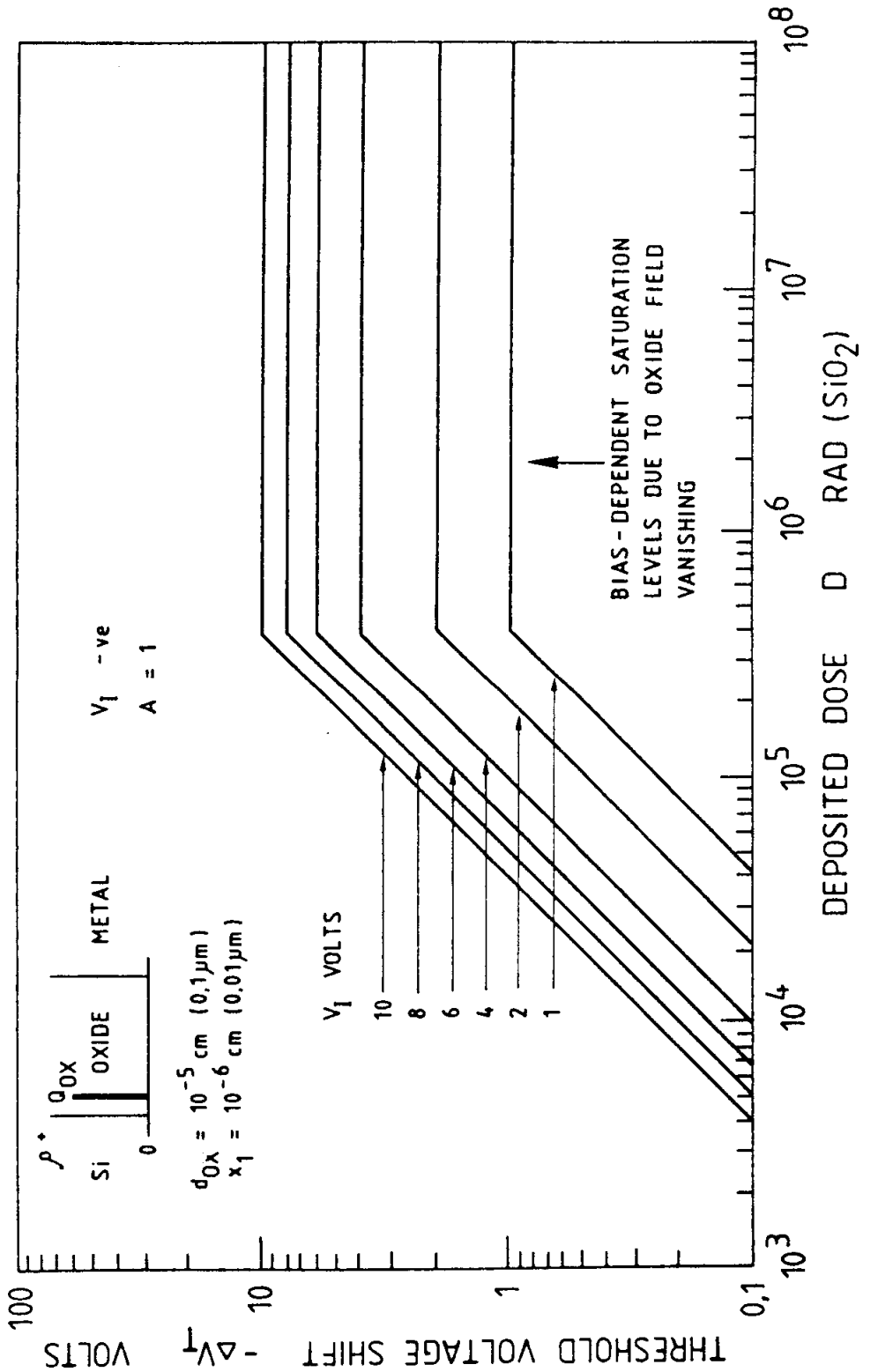

Simple model of threshold shift as a function of dose for several values of negative irradiation bias, with trapping probability equal to unity.

FIGURE 6.11 - ENGINEERING GROWTH CURVES

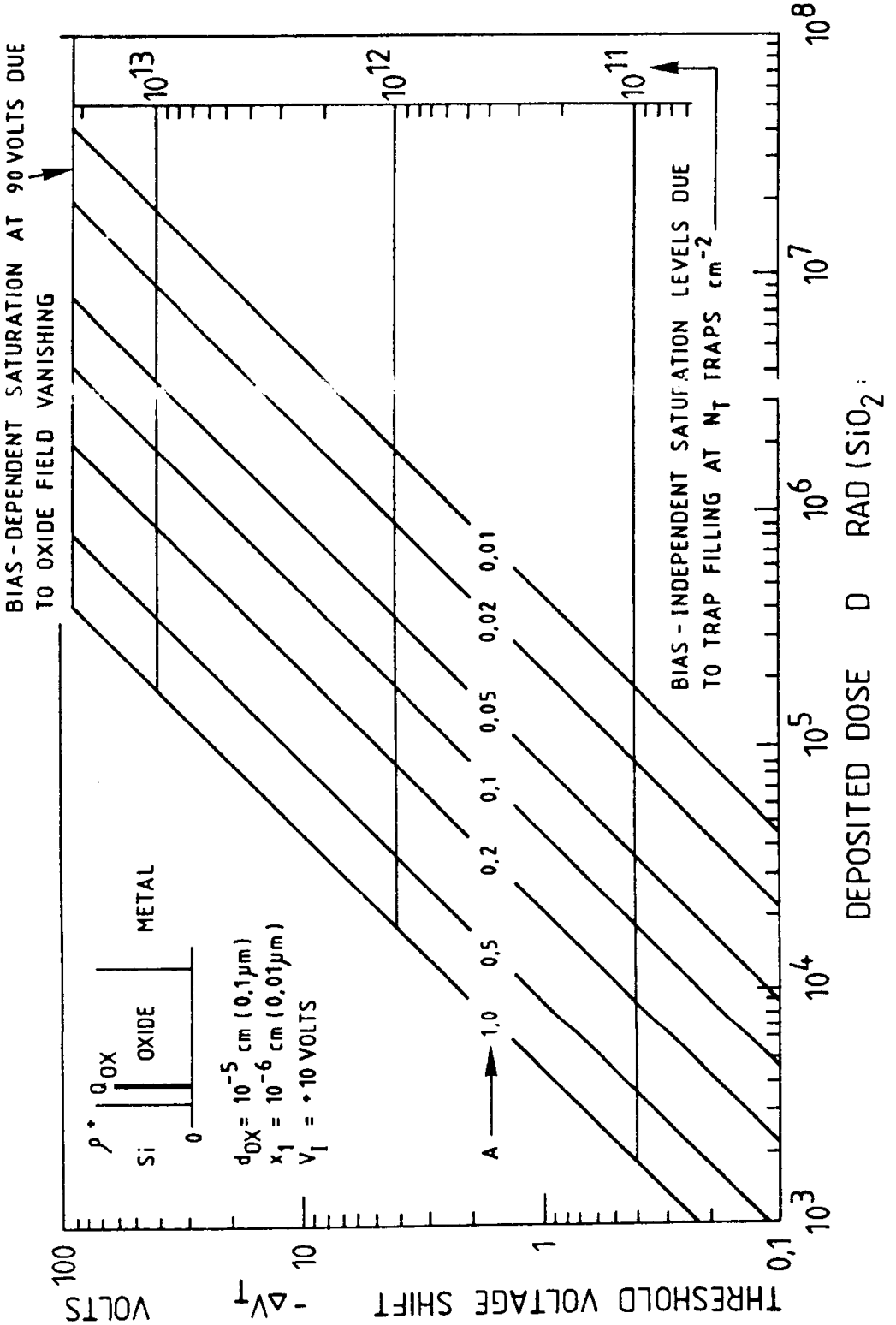

Simple model of threshold shift as a function of dose for several values of trapping probability at +10V bias.

FIGURE 6.12 - ENGINEERING GROWTH CURVES

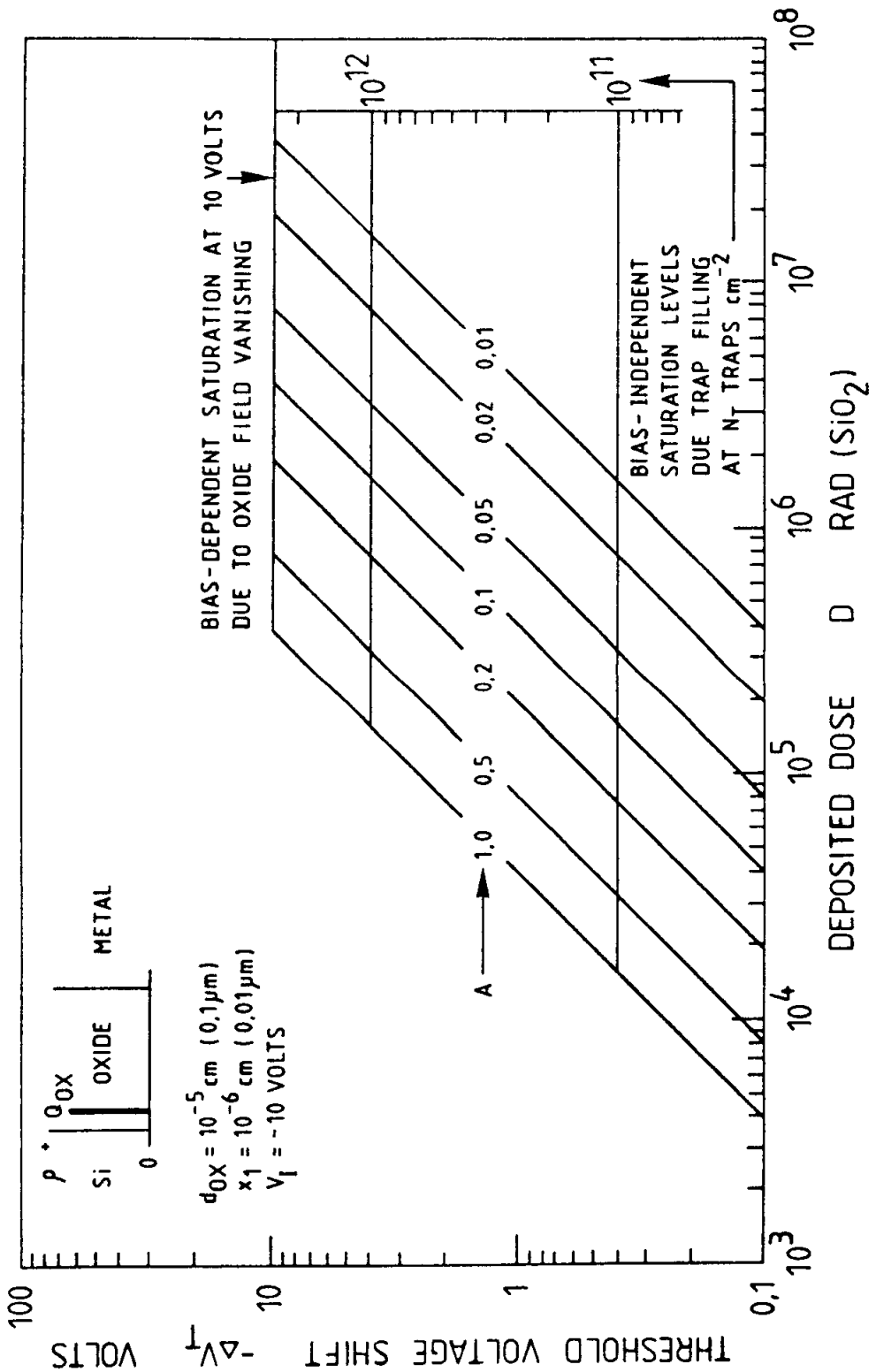

Simple model of threshold shift as a function of dose for several values of trapping probability at -10V bias.

FIGURE 6.13 - ENGINEERING GROWTH CURVES

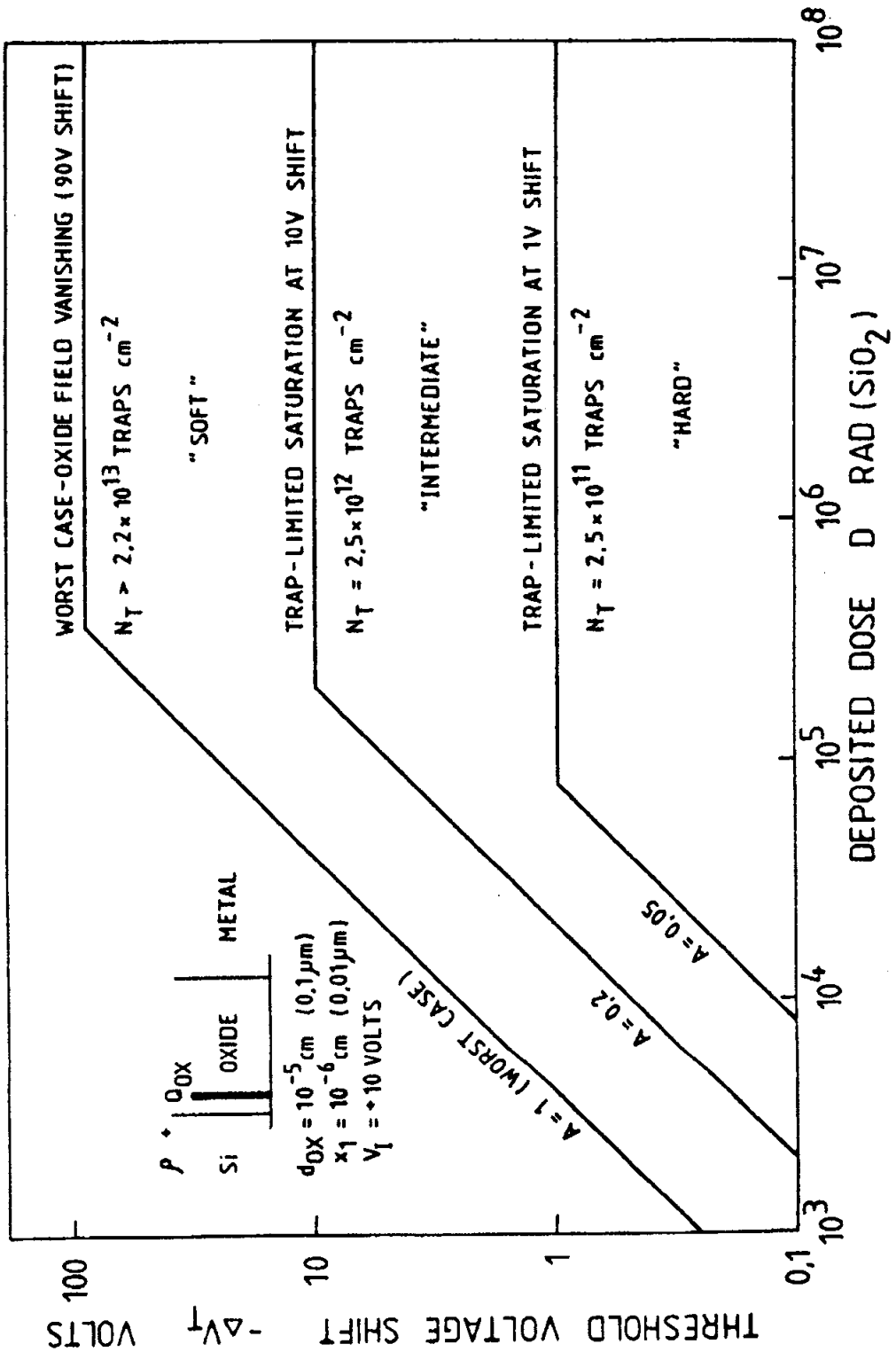

The "growth curve" format divided into proposed areas corresponding to the degree of radiation sensitivity. Devices are under +10V irradiation bias with trapped charge sheet as shown.

FIGURE 6.14 - PRACTICAL MOS DEGRADATION MODEL

6.5. LATE EFFECTS

6.5.1. High-temperature annealing

Early in the investigation of hole-trapping in MOS systems, it was discovered that the trapped charge could be removed ("annealed") without trace by heating the device to a temperature near 300°C.

The "irradiate-anneal" cycle could be repeated many times with little alteration. However, these results were puzzling because they conflicted with the evidence from physics experiments which pointed to a high activation energy required for the trapping of holes. The exact mechanism of thermal annealing has not been established, but Danchenko and colleagues (1968) have proposed that the effect is brought about by electrons being injected into the Si-SiO_2 interface from the silicon. Figure 6.15 shows a comparison between Danchenko's results and some by Holmes-Siedle and Groombridge of irradiation of MOS capacitors with X-rays and V-UV light. Also shown are results by the same authors of the annealing of the interface states.

6.5.2. Room-temperature annealing

6.5.2.1. General

The rate of relaxation of the charge trapped in MOS structures is extremely variable, as is demonstrated by the spread of effects shown in Figure 6.16 (Winokur et al, 1983). Simple CMOS inverters from five different manufacturers were irradiated fairly rapidly and then observed for the next 10^6 seconds (about 11 days). Some n-channel devices had recovered less than 10%; others had undergone a large recovery, with V_T even overshooting the original value (this is known as "rebound"). The p-channel transistors are seen to be degrading further with time ("reverse annealing").

6.5.2.2. Prediction model

Winokur (1983) has produced an analysis of the above recovery effects which is useful for spacecraft design because it allows us to perform tests in a reasonably short time and to extrapolate the results to long times, say, several years in space. By the use of simple linear system theory, a mathematical value - the "annealing slope" - is extracted from the test data. A high slope value implies a rapid recovery characteristic in the laboratory test and predicts a milder degradation in space at low dose rates. If this technique is used in projects, caution has to be exercised in device selection because the same manufacturer may produce batches with different recovery characteristics.

Brucker (1982) and Holmes-Siedle and Adams (1985) have found that p-channel devices are often slower to recover than n-channel ones. Also, interface effects can cause p-channel threshold voltage shifts to become even larger as time progresses. In a 10-year study of ultra-soft p-channel devices used as space radiation dosimeters, a typical recovery over 10 years was between zero and 20%.

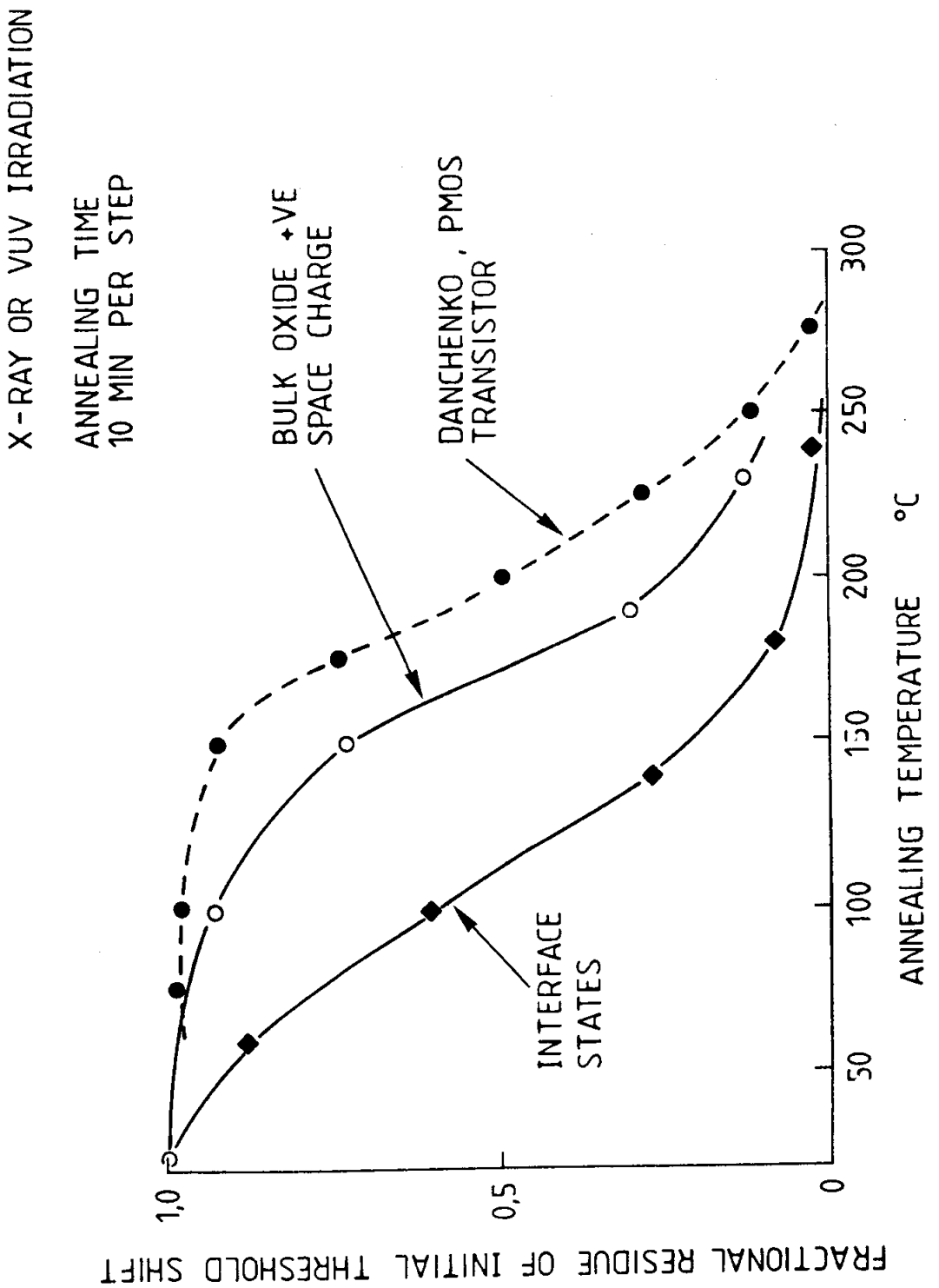

Experimental results showing the fractional residue of radiation-induced threshold shift as a function of isochronal annealing temperature.

FIGURE 6.15 - THERMAL ANNEALING OF THRESHOLD VOLTAGE SHIFT

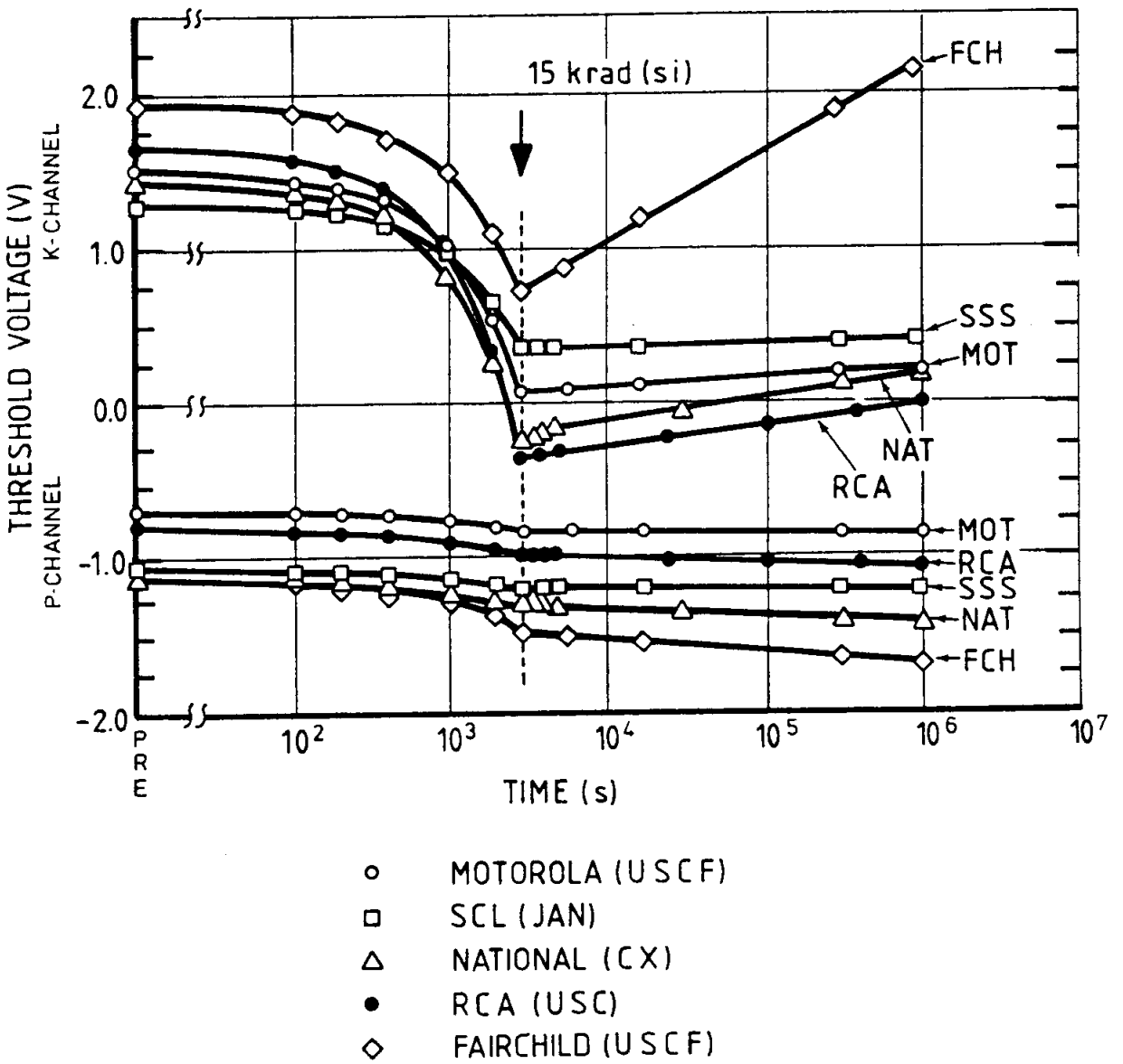

Threshold voltage curves for n- and p-channels of commercial 4007 inverters both during and following a 5-rad(Si)/s ^{60}Co irradiation. Dashed vertical line at 3000 s denotes end of irradiation. (Winokur 1983).

FIGURE 6.16 - THRESHOLD VOLTAGE CURVES FOR N- AND P-CHANNELS

To illustrate the wide variety of possible annealing rates, Figure 6.17 shows some of the results quoted above compared in terms of fractional recovery with log (time). The annealing curves are straight lines on this scale and slopes vary from 3 to 25% per decade of time. Also shown on this chart are p-channel devices exhibiting increased degradation with time (curve 'd'). Both this "reverse annealing" effect and the "rebound" of n-channel devices, mentioned earlier, are explained by the build-up of new interface states with time. See for example Oldham (1984); Schwank et al (1983).

A NASA-sponsored group of investigators (Brucker et al, 1982, 1983; Stassinopoulos et al, 1983, 1984; Danchenko et al, 1968, 1980, 1981) have made extensive studies of late irradiation effects in MOS devices. This work included a detailed investigation into the relative effects of electrons, protons and gamma radiation on a uniform batch of CMOS inverters of the 4007 type. This batch, containing a fairly "soft" type of oxide, exhibited recoveries of V_T shift in the region of 35% in a year. Particle type had some influence on the mode of recovery.

6.5.3. NASA/JPL workshop on "post-irradiation effects"

6.5.3.1 General

Sponsored by NASA, Jet Propulsion Laboratories, Pasadena, USA, held a workshop on "Post-irradiation Effects" in 1983 to assess the impact of room temperature annealing on spacecraft project engineering work such as device and radiation testing specifications. The physics of room temperature annealing is only partly understood, but sufficient testing has been done to enable an approximate mathematical model to be developed for the main recovery effects. If further work proves this model to be reliable, we may be able in due course to apply "annealing coefficients" to devices which are to be operated in space at a very low rate. The workshop discussed these questions with a view to evolving proper methods for handling the recovery and rebound effects in the development of aerospace devices and equipment. Some of the panel's conclusions are given in the following section.

The terms "Late radiation effects" or "Post irradiation effects" are to be preferred to "Room temperature annealing". The latter term implies heating and recovery while irradiated MOS devices may degrade further with time at room temperature or below. The term 'late radiation effects' is already used in medicine.

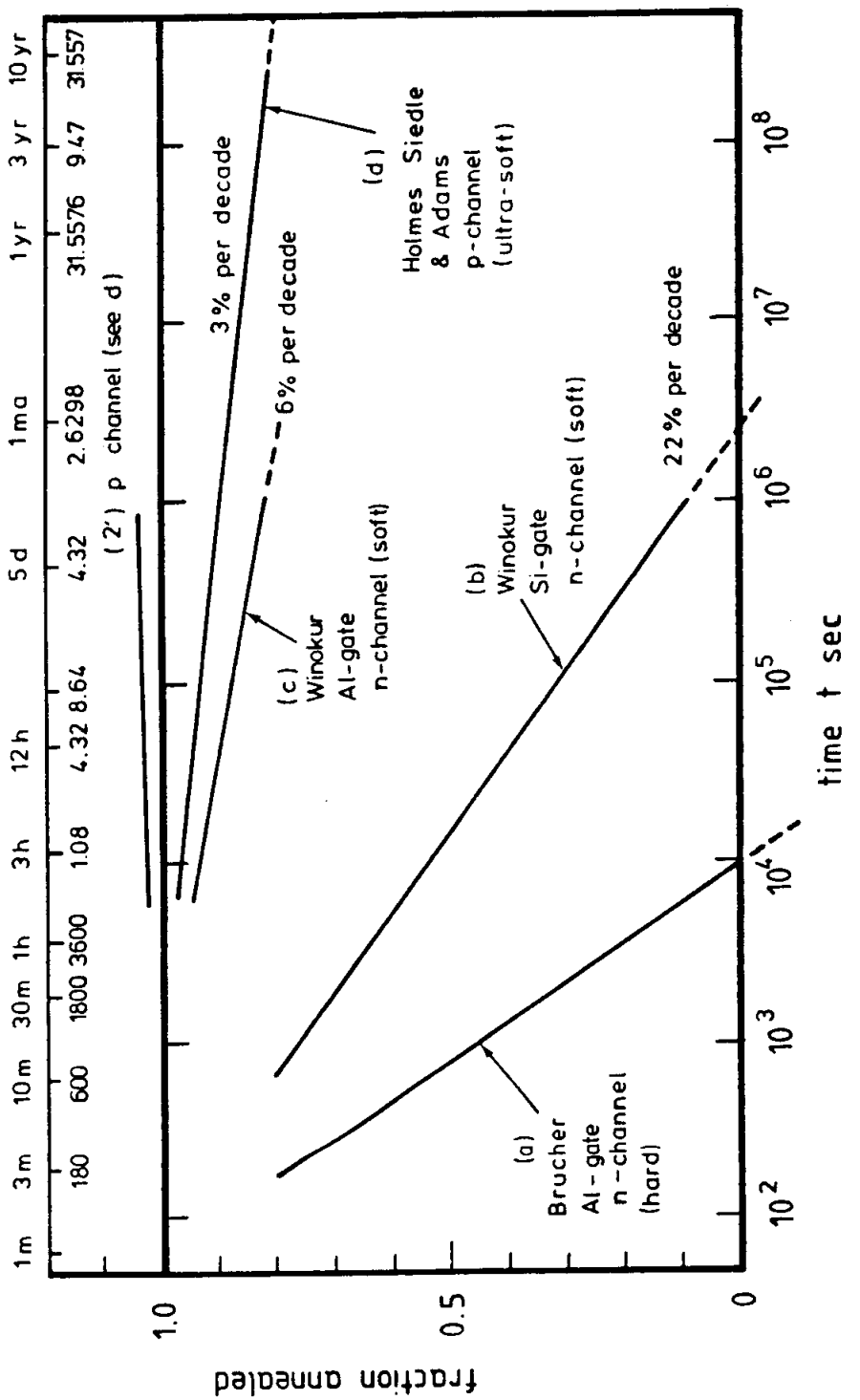

Typical post-irradiation changes in MOS devices as a function of log (time) at room temperature. Trapped charge in the oxide may relax rapidly, especially in "hard" n-channel transistors (a), or very slowly as in the ultra-soft (dosimeter) devices shown in (d). (b) and (c) are examples from an analysis of CMOS devices by Winokur (1983).

FIGURE 6.17 - ROOM TEMPERATURE ANNEALING

One objective of the workshop was to identify the key problem of Late Radiation Effects (L.R.E.) as they vary in detail with the semiconductor device technology in question. While the nature of the mechanisms had to be borne in mind as a unifying factor, the key issue was how best to characterise various technologies with respect to late radiation effects. This may involve research into the improved measurement of device parameters as well as into the development of new sample preparation and irradiation procedures.

6.5.3.2. Technology

The major problems caused by Late Radiation Effects (L.R.E.) derive from the complexity of integrated circuits (ICs) and the multi-function nature of the "anneal" which can include reverse-annealing and rebound effects. As a result, in large-scale ICs, a loss of functionality is sometimes found to occur later. This effect is difficult to predict on a mechanistic basis because of the highly complex relations between IC functionality and the drift of device parameters. The effect is also technology dependent. The IC technologies most significantly affected are:

- CMOS MSI to VLSI,
- NMOS LSI to VLSI,
- Bipolar VHSIC,
- Bipolar analogue.

It is predictable that recessed-oxide technology (e.g. LOCMOS) will introduce several new degradation modes which may contribute to L.R.E.

Other structures in which L.R.E. problems may be expected are:

- GaAs devices (neutron effects) and
- Power MOS devices.

6.5.3.3. Parameters affected

Serious drifts in device parameters with time in the 1 minute to 1 year time-frame include the following:

(a) For a wide range of technologies, the following apply:
  - recovery and overshoot of V_{TN} with time,
  - continued degradation of V_{TP} with time,
  - continued degradation of transconductance or gain with time,
  - continued increase of junction reverse leakages with time,
  - continued build-up of field-oxide inversion paths with time,
  - recovery in propagation delay.

(b) For a limited range of technologies, the following also apply:
- late changes in MOS transistor edge effects (CMOS-SOS),
- the loading of on-chip VBB generators by leakage paths (NMOS),
- tub-to-tub leakage (VHSIC-bipolar ICs),
- nonuniform charge rearrangement on source drain axis during post-irradiation cycling (short-channel devices),
- the reverse annealing of h_{FE} (bipolar analogue),
- degradation of power MOS devices,
- rapid recovery in bit error rates vs time.

6.5.3.4. Measurement technique

As IC elements become smaller, the need to expand the range of device parameters measured becomes urgent (e.g. the conventional meaning of "threshold voltage" becomes too vague). Also, as IC complexity increases, more complex functional parameters (e.g. "shmoo" plots) must be followed as a function of time after irradiation. Therefore, we must attempt to define new post-irradiation measurement procedures for ICs which are appropriately sensitive to post-irradiation drifts and which will permit considerably improved predictions of the drift of IC performance parameters with time. Typical parameters to be considered in new post-irradiation measurement procedures are:

- the minimum operating voltage (V_{DD} (min)) of an IC,
- the "shmoo" plots for an IC,
- effective surface mobility of a transistor channel,
- the "bipolar snap-back" effect in MOS IC's,
- the charge-pumping currents of a transistor.

6.5.3.5. Acceleration techniques

It is possible that accelerated ageing techniques will be combined with improved parameter measurement to improve the accuracy of long-term performance prediction. Research is warranted, especially into the exploitation of modern burn-in techniques and the validity of elevated temperature post-irradiation treatments of various technologies.

6.5.3.6. Use of test patterns

The use of technology test patterns in radiation evaluation will solve some problems in late radiation effects (especially the statistics of failure). In some cases, the adoption of a test-chip evaluation programme by a spacecraft system contractor could allow that contractor to relax the radiation-effect design margins used in system design and, hence, lead to a reduction of the shield weight associated with the design.

The test patterns should include both (a) simple structures such as capacitors and ring-dot transistors and (b) complex networks as appropriate such as logic string, ring oscillators and memory cells.

6.5.4. Annealing of cryogenic devices

MOS devices irradiated at cryogenic temperatures exhibit larger radiation-induced shifts than those irradiated at room temperature. More charge is trapped in the oxide at low temperature, although much of the excess is removed if the device is warmed to room temperature. Boesch and co-workers (1976) have characterised this process.

6.6. DOSE RATE EFFECTS

It has been explained earlier that if a MOS device is prone to "room temperature annealing", then the radiation-induced shift of V_T will be affected by the dose rate used, so long as the shifts are measured immediately after irradiation. It has also been explained that this is not a true dose-rate effect, but the effect of concurrent processes of charge build-up and charge-trapping. Winokur's recent work shows that if allowance is made for the latter factors in the calculation of end-of-life state of the device, the dose rate used in gamma irradiations can be varied between a few rads per hour and thousands of rads per second without affecting the end result many days after irradiation has ceased. In other words, no fundamentally different physical processes occur during accelerated testing compared with the slow rate expected in space.

6.7. OTHER EFFECTS IN MOS DEVICES

6.7.1. Interface states

The effects of radiation-induced states on MOS devices are strong, especially in high-technology IC's having thin gate oxides. The main effects are:

(a) lowering of transconductance,

(b) distortion of I_D-V_G characteristics,

(c) generation of "slow states" and a resulting slow drift of V_T with time (Holmes-Siedle and Adams, 1983).

Effects (a) and (b) have been incorporated in the simple models discussed earlier.

6.7.2. Atomic displacement damage

Transport of carriers in the channel of an MOS device is by majority carrier conduction. The effect of atomic displacement damage on this transport is slight at the levels likely in space and any such changes are almost certain to be swamped by the oxide and interface effects already described. The conduction of majority carriers in the channel of an MOS device is lower than that in bulk silicon due to collisions with interface states. Changes in transconductance of the channel, owing to the ionisation-induced build-up of interface states would therefore be expected to overshadow the effects of changes in resistivity caused by displacement damage in the silicon itself. (Note that this change in transconductance is illustrated by the distortion of the I_D-V_G curves in Figure 6.3(a).

Even though displacement damage will not be a significant factor in the space environment, it is worth while to note very briefly the factors that affect the resistivity of bulk silicon. The resistivity, ρ, of bulk silicon is controlled by majority carrier mobility, μ, (which, in turn, is controlled by the number of centres in the silicon that scatter majority carriers) and by the carrier concentration, N_o.

$$N_o = \frac{1}{q\,N_o} \qquad \text{..... 6(ii)}$$

where q is the charge on the electron.

Defects produced by atomic displacement can reduce the carrier concentration, N_o, by trapping. This effect is called "carrier removal" and is proportional to radiation fluence. Thus, carrier concentration after irradiation, $N\phi$, is given by:

$$N_\phi = N_o - \phi\frac{\Delta n}{\Delta \phi} \qquad \text{.....6 (iii)}$$

'where $\Delta n/\Delta \varnothing$ (for n-type) or $\Delta \rho/\Delta \varnothing$ (for p-type) is termed the "carrier removal rate".

Table 6(3) shows some experimental values for electrons, protons and neutrons. For the silicon of a typical n-channel MOS device, for which N will be about 10^{16} cm^{-3}, it is clear that the effect of 10^{15} damage-equivalent 1 MeV electrons will be a change of only a few percent in concentration.

Damage in most operational orbits is much lower than this (see Section 7.10) and, even at the peak of the proton belt, will not be over 10^{16} damage-equivalent 1 MeV electrons.cm^{-2} per year behind 1 g.cm^{-2} aluminium. At geostationary altitude, because of

the virtual absence of protons, bulk damage rates are completely negligible within the spacecraft.

Concerning changes in the mobility term in equation 6(iii) caused by increased scattering of majority carriers by displacement defects, Gregory (1973) shows that this change would be only a few percent at a neutron fluence of 10^{14} cm^{-2}. This fluence is equivalent to over 10^{15} 1-MeV electrons cm^{-2}. As indicated above, damage in most operational orbits will be much lower than this.

TABLE 6(3) - CARRIER REMOVAL RATES ($\Delta n/\Delta\phi$) FOR 1-OHM CM SILICON UNDER PARTICLE IRRADIATION

Particle	Energy (MeV)	Carrier removal rate (cm^{-1}) $\Delta n/\Delta\phi$		$\Delta n/\Delta\phi$		Ref.
		Cz	Fz	Cz	Fz	
Electrons	1.7	0.31	1.3	0.2	0.2	55
Protons	4.5 - 207	1000	1000	1000	1000	56
Neutrons	0.01	6	9	13	13	55

Cz = Czochralski crystal growth method
FZ = Float-zone refined crystal
Removal rates for protons are approximate

6.8. COMMERCIAL AND HARDENED MOS DEVICES

6.8.1. Processing variables

The key to the radiation sensitivity of MOS devices lies in the preparation of the gate insulator layer, at present invariably grown by various methods of thermal oxidation of the silicon wafer. As explained in Section 6.4, this sensitivity varies with the concentration of hole-traps in this layer and, although research has been intensive, there is still controversy about:

- the exact structure of the hole-trapping defects,
- the exact mechanism of their generation during growth and annealing of the oxide and
- the best methods of controlling their generation.

The important point is that, apparently, small variations in growth temperature, annealing temperature, subsequent metallisation, silicon quality and cleanliness, and oxidation ambient, can make a large difference in hole-trap concentration. Although considerable attention is paid to these "process parameters" in commercial MOS devices, it still appears that the control exercised is often not close enough to maintain a uniform level of radiation sensitivity. V_T shifts for a given dose vary from unit to unit and from batch to batch, giving a serious problem of "scatter".

For a cost-conscious small purchaser of devices, such as a space equipment manufacturer, a still more unfortunate fact is that the MOS process parameters chosen by manufacturers on grounds of profitability are well removed from those which produce low radiation sensitivity. For example, while the current "recipe" for the

best tolerance to radiation calls for such features as slow oxide growth to limited thickness in specially purged dry oxygen furnaces at low temperature, low temperature anneal, deposition of metal without electron beam heating and "tailoring" for high V_T, commercial LSI circuits are often made to a recipe which includes fast oxide growth in non-purged furnaces (for high throughput), thicker oxides (for fewer pinhole defects), silicon gate electrodes (for self-alignment and low V_T) and high temperature anneal (for low V_T and high yield).

Furthermore, competition in the area of switching speed causes the manufacturer to "tailor" V_T to as low a value as possible. While a high-reliability LSI integrated circuit can be easily produced to the first recipe, few manufacturers offer such a device as a commercial product.

Thus, the problem of high and varying sensitivity of commercial devices to total dose may remain for some time. It must be circumvented by a mixture of pre-selection, batch monitoring, protection of components from the external environment and the procurement of special alterations, by the manufacturer, of his process.

6.8.2. Memory technology

For data storage in spacecraft, it is likely that CMOS static RAM's will be the most widely used form of semiconductor memory. First, the static memory configuration is less prone to upset than the dynamic form; second, the low power drain of the CMOS form not only suits the power requirements of the spacecraft, but the drain is so low that a small emergency battery can be used to maintain data if the main spacecraft power fails. The main advantage of the NMOS dynamic memory in the commercial field is very high information-storage density. In spacecraft circuitry, the greatest value is placed on process reliability and tolerance to noise and various radiation effects. CMOS circuitry is preferable in most of these respects so long as "latchup" effects are suppressed. The information density of CMOS devices may have to be limited for space because, at high bit densities, single-event upsets may become too frequent unless specialised measures are taken.

6.8.3. Microprocessor technology

6.8.3.1. General

Data processing and control functions in spacecraft will employ microprocessors distributed throughout the equipment. As with memories, CMOS devices are preferable to NMOS and bipolar forms. However, several relevant differences between memories and microprocessors may also be stated. First, the radiation-

induced power drain due to a few microprocessors is of less importance than that due to a large array of memories.

Second, it is simpler to apply local shielding to single microprocessor chips achieved than to arrays of memories. The choice of microprocessor for radiation environments will rest on total dose functional tolerance and the proneness of the system to errors induced by cosmic rays and other disturbances.

6.8.3.2. Hardened technology

One example of a hardened microprocessor is the 8-bit 80C85RH. This is a hardened CMOS version of the Intel 8085 NMOS microprocessor. It was developed by Sandia National Laboratories and is being marketed in Europe. The 80C85RH offers a functional copy of the NMOS 8085 and is fully software compatible. Power reduction of 90% is claimed and the microprocessor and its peripheral devices have a power supply operation range of 4.5 to 11V. Total dose hardness levels of 10^6 rad (Si) have been recorded on tests.

Latchup-free operation is obtained by the use of an epitaxial substrate as the starting material in the fabrication process. For further reduction in power consumption, the microprocessor clock may be stopped without loss of data because the memory devices are fully static. The peripheral devices include a 256 x 8 RAM, a 2k x 8 ROM, an I/O decoder, a level converter, a bus transceiver and an I/O port.

Further hardened technologies now becoming available in Europe are based on silicon-on-sapphire technology and cover semi-custom gate array and cell-based design as well as Random Access Memories up to 64 Kbits. The SOS technology is extremely hard to total-dose (hundreds of kilorads) as well as being latchup-free and immune to SEU.

6.8.4. Spacecraft system technology

An example of the practical use of MOS memories and microprocessors in complex systems is available in ESA's On-Board Data Handling (OBDH) programme. Figures 6.18 to 6.20 (Walker, 1985) show some aspects of the organisation of this system and the complexity of radiation effects involved. The requirement for tolerance to radiation in this system has given rise to ESA Applied Research Programmes in the radiation-hardening of European MOS technology.

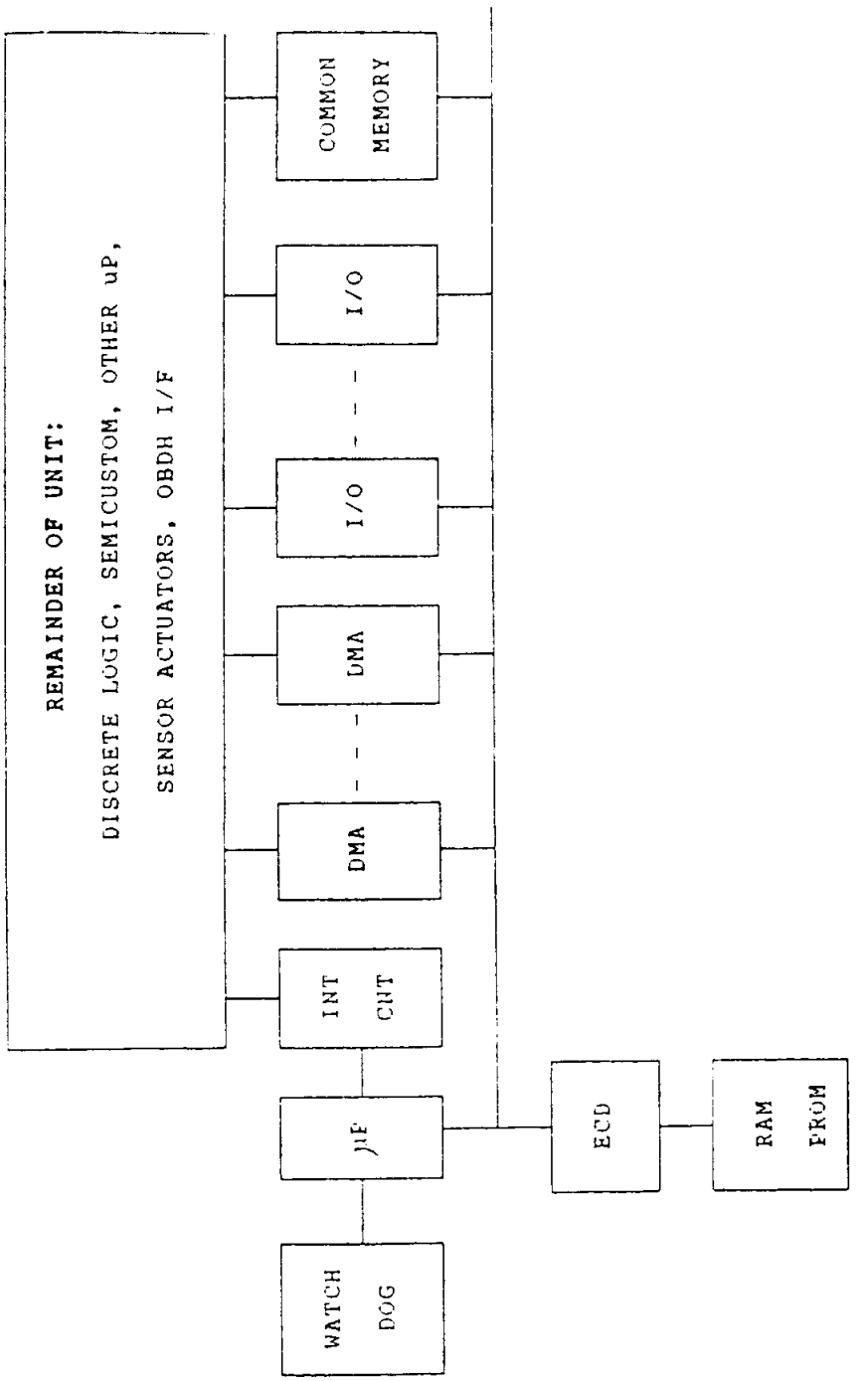

Key

P = Microprocessor
INT CNT = Interrupt Controller
DMA = Direct Memory Access
I/O = Input/Output
I/ED = Interfaces
ICD = Error Correction and Detection

Examples of above

Central Terminal Unit
Intelligent Remote Terminal Unit
On-board Computer
Mass Memory Controller
Sensor Electronics
Attitude Control System

FIGURE 6.18 - TYPICAL FORM OF MICROPROCESSOR - CONTROLLED SPACECRAFT SUBSYSTEM

Device/ character-istics	In orbit as of 1985	Forefront devices 1985	Future	System implications
Micropro-cessors	Various 8-bit μ P's	8086, etc.	80 C 86, 1750, 31750, 80386	-Increasing use of UP + large capacity memory throughput SIC units. -Increasing decision-making capability on-board. -Possibility for more autonomy for mission management, adaptive control and crisis management.
Memories	1 K RAM	16 K RAM	25 K RAM	
Logic	Lp TTL (CMOS)	Lp STTL, CMOS	ALS, CMOS, HCMOS	MOS technology increasing
Periphe-rals	–	– DM INT.	AC CONT., etc.	Hardening by design, if possible.
Semi-custom	–	Circa 5%	Increasing	
Geometry	–	Circa 3 μm	Decreasing	More bit errors
Total rad-iation dose -Majority	2 - 5 K rad	1-12 K rad 20-50 K rad	Increasing	Prediction, test and quality control are problems.
-Special MOS parts	–			
Single events Upsets	–	Several events/day	More events per day	
Testability	–	100%	Unknown	

FIGURE 6.19 - TRENDS OF IN-USE DIGITAL DEVICES ON SPACECRAFT: SYSTEM IMPLICATIONS

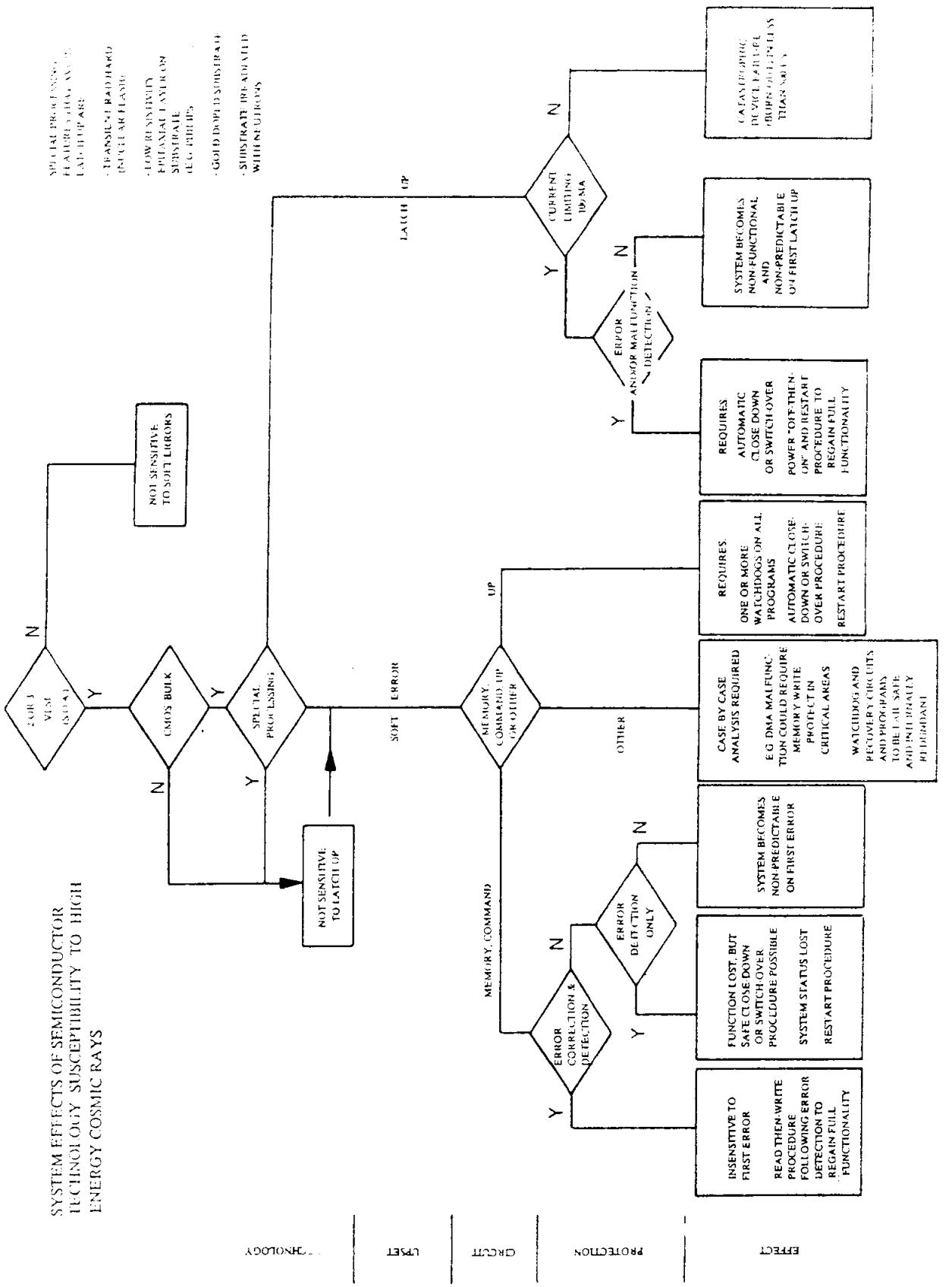

FIGURE 6.20 - SYSTEM IMPLICATIONS OF COSMIC RAY EFFECTS (E > 1000 MeV) FOR DIGITAL TECHNOLOGY

6.9. COMPILATION OF RADIATION DATA

The radiation test data for commercial MOS devices are available, but too voluminous for inclusion. Data banks have been established for the collection and dissemination of such data. These include:

- ESA Radiation Effects Data Base (includes total dose and single event upset data on a wide range of devices,
- Hahn-Meitner Institut, Berlin: "Data Compilation of Irradiation Tested Electronic Components", HMI-B353 (loose-leaf Computer-Printed Data Sheets),
- SPIRE Compilation (available through U.K. Ministry of Defence (AWD), London),
- Kaman-Tempo, Santa Barbara, USA (incorporating the data bank initiated by U.S. Army (HDL), Adelphi, MD, USA),
- NASA (available through Product Assurance Group, Goddard Space Flight Center, Greenbelt, MD, USA),
- SPACERAD Compilation (available through Jet Propulsion Laboratory, Pasadena, CA, USA and accessible via DARPANET electronic mail system).

6.10. CONCLUSIONS

This section has dealt extensively with the radiation sensitivity of MOS devices because this class of devices will be used more and more on spacecraft, the types available will become more varied and complex and the radiation sensitivity of some of these components will continue to present an engineering problem. This can still be said despite the appearance of new recipes for "hard" oxides and their adoption for a few commercial device types. This may alleviate the problem in a few cases, but it is predictable that the suppliers of many desirable MOS devices, including NMOS and CMOS LSI circuits, will not choose to employ these recipes. Thus, the overall radiation problem of MOS devices is likely to remain for many years.

This section is an attempt to state the physical problem and to propose practicable methods of classifying and predicting the response of MOS devices from all quarters of the market place. The effect of processing on mass commercial technology should be understood and applied to the practical schemes outlined here for introducing the required overall "hardness" into a system (i.e. a whole piece of equipment). In this way, the designer retains flexibility in his choice of circuits, but can also take advantage of improved processing technology in an unforced manner as and when this technology reaches the required level of acceptability.

REFERENCES

K.G. Aubuchon, IEEE Trans.Nucl.Sci. NS-18 (6), p. 117 (Dec. 1971)

G.A. Ausman and F.B. McLean, HDL-TR-1720, Harry Diamond Laboratories, Adelphi, MD (Nov. 1975)

A.L. Barry and D.F. Page, IEEE Trans.Nucl.Sci. NS-13 (6), pp. 255-261 (Dec. 1966)

J. Bourrieau, ESTEC Seminar (Sept. 21, 1977)

D.M. Brown and P.V. Gray, J. Electrochem. Soc. 115 (7), p. 760 (1968)

G.J. Brucker, W.J. Dennehy and A.G. Holmes-Siedle, Proc. IEEE (Correspondence) 53, p. 1800 (Nov. 1965)

G.J. Brucker, IEEE Trans.Nucl.Sci. NS-24 (6), pp. 2209-2213 (Dec. 1977)

G.J. Brucker, E.G. Stassinopoulos, O. van Gunten, L.S. August and T.M. Jordan, "The Damage Equivalence of Electrons, Proton and Gamma Rays in MOS Devices", IEEE Trans.Nucl.Sci. NS-29(6), pp. 1966-1969 (1982)

G.J. Brucker, O. van Gunten, E.G. Stassinopoulos, P. Shapiro, L.S. August and T.M. Jordan, "Recovery of Damage in Rad-hard Devices During and After Irradiation by Electrons, Protons, Alphas and Gamma Rays", IEEE Trans.Nucl.Sci. NS-30(6), pp. 4157-4161 (1983)

R.A. Cliff, V. Danchenko, E.G. Stassinopoulos and M. Sing, IEEE Trans.Nucl.Sci. NS-23 (6), p. 1781 (Dec. 1976)

V. Danchenko, U.D. Desai and S.S. Brashears, J.Appl.Phys. 39 (5), p. 2417 (1968)

V. Danchenko, "Radiation Testing of CMOS Integrated Circuits", GSFC Report (1971)

V. Danchenko, E.G. Stassinopoulos, P.H. Fang and S.S. Brashears, "Activation Energies of Thermal Annealing of Radiation-induced Damage in N- and P-channel CMOS IC's", IEEE Trans.Nucl.Sci. NS-27(6), pp. 1658-1676 (1980)

V. Danchenko, P.H. Fang and S.S. Brashears, "Activation Energies of Thermal Annealing of Radiation-induced Damage in N- and P-channel CMOS IC's, Part II", IEEE Trans.Nucl.Sci. NS-28(6), pp. 4407-4412 (1981)

W.J. Dennehy, G. Brucker and A.G. Holmes-Siedle, IEEE Trans.Nucl.Sci. NS-13 (6), pp. 273-281 (Dec. 1966)

W.J. Dennehy, A.G. Holmes-Siedle and K.H. Zaininger, IEEE Trans.Nucl.Sci. NS-14 (6), p. 276 (Dec. 1967)

G.F. Derbenwick and B.L. Gregory, IEEE Trans.Nucl.Sci. NS-22 (6), p. 2151 (Dec. 1975)

G.F. Derbenwick and H.H. Sander, IEEE Trans.Nucl.Sci. NS-24 (6), pp. 2244-2248 (Dec. 1977)

DERTS Internal Report (1975)

R.C. Docherty and S.A. Abbas, IEEE Trans. Electron. Dev. ED-22 (2), pp. 33-39 (Feb. 1975)

C.G. Emms, A.G. Holmes-Siedle, I. Groombridge and J.R. Bosnell, IEEE Trans.Nucl.Sci. NS-21 (6), p. 159 (Dec. 1974)

J.G. Fossum, G.F. Derbenwick and B.L. Gregory, IEEE Trans.Nucl.Sci. NS-22 (6), p. 2208 (Dec. 1975)

F. Gordon and H.E. Wannemacher, IEEE Trans.Nucl.Sci. NS-13 (6), pp. 262-272 (Dec. 1966)

D. Green, J.E. Sandor, T.W. O'Keeffe and R.K. Matta, Appl.Phys.Lett. 6, pp. 3-4 (1965)

B.L. Gregory, IEEE Trans.Nucl.Sci. NS-22 (6), p. 2296 (Dec. 1975)

A.S. Grove and E.H. Snow, Proc. IEEE (Letters) 54, pp. 894-895 (June 1966)

A.S. Grove, "Physics and Technology of Semiconductor Devices", New York, Wiley (1967)

A.G. Holmes-Siedle, RCA Internal Report (1971)

A.G. Holmes-Siedle, ESA Contract Report AHS-ESA-77-1 (Jan. 1977)

H. Hughes, "Gamma Radiation Effects on some MOS Transistors", Paper presented at IEEE Nuclear and Space Radiation Effects Conf., Ann Arbor, Mich. (July 1965)

H.L. Hughes, IEEE Trans.Nucl.Sci. NS-16 (6), p. 195 (Dec. 1969)

G.W. Hughes and R.J. Powell, IEEE Trans.Nucl.Sci. NS-23 (6), p. 1569 (Dec. 1976)

H.L. Hughes, R.D. Baxter and D. Phillips, IEEE Trans.Nucl.Sci. NS-19 (6), p. 256 (Dec. 1972)

H.L. Hughes and R.A. Giroux, Electronics, 37 pp. 58-60 (1964)

E.E. King and R.L. Martin, IEEE Trans.Nucl.Sci. NS-24 (6), pp. 2172-2177 (Dec. 1977)

E.E. King and G.P. Nelson, IEEE Trans.Nucl.Sci. NS-22 (5), p. 2120 (Oct. 1975)

E. Kooi, Philips Res. Rept. (Netherlands) 20, p. 595 (1965)

R.E. Leadon, D.P. Snowdon and J.M. Wilkenfeld, "Radiation Effects in Semiconductor and Insulator Materials", HDL-CR-76-152-1, IRT Corp., San Diego, Cal. (April 1976)

A. London, D.A. Matteucci and R.C. Wang, IEEE Trans.Nucl.Sci. NS-24 (6), pp. 2056-2060 (Dec. 1977)

P. May and F.C. Schiereck, IEEE J. Solid State Circuits, SC-11 (3) (June 1976)

F.B. McLean, H.E. Boesch and J.M. McGarrity, IEEE Trans.Nucl.Sci. NS-23 (6), p. 1506 (Dec. 1976)

G.C. Messenger, E.J. Steele and M. Neustadt, IEEE Trans.Nucl.Sci. NS-12 (5), pp. 78-82 (Oct. 1965)

J.P. Mitchell, IEEE Trans. Electron Dev. ED-14 (11), p. 764 (Nov. 1967)

D.K. Myers, IEEE Trans.Nucl.Sci. NS-23 (6), p. 1721 (Dec. 1976)

D.K. Myers, IEEE Trans.Nucl.Sci. NS-24 (6), pp. 2169-2172 (Dec. 1977)

G.P. Nelson and E.E. King, IEEE Trans.Nucl.Sci. NS-24 (6), pp. 2341-2347 (Dec. 1977)

T.R. Oldham, "Analysis of Damage in MOS Devices for Several Radiation Environments", IEEE Trans.Nucl.Sci. NS-31(6), pp. 1236-1241 (Dec. 1984)

S. Peck and E. Schmid, quoted in J.P. Mitchell and D.K. Wilson, Bell System Tech. J., 46 1 (Jan. 1967)

J. Peden, "Gamma-irradiation of Some Silicon Planar Transistors", Paper presented at IEEE Nuclear and Space Radiation Effects Conf., Seattle (July 1964)

O.G. Pedersen and B. Wensink, ESTEC Internal Report FA 361

C.W. Perkins, K.G. Aubuchon and H.G. Dill, IEEE Trans. Nucl.Sci. NS-15 (6) (Dec. 1968)

A. Pikor and E.M. Reiss, IEEE Trans.Nucl.Sci. NS-24 (6), pp. 2047-2051 (Dec. 1977)

W.J. Poch and A.G. Holmes-Siedle, IEEE Trans.Nucl.Sci. NS-16 (6), p. 227 (Dec. 1969)

W.J. Poch and A.G. Holmes-Siedle, IEEE Trans.Nucl.Sci. NS-17 (6), p. 33 (Dec. 1970)

W.E. Price and A.G. Stanley, IEEE Trans.Nucl.Sci. NS-22 (6), p. 2669 (Dec. 1975)

E.M. Reiss, T.J. Sanders and J. Feldt, priv. comm., IEEE Nuclear and Space Radiation Effects Conference, Williamsburg, Va (July 1977)

T.J. Sanders, IEEE Trans.Nucl.Sci. NS-24 (6), p. 2669 (Dec. 1975)

M. Schlehther, D. Braunig, M. Gartner, F. Gliem and R. Gunzenhauser, ESTEC Seminar (Sept. 21, 1977)

K.M. Schlesier, IEEE Trans.Nucl.Sci. NS-21 (6), p. 152 (Dec. 1974)

J.R. Schwank and W.R. Davies Jr., "Irradiated Silicon Gate MOS Device Bias Annealing", IEEE Trans.Nucl.Sci. NS-30(6), pp. 4100-4104 (Dec. 1983)

L.L. Sivo et al, IEEE Trans.Nucl.Sci. NS-19 (6), p. 313 (Dec. 1972)

E.H. Snow, A.S. Grove and D.J. Fitzgerald, Proc. IEEE 55 (7), pp. 1168-1185 (July 1967)

J.R. Srour, O.L. Curtis and K.Y. Chiu, IEEE Trans.Nucl.Sci. NS-21 (6), p. 73 (Dec. 1974)

A.J. Speth and F.F. Fang, Appl.Phys.Lett. 7, pp. 145-146 (1965)

A.G. Stanley, IEEE Trans.Nucl.Sci. NS-13 (6), pp. 248-254 (Dec. 1966)

A.G. Stanley, K.E. Martin, S. Douglas, "Radiation Design Criteria Handbook", JPL Tech. Mem., pp. 33-763 (Aug. 1976)

A.G. Stanley, K.E. Martin, W.E. Price, "Voyager Electronics Parts Radiation Programme", JPL Publ., Volume 1, pp. 77-41 (Sept. 1977)

A.G. Stanley, K.E. Martin, S. Douglas, "Radiation Design Criteria Handbook", JPL Tech. Mem., pp. 33-763 (Aug. 1976)

E.G. Stassinopoulos, G.J. Brucker, O. van Gunten, A.R. Knudson and T.M. Jordan, "Radiation Effects in MOS Devices; Dosimetry, Annealing, Irradiation Sequence and Sources", IEEE Trans.Nucl.Sci. NS-30(3), pp. 1880-1884 (1983)

E.G. Stassinopoulos, O. van Gunten, G.J. Brucker, A.R. Knudson and T.M. Jordan, "The Damage Equivalence of Electrons, Protons, Alphas and Gamma Rays in Rad-hard MOS Devices", IEEE Trans.Nucl.Sci. NS-30(6), pp. 4363-4367 (1983)

E.G. Stassinopoulos, G.J. Brucker and O. van Gunten, "Total Dose and Dose-rate Dependence of Proton Damage in MOS Devices During and After Irradiation", IEEE Trans.Nucl.Sci. NS-31(6), pp. 1444-1447 (1984)

S.M. Sze, "Physics of Semiconductor Devices", New York, Wiley (1969)

J.R. Szedon and J.E. Sandor, Appl.Phys.Lett. 6, pp. 181-1182 (1965)

B. Wensink and L. Adams, ESTEC Internal WP 988

P.S. Winokur, K.C. Kerris and L. Harper "Predicting CMOS Inverter Response in Nuclear and Space Environments", IEEE Trans.Nucl.Sci. NS-30(6), pp. 4326-4332 (Dec. 1983)

K.H. Zaininger, Appl.Phys.Lett. 8, pp. 140-142 (1966)

K.H. Zaininger, IEEE Trans.Nucl.Sci. NS-13, pp. 237-247 (Dec. 1966)

K.H. Zaininger and A.S. Waxman, IEEE Trans.Electron Dev. ED-16, p. 333 (Apr. 1969)

K.H. Zaininger, RCA Review 27, pp. 341-359 (Sept. 1966)

SECTION 7. DISCRETE BIPOLAR TRANSISTORS

7.1. INTRODUCTION

Bipolar transistors consist of a pair of closely spaced p-n junctions in a single semiconductor structure. The order can be 'NPN' or 'PNP'.

These devices, in both discrete and integrated form, are essential components in many electronic systems, especially in applications (such as in amplifiers) which require a high current gain or considerable "drive" current. Radiation produces degradation of gain and an increase in leakage. The degradation of gain is well understood and derives from degradation of the transport of minority carriers across the base region. We will discuss the effects of electrons, neutrons and gamma rays on this transport, dividing them into those occurring near the surface of the device and those that occur deeper in the material, i.e. bulk effects. In this chapter, we discuss the basic effects with reference to discrete silicon planar transistors. In this structure (see Fig. 7.1), the silicon substrate forms the collector region. Base and emitter regions are formed by the successive introduction of appropriate dopants by diffusion or ion implantation. The junctions are protected by a passivation layer which usually is thermally grown oxide. In general, this layer is thicker than that of MOS devices and accumulates charge when irradiated.

7.2. EFFECTS OF RADIATION ON DEVICE FUNCTION

7.2.1. Gain

The term "gain" can refer to either of two separate parameters in a bipolar transistor. Common-base current gain (α or h_{FB}) is the ratio between collector current and emitter current and has a value rather less than unity. Common-emitter current gain, β or h_{FE}, is the ratio between collector current and base current; it will have a value, typically, of 50 to 2000. In our discussion of gain degradation, we will use the common-emitter current gain term and, for brevity, use the symbol 'β'.

7.2.2. Degradation of gain

Gain degradation and leakage are the most striking and common effects of radiation on bipolar transistors. One cause of gain degradation is atomic displacement in the bulk of a semiconductor. This bulk damage produces an increase in the number of recombination centres and therefore reduces minority carrier lifetime. The other main cause of gain degradation is ionisation in the oxide passivation layer, particularly that part of the oxide covering the emitter-base junction region (see Fig. 7.1). By a

process similar to that in MOS devices, charge-trapping and the generation of new interface states produce degradation of gain. The trapped surface charge and interface states cause an increase in minority carrier surface recombination velocity, reducing gain. Under electron irradiation, such surface-linked degradation often precedes minority carrier effects.

We have seen that two quite distinct processes combine to decrease gain. Thus, degradation can be represented by the equation:-

$$\Delta(1/\beta) = 1/\beta - 1/\beta_o \qquad \text{.....7(i)}$$

where 'β_o' and 'β' are the gain values before and after irradiation.

Gain degradation is often analysed by plotting the change in reciprocal gain $\Delta(1/\beta)$ versus radiation fluence. The term '$\Delta(1/\beta.)$' is known as the "gain damage figure". The effects of bulk and surface damage can be separated as follows:-

$$\Delta(1/\beta) = \Delta(1/\beta)_b + \Delta(1/\beta)_s .$$

where the suffixes 'b' and 's' indicate the bulk and surface contributions respectively. However, while the bulk contribution may be reasonably predicted from analysis of minority carrier lifetime behaviour, the surface contribution is highly dependent upon process factors (see later Sections).

7.2.3. Other permanent effects

Apart from degradation of gain, irradiation also causes other important effects in bipolar transistors. Increases in the junction leakage currents (e.g. collector-base reverse leakage 'I_{CBO}'), like the surface-linked gain degradation already mentioned, result from ionisation in the surface oxide, particularly the region over the collector-base junction (see Fig. 7.1).

It is also found that heavy atomic displacement damage in the semiconductor causes an increase in the collector-emitter saturation voltage '$V_{CE(SAT)}$'. The rate of this increase with fluence is roughly the same as that with which gain decreases, i.e. the fluences producing a 50% change in either parameter are about the same. This is because '$V_{CE(SAT)}$', the voltage at which both transistor junctions are just forward biased, is an inverse function of transistor gain and is thus affected by changes in minority carrier lifetime.

Transistors with high breakdown voltages have high resistivity (low doping) in the collector region. At very high bulk damage levels, the resistivity may be changed noticeably, causing further changes in '$V_{CE(SAT)}$'. Such effects are of less importance in low power transistors such as logic devices because the switching or amplifying action is not affected by relatively high '$V_{CE(SAT)}$' values. On the other hand, the efficient operation of power transistors, especially switching power transistors, requires low '$V_{CE(SAT)}$' values. Donovan et al (1976) indicate that circuit failure of power transistors can be caused by a 50% increase in '$V_{CE(SAT)}$' or a 100-fold increase in 'I_{CEO}' (a surface-controlled leakage). Table 7(1) shows the change in these and other parameters in a bipolar power transistor.

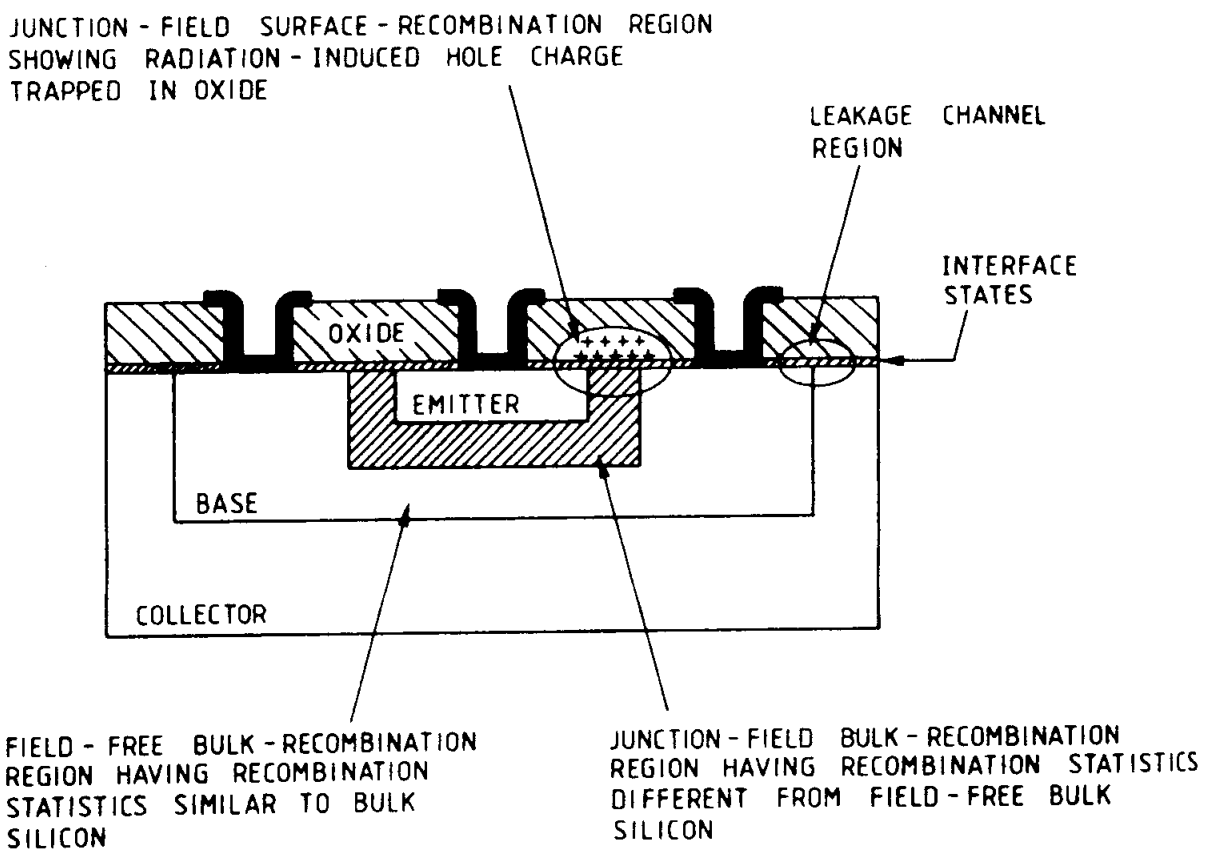

Essential features of device structure showing regions involved in radiation effects

FIGURE 7.1 - PLANAR BIPOLAR TRANSISTOR

TABLE 7(1) - THE EFFECT OF NEUTRON IRRADIATION UPON THREE SAMPLES OF A FAIRCHILD BIPOLAR TRANSISTOR 1970 era (V_{CE} = 5V, V_{CB} = 30V)

Neutron fluence cm^{-2}	I_m amp.	I_m/I_{mo}	β_o at I_{mo}	β/β_o at I_{mo}	β at 1A	V_{CE} (sat) Pre-irrad. V	V_{CE} (sat) Post-irrad. V	I_{CEO} at 30V Pre-irrad. nA	I_{CEO} at 30V Post-irrad. nA	(a) Approx. equivalent 1-MEV electr.fluence cm^{-2}
$1x10^{14}$	1.05 0.85 0.90	0.95 0.88 0.83	35.5 33.5 33.7	0.75 0.73 0.72	25.9 21.1 22.7	0.27 0.30 0.29	0.38 0.43 0.42	1.6 0.5 0.1	6.9 6.9 6.0	$3x10^{16}$
$3x10^{14}$	0.90 1.00 0.90	0.83 0.90 0.89	34.8 34.8 34.3	0.57 0.59 0.59	17.9 20.0 19.1	0.29 0.25 0.25	0.54 0.47 0.49	1.4 0.4 0.7	17.4 15.6 15.3	$9x10^{16}$
$1x10^{15}$	0.90 0.90 0.90	0.44 0.44 0.34	34.3 33.7 34.5	0.31 0.32 0.31	6.3 6.4 6.6	0.26 0.23 0.27	1.19 1.16 1.12	0.4 0.8A 0.5	35.2 1 A 35.7	$3x10^{17}$
$2x0^{15}$	0.90 0.80 0.90	0.17 0.19 0.17	35.3 37.1 34.7	0.15 0.15 0.14	– – –	0.23 0.25 0.25	1.55 2.41 1.86	0.4 1.1 0.4	58.4 58.9 61.7	

β_o = pre-irradiation gain
β = post-irradiation gain
I_{mo} = current at which β_o peaks
I_m = current at which β peaks
(a) : 1 n cm^{-2} is equivalent to approximately 300 e cm^{-2} (1 MeV)

7.2.4. Transient effects

The effect of ionisation on the p-n junction of a bipolar transistor may lead to transient photocurrent effects. The radiation dose rates required to produce significant effects are in the region of 10^6 rad $.s^{-1}$, well above the rates produced by either the natural space environment or typical isotope sources. The response of a bipolar transistor to dose rate is usually controlled by the photocurrent generated in the collector-base junction. These currents may be calculated if the dose rate and junction area are known.

7.3. BULK DAMAGE

7.3.1. General

The effect of atomic displacement in bulk silicon is a reduction in conductivity and minority carrier lifetime. The reduction in lifetime may be represented by the following equation:

$$1/\tau - 1/\tau_0 = K_\tau \phi \qquad 7 \text{ (iii)}$$

'K_τ ($cm^2 .s^{-1}$)' is known as the minority carrier lifetime damage constant for a given type and resistivity of silicon at a given radiation energy, 'ϕ' is the fluence and 'τ_0' and 'τ' are the initial and post-irradiation lifetime values. The value of 'K_τ' is dependent upon material properties, e.g. the value of oxygen-free silicon is significantly less than that of oxygen-rich material.

This picture is complicated by various other factors which depend upon the device geometry, particularly that of the base region. The following are three examples of such complicating factors:-

- The effectiveness of a given recombination centre on lifetime depends upon the charge state of that centre and this, in turn, is controlled by the minority carrier equilibrium pertaining to that point. A diffused junction device contains depletion regions near the junctions. In these regions, the electric fields are high and carriers are swept out rapidly. The material here resembles an intrinsic semiconductor and recombination rates are very low, although the addition of new defects will certainly alter these rates. The actual fields, and hence the carrier equilibria, vary with the bias applied.

- The nature of the production techniques commonly used for transistors is another complicating factor. In a diffused transistor, the base and emitter are regions formed by the diffusion of dopants into the substrate silicon. Thus, the dopant concentration profile (and hence the Fermi level) in the base is far from uniform and varies by orders of magnitude. In an ion-implanted device, different dopant concentration profiles will also be found and, in addition, the implantation itself is likely to cause defects in the silicon.

- When current flows in the transistor, the Fermi level is altered by the presence of excess carriers injected at the emitter-base junction and effectively dependent upon the operating level of the transistor. Therefore, other factors being equal, the value of 'K_τ' in a device carrying a signal current of 1 mA will be different from the 'K_τ' value in a device carrying a current of, say, 10 μA.

Thus, it is a complex task to predict the 'K_τ' value of a device from first principles.

The predicted typical relationship between gain and 1-Mev electron fluence, shown by the dotted lines in Fig. 7.2, derives from equation 7(ii). A change in 'K_τ' is expressed as a translation of the curves along the fluence axis. However, the observed gain degradation in a "planar" (oxide-passivated) bipolar transistor does not follow this predicted course. Instead, many devices are observed to degrade in the manner shown by the solid curve in Fig. 7.2. This is a clear indication that some degrading mechanism other than minority carrier lifetime reduction is affecting gain and this is found to be the surface ionisation effect already discussed.

7.3.2. The influence of base width

In MOS transistors, the oxide thickness is an important device parameter; in bipolar devices, base width is an equally important factor and - as described below - has a significant influence upon gain degradation by bulk damage.

The Webster equation for the gain of a bipolar transistor uses the following term for relating gain 'β' to minority carrier lifetime 'τ':

$$\frac{1}{\beta} = \frac{W_b^2}{2D} + \ldots \qquad \text{.....7(iv)}$$

where 'W_b" is the base width and 'D' is the minority carrier diffusion constant. Other terms in this equation account for the contributions of surface recombination (the surface effect) and emitter efficiency. The base width term is the controlling one for reduction in 'β' (i.e. bulk damage).

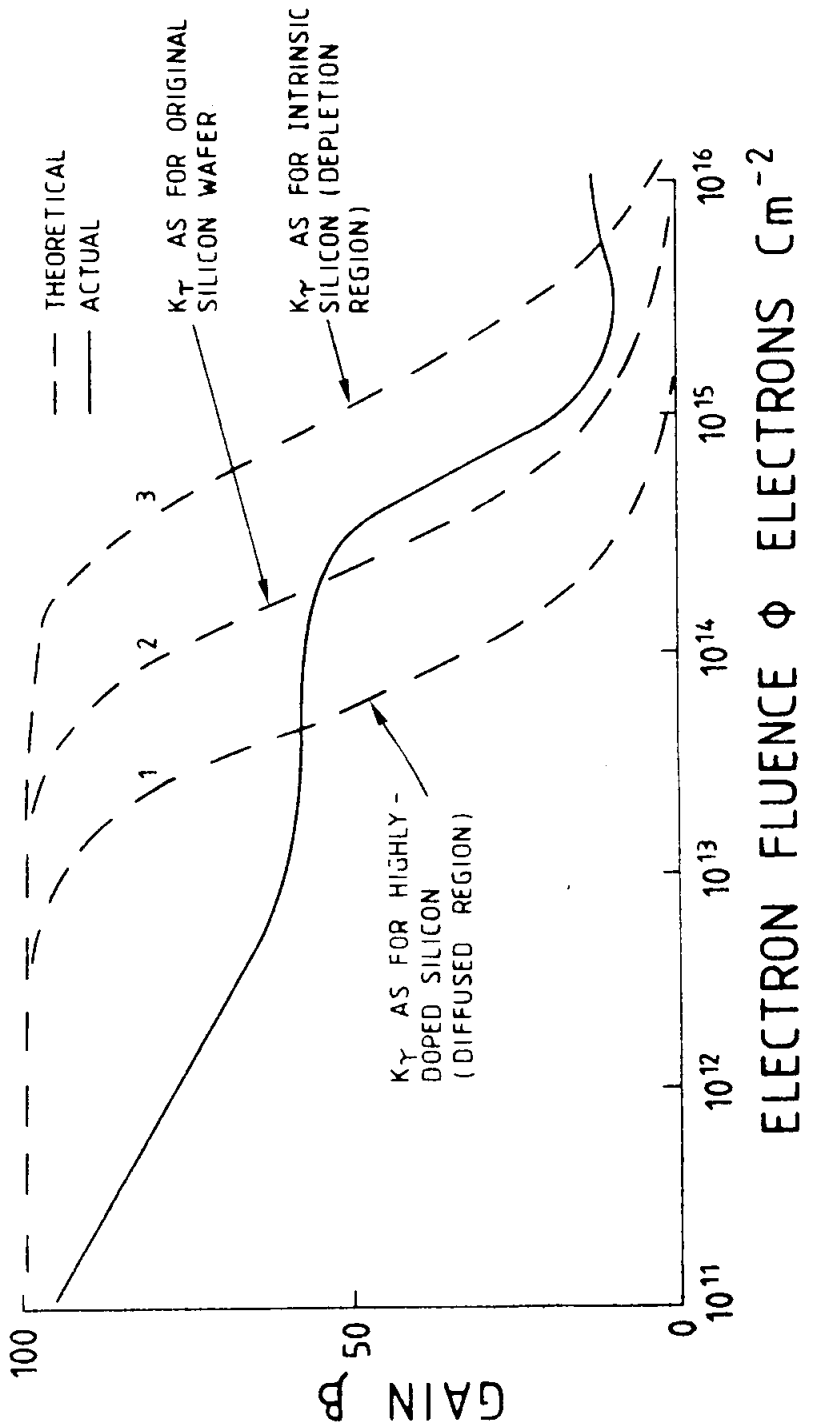

Common emitter current gain as a function of electron fluence. Solid curve shows typical behaviour of a real device indicating the early effects of ionisation in the surface oxide passivating layer.

FIGURE 7.2 - BIPOLAR TRANSISTOR DEGRADATION

Assuming that the surface recombination and emitter efficiency terms remain constant, a combination of the Webster equation and equations 7(i) and 7(iii) produces the following equation for the figure of gain damage caused by bulk damage:

$$\Delta(1/\beta) = \frac{W_b^2}{2D} \cdot K_\tau \cdot \phi \qquad \text{.....7(v)}$$

This equation demonstrates the strong dependence of the gain damage figure upon base width. Thus, it is necessary to measure or calculate this term for devices under consideration. The value of 'W_b' itself cannot be measured easily; however, the cut-off frequency 'f_α' (the frequency at which common-base current gain 'α' falls to one-half of its low-frequency value, say at 1 kHz) bears a close relation to 'W_b'. By using this dependence, Messenger and others (1965) derived the following prediction for the effect of bulk damage on transistors:

$$\Delta(1/\beta) = \frac{K_\tau \phi}{2\pi f_\alpha} \qquad \text{.....7(vi)}$$

Here, gain degradation has been related to more easily measurable parameters. For the purpose of the prediction, 'K_τ' must be determined at least one type of particle for any given bipolar transistor technology.

Typical figures for 'K_τ', measured for diffused NPN and PNP transistors under 1 MeV electron irradiation, are 1×10^{-8} and 3×10^{-8} $cm^2.s^{-1}$ respectively and, for reactor neutrons, 1×10^{-6} and 3×10^{-6} $cm^2.s^{-1}$ respectively.

As might be expected from solar cell investigation ('P' diffusion on N- type base is more sensitive than 'N' on 'P'), PNP transistors are more sensitive than the NPN-type by a factor of about 3 (the fluence required to yield a given degradation value is three times lower).

Although the cut-off frequency 'f_α' is included in the equation for gain prediction, an alternative parameter 'f_T' (the gain bandwidth product) is more easily measured and also most commonly quoted for transistors. It is the product of common-emitter gain 'β' and the frequency of measurement when the frequency lies on the descending part of the gain frequency curve.

The value of f_T is also the frequency at which 'β' falls to unity. Table 7(2) gives examples of the relationship between 'f_T' and base width 'W_b'.

The frequencies 'f_α' and 'f_T' are not exactly equal, 'f_T' being slightly lower. The ratio between them depends on the doping profile. For ideal step junctions, 'f_α' = $\sqrt{1.22\, f_T}$; for diffused junctions, the ratio is 1.33. thus, in practice, the error introduced by using 'f_T' in the prediction of $\Delta(1/\beta)$ is not often significant and, in any case, errs on the side of safety. In recent publications, 'f_T' is used in place of 'f_α' for diffused transistors, without any correction factor (Cooper et al, 1979; Berger et al, 1978).

It is often convenient to express transistor damage as "a gain damage factor" ('K_b') without normalising for base width, 'f_T', etc. Thus:

$$1/\beta - 1/\beta_o = 1/\beta = K_b\phi \qquad \text{.....7(vii)}$$

TABLE 7(2) - CALCULATION OF BASEWIDTH FROM BASE TRANSIT TIME OR APPROXIMATE GAIN-BANDWIDTH PRODUCT (GBP)

Approx. GBW Product (1) f_T (MHz)	Base transit time (2) t_b (ns)	$\sqrt{33.2\, t_b}$ (s)	$33.2\, t_b$ (cm)	Base width NPN (2) W_b (μm)	Base width PNP W_b (μm)
1000	0.16	5.28×10^{-9}	7.26×10^{-5}	0.73	0.63
500	0.32	1.05×10^{-8}	1.02×10^{-4}	1.02	
200	0.80	2.63×10^{-8}	1.62×10^{-4}	1.62	
100	1.59	5.28×10^{-8}	2.30×10^{-4}	2.29	2.0
50	3.18	10.5×10^{-8}	3.24×10^{-4}	3.24	
20	7.95	26.3×10^{-8}	5.13×10^{-4}	5.12	
10	15.9	52.8×10^{-8}	7.26×10^{-4}	7.26	6.3
1	1.59	5.28×10^{-6}	22.9×10^{-4}	22.9	20

(1) Ignoring t_e, t_c, etc.; GBW = gain bandwidth;
(2) using relations:

$$t_b \simeq \frac{2\pi ft}{1}$$

$$W_b = \sqrt{2D_n t_b} = \sqrt{33.2\, t_b}$$

$$D_n = 16.6\ cm^2\ s^{-1}\ (D_p = 12.5\ cm^2\ s^{-1})$$

See F. Larin, "Radiation Effects in Semiconductor Devices" (pp. 18, 67, 04); Wiley, 1968

Gain after a given irradiation can be calculated:

$$\beta = \frac{\beta_0}{1 + \beta_0 k_b \phi} \qquad \text{.....7(viii)}$$

A simple relation between 'K_b' and K_τ' is derived from equation 7(vi):-

$$K = 2\pi\ K_b.\ f_T = 6.28\ K_b.\ f_T \qquad \text{.....7(ix)}$$

7.3.3. The influence of type and energy of radiation

The atomic displacement process which causes bulk damage is, unlike the process causing surface damage, quantitatively dependent upon the momentum of the radiation. It is useful to consider briefly the effects of energy and particle type because this enables the test results of a large range of particle types and energies, including many results for reactor neutrons, to be found. Moreover, the particle spectrum in space is very broad.

The following equations summarise four important "damage constants" ('K') which relate the relevant "damage figure" to particle fluence. Minority carrier lifetime damage constant, 'K' (cm 2 .s^{-1}):

$$\Delta(1/\tau) = K_\tau\phi \qquad \text{.....7(x)}$$
(see also 7(iii))

Gain damage constant, 'K_b' (cm^2):

$$\Delta(1/\beta) = K_b\phi \qquad \text{.....7(xi)}$$
(see also 7(vii))

Diffusion length damage constant (for solar cells), 'K_L' (cm^2 per cm^2):

$$\Delta(1/L^2) = K_L\phi \qquad \text{.....7(xii)}$$

Carrier removal rate, '$\Delta n/\Delta\phi$ (or Δ p/$\Delta\phi$' (cm^{-1}))

$$n(\phi) = n_o \frac{\Delta n}{V\phi} \qquad \text{.....7(xiii)}$$

These constants all change with particle type and energy and this section will discuss mainly the variation of the lifetime and gain damage constants in bipolar transistors. Figure 7.3 shows the experimental results of exposing a 2N1613 transistor to several different types of radiation. The form of degradation is the same for each type of radiation except that (1/ϕ) is displaced along the flux scale (i.e. 'K_b' is different). Thus, it may often be possible to employ test results using one particle type or energy to predict the effects expected under irradiation by another particle type or energy.

Figure 7.3 also shows that in all cases some slowly developing non-linear degradation takes place well before a linear growth of

gain damage with fluence (indicated by a dotted line) is observed to occur. This early degradation is the "surface effect" due to the ionising component of the radiation.

The constant 'K_b' can be measured from the linear portion of Figure 7.4. 'K_b' for reactor neutrons is seen to be over 100 times greater than for electrons. It is fortunate that low-energy protons are filtered out by normal device packaging as otherwise the high 'K_b' value shown for 2 MeV protons would cause a serious effect in space. The long "tail" of the ^{60}Co gamma-radiation curve indicates that ionisation (surface effect) is the major effect of this radiation although bulk damage from Compton electrons is evident at very high doses (10^8 rad (Si)).

Table 7(3) lists a more complete set of results by Brown and colleagues (1964, 1967), giving 'K_b' for a number of bipolar transistors and six different radiation sources. To normalise for base width, 'K_b' has been converted to 'K_τ' with the aid of equation 7(ix).

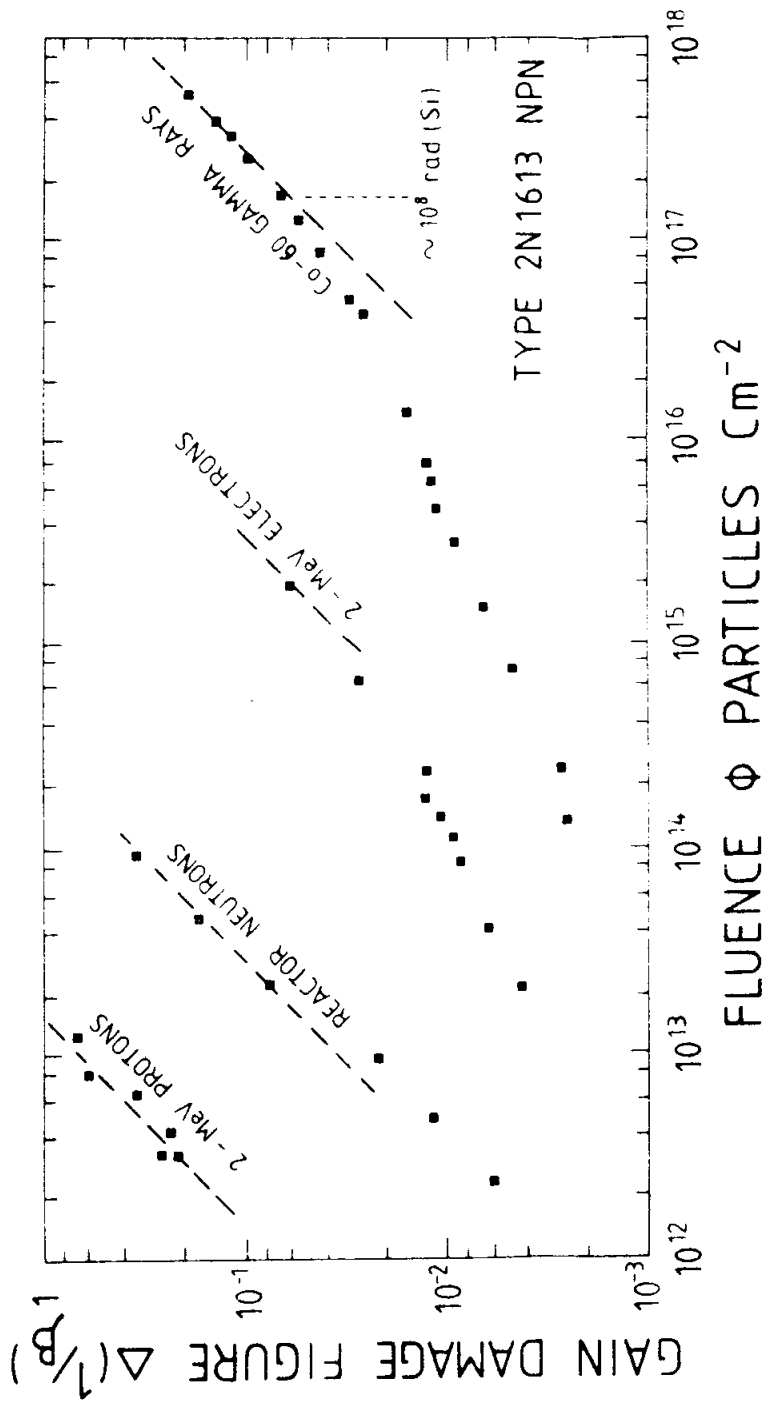

Gain damage figure for 2N1613 devices as a function of radiation fluence, showing the effect of radiation-type (data from Brown, 1964)

FIGURE 7.3 - THE INFLUENCE OF RADIATION TYPE (FROM BROWN 1964)

TABLE 7(3) - BROWN'S DAMAGE CONSTANTS FOR A NUMBER OF TRANSISTORS SUBJECTED TO VARIOUS TYPES OF IRRADIATION

Device type	f_T MHz	Protons[a]		Reactor neutrons	Electrons		Gamma rays
	(nom)	2-MeV	10-MeV	>10KeV	2-MeV	5-MeV	Co-60
A. Transistor gain damage constant K_b(cm^2) for various types of radiation (after Brown et al (11, 12); Collector current 2mA							
2N336 NPN	7	–	70E-15	2.5E-15	4.0E-17	2.5E-17	9.0E-19
2N1132A NPN	60	5.5E-14	–	–	2.5E-17	–	7.0E-19
2N1613 NPN	60	7.0E-14	5.0E-15	2.5E-15	4.0E-17	7.0E-15	4.0E-19
2N2107 NPN	150	–	–	–	4.50E-17	–	3.5E-19
2N2217 NPN	100	–	–	8.0-16	1.5E-17	1.7E-17	1.0E-19
B. Nominal minority-carrier lifetime damage constant K_τ (cm^2 $s.^{-1}$) calculated from the values of K_b above[b]							
2N336 NPN	7	–	2.5E-7	9.0E-8	1.4E-9	9.0-10	3.2E-11
2N1132A PNP	60	1.7E-5	–	–	7.7E-9	–	2.2E-10
2N1613 NPN	60	2.2E-5	1.6E-6	7.8E-7	1.2E-8	2.1E-8	1.3E-10
2N2107 NPN	150	–	–	–	3.5E-9	–	2.7E-10
2N2217 NPN	100	–	–	4.1E-7	7.6E-9	8.7E-9	5.1E-11

a. Proton irradiation with cans removed.

b. Calculated from equation 5(ix) assuming f_T equal to f_α.

The uncertainty ascribed by Brown to his K_b values is typically ± 30%.

The notation "E-14" indicates "10^{-14}" (etc.).

TABLE 7(4) - BRUCKER'S DAMAGE CONSTANTS FOR A NUMBER OF TRANSISTORS SUBJECTED TO VARIOUS TYPES OF IRRADIATION

(with pre-irradiation to saturate surface effects - see text)

Device type	f_T MHz (nom)	Protons 16.8 MeV	Reactor neutrons >10 keV	Electrons 1 MeV	Collector current mA
A. Gain damage constant, Kb (cm^2) for various types of radiation (after Brucker ([13]))					
2N2102 NPN	100	1.5E-14 8.0E-15 –	4.6E-15 2.9E-15 4.9E-15	1.9E-17 1.8E-17 4.1E-17	1 10 100
2N1132 PNP	100	1.8E-14 1.2E-14 –	4.5E-15 2.4E-15 3.4E-15	7.4E-17 6.2E-17 6.8E-17	1 10 100
B. Nominal minority-carrier lifetime damage constant, K_τ ($cm^2.s^{-1}$) calculated from the values of K_b above					
2N2102 NPN	100	7.7E-6 4.1E-6 –	2.4E-6 1.5E-6 2.5E-6	9.7E-9 9.2E-9 2.1E-8	1 10 100
2N1132 PNP	100	9.2E-6 6.2E-6 –	2.3E-6 1.2E-6 1.7E-6	3.8E-8 3.2E-8 3.5E-8	1 10 100

a. Calculated from equation 5 (ix) with f_T assumed equal to f_α.

Damage efficiency of protons and neutrons compared with 1 MeV electrons at collector current of 1mA (energies as above).

Device	K_τ (p,n) /K_τ (e)	
	Protons	Neutrons
2N2102 NPN	790	240
2N1132 PNP	240	60

Brucker ascribes an uncertainty to Kp values of typically ± 20%.
The notation 'E-14' indicates 'x 10^{-14}' (etc.).

The 'K_τ' values of three of the NPN devices fall within the range given by Van Lint and co-workers (1975) for 3 MeV electrons in 1 ohm/cm silicon, namely 2 to 8×10^{-9} $cm^2 .s^{-1}$.

It is not clear whether the variations from type to type are due to variations in resistivity in the base region, different impurities or other dissimilarities between experiments. The data quoted by Van Lint (1975) are largely for the base regions of solar cells or other uniformly doped silicon. In the circumstances, the correlation is quite good.

Brucker (1965, 1967) performed a set of irradiation tests similar to those carried out by Brown, but added a preliminary heavy irradiation with 125 keV electrons. This caused no displacement damage, but virtually saturated the surface damage. As a result, 'K_b'could be determined over a wider range of fluence because the obscuring influence of surface effects had been removed. The Brucker 'K_b' values, which have again been converted into 'K_τ', are shown in Table 7(4). The electron result for an NPN transistor at 1 mA again lies near Van Lint's figure. Both protons and neutrons yield 'K_τ' values higher than those of Brown's devices. Brucker also studied the effect of varying electron energy over the range 0.275 to 1 MeV and found that the energy dependence of 'K_τ' in solar cells was similar to that found by other workers.

The influence of displacement defects on 'τ' is well known to be affected by the concentration of minority carriers ("injection level") in the device. This can be explained by the Shockley-Hall-Read recombination theory. Irradiation results from mesa and wide-base power transistors at 1 MeV and 8 MeV suggest that damage constants of the order given above can be used for these devices despite their very different structures. In Europe, Lambert et al (1975) report the testing of a wide range of discrete and integrated devices (including operational amplifiers) under neutrons, high-energy protons and ^{60}Co gamma radiation, but do not apply the analytical treatments discussed here.

7.3.4. Irradiation results

Table 7(5) lists the results of an extensive series of nuclear reactor exposures performed in the U.K. under the sponsorship of the U.K. Government. Listed in the first group are the maximum values of 'K_b' for the fluence range 10^{12} to 10^{13} reactor neutrons.cm^{-2} (E > 10 keV). Where possible, we have selected an 'I_c' value of 1 mA. 'K_b' is the experimental value and we have calculated the "apparent K_τ" value from 'K_b' as in equation 7(ix). The variations in this value are unlikely to be due to a true difference in lifetime degradation. The high values probably contain a contribution to

$\Delta 1/\beta$ from effects at the surface and in the emitter-base depletion region. The quoted value of 'f_T ' is not a measured value, but the minimum value quoted in the manufacturer's data sheet. It is quite likely that some of the samples tested had a higher value than that specified. Hence, both high values of apparent 'K_τ' and some variability are to be expected.

TABLE 7(5) - COLLECTED VALUES OF DAMAGE CONSTANTS FOR COMMERCIAL PLANAR SILICON TRANSISTORS AND REACTOR NEUTRONS

1 Device type nr. (d)	2 Manu-facturer (d)	3 Polarity	4 Nominal cutoff Frequency(a) f_T (MHz)	5 IC Value for Meas. I_C (mA)	6 Exptl. Beta-damage Const. (b) K_b ($10^{-15}cm^2n^{-1}$)	7 $K_b \times f_T$ ($10^{-9}cm^2n^{-1}s^{-1}$)	8 Lifetime damage constant (low I_C) (c) K col 7 x 2 ($10^{-6}cm^2n^{-1}s^{-1}$)
2N720A	TEX	NPN	50	1	9.8	490	3.27
2N918	TEX	NPN	900	1	0.71	639	4.26
2N930	TEX	NPN	45	1	1.9	86	1.84
2N1486	RCA	NPN	1.2	10	110.0	132	0.88
2N1613	TEX	NPN	60	1	6.7	402	2.68
2N2219	TEX	NPN	250	1	0.99	248	1.65
2N2219	SGS	NPN	250	1	1.1	275	1.83
2N2219A	FAI	NPN	250	3	0.67	168	1.12
2N2222A	FER	NPN	250	1	1.6	400	2.67
2N2223A	TEX	NPN	50	1	6.6	330	2.20
2N3055	FER	NPN	20	100	44.0	880	5.87
2N3055	MUL	NPN	20	100	69.0	1380	9.20
2N2905	NAT	PNP	200	3	0.95	190	1.27
2N2905A	TEX	PNP	200	3	0.57	114	0.76
2N2906	TEX	PNP	200	3	2.1	420	2.80
2N2906	TEX	PNP	200	1	3.2	640	4.26
2N2907A	TEX	PNP	200	1	3.4	680	4.53
2N4901	TEX	PNP	4	100	8.7	34.8	0.23
2N4904	MOT	PNP	4	100	10.13	0.52	0.003
2N1132	TEX	PNP	90	3	4.0	360	2.40
2N2303	FAI	PNP	60	1	2.7	162	1.08
2N2412	TEX	PNP	200	1	1.7	340	2.27
2N2894	FAI	PNP	370	1	0.51	189	1.26
2N4028	FAI	PNP	150	3	2.2	330	2.20
2N5883	MOT	PNP	4	30	35.0	140	0.93
Cooper, Retzler and Messenger 1979, (e)							
2N222A	–	NPN	300	0.51	1.4	467	3.11
2N2907A	–	PNP	200	1	0.54	108	0.72
2N2369A	–	NPN	500	10	0.20	100	0.67
2N4150	–	NPN	15	1000	3.68	55	0.37
2N5666	–	NPN	20	1000	5.75	115	0.77

See next page.

a) Quoted on data sheets: Specified minimum, not actual

(b) $K_b = \left[\frac{1}{\beta} - \frac{1}{\beta_0} \right] - \phi_n$

(c) $K = 2\pi K_b f_T$

(d) Herald reactor, UK; maximum K_b observed:
$\phi_n = 10^{12}$ to 2×10^{13} cm^{-2};
isotope γ-rays: 3000 to 30 000 rad (Si).

(e) Equiv. 1 MeV neutrons quoted. $\phi_n = 2$ to 5×10^{13} cm^{-2}.

7.3.5. Prediction of degradation

Once decided, lifetime damage constants can be turned into a master set of prediction curves. For example, those shown in Fig. 7.4 are for an NPN device, having an original gain 'β_O' of 100, exposed to 1 MeV electrons. These curves apply to that one value of gain only, but the trends are the same for all values of gain.

To predict the degradation of a given device numerically, the value of $\Delta(1/\beta)$ may be calculated from equations given earlier. This value of $\Delta(1/\beta)$ may then be converted by calculation to the final value of 'β'. A convenient ready reckoner for this conversion is given in Table 7(6).

Table 7(7) shows some calculations of degradation in space, using three values of electron fluence such as might be calculated for a spacecraft in a high-radiation orbit.

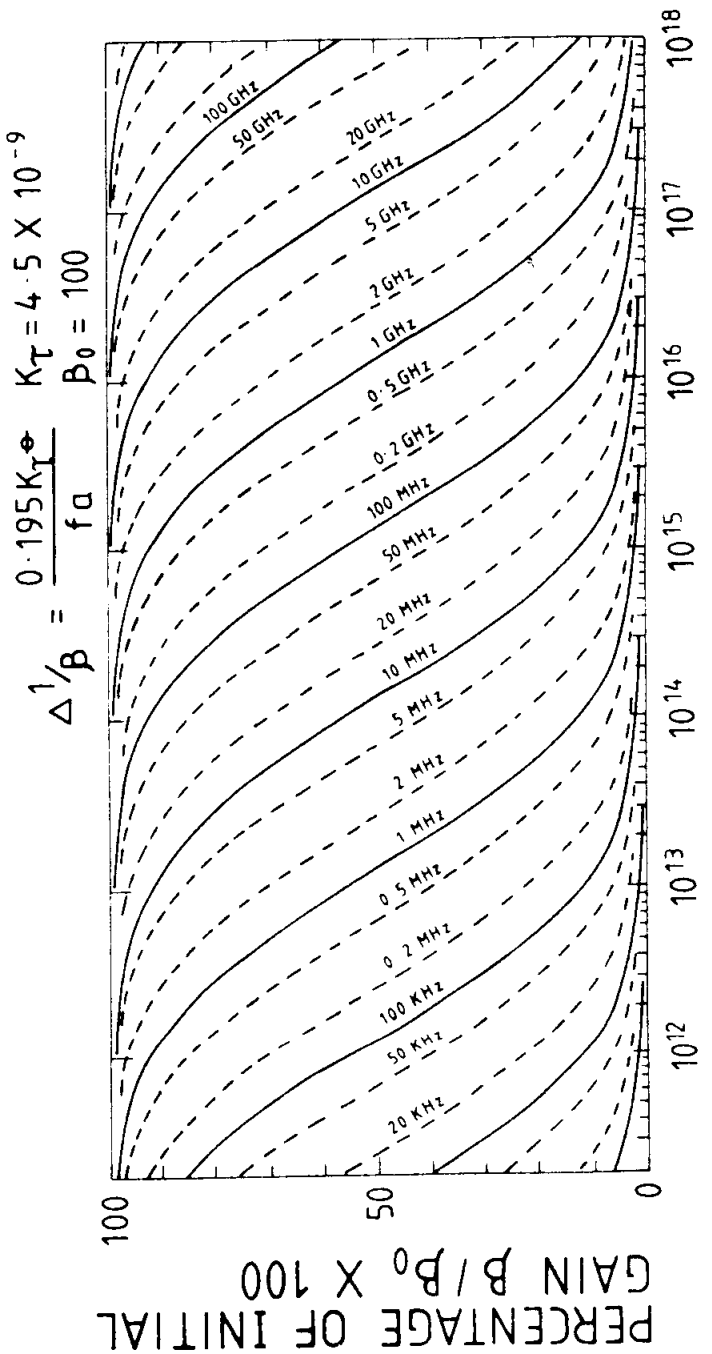

Degradation of gain as a function of electron fluence showing variation with alpha cut-off frequency Fα (a function of base width).

FIGURE 7.4 - THE INFLUENCE OF BASE WIDTH.

TABLE 7(6) - FINAL VALUES OF TRANSISTOR GAIN 'β', GIVEN INITIAL GAIN 'β_o' AND DAMAGE FIGURE '$\Delta 1/\beta$' (BASED ON $\Delta 1/\beta = 1/\beta - 1/\beta_o$)

Original values of gain, β_o →

$\Delta 1/\beta$	10	12	15	20	25	30	35	40	45	50	55	60	65	70	75	80	85	90	95	100	110	120	130	140	150	170	200	250	300	350	400
.0005	9.95	11.9	14.9	19.8	24.7	29.6	34.4	39.2	44.1	48.8	53.6	58.1	62.9	67.6	72.5	76.9	81.3	86.2	90.9	95.2	104	114	122	132	139	156	182	222	263	294	333
.0007	9.93	11.9	14.9	19.7	24.6	29.4	34.1	38.9	43.7	48.3	53.3	57.5	61.7	66.7	71.4	75.8	80.0	84.8	89.3	93.5	102	111	119	128	135	152	175	212	250	278	313
.001	9.90	11.9	14.8	19.6	24.4	29.2	33.8	38.5	43.1	47.6	52.1	56.6	61.0	65.4	69.8	74.1	78.1	82.6	87.0	90.9	99.0	107	115	124	130	145	167	200	233	256	286
.0015	9.85	11.8	14.7	19.4	24.1	28.7	33.2	37.7	42.2	46.5	51.8	55.0	59.2	63.4	67.6	71.4	75.2	79.4	83.3	87.0	94.3	102	109	116	122	135	154	182	208	227	250
.002	9.80	11.7	14.6	19.2	23.8	28.3	32.7	37.0	41.3	45.5	49.5	53.6	57.5	61.4	65.4	69.0	72.5	76.3	80.0	83.3	90.1	96.8	103	110	115	127	143	167	189	204	222
.0025	9.76	11.7	14.5	19.0	23.5	27.9	32.2	36.4	40.5	44.4	48.3	52.2	55.9	59.6	63.3	66.7	69.9	73.5	76.9	80.0	86.2	92.3	98.0	104	109	119	133	154	172	185	200
.003	9.71	11.6	14.3	18.9	23.3	27.5	31.7	35.7	39.7	43.5	47.2	50.8	54.4	57.9	61.4	64.5	67.6	70.9	74.1	76.9	82.6	88.2	93.5	99.0	103	112	125	143	159	170	182
.0035	9.66	11.5	14.3	18.7	23.0	27.2	31.2	35.1	38.9	42.6	46.1	49.5	52.9	56.2	59.5	62.5	65.4	68.5	71.4	74.1	79.4	84.8	89.3	94.3	98.0	106	118	133	147	156	167
.004	9.62	11.5	14.1	18.5	22.7	26.8	30.7	34.5	38.2	41.7	45.1	48.4	51.6	54.7	57.8	60.6	63.3	66.2	69.0	71.4	76.3	81.1	85.5	90.1	93.8	101	111	125	137	145	154
.005	9.52	11.3	13.9	18.2	22.2	26.1	29.9	33.6	36.8	40.0	43.1	46.2	49.0	51.9	54.6	57.1	59.5	62.1	64.5	66.7	70.9	75.0	78.7	82.6	85.7	91.7	100	111	121	127	133
.006	9.43	11.2	13.8	17.9	21.7	25.5	29.0	32.3	35.5	38.5	41.3	44.1	46.7	49.3	51.8	54.1	56.2	58.5	60.6	62.5	66.2	69.8	73.0	76.3	79.0	84.0	90.9	100	108	112	118
.007	9.35	11.1	13.6	17.5	21.3	24.8	28.1	31.3	34.3	37.0	39.7	42.3	44.6	47.0	49.3	51.3	53.2	55.2	57.1	58.8	62.1	65.2	68.0	70.9	73.2	77.5	83.3	90.9	97.1	101	105
.008	9.26	11.0	13.4	17.2	20.8	24.2	27.4	30.3	33.1	35.7	38.2	40.5	42.7	44.9	47.0	48.8	50.5	52.4	54.1	55.6	58.5	61.2	63.7	66.2	68.2	71.9	76.9	83.3	88.5	91.7	95.2
.009	9.17	10.8	13.2	16.9	20.4	23.6	26.6	29.4	32.1	34.5	36.8	39.0	41.0	42.9	44.8	46.5	48.1	49.8	51.3	52.6	55.3	57.7	60.0	62.1	63.8	67.1	71.4	76.9	81.3	84.0	87.0
.010	9.09	10.7	13.0	16.7	20.0	23.1	26.0	28.6	31.1	33.3	35.5	37.5	39.4	41.2	42.9	44.4	45.9	47.4	48.8	50.0	52.4	54.5	56.5	58.5	60.0	62.9	66.7	71.4	75.2	77.5	80.0
.011	9.01	10.6	12.9	16.4	19.6	22.6	25.3	27.7	30.1	32.3	34.3	36.1	37.4	39.5	41.1	42.6	43.4	45.3	46.5	47.6	48.7	51.2	53.5	55.3	56.5	59.2	62.5	66.7	69.9	71.9	74.1
.012	8.93	10.5	12.7	16.1	19.2	22.1	24.7	27.0	29.2	31.3	33.1	34.9	36.5	38.1	39.5	40.8	42.0	43.3	44.4	45.5	47.4	49.2	50.8	52.4	53.6	55.9	58.8	62.5	65.4	67.1	69.0
.013	8.85	10.4	12.6	15.9	18.9	21.6	24.1	26.3	28.4	30.3	32.1	33.7	35.2	36.6	38.0	39.2	40.3	42.5	43.5	44.6	45.3	47.0	48.3	49.8	50.8	52.9	55.6	58.8	61.4	62.9	64.5
.014	8.77	10.3	12.4	15.6	18.5	21.1	23.5	25.6	27.6	29.4	31.1	32.6	34.0	35.1	36.6	37.7	38.8	39.8	40.8	41.7	43.3	44.0	46.1	47.4	48.3	50.3	52.6	55.6	57.8	59.2	60.6
.015	8.70	10.1	12.2	15.4	18.2	20.7	23.0	25.0	26.9	28.6	30.1	31.6	32.9	34.1	35.3	36.4	37.3	38.3	39.2	40.0	41.5	42.9	44.1	45.3	46.2	47.9	50.0	52.6	54.6	55.9	57.1
.017	8.62	10.0	12.0	14.9	17.5	19.9	21.9	23.8	25.5	27.0	28.4	29.7	30.9	32.0	33.0	33.9	34.7	35.6	36.4	37.0	38.3	39.5	40.5	41.5	42.2	43.7	45.5	47.6	49.3	50.3	51.3
.020	8.33	9.67	11.5	14.3	16.7	18.8	20.6	22.2	23.7	25.0	26.2	27.3	28.3	29.2	30.0	30.8	31.5	32.2	32.8	33.3	34.4	35.3	36.1	36.9	37.5	38.6	40.0	41.7	42.9	43.7	44.4
.025	8.00	9.23	10.9	13.3	15.4	17.2	18.7	20.0	23.4	22.2	25.8	24.0	27.9	25.5	29.6	26.7	27.2	27.7	28.2	28.6	29.3	30.0	30.6	31.2	31.6	32.4	33.3	34.5	35.3	35.8	36.4
.030	7.69	8.82	10.3	12.5	14.3	15.8	17.1	18.2	21.9	20.0	20.8	21.4	22.0	22.8	23.1	23.5	23.9	24.3	24.7	25.0	25.6	26.1	26.5	27.0	27.3	27.9	28.6	29.4	29.9	30.4	30.8
.035	7.41	8.48	9.83	11.8	13.3	14.6	15.8	16.7	21.7	18.2	20.5	19.3	19.8	20.3	22.8	21.0	21.4	21.7	22.0	22.2	22.7	23.0	23.4	23.8	24.0	24.5	25.0	25.6	26.1	26.4	26.7
.040	7.14	8.11	9.38	11.1	12.5	13.6	14.6	15.4	21.4	16.7	17.2	17.6	18.0	18.4	18.8	19.0	19.3	19.6	19.8	20.0	20.4	20.7	21.0	21.2	21.4	21.8	22.2	22.7	23.1	23.3	23.5
.050	6.67	7.50	8.57	10.0	11.1	12.0	12.7	13.3	21.2	14.3	14.7	15.0	15.3	15.6	15.8	16.0	16.2	16.4	16.5	16.7	16.9	17.2	17.3	17.8	17.6	17.9	18.2	18.5	18.8	18.9	19.1
.060	6.25	6.98	7.89	9.09	10.0	10.7	11.3	11.8	21.0	12.5	12.8	13.0	13.3	13.5	13.6	13.8	13.9	14.1	14.2	14.3	14.5	14.6	14.8	14.9	15.0	15.2	15.4	15.6	15.8	15.9	16.0
.070	5.88	6.52	7.32	8.33	9.09	9.71	10.1	10.5	20.8	11.1	11.3	11.5	11.7	11.8	12.0	12.1	12.2	12.3	12.4	12.5	12.6	12.8	12.9	13.0	13.0	13.2	13.3	13.5	13.6	13.7	13.8
.080	5.56	6.12	6.82	7.69	8.33	8.85	9.21	9.52	20.5	10.0	10.2	10.3	10.5	10.8	10.7	10.8	10.9	11.0	11.1	11.1	11.2	11.3	11.4	11.5	11.5	11.6	11.8	11.9	12.0	12.1	12.1
.090	5.26	5.77	6.38	7.14	7.69	8.13	8.42	8.70	20.3	9.09	9.25	9.38	9.49	9.59	9.68	9.76	9.83	9.89	9.95	10.0	10.1	10.2	10.2	10.3	10.3	10.4	10.5	10.6	10.7	10.8	10.8
.100	5.00	5.45	6.00	6.67	7.14	7.52	7.81	8.00	20.1	8.33	8.46	8.57	8.67	8.75	8.83	8.89	8.95	9.00	9.05	9.09	9.17	9.23	9.29	9.34	9.38	9.44	9.52	9.62	9.68	9.72	9.76

← $\Delta 1/\beta$ →

← Final values of gain, β_o →

TABLE 7(7) - PREDICTED DEGRADATION OF BIPOLAR TRANSISTORS IN SPACE RADIATION

Device type	Damage constants		Gain (β) after given 1-MeV electron fluence (cm^{-2})		
	K $cm^2.s^{-1}$	K cm^2	10^{13}	10^{14}	10^{15}
60 MHz transistor					
NPN (e.g. 2N1613	5.84E-9	1.0 E-17a	98.6	87.3	40.7
PNP (e.g. 2N1132)	2.27E-8	7.4 E-17a	93.1	57.5	11.9
200 MHz transistor					
NPN (e4.g. 2N2222A)	5.84E-9	5.71E-18	99.4	94.6	63.7
PNP (e.g. 2N2907A)	2.27E-8	2.22E-17	97.8	82.0	31.3
1.2 MHz power transistor					
NPN (e.g. 2N1485)	4.2E-9	6.6E-16	58.8	12.5	1.5

NOTE that "E-9" signifies "x10-9", etc.

$$(1/\beta) = \frac{0.195K}{f}\phi = K_b\phi$$

7.3.6. Selection rules for bipolar transistors

In general, the longest survival time of a transistor will be achieved if the following selection rules are applied:

- Where possible, use low-gain transistors at fairly high collector current levels;
- When heavy particle irradiation is involved (near a space nuclear power system), employ - where possible - high-frequency NPN devices.

7.4. SURFACE-LINKED DEGRADATION IN GAIN

7.4.1. Introduction

In previous sections, it has been shown how gain degradation is made up of surface and bulk contributions. While the bulk damage figure $\Delta(1/\beta)_b$ can be predicted fairly well by means of the analytical techniques described, the value of the surface damage figure

$\Delta(1/\beta)_S$ produced by a given radiation dose is much less easily predicted for a given transistor design. The latter value is highly dependent upon the surface preparation used, which usually consists of the growth of a passivating oxide in steam. Each manufacturer tends to use a slightly different process and, even when meeting ultra-high reliability specifications, is liable to vary the process significantly from time to time.

Figure 7.5 shows the gain degradation exhibited by a batch of transistors from one day's production, as a function of dose during gamma irradiation, which produces mainly surface effects at the doses shown. Units with identical functional specifications, but from different manufacturers, may vary even more widely after irradiation. For these effects, the "surface damage figure", $(1/\beta)_S$, was found to be a useful tool in that it provides a routine method of recording and characterising the surface effect. An example of the variation of surface damage figure with the collector current 'I_C' used for measurement (equivalent to emitter injection level) is shown in Figure 7.6. A reasonably close linear relationship between 'I_C' and damage figure is demonstrated.

All transistors exhibit lower gain values at low current than at high current. This is because, at low currents, the flow of minority carriers is greater near the surface. The recombination of carriers at the surface removes carriers more effectively at low currents. It appears that this surface gain factor is always present and is simply increased by irradiation, an unexpected result since interface states are surface recombination sites and these are increased by irradiation. The change in gain can thus be interpreted as a change in the surface recombination term in the well-known Webster equation for the bipolar transistor. Stanley and co-workers obtained a large amount of data on the surface effect in bipolar transistors as part of the hardening programme for the Voyager project. $\Delta(1/\beta)$ versus collector current after irradiation by electrons of energy near 2.5 MeV was measured and found to vary from type to type by as much as 100 times.

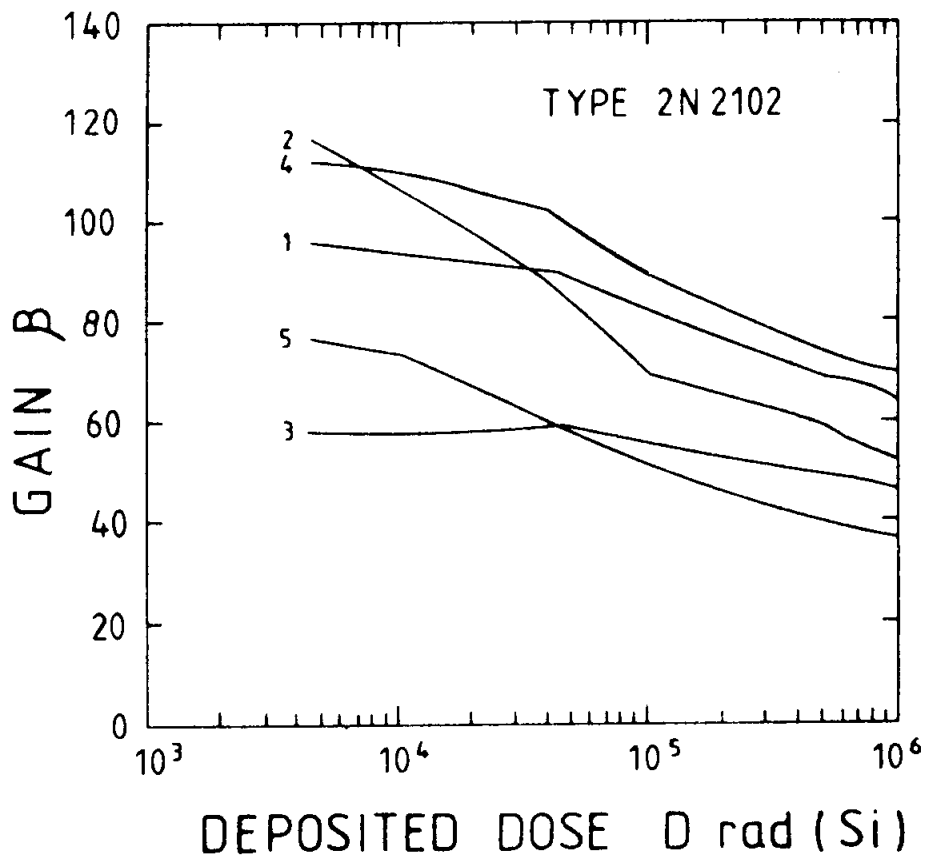

The variability of gain degradation due to the surface ionisation effect is shown by the results of tests on a batch from one day's production. Irradiation was by ^{60}Co gamma radiation and the collector current was 10 mA (after Poch and Holmes-Siedle, 1968).

FIGURE 7.5 - VARIABILITY OF SURFACE EFFECT GAIN AS A FUNCTION OF DEPOSITED DOSE IN NPN BIPOLAR TRANSISTOR, TYPE 2N2102

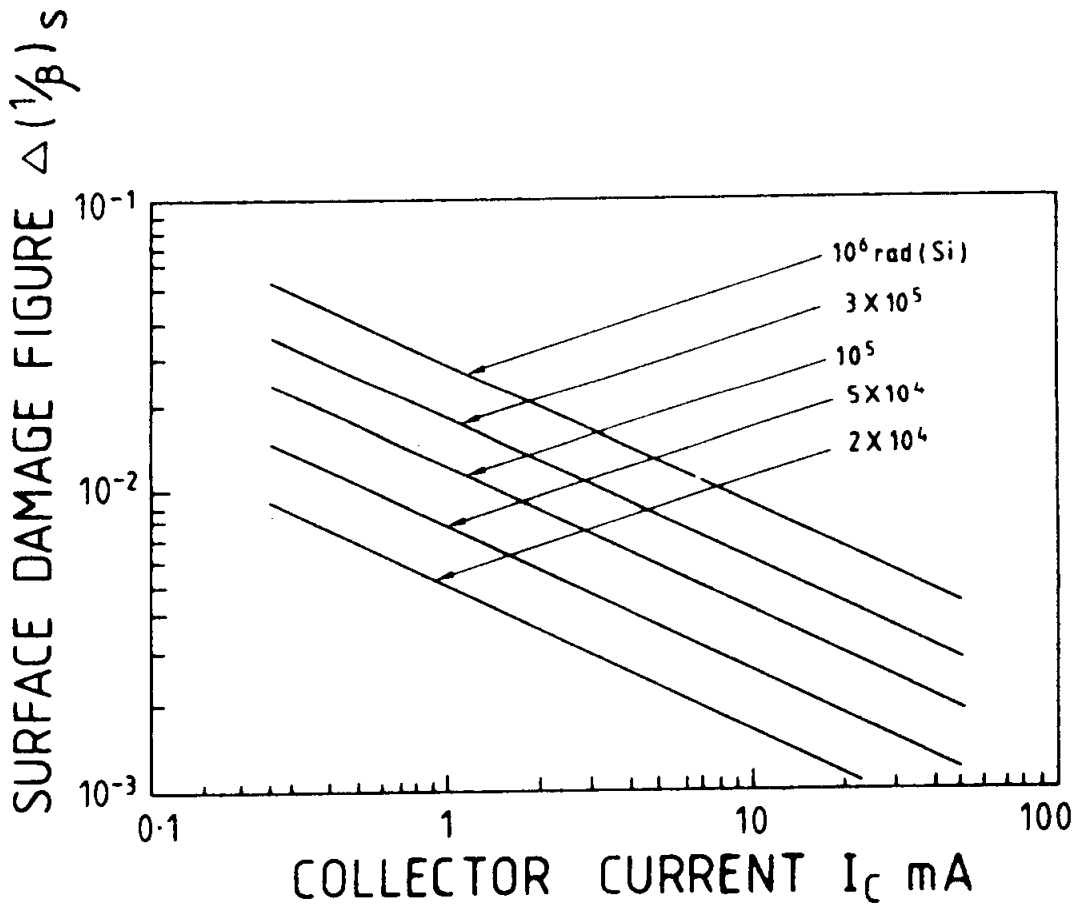

Form of an engineering specification for "worst case" of surface damage figure as a function of collector current in 2N916 transistors of a given manufacturer. The specification is for a 99% probability of staying below the indicated degradation level (after Poch and Holmes-Siedle, 1968).

FIGURE 7.6 - SPECIFICATION OF SURFACE DAMAGE FIGURE IN BIPOLAR TRANSISTOR

7.4.2. Statistical prediction of surface damage

The radiation-induced loss of gain for a batch of devices analysed statistically, with $\Delta(1/\beta)_S$ as a measure of damage, has been found to have a frequency distribution fitting the normal Gaussian curve. For example, a set of 32 2N2102-type planar NPN transistors was irradiated to a dose level of 10^6 rads gamma radiation. When 'β' and 'β'_0 were measured at a collector current of 0.7 mA, the mean value of the damage figure was 22×10^{-3} and the standard deviation 7.4×10^{-3}.

If the assumption of normal distribution is valid and this 2N2102 sample can be considered typical of the entire population, then the probability that the anticipated value of the ionisation damage figure will not exceed a specified maximum at a specified radiation dose can be calculated. Values of $\Delta(1/\beta)_S$ determined in this manner can be treated as a "worst case" upper limit of anticipated transistor gain degradation. It is therefore feasible to predict degradation in the form of a "worst expected surface damage figure" plotted against collector current. This form of prediction may be a useful method of specifying surface effects in design documents.

7.4.3. Collector-base leakage currents

Increase in collector-base leakage currents I_{CBO} is usually due to the formation of a surface channel. Although slight increases in the 'I_R' term for the collector-base junction are produced by a reduction in the minority carrier lifetime, the values are usually a minor component of the reverse leakage. By contrast, a charge build-up in the oxide layer over the junction can produce a surface channel which conducts strongly. As a result, I_{CBO} values which, for planar transistors, are usually 10^{-9} or thereabouts, may increase tenfold for a dose in the 10^4 rad range. Onset as a function of dose is often quite sudden and probably not amenable to statistical treatment. Figure 7.7 shows a case of sudden onset and scattered results in a batch of 5 specimens.

7.4.4. The "Maverick" device

Unfortunately, one of the characteristics of bipolar transistor performance is the occurrence of the "maverick" or anomalous device. Such a device may be discovered in an otherwise normal batch, all processed in an essentially similar manner. It is anomalous in that it exhibits a radiation-induced gain degradation much more severe than the "worst expected case". While most of the devices follow a well-defined band of surface-damage figure, the anomalously sensitive unit may show a degradation level which is higher by a factor of 50 or more. To design all circuits and

associated shielding to tolerate this abnormal sensitivity and wide range of degradation characteristics would impose severe penalties with regard to size, weight, power drain and complexity. On the other hand, the occurrence of such a degree of degradation in a particularly vital component would be catastrophic to equipment performance. The existence of a "maverick" could easily be missed if small-sample tests were performed and, therefore, preselection test programmes should - if possible - specify large statistical samples of devices.

7.4.5. Annealing of surface effects

The thermal annealing of the surface effects in bipolar transistors follows the same trends as that in MOS devices. Interface states should anneal out at temperatures in the 100 to 200°C range and trapped charge should be removed between 150 and 300°C. Some relaxation may occur even at room temperature. Many, but not all, bipolar devices can be annealed by baking although quite a large amount of damage persists in some types. Thermal annealing as a basic preselection technique is not widely used.

The Irradiate-Anneal (IRAN) preselection procedure involves testing the entire quantity of any device proposed for use. On the basis of test results and design criteria, in the form of specified allowable degradation, the acceptable devices are retained (those that degraded within acceptable limits) and the unacceptable ones set aside for other, less critical, uses. Normally, the original (pre-irradiation) electrical characteristics can be restored, through an annealing process, to the samples selected for use without unacceptable loss of reliability. It must then be assumed that any subsequent in-flight irradiation to the same dose levels will cause the devices to degrade to approximately the same extent as during the test in the simulated environment. Following this procedure, the engineer has the added advantage of knowing in advance exactly what the degradation will be. Experiments by RCA and JPL to further evaluate the feasibility of this technique showed that IRAN preselection has limitations. JPL experience uncovered a number of cases where the degradation of devices subjected to re-irradiation was not the same as that of the original IRAN irradiation. From the JPL and RCA results, it would appear that the technique works only for certain bipolar devices.

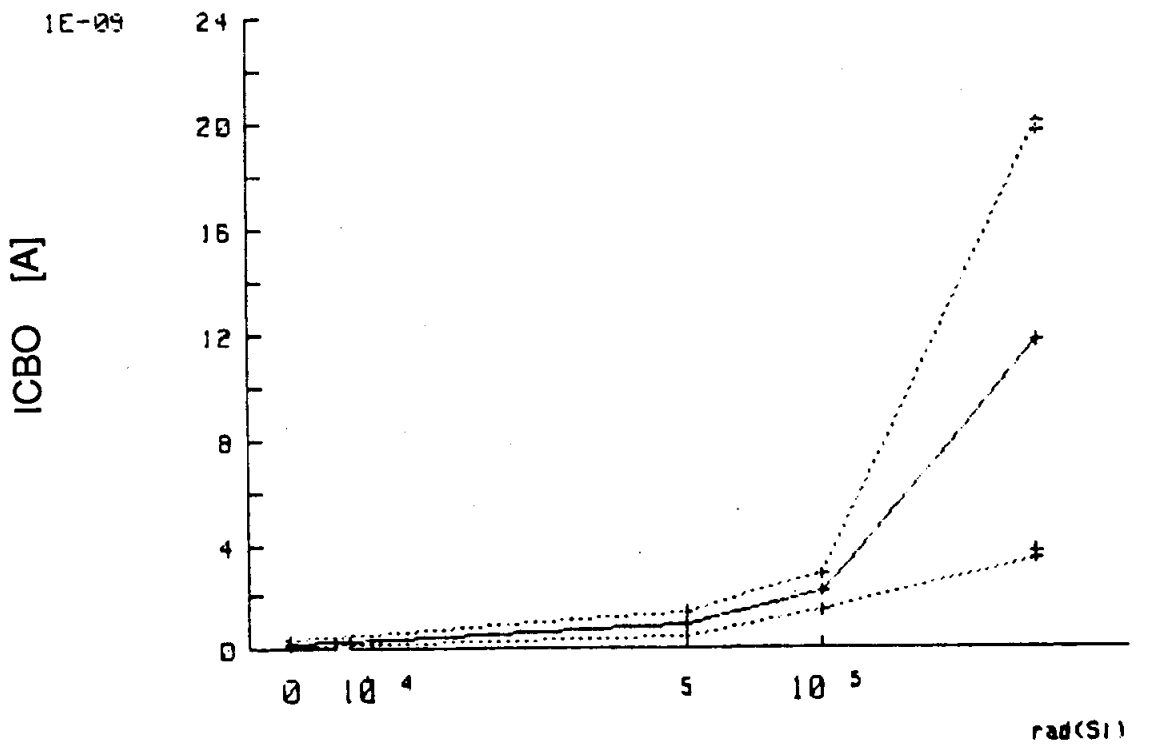

FIGURE 7.7 - EXAMPLE OF RADIATION-INDUCED LEAKAGE CURRENT IN A BIPOLAR TRANSISTOR

7.4.6. Thermal annealing of bulk damage

Radiation-induced displacement defects (bulk damage) in silicon do not anneal easily because the vacancies and interstitials created by the radiation are usually complexed with an impurity atom (oxygen or dopant). The defects which concern us most are those that are stable at room temperature, e.g. the 'A' centre (complex of a vacancy with oxygen) and the centres designated 'E' (phosphorus vacancy complex), 'J' (di-vacancy) and 'K' (divacancy-oxygen complex). These centres are completely stable at temperatures below 200°C, but the damage often anneals between 200 and 450°C completely. It is not easy to diagnose the damage effect in a commercial device. However, some information on the defects involved in transistor damage has been obtained by isochromal annealing in which devices are heated for the same time at several evenly spaced temperature steps.

7.4.7. Saturation voltage

The well-known "knee" in a plot of 'I_C' versus 'V_{CE}' with 'I_B' constant) for a bipolar transistor occurs at a low value of 'V_{CE}' (typically 0.1 to 1V). "Saturation" occurs when 'V_{CE}' falls to the same order of voltage as the forward voltage on the base-emitter junction 'V_{BE}'. As 'V_{CE}' falls, the collector-base junction, which must be biased in the reverse direction in order to produce high gain, becomes forward-biased. The transistor is then said to be in "saturation". As a result the gain falls dramatically, producing the "knee" in the 'I_C' and 'V_{CE}' curves. For certain types of application (saturated switches, power transistors), it is necessary for transistors to operate in saturation. An increase in the saturation voltage '$V_{CE(SAT)}$' is usually harmful. By decreasing gain and increasing the resistivity of the silicon, particle irradiation can increase the '$V_{CE(SAT)}$' value. For measurement purposes, '$V_{CE(SAT)}$' is usually defined as the 'V_{CE}' value required to produce a given value of 'I_B/I_C' ("forced gain") near the "knee" described above. Figure 7.8 shows the changes induced in the saturation region by neutron irradiation. Owing to the effects described earlier, gain has fallen, but increases in silicon resistivity have also affected the 'V_{CE}' values required for a given ratio of 'I_B' to 'I_C' in saturation. For example, at 'I_B' = 50 mA (forced gain = 2), the required 'V_{CE}' value has been changed from 0.2 to 1.3V by an exposure of 1.3×10^{14} n.cm^{-2} (reactor neutrons).

An increase in the values of '$V_{CE(SAT)}$' under particle irradiation is important for "saturation bipolar logic" devices such as the TTL series. In logic devices, when the pull-down transistor is turned hard "on", the value of the voltage drop across the device is low and equal to '$V_{CE(SAT)}$'. If the silicon forming those junctions increases in bulk resistivity, then that voltage drop will increase. This effect, in

turn, causes a change in logic output and moreover produces higher power dissipation in the silicon.

In power transistors, changes of the above sort are also serious because, in "high-voltage types", silicon of low resistivity is employed in the collector so that low values of breakdown are avoided. When the initial doping levels are low, a given particle fluence will alter the resistivity of the silicon more radically than that of a heavily doped material. Thus, in high-voltage power transistors, the increase in 'V_{CE}(SAT)' proceeds more rapidly under neutron exposure than in "low-voltage" amplifying or "fast" logic devices possessing heavily doped collectors. For example, a fluence of 10^{12} n.cm^{-2} may cause a "high-voltage" device to undergo 100% change in 'V_{CE}(SAT)' while a "low-voltage" device may undergo only a few per cent change.

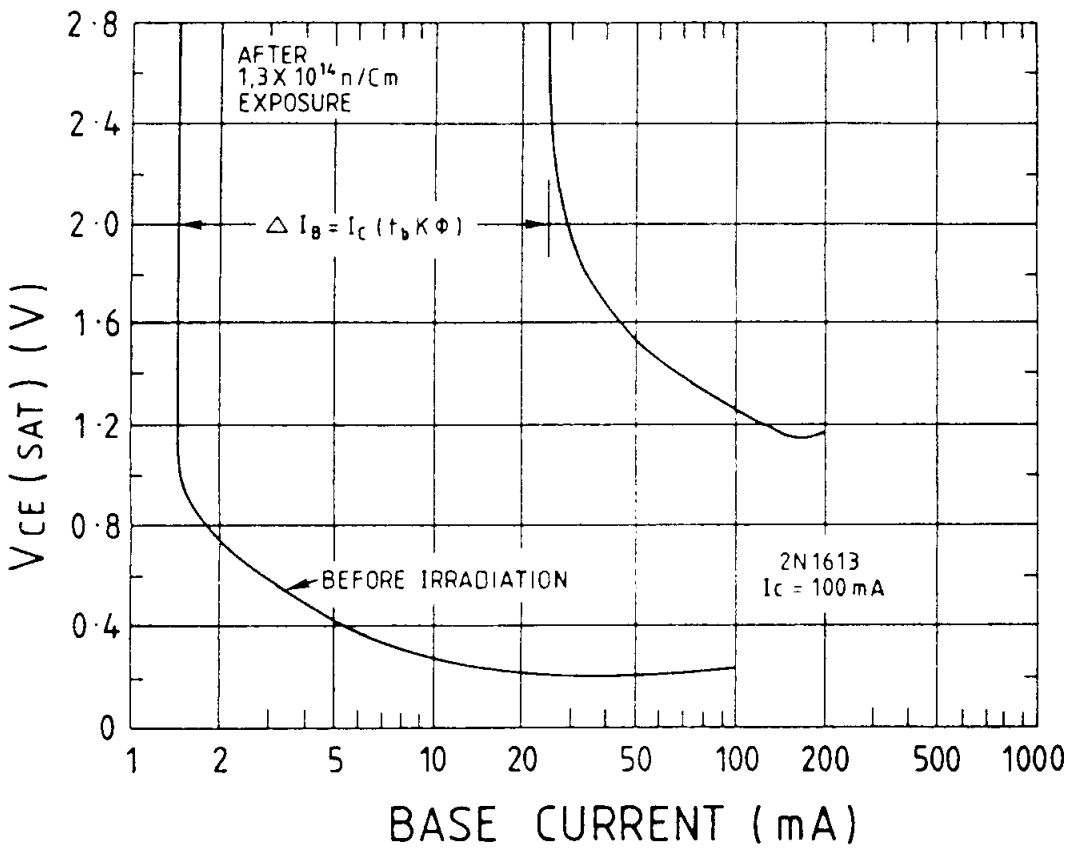

(1.3 x 1014 n cm^{-2} ; E > 10 keV) (after Larin)

FIGURE 7.8 - CHANGE IN SATURATION VOLTAGE OF A SILICON NPN MEDIUM POWER BIPOLAR TRANSISTOR (2N1613) UNDER REACTOR NEUTRON/GAMMA IRRADIATION

7.5. BIPOLAR TRANSISTORS - SUMMARY

The effects of radiation on bipolar transistors can be divided into surface bulk effects as follows:

Type of effect	Phenomenon	Deleterious effects	Important radiation types	Damage units
Surface effects	Ionisation in oxides Photocurrent	Changes in surface properties	- Space - Gamma radiation - Electron beams	rad (Si)
Bulk effects	Atomic displacement	Changes in current-carrier properties (bulk damage)	- Nuclear reactors - Nuclear weapons - Particle beams	Equivalent 1 MeV electrons or neutrons
Transcient effects	Photocurrent generation	No long-lived effects unless latch up or burn out levels are reached	- Pulsed radiation	Not applicable

Physical analysis of these responses is possible and methods of systematic prediction and control of the responses are available. It should be mentioned that these methods require detailed knowledge of process techniques and solid-state physics.

REFERENCES

W.M. Webster, Proc. IRE 42 914-920 (1954).

L.L. Sivo, "Relative Role of Charge Accumulation and Interface States in Surface Degradation (NPN Planar Transistors)", paper presented at IEEE Nuclear and Space Radiation Effects Conference, Seattle, Wash. (July 1962).

W.C. Cooley and R.J. Janda, "Handbook of Space Radiation Effects on Solar Cell Power Systems", NASA Report SP-3003 (1963).

R.R. Brown, "Proton and Electron Permanent Damage in Silicon Semiconductor Devices", Boeing Report D2-90570 (1964).

G.J. Brucker, W.J. Dennehy and A.G. Holmes-Siedle, IEEE Trans. Nuc. Sci., NS-12 (5), pp. 69-7 (Oct. 1965).

G. Messenger and J. Spratt, IEEE Trans.Nucl.Sci. NS-12(2), pp. 53-74 (April 1965).

J.E. Drennan and D.J. Hamman, "Space Radiation Damage to Components and Materials", REIC Rept. 39, Battelle Memorial Institute, Columbus, Ohio (Jan. 1966).

R.R. Brown and W.E. Horne, "Space Radiation Equivalence for Effects on Bipolar Transistors", NASA CR-814, U.S. Dept. of Commerce, Washington D.C. (July 1967).

G.J. Brucker, "Correlation of Radiation Damage in Silicon Transistors Bombarded by Electrons, Protons and Neutrons", Proc. Symp. of Radiation Effects in Semiconductor Components, Toulouse, France (March 1967).

J.P. Mitchell and D.K. Wilson, Bell System Tech. J. 46(1) (1967).

F. Larin, "Radiation Effects in Semiconductors", London, Wiley (1968).

H.J. Stein and R. Gereth, J. Apply. Phys. 39 (6) pp. 2890-2904 (1968).

F. Larin, "Radiation Effects in Semiconductor Devices", Wiley (1968).

W.J. Poch and A.G. Holmes-Siedle, IEEE Trans.Nucl.Sci., NS-15(6), p. 213 (Dec. 1968).

W. Dennehy, A. Holmes-Siedle and K.H. Zaininger, "Digital Logic for Radiation Environments", RCA Review 30(4), pp. 668-708 (Dec. 1969).

A. Holmes-Siedle and W.J. Poch, "The Design of a Weather Satellite to Withstand the Radiation Environment", J.B.I.S. 24(5), pp. 273-288 (1971).

E.H. Snow, H.P. Albus, A.Y.L. Yu, R.E. Hurslson, D.A. Tremere, "Study of Radiation Effects on Novel Semiconductor Devices", AFCRL-70-0586, Fairchild Res. & Dev., Palo Alto, Cal. (Aug. 1970).

F. Coppage, IEEE Trans.Nucl.Sci. NS-22(6), pp. 2336-2339 (Dec. 1975).

V.A. Van Lint, G. Gigas and J. Barengoltz, IEEE Trans.Nucl.Sci. NS-22(6), pp. 2663-2668 (Dec. 1975).

W.E. Price and A.G. Stanley, IEEE Trans.Nucl.Sci. NS-22(6), p. 2669 (Dec. 1975).

R.C. Waggit, Electron, pp. 57-58 (Dec. 1975).

R.F. Donovan, J.R. Hauser and M. Simons, "A Survey of the Vulnerability of Contemporary Semiconductor Components to Nuclear Radiation", AFAL-TR-74-61, U.S. Air Force Avionics Laboratory, Dayton, Ohio (May 1976).

U.K. Ministry of Defense, Report No. SSWL-1291, "Transient Radiation Effects on Electronics; Semiconductors: Data Summary (AWRE 1976).

M. Hartley-Jones, "A Practical Introduction to Electronic Circuits", Cambridge U.P. (1977).

A.G. Holmes-Siedle and R.F.A. Freeman, "Radiation Effects Engineering Handbook", Report R730/8, Fulmer, Stoke Poges (Apr. 1978).

R.A. Berger, J.L. Azarewicz and H. Eisen, IEEE Trans.Nucl.Sci. NS-25, pp. 1555-1560 (1978).

A.G. Stanley and K.E. Martin, Radiation Physics and Chemistry 12, pp. 133-142 (1978).

A.R. Hart, J.B. Smyth Jr., V.A.J. Van Lint, D.P. Snowden and R.E. Leadon, "Hardness Assurance Considerations for Long-Term Ionising Radiation Effects on Bipolar Structures", IEEE Transactions on Nuclear Science NS-25(6), pp. 1502-1507 (Dec. 1978).

R.A. Berger, J.L. Azarewicz and H. Eisen, "Hardness Assurance Guidelines for Moderate Neutron Environment Effects in Bipolar Transistors and Integrated Circuits", IEEE Transactions on Nuclear Science NS-25(6), pp. 1555-1560 (Dec. 1978).

M.S. Cooper, J.P. Retzler and G.C. Messenger, IEEE Trans.Nucl.Sci. NS-26 4758-4762 (1979).

A.H. Johnston and C.A. Lancaster, "A Total Dose Homogeneity Study of the 108A Operational Amplifier", IEEE Transactions on Nuclear Science NS-26(6), pp. 4769-4774 (Dec. 1979).

E.E. King and C.J. Manzo, "Total Dose Failure Levels of Some VLSIC's", IEEE Transactions on Nuclear Science NS-27(6), pp. 1449-1453 (Dec. 1980).

W.E. Price, K.E. Martin, D.K. Nichols, M.K. Gauthier and S.F. Brown, "Total-Dose Radiation Effects Data for Semiconductor Devices", Report No. 81-66, Vols I to III, Jet Propulsion Laboratory, Pasadena, Cal. 91109 (1981 to 1982).

D.R. Alexander and E.W. Enlow, "Predicting Lower Bounds on Failure Power Distribution of Silicon NPN Transistors", IEEE Transactions on Nuclear Science NS-28(6), pp. 4305-4310 (Dec. 1981).

R.D. Blice and J.H. Collins, "Analysis of the Behaviour of Integrated Schottky Logic in Neutron Total Dose and Dose Rate Environments", IEEE Transactions on Nuclear Science NS-28(6), pp. 4366-4375 (Dec. 1981).

D. Bräunig, F. Wulf, W. Gaebler and A. Boden, "GfW Handbook: Irradiation Test Guidelines for Radiation Hardness of Electronic Components", 1st Edition". GfW Report No. TN 53/10, HMI Report No. HMI-B380, Hahn-Meitner Institut für Kernforschung, Berlin GmbH (Dec. 1982).

SIRE Data Book (Semiconductor Index of Radiation Effects), issued by U.K. Ministry of Defence (PE), TS(NUC)3a, Whitehall, London SW1A 2EU, U.K. (Issue 1, April 1982).

F.W. Poblen, R.G. Carroll, D.A. Whitmire, B.W. Cheney and D.L. Walthall, "Total Dose Response of STL and 1 L Logic Devices", IEEE Transactions on Nuclear Science NS-29(6), pp. 1727-1732 (Dec. 1982).

N.E. Baxter, I. Collings, C.J. Hill and B.C. Roberts, "Evaluation of the Radiation Hardness of the Ferranti F100-L Microprocessor in an Operating System", IEEE Transactions on Nuclear Science NS-29(6), pp. 1737-1739 (Dec. 1982).

J.P. Woods and J.V. MacPhee, "Total Dose Susceptibility of the SBP 9989 Microprocessor", IEEE Transactions on Nuclear Science NS-29(6), pp. 1740-1745 (Dec. 1982).

"Semiconductor Index of Radiation Effects (SIRE)", issued by U.K. Ministry of Defence (PE) Dept., TS (NUC) 3a, London SW1A 2 EU, England (Issue 1, April 1982).

R.L. Pease, R.M. Turgler, D. Platteter, D. Emily and R. Blice, "Total Dose Effects in Recessed Oxide Digital Bipolar Microcircuits", IEEE Transactions on Nuclear Science NS-30(6), pp. 4216-4223 (Dec. 1983).

M.K. Gauthier and D.K. Nichols, "A Comparison of Radiation Damage in Linear IC's from Cobalt-60 Gamma Rays and 2.2 MeV Electrons", IEEE Transactions on Nuclear Science NS-30(6), pp. 4192-4196 (Dec. 1983).

Werner, J. Electrochem. Soc. 123 (4), pp. 5

PAGE INTENTIONALLY LEFT BLANK

SECTION 8. DIODES

8.1. INTRODUCTION

The semiconductor diode performs a large variety of electronic functions. These include rectification or "blocking", switching, photo-current generation, light emission and Zener breakdown at an electronic barrier, most commonly a diffused p-n junction (Grove, 1967). Other barriers include epitaxial and implanted junctions, the heterojunction and the Schottky barrier. Materials include silicon, germanium and all the compound semiconductors. P-n junctions form sub-elements of all integrated circuits (e.g. source/drain junctions of MOS devices), but this section will discuss mainly the discrete silicon p-n junction diode.

Unless heavy neutron irradiation is involved, rectifying action is not affected seriously by radiation; optical diodes, however, may be seriously affected (see e.g. Martin et al (1983); Eisen & Wengen (1982)).

8.2. MECHANISMS

The changes in minority-carrier lifetime, τ, and resistivity, ρ, produced in silicon by bulk radiation damage are reflected in the response of p-n junction devices to radiation. In a p-n junction, both forward and reverse I-V characteristics contain lifetime terms. For forward current:

$$I_F \propto \frac{\sqrt{\rho}}{\tau} \qquad \text{.....8(i)}$$

where I_F is the forward current for a given voltage. The reverse current is composed of diffusion and generation current.

The latter is increased if τ is reduced:

$$I_{gen} \propto \sqrt{\frac{1}{\tau}} \qquad \text{.....8(ii)}$$

The reverse diffusion current which flows when a diode is illuminated also contains a lifetime term:

$$I_{diff} \propto \frac{1}{\tau} \qquad \text{.....8(iii)}$$

Thus, we can estimate the effects which a given amount of lifetime damage will produce although, in the case of reverse leakage current, the magnitude of surface leakage is usually greater than either of the above terms and less predictable. Carrier removal will,

of course, also increase the voltage drop produced by a current flowing across the base region of a diode. The principles described above apply also to the metal-semiconductor junction diode (Schottky barrier) used in some nuclear diodes, photodiodes and integrated circuits.

"Surface effects" on several device structures (e.g. rectifier diodes and transistors) are described later. The term embraces a wide range of effects which vary with the treatment applied to p-n junctions where they meet a surface. In oxide-passivated ("planar") diodes, it is predictable that surface leakage will be increased by irradiation. Normally, the magnitude of surface effects will be determined by the ionising dose received, such dose having an ionisation, not a bulk damage effect.

8.3. EQUIVALENT FLUENCES

It is often possible to "simulate" the effect of irradiation of one particle by using another, more easily available, type of particle. This is discussed more fully under bipolar transistors. However, much of the research into this principle was performed with solar cells as test vehicles (see e.g. G.J. Brucker and B. Markow (1967); B.L. Gregory and F.L. Vook (1968); W. Rosenzweig (1962); J.R. Carter Jr. and H.Y. Tada (1977)).

Table 8(1) shows the relative effect of various particles on solar cells. In the diodes in question, a given fluence of reactor neutrons "is equivalent to" a larger fluence of 10 MeV electrons and a still larger fluence of 1 MeV electrons. In the case shown in Table 8(1), one reactor $n.cm^{-2}$ is equivalent to 2000 normally incident 1 MeV $electrons.cm^{-2}$: a useful conversion when test results are compared.

This convenient principle of equivalent fluences applies to most solar cells because, given this structure, atomic displacement effects ("bulk damage") are dominant degradation mechanisms. The principle need not apply if surface or interface effects are significant, as is the case with many blocking diodes, especially those with the oxide passivated (planar) structure. Some of the data of diodes and transistors presented in this document originate from U.K. defence programmes (Martin et al (1983)). They describe devices tested in the HERALD and VIPER reactors at neutron fluence values in the range 10^{12} to 10^{13} $n.cm^{-2}$ (E_n 10 keV). On the basis of Table 8(1), one could assume the damage-equivalent fluences for a test in a 1 MeV electron beam at 90° incidence to be 2×10^{15} and 2×10^{16} $e.cm^{-2}$ respectively. In comparison with the exposure levels inside spacecraft (less than 10^{13} $e.cm^{-2}$ or 300 Krad), these are very high. The reactor test data are therefore mainly useful in that they provide the design engineer with some documentary evidence of the comparative severity of radiation problems with one device type or another in the space environment

and with guidance as to how to structure the evaluation of radiation at the calculated mission exposure levels.

As Van Lint(1980) says: "The most common need is to establish an upper limit for the damage produced by one particle type (using) experimental data (obtained from) another particle type". He stresses that calculation, although an approximate procedure, is a useful one.

8.4. SOLAR CELLS

The cells in solar-cell arrays on spacecraft are protected by thin cover glasses. The resistivity of the silicon base region may be 1 to 10 ohm.cm, n- or p-type, with various refinements of diode structure. When cells are exposed to space radiation, all of these factors affect their degradation. Degradation versus time predictions in a given orbit are made by a computer program in which all these factors are adjusted (Debruyn and Jensen (1983)). Other forms of optoelectronic diodes are dealt with in later sections.

TABLE 8(1) - CRITICAL PARTICLE FLUXES, ϕCRIT, REQUIRED TO PRODUCE 25% AND 50% DEGRADATION OF SHORT-CIRCUIT CURRENT UNDER AM = 0 ILLUMINATION OF 10 OHM.CM N-ON-P SILICON SOLAR CELLS (1)

	ϕ crit (25%)	Damage ratio $\frac{K\tau \text{ (particle)}}{K\tau \text{ (1 MeV)}}$	ϕ crit (50%)	Damage ratio
10 MeV protons	8.0×10^{12}	6250	1.8×10^{13}	6666
Reactor neutrons	2.5×10^{12}	2000	6.0×10^{13}	2000
10 MeV electrons	3.0×10^{14}	16.7	8.0×10^{15}	15
1 MeV electrons	5.0×10^{15}	1.0	1.2×10^{17}	1.0
Co-60 gamma rays	1.8×10^{18}(2)	0.003	–	–

NOTES

1. Values taken from "The Solar Cell Radiation Handbook", Report No. 21945-6001-RU-00 (TRW Systems Group, Redondo Beach, Cal., USA, 28 June 1973: Fig. 3-6, pp. 3-21).

2. This fluence yields a dose of approx. 10^9 rad (Si).

8.5. LOW-POWER RECTIFIER DIODES

Low-power rectifier diodes are usually of a planar structure and exhibit low leakage before irradiation. Thus, small radiation-induced alterations in surface charge may produce noticeable effects on the measured leakage even though such leakage does not often become a serious functional hazard. A typical result of electron beam irradiation, carried out by JPL on a sample group of GE 1N4148 signal diodes, is given by Stanley et al (1976) and Price et al (1981/82). After a fluence of 10^{13} electrons.cm^{-2} of energy 2.2 MeV, an ionising dose of approx. 300 Krad (Si), the mean reverse leakage current at 15V increased from a fraction of a nanoampere to about 1 nA. However, the device did not exceed the specified value of 25 nA. Only a very small change in the forward characteristic was observed. The authors of the JPL test report comment elsewhere (Price et al (1981/82)) that diodes, when exposed to such doses as used, exhibit "inherent radiation hardness" and that consequently not many tests on diodes were performed. The above is borne out by test results from other European programmes. However, Bräunig et al (1981) also discuss elsewhere the occurrence of "mavericks", i.e. exceptionally sensitive diodes (Wagemann et al (1973)).

One U.S. manufacturer advertises a radiation-characterised form of diode, type 1N5430. This diode has a guaranteed performance after a fast neutron dosage, ϕn , of 10^{14} n.cm^{-2} ($\Sigma > 10$ keV; isotope gamma rays of the order of 10^5 rads can be assumed to accompany the neutron). Typically, the reverse current at 50V increases from 20 to 22 nA at $\phi n = 10^{14}$ cm^{-2} and 32 nA at $\phi n = 10^{15}$ cm^{-2}. Minimum and maximum limits of certain post-irradiation parameters are given in the data sheets.

Generally, low-power silicon rectifiers exposed to a fluence of 3×10^{12} reactor neutrons.cm^{-2} show a small change in forward voltage drop of the order of ±5%. Such a change can normally be neglected. On the other hand, in some tests (Eisen and Wenger (1982)), changes in reverse leakage were found to be as large as 500% if the initial leakage was low, e.g. in the 10 nA range, the post-irradiation values being in the region of 100 nA. In this case, the effect would be produced by the ionisation accompanying the reactor neutron fluxes used for testing.

It is to be expected that reverse leakage currents will be both noticeable and more severe when a diode is under a high reverse voltage or when low leakage currents may affect the circuit as, for example, in photomultiplier circuitry.

8.6. HIGH-POWER RECTIFIER DIODES

In high-power diodes, an increase in the forward voltage drop may be of greater significance than in low-power devices because power dissipation will increase noticeably. After 3×10^{-2} n.cm^{-2} (reactor), an increase in forward voltage drop as large as 100% at 1A was observed in some power rectifiers (Eisen and Wenger (1982)). It is probable that types which exhibit a much smaller change are available.

8.7. ZENER DIODES

At reactor neutron exposures in the 10^{12} cm^{-2} range, Zener breakdown voltages do not change more than 10 mV, well within the limits of the usual commercial devices.

Bräunig et al (1981) show a similar change from a fluence of 10^{13} cm^{-2} of 2.2 MeV electrons.

8.8. LIGHT-EMITTING, PHOTO- AND NUCLEAR DIODES

These devices degrade quite strongly under particle radiation. They are discussed in detail in a later Section.

8.9. CONCLUSIONS

Although the reaction of diodes to irradiation is generally much less profound than that of transistors, semiconductor diodes have active junctions and may develop leakages or undue forward resistance when irradiated heavily under demanding stress conditions.

REFERENCES

D. Bräunig, W. Gaebler, W.R. Fahrner and H.G. Wagemann (1981) "GfW Handbook for Data Compilation of Irradiation-tested Electronic Components, 1st Edition", Report No. HMI-B248 (TN 53/08) DFVLR/BPT and Hahn-Meitner Institut für Kernforschung, Berlin, W.Germany (Nov. 1977); 2nd Edition by F. Wulf, D. Bräunig and W. Gaebler, HMI-B353 (June 1981)

G.J. Brucker and B. Markow, Proceedings of 6th IEEE Photovolta ic Specialists' Conference, Florida, March 1967 (IEEE, New York, 1967)

J.R. Carter Jr. and H.Y. Tada, "Solar Cell Radiation Handbook", JPL Publication 77-56 (TRW Systems Group, Redondo Beach, Cal., USA and Jet Propulsion Laboratory, Pasadena, Cal. 91109, November 1, 1977)

J.D. Debruyn and L.H. Jensen, "The Uniflux System", ESTEC - EWP-1309 (European Space Technology Centre, Noordwijk, The Netherlands, July 1983)

H. Eisen and C. Wenger (1982), "Radiation Effects on Semiconductor Devices (Data Summary), Report No. HDL-DS-82-1 (Component Response Information Center, Harry Diamond Laboratories, Adelphi, MD October 1982)

B.L. Gregory and F.L. Vook (ed.), "Radiation Effects on Semiconductors" (Plenum, New York, 1968)

A. Grove (1967), "Physics and Technology of Semiconductor Devices", (Wiley 1967)

R. Martin et al (1983), SIRE Data Book (Semiconductor Index of Radiation Effects), issued by U.K. Ministry of Defence (PE), TS (NUC)3a, Whitehall, London SW1A 2 EU, UK (Issue 1, April 1983)

Note: the information in this report is not secret, but distribution may be restricted to certain agencies.

W.E. Price, K.E. Martin, D.K. Nichols, M.K. Gauthier and S.F. Brown, "Total Dose Radiation Effects Data for Semiconductor Devices", Report No. 81-66, Vols I to III (Jet Propulsion Laboratory, Pasadena, Cal. 91109, 1981 to 1982)

W. Rosenzweig, Bell Sys.Tech. J., 41 1573-1588 (1962)

A.G.Stanley, K.F. Martin and S. Douglas, "Radiation Design Criteria Handbook", Techn. Memo 33-763 (Jet Propulsion Laboratory, Pasadena, Cal. 91109, Aug. 1, 1976)

V.A. Van Lint, T.M. Flanagan, R.E. Leadon, J.A. Naber and V.V. Rogers (1980), "Mechanisms of Radiation Effects in Electronic Materials", Vol. I (Wiley, New York, 1980)

H.G. Wagemann, A. Spencker, D. Bräunig, J.C. Roncin and G. Pelous (1973), "Radiation Test and Preselection of Maverick Diodes for the Project Symphonie Satellite", Microelectronics and Reliability, 12 467-472

PAGE INTENTIONALLY LEFT BLANK

SECTION 9. JUNCTION FIELD-EFFECT TRANSISTORS

9.1. INTRODUCTION

The silicon junction field-effect transistor (JFET) has many of the characteristics required to withstand heavy radiation damage. Amplification is produced by the transport of majority carriers through a channel which is quite heavily doped. Unlike the MOSFET, current flow is remote from the surface of the silicon. Thus, both the major effects which degrade bipolar and MOS transistors in a radiation environment (ionisation and bulk damage) are absent. Commercial JFET devices have indeed proved in practice to be tolerant of the effects of heavy ionisation and bulk damage, and some work has also been done in the USA to produce special JFET devices which are even more tolerant of neutrons. Despite these advantages, the use of the JFET in "hardened" equipment has not been extensive. For space environments, where ionisation is dominant, the advantages are not as great as in nuclear environments. However, in the field of instrumentation amplifiers, the properties of the silicon JFET as a low-noise, high-impedance input device have already been appreciated in commercial use and are attractive for some uses in space. The gallium arsenide JFET is now increasingly used in microwave circuits.

As expected, gamma and particle irradiations to a total dose of 10^6 rads cause only minor degradation in JFET (Martin, 1985; Rudie, 1972). Normally, transconductance, pinch-off voltage, "on" resistance and other channel parameters are practically unchanged. Due to oxide charge build-up, surface leakage may manifest itself as an increase in I_{GSS} , but this appeared to remain in the nanoampere range under the highest doses used. Reactor neutron irradiation causes minor degradation at 10^{13} n.cm^{-2}. , but severe degradation at 10^{15} n.cm^{-2}.

Notthoff (1971) finds that matched pairs of discrete commercial JFET devices, which are suitable as input devices for a differential amplifier, operate well after exposure to a reactor neutron fluence of about 10^{14} n.cm^{-2}.. Compared with bipolar equivalents, integrated operational amplifiers with JFET structures as input devices may therefore be preferred for very high radiation environments. Other radiation-hardened circuits that include JFET's are multiplexers and ladder networks for data-acquisition circuits. An application which suggests itself for future space use is as the amplifying element for a highly exposed photodetector, say in the parts of a data link which must survive for a long time in a robot exposed to reactor or RTG radiation. A "Photo JFET" would consist essentially of a photodiode with built-in amplification by the JFET mechanism. No test data are available for this type of device. However, if radiation problems associated with amplification or light detection arise in future

projects, the possibilities of JFET devices should be investigated in some detail.

A more specialised device that has been finding commercial use lately is the microwave JFET in silicon or gallium arsenide. The mobility of III-V semiconductors leads to good high-frequency operation. GaAs FETs are used routinely as low-noise input devices for microwave amplifiers, while very fast logic devices are under development. Several investigations have shown that neutron irradiation of GaAs FETs has the effects predicted. Studies of bulk properties on III-V compounds, for example, have shown the reduction of conductivity. As for silicon devices, the resulting device degradation only becomes apparent in the range 10^{14} to 10^{15} $n.cm^{-2}$ (1 MeV).

Several authors emphasise that the JFET structure is "hardenable" and the choice of electronic devices in very high particle fluxes may often lie between vacuum tubes and specially "hardened" JFETs. This choice applies to amplification, switching and light detection.

REFERENCES

J.M. Borrego, R.J. Gutmann, B. Moghe and M.J. Chudzicki, "Radiation Effects on GaAs MESFET's, IEEE Transnucl.Sci. NS-26 (6), pp. 1436-1443 (Dec. 1978)

J.M. Borrego, R.M. Gutmann and S.B. Moghe, IEEE Trans.Nucl.Sci. NS-26 (6), pp. 5092-5100 (Dec. 1979)

B. Buchanan, R. Dolan and W. Shedd, IEEE Proceedings 55 (12) (Dec. 1967)

W.L. George, IEEE Trans.Nucl.Sci. NS-16 (6) (Dec. 1969)

D. Long, IEEE Trans.Nucl.Sci. NS-18 (6), pp. 332-339 (Dec. 1971)

K.E. Martin et al, "Total Dose Radiation Effects Data for Semiconductor Devices" JPL Publication 85-43, Vol. 1, NASA-JPL, Pasadena, CA (1985)

D. Neamen, W. Shedd and B. Buchanan, IEEE Trans.Nucl.Sci. NS-22 (6), pp. 2203-2207) (Dec. 1975)

D.M. Newall, P.T. Ho, R.L. Mencik and J.R. Pelose, "Total Dose Hardness of Microwave GaAs Field-Effect Transistors", IEEE Trans.Nucl.Sci. NS-28 (6), pp. 4403-4406 (Dec. 1981)

J.K. Notthoff, IEEE Trans.Nucl.Sci. NS-18 (6), pp. 397-403 (Dec. 1971)

N. Rudie, "Principles and Techniques of Radiation Hardening", (Western Periodicals (1972))

W. Shedd, B. Buchanan and R. Dolan, IEEE Trans.Nucl.Sci. NS-16 (6) (Dec. 1969)

M. Simons, IEEE Trans.Nucl.Sci. NS-26 (6), pp. 5080-5086 (Dec. 1979)

R. Zuleeg and K. Lehovec, IEEE Trans.Nucl.Sci. NS-25 (6), pp. 1444-1449 (Dec. 1978) IEEE Trans.Nucl.Sci. NS-26 (6), pp. 1436-1443 (Dec. 1978)

R. Zuleeg and K. Lehovec, "Neutron Degradation of Ion-implanted and Uniformly Doped Enhancement Mode GaAs JFET's", IEEE Trans.Nucl.Sci. NS-25 (6), pp. 1444-1449 (Dec. 1978)

R. Zuleeg, J.K. Notthoff and G.L. Troeger, "Ionising Radiation Response of GaAs JFET's and DCFL Circuits", IEEE Trans.Nucl.Sci. NS-29 (6), pp. 1656-1661 (Dec. 1982)
R. Zuleeg, J.K. Notthoff and G.L. Troeger, "Channel and Substrate Currents in GaAs FET's due to Ionizing Radiation", IEEE Trans.Nucl.Sci. NS-30 (6), pp. 4151-4156 (Dec. 1983)

SECTION 10. POWER DEVICES

10.1. GENERAL

The power subsystems of large space equipment, radiation-generating equipment and nuclear power sources are frequently required to be capable of handling high currents and voltages greater than the kilowatt range.

Additionally, the other subsystems require local regulation by power transistors, thyristors, large rectifiers etc. Silicon power devices of the type described operate on the same general principles as the junction devices discussed earlier, but their construction is often different: the chip is larger and may even be in the form of a "pellet" having the full diameter of the source ingot (say, 30 mm). Epitaxial growth is used more extensively in power devices, while special doping (e.g. neutron transmutation) and unusual geometry are required to achieve a high junction breakdown voltage, low "on" resistance and good heat removal. In general, locally low levels of doping are required for high-voltage devices and, in terms of radiation-effect engineering, this is significant because carrier removal due to particle irradiation will be more noticeable. Also, in order to accommodate large depletion regions, large values of base width are required in the design of power transistors and thyristors. This can impart unusually high sensitivity to gain degradation (see Section "Bipolar Transistors").

In some respects, the power MOS device is also structurally different from its low-power relatives (see, for example, "VMOS" and "HEXFET" construction). Nevertheless, the response of the gate oxide layer - probably the dominant effect in space and gamma rays - can still be predicted by the methods described earlier.

10.2. BIPOLAR POWER TRANSISTORS

The degradation of gain in transistors under particle irradiation has been discussed earlier and details of commercial power transistors were given. It can be seen that unless these devices are carefully selected, neutron-induced damage becomes serious below a fluence value of 10^{12} n. cm^{-2} (1 MeV). To understand the generally high radiation sensitivity of power devices, it is necessary to outline the theory of transistor breakdown and its influence on base width. The avalanche breakdown voltage of the collector-base junction of a silicon transistor, BV_{CBO}, is highest when the collector region is very lightly doped. To a first approximation:

$$BV_{CBO} = \frac{2 \times 10^{17}}{N_{coll}} \qquad \text{.....10(i)}$$

where N_{Coll} is the doping concentration in units per cm^3 in the collector region. Thus, for a breakdown voltage greater than 100V, a doping level of less than 2.5×10^{15} cm^{-3} is necessary. This is equivalent to a resistivity higher than 2 ohm. cm.

Now, the practical limit of collector-to-emitter voltage in transistor operation is, in fact, lower than this value. The reason is that two collective effects occur in the npn or pnp structures, the "punch-through" and the "open-base" effect. At high collector-base voltages, the depletion region of the collector-base junction extends completely through the base region. If this occurs, the collector-emitter voltage is, in a sense, "shorted" because the p-type base region, once depleted, no longer rectifies. A large current, I_{CE}, flows between emitter and collector. This punch-through conduction is at its highest when the base contact is "open". The base region is then floating (i.e. capable of taking up the potentials due solely to I_{CE}) and the net result is that I_{CE} (in this case termed I_{CEO}) is increased further by the amplifying action of the npn structure. As a result, the "breakdown value of V_{CE} with base open" (BV_{CEO}) is lower than BV_{CBO} with a ratio:

$$\frac{BV_{CBO}}{BV_{CEO}} = (h_{FE}), \qquad \text{.....10(ii)}$$

where h_{FE} = is the forward gain of the transistor.

To achieve a high value of V_{CE} before punch-through occurs, a wide base is required. Other factors being equal:

$$BV_{PT} \propto W_B \qquad \text{.....10(iii)}$$

where BV_{PT} is the punch-through value of V_{CE} and W_B is the base-width.

The above rationale leads to the conclusion that, for the design of high-voltage power transistors (devices in which the value of the rated V_{CEO} is high), we require two physical features which lead to high sensitivity to neutron irradiation, namely:

(a) a low doping level for the collector and
(b) a high base width.

Additionally, and in accordance with equation 10 (ii), the initial value of h_{FE} must be kept intentionally as low as possible. Thus, only a small "margin" for neutron-induced degradation will exist. Typical values for the rated parameters of a power transistor are:

Device type	V_{CEO} (max) (V)	h_{FE} (max) (I_C/I_b)	f_T (min) (MHz)	Power (max) (W)	Process specification
1	400	40	50	10	P 48
2	100	120	2	120	P 4A

To give an example of particle effects at neutron fluences of 2×10^{12} and 7×10^{11} cm^{-2}, a transistor of type 1 would lose respectively about 50 and 10% of its gain, while a specimen of type 2 would lose respectively 99 and 90%. This illustrates how voltage and power specifications alter the "hardness" obtainable from bipolar power transistors.

Despite the large junction areas, it is unlikely that transient, ionisation-induced leakage currents will be of any importance at the expected dose rates in space. A typical response to ionising dose rate is 5×10^{-9} A.rad.s. Similarly, at the high values of "drive" used, the impact of surface effects on gain and leakage (which are induced by ionisation and are important for low-power transistors - see earlier) is unlikely to add significantly to the large particle effects described above.

In the USA, radiation-hardened power transistors have been developed. Epitaxial collector regions are carefully adjusted for doping level and minimum acceptable widths (to minimise change in $V_{CE(SAT)}$) and base regions are adjusted to the minimum acceptable width (to minimise gain degradation). An example of the data for some advanced power transistors capable of operating reasonably well after a neutron fluence of 10^{14} $n.cm^{-2}$ has been given earlier. Ferranti have performed comparative neutron tests in the 10^{-12} to 10^{13} $n.cm^{-2}$ range on single diffused and planar-epitaxial power transistors.

10.3. THYRISTORS (previously known as silicon controlled rectifiers)

To perform triggering functions, the 4-layer thyristor structure requires high values of gain in the overlapping npn and pnp structures of which it is composed. Similar arguments indicate the need for:

- high base widths and resistivity values, as described for power transistors,
- a high doping uniformity to avoid the local triggering which is often induced if local regions of low resistivity are present,
- low minority carrier lifetime values in certain junction regions to avoid charge storage effects which induce slow turn-off.

Optically triggered thyristors are becoming widely used.

In these devices, one should anticipate some severe radiation-induced effects, arising in both the optical and the semiconductor media. For reactor neutron fluences higher than 10^{12} n.cm^{-2} (1 MeV), it has been shown (SPIRE, 1980) that the characteristics of switching may change radically in existing commercial thyristors. The gate current at the triggering point may increase over 10 times and also the "holding current", while the forward voltage drop in the "on" condition may double owing to resistivity effects. Boswell and Widdows (1976) also found that, for certain commercial thyristor types, triggering parameters degrade suddenly as the neutron dose is increased. Few problems appear until a fluence of 2 x 10^{12} has been passed but, thereafter, parameters change at a rate more than linear.

10.4. POWER MOS FETs

10.4.1. Introduction

While MOS transistors for logic switching are being reduced to outline dimensions smaller than 10 µm on a side for VLSI chip technology, MOS transistors for power control are being enlarged to sizes up to 10 mm on a side. However, the power MOS transistor actually comprises many thousands of vertical MOS structures connected in parallel (typically, over 50,000). Hence, the technology bears some resemblance to that of integrated circuits. The gate oxide technology is similar to MOS integrated circuits and, hence, the same rules as for radiation hardness apply. Although some research efforts have been made to achieve radiation hardening (Roper and Lowis, 1985), no hardened MOS power devices are available commercially at the time of writing (1986).

10.4.2. Parameter changes under irradiation

The response of power MOS devices to radiation is mainly characterised by:

1. Threshold voltage shift,
2. Transconductance degradation and
3. Reduction in breakdown voltage.

(a) Threshold voltage shift.
As for other MOS devices, the shift of threshold voltage, V_T, is negative and shows a significant bias dependence (Seehra and Sluzark, 1982; Adams and Minnee, 1982). The following are typical test data of an 100V, 40 A, n-channel commercial MOS power transistor:

Bias during irradiation (V_I)	Failure dose (Krads)
+10V d.c.	25
+10V to 0V (switched, 50% cycle)	30
-10V d.c.	25
+5V d.c.	30
-5V d.c.	45
0V	100

(b) Transconductance degradation.
This occurs as a result of mobility reduction due to interface state generation. However, significant changes in transconductance occur only at comparatively high doses - above 1 Mrad (Roper and Lowis, 1983).

(c) Reduction in breakdown voltage (BV).
Drain-source breakdown voltage (BV_{DS}) shows significant reduction as a function of total dose. The mechanism is believed to be charge trapping in the field oxide and generation of interface traps at the field oxide/silicon interface (Blackburn et al, 1983). The trapped charges alter the potential at the surface of drain and source junctions and hence become part of the junction termination and influence the breakdown voltage. The reduction of breakdown voltage is a strong function of the drain-source voltage applied during irradiation.

Typical changes in BV, noted during irradiation of a 500V n-channel device, are -40V at 1 Mrad for zero bias and -140V at 50 Krads for 300V bias. The behaviour at high drain-source voltages (>200V) during irradiation shows a sharp decrease in BV at low voltages and then an increase at about 150 Krads, followed by a small, gradual decrease. This implies that, in the rather low total dose environment of space, the reduction in breakdown voltage may be significant and must be considered in conjunction with normal derating requirements.

10.4.3. Radiation-tolerant power MOS circuits

Scope exists for radiation tolerance to be introduced as part of the circuit-design procedure when power MOS is used. In view of the earlier discussion of V_T and BV_{DS} bias dependence, it is clear that circuit designs should minimise both the magnitude and the

application time of bias voltages. For example, "overdrive" (i.e. the use of a negative gate voltage to turn off an n-channel transistor) should be applied with caution because the enhanced radiation sensitivity resulting from the use of gate bias may dominate (Adams and Minnee, 1983). Inverter circuits should be tested as complete circuits as it is found that a combination of dynamic switching and self-heating of transistors leads to a higher tolerance to radiation than simple assessments would indicate.

10.5. CONCLUSIONS

Of the many classes of semiconductor devices used in space equipment and other lightweight electronics, silicon power devices are among those few whose high sensitivity to damage from specific particles must be given major consideration. Calculations given in earlier chapters show that because of the high base-width values of such devices, electron and neutron fluences as low as 10^{14} and 10^{11} cm^{-2} respectively may cause significant degradation in bipolar junction devices. The behaviour of the power MOS device resembles that of its corresponding smaller relation, the MOS switching device.

REFERENCES

L. Adams and J. Minnee, "Radiation Evaluation of Application Circuits for Power MOSFET Technology", ESTEC Report MISC 235 (Oct. 1983)

L. Adams and J. Minnee, "Bias Dependence of IRF 150 HEXFET Transistors under Ionising Radiation", ESTEC Report MISC 197 (May 1982)

D.L. Blackburn et al, "The Effect of Ionising Radiation on the Breakdown Voltage of Power MOSFET's", IEEE Trans.Nucl.Sci. NS-30 (6), pp. 4116-4121 (Dec. 1983)

J. Bosnell and S. Widdows Royal Signals and Radar Establishment (1976)

H.H. Fry et al, IEEE Spectrum, pp. 57-60 (March 1980)

A. Grove, "Physics and Technology of Semiconductor Devices", Wiley, New York (1967)

A. Holmes-Siedle, Fulmer Report R 829/2 (1979)

F. Larin, "Radiation Effects in Semiconductor Devices", Wiley, New York (1968)

J. Minnee, "Radiation Sensitivity of Power MOSFET HEXFET Transistors IRF 150, 350 and 9132", ESTEC Report MISC 148 (1982)

Nat. Semiconductor Corp., "Discrete Databook", Sta Clara, USA, pp. 46 et seq. (1978)

P. Noll, Personal communication

G.B. Roper and R. Lowis, "Development of a Radiation-hard N-channel Power MOSFET", IEEE Trans.Nucl.Sci. NS-30 (6), pp. 4110-4115 (Dec. 1983)

S. Seehra and W.J. Slusark, "The Effect of Operating Conditions on the Radiation Resistance of VDMOS Power FET's", IEEE Trans.Nucl.Sci. NS-29 (6), pp. 1559-1564 (Dec. 1982)

SPIRE Data Compilation, U.K. Ministry of Defense (1980)

R.C. Waggitt, Electron, pp. 57-58 (Dec. 1975)

PAGE INTENTIONALLY LEFT BLANK

SECTION 11. OPTICAL MEDIA

11.1. GENERAL

The generation of colour centres in optical media by displacement and ionisation effects has been mentioned earlier under the heading "Dielectrics" in the overall survey of radiation-induced responses and is discussed below. In this Section, the windows, lenses and coatings likely to be used in radiation environments are considered. The special subject of optical fibres is dealt within Section 12. The optical path lengths in the media discussed here range from a few micrometres (coatings) to a few centimetres (lenses). Unless otherwise stated, it will be assumed that the pieces of glass or other optical medium considered are in the thickness range 1 mm to 1 cm and that the performance losses of interest are greater than about 20%, such as may be evidenced by visible darkening under irradiation. Translated into other absorption units, the range of concern constitutes values greater than the following:

Absorption:	20%
Absorption :	1 dB
Loss rate:	1 dB mm^{-1} or 10^6 dB.km^{-1}
Optical density:	0.1
Absorption coefficient:	0.2303 cm^{-1} or 2303 μm^{-1}
Transmission :	90% (assuming 100% initially)

11.2. COLORATION IN OPTICAL MATERIALS

Transparent solids are normally insulators which also have the property of good light transmission. This is because the forbidden energy gap in these materials is sufficiently large to prevent visible light easily exciting electrons from the conduction to the valence band. However, if radiation or impurities produce defects in the material, visible light may be absorbed because it can now excite electrons into the defects. The intrinsically clear material then becomes coloured. For this reason, optically-absorbing, radiation-induced defects in transparent solids are known as "colour centres".

The original work on colour centres concerned alkali halides, which are particularly susceptible to the formation of defects under irradiation. Since then, the field has been extended to cover transparent oxides, such as silica and magnesium oxide and their glassy derivatives. Some colour centres are even used in generating laser beams.

The type of centre most commonly associated with radiation-induced coloration is an ionic vacancy produced by the radiation in the lattice of a crystalline material. However, in many engineering materials, defects exist in the material as processed, and irradiation merely serves to excite electrons into these defects. The latter is the

case for most optical glasses, many of which become deeply coloured on exposure to several kilorads of gamma rays or particles. The effect is also turned to good use in some types of dosimeter, which use either the absorption or the associated luminescence as a means of measuring dose.

The nomenclature for simple colour centres is as follows. Anion vacancy centres are known as F centres; these may exist in charged, uncharged or aggregated forms, which bear appropriate subscripts. Cation vacancies are known as V centres, of which there is also a variety.

The effect of composition on radiation-induced absorption in multicomponent glasses is reviewed by Lell et al. (1966) and Stroud et al (1965). Figure 11.1 shows absorption curves from Lell et al. (1966) which demonstrate the variety of absorptions to be expected from optical media and the effect of alkali.

The examples shown are "soft" alkali silicate glasses, but the principles also hold for optical glasses although absorption is often less in the latter. In Figure 11.2 and Table 11(1), Sigel and co-workers at NRL (Evans and Sigel, 1975) have compared the radiation-induced losses in a variety of useful optical glasses. The relevant values at 800 nm vary between approximately the same sensitivity as that of the soft glasses shown in Figure 11.1 (e.g. a loss for lead-flint glass of 1.3 $dB.km.^{-1}$ rad^{-1}) and a sensitivity 300 times lower (zinc crown at 0.04 $dB.km.^{-1}$ rad^{-1}).

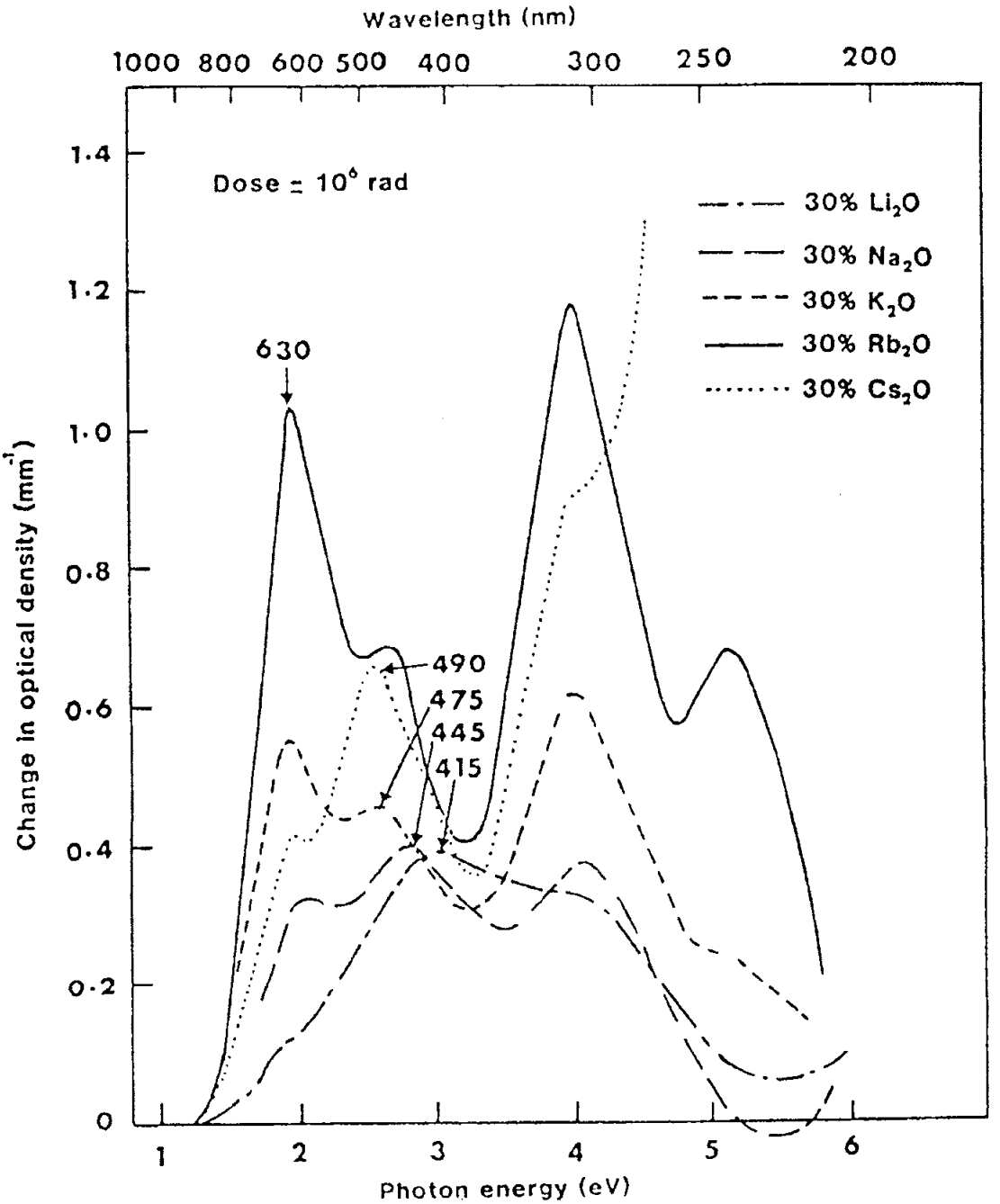

Radiation-induced absorption of various alkali silicate glasses about 1 mm thick. All appear to have a specific radiation response at 820 nm of the order 1 dB.km.$^{-1}$ rad^{-1} and exhibit an absorption peak near 630 nm (after Kats and Stevels).

FIGURE 11.1 - RADIATION-INDUCED ABSORPTION OF VARIOUS ALKALI SILICATE GLASSES ABOUT 1 MM THICK

TABLE 11(1) - RADIATION-INDUCED LOSS PER UNIT DOSE IN SELECTED BULK GLASSES AND FIBRES (AFTER EVANS AND SIGEL, 1974/1975)

SOURCE	CODE	TYPE	CORE MATL.	FORM OF GLASS	RESPONSE[a] - (dB(km-rad(Si))$^{-1}$		
					λ = .8μm	.9μm	1.05μm
Corning	(CGW)	5010	Pb FLINT	FIBER	5.4	2.5	0.50
Pilkington	(PBL)	HYTRAN	Pb FLINT	FIBER	4.5	1.9	0.50
Galileo	(G)	0001AA	Zn CROWN	FIBER	1.5	0.49	0.25
Schott	(S)	F2	Pb FLINT	BULK	1.3	0.69	0.21
dividing line for values above and below 1 dB/km at λ = 0.8μm.							
NRL		GL2382	BaLa CROWN	BULK	0.65	0.35	0.16
Galileo	(G)	0001AB	Zn(.3% Ce) CROWN	FIBER	0.27	0.0062	0.0026
NRL[b]	-	GL2364	BaLa(1% Ce) CROWN	BULK	0.21	<0.18	---
Owens Corning	(OCF)	X-4147A	Zn CROWN	BULK	0.040	0.020	<0.016
Schott[c]	(S)	F2G12	Pb(1.2% Ce) FLINT	BULK	<0.01	---	---
Schott	(S)	R1	Pb(~1% Ce)	FIBER	0.0031	0.0015	0.0010
Corning	-	-	SiO_2(Ti)	FIBER	8×10^{-1}	-	-
Corning	-	-	SiO_2(Ge)	FIBER	1.4×10^{-2}	-	-
NRL	-	-	Soda-lime Silicate glass	BULK	1×10^{-2}	-	-
NRL	-	-	Suprasil I	BULK	$<1\times10^{-5}$	-	-

(a) Except where mentioned, readings made 1 hour after γ-irradiation

(b) 30 min after γ-irradiation (c) 9 min after γ-irradiation

As regards the visible spectrum, virtually all multicomponent silicate glasses behave like silica in that the radiation-induced absorption in the blue end of the spectrum is much higher than in the red (see Figure 11.2). The radiation-induced loss at 400 nm is usually 10 times higher than at 800 nm. Thus, 20% loss at 800 nm would imply 50% loss at 600 nm and 90% at 400 nm. For these values of loss, samples have a pronounced red-brown or deep yellow colour, depending on the exact spectral shape. A 10-component camera-lens system, irradiated to 10^5 rad, suffered initially similar values of loss, but the coloration faded by about 50% over a few months. Some elements appeared gray rather than brown (Holmes Siedle, unpublished work).

In the design of optical systems tolerant to radiation, the implication is that light in the blue or UV region will be more difficult to handle than red or near IR. Lenses should be tested for radiation-induced loss and for the post-irradiation fading of that loss with time.

"Hardened" optics, pure sapphire and synthetic fused silica have been shown to be extremely insensitive to radiation-induced losses in the visible region (see, for example, Yale, 1968 and Cooley et al., 1963).

11.3. COATINGS

The small optical path length in a typical optical coating (order of micrometres) prevents the development of serious radiation-induced losses in the visible region. The optical properties of films and the effects of radiation on film-forming glasses are reviewed by Wong and Angell (1976). It is unlikely that changes of refractive index, shrinking or swelling will affect optical coating performance under exposure to nuclear and space environments.

11.4. CONCLUSIONS

In the thickness range 1 - 10 mm, many glasses show measurable losses in the dose range 10^4 to 10^6 rads. Thus, optics exposed to space and nuclear radiation may suffer significant losses. Some "hardened" optical glasses are available commercially.

The data given in this section are illustrative only and variation may be expected between batches of material. Samples from batches of material selected for flight use should be tested to verify radiation response.

Since optical media may be subject to "annealing", both temperature and dose rates are important test parameters.

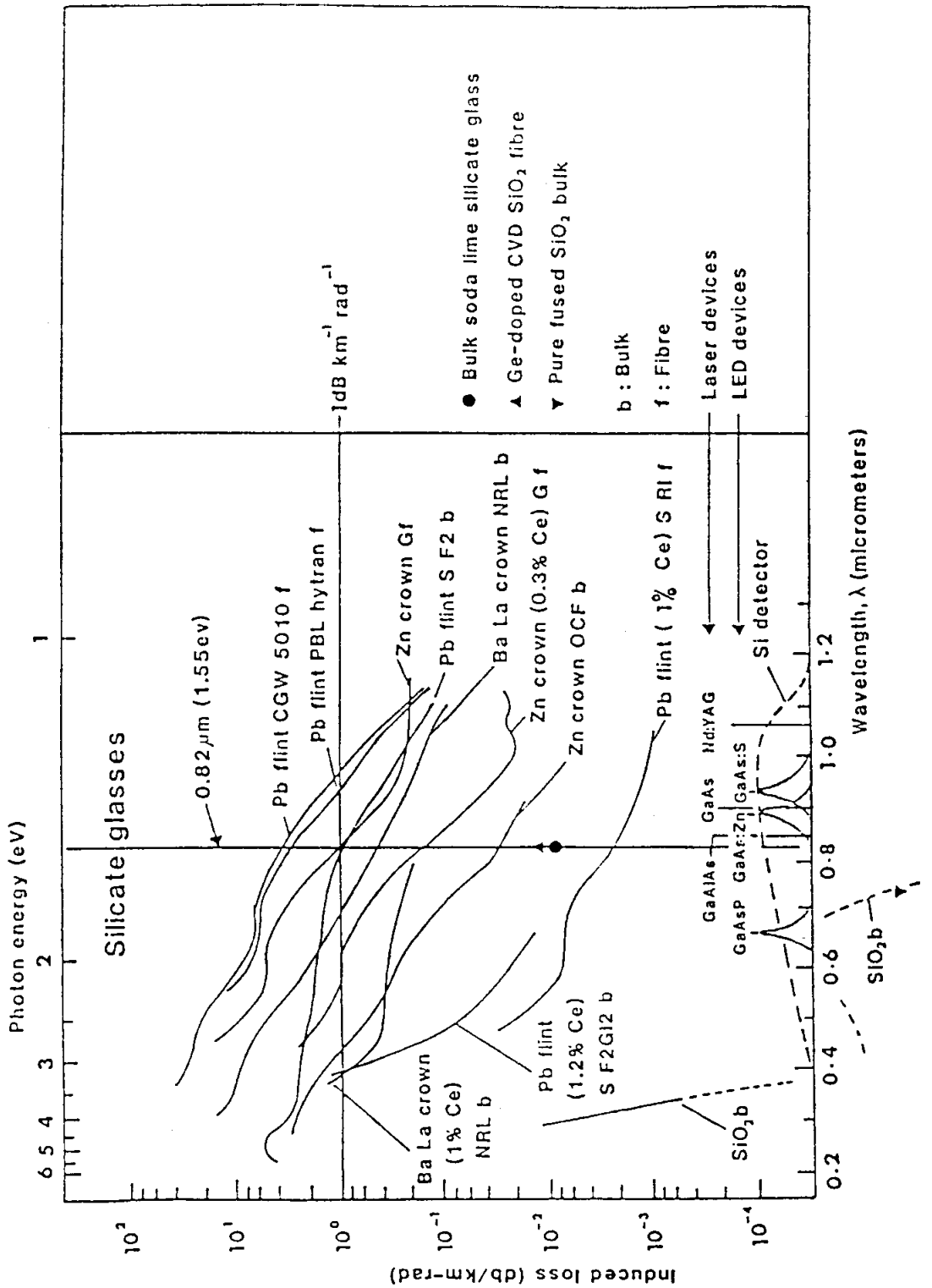

Radiation-induced losses in bulk silicate glasses and fibres one hour after short room-temperature irradiations. Doses ranged from 2 x 10^3 rads (Si) to 5 x 10^5 (Si); at 7 x 10 rads (Si)/s. All curves from Evans and Sigel (1975). Data points from Sigel and Evans (1974), also given on Table 13(1).

FIGURE 11.2 - RADIATION-INDUCED LOSSES IN BULK SILICATE GLASSES AND FIBRES ONE HOUR AFTER SHORT ROOM-TEMPERATURE IRRADIATIONS

REFERENCES

W.C. Cooley and R.J. Janda, "Handbook of Radiation Effects in Solar Cell Power Systems", NASA SP-3003, Appendix A (1963)

B.D. Evans and G.H. Sigel Jr, IEEE Trans.Nucl.Sci. NS-22 (6), pp. 2461-2462 (Dec. 1975)

E. Lell, N.J. Kreidl and J.R. Hensler, Prog. Ceram. Science 4, pp. 1-93 (1966)

W.J. Poch and A.G. Holmes-Siedle, "TOS Radiation Program Report, NAS 5-9034, RCA AstroElectronics Div., Princeton, USA (Sept. 1965)

J.S. Stroud, J. Chem. Phys. 37, pp. 836-841 (1962)

J.S. Stroud, J.W.H. Schreurs and R.F. Tucker, 7th. Intern. Congress on Glass, pp. 42.1-42.18, Gordon and Breach, N.Y. (1965)

J. Wong and C.A. Angell, "Glass: Structure by Spectroscopy", Dekker, Basel (1976)

G.A. Yale, Optical Spectra, pp. 17-23 (Sept./Oct. 1968)

PAGE INTENTIONALLY LEFT BLANK

SECTION 12. OPTICAL FIBRES

12.1. INTRODUCTION

The transmission of digital or analogue information by conversion of the information into the modulations of a light beam is a useful technique for long-range communication or in an electrically noisy environment. RF radiation and magnetic fields can produce electrical transients in metallic conductors, leading to the corruption of data. RF and magnetic fields have no effect on light beams. Plastic and hollow waveguides are sometimes used, but for ruggedness, reliability and high data rates, fibres made from silica glasses are the most highly developed form of optical link. The effect of radiation on silica glasses has been intensively studied and it is possible to say at the outset that, although the effect of radiation on silica materials is considerable, it is tolerable if materials control is exercised. Apart from a general discussion of radiation effects in silica fibre materials, this Section also contains an account of some models for predicting optical loss in fibres.

12.2. DEFECT CENTRES AND ABSORPTION SPECTRA IN SILICA AND GLASSES

12.2.1. General

In this discussion, optical fibre materials will be regarded as being composed of a glassy silica network (O-Si-O-Si structures) in which varying degrees of imperfection are introduced by bond strain or network disrupting atoms. Initially, then, exposure of an ideal silica network, crystalline or amorphous, to ionising radiation should produce no coloration whatsoever, because all bonds are satisfied. Ionisation does not give rise to the displacement of any atoms (as it does in the case of alkali halides) and hence no "colour centres" are formed. In fact, the purest form of silica, pyrolytic fused silica, can be irradiated to a very high dose (10^8 rad) without visible coloration appearing. While pure synthetic crystalline silica (quartz) undergoes no visible coloration, spectroscopy in the UV region reveals a radiation-induced absorption peak. This is probably due to impurities remaining from the additives used for crystal growth. Natural quartz is very impure; when irradiated to a dose of 10^5 rads, strong "smoky" brown coloration is produced. As will be seen later, pyrolitic silica, when intentionally doped or even when subjected to strains during fibre drawing, displays colorations which, in the 10^6 rad range, are visible to the naked eye and may be significant at doses as low as 10^3 rad.

12.2.2. Ionisation effects

Most of the radiation effects in optical fibres are caused by impurities (or strains) introduced intentionally or unintentionally during fabrication. The fabrication process often consists of many stages and is becoming increasingly sophisticated. For example, Figure 12.1 shows the absorption spectra of pure and doped silica material irradiated with ionising radiation (Lell, 1962). Whereas there are two optical absorption peaks in pure fused silica, the alkali-doped samples exhibit three such peaks. The intensities of the latter are larger by at least a factor of 10, having a specific radiation-induced loss value of 1 $dB.km^{-1}$ rad^{-1} in the UV region versus 0.2 $dB.km^{-1}$ rad^{-1} for pure silica and a value of about 0.8 at 600 nm versus 0.1 dB km^{-1} rad^{-1} for pure silica. Aluminium doping, also shown in Figure 12.1, shows the type of effect which the addition of other intentional network-forming dopants can produce. The contrast between alkali and aluminium illustrates a characteristic difference between network disrupting agents (such as alkali) and network formers (Al, B, P). Each disrupting alkali atom produces a non-bridging Si-O group which can then trap a radiation-generated free hole before it recombines. These same trapped-hole species appear to be present in vapour-deposited silica fibre and other heat-treated silicas, probably because thermal treatments can break Si-O-Si bonds and hence create non-bridging oxygens. The hole is trapped in one of the p-orbitals of the oxygen atom.

A common radiation-induced effect in glasses is the production of a yellow or "smoky" coloration. This is produced by the "tail" of a UV absorption peak which intersects the visible region in the blue. An Al colour centre is thought to be the main defect in "smoky" quartz (O'Brien, 1955). Other workers (Friebele et al., 1978) find a similar state of affairs in their spectral measurements for phosphorus-doped optical fibres.

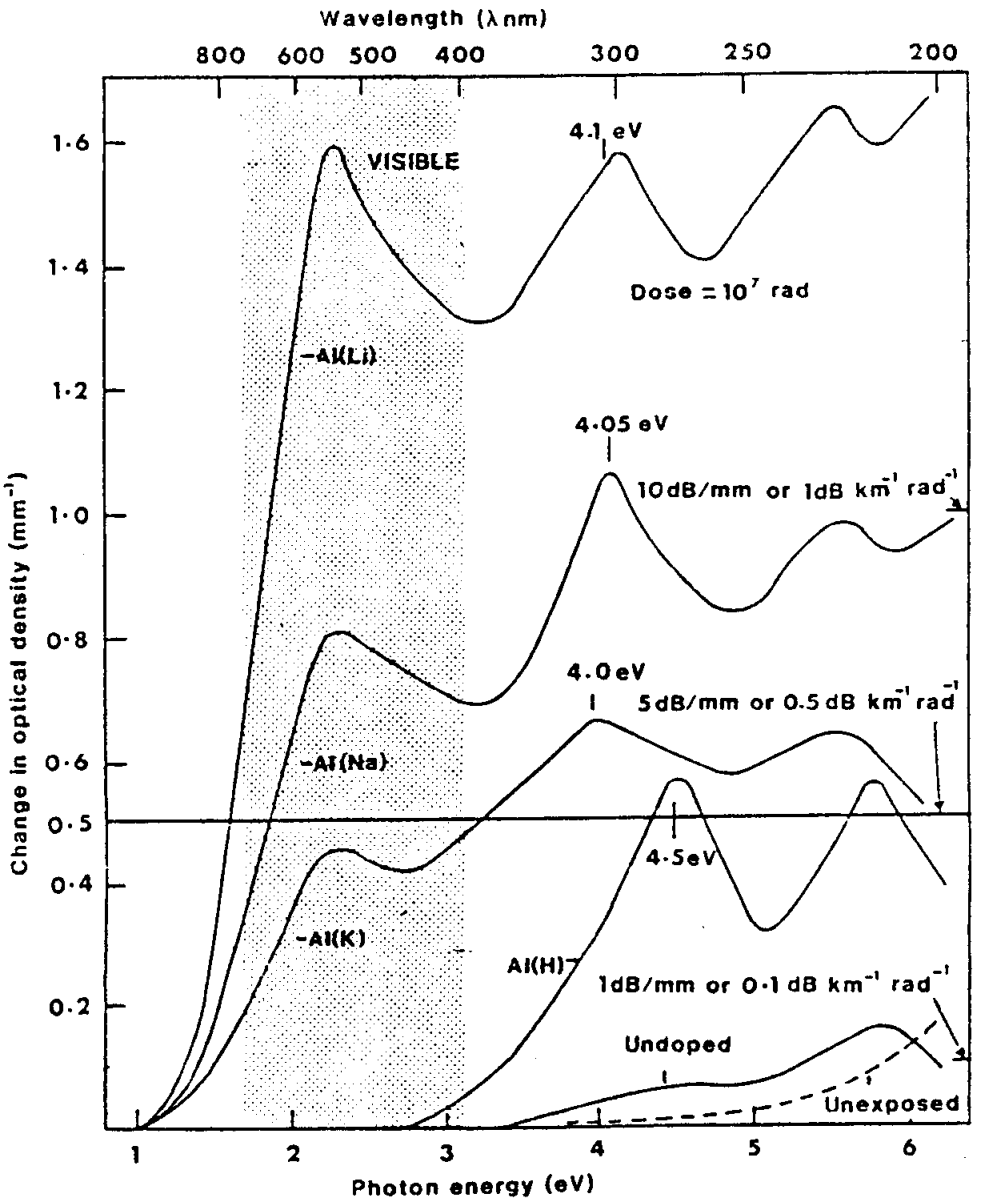

Approximate specific radiation-induced loss values are noted

FIGURE 12.1 - TYPICAL RADIATION-INDUCED LOSS PEAKS IN FUSED SILICA DOPED WITH ALUMINIUM AND ALKALI METALS, FROM 200 to 900 nm (AFTER LELL)

The absorptions occurring in multicomponent optical glasses are usually orders of magnitude stronger than those which occur in the pure or doped silicas discussed above (see Section 11). This is understandable when it is realised that such glasses contain relatively large percentages of alkali or other network-disrupting oxides (Na_2O, CaO, BaO etc.). Each atom of the metal can support a non-bridging oxygen ion of the type which can trap holes. Thus, soda glass is visibly affected at a few thousand kilorads while the effect of a few hundred rads on lead-oxide glass fibre is large enough for a fraction of a metre to provide the sensing element of a personnel dosimeter now under development in the USA. Fulmer Research Laboratories have tested some multicomponent glasses developed for fibre cores by British Telecom. Based on US results, it is expected that, if the exposure dose is in the kilorad range, the use of multicomponent glasses will not even be possible for short runs of fibre.

12.2.3. Particle-induced defects

The studies which have contributed most to our understanding of bulk damage in silica were performed by Arnold and co-workers (1973), using electrons and ions. Studies by Levy (1960) have confirmed that reactor neutrons produce similar defect centres. Early work suffered from the fact that the silica used was often relatively impure.

For present purposes, we need only note that a significant rate of generation of new displacements will only occur in silica samples operating in intense particle beams (e.g. in nuclear equipment). For example, Primak (1980) has described the heavy irradiation of fused silica bars in a fusion-neutron simulation source and calculated the relative defect production rates for neutrons in the fusion energy range. It is not likely that the electron and proton fluxes found within spacecraft will generate a significant number of new defects.

12.3. PREDICTION MODELS FOR OPTICAL FIBRE LOSS VERSUS DOSE

12.3.1. Fundamentals

As mentioned earlier, the fundamentals of the production of colour centres in silica-containing materials have been worked out in great detail by, amongst others, Mitchell and co-workers of Reading University (1956); Weeks and co-workers at Oak Ridge (1960, 1964) who investigated bulk silica, and groups at Reading and Fulmer, including Holmes-Siedle (1974, 1980), who studied thin-film silica physics. These investigations form a body of work which provides a base for models of the effect of radiation on the optical properties of fibres. A preliminary prediction model is outlined below.

An engineering term for the deterioration of optical performance is introduced here, namely dB of loss per kilometre per rad, L_O. The sense of this term, used in engineering for comparing fibres, must be limited because of the known saturation of radiation-induced loss at high doses (10^5 to 10^6 rads) and the decay of loss with time after a pulse of radiation. However, as a means of conveying orders of magnitude in sensitivity - as in the present discussion - the term is useful. Radiation-induced absorptions in fibres in the 0.4 to 1.5 μm range tend to lie in the range 10^{-2} to 10 $dB.km^{-1}.rad^{-1}$. Figure 12.2 shows the simple arithmetical relations between transmission, optical density and loss (loss in dB is found by multiplying optical density by 10; absorption coefficient is a scientific unit which can be easily related to oscillator strength). Figure 12.3 shows how the optical path length of the irradiated sample bears a linear relation to the loss expressed in the usual engineering term, dB per km. We can thus extrapolate simply from short lengths to kilometre distances.

Finally, if radiation-induced loss increases linearly with dose, we can express the characteristic radiation sensitivity of a fibre in terms of "specific radiation-induced loss" in $dB.km^{-1}.rad^{-1}$ at a given wavelength. This should be a characteristic of the material, not altered by sample thickness or type of ionising radiation; it constitutes a useful performance parameter for a fibre system.

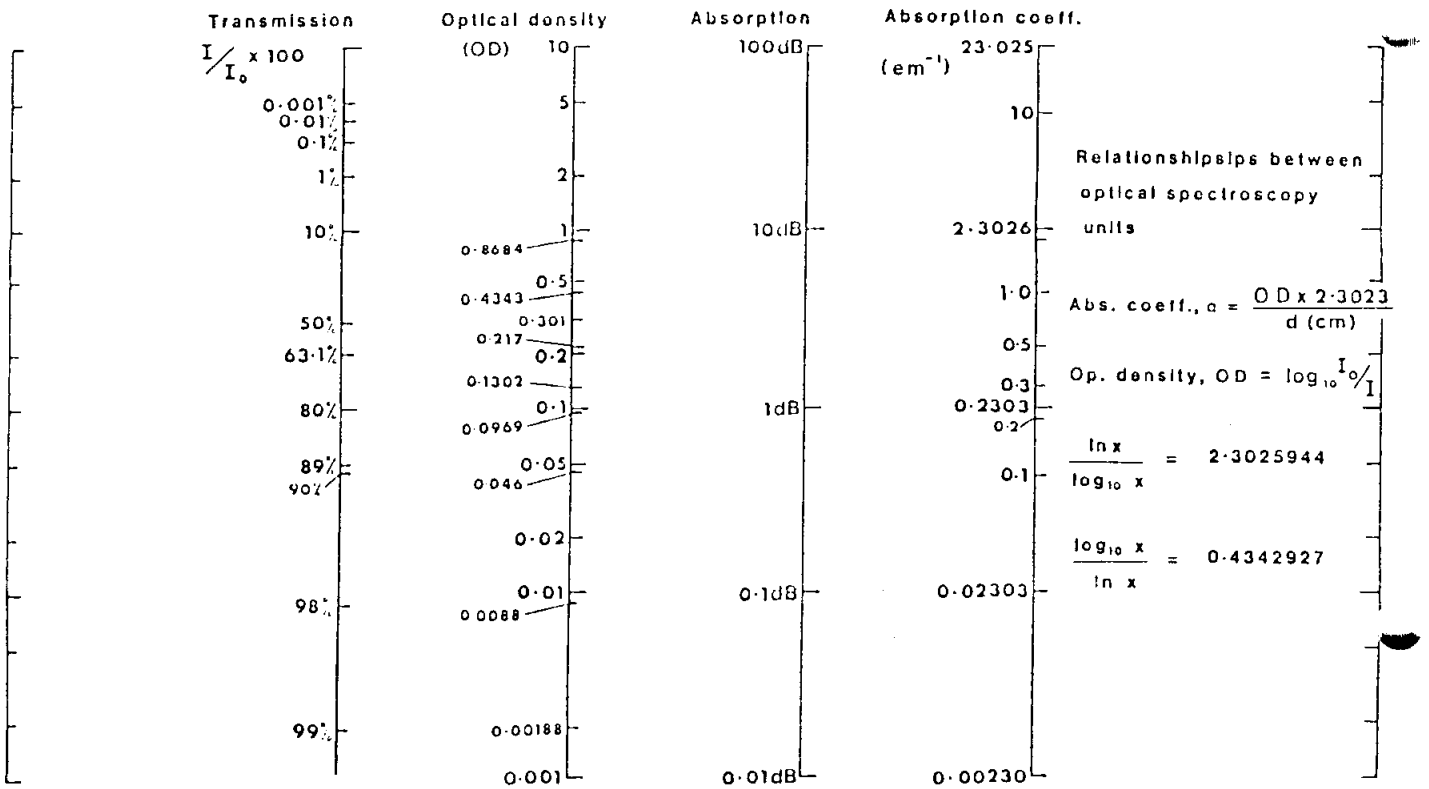

FIGURE 12.2 - CONVERSION CHART FOR FINDING RELATIONSHIPS BETWEEEN OPTICAL ABSORPTION UNITS

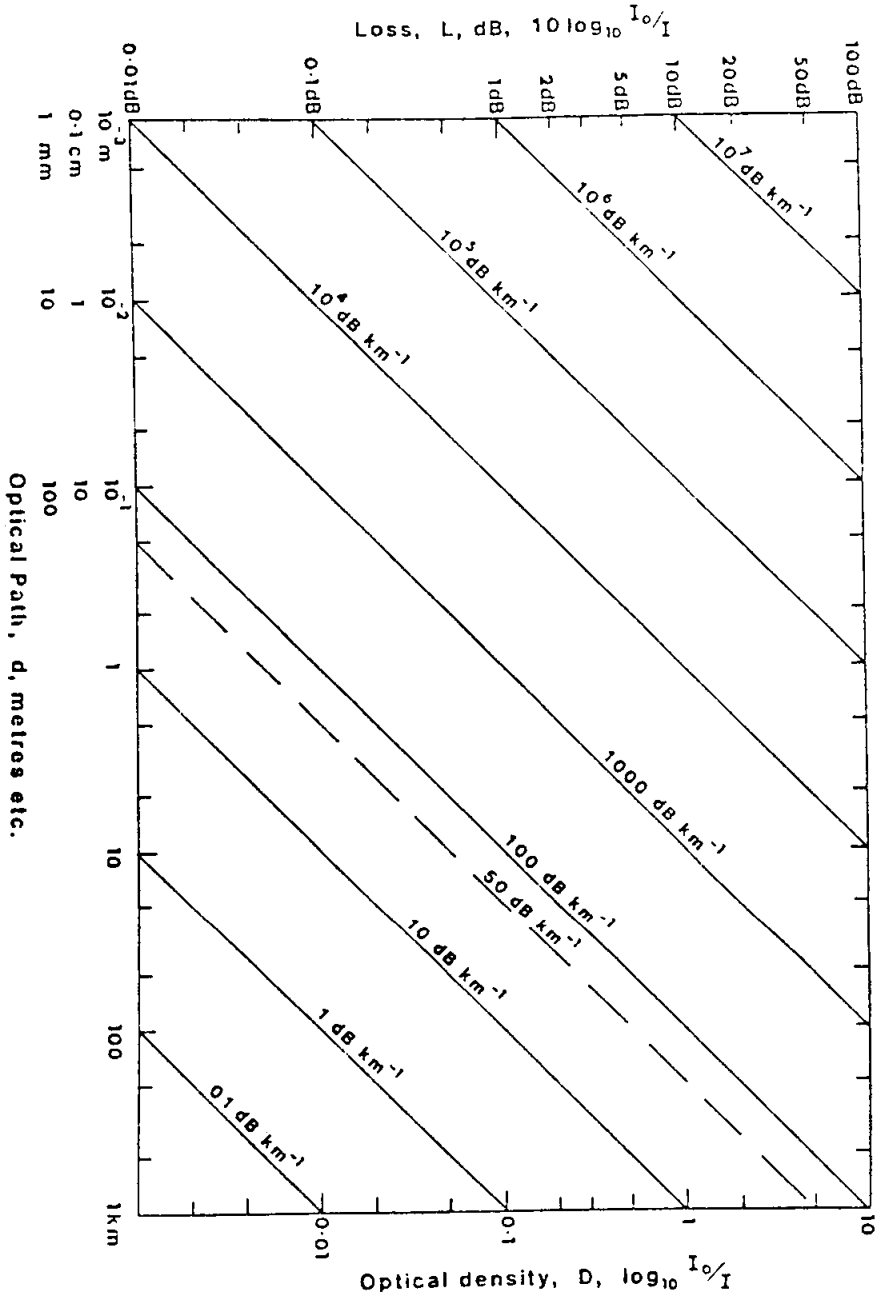

FIGURE 12.3 - CHART FOR CALCULATING LOSS PER KM FROM VALUES OF ABSORPTION AND PATH LENGTH

12.3.2. Simple mathematical model

It is reasonable to expect the build-up in the number of occupied colour-centre defects in (and, hence, the optical absorption of) irradiated silica to be proportional to dose if the fraction occupied is small. The plot or "growth curve" of detectable absorption against dose could thus have the form of a straight line over several decades before the fraction occupied becomes large. At this point, the curve will first become sublinear and finally saturate (become flat). A review of the data of Friebele (1979) shows that the loss versus dose curves do follow this scheme. It appears that the low-dose, linear regions of the curves in a variety of different silica materials have a slope lying between 10^{-2} and 1 $dB.km^{-1}.rad^{-1}$ for the wavelength value 0.82 μm.

Thus, as a model for fibre degradation, upper and lower limits can be postulated as shown in Figure 12.5. This corresponds to an equation:-

$$L = L_0 D \qquad (L \ll L_{sat}) \qquad \text{.....12(i)}$$

where L = loss and D = dose.

The slope L_0, representing the "specific radiation-induced loss", is constant for a given material and, at a light wavelength of 0.82 μm, has the values 1.0 and 10^{-2} for the upper and lower bounds respectively. L_{sat} is the saturation value of loss.

L_0 will be a function of defect concentrations N_1, N_2, etc., the peak absorption wavelength, λ_{peak}, the wavelength of observation, λ_{obs}, the oscillator strength of the defect, S, and the capture cross-section of the defect for charge-carriers. If 'f' is a function of the shape of the absorption band (i.e. of the broadening and "tailing") and the separation between λ_{obs} and λ_{peak}, then the form might be:

$$L_0 \propto S_1 \sigma_1 N_1 f(\lambda) + S_2 \sigma_2 N_2 g(\lambda) \nu \text{ ., etc.} \qquad \text{.....12(ii)}$$

The CVD silica used in fibres is deposited rapidly in layers containing varied amounts of dopant, subjected to several transient heat treatments and then to collapsing and drawing stresses. Therefore, it may not behave as simply as these models imply. For example, the experimental growth curves given by Friebele (1979) show signs of at least two saturating processes. Such effects can be handled mathematically by providing in the equations for the filling of several centres. The question of the creation of new centres by particles can be accommodated by making L_0 a function of particle flux. Some preliminary experiments by Mattern and co-

workers (1975) suggest that neutron displacement effects are of small significance, even in intense reactor environments.

12.4. MODERN VAPOUR-DEPOSITED FIBRE TECHNOLOGY

Figure 12.4 shows a graph compiled after review of the results of recent irradiation of communications fibres of the more advanced type. Such fibres are all made by the successive deposition of silicon dioxide layers on a former or "bait". The constituents used are of the very highest purity, but the refractive indices of different regions are manipulated by the addition of dopants to the stream of silicon tetrachloride which is the source of the silica. The common dopants are gases containing germanium, phosphorus and fluorine. Some forms have as their core section an ultrapure undoped silica, very similar to Suprasil (e.g. the fibre marked "SiO_2: SiO_2(F)" in Figure 12.4). The two solid lines marked "worst case expected" (A) and "best case expected" (B) form approximate boundaries for all of the data of the above type which was included in a survey by Holmes-Siedle (1980). It will be seen that, initially, the curves rise in a linear fashion and, in case B, with a slope of 10^{-2} dB.km^{-1} .rad^{-1}.

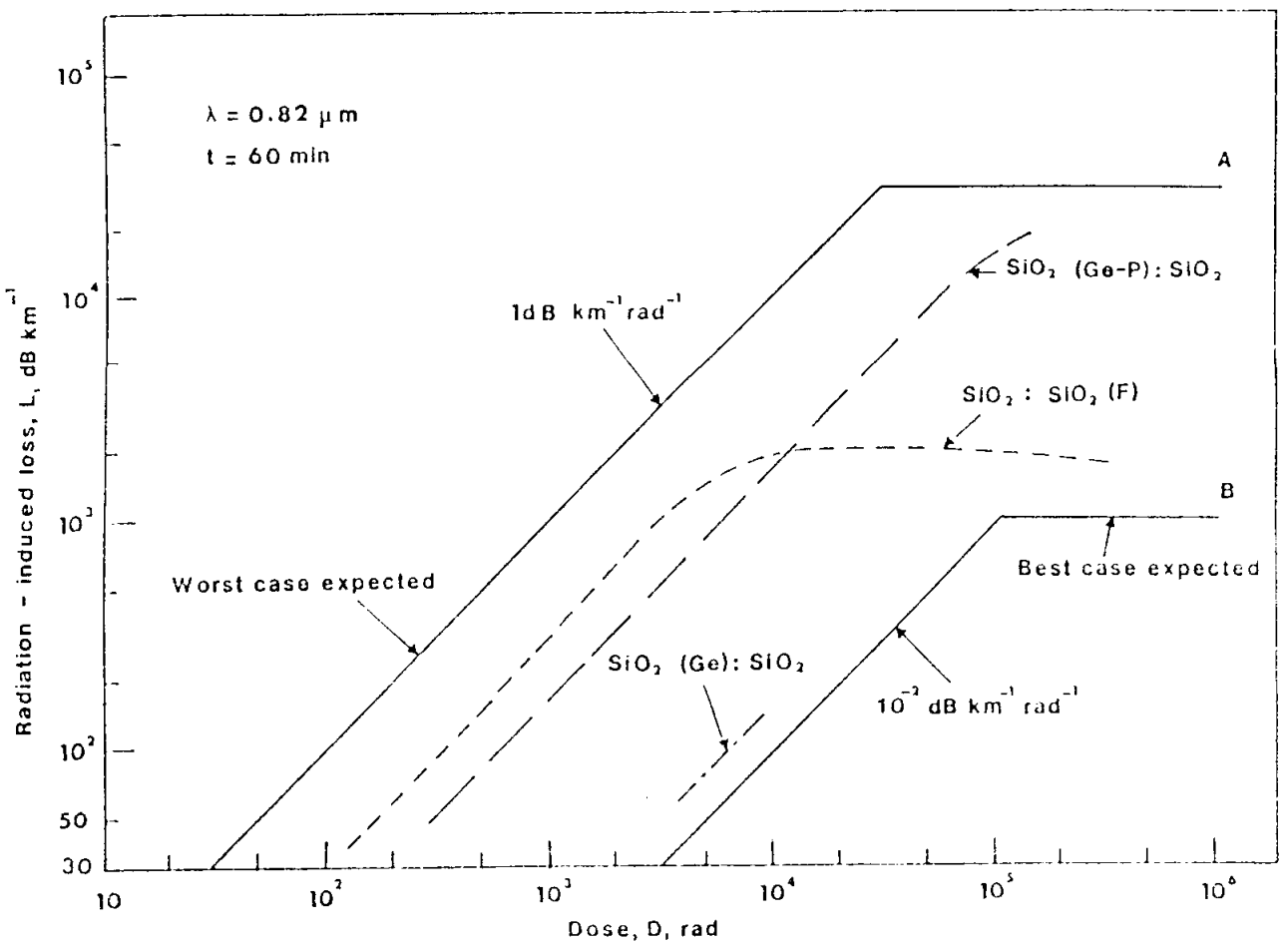

Upper and lower limits (lines A and B respectively) found during a survey of radiation-induced loss in all-silica optical fibres (mainly those tested by E. Friebele, plus some Fulmer experiments). Some examples of experimental results are given, showing the influence of core doping. The first set of symbols represents the core material with doping in brackets: the second represents the cladding material, with doping, if any, again in brackets.

FIGURE 12.4 - UPPER AND LOWER LIMITS

12.5. FIBRES DRAWN FROM SUPRASIL RODS

Plastic-coated silica (PCS) fibres are quite different from the above in several respects. Fabrication is less sophisticated and the fibres produced are not so rugged under the conditions used for splicing or interconnection. A silica rod (of "bulk" - Outer surface Vapour-deposited - OVPO-type, made for many years for other purposes such as optical blanks and made of Suprasil, Amersil, Spectrosil, Corning 7940 or one of the other long-used synthetic silicas) is drawn in an oxyhydrogen flame and then immediately passed through a bath of coating polymer. These PCS fibres are quite low in cost but, with this method, it is difficult to achieve numerical apertures less than 0.15. Low numerical apertures are required for high-rate communication. However, diagnostic instruments and local area networks may not require high data-rate transmission and could employ PCS fibres.

Data for Suprasil by Mattern et al (1975) together with the "best case" line B from Figure 12.4 are plotted in Figure 12.5. The curves for the build-up of absorption as a function of dose for undrawn rods of Suprasil fall below this line. As might be expected, there is an opportunity during the drawing procedure for impurities to be diffused or stresses to be introduced into the fibre. The radiation-induced loss in silica is known to be associated with the presence of impurities (alkalis, hydrogen, etc.). It is therefore not surprising that the one point recorded for "BTL fibre", made from Suprasil, lies above that for the bulk Suprasil road and near to the "best case" line, i.e. the loss is worse because defects have been introduced by processing. In a fibre made from pure Suprasil, coated with plastic (PCS), by Galileo Corp., which was tested by Friebele, Sigel et al in 1978, the loss is already 5 $dB.km^{-1}$ at a dose of 10^2 rads. As can be seen from the diagram, the build-up curve peaks at 10^4 rads and then reduces again. Another curve, F, has a similar shape, but shows a lower loss at all points. The data show a difference of three orders of magnitude in the radiation-induced loss to be found in ultrapure silica rods at the same dose level (as is illustrated by the response of Suprasil SS1, Suprasil SSWF (curve C) and Corning 7940 at 10^8 rads (Point 'o' in Figure 12.5). Even nominally pure silica fibres should therefore be carefully selected and tested.

The effort devoted to the selection of fibres will be influenced by the loss which can be tolerated, the lengths which are in highly exposed locations and the total lengths used.

Radiation-induced loss of ultrapure silica in bulk and fibre forms as a function of radiation dose. Curve B is the lower limit, found by A.Holmes-Siedle in an earlier survey of all-silica (non-plastic fibres. Apart from point D, all other results are for gamma rays at low dose rate (about 100 rad.sec^{-1}). Dotted line, solid lines and open circles - from Mattern et al 1974; chain-dotted and curve E - Evans and Sigel, 1978; curve F -Sigel et al 1979; filled circle - Evans and Sigel, 1975.

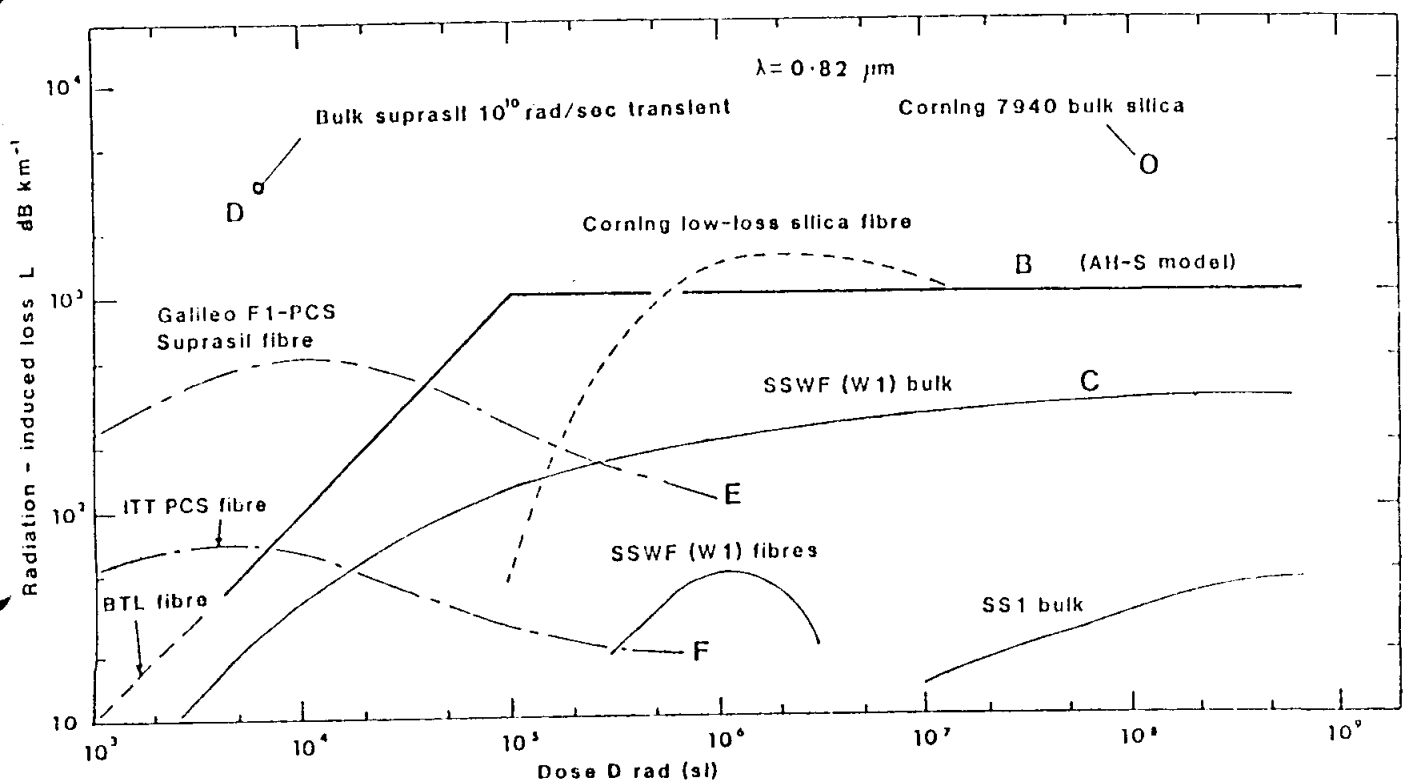

FIGURE 12.5 - RADIATION-INDUCED LOSS OF ULTRA-PURE SILICA

12.6. RECENT DEVELOPMENTS

Modern long-wave IR fibre materials, based on ZrF_4, have been irradiated (Tanimura, Sibley et al, 1985) with 1.7 MeV electrons.

At 10^8 rads, there was intense absorption in the UV and visible regions (absorption coefficient over 100 cm^{-1}).

12.7. FIBRE LUMINESCENCE

Mattern and co-workers (1975) measured the radiation-induced luminescence energy delivered to a photosensor connected to a fibre during a pulse of X-rays. The dose rate was over 10^{10} $rad.s^{-1}$ The constant calculated for the light yield from Corning Type B silica fibre at 800 m was:

$$2 \times 10^{-14} \text{ mJ.cm}^{-1}.\text{nm}^{-1} .\text{rad}^{-1}.$$

We will assume the following values for a fibre cable exposed to a dose rate of 1 $rad.s^{-1}$:

Dose rate:	1 rad.s ,
Length of cable:	10^4 cm (100 metres),
Bandwidth of sensor:	300 nm,
Responsivity of photodiode:	1 A/W

The calculated output of a photosensor under these conditions is 6×10^{-11} A. This is unlikely to produce any problems in the form of "background" interference in normal electrical or light signals which would normally generate far higher current values. On the other hand, Mattern mentions that other materials may yield higher efficiencies. However, Lyons et al (1980) find that the luminescent efficiency of five modern fibre types is even lower than the above. Both neutron and X-ray pulses in the 10^2 - 10^4 rad range produced results indicating luminescence yields in the range 10^{-17} to 3×10^{-15} $mJ.cm^{-1}.nm^{-1}.$ rad^{-1}. Thus, the above value of 2×10^{14} $mJ.cm^2.nm^{-1}.rad^{-1}$ is the highest so far found. The luminescence spectrum of one case is shown in Figure 12.6.

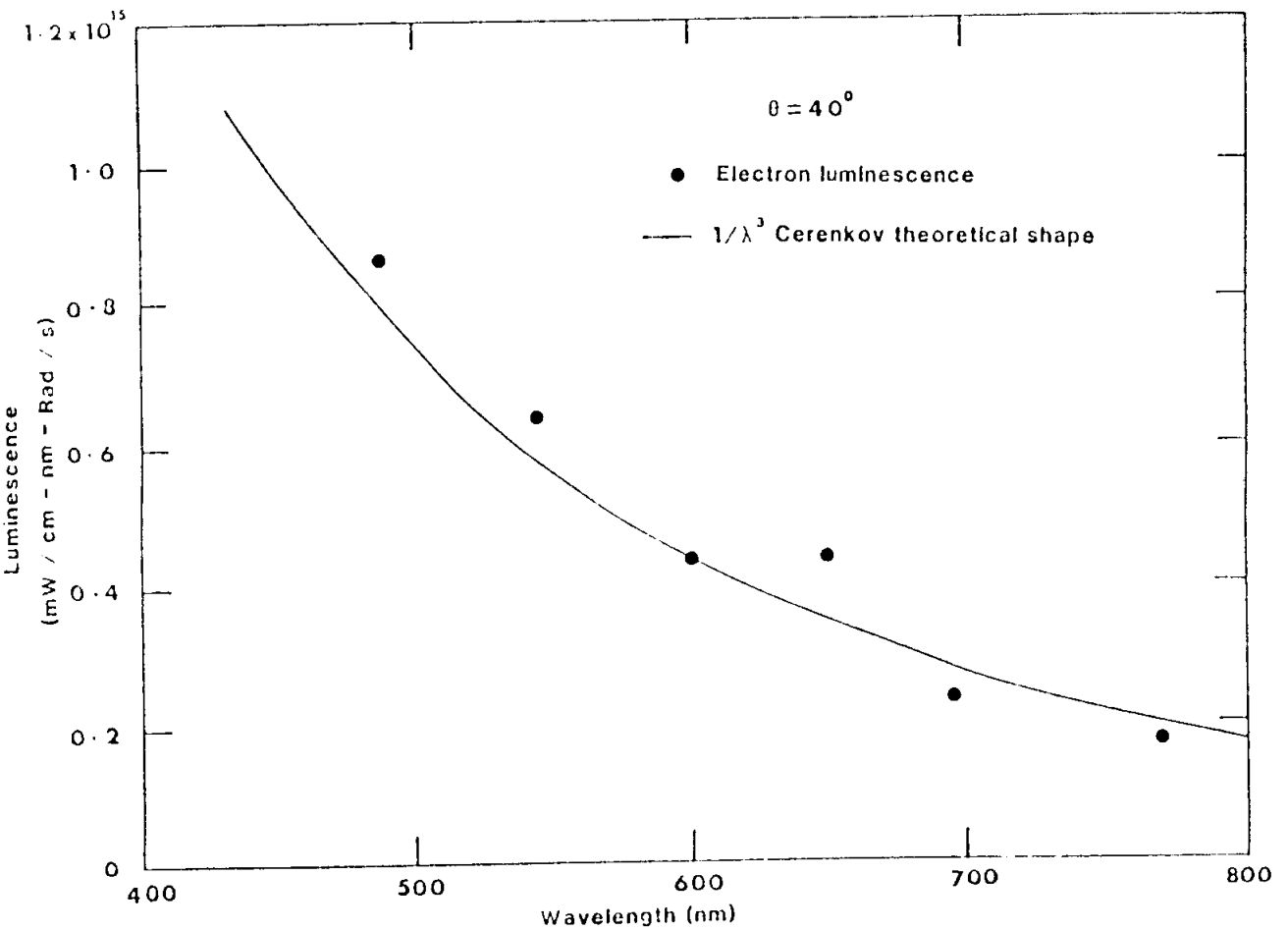

Luminescence induced by pulsed electron irradiation in a step-index fibre vs. emission wavelength. The solid curve is the theoretical Cerenkov shape and the points are experimental (after Lyons et al).

FIGURE 12.6 - LUMINESCENCE INDUCED BY PULSED ELECTRON IRRADIATION

12.8. CONCLUSIONS

As the optical paths in fibre optic systems may be very long, radiation-induced loss effects due to space or reactor radiation may be quite severe. Multicomponent glass fibres will show greater loss under radiation than ultrapure synthetic silica fibres. Selection by means of radiation testing is strongly advised.

Optical fibres may be subject to "annealing" and test programmes should take this into account in defining temperatures and dose rates. High dose rate testing may not adequately represent a low dose rate service environment.

Considering that, at the present time, European manufacturers and users have no procedures for the "Hardness Assurance" of fibres, there is a need to establish a programme for radiation testing of European fibre technology.

REFERENCES

G. Arnold, IEEE Trans.Nucl.Sci. NS-20 (6), pp. 220-228 (Dec. 1973)

G. Arnold and D. Compton, Trans.Farad.Soc.

J.R. Bosnell, IEEE Trans.Nucl.Sci. NS-21 (6), pp. 159-166 (Dec. 1975)

G. Brucker, "TFTR Diagnostics Engineering Report No. 2", Report No. PH-I-001 (Plasma Phys.Lab., Princeton, N.J. (1977)

C.G. Emms, I. Groombridge, A.G. Holmes-Siedle and J.R. Bosnell, IEEE Trans.Nucl.Sci. NS-21 (6), pp. 159-166 (Dec. 1975)

B. Evans and G. Sigel, IEEE Trans.Nucl.Sci. NS-22, pp. 2462-2467 (1975)

B.D. Evans, G.H. Sigel Jr and J. Langworthy, IEEE Trans.Nucl.Sci. NS-25 (6), pp. 1619-1624 (Dec. 1978)

E.J. Friebele, Opt.Eng. 18 (6), pp. 552-561 (Nov./Dec. 1979)

E.J. Friebele, G.H. Sigel Jr and M.E. Gingerich, IEEE Trans.Nucl.Sci. 25 (6), pp. 1261-1266 (Dec. 1978)

I. Groombridge and A. Holmes-Siedle, Thin Solid Films 27, pp. 165-170 (1975)

A. Holmes-Siedle, Nucl.Instr. & Methods 121, pp. 169-179 (1974)

A. Holmes-Siedle, "Radiation Effects on the Joint European Torus; Guidelines for Preliminary Design", Fulmer Report No. R 857/2, Fulmer Research Inst., Stoke Poges England (Sept. 1980)

E. Lell, Physics and Chemistry of Glasses 3, pp. 84-94 (1962)

P.J. Mattern et al, IEEE Trans.Nucl.Sci. NS-22, pp. 2468-2474 (1975)

E.W. Mitchell and E.G. Paige, Phil. Mag. 1, p. 1085 (1956)

M.C. O'Brien, Proceeding Royal Society (London), A231, p. 404 (1955)

W. Primak, Nucl.Eng. 73, pp. 29-34 (1980)

G.H. Sigel, E.J. Friebele, M.E. Gingerich and L.M. Hayden, IEEE Trans. Nucl.Sci. NS-26, pp. 4796-4801 (Dec. 1979)

K. Tanimura, W.A. Sibley, M. Suscavage and M. Drexhage, J.Appl.Phys. 58, pp. 4544-4551 (Dec. 1. 1985)

R.A. Weeks and C.M. Nelson, J. American Ceram. Soc. 43, pp. 399-404 (1960)

R.A. Weeks and E. Lell, J. Appl.Phys. 35, pp. 1932-1938 (1964)

SECTION 13. OPTOELECTRONIC DEVICES

13.1. INTRODUCTION

The term optoelectronic devices is taken here to mean devices which are activated by, or emit, light. Frequently, a pair of these devices are used together as a transmitter and a receiver of light signals. Optical fibres have been dealt with in a separate section, as have passive optical media. We will not discuss display devices which are unlikely to play a major part in equipment exposed to space or nuclear radiation. Most of the devices subject to exposure will be of the semiconductor type, but brief mention will also be made of light sensors of the vacuum-tube type. In general, vacuum tubes and other devices with glass envelopes are tolerant to radiation, but rarely used due to their bulkiness and high electrical power consumption and high voltage supply requirement.

Optoelectronic devices, in which the active elements are semiconductors, are frequently sensitive to radiation because the absorption or generation of light in a solid medium is often influenced by the defect structure of that medium (hence, the first studies of radiation damage were "on colour"; see section on "optical media"). For example, light-emitting diodes operate by the recombination of excess carriers via impurity centres in a III-V compound. Neutron-induced centres can interfere with this process. The detection of light in silicon usually operates by the collection of the minority carriers generated by the light. Neutron or surface damage can interfere with this collection process. The darkening of transparent coatings or encapsulations around a semiconductor chip (glass or polymer) is also a possibility. In the case of vacuum tubes, such as TV or multiplier tubes, the mechanisms of light generation and sensing are not as strongly affected by radiation damage, but one must always ensure that the transparent envelope is not darkened in the window region. A major radiation characterisation programme for visible and IR LEDs, photo-transistors and optocouplers was carried out for ESA by Crouzet in 1980 and updated in 1985.

13.2. LIGHT-EMITTING DIODES (LEDs)

When a p-n junction in a III-V semiconductor is forward biased, the carriers pass into and across the junction, and recombine near the junction. Given suitable defect centres, the recombination is accompanied by light of a photon energy slightly less than the band-gap energy of the semiconductor. The efficiency of conversion of electrical power into photon events is directly proportional to the minority carrier lifetime in the active regions of the diode. Particles can affect the light output efficiency of the system in two ways:

1. as for transistors, neutron damage reduces the minority carrier lifetime in the active regions and

2. as particles produce new defects (recombination centres), the radiation-induced defects compete for carriers with the pre-existing luminescent defects. This may further reduce the light output efficiency.

The importance of the two damage effects will vary quite strongly with the impurities used and it is not surprising therefore that some designs of light-emitting structure are found to be more affected by neutron irradiation than others. The more sophisticated epitaxial structures (often multilayer ones) are often strongly affected by a neutron exposure of 10^{12} n.cm^{-2} (1 MeV). The non-epitaxial zinc-diffused gallium arsenide diodes are less strongly affected, while Si-doped GaAs diodes are damaged in the same way as the epitaxial type. Barnes has studied neutron/gamma effects (1972) and Stanley tested LEDs using high-energy electrons (1970). JPL has also explored LEDs to 2.5 MeV electrons (1985). Thompson and Janssens (1978) showed that there is significant injection annealing of LEDs which may balance the radiation degradation. Judicious choice of forward current and duty cycle could extend the life of LEDs in the space environment.

In the photovoltaic mode, the photodiode operates on the same general principle as the solar cell. Minority carriers, generated by light, diffuse to the p-n junction and are collected. The region from which carriers can be collected is determined by the diffusion length, L, of minority carriers in the base (low-doped) region of the diode. L^2 is equal to $D\tau$, where 'τ' is the minority carrier lifetime and D is the minority carrier diffusion constant. As described earlier, particles degrade minority carrier lifetime. Thus, the fractional photovoltaic efficiency n/n_0 of a diode as a function of neutron fluence can be predicted from first principles by a method similar to that described earlier for the degradation of transistors. The photovoltaic mode is useful when the signal amplitude is to reproduce the variations in light intensity. The speed of response, however, is limited by the time taken for carriers in the base to diffuse to the junction.

In the photoconductive mode, only the carriers created within the electric field of the junction (depletion region) are collected, which increases speed of response. In addition, this removes some of the dependence of the performance on minority carrier lifetime and thus reduces the effect of neutron bombardment. Some effects will still occur because leakage and series resistance are also increased by neutron bombardment and affect the light-generated signal.

According to the "SIRE" data compilation, reactor neutron fluence of about 3 x 10^{12} n.cm^{-2} (1 MeV) reduces the photo-current (presumably in the photovoltaic mode at "short circuit") of type TIL78 and other devices.

At this fluence, the photo-current was reduced by about 90%. In another device, the Ferranti MS7B, operated at open circuit (roughly equivalent to photoconductive mode), the signal decreased by 32% for the same order of neutron fluence. As the mechanisms of photodiode degradation are understood, it should theoretically be feasible to generate engineering prediction curves of performance versus time in space (or particle fluence).

13.3. PHOTOTRANSISTORS

A phototransistor consists of an npn or pnp structure designed in such a way that the base region is efficiently exposed to a light beam. The minority carriers produced constitute the signal normally supplied electrically by the base contact and, when the normal V_{CE} bias is supplied, collector current flows at a value proportional to the light intensity. The "base current" is, of course, amplified by h_{FE} (see Section 5) and neutron damage will accordingly affect the responsivity of phototransistors. The gain of a phototransistor is, in fact, directly proportional to the minority carrier lifetime in the base region (A.G. Stanley, 1970). Under neutrons, light-activated relays (thyristors, etc.) should behave in the same general way as phototransistors.

The degradation of the output current of an LS600 phototransistor after exposure to 2 x 10^{12} reactor neutrons.cm^{-2} was 80% (SIRE). Given the above direct dependence on minority carrier lifetime, it is unlikely that phototransistors of greatly improved tolerance to radiation can be found and this form of light sensor should be dispensed with when the predicted degradation cannot be tolerated. Since a phototransistor can be considered as a photovoltaic diode with a built-in amplifier, it is reasonable to assume that most signal applications, normally dealt with by the use of phototransistors, can be achieved by means of a photodiode followed by a radiation-tolerant amplifying device (junction FET, high-frequency transistor). Photosensitive field-effect transistors are obtainable, but no radiation test data are available at present.

As for photodiodes, prediction curves for phototransistors can be produced.

13.4. OPTOCOUPLERS

Optocouplers (opto-isolators) are devices which employ a light beam to achieve electrical isolation between a signal input and the rest of an electronic circuit. The usual types consist of a light-

emitting diode facing a photodiode or phototransistor chip across a small thickness of an optical medium such as polymer, glass or, in some cases, air. A new series of "photologic" consists of an optical-fibre input and an electrical output, usually a logic voltage. The response of these devices to radiation damage is simply a combination of the degradation of the component parts. Thus, for example, it is not surprising that isolators employing phototransistors are more sensitive than those employing photodiodes (see earlier parts of this section).

A degradation of about 70% in the current transfer ratio (I_{in} vs I_{out}) was found after exposure of a phototransistor (type TIXL 101) to a neutron fluence of 2×10^{12} reactor neutrons.cm^{-2}. Because of surface effects, 10^5 rad gamma rays also produced degradation. Brucker (1978) estimates the threshold of damage to optoisolators to be in the region of 5×10^{10} for the photodiode types and of 10^{10} for phototransistor types. He derives these estimates from data by Barnes on light-emitters (threshold of damage 10^{11} n.cm^{-2} (14 MeV)) and some of his own data on p-i-n diodes, showing some degradation at 10^{11} n.cm^{-2} (14 MeV) by use of a factor of two for relative damage effect. Brucker (1978) thus gives a figure of 5×10^{10} n.cm^{-2} (14 MeV) for optoisolators, but the above explanation shows that this is very much a worst case, i.e. the fluence at which the first detectable damage is observed in quite sensitive devices. The data on the TIXL 101 shows that, for some types of optoisolators, circuits which will survive much higher levels than 5×10^{10} n.cm^{-2} could, in fact, be designed even with commercial devices.

13.5. IMAGING CHARGE-COUPLED DEVICES (CCDs)

These devices find application in control and stabilisation systems such as star-trackers and as imaging elements in the focal plane of camera-type instruments.

Certain scientific CCD types have a response to X-rays which is useful for astronomy, including spectroscopy. X-ray telescopes with cooled CCDs at the main focus are being adopted for several US and ESA projects (see, for example, ESA SP-1097; Lumb and Holland 1988a). Other applications of X-ray imaging are also being investigated.

Most imaging CCDs are comparatively radiation-sensitive with typical failure levels in the range of 3 to 10 kilorads. Some work has been performed on radiation-hardening and a hardened array is offered by Texas Instruments for military applications.

The most noticeable consequence of radiation damage is an increase in dark current due to interface state generation (Saks,

1980; Debusschere, 1984) and this is generally the main reason for device "failure".

For X-ray astronomy missions, a cooled CCD is used in the photon-counting mode. In this mode, the device is very sensitive to radiation-induced defects in the silicon. These defects may retain part of the signal charge, which may only consist of a few hundred electrons. As a result, the measurement of X-ray energies may be seriously affected by a total dose of a few kilorads (see, for example, J.R. Janesick 1988). However, methods of minimising this effect are being developed by ESA projects (see, for example, Lumb and Holland, 1988b).

When CCDs are used a star trackers, particle radiation can produce signals which could be mistaken for stars. An analysis of this type of interference should be made of any mission passing through radiation belts (see, for example, J. Daniels and A.D. Holland, 1987).

Using 150 kV X-rays, ^{60}Co and protons to 50 MeV, it has been found that the damage is independent of the type of radiation and only a function of total dose (Debusschere, 1984). Some initial studies, also carried out by Debusschere, evidenced that imaging CCDs can be hardened using the well-established MOS hardening techniques.

13.6. ELECTRO-OPTIC CRYSTALS

Inorganic and organic materials possessing certain types of crystal symmetry may demonstrate the electro-optic effect. Examples of this effect are bi-refringence, doubling of laser light frequency, light valve, piezoelectric and pyroelectric action and other ferroelectric effects. Little study has been performed of space radiation effects on these materials as a class. Apart from a predictable darkening of some crystals due to colour centres or radiolysis, no known pattern exists in the radiation effects to be found in the megarad range. Test data, especially for quartz, will be found in many compilations.

REFERENCES

C.E. Barnes, Appl.Phys.Lett. 20, 3.1 (Febr. 1972)

C.E. Barnes, IEEE Trans.Nucl.Sci. NS-18(6), pp. 322-331 (Dec. 1971)

C.E. Barnes, IEEE Trans.Nucl.Sci. NS-24(6), pp. 2309-2314 (Dec. 1977)

G.J. Brucker, "TFTR Diagnostics Engineering Report No. 3", Report No. PH-I-004, Princeton Plasma Lab., USA (May 1978)

G.J. Brucker, A. Rosen and A. Schwarzmann, IEEE Trans.Nucl.Sci. NS-25(6), pp. 1528-1533 (Dec. 1978)

Crouzet, "Evaluation de Composants Optoélectroniques Destinés aux Applications Spatials", ESA Contract Report CR(X)-1442 (1980); Updated Report under Contract 5799/84 (Jan. 1985)

I. Debusschere, "Radiation Evaluation of the ESA 512 Imaging Technology", ESTEC Contract 5170/82/NL/MS, Leuven University (1984)

K. Marlin, M. Gauthier, J.R. Coss, A.R.V. Dantas and W.E. Price, "Total Dose Radiation Effects Data for Semiconductor Devices", JPL Publ. No. 85-43, Vol. 1, NASA-JPC, Pasadena (Oct. 1985)

W.J. Poch and A. Holmes-Siedled, "TOS Radiation Program Report", RCA Astroelectronics Div., Princeton, N.J., USA (1967)

N.S. Saks, "A New Technique for Hardening CCD Imagers by Suppression of Interface State Generation", IEEE Trans.Nucl.Sci. NS-27(6), pp. 1727-1734 (Dec. 1980)

SIRE, Data Compilation, U.K. Ministry of Defence, London

A.G. Stanley, IEEE Trans.Nucl.Sci. NS-17(6), p. 239 (1970)

S.M. Sze, "Physics of Semiconductor Devices", Wiley (1969)

I. Thompson and G. Janssens, "Radiation Sensitivity and Recovery Characteristics of 1 MeV Electron-irradiated Optocouplers and GaAs LED's", ESTEC Internal Report MISC 078 (Febr. 1978)

D.H. Lumb and A.D. Holland, 1988a, "X-ray Imaging Spectroscopy with EEV CCDs" Proc. SPIE, Vol 982 in press

D.H. Lumb and A.D. Holland, 1988b, University of Leicester Reports ESTEC Contract No. 6906/86/NL

J. Daniels and A.D. Holland, 1987, "Background Charged Particle Effects in the ROSAT Wide Field Camera Star Tracker", University of Leicester Report No. WFC/UL/TN87-01(1987)

M.M. Blouke, F.H. Yang, D.L. Heidtmann and J.R. Janesick (1988), "Traps and Deferred Charge in CCDs" SPLE Conf. on Instrumentation for Ground Based Optical Astronomy ; Present and Future, 1988 AH-S 10/10/88

ESA Special Publication SP-1097 (1988) "The high Throughput X-ray Spectroscopy Mission – The Mission - Science Report

PAGE INTENTIONALLY LEFT BLANK

SECTION 14. TRANSDUCERS AND OTHER COMPONENTS

14.1. TRANSDUCERS

14.1.1. General

Electronic transducers can be described as devices which perform measurements. Space vehicles, remote scientific equipment and other forms of automated apparatus working in radiation are likely to require transducers. Transducer technology covers a very large variety of types and it is therefore difficult to predict the effects of radiation. Moreover, there is usually a close link between requirements for performance and individual measurement requirements.

Optical transducers have been dealt with under other headings. Further classes likely to be important for space vehicles include:

- mechanical sensors (strain gauges, displacement sensors, pressure gauges),
- temperature sensors (thermistors, thermocouples),
- particle sensors and
- magnetic sensors (including Hall devices).

The requirements for sensitivity are very variable but, clearly, radiation effects will have more impact on the high-sensitivity applications. Radiation-induced degradation is likely to cause inaccuracy and the associated high-gain instrumentation amplifiers and oscillators may be more vulnerable. Radiation-induced noise may be important at low levels of signal.

The science of transducers is growing and new designs appear frequently. Therefore, in project studies, each new design with its associated electronic preamplifiers etc. should be carefully examined for sensitivity to radiation before it is adopted for operation in radiation environments.

14.1.2. Previous transducer studies

No reports exist of previous studies of the impact of space radiation on transducers. However, in the nuclear field, Brucker (1977/78) wrote a useful report on his survey of piece parts used in diagnostic equipment on nuclear reactors. Its contents are mainly based on a search of the literature and followed by recommendations for choices wherever two device types are available. In Table 14(2), the sensors appear to fall into two classes, those which are useless at 10^{14} n.cm^{-2} (14 MeV) and those which still operate with little or no degradation. In the former group are opto-isolators (see Section 10 for further comment); charge-coupled devices (CCD) and a piezoelectric pressure transducer employing $BaTiO_3$ used in the shear mode. In the "resistant" class fall ZnS scintillators, InSb

devices for sensing heat radiation, silicon thermistors and lead zirconate titanate pressure transducers used in the compression mode. At high particle fluences, germanium devices are not advisable.

Tables 14(3), (4) and (5) give some test data and basic information on the "corruption" of the signals from transducers by transient, radiation-induced ionisation or leakage effects. The two radiation sensors shown in Table 14(3), HgCdTe and a pyroelectric detector are the most sensitive to noise. The signal amplitude would have to be known for a proper noise evaluation to be made.

Table 14(5) records a calculation of current generation and Table 14(6) notes some measurements/calculations by the Princeton Fusion Experiment Group which may prove useful in defining background interference in X-ray detectors, including photomultipliers.

Two careful studies of space radiation effects in photovoltaic devices have some relevance to spaceborne sensors (Cooley and Janda, 1963; Tada et al, 1972). These studies explain damage in solar cells and give results for transparent materials.

TABLE 14(1) - RADIATION DAMAGE THRESHOLDS FOR DIAGNOSTIC SENSORS (After Brucker)

Director	Application	Threshold fluence $n.cm^{-2}$ (1 MeV eqt)	Threshold dose (rad (Si))
HgCdTe	Photovoltaic	5×10^{11}	10^6
InSnTe	Photovoltaic	5×10^{11}	10^6
GaAs	Photovoltaic	10^{12}	10^6
Si(Li) or Ge(Li) (1)	Reverse biased diode	10^{10}	3×10^5
Surface barrier diode	Reverse biased diode	10^{10}	10^7
Pyroelectric	Temperature change	10^{14}	10^7
Schottky diode (2)	Reverse biased diode	10^{14} to 10^{15}	5×10^5 to 10^8
Crystal Ge (Cu or Hg-doped)	Photo-conductive	5×10^{13}	10^6
NaI	Scintillator	10^{14}	10^5

NOTES:

(1) Both these detectors can be annealed back to their initial state by high temperature.

(2) Depending on construction details, the minimum or maximum value applies.

TABLE 14(2) - THRESHOLD DAMAGE LEVELS: PERMANENT DAMAGE EFFECTS IN PARTS FOR DIAGNOSTICS (After Brucker)

Detector or device	Ionisation (rad)	Bulk damage (n/cm^2) (1 MeV eqt.)
Optical isolator (PD)	10^6	5×10^{10}
Optical isolator (PT)	5×10^4	10^{10}
Zinc sulfide	–	10^{14}
Indium antimonide (doped 10^{15} atoms/cm^3)	10^8	10^{14}
Germanium bolometer (doped 10^{15} atoms/cm^3)	10^7	2×10^{13}
Germanium (PV) (Gallium-doped)	3×10^6	10^{12}
Germanium (PC) (Gallium-doped)	6×10^7	5×10^{13}
Diamond	–	10^{14}
CCD (SC) (dark-current failure)	10^4	10^{11}
CCD (BC) (dark-current failure)	10^4	5×10^{10}
Silicon thermistor (Boron-doped)	–	10^{14}
RCA memory CDP 1821	5×10^3	10^{15}
Harris memory HMI 6508	10^3	10^{15}
RCA memory CD 4061	10^5	10^{15}
NMOS memory - 4 kilobit	10^3	10^{15}
Barium titanate	9.5×10^6	7.6×10^{10}
Lead zirconate titanate	4×10^{10}	3.6×10^{18}
Quartz crystal (X-ray diffraction effects)	–	10^{19}

NOTES:

Channeltron: temporary fatigue commences after 10^{10} counts; gain can be restored by a clean-up treatment.

PD = photodiode
PV = photovoltaic
PT = phototransistor
PC = photoconductive

TABLE 14(3) - DETECTOR RADIATION NOISE THRESHOLDS (After Brucker)

Material or detector	Threshold flux or dose rate
Hg Cd Te	10^2 rad s^{-1}
Fibre optics	10^{10} rad s^{-1}
Pyroelectric	3×10^{-3} rad s^{-1}

TABLE 14(4) - THRESHOLD DAMAGE (DATA UPSET) LEVELS (after Brucker)

Detector or device	Dose rate (rad/s)	Neutron rate ($n.cm^{-2}.s^{-1}$)
Optical isolator	10^4	–
CCD (scramble of data in a register)	10^5	–
RCA memory CDP 1821	6×10^{10}	–
Harris memory HMI 6508	8×10^7	–
Intersil memory IM 6508	8×10^7	–
RCA memory CD 4061	10^8	–
Kilobit NMOS memory	5×10^8	–
Barium zirconate titanate	–	2.1×10^{14}
Lead zirconate titanate	–	1.2×10^{12}

TABLE 14(5) - CARRIER GENERATION RATES AND CURRENTS FOR EXPOSURE TO A UNIT DOSE RATE (rad/s) (after Brucker)

Detector or device	Generation (carrier/cm^3.s)	Current (A/cm^3)
Silicon	4×10^{13}	6.4×10^{-6}
Germanium	10^{14}	1.6×10^{-5}
In Sb	4×10^{14}	6.4×10^{-5}
Diamond	10^{13}	1.6×10^{-6}
Channeltron	6.4×10^{-5} e.cm^{-2}.s^{-1}	10^{-13} A

TABLE 14(6) - NEUTRON AND GAMMA RAY RESPONSE BY SOME DETECTORS (after K.W. Hill, quoted by Brucker, 1977)

Detector	Material	Radiation	Signal	Units
SPMT	ZnS	Reactor n	54	$\frac{(eV.cm^2)}{n.mg}$
IC	Argon	Reactor n	8	n.mg
PMT	Glass	Reactor n	2.4	Electrons/n (*)
PMT	Quartz	Reactor n	.28	Electrons/n (*)
PMT	Glass	.662 meV	6×10^{-3}	Electrons/(*) photon
IC	Argon	2.5 meV n	2.8	$\frac{(eV.cm^2)}{n.mg}$

(*) Photocathode electrons

PMT = Photomultiplier
IC = Ionisation chamber
SPMT = Scintillator optically coupled to PMT

14.1.3. Temperature sensors

ESA experience has shown that thermocouples are very insensitive to typical space radiation levels. Thermocouples can be used even inside nuclear reactors (say, fluences of 10^{20} n.cm^{-2}) as long as the wire insulation associated with them (e.g. glass and ceramic tube) does not become leaky (Ricketts, 1972). The same general statements apply to platinum resistance thermometers.

Thermistors are composed of semiconductors but, again, the wire insulation is usually the most sensitive element and most devices will withstand megarad doses (Ricketts, 1972). Modern fibre-optic temperature sensors will, of course, exhibit the optical darkening discussed elsewhere.

14.1.4. Hall-effect sensors

Hall-effect sensors are small "Hall bars" made of ferrite (e.g. type SBV 566). When a "control current" of about 50 mA is passed through the bar and a magnetic field, B, is applied perpendicular to the current, a Hall voltage, V_H , of a few mV appears across the voltage output arms at right angles to the current flow and field direction, which is proportional to current and field. An operational amplifier with feedback - frequently placed in the same package as the Hall bar - is used to amplify V_H to a few volts. Diverse transistors (e.g. 2N2222) can be added to act as relays or to give a TTL logic voltage.

The transport properties of ferrite (mobility, etc.) will not be greatly affected by neutrons in the 10^{15} n.cm^{-2} (1 MeV) range. Thus, the site of any degradation suffered is more likely to be in amplifier circuits. The latter is essential for read-out. The Hall bar can be connected remotely to the amplifier chip by means of a cable but, of course, the low value of the original Hall voltage means that - as the leads become longer - so the Hall effect sensitivity is reduced by noise, voltage drop, thermal EMFs etc.

14.1.5. Mechanical Sensors

14.1.5.1. General

Transducers of mechanical movement include sensors for displacement, pressure, acceleration, vibration, sound etc. The effect of radiation depends, of course, on the principle used to measure the movement. The earliest electrical types were moving coils. Later, strain gauges made of metal and silicon were developed. More recently, use has been made of optical fibres and piezoelectric effects in ceramics and polymers, and of silicon microstructures for the manufacture of accelerometers, pressure gauges, tactile sensors, oscillators etc.

In coil solenoid sensor structures, the effects of radiation will centre on the degradation of the coil insulation and the mechanical linkages (e.g. the polymeric parts). In optical types, darkening of glasses will be most important. Metallic and ceramic strain gauges are unlikely to be affected. The piezoelectric polymer film, PVF2 , has been shown to survive doses of more than 10^7 rads without loss of performance, but degrades at higher doses with evolution of HF (HolmesSiedle, 1985). Note that PVF2 appears much less sensitive to radiation than PTFE.

14.1.5.2. Silicon micromechanisms

As the mechanical properties of silicon are not affected by even large doses of electrons, protons, neutrons or gamma rays, it is probable that radiation-tolerant, silicon, micromechanical devices can be built. However, these often incorporate diffused junctions or even integrated transistors which, as discussed elsewhere, must of course be considered in the usual way. Discrete strain gauges, capacitive pressure sensors and accelerometers, however, should not be severely affected by typical space radiation levels.

14.2. OTHER ELECTRONIC COMPONENTS

14.2.1. General

Devices included in this section are those that either have a relatively high tolerance to radiation or cannot logically be categorised under any other section. Examples of the first category are non-semiconductor components such as resistors, inductors and electron tubes. To the second category belong connectors and various mechanical devices.

Table 14(7) shows a list of components and materials known to be sensititive to radiation. This section includes several of these, but more general information is given in Section 5. Information on reactor tests of miscellaneous components can be found in a number of handbooks on nuclear hardening (see e.g. Rudie (1976); Ricketts (1972) and references therein) as well as in the bibliography given in Appendix B to this handbook and the Data Bank compilations listed elsewhere.

TABLE 14(7) - MATERIALS AND DEVICES WITH GENERALLY POOR RADIATION TOLERANCE

Semiconductors
Optical lenses
Optical fibres
Optical windows (e.g. encoder plates)
Elastometers (e.g. plastic bellows)
Plastic bearings
Lubricants
Adhesives
Hydraulic fluids
Paints
Reflective coatings
Wood, paper, string and cloth
Thin insulators
Photosensitive materials
Gas sensors
Liquid-ion sensors
Surface-active reagents
Piezoelectric transducers
Micropositions

14.2.2. Capacitors

14.2.2.1. General

Capacitors consist of large areas of conductor separated by a thin insulator. It is usually desirable for the insulator to exhibit very low leakage (R(insulation) $>10^{13}\Omega$). Total dose permanently degrades the insulation resistance of organic insulators, but barely at all in the case of air or ceramic. On the other hand, if the dose rate is significant, the insulator can exhibit "transient photoconductivity". In solid capacitors, some charge becomes trapped during irradiation and may be released slowly some time later to produce a small, long-term conductivity after irradiation has ceased.

14.2.2.2. Total-dose effects

The electrical effects of total dose become severe in capacitors until a dose of about 10^7 rads is reached. Plastic and paper capacitors are the most likely to exhibit radiation-induced changes in leakage and dielectric loss. Glass and ceramic capacitors may be unaffected up to 10^{10} rads. For reactor irradiation, damage thresholds are in the region of 10^{14} to 10^{16} n.cm^{-2} (E>10 keV) (Ricketts, 1972) and it is likely that the source of damage in this case is the accompanying gamma-ray dose.

14.2.2.3. Dose-rate effects

Electrolytic capacitors are subject to an unusual photovoltaic type of leakage (Rudie, 1978) but, in fact, leak less than plastic and paper ones (Ricketts, 1972).

Natural radiation dose rates in space are, normally, not high enough to yield significant radiation-induced conductivity (RIC) in capacitors' dielectrics. The order of magnitude for RIC was given in the section on "Polymers".

14.2.3. Resistors and conductors

Most of the effects of radiation on resistors were being observed during irradiations of very high intensities in nuclear reactors or flash X-ray machines. Most of the changes observed are due to the breakdown of encapsulating media such as silicone potting compounds. Only mild resistance changes take place at a fluence of 10^{13} fast neutrons in carbon resistors which are the most sensitive class. The dose rates required to give transient changes are of the order of 10^{10} rad.s^{-1}. Precision wire-wound resistors are many orders less sensitive.

Conduction in metals is not affected by gamma rays or space particles. In reactor irradiation, changes are observed in the ultra-high fluence range (10^{20} n.cm^{-2} and above) due to alterations in crystal lattice structures.

14.2.4. Radiofrequency devices

14.2.4.1. Oscillator crystals

The piezoelectric properties of quartz and most other single crystals are not catastrophically affected by neutrons, even at 10^{18} n. cm^{-2}. However, oscillator frequencies must often be accurate to extremely close limits (say 1 part in 10^6) and neutron damage to the lattice in the range 10^{12} n.cm^{-2}, and gamma doses in the 10^5 rad range can produce permanent changes in oscillation frequency of about 1 part in 10^7. Thus, ultra-high-precision oscillators may experience inconvenient drifts, but predictable drift of this sort can probably be adjusted by recalibration.

High-grade synthetic quartz, suitable for oscillators and having a reproducible response to radiation, is now available commercially. King (1974), in a review of the effect of radiation on 5 MHz, 5th-overtone resonators, notes a negative change of 50 ppm in frequency for 10^6 rads in natural quartz and one-fifth of this amount in Z-growth electronic-grade synthetic quartz, in the positive direction. Neutron damage produces positive shifts at rates which

vary from 0.56 x 10^{-15} to 3 x 10^{-15} ppm/n/cm^{-2} for unpurified synthetic quartz. Many important literature references are given in King's review.

14.2.4.2. Vacuum tubes

Despite the large power drain and size of vacuum tubes, their use in very high neutron/gamma environments has proved to be useful. For amplifying tubes (valves), no known degradation mechanism (except outgassing in some cases) provides an upper fluence limit to operation. Imaging devices, of course, suffer optical-path and possibly photosensor degradation, but vidicons are used in reactors and have been tested for use in space missions.

14.2.4.3. Microwave devices

Both silicon and III-V semiconductors are used for microwave signal generation, switching and amplification. Amplifiers are dealt with in our discussion of transistors. The other two microwave device types employ the action of majority-carriers and fall into a different, lower class of radiation sensitivity.

The main effects of radiation on the above class of device are:

(a) Reduction of majority carrier concentration by bulk displacement damage and
(b) Transient increase in majority carriers produced by a burst of radiation.

In ESA's experience, the above effects have not produced significant problems in geostationary orbit. The effects of intense neutron and flash X-ray irradiation on Gunn diodes and silicon p.i.n. switches have been investigated by Berg and co-workers (1970, 1971) and Chaffin (1971).

14.2.5. Miscellaneous hardware

The term "miscellaneous hardware" includes connectors, cables, gaskets, O-rings, switches and so on.

In this range of hardware, an approach to prediction is to examine data of the plastic materials used in their construction. Normally, the mechanical properties of structural plastics show the onset of damage in the range 10^7 to 10^8 rads. Elastomers are more sensitive than rigid plastics, owing to the larger cross-linking changes in the former. Leakage effects in connectors and cables are dealt with by calculation of radiation-induced conductivity (see "Polymers" section).

REFERENCES

TRANSDUCERS

G.J. Brucker, "TFTR Diagnostic Engineering Report No. 2", Report No. PH-I-001, Princeton Physics Lab. (1977)

G.J. Brucker, ibid, No. 3, Report No. PH-I-004 (May 1979)

J.R. Carter and H.Y. Tada, "Solar Cell Radiation Handbook", JPL-NASA, Pasadena (1972)

W.C. Cooley and R.J. Janda, "Handbook of Radiation Effects in Solar Cell Power Systems", NASA SP-3003, Appendix A (1963)

R. Grube et al (on Pulse Shape in Proton-damaged Silicon Surface Detectors) Nucl.Instrum. & Methods 101, p. 92 (1972)

E.E. Haller et al (on Germanium Detectors), IEEE Trans.Nucl.Sci. NS-19(3), p. 271 (1972)

H.M. Heijne et al, "TSC Defect Levels in Silicon Produced by Irradiation with Muons of GeV Energy", Radiation Effects 29, p. 25 (1976)

A. Holmes-Siedle, "Radiation Effects in the Joint European Torus: Guidelines for Preliminary Design", Fulmer Report No. R 857/2, Fulmer Research Inst., Stoke Poges, England (Sept. 1980)

A. Holmes-Siedle, Unpublished work on irradiation of PVF2 (1985)

H.N. Norton (Member of JPL Techn. Staff),
(a) "Sensor and Analyser Handbook" (1982)
(b) "Biomedical Sensors" (1982)
(c) "Sensor Selection Guide" (1984)
Elsevier Sequoia, Lausanne

A. Stefanini (ed) "Miniaturisation of High-Energy Physics Detectors", Plenum, New York (1983)

OTHER COMPONENTS

L. Adams and A. Holmes-Siedle, "The Development of an MOS Dosimetry Unit for Use in Space", IEEE Trans.Nucl.Sci. NS-25(6), pp. 1607-1612 (Dec. 1978)

D.J. Allen, T.F. Wrobel, F.N. Coppage and G.L. Hash, "Gamma-induced Leakage in Junction Field-effect Transistors", IEEE Trans.Nucl.Sci. NS-31(6), (Dec. 1984)

C.E. Barnes and J.J. Wiczer, "Neutron Damage Effects in AlGaAs/GaAs Solar Cells", IEEE Trans.Nucl.Sci. NS-31(6), (Dec, 1984)

N. Berg and H. Dropkin, "Neutron Displacement Effects in Epilaxial Gunn Diodes", IEEE Trans.Nucl.Sci. NS-17(6), pp. 233-238 (Dec. 1970)

N. Berg and H. Dropkin, "The Effect of Ionising Radiation on Gunn Diode Oscillators", IEEE Trans.Nucl.Sci. NS-18(6), pp. 295-303 (Dec. 1971)

D.M. Binkley, "A Radiation-hardened Accelerometer Preamplifier for 2 x 10 Rads(Si) Total Dose", IEEE Trans.Nucl.Sci. NS-29(6), pp. 1500-1507 (Dec. 1982)

G. Brucker and A.D. Cope, IEEE Trans.Nucl.Sci. NS-19(6), p. 147 (Dec. 1972)

R.J. Chaffin, "Permanent Damage in PIN Microwave Diode Switches", IEEE Trans.Nucl.Sci. NS-18(6), (Dec. 1971)

S.C. Chen and J.R. Srour, "Ionising Radiation Effects on Indium Antimonide MIS Devices", IEEE Trans.Nucl.Sci. NS-26(6), pp. 4824-4827 (Dec. 1979)

W.R. Dawes Jr and J.R. Schwank, "An IC Compatible Ionising Radiation Detector", IEEE Trans.Nucl.Sci. NS-28(6), pp. 4152-4155 (Dec. 1981)

B.D. Evans, G.H. Sigel Jr., J.B. Langworthy and B.J. Fararday, "The Fiber Optic Dosimeter on the Navigational Technology Satellite 2", IEEE Trans.Nucl.Sci. NS-25(6), pp. 1619-1624 (Dec. 1978)

J.E. Ferl and E.R. Long Jr, "Infrared Spectroscopic Analysis of the Effects of Simulated Space Radiation on a Polymide", IEEE Trans.Nucl.Sci. NS-28(6), pp. 4119-4124 (Dec. 1981)

R.G. Fraas and R.W. Tallon, "Use of a Metal-Nitride-Oxide Semiconductor as the Detector for a Radiation Dosimeter", IEEE Trans.Nucl.Sci. NS-25(6), pp. 1613-1618 (Dec. 1978)

A.R. Fredrickson and S. Woolf, "Electric Fields in KeV Electron Irradiated Polymers", IEEE Trans.Nucl.Sci. NS-29(6), pp. 2004-2011 (Dec. 1982)

L.E. Halliburton, M. Markes, J.J. Martin, S.P. Doherty, N. Koumvakalis, W.A. Sibley, A.F. Armington and R.N. Brown, "Radiation Effects in Synthetic Quartz: The Role of Electrodiffusion and Radiation-induced Mobility of Interstitial Ions", IEEE Trans.Nucl.Sci. NS-26(6), pp. 4851-4857 (Dec. 1979)

A.H. Kalma and M.A. Hopkins, "Ionising Radiation Effects in HgCdTe MIS Capacitors", IEEE Trans.Nucl.Sci. NS-28(6), pp. 4083-4087 (Dec. 1981)

A.H. Kalma, R.A. Hartmann and B.K. Kanousek, "Ionising Radiation Effects in HgCdTe MIS Capacitors Containing a Photochemically Deposited SiO 2 Layer", IEEE Trans.Nucl.Sci. NS-30(6), pp. 4146-4150 (Dec. 1983)

J.C. King, "Hardening Quartz Resonators to Ionising Radiation - A Review", Report No. SAND 74-0136, Sandia Labs, Albuquerque, NM 87115, USA (Sept. 1974) and Proc.Intl. Conf. on Evaluation of Space Environ- ment on Materials, June 17-21, 1974, CNES, Toulouse, France

G.H. Marcus and H. Bruemmer, "Radiation Damage in GaAs Gunn Diodes", IEEE Trans.Nucl.Sci. NS-17(6), pp. 230-232 (Dec. 1970)

D.K. Meyers and W. Herzog, "Feasibility Study on the Design and Radiation Testing of Complex Functions for 2 x 10 Rads(Si)", IEEE Trans.Nucl.Sci. NS-29(6), pp. 1508-1511 (Dec. 1982)

J.R. Norton, J.M. Cloeren and J.J. Suter, "Gamma Ray and Proton Beam Radiation Testing of Quartz Resonators", IEEE Trans.Nucl.Sci. NS-31(6), (Dec. 1984)

P. Pellegrini, F. Euler, A. Kahan, T.M. Flanagan and T.F. Wrobel, IEEE Trans.Nucl.Sci. NS-25(6), pp. 1267-1273 (Dec. 1978)

W. Poch and A. Holmes-Siedle, TOS Radiation Program Report NAS 5-9034, RCA Astro-Electronics, Princeton, N.J. 08540 (Sept. 1965)

RCA, "Nuvistor" Application Notes (1965)

W.F. Rees Ltd., Woking, U.K., Private communication

L.W. Ricketts, "Fundamentals of Nuclear Hardening of Electronic Equipment", Wiley (1972)

L. Varnell and D.E. Langford, "Radiation Effects in IRAS Extrinsic Infrared Detectors", IEEE Trans.Nucl.Sci. NS-29(6), pp. 1551-1554 (Dec. 1982)

J.J. Wiczer, T.A. Fischer, L.R. Dawson, G.C. Osbourn, T.E. Zipperian and C.E. Barnes, "Pulsed Irradiation of Optimized, MBE Grown AlGaAs/GaAs Radiation hardened Photodiode", IEEE Trans.Nucl.Sci. NS-31(6), (Dec. 1984)

PAGE INTENTIONALLY LEFT BLANK

SECTION 15. POLYMERS AND OTHER ORGANICS

15.1. INTRODUCTION

15.1.1. General

Organic compounds are sensitive to radiation by virtue of the irreversible chemical processes which take place when covalent bonds, in this case C-C and C-H bonds, are excited or ionised by irradiation. Frequently, the bonds are ruptured and the reactive fragments then form new compounds; a process known as radiolysis. One very common effect is the combination of hydrogen atoms from two ruptured C-H bonds to form hydrogen gas. This provides a simple measure of the type and degree of chemical reaction occurring in the organic material. The variety of other possible radiolytic reactions is so large that understanding them is a science in its own right. Naturally, the interpretation of effects in extended structures such as macromolecules (polymers, proteins, etc.) is particularly complex. In this section, we give a brief description of permanent radiation effects in different classes of polymer and discuss also radiation-induced photocurrents in cables, connectors and capacitors.

For electronic systems within spacecraft enclosures, the integrated doses are usually well below the threshold for serious permanent degradation in electrical and mechanical properties (a level of 10^7 rad or more). Also, the dose rates in the enclosures rarely produce photocurrents which affect the operation of equipment. However, some exceptions may be quoted:

- In space, polymers will be directly exposed to bombardment at the surface of the spacecraft and hence receive a high dose;
- Optical properties of some polymers may degrade at doses as low as 10^4 rad, especially in optical fibres.
- Polymeric transducers (e.g. photoconductors) may be extra sensitive to damage;
- Remote manipulators on spacecraft will have to work in especially severe environments, e.g. when changing the isotope charge in a power generator.

In ground installations (accelerators, nuclear-fuel handling, fusion reactors, etc.), radiation-induced effects in polymers will be encountered more frequently.

We will use the term "ionisation effects" to cover the broad range of excitation effects described above. Although damage to properties occurs in organic compounds, the mechanisms are very different from the collisional processes which cause "bulk damage" in electronic crystals. In organic materials, the chemical rearrangements occur after a chain of events which includes

ionisation in the form of low-energy electrons emanating from one high-energy particle or photon. This is why the effects of irradiation with different particles in polymers are qualitatively similar. The degree of damage can be predicted if the energy deposited in rads(C) (or Gy(C)) is calculated, the distribution of dose with depth and the influence of the ambient atmosphere being taken into account.

15.1.2. Bombardment of external coatings

The surfaces of spacecraft are bombarded by photons, electrons, protons and alpha particles. The numbers and energies of these particles are such that, in a skin layer of the order of 0.1 mm, chemical disruption and electrostatic charging effects are produced. The effects will be most pronounced in polymeric insulators and special research is done to ensure that thermal blankets and paints will withstand these effects over the required mission period.

15.2. LONG-LIVED DEGRADATION IN POLYMERS

15.2.1. Relative sensitivity

There are many books and handbooks on the long-lived effects of radiation on the engineering and chemical properties of commercial and pure polymers. Detectable degradation of the mechanical, optical and electrical properties of polymers usually appears at a dose value lower than 100 megarads (10^6 Gy). In some cases, doses less than this can actually improve toughness. Doses in the 3-megarad range are actually used for the routine sterilisation of surgical plastics. An exception to this is the case of fluoropolymers, some of which show catastrophic mechanical degradation if exposed in air at megarad doses. In most polymers, long-lived electrical leakage and increased dielectric loss are likely to appear well before mechanical degradation occurs. Different forms of radiation normally produce the same qualitative effects in polymers, namely the rupture of chemical bonds, the evolution of gaseous molecules, destruction of crystallinity and change of colour. All of these are ionisation effects. Not unexpectedly, the quantitative effect for different forms of radiation can be predicted by calculating the dose.

In polymers, the rupture of chemical bonds results in one of two sequels - cross-linking or scission. Table 15(1) lists the polymer types most likely to undergo cross-linking or scission, as the case may be. As the radiation dose increases, polymers which tend to cross-link show an increase in strength and toughness; however, they ultimately become brittle. Those tending to scission will become steadily weaker and may eventually liquefy. In both groups, hydrogen gas is evolved and colorations are produced due to complex side-reactions.

As may be imagined from the very large variety of plastic compositions, engineering plastics differ greatly from one to the other in radiation tolerance. The threshold dose for radiation damage varies by at least three orders of magnitude. Because the demands made on plastics in different applications are so diverse, it is often difficult to predict degradation effects except by considering individual cases and by radiation testing. Most of the "league tables" compiled are based on the measurement of tensile properties (see e.g. Schönbacher and co-workers, 1979-1982). Kapton, polystyrene, phenylsilicones, polyethylene, Mylar and epoxy are usually near the top of any such tables, while nylon, polyvinylchloride and all elastomers are usually near the bottom.

15.2.2. Polymers in electronics

Polymers are used very widely as sub-elements of electronic piece parts and circuits, e.g.:

- Epoxy resins are used in circuit boards as adhesives and "potting" or encapsulation compounds;
- Mylar, polycarbonate and polystyrene are used in capacitors;
- enamels are used for coil insulation;
- silicones and polyamides have many specialised electronic applications;
- PVC, PTFE and sulphones are used in sockets, connectors and wires.

15.2.3. Effect of additives and fillers

The long-lived effects of radiation on plastics can be strongly affected by the chemical additives used, especially by the quantity of antioxidant and plasticiser present. In both cases, the additives delay the onset of mechanical and other effects caused by oxidation, chain scission and embrittlement. Therefore, to increase radiation tolerance in plastics, we can specify plastics which are rich in these additives. Filler and pigments may sometimes alter the radiation-induced behaviour of the polymeric matrix.

15.2.4. Combined effects of stress (fields, vacuum, temperature) and ageing with irradiation

All plastics age on storage, owing to the evaporation or depletion of antioxidants and plasticisers. Hostile environments may accelerate radiation-induced effects. For example, if plasticisers vaporise in a plastic irradiated in vacuo, then radiation-induced embrittlement can be said to be accelerated by the use of vacuum; however, since oxygen is gradually removed from a plastic in vacuum, oxidative scission may be greatly reduced. Increased temperatures will encourage oxidative attack and outgassing. Exposure to an electrical field or light is also likely to accelerate these effects. PVC

cable material is more severely affected by radiation if irradiated slowly at increased temperature.

15.3. RADIATION TOLERANCE OF PLASTICS ACCORDING TO TECHNOLOGY

15.3.1. General

Engineering plastics are frequently grouped according to the manufacturing processes used and the function required. Broad process classifications are thermoplastics, thermosets and elastomers. Functional classifications include structural, insulating, coating, adhesive and optical. Demands on mechanical, electrical and optical properties vary very widely in these functional groups. Thus, the "bar charts" commonly compiled, which quote the effects of a given dose and use phrases such as "negligible damage" or "severe damage", can be misleading unless the properties measured and the tolerances allowed are specified. For example, bar charts suggest that few plastics show damage in vacuum at doses below 10^6 rad (10^4 Gy). On the contrary, long plastic optical fibres may be rendered useless by a dose of 10^4 rads (10^2 Gy). Therefore, we do not reproduce bar charts here, but give comments derived from them.

15.3.2. Thermoplastics

15.3.2.1. Structural plastics

A very large variety of parts of machines and electronics are made by the injection-moulding of thermoplastics. Radiation tolerance estimates related to the mechanical performance of about 35 different types of polymer are listed by Schönbacher. These indicate that very few thermosetting plastics show damage effects below a dose of 1 megarad(10^4 Gy). Those that may show damage at this dose include polypropylene, polyformaldehyde (Delrin) and PTFE. In the case of PTFE, the results quoted above are for irradiation in air. In vacuum, the tolerance of PTFE is increased tenfold. The most tolerant thermoplastics include polyimides (Kapton), Mylar and polystyrene. In all halogenated polymers (PTFE, PVdF, PVC), the possibility of release of halogen acid vapour must be considered. Rupture strength and elasticity are usually the properties of most interest in this group.

15.3.2.2. Plastic films as dielectrics and coatings

Thin, thermoplastic films (usually extruded or solution-cast) are often used at the limit of their mechanical or electrical strength in capacitors, varnishes or wrappings. Polyester (Mylar) and polyimide (Kapton) films are found to be very stable under irradiation. Little degradation is found at doses of 10^9 rads.

Polyethylene film develops an odour at about 10^7 rads and loses some mechanical strength at 10^8 rads; polypropylene is worse in this respect and becomes brittle. Halogen-containing polymers evolve acid vapours at dose values below 10^8 rads. For example, aluminised PVdF was found to maintain its strength at this dose, but etching of the aluminium occurred as a result of HF evolution. The polyvinylidene series of polymers is said to be less stable than the polyvinyl series.

15.3.3. Thermosetting plastics

Thermosetting plastics are usually formed by the mixture of a fluid prepolymer with an agent which initiates polymerisation (hardener, etc.). This produces highly cross-linked polymer. Composite structural elements, PCBs (printed circuit boards) and adhesives are made from this class of polymer. The manufactured formulas are very varied and, therefore, response to radiation is diverse. However, the radiation tolerance is often good because of the original cross-linking present. Epoxy adhesives lose only about 10% of their tensile shear strength at a dose of 10^9 rads in air. Epoxy glass laminates also show good performance at this dose level.

15.3.4. Elastomers

The need to maintain elasticity is of course the critical property in this group. The most stable elastomers are polyurethanes and phenylsilicones (usable to well above 10^8 rads). Nitriles, butadiene styrenes and natural rubbers also can be used up to 10^8 rads. Butyl rubber liquefies and neoprene evolves HCl at similar dose levels. Most proprietary polyurethane foam rubbers can be used as electrical encapsulant materials at a dose level of 10^9 rads in vacuum at temperatures between -85 and +250°C. Silicone and polysulphide sealants are probably less radiation tolerant.

15.4. RADIATION-INDUCED CONDUCTIVITY IN INSULATORS

The exposure of solids to ionising radiation produces current carriers in the form of electrons and holes. If the original conductivity is small, then the presence of carriers produces an observable increase in the background conductivity of the material σ_B. The increases follow the rules of normal conduction and we can thus calculate a "radiation-induced conductivity" (RIC) value R. Ideally, this will increase instantaneously to a steady level when exposure starts and decay when it stops. If R is large and σ_B is small, we can use the simple formula:

$$R_R = \frac{L}{\sigma_R . A} \qquad \text{.....15(i)}$$

where L is the sample length, A is the sample area and R_R is the resistance of the insulator during irradiation (assumed to be very much greater than the background resistance).

We can say that a new resistor R_R appears in parallel with resistor R_B which represents the small background conductivity.

The expected magnitude of this new resistor R_R can be found from the curve in Fig. 15.1. The ideal radiation-induced response of a polymer is given by the curve:

$$R = 10^{-18} \cdot \sigma_R D \qquad \text{.....15 (ii)}$$

where D is the dose rate in rad min^{-1} and R is the response in $ohm^{-1} .cm^{-1}$.

The measured results for many polymers lie about the curve and the linear formula may be used for approximate predictions of RIC. The photocurrent I_R is of course calculated from R_R by Ohm's Law. For some polymers, the dependence of R_R on D is however not linear, e.g. the points given in Fig. 15.1 for polyethylene show R_R to be proportional to $D^{0.7}$.

In Fig. 15.1, some representative dose rate values for space vehicles, fusion reactors and gamma pulses from nuclear bursts are marked on the bottom scale. The radiation-induced conductivity values for these three conditions are respectively 10^{-18}, 10^{-13} and 10^{-6} $\Omega^{-1} . cm^{-1}$. We can see that, for a 1 cm cube of polymer, these represent R_R resistors of values 10^{18}, 10^{13} and 10^6 Ω respectively. As regards the practical impact, we can see that probably only in the last case would this resistance change produce any noticeable reduction in the performance of a polymer as an insulator. This is because the insulation resistance R_B will be typically of the order of 10^{13} Ω. Adding a resistor of the same, or higher, value in parallel will not produce a serious disturbance of the insulator's function.

The linear formula shown above (15(ii)) gives us a simple engineering approach to apply to leakage questions for space systems or ground installations. However, Fig. 15.1 shows us that it may not give the "worst case" RIC value for low dose rates.

15.5. SUMMARY

Radiation effects on polymers include permanent degradation and transient conductivity. In spacecraft, internal plastics should not normally be severely affected mechanically or electrically, but optical and other electronic properties may be changed. At the spacecraft surface, heavy particle bombardment may have severe effects on plastic sheeting or coatings.

The commonly published bar charts refer mainly to effects on mechanical properties, not to electrical or optical effects which may be more severe. In engineering terms, designers should recognize that polymeric materials in special high-performance uses may be subject to radiation-induced degradation and, as in the case of electronic piece parts, this should induce them to carefully scrutinise plastic items intended for such use.

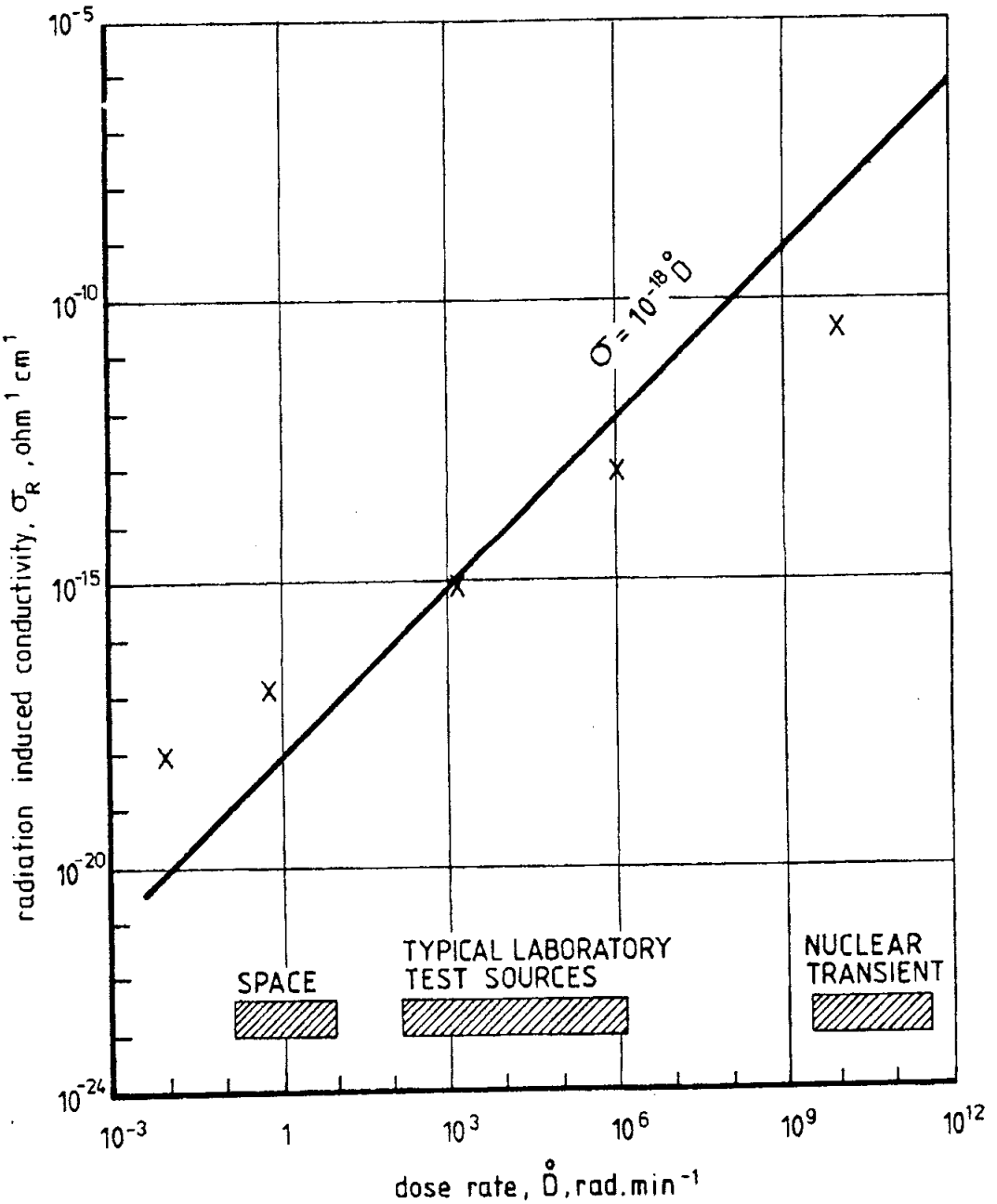

(The crosses show an exception, polyethylene)

FIGURE 15.1 - PREDICTION CURVE FOR RADIATION-INDUCED CONDUCTIVITY IN MANY POLYMERS

REFERENCES

P. Beynel, Maier, P. and H. Schönbacher, "Compilation of Radiation Damage Test Data, Part III: Materials Used around High-Energy Accelerators", Report No. CERN 82-10, CERN, Geneva (Nov. 1982)

F.J. Campbell, "Radiation Damage in Organic Materials", Radiation Physics and Chemistry 18 (1-2), (1981)

"The Particle and Ultraviolet (UV) Radiation Testing of Space Materials", (J. Dauphin), ESA PSS-01-706 (1983)

C.L. Hanks, and D.J. Hamman, "The Effects of Radiation on Electrical Insulating Materials", Report No. REIC-46, Radiation Effects Information Center, Battelle Memorial Institute, Columbus, Ohio (June 1969)

J. Hitchon, "Radiation Stability of Plastics and Rubbers", Report No. AERE M-3251, U.K. Atomic Energy Research Establishment, Harwell, Didcot, U.K. (1983)

H. Schönbacher, and A. Stolarz-Izycka, "Compilation of Radiation Damage Test Data, Part I: Cable Insulating Materials", Report No. CERN 79-04, CERN, Geneva (June 1979)

H. Schönbacher, and A. Stolarz-Izycka, "Compilation of Radiation Damage Test Data, Part II: Thermosetting and Thermoplastic Resins", Report No. CERN 79-08, CERN, Geneva (August 1979)

A.J. Swallow, "Radiation Chemistry", Longman, London (1973)
M.H. Van de Voorde, "Effects of Radiation on Materials and Components", Report No. CERN 70-5, CERN, Geneva (Febr. 1970)

M.H. Van de Voorde, and C. Restat, "Selection Guide to Organic Materials for Nuclear Engineering", Report No. CERN 72-7, CERN, Geneva (May 1972)

L.A. Wall, "Fluoropolymers", Wiley Interscience, New York (1972)

PAGE INTENTIONALLY LEFT BLANK

SECTION 16. THE INTERACTION OF RADIATION WITH MATERIALS

16.1 INTRODUCTION

Previous sections have described the radiation environment to which Earth-orbiting electronic devices may be exposed, and have indicated how these devices react to that exposure. It will now be useful to describe the physical principles which govern the transfer of energy from the incoming radiation flux to the device materials. Of fundamental importance in this respect is the estimation of the attenuating effect of other materials protecting the device from the external radiation environment. This protection may be provided fortuitously ("built-in absorber") by spacecraft structural members or covers, or may have to be added specifically for protection ("add-on absorber").

This section describes some of the physical processes involved in radiation transport through matter, its attenuation, scattering and generation of secondary radiation.

Radiation attenuation data for the most important parts of the Earth's radiation environment are given in graphical form. These data should allow evaluation of radiation doses in simple geometries, given the input electron and proton energy spectra.

These data supersede those presented by Holmes-Siedle and Freeman (1978).

Subsequent sections will discuss ways of making the best use of shielding material at minimum cost and weight penalty, and describe computerised methods which deal with the complexity of some radiation-dose calculations for spacecraft.

16.2 PARTICLE RADIATION TRANSPORT

Energetic particles passing through material can undergo a variety of interactions leading to energy-loss, scattering and/or the generation of secondary particles. In Section 3 it was seen that the principal components of the Earth's radiation environment are energetic electrons and protons. Interactions involving these particles are summarised below.

16.3 ELECTRONS

Electrons interact with material mainly at the atomic level, producing excitation and ionisation while losing energy and being scattered in the process. Because of their low mass relative to nuclei, electrons are readily scattered through large angles and complete "backscattering" of electrons from materials can be significant, especially in high-Z materials. Electron acceleration in the strong electric fields of the atom result in the generation of energetic photons, a process known as "bremsstrahlung" (braking radiation).

Figure 16.1 illustrates electron/bremsstrahlung behaviour in matter. Electron and bremsstrahlung photon trajectories are shown in both aluminium and in lead. These trajectories were computed by Daly using the CERN Monte-Carlo code GEANT (see Section 18 for a discussion of computational methods). The figure shows clearly the tortuous nature of electron motion and the production of penetrating bremsstrahlung. Lead is clearly a better absorber of electrons than aluminium.

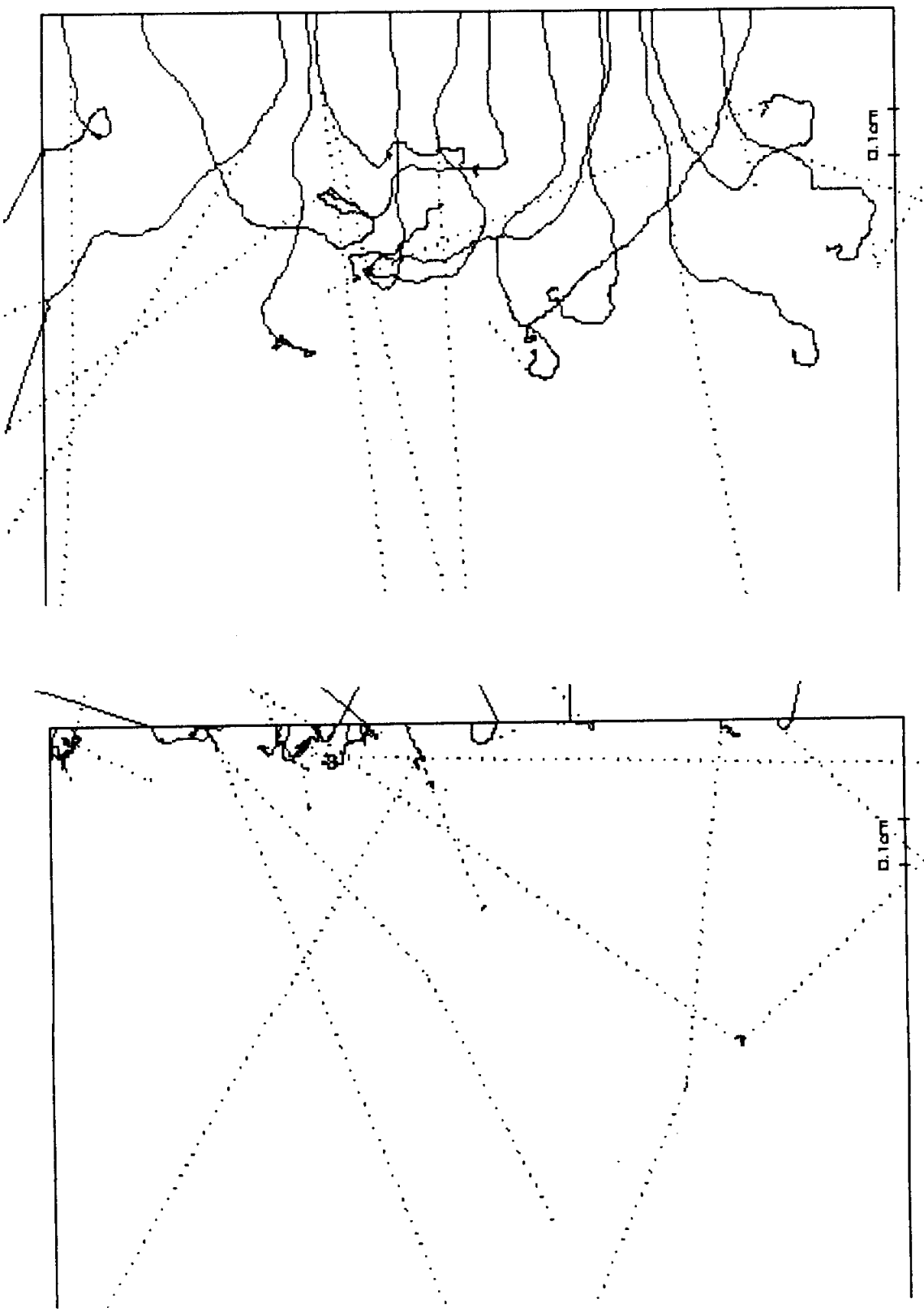

Trajectories of 5 MeV electrons in (a) aluminium and (b) lead as computed with the GEANT Monte-Carlo code. Electrons are injected normally from above. Dotted lines indicate the paths of bremsstrahlung photons induced by the electrons.

FIGURE 16.1

16.3.1 Transmission coefficients for electrons

We have already indicated that the transmission of electrons through material is a highly complex process. They do not travel in continuous straight lines, but follow highly scattered paths. The degree of scattering depends, for example, upon the material, the incident particle energy and the angle of incidence. A number of sophisticated analytical treatments have been developed to estimate the dose deposited and the residual flux after transmission of electrons through material of given "stopping power". Among the best known are the various "Monte Carlo" methods, whereby an electron track through a material is divided into a large number of "steps" very similar to the real case. In a typical treatment of an aluminium medium, as described by Berger & Seltzer (1968), the step size is chosen such that the electron energy decreases on average by a factor of 2^{-8} per step.

When a stream of "mono-energetic" electrons passes through a material, the energy and particle flux are both reduced. The emergent energy spectrum is broadened and somewhat asymmetric; however, a clearly dominant peak or "most probable energy" is preserved and its value will be less than the incident energy.

Number Transmission Coefficient (NTC) is the ratio between the total emergent particle fluence N_e and the total incident particle fluence, N_i :

$$NTC = N_e/N_i \qquad \text{.....16(i)}$$

Values of NTC for the transmission of omnidirectional electrons of energy 0 - 6 MeV through plane aluminium shielding of various thicknesses are tabulated by Berger & Seltzer (1968). These values are derived from the work of Hardy et al (1967) at NASA.

Figure 16.2 shows a graphical presentation of values of NTC as a function of aluminium absorber thickness (actually mass thickness in g. cm^{-2}) for various incident energies. A feature of each curve is the "tail", an effect of "straggling electrons" which penetrate further than might otherwise be expected. The tails of the curves cut the thickness axis at the "maximum range" for a particular energy. The broken lines, which neglect the straggling effect, cut the axis at the "Practical range". The practical ranges indicated in Figure 16.2 agree well with those given for aluminium by, for example, Linnenbom (1962).

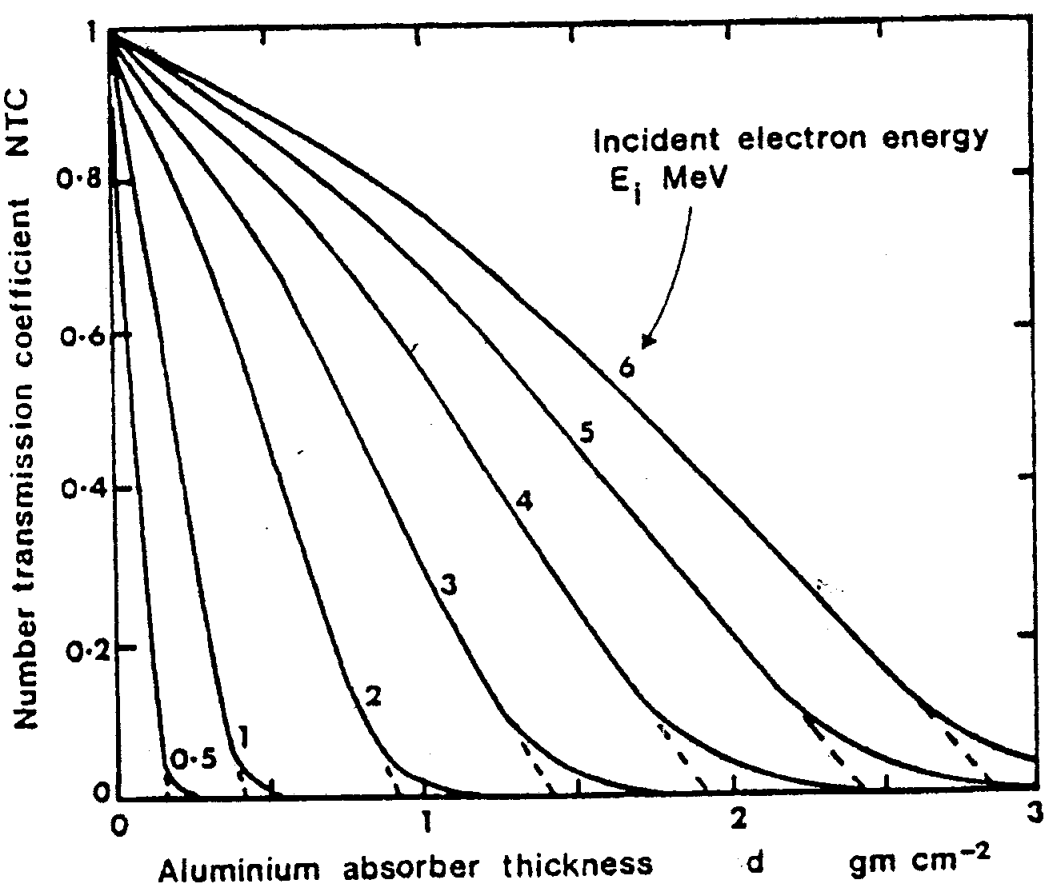

Number Transmission Coefficient (NTC) of omnidirectional electrons through plane aluminium absorber as a function of thickness.

FIGURE 16.2 - ELECTRON TRANSMISSION

16.3.2 Stopping power

For electrons in the energy range less than 5 MeV, typical of the Earth's trapped radiation belts, almost all energy loss during passage through material is by interaction mechanisms that result in ionisation of the material, i.e. the creation of electron-hole pairs with no momentum transfer to the atoms. The rate of loss of energy with distance traversed, known as the "stopping power" of the material, is given by the following equation (Berger and Seltzer, 1982):

$$\frac{dE}{dx} = \frac{2\pi e^4 z^2 N_A Z}{mv^2 A} .Be \qquad .....16(ii)$$

when ρN_A is the number of atoms per unit volume, where N_A ($\sim 6 \times 10^{23}$) is Avogadro's number atoms/mole, v is the velocity of the electron, e and m are the charge and mass of an electron, and x = "path length" or distance measured along the track of an electron.

B_e is known as the "electron stopping number" of the material; it is a function of particle energy, but rises only slowly with E. Therefore, dE/dx at first falls rapidly with increasing E (and hence v), being dominated by the $1/v^2$ dependence. It reaches a minimum as v approaches a limit at the speed of light. At higher energies (corresponding to a relativistic increase in electron mass), dE/dx rises slowly with the now dominant B dependence, since v is now limited.

The minimum stopping power for electrons occurs at energies in the range 1 - 2 MeV; electrons at this energy are said to be "minimum ionising". The amount of data available on stopping power for various materials is considerable (Berger & Seltzer, 1982). Note that, normally, stopping power is quoted in units of energy lost per unit "mass thickness" measured along the particle path in $MeV.g^{-1}.cm^2$ $\left(\frac{1}{\rho}\frac{dE}{dx}\right)$.

In addition to energy loss by collision, there is a further contribution to stopping power due to radiation loss (i.e. bremsstrahlung generation). At energies below 1 MeV, this is extremely small when compared with collision loss as a mechanism for stopping electrons. It is a rising function of energy, but does not dominate over collision loss except at energies well over 10 MeV. For the typical near-Earth electron spectrum (1 - 4 MeV), only a very small fraction of the energy passes into bremsstrahlung, but the latter radiation is so much more penetrating that it emerges as a significant remaining "background" when all electrons have been stopped.

16.3.3 Internal spectrum

The energy spectrum of the particle radiation emerging from the inner surface of an absorber will clearly be a degraded form of the incident external spectrum. Particles of lower energy, having ranges less than the shield thickness, may be completely stopped while at higher energies there will be a reduction in flux.

Figure 16.3 shows the effect on a flat incident isotropic electron spectrum of planar aluminium shielding. This behaviour was computed with the ITS/Tiger Monte-Carlo code by Daly. The change in the electron spectrum is shown in Figure 16.3(a), while Figure 16.3(b) shows how the emerging spectrum depends on direction.

Note that the fluxes shown are normalised to unit incident current and are differential in energy. On average, it takes 4 electrons distributed isotropically to produce unit current, 2 of which are moving away from the medium. In addition to this, 20 groups are used, each with a width of 0.25 MeV. Therefore, the unshielded flux is 0.4 electrons/MeV/unit incident current (20 X 0.4 X 0.25 MeV = 2 electrons).

Figure 16.3(a) shows that with small amounts of shielding, the upper edge of the spectrum is degraded but that this is accompanied by an enhancement of the low-energy portion of the spectrum, because of secondary electrons. As the shielding increases, both low and high-energy electrons are attenuated and lose energy, producing a rounding of the spectrum. Figure 16.3(b) shows that a significant fraction of the emerging electron flux is at relatively large angles to the normal direction.

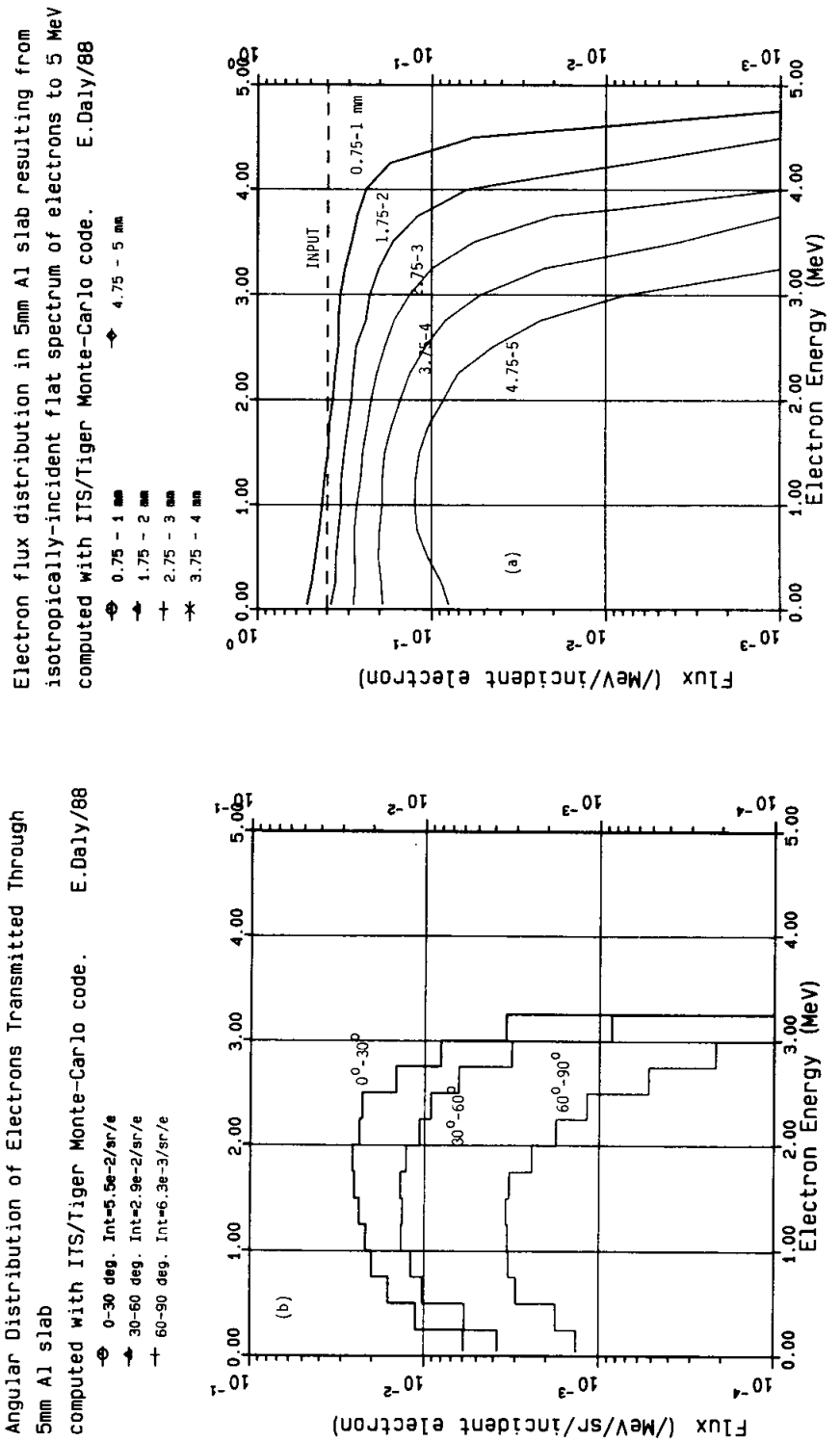

Variation of electron spectra in a 5mm slab. The input electrons are isotropic, with a uniform spectrum up to 5 MeV (indicated by the dotted line in (a)). (a) shows spectra at various depths. The fluxes are differential in energy and normalised to unit incident current. (b) shows the transmitted spectra in three ranges of angles to the slab normal. These fluxes are differential in both energy and solid angle.

FIGURE 16.3

16.4 ELECTROMAGNETIC RADIATION - BREMSSTRAHLUNG, X AND GAMMA RAYS

In spacecraft engineering and operations, energetic electromagnetic radiation can be encountered in a number of forms:

(a) Bremsstrahlung radiation produced by the slowing of energetic electrons in the atomic electric fields of a material. The electrons may be either from the space environment or from ground-testing electron beams.

(b) X-radiation produced by electron-beam excitation of atomic transitions.

(c) Nuclear emissions, Cerenkov radiation, etc..

The interaction of electromagnetic radiation with matter is thus a topic of some importance to those predicting or testing the response of devices to radiation, particularly where device electrode materials of high atomic number, such as gold and molybdenum, lie in close relation to the active region of the device. A discussion of the relevant general features of interactions is given here, while discussions of specific problems such as dose enhancement and package attenuation are given in other sections.

Since bremsstrahlung, X-rays and other electromagnetic radiation are just differing manifestations of the same type of radiation, they are absorbed according to the same laws. However, whereas bremsstrahlung is usually spread over a broad spectrum, X-rays and gamma-rays have well-defined energies, corresponding to atomic and nuclear energy states.

16.4.1 Bremsstrahlung

Photons produced by the bremsstrahlung mechanism are a significant problem in space applications because the ranges of the photons are generally greater than those of the primary electrons themselves. The production of bremsstrahlung is higher in materials of high atomic number, Z, and is proportional to the square of Z. Bremsstrahlung attenuation depends strongly on energy; photoelectric absoption usually dominates at energies below 0.1 MeV, Compton scattering at energies around 1 MeV and pair-production at high energy, above 10 MeV. These processes all result in the production of further electrons.

Figure 16.4(a) shows the bremsstrahlung spectra resulting from the flat electron spectrum shown in Figure 16.3(a). These were also produced with the ITS/TIGER Monte-Carlo code by Daly. Clearly there is a bias towards the production of low-energy photons, and while the shielding is less than the electron range, the continuing

production of bremsstrahlung leads to an increasing photon flux. Figure 16.4(a) shows that a significant fraction of the transmitted bremsstrahlung photon flux is at large angles from the slab normal.

16.4.2 X-rays

X-rays are produced by electron transitions in the atom. These can be stimulated by bombardment of material by an energetic electron beam, as occurs in X-ray tubes.

16.4.3 Other electromagnetic radiation

In passing through optical materials, energetic charged particles can also give rise to Cerenkov radiation. This is a result of particles travelling faster than the speed of light in the medium; the result is electromagnetic radiation emission which may interfere with the optical system's detectors.

Nuclear interactions can also give rise to gamma-radiation which can be troublesome, as mentioned in the next subsection.

Finally, gamma-radiation will be present if radioisotopes are used on-board a spacecraft. For example, radioisotope thermoelectric generators are used in deep-space interplanetary missions.

16.4.4 Production and attenuation of electromagnetic radiation

16.4.4.1 Production

Figure 16.5 (from Wayard) shows the spectrum of bremsstrahlung X-ray photons generated when a 1 MeV electron beam strikes a considerable thickness of material. As described later, this broad spectrum results from a complex process, but it will be seen that the peak of the spectrum emitted is at a photon energy of about half the energy of the impinging particle. Because it is broad, the emission is sometimes called "White Radiation".

Bremsstrahlung-generating efficiency is strongly dependent upon material; a heavy element will generate bremsstrahlung much more effectively than a lighter one. This efficiency is roughly in proportion to the atomic number. This dependence is not followed so simply, however, when attenuation of bremsstrahlung is dealt with, as described below.

Superimposed on the white radiation described above are the characteristic emission lines of the target material concerned. Table 16(1) gives some wavelengths for common target materials. For most materials, the cluster of K lines will be of greatest interest to us. However, for tantalum, tungsten, gold, platinum and lead, the L lines, which have photon energies in the 7-10 keV region, may also be of significance, especially in testing practices.

Figure 16.6 shows the photon spectra for a tungsten target on a commercial radiographic X-ray machine. The K emission appears as a complex set of lines. It can be seen that a copper filter greatly modifies or "hardens" the spectrum and reduces the influence of the characteristic lines.

Figure 16.7 shows another spectrum for a low-energy X-ray tube operating at 25kV. Here, the 'L' lines are seen and, because of the low beam voltage, the K lines are not excited. Both types of X-ray tube are currently being used for device testing (see later sections).

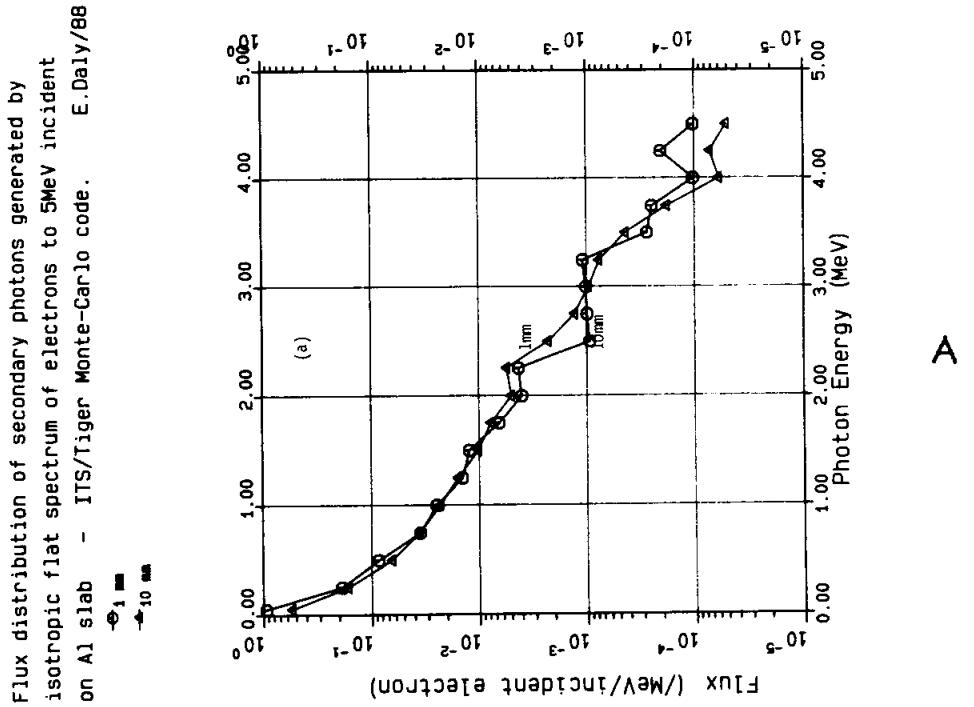

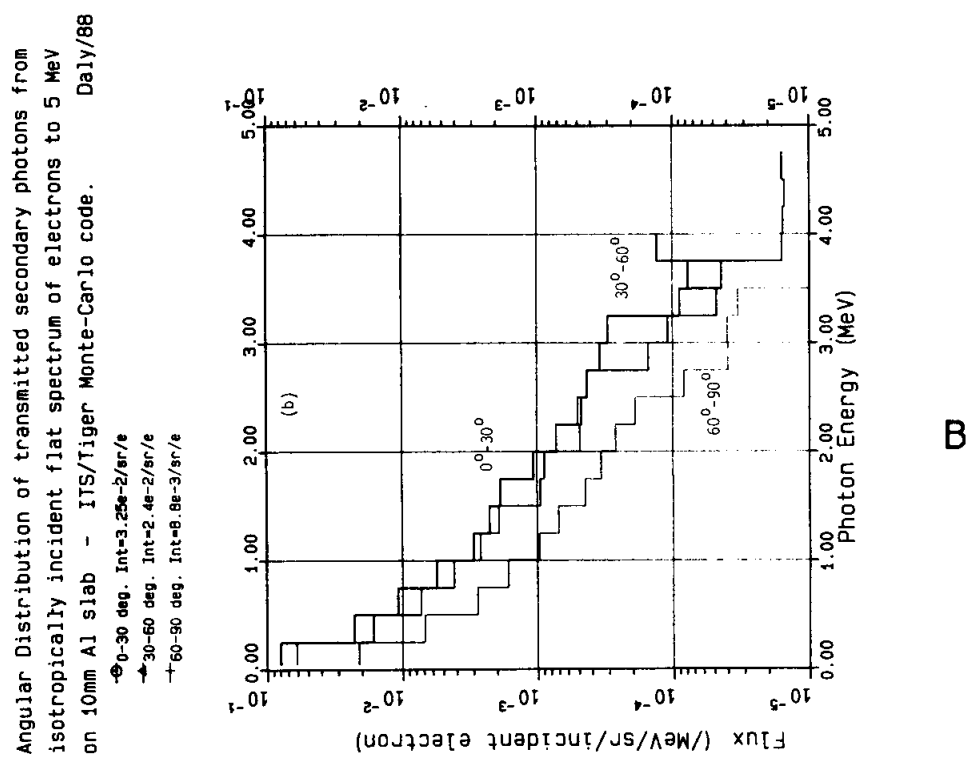

Bremsstrahlung spectra resulting from the flat electron spectrum of Figure 16.3. (a) shows spectra at 1mm and 10mm. The fluxes are differential in energy and normalised to unit incident current. (b) shows the transmitted spectra in three ranges of angles to the slab normal. These fluxes are differential in both energy and solid angle.

FIGURE 16.4

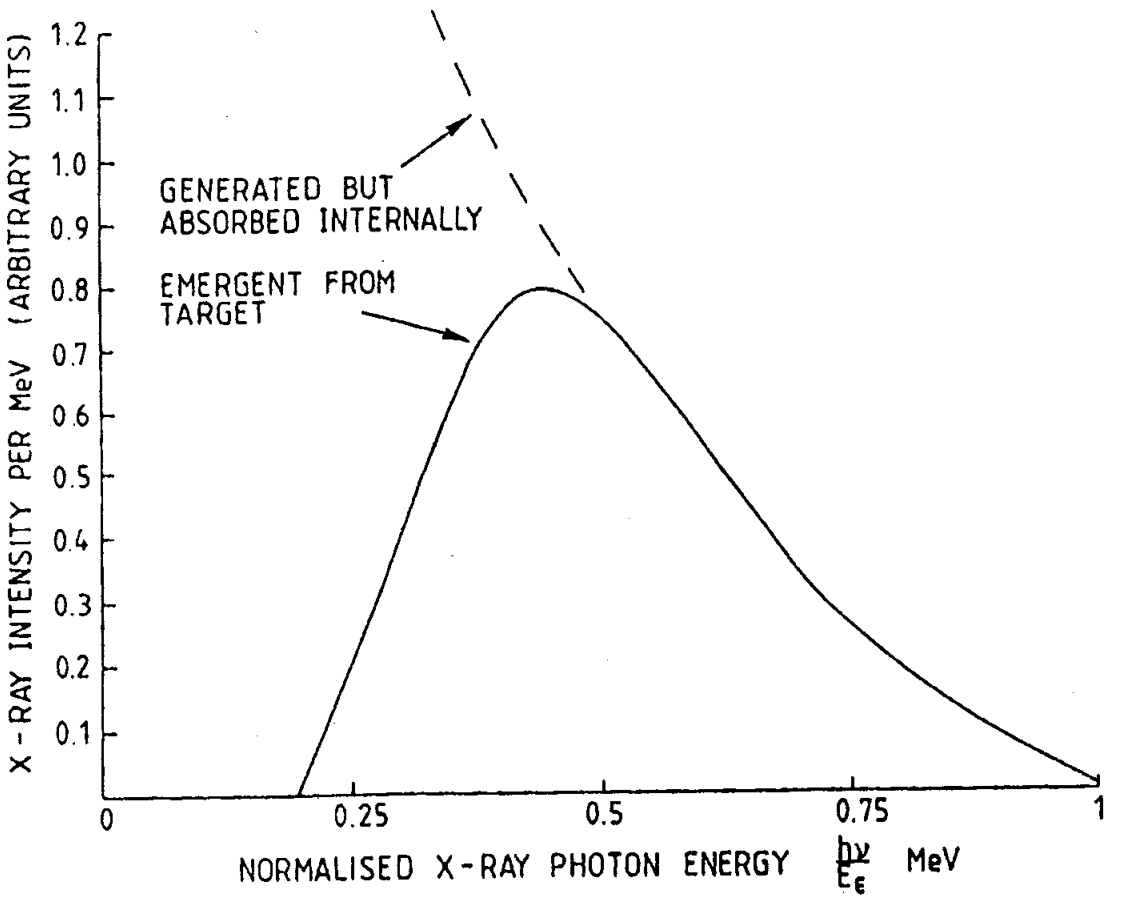

Spectrum of bremsstrahlung X-ray photons generated when electrons are slowed down in a material. For a 1 MeV electron, the energy scale can be read in MeV. The intensity expressed in rads integrated over the whole emergent spectrum will then be of the order of 10^{-12} rad(Si) per unit incident flux.

FIGURE 16.5 - GENERATION OF BREMSSTRAHLUNG

TABLE 16(1) - TYPICAL CHARACTERISTIC X-RAY EMISSION LINES FOR ELEMENTS OF IMPORTANCE IN SPACECRAFT AND DEVICES

Element	Atomic nr. (Z)	Highest 'K' line (keV)	Highest 'L' (keV)
Be	5	0.11	-
C	6	0.28	-
O	8	0.53	-
Al	13	1.56	0.07
Si	14	1.84	0.09
Ti	22	4.96	0.46
Cr	24	5.99	0.65
Mn	25	6.54	0.64
Fe	26	7.11	0.79
Co	27	7.71	0.79
Ni	28	8.33	0.94
Cu	29	8.98	1.02
Mo	42	20.00	2.51
Ta	73	67.42	11.67
W	74	69.48	12.10
Pt	78	78.34	13.56
Au	79	80.66	14.78
Tl	81	85.45	15.33
Pb	82	88.06	15.84
U	92	115.39	21.66

Adapted from R.C. Weast (Ed), "CRC Handbook of Chemistry and Physics" (CRC Company, Cleveland, Ohio, 1973).

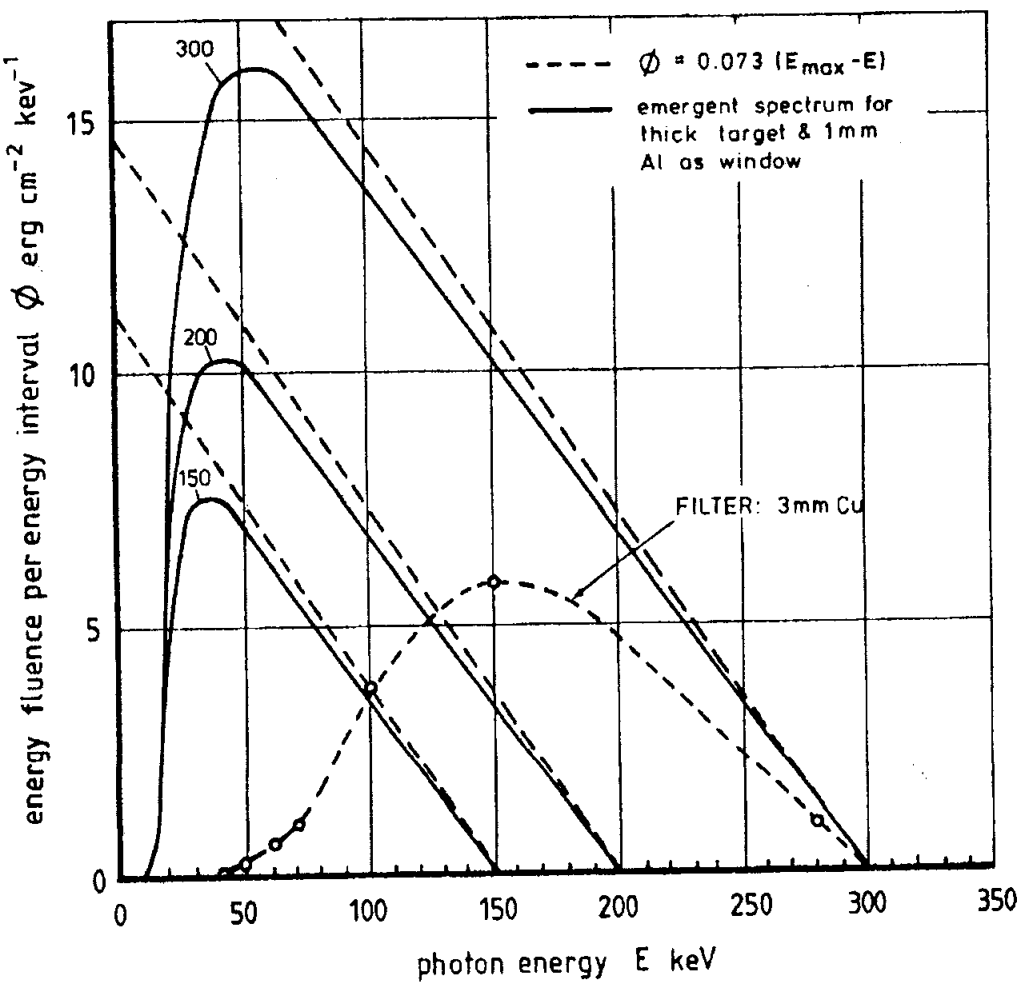

Ideal transmission of high-energy X-ray photons through plastic, aluminium and tungsten. No "build-up" included.

FIGURE 16.6 - BREMSSTRAHLUNG TRANSMISSION

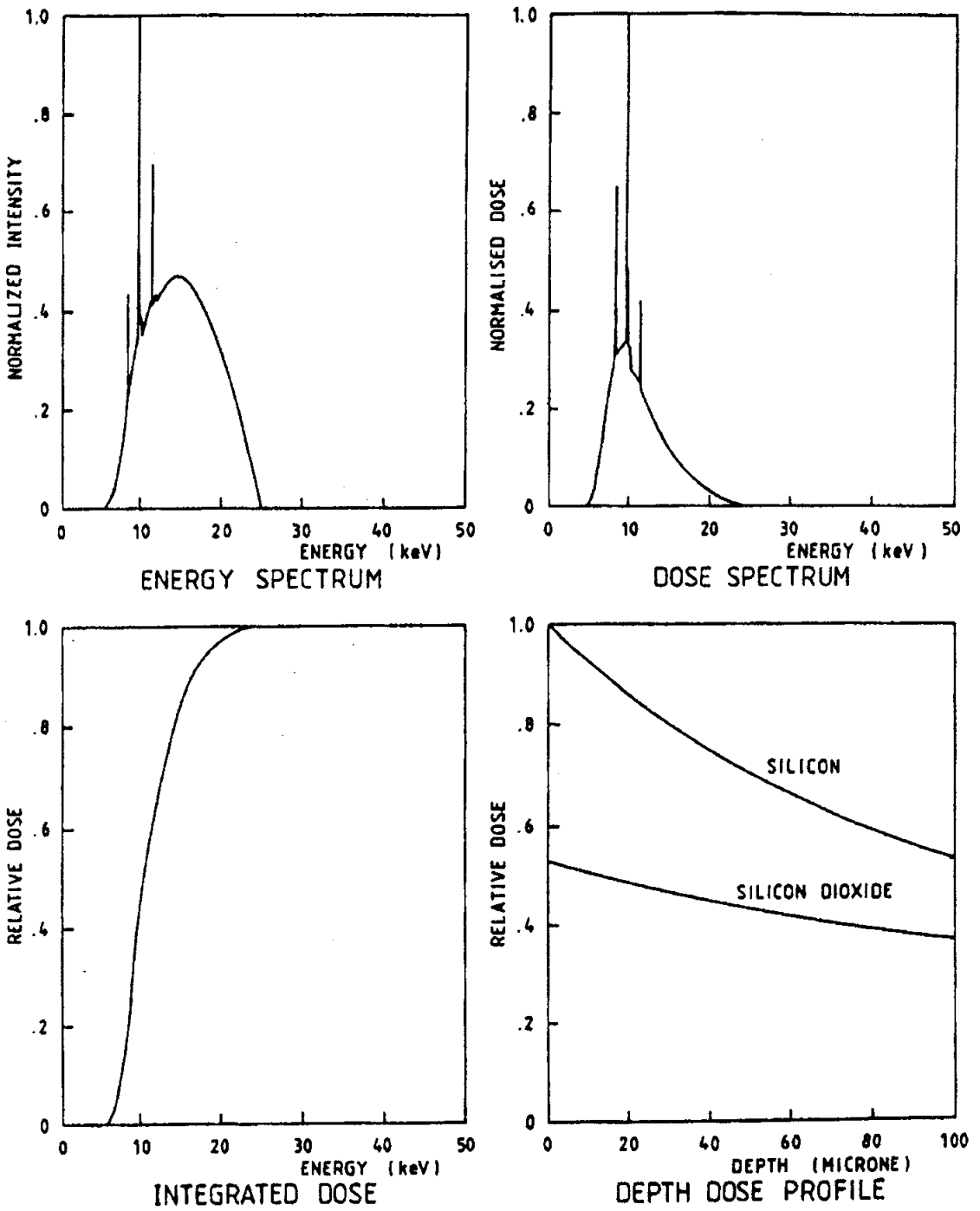

(Courtesy of Aracor Inc.)

FIGURE 16.7 - X-RAY ENERGY SPECTRA AND DOSES DEPOSITED BY A LOW-VOLTAGE MACHINE: 0.006" A.C. FILTER

16.4.4.2 Attenuation

An important feature of electromagnetic radiation in the 5 to 1000 keV range (X-rays) is the strong difference in attenuation from material to material and the very wide range of attenuation per unit thickness over that energy span. We will illustrate this with a few cases.

In ideal circumstances, known as "narrow geometry", X-rays are attenuated according to Lambert's Law:

$$I = I_0 e^{-\mu_m x_m} = I_0 e^{-\mu x} \qquad \text{.....16(iii)}$$

where $x_m = x$ is the areal density (thickness normalised to material density ρ, expressed in g/cm^2 or kg/m^2); μ is linear absorption coefficient and $\mu_m = \mu/\rho$ is the mass absorption coefficient.
μ is the attenuation coefficient for the material and is a total of the energy absorption and scattering powers of the constituent atoms.

μ is derived from the sum of all the interactions of a photon with a material (photoelectric absorption, Compton scattering etc.) and is often expressed in the form of a cross-section (a probability) of these interactions:

$$\sigma_{tot} = \sigma_1 + \sigma_2 \ldots \text{etc.} \qquad \text{.....16(iv)}$$

where σ tot is the total cross-section (probability) per atom and σ_1, σ_2 etc. are the probabilities for particular physical processes.

The relation of attenuation coefficient to the above is:

$$\mu = \frac{N_A Z}{A} \sigma \text{ for electron scattering} \qquad \text{.....16(v)}$$

The attenuation coefficient is sometimes given as the "mass attenuation coefficient" μ/ρ in units of $cm^2 .g^{-1}$.
For dosimetric calculations, another form of μ is used, namely the "energy absorption coefficient" which includes only radiation energy absorbed and ignores attenuation due to scattering.

A list of mass attenuation coefficients for megavolt photons is tabulated in Appendix D. The table shows that, in the region of 1MeV, the dependence of absorption upon atomic number is quite weak.

Thus, for example, 1 $gm.cm^{-2}$ of lead (0.1 mm) will produce 7% attenuation of 1 MeV photons while the same "mass thickness" of aluminium (3.7 mm) will produce 6%. Only large thicknesses of

aluminium (3.7 mm) will produce 6%. Only large thicknesses of shield material will significantly attenuate photons of these energies produced by Van Allen belt electrons.

It has been mentioned above that all materials are roughly equivalent in the efficiency of stopping X-rays in the megavolt range. Unfortunately, this statement ceases to hold at lower energies. At 100 keV, for instance, very great differences in absorption exist between, say, steel, plastic and biological materials. These differences are also tabulated in Appendix C. They greatly complicate testing with X-rays and make all dosimetry more complex. For example, the attenuation of X-rays at 5 keV is typically 10,000 times higher than at 1 MeV. This large factor implies that radiation testing procedures are less complex when high photon energies are used because package attenuation and scattering are less important.

16.4.4.3 "Build-up"

In calculating bremsstrahlung doses in spacecraft, it must be remembered that the "narrow geometry" required for the exact use of Lambert's Law does not hold. Higher doses will be obtained as a result of scattering effects, sometimes called "build-up", that increase the number of transmitted photons by a factor of 2 at all depths greater than about 5 mm.

Another effect of scattering is also referred to as "build-up"; in gamma radiation testing. "Build-up material" is placed around a sample to promote scattering equilibrium.

16.5 PROTONS AND OTHER HEAVY PARTICLES

16.5.1 Interactions

Energetic protons and ions, being heavier particles, are not subject to the high degree of scattering experienced by electrons and normally follow virtually straight paths. It is relatively easy to compute their slowing and energy deposition in materials and they have well-defined ranges.

There is a small, but not negligible, probability of protons and other ions interacting with atomic nuclei, causing fragmentation of the nucleus or emission of secondary neutrons and protons. Such fragments and secondaries are hazards which cannot be ignored in some circumstances, such as in manned missions or single-event processes. Secondary neutrons produced in spacecraft materials, or even the upper atmosphere, can again interact "inelastically" with nuclei, producing gamma-rays which may interfere with gamma-ray telescopes.

16.5.2 Energy loss and attenuation

The rate of ion energy loss is, as for electrons, defined by a "stopping power" formula (Berger and Seltzer, 1982):

$$\frac{dE}{dX} = \frac{4.\pi\, e^4\, z^2 \rho N_A Z}{m_o v^2\, A} B_i \qquad \text{.....16(vi)}$$

where z is the ion charge number and Z is the material atomic number, B_i is the ion stopping number, N_A is Avogadro's number (6×10^{23}) and A the atomic mass number. $\rho N_A/A$ is the number of atoms per unit volume. Clearly, fully ionised energetic ions, such as cosmic rays, deposit energy very rapidly in a material and this gives rise to single-event phenomena (SEU, latchup and radiobiological damage). This energy loss expression can be readily evaluated to give particle ranges, residual energies and energy deposit, the latter relating to dose and upset.

16.6 RADIATION ATTENUATION BY SHIELDING AND DOSE-DEPOSITION IN TARGETS

16.6.1 Dose

Ionisation induced by the various particles described above on reaching a device results in damage as described in Section 5. Dose, the energy deposited per unit mass of material, is the basic parameter for evaluating ionisation-induced damage. More precisely, this is the "physical absorbed dose". The dose deposited in a "target" depends on the particle type and on the energy which it retains after passing though any surrounding material "shielding". The dose is simply computed from the product of the particle fluence at a particular point and the restricted stopping power of the particle. The qualifier "restricted" means that only the energy loss which results in *locally* deposited energy is considered; the generation of secondaries which travel some distance before depositing their energy is excluded (Berger and Seltzer, 1982).

Evaluation of biological effects of radiation normally involve the use of the quantity "dose equivalent". This quantity attempts to account for the differences in the effects of the same absorbed dose of different radiation types. It is related to absorbed dose by quality factors and dose modifying factors :

$$D_{bio} = \sum_{\text{radiations}} D_{phys} \cdot Q(LET) \cdot DMFs \qquad \text{.....16(vii)}$$

International standards exist for quality factors ; for electrons, X-and gamma-radiation, they are unity, whereas for ions they are a

function of particle stopping power (LET) and reach a value of 20. For fast neutrons, a value of 20 has been set by the ICRP.

There is some uncertainty attached to quality factors, dose modifying factors and to the applicability of the dose concept to heavy ions which have unique biological effects. There are a variety of biological effects over short and long time scales and at high and low dose rates (Bucker and Facius, 1988). This is clearly a highly complex field and beyond the scope of the present document.

16.6.2 Range

The range of a particle in a material is the thickness of material penetrated before the particle loses all its energy. "Practical range" (R_p) is the most probable range of a particle of a given incident energy. Some electrons, in particular, clearly penetrate thicknesses greater than R_p and are often termed "straggling electrons". The term "maximum range" takes this into account ; the distinction will be illustrated more clearly in the subsequent discussion of transmission coefficients.

Range may be expressed either in units of depth (length) or, more commonly, as the product of depth and density ($g.cm^{-2}$). This unit is equivalent to mass per unit area and is used frequently in radiation studies as a measure of absorber thickness (may be termed "shield thickness" in some diagrams). For convenience, we shall henceforward refer to this unit as "mass thickness". Some range values for electrons and proton ranges in aluminium are tabulated in an appendix to this document.

The range of a particle at a given incidence particle energy, when expressed in $g.cm^{-2}$, is closely similar for all materials. There are second-order effects dependent on excitation potential and atomic number, but - at the energies likely to be encountered in the space environment - the spread in range is no more than a factor of two. Plots of the practical ranges of electrons and protons in a number of materials are shown in Figure 16.8. The data of both particles in Si is taken from Berger and Seltzer (1964 and 1966) and from Barkas and Berger (1964). Ranges in aluminium are given by Linnenbom (1962) and proton ranges in aluminium are also given by Cooley and Janda (1963). Data of electron and proton range in various other materials, including germanium and liquid propane, are also given by Berger and Seltzer (1971). When expressed in $g.cm^{-2}$, these ranges are almost coincident with those shown in Figure 16.8 and have therefore been omitted for the sake of clarity.

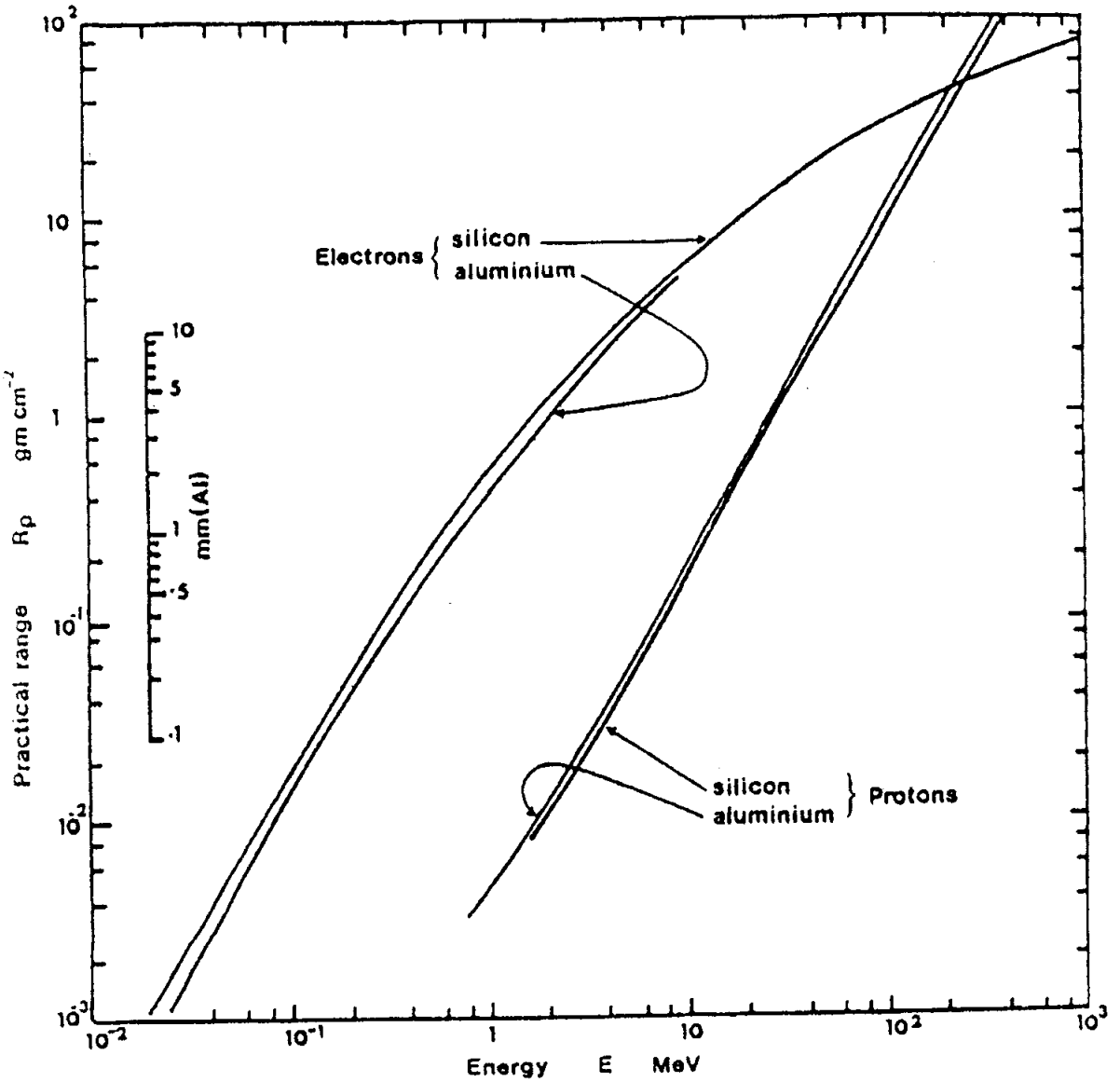

The range of electrons and protons in aluminium and silicon as a function of incident energy.

FIGURE 16.8 - PARTICLE RANGE IN MATERIALS

16.6.3 Relationship between incident flux and deposited dose

In performing evaluations of radiation environments, it is often most convenient to consider a silicon target shielded by aluminium since this relates closely to typical electronic devices in spacecraft and is the basis for much testing work and calculation. The effect of shielding is generally to reduce fluxes of primary particles, to lead to creation and subsequent absorption of secondary radiations and to change the energy spectra of the radiation. Therefore the dose in a target depends on the amount of shielding in a way that is not simple to calculate.

For engineering purposes, a "dose-depth" curve is often used to represent the space radiation environment, its modification by shielding and the resulting dose in components. This gives the dose, either for the individual components of the environment (protons, electrons, bremsstrahlung etc) or the sum of the components, as a function of the thickness of shielding material, usually aluminium. This removes all information about particle energies or even particle type and is usually an integration over orbits or complete missions.

This subsection provides data with which the dose in silicon can be calculated for various thicknesses of aluminium shielding. Computer programs for such purposes are readily available and readers who have a continuing need for such calculations are advised to obtain copies of these programs. Section 18 contains details on programs and how to obtain them.

We will now consider how to calculate the dose which is produced behind a given thickness of aluminium shielding by electrons, electron-induced bremsstrahlung and protons resulting from the broad spectra of electrons and protons found in space.

Seltzer (1979) used the ETRAN Monte-Carlo computer code, simulating the propagation of electrons and photons (bremsstrahlung), to compute the dose generated at different depths in planar, semi-infinite (one-dimensional) aluminium shielding for a range of incident *isotropic, monoenergetic* electron energies. The d(x,E) data set thus created allows an arbitrary input spectrum f(E) to be folded with d(x,E) to yield a sum dose at depth x due to the spectrum. This is normally done by the SHIELDOSE computer program, but can be done manually, given the data. In addition to electrons and bremsstrahlung, Seltzer's data set includes doses from protons, computed by means of the straight-ahead, continuous-slowing-down approximation.

The data set is organised in normalised form, with the depth scale normalised with range and the doses energy-, range- and current-normalised and made dimensionless.

For each type of use, these have been converted to dose (Si) per unit incident isotropic (4 π) electron or proton flux and are shown in Figures 16.9-16.11. There is a pair of curves for each of the important radiation types; electrons, electron-induced bremsstrahlung and protons. For each type, the curves (a) give the doses as functions of incident particle energy for various shielding depths while the curves (b) give the doses as functions of shield depth for various incident particle energies.

In performing an evaluation of the expected radiation dose on a space mission, the shielding geometry should be given some thought. It should be recognized that the doses provided in these figures are for a *planar shield* where, clearly, radiation comes principally from one side and paths which are not normal to the face encounter increased amounts of shielding.

The popularity of planar and slab geometries arises from the efficiency with which Monte-Carlo analyses can be performed with them. A less optimistic basis for the evaluation of shielding effects is to assume spherical shielding. When the dose point is located at the centre, minimum shielding is encountered in all directions. This is preferable for initial evaluation except where there is good justification for the assumption of planar shielding, for example when considering surface materials.

Dose at the centre of a solid sphere of radius z can be derived from the planar dose at depth z by means of the approximation (Seltzer, 1979):

$$D_{sp}(z) = 2D_{pl}(z) \cdot \left(1 - \frac{d\ \log(D)}{d\ \log(z)}\right) \qquad \text{.....16(viii)}$$

If solid-angle sectoring is employed for analysis of complex geometries, doses based on spherical shielding should be used.

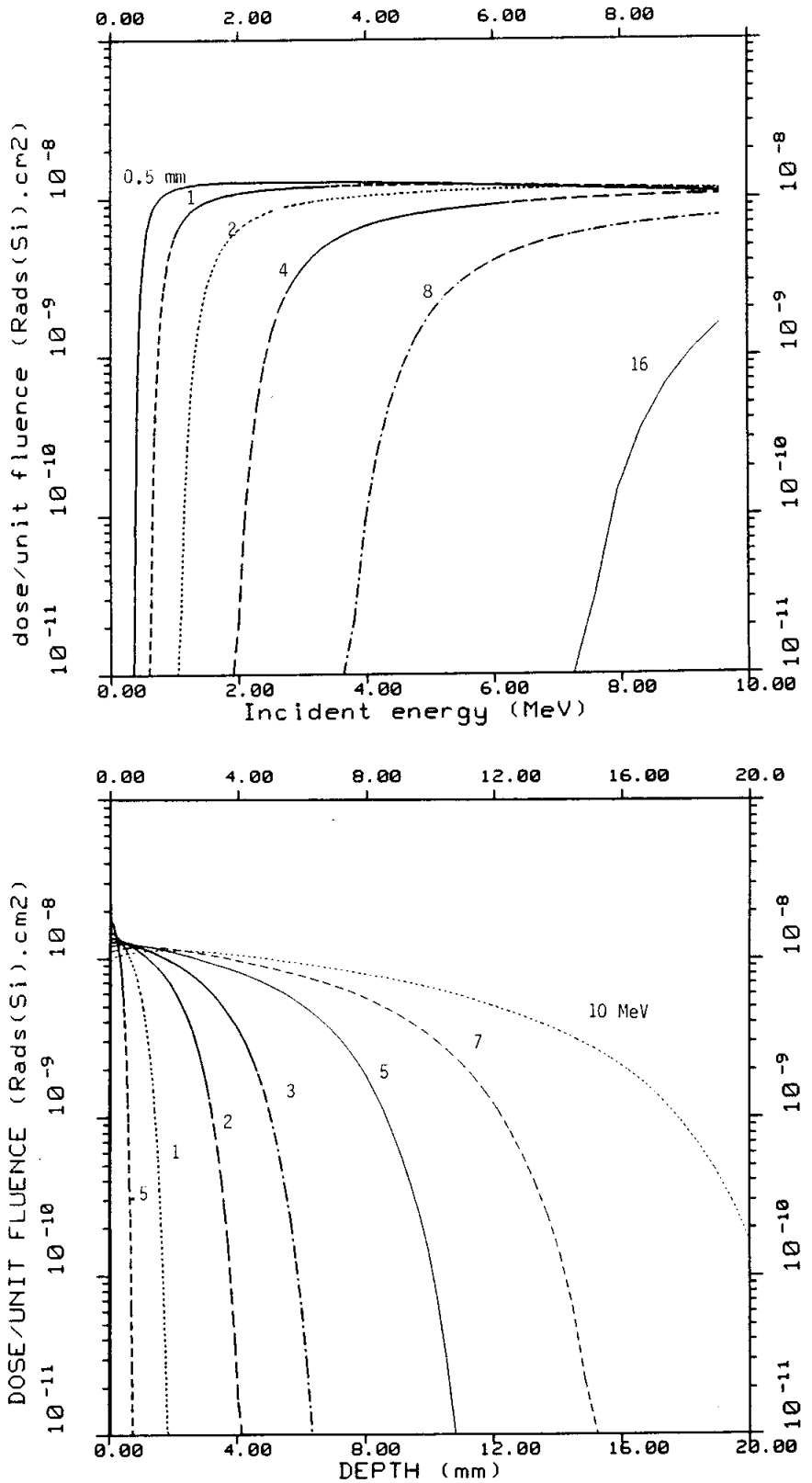

Electron dose deposition in planar semi-infinite aluminium shielding (a) as functions of incident electron energy for different shield depths (mm) and (b) as functions of shield depth for different incident electron energies (MeV). Dose is for silicon and is normalised to unit incident isotropic flux.

FIGURE 16.9

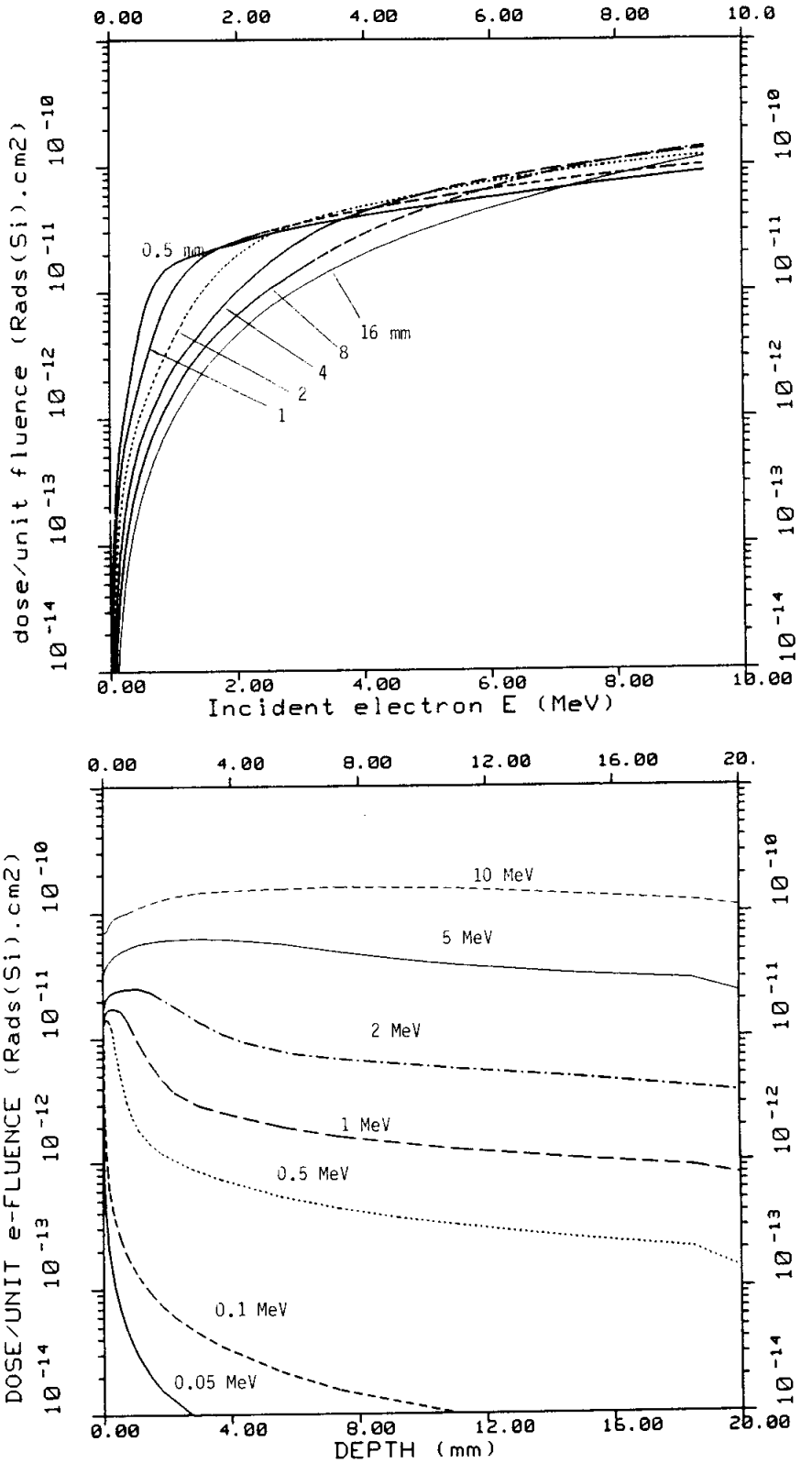

Bremsstrahlung dose deposition in planar semi-infinite aluminium shielding (a) as functions of incident electron energy for different shield depths (mm) and (b) as functions of shield depth for different incident electron energies (MeV). Dose is for silicon and is normalised to unit incident isotropic electron flux.

FIGURE 16.10

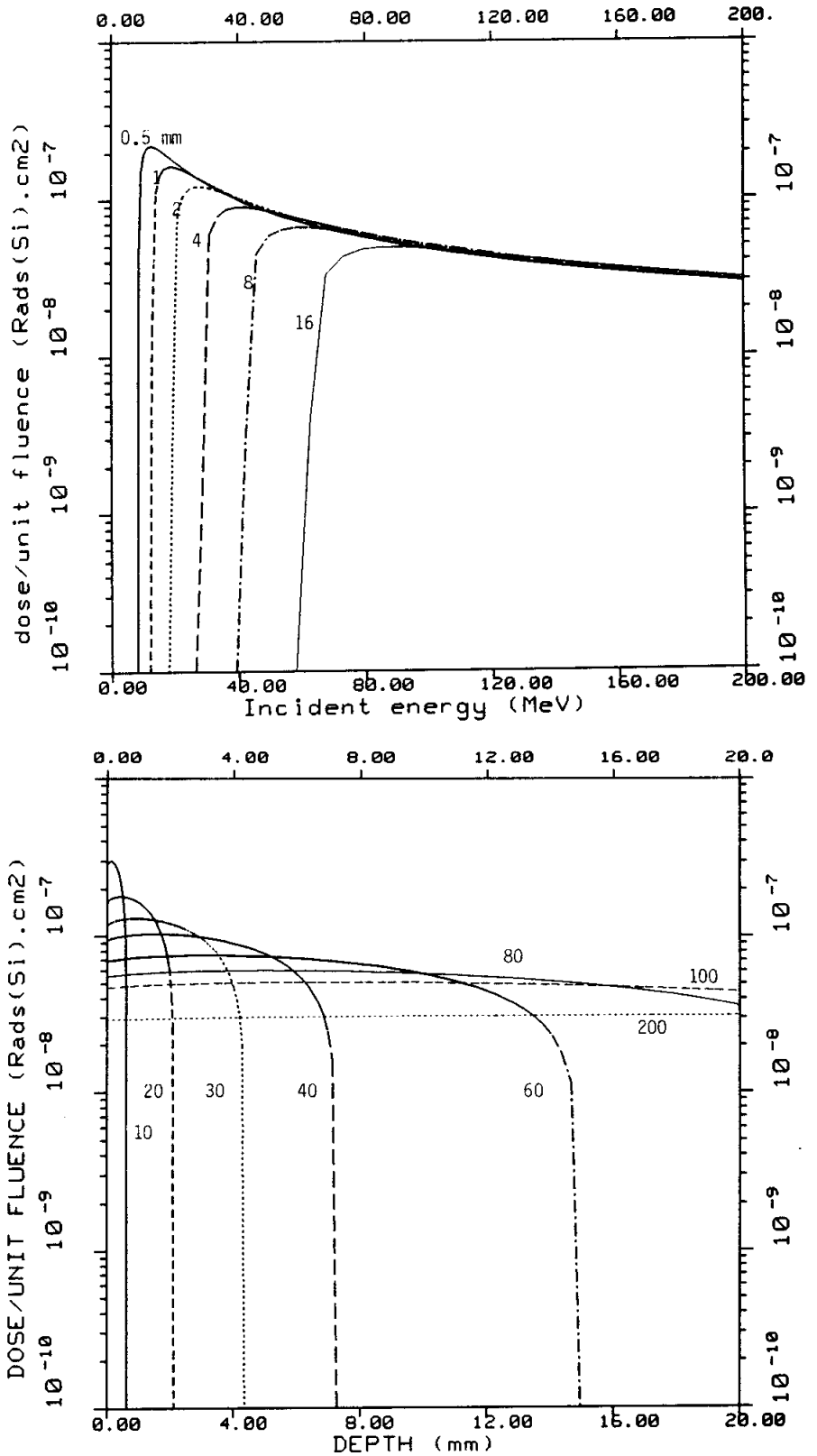

Proton dose deposition in planar semi-infinite aluminium shielding (a) as functions of incident proton energy for different shield depths (mm) and (b) as functions of shield depth for different incident proton energies (MeV). Dose is for silicon and is normalised to unit incident isotropic flux.

FIGURE 16.11

16.6.4 Dose calculation procedure

It is now possible to calculate the relationship between ionisation dose and the depth of absorber (for the time being, only the special case of silicon shielded by aluminium is considered) for any spacecraft orbit where the integrated flux vs energy spectrum is known. The calculation is performed by combining the particle spectrum with the relevant dose transmission curves (Figures 16.9 to 16.11). In principle, the procedure described below is identical for electrons, electron-induced bremsstrahlung and protons.

Given:

(a) Spectrum of omnidirectional integral flux, ϕ (>E) versus energy E,

(b) Dose per unit fluence curves, D_F (d), showing dose per unit particle fluence versus incident energy at a specified depth (or "mass thickness").

Procedure:

(i) Calculate flux element in a small energy interval of width ΔE and of mean energy E_m .

$$\Delta\phi(E_m) = \phi(>E_1) - \phi(>E_2) \qquad \text{.....16(ix)}$$

where

$$E_1 - E_2 = \Delta E$$

Alternatively, if differential spectra are available:

$$\Delta\phi(E_m) = \frac{d\phi(E_m)}{dE} \times \Delta E \qquad \text{.....16(x)}$$

(ii) Read the dose per unit fluence, D_F (d), at energy E_m for the appropriate absorber thickness d.

Calculate the dose contribution ΔD (per unit time) due to the flux element in energy interval:.

$$\Delta D(dE_m) = D_F(d,E_m) \times \Delta\phi(E_m) \qquad \text{.....16(xi)}$$

Note here that multiplication of the dose per unit fluence by the flux (fluence per unit time) yields, strictly, a dose rate. The time unit for dose rate is often given as the mission duration (e.g. 7 years); in this context, the term "total dose" is often used to describe mission dose.

(iii) Calculate the total dose for thickness d by adding dose contributions from the energy intervals covering the whole energy spectrum.

Thus, the total dose $D(d) = \sum_{E_m} \Delta D(d,E_m)$ at all E.

(iv) Repeat the procedure for several values of thickness d. Plot D(d) against d, giving the "Dose-depth" curve.

(v) Repeat the procedure for each component of the environment, trapped protons and electrons, and solar flare protons. Note that for calculating the bremsstrahlung dose, the electron flux is used together with the bremsstrahlung dose data.

We are free to choose the width of the "small" energy intervals and of the energy spectrum over which to collect dose contributions. Clearly, more accurate results are obtained by considering larger numbers of energy intervals of smaller width.

The "hardness" of the flux spectrum, dependent upon the rate of change of flux with energy, is an important factor in the actual choice (a "hard" spectrum is one showing little change with energy). As far as the spectrum width is concerned, it is clear that the lower limit is set by the thickness (and therefore particle range) being considered. The higher limit is effectively reached when dose contributions from successive energy intervals cease to be a significant part of the total. Thus, for non-computerised calculations, a certain degree of trial and error is necessary.

16.7 ATOMIC DISPLACEMENT DAMAGE

The degradation of energy and number of particles as they proceed through a slab of absorber has been explained in detail in preceding sections dealing with the ionisation dose versus depth relations for absorbers surrounding electronic equipment. Curves analogous to those for dose transmission may sometimes be required for a limited range of electronic devices which are also sensitive to displacement damage. Thus, in the same way as before, generalised damage tramsmission versus energy curves may be made first so that "damage-depth" curves can be calculated for a given set of particle spectra. Brown, Gabbe and Rosenzweig constructed such curves on the same general basis as our dose transmission shown here as Figures 16.12 and 16.13. They are useful in, for instance, studies of solar cells.

For a complete description of solar cell degradation and the concept of damage equivalence for evaluating such degradation, the reader is referred to Tada et el. (1982). They also give, for a variety of solar cells, the degradation to be expected in cell output

Data handling equipment employs high-speed bipolar transistors which are insensitive to the displacement effect by virtue of their design.

The narrow base region confers this insensitivity (see Section 7). Some power transistors have base regions wide enough to experience damage-induced gain degradation, but the use of these in the power units of a spacecraft can usually be avoided. Finally, an order of magnitude calculation shows that, except for the very inhospitable inner-belt "heart" region, vehicles in 5-year circular equatorial orbits will not experience sufficient exposure for serious damage to occur in transistors of medium-power design (frequency cut-off about 100 MHz). "Serious damage" here may be taken to represent a decrease of 10% in gain. For dealing with such transistors, or even more sensitive ones of wider base (lower frequency cut-off), the "BGR" damage curves will suffice so long as the vertical scale is multiplied by 2 to allow for non-infinite back-shielding. It should be noted that in typical fast-switching transistors in space, the "surface effect" due to ionisation will be more problematical than the atomic displacement effect.

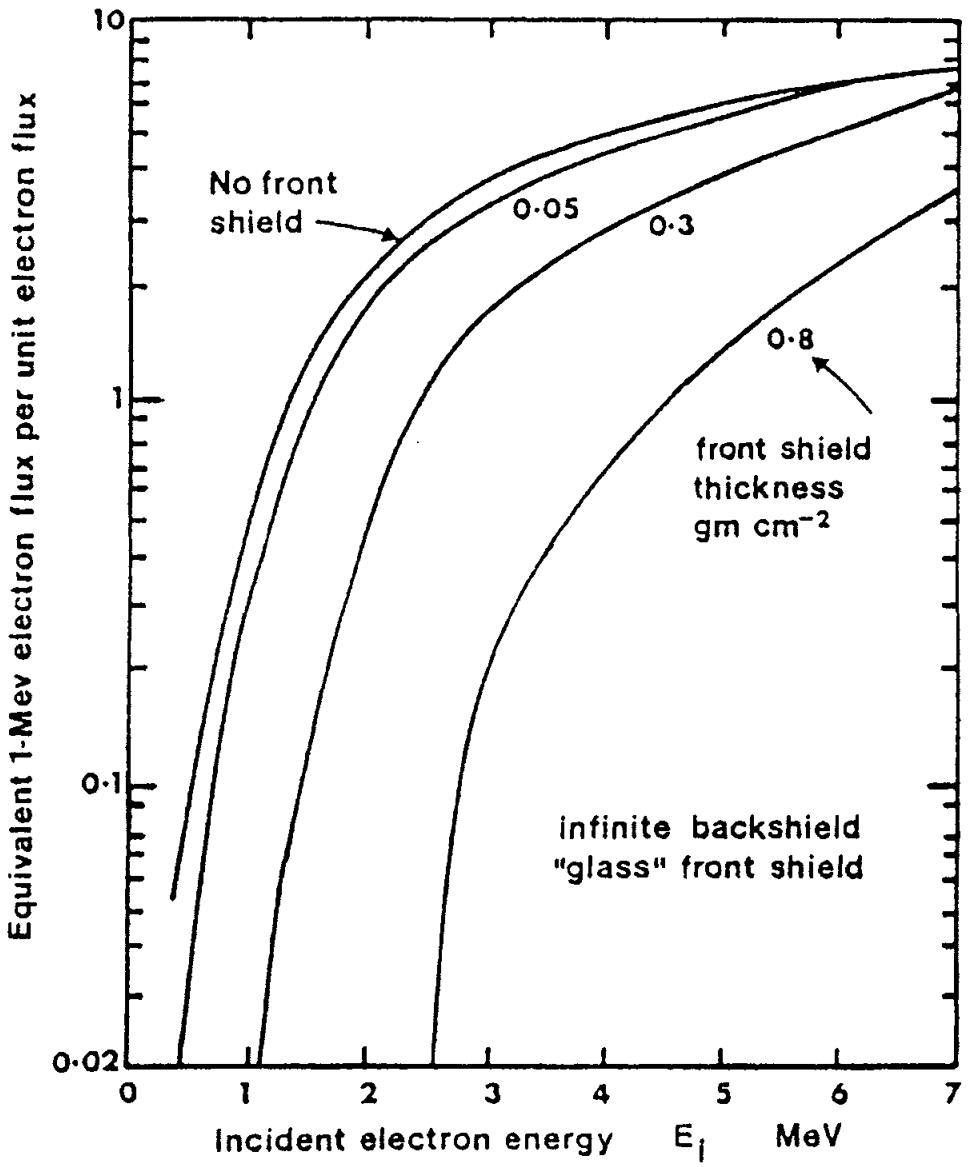

The "BGR" damage transmission curves, giving the damage-equivalent 1-MeV electron flux as a function of the energy of a monoenergetic isotropic flux of electrons incident upon n-on-p solar cells with various front shielding. The back-shield is assumed to be infinitely thick. For uniform all-round shielding, the vertical scale should be multiplied by two. The front-shielding would be a typical solar-cell cover glass.

FIGURE 16.12 - ELECTON DAMAGE TRANSMISSION

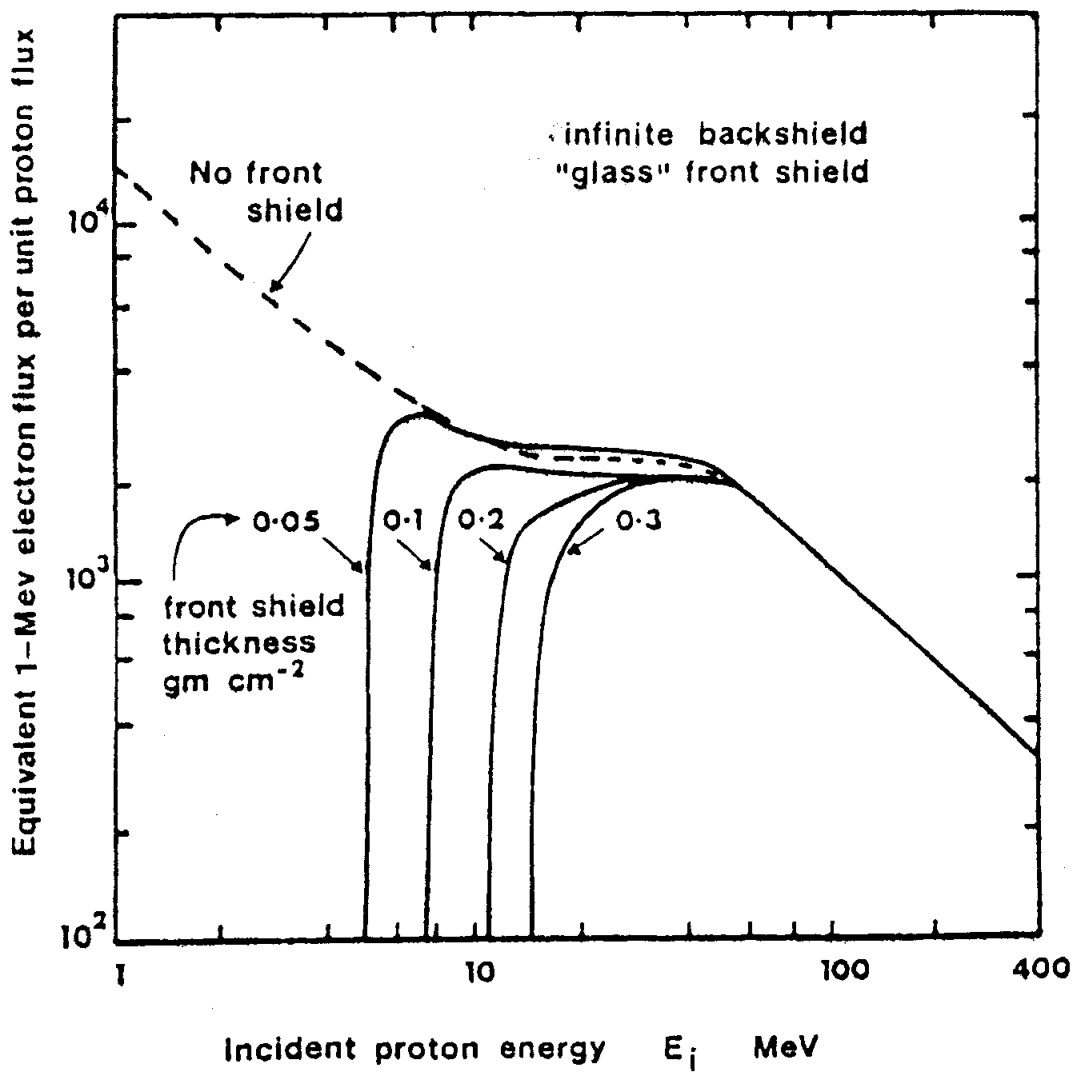

The "BGR" damage transmission curves, giving the damage-equivalent 1-MeV electron flux as a function of the energy of a monoenergetic isotropic flux of protrons incident upon n-on-p solar cells with various front shielding. The back-shield is assumed to be infinitely thick. For uniform all-round shielding, the vertical scale should be multiplied by two. The front-shielding would be a typical solar-cell cover glass.

FIGURE 16.13 - PROTON DAMAGE TRANSMISSION

16.8 MATERIAL EFFECTS

16.8.1. Deposition of dose

The procedure for deriving the dose-depth curves described in the preceding sections has been applied to the typical case of a silicon device protected by an aluminium absorber. To estimate doses deposited in materials other than silicon, the appropriate "stopping power" data should strictly be used as the basis of the dose per unit fluence calculation. In practice, however, stopping power (when expressed in "mass thickness" units) does not vary greatly from material to material.

Figures 16.14 and 16.15 show electron and proton stopping powers for various materials normalised, for convenience, to the values for aluminium. Stopping power values for silica, for instance, are not available, but it is reasonable to assume that they are no more than a few percent greater than those for silicon. Clearly, it would be essential to make the appropriate corrections when calculating the dose in materials such as water (human tissue), polyethylene or heavy materials such as gold, where stopping power values are further removed from those of silicon or aluminium.

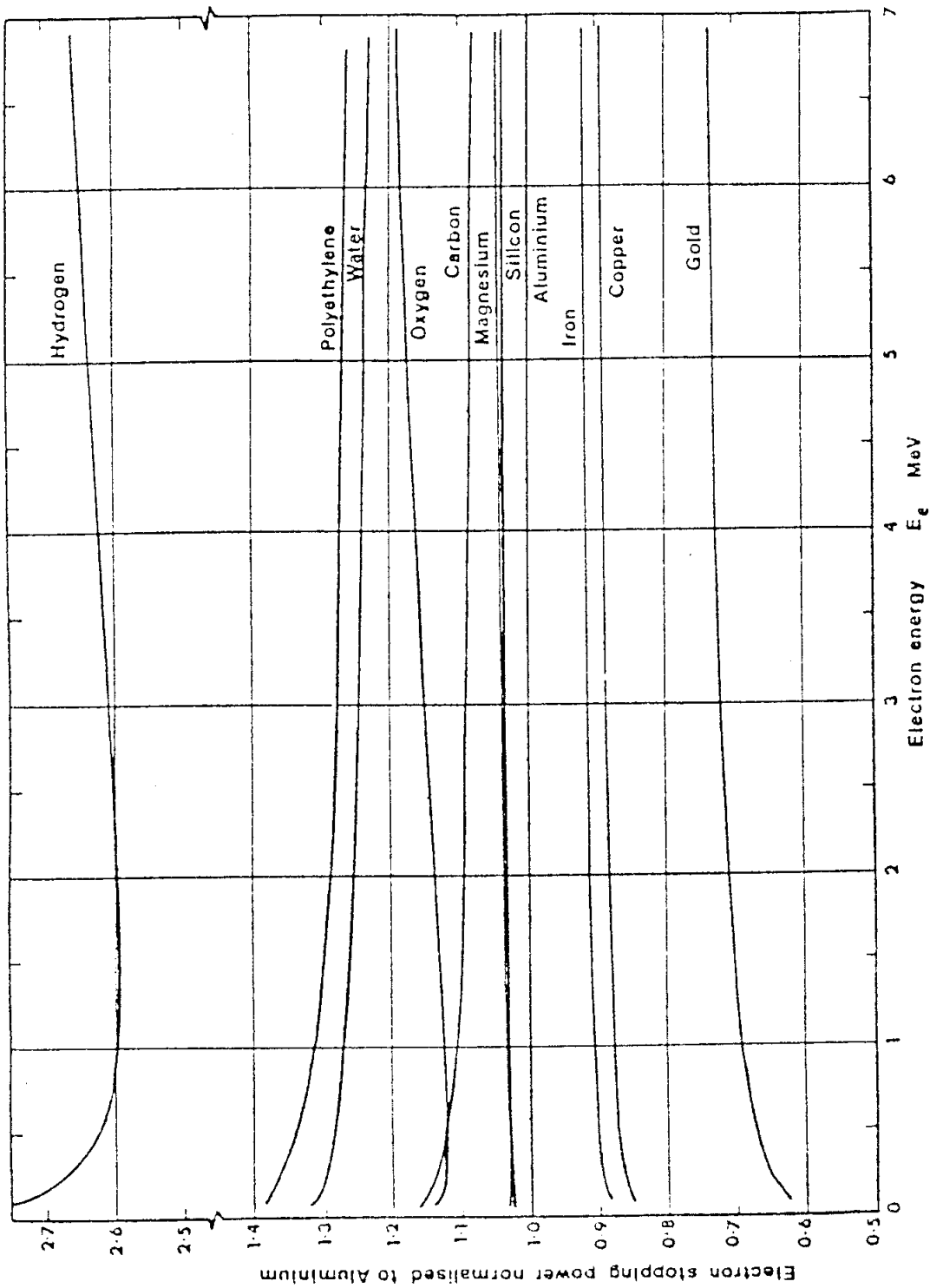

The electron stopping power for various materials, normalised against aluminium, as a function of incident energy.

FIGURE 16.14 - ELECTRON STOPPING POWER; EFFECT OF DIFFERENT MATERIALS

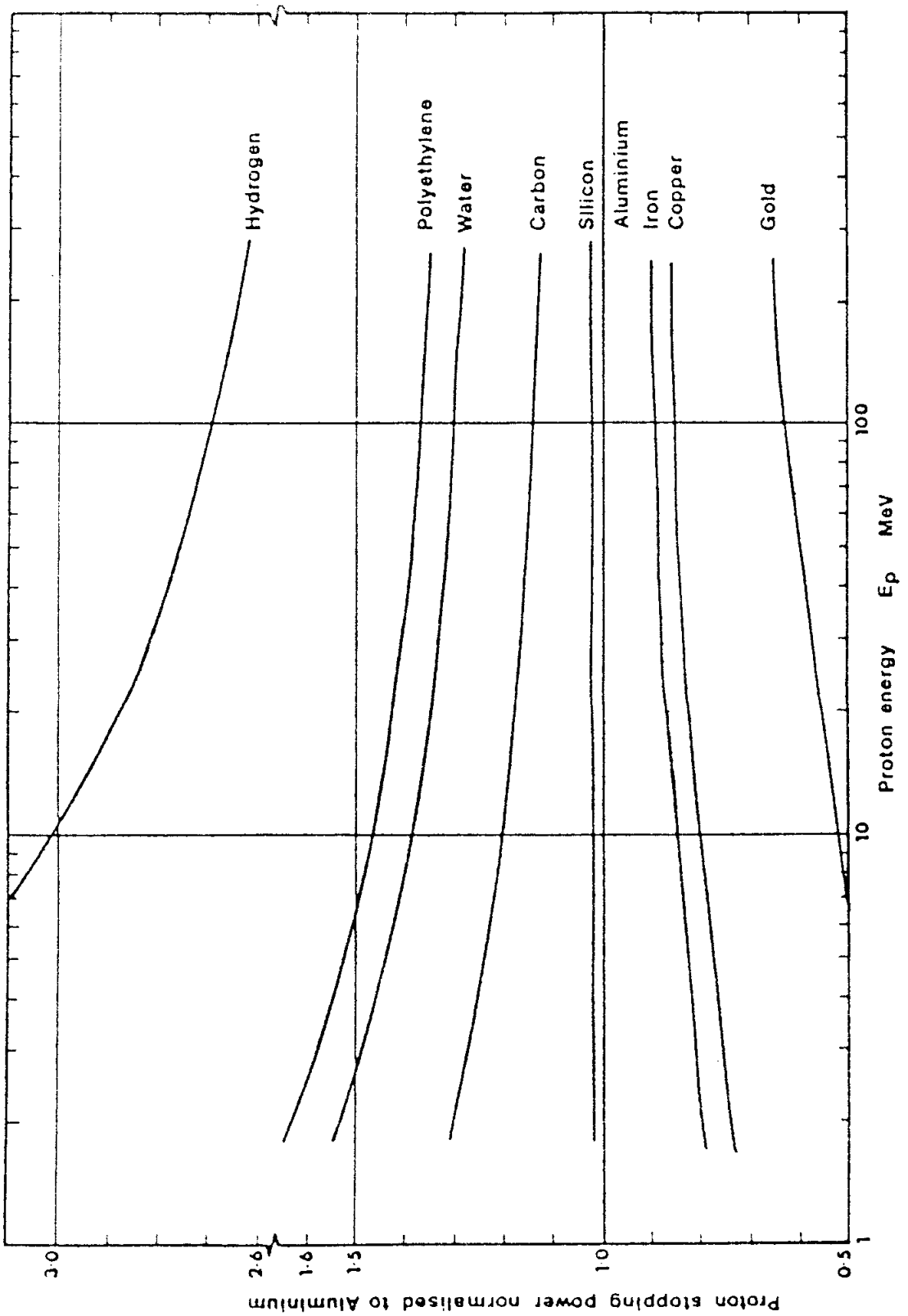

The proton stopping power for various materials, normalised against aluminium, as a function of incident energy.

FIGURE 16.15 - PROTON STOPPING POWER; EFFECT OF DIFFERENT MATERIALS

16.8.2. Other shielding materials

For the calculation of radiation doses behind different absorbing or shield materials, it has often been practice "to convert" all materials to equivalent aluminium thickness by making the appropriate density correction. The use of an alumium dose-depth curve for all materials thus requires the assumption that transmission coefficients for a given "mass thickness" will be the same for any material. This may lead to considerable error, especially in the case of electron doses.

In certain circumstances, and especially in orbits such as geostationary where electron and bremsstrahlung doses dominate, the reduction of all materials to "aluminium equivalent" can lead to significant error. Evaluation based on aluminium equivalents is useful for initial analysis to identify potential problem areas. A more rigorous analysis which may subsequently be required should account for the different materials, possibly by application of the computer programs described in Section 18 to "multi-layer structures".

The need for the multilayer approach arises from the strong degree of scattering of electrons by matter and the strong dependence of this effect on atomic number. As a result, a slab of material of high atomic number transmits fewer electrons than one of low atomic number with the same "mass thickness". Figure 16.16 shows this effect for several different materials (Mar, 1966). The electrons are scattered out of the transmitted beam; many, in fact, in a backward direction. Figure 16.17, based on data from Wright and Trump (1962) shows experimental results for the back-scattering of megavolt electrons from thick targets. It will be seen that lead is 5 to 10 times more efficient at back-scattering than aluminium. It is not surprising, therefore, that the opposite, but far weaker dependence of electron "stopping power" on atomic weight is swamped by the scattering effects.

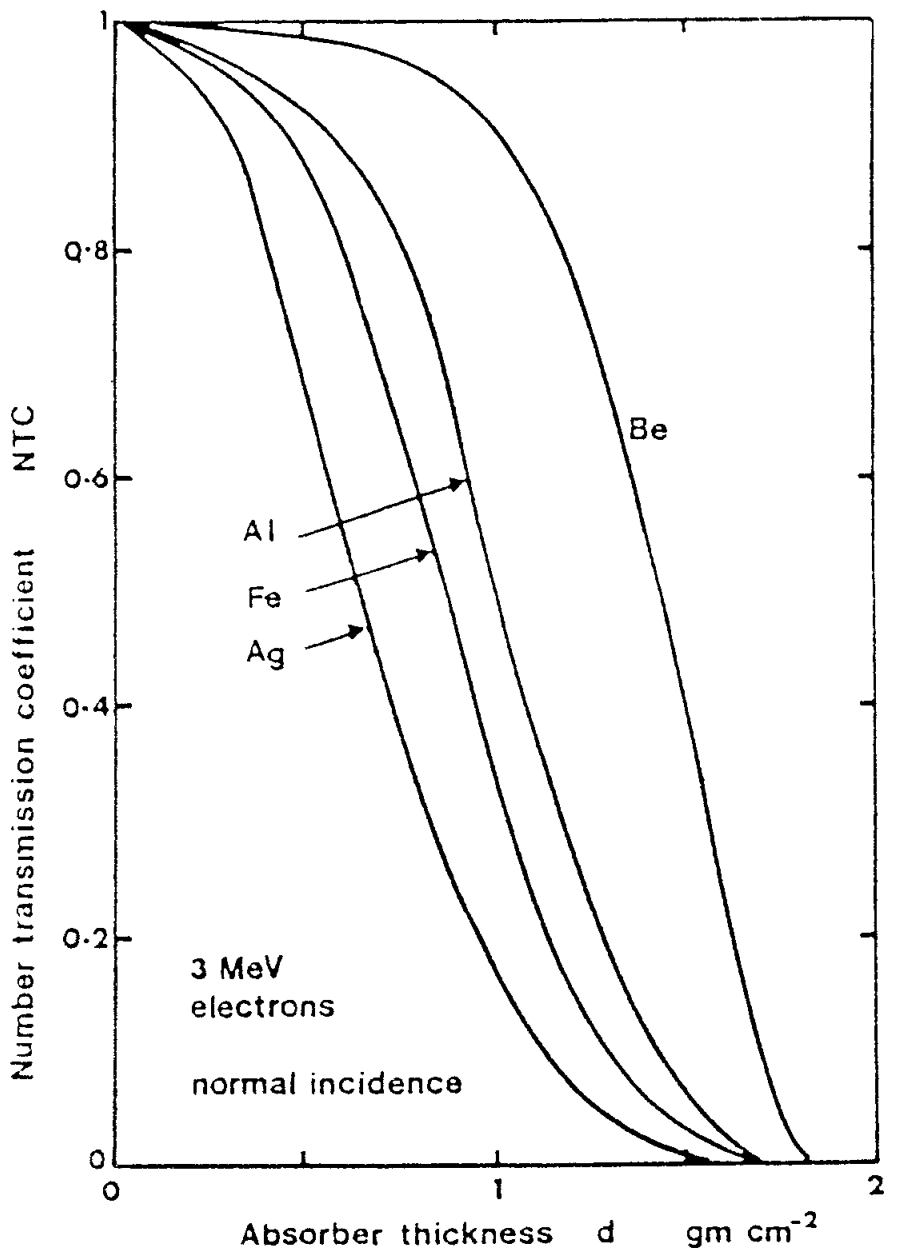

Number transmission coefficient for 3 MeV electrons as a function of absorber thickness for several absorber materials.

FIGURE 16.16 - ELECTRON TRANSMISSION; EFFECT OF DIFFERENT MATERIALS

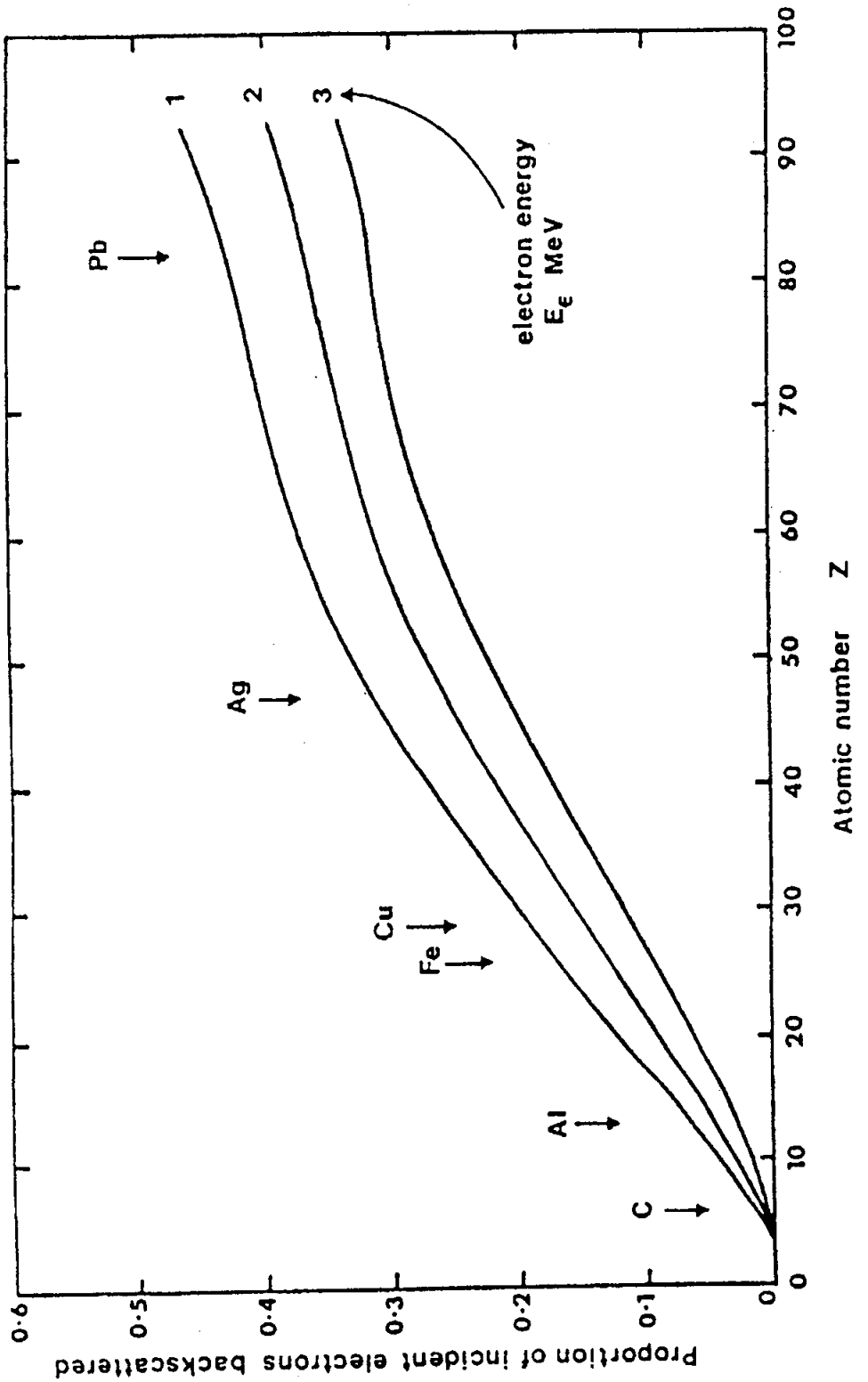

The fractional backscattering of electrons as a function of atomic number of absorber material.

FIGURE 16.17 - ELECTRON BACK SCATTERING

As an illustration of the effect of heavier shielding material on back scattering and bremsstrahlung generation, Figure 16.18 shows dose-depth curves (for electron and bremsstrahlung doses) for equivalent mass-thicknesses of aluminium and lead absorbers in the geostationary orbit environment. It can be seen that, for shield thicknesses less than 1 $g.cm^{-2}$, lead is a more efficient absorber. However, this degree of protection will be satisfactory only for devices that tolerate total doses of greater than 10^4 rad(Si) over a 7-year mission. For more sensitive devices requiring greater protection, the bremsstrahlung generated by lead is likely to provide an irreducible and unacceptable background. The same strong dependence on atomic weight does not hold for protons on account of their greater mass.

These curves are derived from old electron models and an approximate dose calculation and are intended only to demonstrate a trend and should not be used directly in generating design rules. They represent the artificial, simplified case of a uniform absorber of a single material.

If we consider the case of a composite absorber consisting of, say, lead and aluminium layers, then the composite dose-depth relationship would clearly be expected to lie somewhere between the extremes of lead and aluminium, and would depend upon the proportion of the overall mass-thickness contributed by each material. It must be remembered, however, that most of the bremsstrahlung is generated in the outermost part of the absorber where the lower-energy electrons are stopped. Therefore, the effect of adding lead to the outside of aluminium shielding would be to limit the minimum dose to something close to the lead bremsstrahlung level. If, on the other hand, lead were the innermost component of the composite, the two advantages of the better electron shielding of the lead and the lower bremsstrahlung generation in the aluminium could, in principle, be combined. In practice, a large amount of absorber will often consist of epoxy-glass laminate (see Appendix C) with transmission coefficients lying between the values for carbon and aluminium.

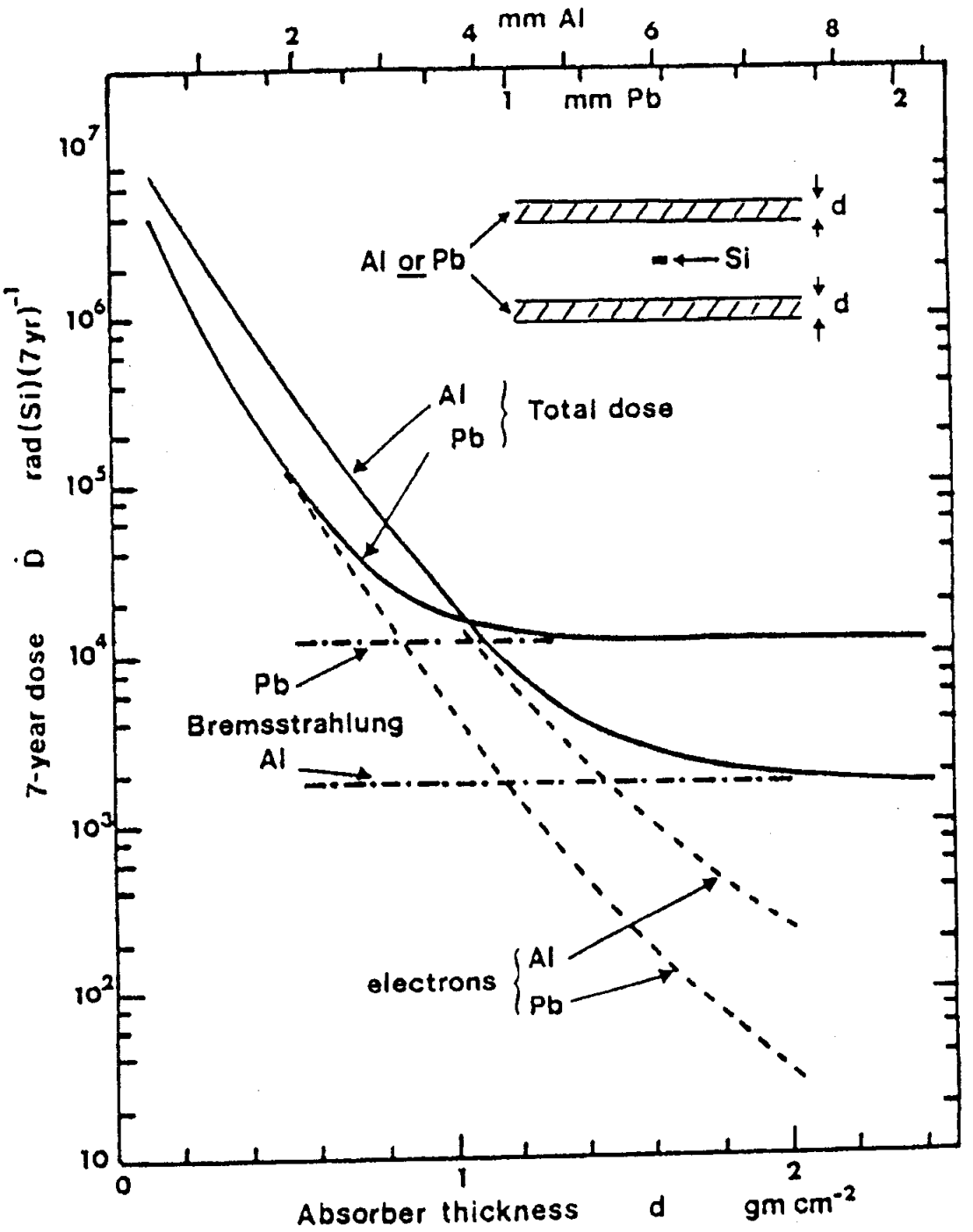

Dose-depth curves for the geostationary orbit showing the effect of different absorber materials. The curve for lead absorber is a provisional estimate.

FIGURE 16.18 - DOSE-DEPTH CURVES; EFFECT ON DIFFERENT ABSORBER MATERIALS

Using Monte Carlo calculation methods, Mar (1966) has made a study of electron transmission as a function of atomic number and derived complex expressions for number transmission coefficient and transmitted flux/energy distribution for monoenergetic incident electrons.

$$NTC(E,Z,X) = \exp\left\{ -\left(\frac{0.634\ EZ^{0.23}}{X^{0.848}} \right)^{-K} \right\} \qquad \text{.....16(xii)}$$

where $k = 7(Z-3.25)^{-0.24}$ and where E, Z and X are incident electron energy, atomic number and shield thickness respectively. The transmitted differential flux distribution is represented by the expression

$$\phi(E_e, Z, X)dE = A\,[\exp[-b(E - E_e)]]\,dE,$$

where

E_e = emergent electron energy,
A = a constant,
$b = (X/E)^{-1.46}(1.53 - 0.0147\ Z)/E$.

A boundary condition, $\phi dE = 0$ for $E_e > E_{max}$, applies to this formula, where E_{max} is the peak or "most probable" transmitted energy. This expression reflects therefore the finite width of the emergent energy spectrum after transmission of a monoenergetic incident flux (see Section 16.3).

Mar's approximation in this case is to consider the transmitted spectrum as a vertical edge (E_{max}) with an exponentially decaying distribution at energy less than E_{max}. This is in order except that as shield thickness increases, the transmitted energy spectrum becomes broader and the vertical-edge approximation less appropriate.

16.8.3. Routine calculation of particle transmission

It has been demonstrated that because of heavy scattering effects, electron transmission in different materials is extremely variable. Merely to use "stopping powers" and Number Transmission Coefficients (NTC) in estimating shielding effects can lead to errors. This is best achieved through computer calculation. The calculation of bremsstrahlung is also highly complex and best performed by computer. Section 18 gives details of suitable computer codes.

16.9 ORBITAL DOSE AND DAMAGE DATA

16.9.1. Orbital dose-depth curves

In the preceding subsections, the interactions of radiation with matter, shielding and resultant dose and damage caused by the radiation were discussed. Section 3 described the radiation environment external to the spacecraft, in terms of particle fluxes and showed how environment models could be used to provide "orbital integrations" which describe the environment in terms of orbit-average particle flux-vs-energy spectra. Using the data presented in Subsection 16.6, these orbital environments can be translated into dose behind given amounts of shielding. In fact, the SHIELDOSE program has been used to do this automatically.

Figures 16.19 and 16.20 show typical results of the process: the orbital dose-depth curves. These show the annual doses expected in Low Earth Orbit (LEO) at solar minimum and in geostationary orbit at solar maximum as functions of spherical aluminium shield thickness. The contributions of the various radiation species to the total doses are also shown. These represent very different regimes of the radiation environment.

LEO orbits encounter very energetic radiation-belt protons, but a "soft" electron environment and therefore relatively low bremsstrahlung doses. Solar flare particles cannot penetrate to LEO orbits because of geomagnetic shielding (see Section 3). The proton dose becomes very flat with shields more than about 4 mm thick and clearly the effectiveness of additional shielding is then poor.

Geostationary orbits are beyond the proton radiation belt, but are exposed to quite a severe electron environment. This results in much higher doses than in LEO for shield thicknesses below 6 mm, before the electrons become attenuated. The electrons generate bremsstrahlung which is not so easily attenuated, resulting in a slowly decreasing dose as the shielding is increased. Also shown are doses expected from energetic protons from a single anomalously large solar flare event. Care should be taken not to scale this contribution with time since such events are infrequent. The flatness of the bremsstrahlung and solar proton dose-depth curves means that, as in LEO, the efficiency of additional shielding for shields thicker than about 7 mm is low, although the causes are different in the two cases. To affect such bremsstrahlung doses significantly would require the use of high-Z shielding materials.

Annex F contains a full selection of dose-depth curves for various orbits. These show that other orbits are generally a combination of the two cases presented above. Elliptical orbits and polar orbits, for example, encounter inner-zone protons and outer-zone electrons and are partially exposed to particles from solar-flare events.

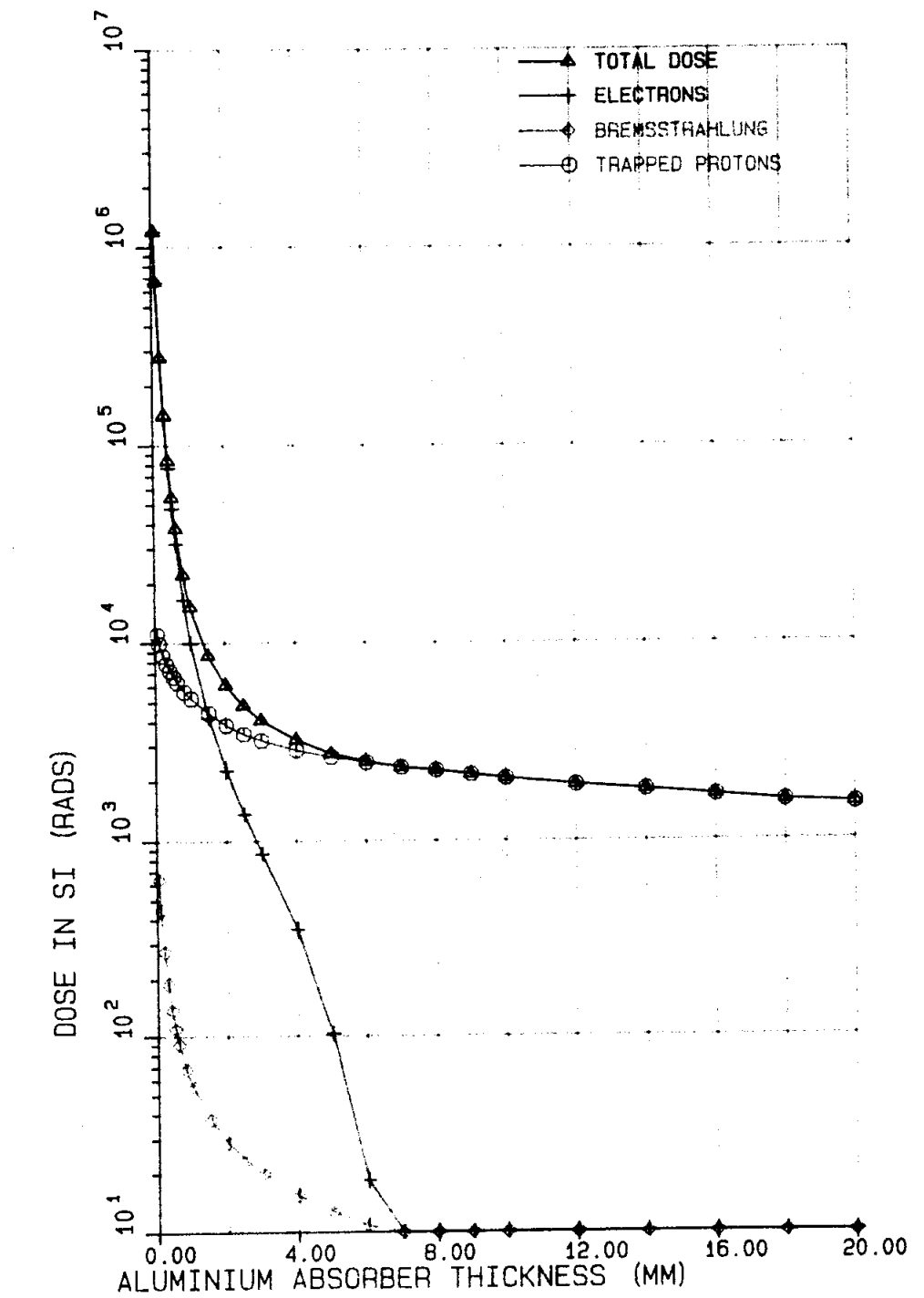

Annual dose as a function of spherical aluminium shield thickness for Low Earth Orbit: 1000 km circular at 28.5 degrees inclination. Protons dominate the dose for shields greater than 2 mm thick. Computed with the SHIELDOSE program. Solar minimum environment models AE8MIN and AP8MIC were used.

FIGURE 16.19

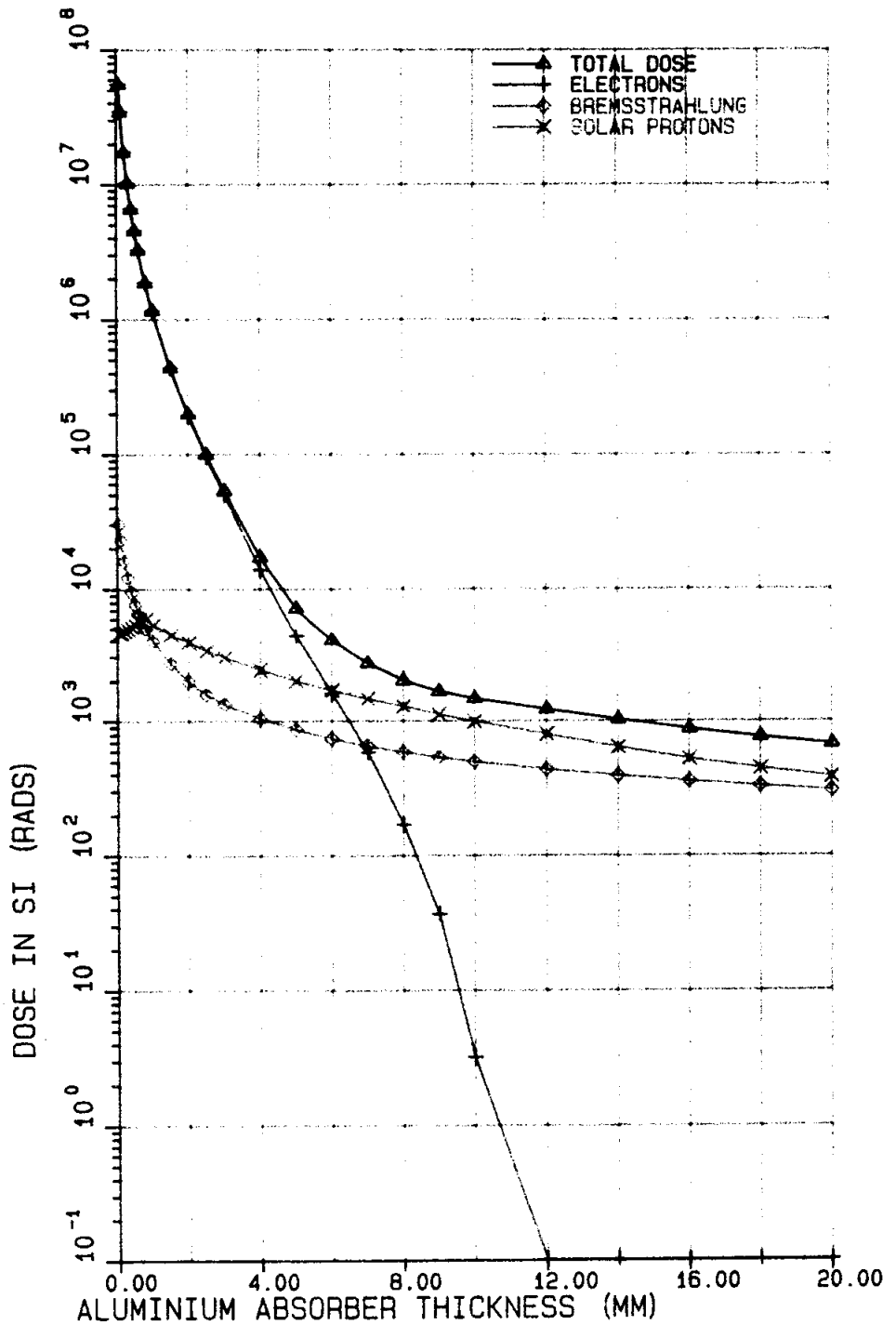

Annual dose as a function of spherical aluminium shield thickness for geostationary orbit: 35786 km circular equatorial. Electrons dominate the dose for shields less than 6 mm thick. Computed with the SHIELDOSE program. Solar maximum environment model AE8MAX and AP8MAC were used.

FIGURE 16.20

16.9.2. Radial-altitude profiles for dose and damage

The variation of orbit-integrated particle fluxes with altitude was discussed in Section 3, where "radial profiles" of electron and proton fluxes were shown. It is instructive to treat the resulting dose within shielding in a similar way. Figure 16.21 shows the radial profiles of dose accumulated in silicon within spherical aluminium of various thicknesses, (a) trapped electrons, (b) electron-induced bremsstrahlung, (c) trapped protons and (d) the total. These are for single circular equatorial orbits and are only included for illustrative purposes. The radiation-belt structure of the environment and the shielding effects on the various radiation species are clear.

Figures 16.22 and 16.23 give similar radial profiles of damage-equivalent 1 MeV electron flux in aluminium behind various thicknesses of aluminium for trapped electrons and protons. The belt structure is again shown. The concept of equivalent 1 MeV electron flux relates to atomic displacement damage and has been explained earlier. This particular effect is unlikely to be significant in the type of device which is the main concern of this document.

Dose and damage profiles calculated for orbits of high inclination show higher integrated doses at low altitude and a less pronounced minimum in the "slot" region (8000 km altitude). We can explain this with the example of a polar (90°) orbit. This cuts the horns of the outer belt (see Figure 3.2) four times per orbit. Orbits as low as 300 km pick up significant doses from these horns, whereas doses from the heart region are negligible at this altitude.

In Figure 16.24, some of the other useful features of radial dose profiles are also demonstrated. The dose profiles for 4 mm of aluminium absorber have been replotted; proton and electron doses have been summed. An attempt has also been made to give a visual guide to "no go" areas of space for specific spacecraft configurations.

The first point of interest demonstrated is that doses in low near-equatorial orbits are proton dominated. This dominance persists past the inner electron peak dose region at 3000 km and on to about 9000 km, after which the influence of protons is negligible. The outer peak region is electron-dominated and, surprisingly, yields the highest dose levels of all. Thus, for electronics, the least healthy "slot" in space appears to be around an altitude of 20000 km. For missions lasting more than one year, doses of over Megarad are possible.

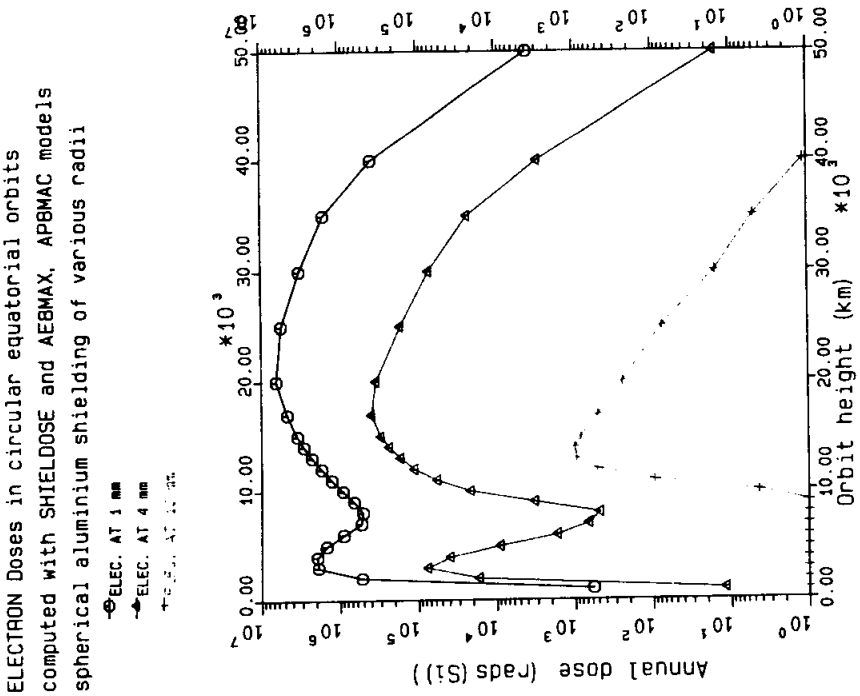

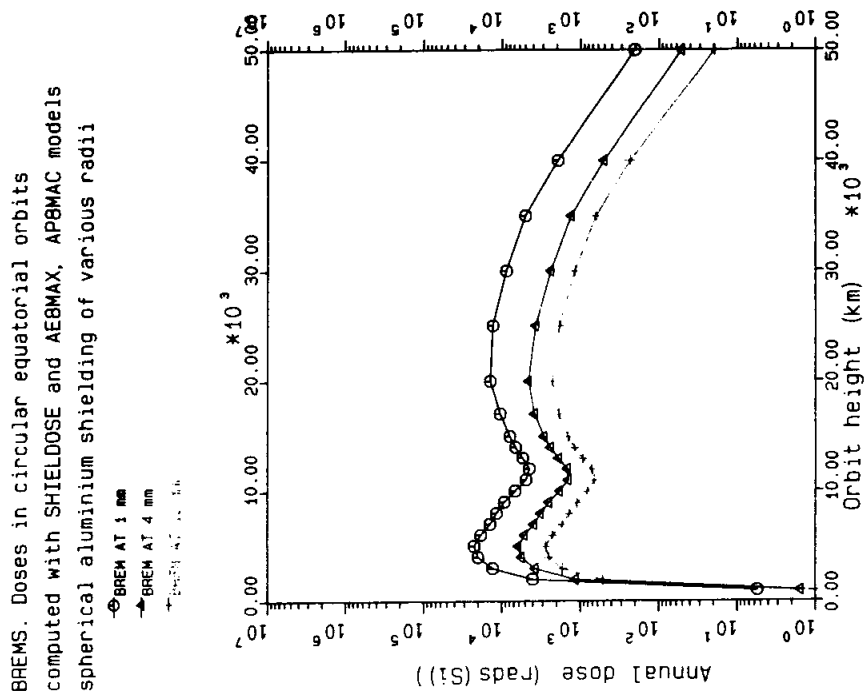

Radial doses (Si) profiles showing annual dose accumulated in silicon within spherical aluminium shields of thicknesses 1, 4 and 10 mm as functions of altitude of single circular equatorial orbits. (a) due to trapped electrons, (b) due to electron-induced bremsstrahlung,..

FIGURE 16.21

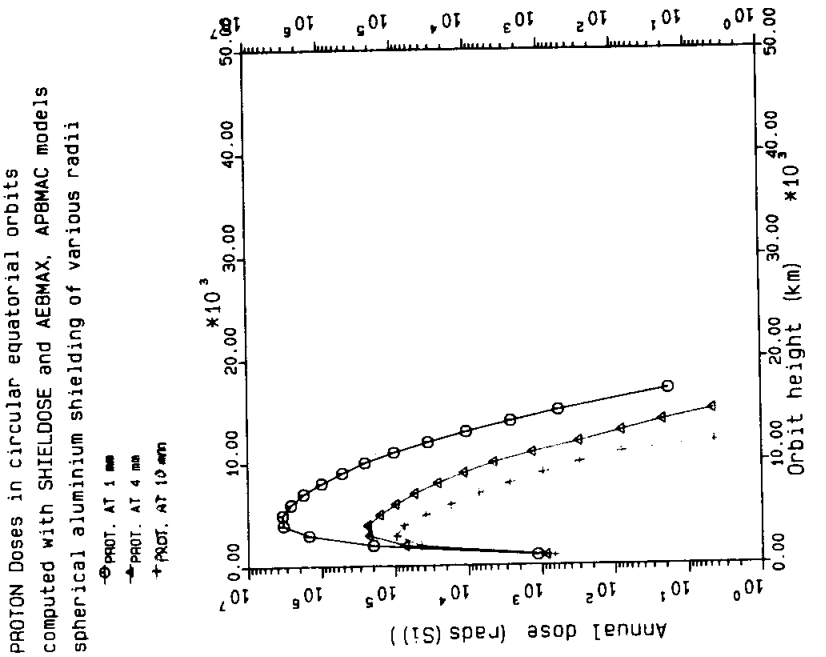

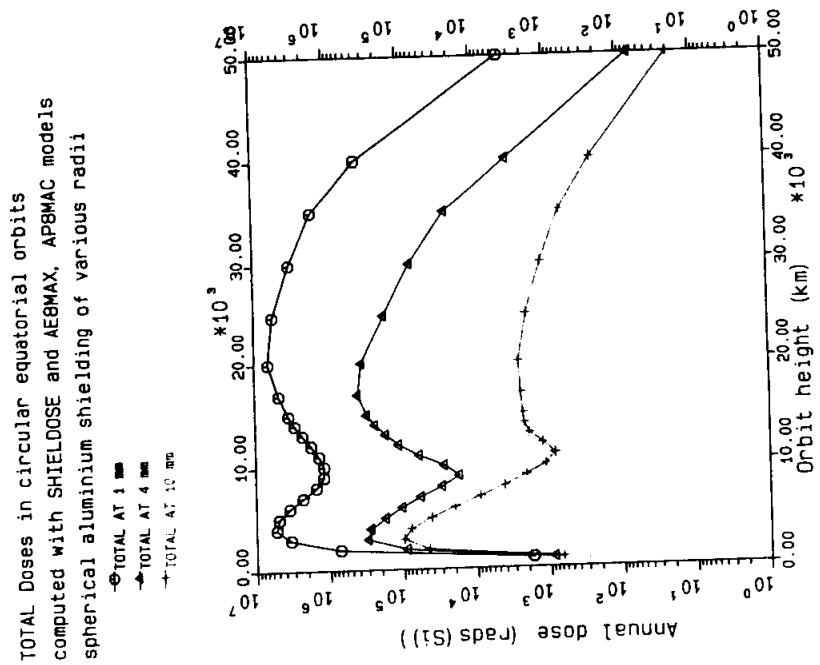

(c) due to trapped protons (d) total dose

FIGURE 16.21 (continued)

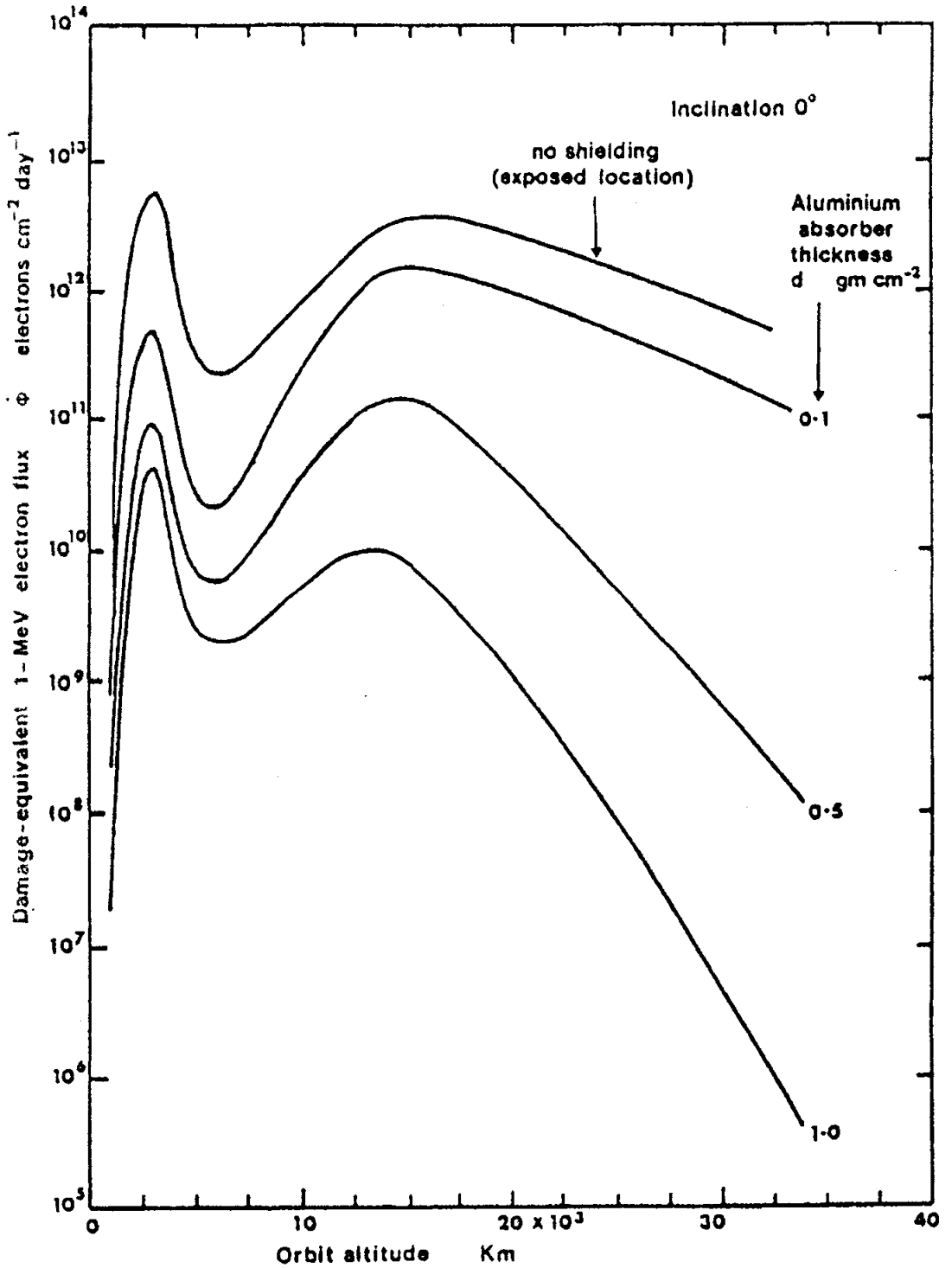

The damage-equivalent 1 MeV electron flux resulting from the trapped electron environment behind various thickness of aluminium absorber as a function of altitude in a circular equatorial orbit. AE-2 environment model.

FIGURE 16.22 - ELECTRON DAMAGE RADIAL-ALTITUDE PROFILES

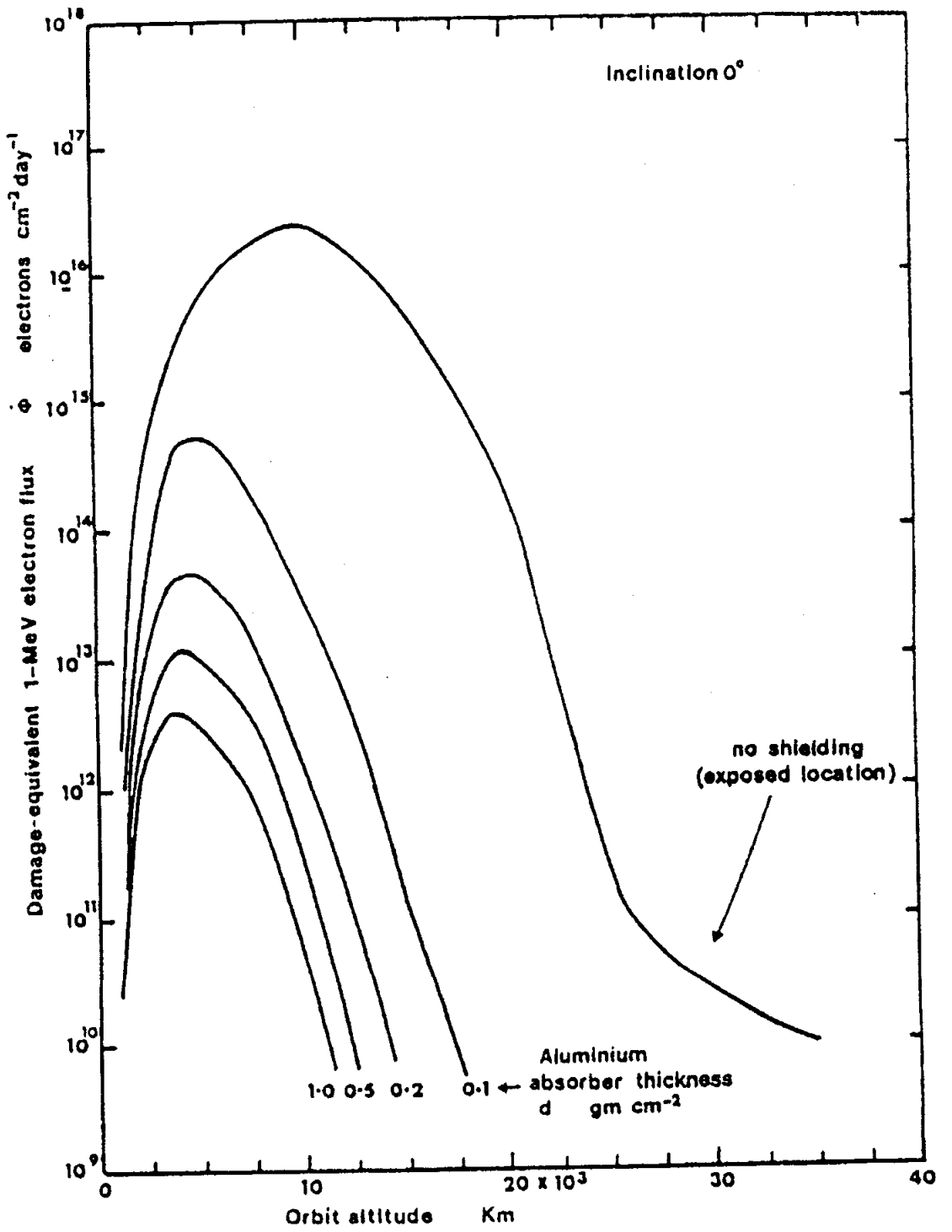

The damage-equivalent 1 MeV electron flux resulting from the trapped proton environment behind various thickness of aluminium absorber as a function of altitude in a circular equatorial orbit. AE-2 environment model.

FIGURE 16.23 - PROTON DAMAGE RADIAL-ALTITUDE PROFILES

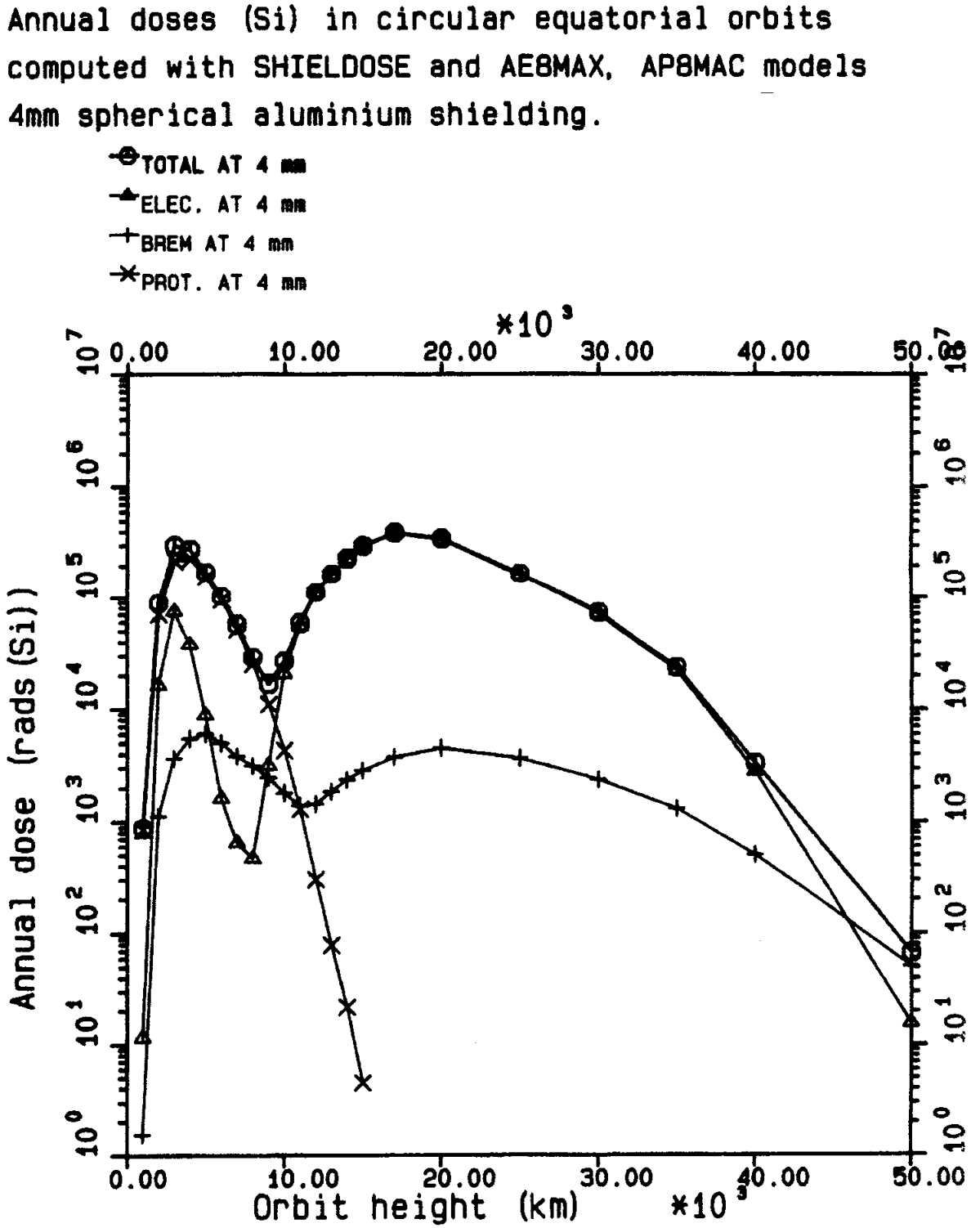

Annual doses (Si) within 4 mm special aluminium shielding as functions of altitude. Contributions from electrons, bremsstrahlung and protons are shown.

FIGURE 16.24

16.10 Nuclear reactions and other effects

Most of the mechanisms involved in the transport of radiation in a medium dealt with thus far have concerned interactions mainly at the atomic or molecular level: ionisation is a removal of atomic electrons; bremsstrahlung is produced by electron scattering in atomic fields; displacement damage results from atoms from a solid lattice. A small fraction of the incident particle flux may penetrate to atomic nucleii of the medium and initiate a nuclear reaction. Although these interactions are infrequent compared to ionisation interactions, the results can be important. The nucleus may break apart with the fragments causing intense local ionisation, or it may emit secondary protons and neutrons, or it may stay for some time in an "excited" state, followed by a delayed emission or radiation (the material is then said to be "activated").

16.10.1. Proton-induced SEU/Latchup

When the result of a nuclear interaction is the break-up of the nucleus, the charged fragments usually have short range and, if the interaction occurs in a sensitive region of a logic device, may lead to single-event upset (SEU) or latchup like that caused by a heavy-ion's ionisation track. In-flight observations of the locations of spacecraft when on-board components exhibit SEU have shown that a significant fraction of the total number of events occurs while satellites are in the proton radiation belt. Upset rates on CRRES (Campbell, 1991) and UoSAT-2 (Harboe-Sorensen et al., 1990) were much higher in the proton belts than in regions of space exposed to cosmic rays alone. Moreover, the CRRES data appear to show that multiple upsets, where the charge generation "contaminates" more than one logic cell, are more likely in the proton environment.

McNulty et al. (1980) and Peterson (1981) provided some of the early analysis of the processes. Evaluation of the problem can be made using Monte-Carlo computer simulation methods where the products of the interaction are determined statistically on the basis of fragmentation cross-section data such as those from Silberberg et al. (1985). Knowing the energies and ion species of the products, one can compute the energy deposition in a region and the upset rate (e.g. Bion and Bourrieau, 1989).

As with ion-induced SEU, testing in a representative ground-simulation environment is vital to the evaluation process. Bendel and Petersen (1983) have described a method for making predictions of in-orbit proton-induced error-rate which is simple provided the upset cross-section of a device as a function of proton energy is available from ground-tests. Harboe-Sorensen et al. (1990) show that this is less easy in practice and can result in predictions in disagreement with in-flight observation.

Recently an instrument on the ERS-1 satellite failed as a result of latchup in a memory while the satellite was passing through the South Atlantic anomaly where the proton radiation belt comes to its lowest altitude (Adams et al., 1992). This, together with the CRRES, UoSAT and much other experience, indicates that proton-nuclear reaction effects are a very important part of the overall radiation hazard.

16.10.2. Radiation-induced detector backgrounds

Primary energetic particles and their secondaries also interfere with payloads, most notably with detectors on astronomy missions where they produce a 'background' signal which may not be distinguishable from the proton signal being counted or which can overload the detector system. All astronomy missions, from infrared (e.g. ISO), through visible (e.g. HST, Hipparcos [Clausen and Perryman], 1989, UV (e.g. IUE) and X-ray (e.g. Exosat, RoSAT, XMM [Danner, 1992] and AXAF) to γ-ray (e.g. GRO, Cos-B, Integral [Dyer et al., 1988]) wavelengths, are or will be affected. The interference mechanism can be one of several, including bremsstrahlung radiation generated by electron slowing in material, Cerenkov radiation emitted when relativistic particles passed through optical materials; and delayed emissions of gamma-rays from the nuclei of activated spacecraft materials.

16.11 CONCLUSIONS

This section has described some of the physical principles involved when radiation interacts with materials and has indicated the approaches required to estimate the dose deposited in a sensitive device material which is protected from the direct action of the radiation environment by other absorber or "shield" materials.

We have demonstrated the complexity of the physical processes and noted the approximations which may be necessary. We should note particularly that some approximations which may be justifiable in preliminary calculations, when order of magnitude is the main question, should be removed in later, detailed calculations where compromises between weight and life are required.

Later sections deal more specifically with practical aspects of spacecraft equipment and the computer methods recommended when a large number of calculations must be performed (e.g. for a compromise estimation) or when the engineering decisions in question demand accuracy outside the scope of the manual methods described.

REFERENCES

L. Adams, E.J. Daly, R. Harboe-Sorensen, R. Nickson, J. Haines, W. Schafer, M. Conrad, H. Griech, J. Merkel, T. Schwall and R. Henneck, "A Verified Proton Induced Latchup in Space", IEEE Trans. Nucl. Sci. NS-38, 6 (1992)

W.H. Barkas and M.J. Berger, "Tables of Energy Losses and Ranges of Heavy Charged Particles", NASA Publication 1113, pp. 103-107, National Academy of Sciences, National Research Council, Washington DC (1964)

M.J. Berger and S.M. Seltzer, "Tables of Energy Losses and Ranges of Electrons and Positrons", NASA Publication 1113, pp. 205-269, National Academy of Sciences, National Research Council, Washington DC (1964)

M.J. Berger and S.M. Seltzer, "Stopping Powers and Ranges of Electronics and Protons", NBSIR-82-2550A, National Bureau of Standards (1982)

M.J. Berger and S.M. Seltzer, "Additional Stopping Power and Range Tables for Protons, Mesons and Electrons", NASA SP-3036, Office of Technology Utilisation, Washington DC (1966)

M.J. Berger and S.M. Seltzer, "Penetration of Electrons and Associated Bremsstrahlung through Aluminium Targets", NASA SP-169, pp. 285-322, Office of Technology Utilisation, Washington DC (1968)

H.A. Bethe, Handb. Phys. 24(1), p. 273 (1933)

T. Bion and J. Bourrieau, "A Model for Proton-Induced SEU", IEEE Trans. Nucl. Sci. NS-36, 6 2281 (1989)

W.L. Brown, J.D. Gabbe and W. Rosenzweig, "Results of the Telstart Radiation Experiments", The Bell System Technical Journal 42(4), pp. 1505-1559 (1963)

G.J. Brucker, "Correlation of Radiation Damage in Silicon Transistors Bombarded by Electrons, Protons and Neutrons", Paper presented at Conf. on Radiation Effects in Semiconductors, Toulouse (March 1967)

H. Bucker and R. Facius, "Radiation Problems in Manned Spaceflight with a View Towards the Space Station", Acta Austronautica (1988)

A.B. Campbell, "SEU Flight Data from the CRRES MEP", IEEE Trans. Nucl. Sci., NS-38, 6, 1647 (1991)

J.B. Cladis, G.T. Davidson, and L.L. Newkirk (Eds), "The Trapped Radiation Handbook", Report DNA 2524H, General Electric Co., Santa Barbara (1973)

K.F. Clausen and M.A.C. Perryman, "The Hipparcos Mission", IAF Paper 89-459, 40th. International Astronautical Congress, Malaga, Oct. 1989

R.A. Cliff, V. Danchenko, E.G. Stassinopoulos, M. Sing, G.J. Brucker and R.S. Ohanian, "Prediction and Measurements of Radiation Damage to CMOS Devices on board Spacecraft", X-700-76-227, NASA Goddard SFC (Oct. 1976) and IEEE Trans.Nucl.Sci. NS-23(6), pp. 1781-1788 (Dec. 1976)

W.C. Cooley, and R.J. Janda, "Handbook of Space Radiation Effects on Solar Cell Power Systems", NASA SP-3003, U.S. Dept. of Commerce, Washington DC (1963)

R. Danner, "Charged Particle Induced Background Expected on XMM", Estec Working Paper EWP 1674, ESTEC/WMA, 1992

C.S. Dyer, P.R. Truscott, A.J. Sims, C. Cumber and N.D.A. Hammond, "Particle Transport Simulation for Spaceborne, NaI Gamma-ray Spectrometers", IEEE Trans. Nucl. Sci. NS-35, 6, 1407, 1988

T.B.M. Dyer, proton nuclear reading: Petersen E.L. "Nuclear Reactions in Semiconductors", IEEE Trans. Nucl. Sci NS-27, 6, 1494 (1980) N.L. Bendel and E.L. Petersen, "Proton Upsets in Orbit" IEEE Trans. Nucl. Sci NS-30, 6, 4481 (1983) Harboe Sorensen et al.

R. Harboe-Sorensen, E.J. Daly, C.I. Underwood, J. Ward and L. Adams, "The Behaviour of Measured SEU at Low Altitude During Periods of High Solar Activity", IEEE Trans. Nucl. Sci. NS-37, 6, 1990

A.C. Hardy, M.D. Lopez and T.T. White, Trans.Am.Nuclear Soc., 10, p. 383 (1967)

A.G. Holmes-Siedle and W. Poch, JBIS 24(5), p. 273 (1971)

A.G. Holmes-Siedle, ESA Contract AHS-EXO-77-1 (Febr. 1977)

A.G. Holmes-Siedle and R.F.A. Freeman, "Radiation Effects Handbook", ESA Contract Report No. CR(P)-1067, Fulmer Research Inst., Slough, U.K. (April 1978)

H.E. Johns and J.R. Cunningham, "The Physics of Radiology", Thomas (1971)

F.L. Keller and R.G. Pruett, "The Effect of Charged Particle Environments on Manned Military Space Systems", NASA SP-71, U.S. Dept. of Commerce, Washington DC (1965)

D.W. Kingsland, Private communication

G.F. Knoll, "Radiation Detection and Measurement", Second edition, John Wiley and Sons, New York, 1989

V.J.L. Linnenbom, NRL Report 5828 (1962)

B.W. Mar, Nuclear Science and Engineering 24, pp. 193-199 (1966)

P.J. McNulty, G.E. Farrell, R.C. Wyatt, P.L. Rothwell, R.C. Filtz and J.N. Bradford, "Upset Phenomena Induced by Energetic Protons and Electrons", IEEE Trans. Nucl. SCI NS27(6) (1980)

E.L. Petersen and W.L. Bendel, " Protons Upsets in Orbit", IEEE Trans. Nucl. SCI NS30(6) (1983)

E. Peterson, "Soft Errors due to Protons in the Radiation Belt", IEEE Transactions on Nuclear Science, NS28(6), (Dec. 1981)

W. Poch, Private communication

S.M. Seltzer, Private communication, via M.J. Teague, NSSDC

S.M. Seltzer, "Electron, Electron-Bremsstrahlung and Proton Depth-Dose Data for Space Shielding Applications", IEEE Trans. Nucl. SCI NS26(6) (1979)

R. Silberberg, C.H. Tsao and J.R. Letaw, "Improved Cross Section Calculations for Astrophysical Applications", Astrophys. J. Suppl. 58, 873 (1985)

J.R. Srour, S. Othmer and K.V. Chiu, ibid., pp. 2656-2662

H.Y. Tada, J.R. Carter, B.E. Ansprangh and R.G. Downing, "Solar Cell Radiation Handbook", JPL Publication 82-69 (1982)

M.J. Teague, Private communication

V.A.J. Van Lint, G. Gigas and J. Barengoltz, IEEE Trans.Nucl.Sci. NS-22(6), pp. 2663-2668 (Dec. 1975)

K.A. Wright and J.G. Trump, J.Appl.Phys. 33, p. 687 (1962)

S.J. Wyard, Proc.Phys.Soc. A65, p. 377 (1952)

W.R. Yucker and J.R. Lilley, "Charge Code for Space Radiation Shielding Analysis", Report DAC-62231, McDonnell Douglas Astronautics Co. (1969)

SECTION 17. EQUIPMENT DESIGN PRACTICE

17.1. INTRODUCTION

The most common starting-point for equipment radiation effects and shielding analysis is the dose-depth curve for the particular mission. A first-cut at the shielding analysis can be made by determining the dose corresponding to the most lightly shielded part of the subsystem under evaluation. If the dose is tolerable then clearly no further analysis is necessary. Tolerability is obviously determined on the basis of device testing which is crucial. It must be borne in mind that, apart from dose, an evaluation of single-event upset and latchup, and possibly displacement damage effects, may need special consideration. A device-and-location combination which appears satisfactory from a total dose perspective is not necessarily immune from all radiation effects. If a problem is identified, more extensive analysis of shielding will be necessary, possibly including a detailed sector-analysis of the whole or a part of the spacecraft.

17.1.1. Materials

Among the large variety of synthetic materials which go into a spacecraft, there is a wide spread of radiation tolerance. Materials with high tolerance include all metals, many ceramics and inert gases. Tolerance in the semiconductor, optics and polymer fields ranges from "fair" to "very poor". To the former class belong bipolar ICs, rectifying diodes and "hardened" MOS circuits; to the latter, devices such as commercial MOS circuits, analogue devices, power transistors and solar cells. At the present time, the degradation of materials other than semiconductor devices, optics and polymers is, where typical space missions are concerned, generally considered as a secondary problem.

It is certain, however that degradation will present a major problem in future missions involving, for example, high-performace electronics and sensors, spaceborne nuclear power sources and particle accelerators.

17.1.2. The importance of layout

In previous sections, we have predicted the likely amount of degradation for various types of semiconductor devices in a spacecraft, where they usually lie behind a structure which attenuates the radiation. It is clear that the designer must always attempt to put equipment boxes containing the more sensitive devices in protected locations; to surround them with structures containing less sensitive materials.

This implies that equipment layout and system sensitivity to space radiation are intimately connected. Layout, packaging and circuit

design all contribute to the radiation tolerance of a spacecraft and, hence, its life expectancy in space. Thus, if a high-radiation mission is planned, a complex "radiation effects engineering" process has to be brought into equipment design practice. The aim of this discipline is to produce a space vehicle of maximum capability (for example with the maximum number of communication channels or scientific experiments) which will survive for a maximum period of time at minimum penalty (attributable to the radiation environment) in cost and launch weight. This section introduces some design rules which may be applied and gives also some examples of current practice in analysing existing spacecraft.

17.1.3. Built-in versus add-on shielding

To avoid confusion, a strict distinction is made here between the "built-in" and "add-on" protection of components. Although all mass surrounding a specific component can be regarded as "shielding" or protection, much of that mass serves some other primary, usually structural, purpose. We will describe this type of protection as "built-in" as opposed to "add-on" shielding. In this context, a neutral term used here for radiation-stopping material is "absorber". (Owing to its ambiguity, the term "screening" is not recommended.)

The ultimate aim of the design practice described in this section is to use "built-in" shielding such that the need for "add-on" shielding is minimised. In other words, layout has a fundamental importance in the design of a radiation-tolerant spacecraft.

17.2. TYPICAL SPACECRAFT CONFIGURATIONS AND MATERIALS

17.2.1. General

The detailed layout of a spacecraft may have quite a strong influence on the radiation dose reaching the silicon chips which are the focus of our interest. For example, if the system designers opt for a spinning satellite, the solar array will be drum-shaped and act as shielding.

The shielding effect of a wrap-around solar array will be the equivalent of 3 to 4 mm of aluminium. As we shall see later, this is a significant addition (possibly 30 kg) to the built-in shielding provided by platforms, box covers and circuit boards. To give another example: an integrated circuit in the centre of a stack of printed circuit boards may be exposed to only one-tenth of the dose received by the same circuits on the uppermost board of a stack. Similarly, equipment boxes near the edge of a platform receive more dose than those near the centre. As an example, Figure 17.1 shows the lay-out of the OTS satellite, the forerunner of the Olympus series, which operates in a geostationary orbit. The equipment is secured to two parallel platforms attached to a central

cylinder which, in turn, is jointed to the launcher via a conical transition section.

The apogee boost motor provides good built-in protection from at least one sector.

17.2.2. Box covers

Many equipment boxes designed by European industry are made up of sections milled out of solid aluminium with certain parts milled very thin as a weight-saving measure. As will be explained later, such an absorber array gives less protection than the uniform sheet-metal enclosures more common in the USA. This is a case of the general rule that good built-in protection from radiation is a matter of total mass as well as efficient mass distribution. This same rule applies not only to box structures, but also to the arrangement of masses around a box containing sensitive devices. Clearly, some point such as 'X' in Figure 17.1 is a suitable one for the placing of radiation-sensitive equipment while points such as those marked 'Y' are not suitable because they do not make good use of the built-in spacecraft mass.

To calculate the dose levels at a given point within a given box, all radiation-absorbing masses present in the satellite have to be taken into account. These, of course, constitute an extremely complex array of masses, but we must calculate as closely as possible how they contribute to radiation-stopping. This is done by "sector analysis" - calculating the solid angle subtended at a given point of interest ("dose point") by a given mass. Computer programs to perform this task are widely available and are described in Section 18.

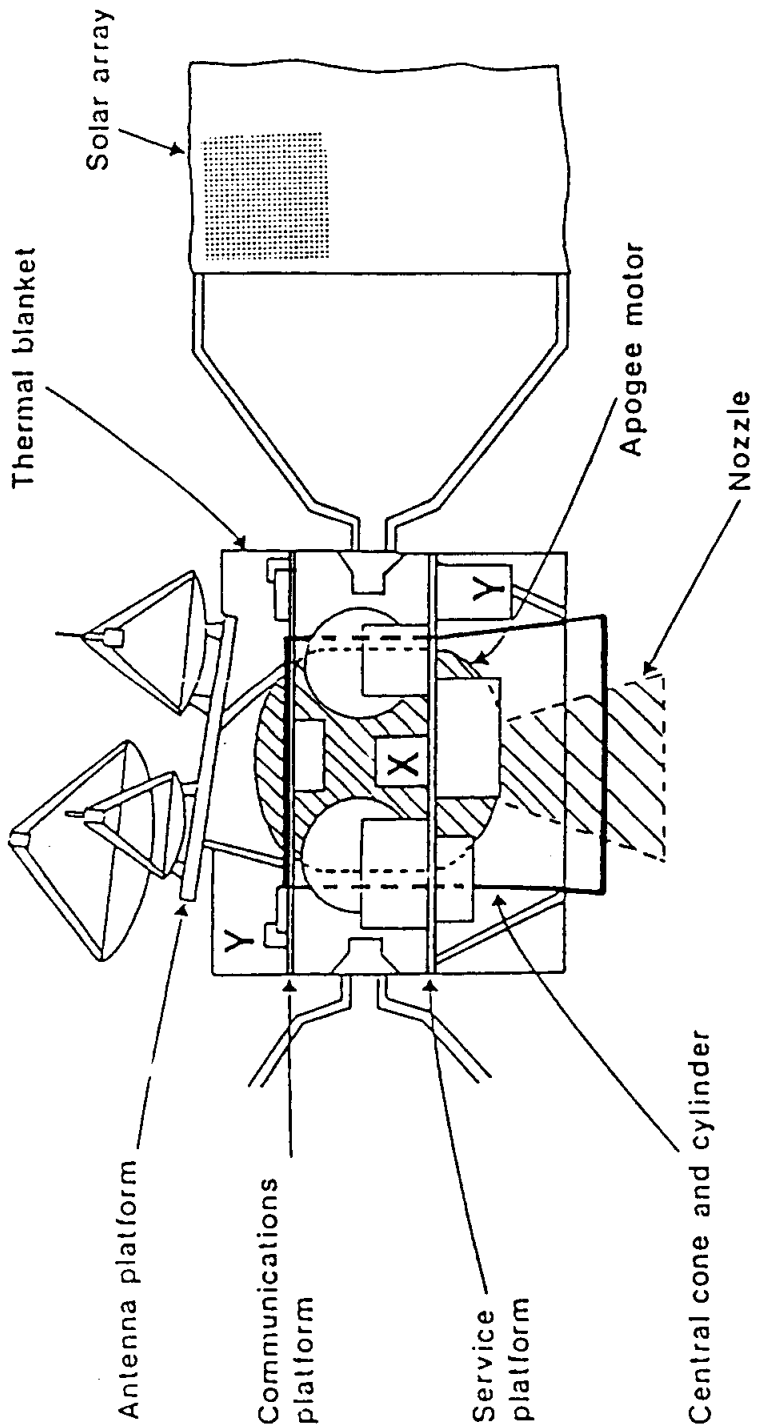

The central core of the satellite, by which it is attached to the launch vehicle, carries parallel platforms to which electronic equipment is secured.

FIGURE 17.1 - LAYOUT OF THE OTS SATELLITE

17.2.3. Radiation-absorbing properties of a spacecraft structure

17.2.3.1. A light weight structure (SMOP)

Figure 17.2 shows the dimensions of a typical spacecraft core structure (platforms, central cylinder and thrust cone with struts) which was designed by Contraves to give optimum structural mass for a 720 kg, Thor-Delta launched, spacecraft. This design, named SMOP, provides for a mass of 20.6 kg, distributed as follows:

- centre cylinder + core: 7.3 kg,
- lower platform: 7.1 kg,
- upper platform: 5.4 kg,
- struts : 0.8 kg.

The average mass density of the platform appears to be between 0.22 and 0.28 $g.cm^{-2}$, equivalent to between 0.8 and 1.0 mm of Al. In fact, the platform deck itself will contain even less absorber than this since much mass will be concentrated in attachment points, mechanical connectors and stiffeners. The facings ("shims") of the carbon fibre honeycomb used were only 0.15 mm thick; those on OTS were of similar thickness, but made of aluminium foil (2). Thus, the shielding capability of a platform is very low, probably less than 0.5 mm Al equivalent. The core of the SMOP design was made of aluminium sheet of less than half the thickness used for OTS (e.g. 0.15 versus 0.4 mm for the cylinder; 0.2 versus 0.6 mm for the core).

17.2.3.2. The apogee motor as an absorber

The spent apogee-kick motor within the central structural cylinder of a space vehicle forms a large part of a geostationary spacecraft mass. A description of the OTS motor and its treatment as an absorber of radiation is given here for guidance in future projects.

The "total inert" material in the OTS motor (Aerojet SVM-7A) has a mass of 32.237 kg, approximately 3% of the total system weight. The fuel compartment can be represented as a fibre-reinforced plastic cylinder (780 mm in diameter and 682 mm in length) which is, in fact, rounded at the ends. The nozzle, composed of carbon felt and reinforced plastic, is a cone extending about 700 mm at one end. The fuel compartment fits within the central cylinder and thrust cone of the space vehicle.

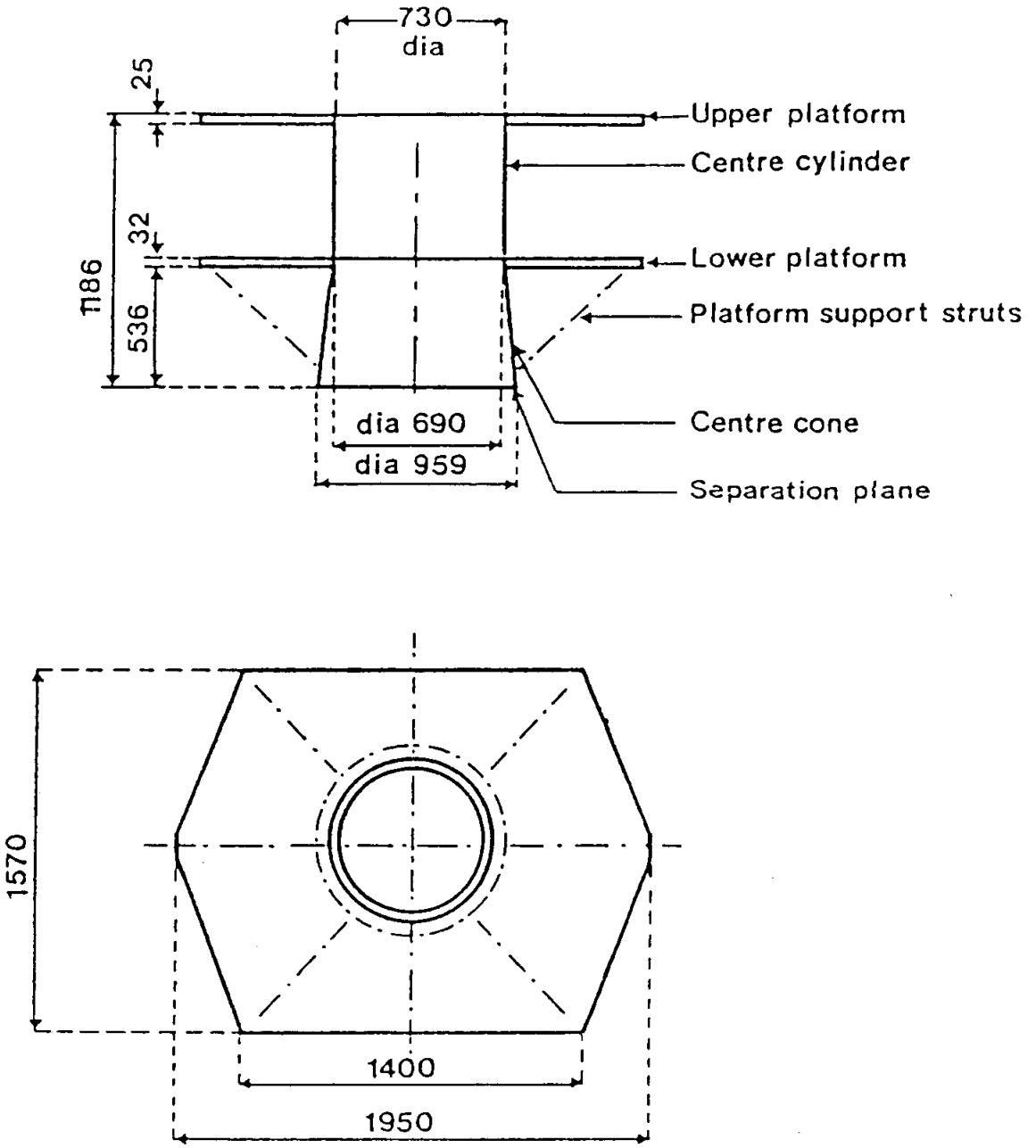

FIGURE 17.2 - A TYPICAL SPACECRAFT (SMOP STUDY)

The central cylinder and thrust cone are made of aluminium honeycomb and corrugated aluminium sheet. The cylinder has an outer diameter of 816 mm and a length of 770 mm, and the cone flares from the same diameter to one of 972 mm in a length of 457 mm.

In a normal sector analysis, the radiation-absorbing mass of the fuel chamber is represented by a cylinder of aluminium sheet of about 2 mm thickness and the nozzle by a cone of about 3 mm thick aluminium sheet. The central structural cylinder and cone can be represented as being of 0.6 thick aluminium sheet. Thus, a particle passing radially through the central part of the space vehicle will have traversed an amount of absorber equivalent to at least 5-6 mm of aluminium. For a box on one of the equipment platforms, especially one of those on the inner faces of the platforms, the central column may subtend more than π steradians (i.e. more than a quarter of the whole sphere). Clearly, the excellent protection given by this large absorber of radiation should be assessed carefully and included in sector analysis calculations. When designing add-on shields, considerable weight can be saved by reducing added mass on the side of the box protected by the motor and column.

17.2.3.3. Antennae as absorbers

On OTS, the six communication antennae are very light dish structures, their thickness being equivalent to about 0.2 mm discs of aluminium, covering less than 50% of the top platform area. The antennae platform is also of light honeycomb of total thickness equivalent to about 0.3 mm aluminium and covering only the centre portion of the top platform.

17.2.4. Typical spacecraft materials

A space vehicle is composed of a large number of small components of widely varying materials. Annex C lists the materials used by one spacecraft contractor and likely to be included in the electronic subsystems and a table of polymers likely to be used in spacecraft. It will be impossible to assign a solid angle to every component in the spacecraft and some form of "homogenisation" of the small parts into an equivalent solid sector of representative atomic number will be necessary for a "manual" calculation of dose.

17.2.5. Conclusions

The analysis of typical designs of geostationary spacecraft shows that:

a) Shielding power often resides mainly in the central structure and not in the equipment platform, and

b) Refinements in mechanical design reduce the built-in protection from some quarters.

The reason why it is difficult to assess the true protection given by the built-in mass is the fact that the mass is divided between a few large structures and a large number of small components.

17.3. SECTOR ANALYSIS

As stressed previously, the application of "single material" dose-depth curves, while useful for preliminary estimation, is not entirely adequate for the detailed design of engineering models. With this limitation in mind, the manual estimation of doses received by devices within sectored structures will now be considered, so that rules for reliable predictions of operating lifetime may be developed. Considering that each part of the spacecraft acts as a radiation shield, even though this may not be its prime function, the need for "sector analysis" is obvious.

A device in operation will clearly not be surrounded by a uniform thickness of material, but by a complex array of spacecraft components and structures as well as the material associated with the mounting of the device itself. It will be necessary to divide the complete structure into a number of sectors, each subtending a solid angle at the device or "dose point". Within each of these sectors, the shielding should be roughly uniform. The dose at the "dose point" arising from radiation through each sector is derived from the appropriate dose depth curve, taking into account the characteristic thickness and, if possible, atomic number of absorber in that sector. The sector dose will be the appropriate fraction of the dose arising from uniform "all-round" shielding and the "total dose" will be the sum of all sector doses.

Obviously, there is scope for considerable variation in the degree of sophistication with which this technique is applied, but some such sectoring method must be used if the life of a component in space use is to be estimated. The choice between the "single layer" approximation as described here and the more complex "multilayer" calculation has been discussed earlier.

A simplified sector analysis which has been used in preliminary design studies is described here as an illustration. In this case, the solid angle subtended by each sector has been estimated as a simple fraction of 4 π. A more rigorous calculation of solid angle may be made, for example, by using the following trigonometric expression:

$$\text{solid angle } \Omega = 4 \arctan \pi \frac{ab}{c(a^2+b^2+c^2)} \qquad \text{.....17(i)}$$

where the solid angle is subtended at the dose point by a rectangle 2a x 2b. The dose point is at a perpendicular distance c from the centre of the rectangle. For small sectors, this expression approximates to:

$$\Omega = 4ab/c^2 . \qquad \text{.....17(ii)}$$

Employing a computer to perform detailed sector analysis is obviously easier than calculating by 'hand'. Various methods are described in Section 18. An important prerequisite for such an analysis is the mass breakdown and dimensions of the spacecraft elements. Once these are available, the computerised geometrical model can be established, the mass values being used to ensure correct allocation of shielding.

The ideal situation is where the prime contractor's layout of the spacecraft is available in computerised form for subcontractors, experimenters or others to perform a detailed computerised sector-analysis. The most important detail in a sector-analysis is the region close to the point of concern. Therefore the subsystem engineer or experimenter can take the 'global' satellite model, including the masses of all the elements, and introduce the detailed description of the contents of his "box" and its immediate surroundings. This was been done for Cluster by Dornier, using ESABASE (see Section 18) to establish the model which was then communicated by ESTEC to experimenters via computer network.

Once a model is established, various parametric analyses are possible, including optimisation of orbit and design of special shielding elements. This was done during the process of orbit selection for XMM (Daly et al., 1992). Apart from predicting dose (or flux) levels at a point, computerised sector analysis can give graphical information on directions which are poorly shielded, and indeed a full distribution of shielding thicknesses.

An important point to bear in mind when performing sector analysis is that it may not always be appropriate to consider the external environment to be isotropic (uniform in all directions). This was discussed in detail in Section 3. This is a particular problem at low altitudes where there are very strong east-west and pitch-angle anisotropies. Gravity-gradient stabilisation on LDEF, for example, and a similar attitude control on the Space Station mean that different parts of these spacecraft are exposed to very different environments. Therefore it must be emphasised that it makes almost no sense to perform a sectoring shielding analysis unless the anisotropy is accounted for at the same time.

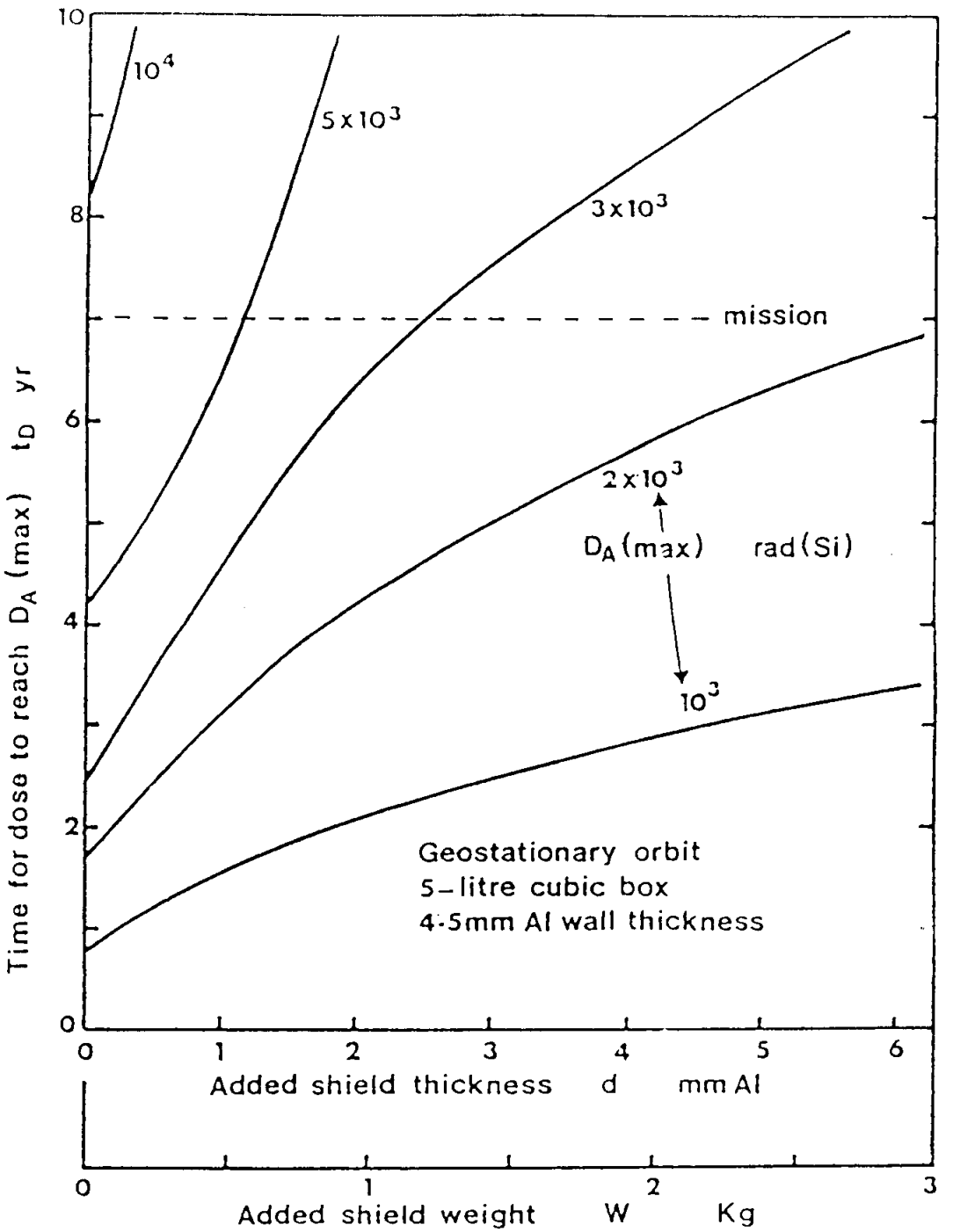

Time taken to reach "maximum acceptable dose" as a function of added shielding. The sensitive component is within a 5 litre cube of initial wall thickness 4.5 mm aluminium. Additional thickness is added uniformly.

FIGURE 17.3 - TRADE-OFF CURVES - GEOSTATIONARY MISSION

17.4. ADD-ON SHIELDING

17.4.1. Introduction

If built-in mass on the spacecraft cannot be arranged so as to protect all sensitive components, then - as a last resort - some "add-on" absorber may have to be judiciously added. The choices that have to be made include:

(a) The elemental composition,
(b) The location,
(c) The method of attachment.

The question of elemental composition has been discussed earlier. Here, the possibilities for add-on shielding are classified by its location and method of attachment. Added shielding can be considered as either "local" or "whole box". Figure 17.3 shows a reasonable scheme for subdividing types of protection. It should be noted that "efficient use of "built-in (existing) mass" is put first. The use of add-on shielding should be regarded as a last resort after the former approaches have been exhausted, essentially because of the high price of payload per kg and the high "revenue" which useful payload can earn. The saving in deadweight can thus be equated to the increase in "revenue", whether this be cash from telecommunications traffic or scientific returns from experiment packages.

The first aim of add-on shielding is to interpose a few millimetres of any suitable material between the device of interest and the external environment. If the array of devices to be shielded is small, we can save weight by enclosing the array in a compact shield rather than build the same thickness onto the outside of the equipment. This is the idea of "local" shielding: simply to obtain a given dose reduction in a given volume for the minimum weight penalty. For instance, a single integrated circuit would best be protected by a blob of filled plastic applied directly to the package or by using thicker Kovar for the covers. We will call this type of shield a "spot shield".

The particle-scattering property of materials has some dependence on the atomic weight. This is weak in the case of protons and strong in the case of electrons. Thus, the choices of atomic weight for an add-on shield in a proton-dominated orbit such as that of Exosat might differ from that for an electron-dominated orbit such as the geostationary case where high-Z materials can dramatically attenuate electron and bremsstrahlung doses (see Section 16).

17.4.2. On-PCB Shielding

17.4.2.1. Spot-shielding

The simplest type of shield is one totally surrounding the device and lying close to it. Alumina-filled plastic would have the insulating power needed and could be given suitable mechanical strength to resist vibration. With ICs, the shield might have to be in two parts: one above and one below the board. Screw-on fins have been designed for ICs, so screw-on shields could also be designed. The USAF has successfully procured CMOS devices with Kovar lids about twice the usual thickness.

A new design of package incorporating radiation shielding has been developed for the USAF (Schmid et al, 1985); for the U.K. AMPTE satellite, tantalum spot-shielding was applied to the lids of certain CMOS circuits. Calculations of layered shield have shown that the dose in geosynchronous orbit can be reduced to 200 rads for 10 years.

17.4.2.2. Edge of board

Under the heading of "Efficient Use of Built-in Mass" comes the use of other active components on the same board. These, if arranged properly, can supply absorber mass in exactly the most critical direction - the line of view through the thin box walls. However, only the middle area of the board gets full benefit of this mode of shielding. On the other hand, if we put add-on mass around the edge of the device area, the whole of the board gains full benefit.

17.4.2.3. Internal slabs

The types of shield so far described protect only one plane of a single component. If a whole plane or several planes are sensitive to radiation, then the region involved can be sandwiched between two slabs of material. Such a slab would be bolted onto the lower frame element where the clearance with respect to the next board allows this. In certain cases, foam sheets could be inserted or potting compound could be poured into the module after fabrication. In extreme cases, an empty module - carrying only the add-on absorber - could be inserted.

17.4.3. Whole box shielding

17.4.3.1. Bolt-on slabs

The simplest way of adding mass to a box might appear to be by bolting a slab of plastic or metal to the outside. In fact, this is rarely convenient because:

a) Suitable bolting may not be available on the outside of the box and

b) The shield may foul other boxes or cables lying close to the sensitive box.

The latter difficulty may sometimes be dealt with by using a very dense material such as lead, tungsten or tantalum, but these may generate excessive bremsstrahlung if the low-energy electron fluxes from space impinge directly. High-Z materials perform best once an initial 1-2 mm aluminium shielding has removed these electrons so that fresh bremsstrahlung generation is minimised.

17.4.3.2. Thickened walls

If the precise amount of shielding needed is known at the beginning of the design, then box walls can be designed to the required thickness over and above that needed for mechanical strength. Many boxes are milled out of solid metal and hence this need not present mechanical difficulties. It has already been noted that, for radiation-sensitive boxes, thin areas of box wall are to be avoided. Such thin areas are sometimes produced when mechanically unnecessary material is milled away. As discussed, the thickening of a whole box is likely to be uneconomical in weight unless every component in the box requires shielding.

17.4.4. The quantitative effect of add-on shielding

Table 17(1) shows the range of doses for typical locations in a geostationary satellite.

For Exosat, the mission dose for a component within the Star Tracker electronics box was calculated as 4.4 krad. This dose was equivalent to an even thickness of 3.3 mm aluminium completely surrounding the component. It is instructive to calculate the effect on total dose of adding "whole box" shielding to this component. Table 17(2) shows the result of adding such aluminium shielding in successive 1 mm steps.

It is clear from the table that successive additions of shielding results in smaller reductions in accumulated dose. This is due to the bremsstrahlung background. The addition of further shielding in excess of 4 mm will have an insignificant effect on dose. The added weight will, of course, continue to penalise performance. It is therefore recommended that always a comparison be made between the penalties and benefits of added shield weight.

17.4.5. Conclusions

Shield types can be classified as "local", "whole-board" and "whole-box"; each may be needed at different times. Modularity in these

shields is useful, but not essential. The shields used must be simple and easily applied. There is a strong incentive to apply the shielding only to the volume which really requires it (e.g. only one area of a printed circuit board); this arises from the cubic relationship between weight and linear dimension. In different cases, the shield may be poured or moulded plastic, aluminium or a very dense metal. Attachment to the device lid by adhesive has been found acceptable for some spacecraft. Complex layered shields have been designed.

17.5. TRADING-OFF SHIELD WEIGHT AGAINST DEVICE ALTERATION

For long-term geostationary missions, as shown in Figure 17.4, the control of radiation tolerance of devices is critical. In the example illustrated, a sensitive component is placed inside a 5 litre cubic aluminium box with a 4.5 mm wall thickness. The time required for the maximum acceptable dose, D_A (max), to be reached is shown as a function of added shielding. For a device with a D_A (max) value of 10^3 rads, it is impossible to add sufficient shielding to make the device survive the desirable 7-year mission. Even with thick shields (3 kg), it will barely survive half the mission. Raising D_A (max) to 3×10^3 rads allows 7-year survival by applying less than 1.5 kg of shielding; when D_A (max) is raised to 5×10^3 rads, only about 0.5 kg will be necessary. The "hardening" has occurred at the best point in the system, namely in the device. The cost penalty of "hardening" to this rather low level may only amount to that incurred by the radiation testing involved. The cost saving in weight reduction or life enhancement may be many times the cost of a well-designed series of laboratory tests.

Figure 17.5 shows similar curves for a hypothetical, exposed Exosat box. Here, unlike the geostationary case, the most sensitive device can survive the mission with 2 kg of shielding while, with D_A (max) of 10^4 rad, scarcely any special absorber is necessary.

The curves shown are, of course, only examples and specific to one particular component location on one space vehicle. However, they present the combined information on sector analysis, testing results (including recovery), physics theory and circuit analysis in a concise form that the system engineer will find useful.

TABLE 17(1) - SUMMARY OF DOSES WITHIN SPACECRAFT STRUCTURES

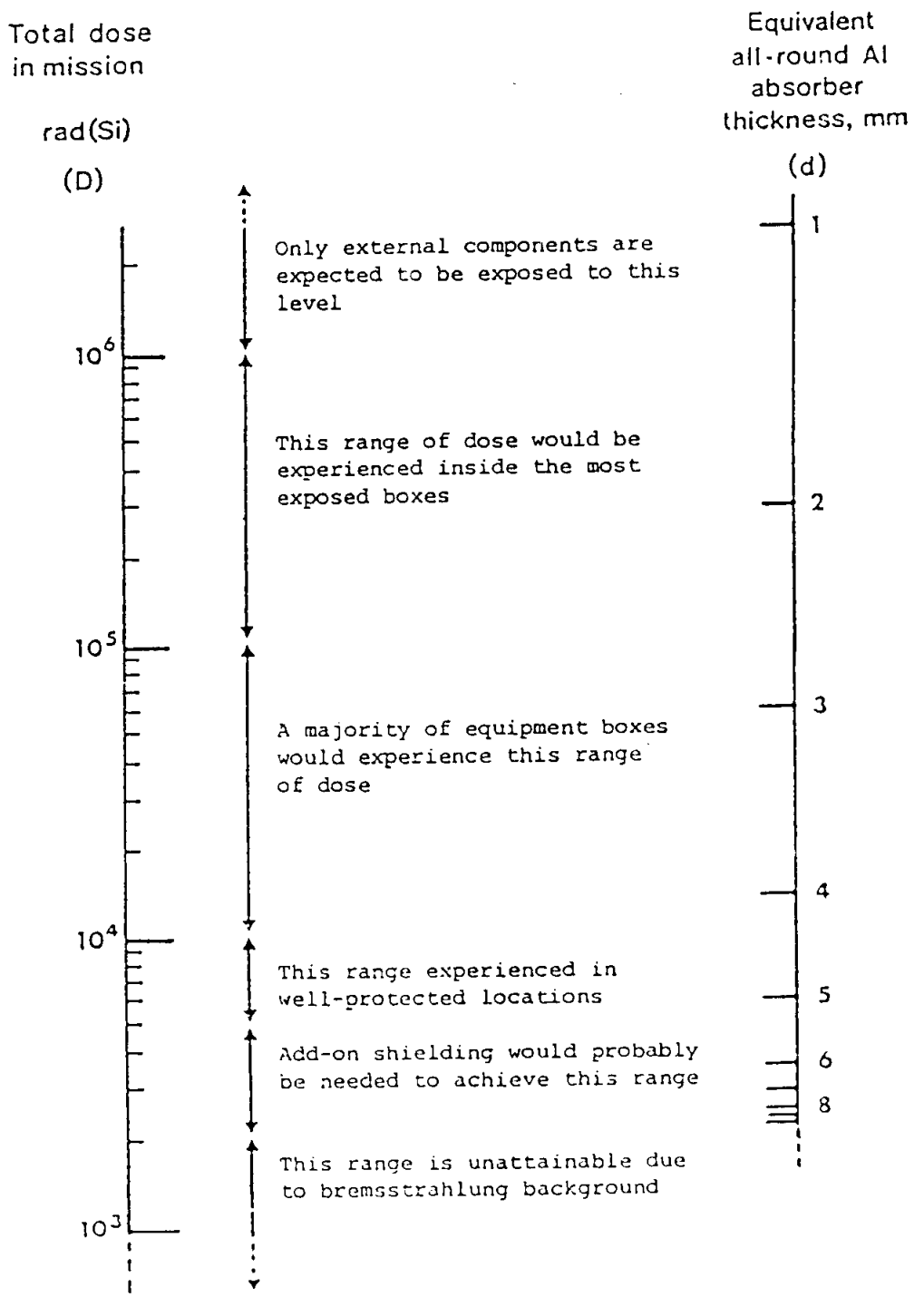

7-year Geostationary Mission

TABLE 17(2) - THE EFFECT OF ADDITIONAL SHIELDING ON THE EXOSAT STAR-TRACKER ELECTRONICS BOX

Total protection	2-Year dose krad (Si)	Dose reduction effected by added shielding
As designed	4.4	–
+ 1 mm Al*	2.4	45%
+ 2 mm Al	1.6	64%
+ 3 mm Al	1.15	74%
+ 4 mm Al	0.92	79%
+ 5 mm Al	0.89	80%

(*) all-round protection

17.6. ON-BOARD RADIATION MONITORING

17.6.1. The need for monitoring

The extensive analytical methods described in this handbook inevitably involve a large number of approximations and may thus be subject to quite large percentage errors in the prediction of radiation exposure at a given dose point and the resulting device degradation. Just as thermal-control calculations are ultimately verified by the installation of thermocouples in space vehicles and telemetry of temperatures in orbit, it is desirable to install small radiation monitors in equipment boxes both to check predictions for future reference and to provide operations staff with guidance on stressing and life of equipment during the mission. Until now, only bulky power-consuming particle pulse detectors such as nuclear diodes and geiger counters have been used and then only as special payload on scientific satellites.

17.6.2. The development of a radiation monitoring unit (RMU)

A concept for such a sensor has only recently become available. ESTEC has designed a trial RMU which may be installed on several spacecraft as a non-interfering "passenger". Figure 17.6 illustrates the principle of a device which was installed on the GEOS-2 spacecraft. The RMU contained five MOS transistors especially processed for high sensitivity to radiation (Holmes-Siedle, Adams, Pauly & Marsden, 1985). Different devices are shielded by different thicknesses of aluminium. Power, mass and data requirements of such devices are very low.

Information from these RMUs was telemetered periodically and served to verify the basic dose-depth curves for the mission. A more

accurate adjustment of shielding mass can be made in future missions and possibly also a cost-saving relaxation of radiation specifications on devices. Future versions placed inside operating boxes near key MOS LSI devices will give evidence of the precise operating conditions of these crucial control circuits and indicate when control should be switched to back-up units (e.g. if radiation-induced functional failure appears imminent).

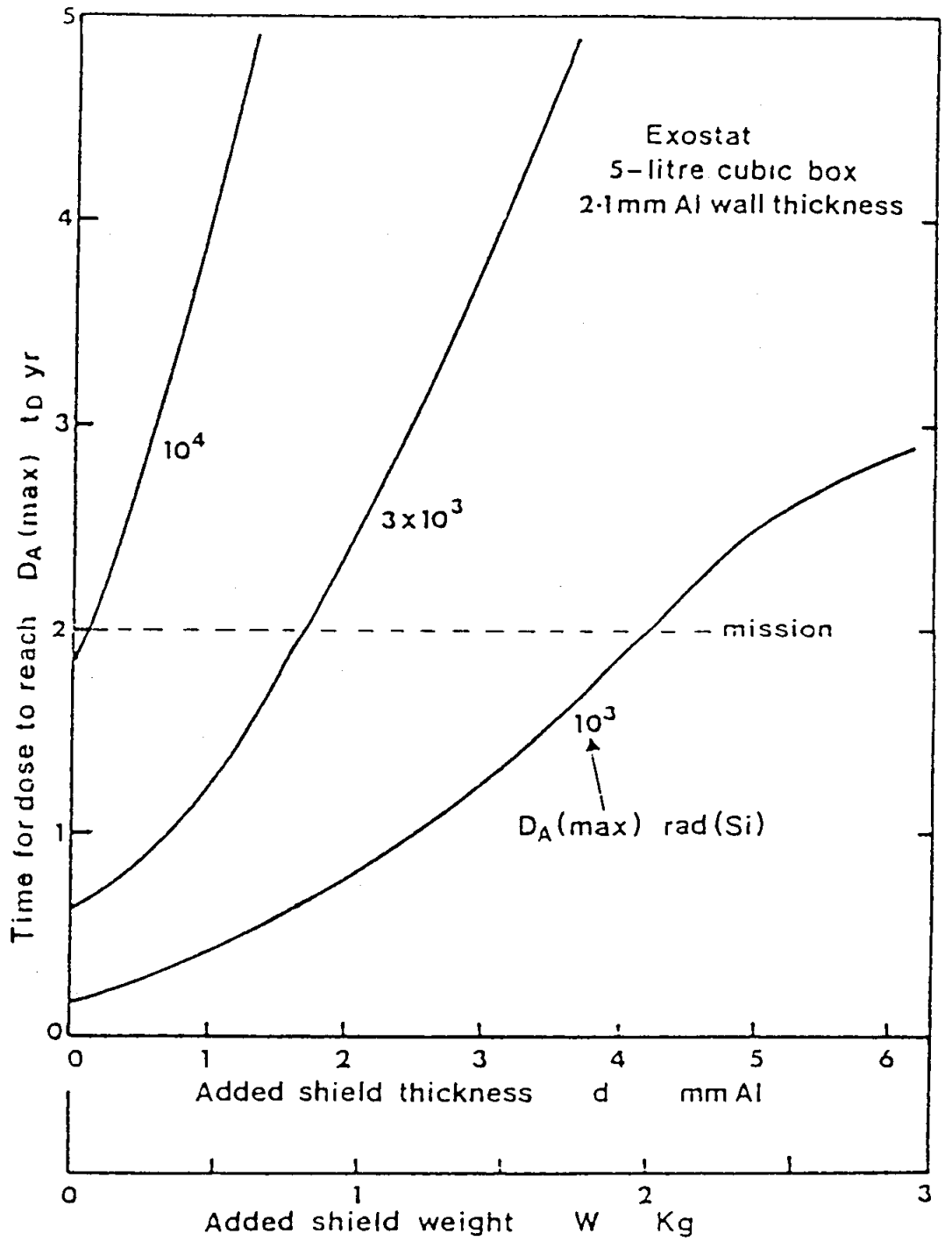

Time taken to reach "maximum acceptable dose" as a function of added shielding. The sensitive component is within a 5 litre cube of initial wall thickness 2.1 mm aluminium. Additional thickness is added uniformly.

FIGURE 17.4 - TRADE-OFF CURVES – EXOSAT MISSION

17.6.3. Particle counting monitors

Small semiconductor counting detectors are useful when temporal data are required, or when particle species or energy discrimination is required. Charge pulses generated by particles passing through the semiconductor material are pulse-height analysed and counted (see e.g. Knoll, 1989). An example of this type of monitor is the Radiation Environment Monitor (REM) built by CIR and PSI for ESA (Daly et al., 1992). The price paid for the flexibility and more comprehensive data return of such devices is the requirement for power (~2W) and mass (~1kg) to accommodate them.

17.7. SUMMARY OF DESIGN RULES

17.7.1. General rules

(a) Device degradation predictions must be prepared in time to influence lay-out and circuit design;

(b) Device selection can increase spacecraft life for no increase in weight.

17.7.2. Measures at device level

(a) Introduce redundancy as widely as possible: this can be "on-chip" (gate functions reassigned periodically) or "standby redundancy" of whole subsystems. The object is to allow "time off" for active recovery of charge build-up.

(b) Favour LSI where reasonable. This allows larger numbers of functions to be shielded with a small mass. However, note that LSI technology is sometimes less tolerant to radiation than the corresponding SSI.

(c) Avoid a mixture of logic technologies (e.g. TTL, CMOS and PMOS) as compatibility may be degraded by radiation. Also, the supply voltages may have to be higher than strictly necessary.

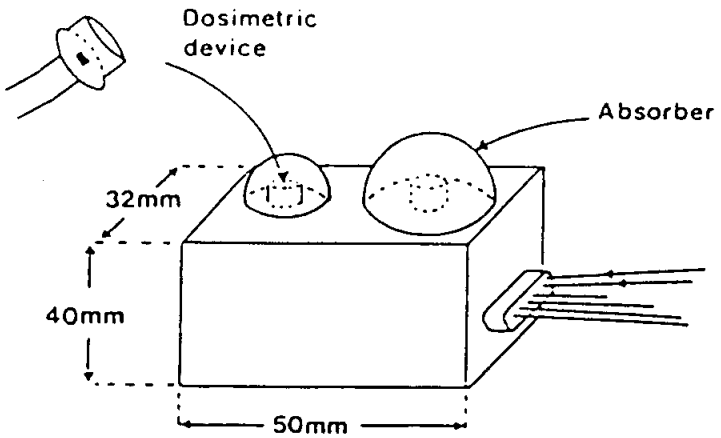

note: 5 devices actually
fit on top

a) ESA self-contained radiation
measurement unit (RMU, ESA, 1977)

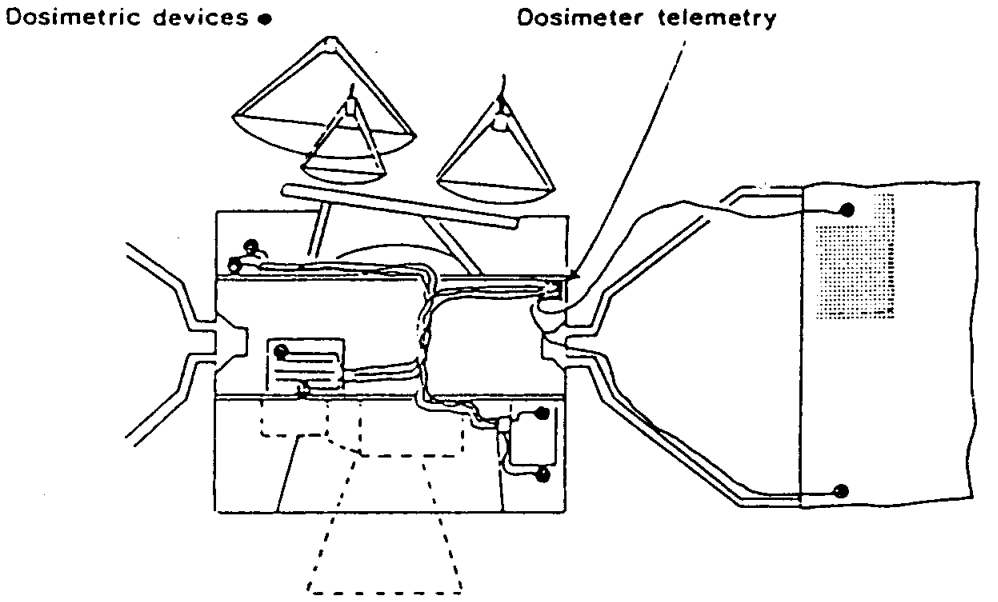

b) Distributed dosimeters
(Future)

Design and distribution of on-board dosimetry:
(a) Current version,
(b) Future distribution of miniature-head version.

FIGURE 17.5 - RADIATION MONITORING UNIT

17.7.3. Circuit design rules

(a) Discrete bipolar transistors

1. Predict and prescribe allowances for degradation of gain, increase of junction leakages, etc.
2. Select by manufacturer and lot.

(b) Bipolar digital circuits

1. Prescribe decreased fan-out.
2. Prescribe minimum collector current (especially with I^2L).

(c) MOS circuits

1. Classify devices by the values of parameters A and $\Delta VT(sat)$.
2. Predict device life and trade shielding against cost, etc.
3. Minimise electrical stress (V_{DD}, "Time On", etc.).
4. Decrease speed and output drive requirements.

(d) Bipolar analogue circuits

1. Prescribe allowances for:
   (i) decrease in open loop gain,
   (ii) input offset currents and voltages,
   (iii) output drive and maximum slow rate.
2. Make trade-offs as for MOS.

(e) CCDs and image sensors

1. Decrease storage times.
2. Allow for an increased dark current.
3. Trade off as for MOS.

(f) Other components - assessment

Perform radiation tests on:

- Voltage regulators,
- Diodes,
- Thyristors,
- Optoisolators,
- Other photosensors and LEDs,
- Glass optical components,
- Other classes of device deemed to be of dubious tolerance to radiation.

17.7.4. Layout for optimisation of built-in protection

(a) Avoid placing sensitive components on top of boards.

(b) Assemble as many sensitive components together as possible for mutual protection and site the box containing them near massive structural elements. Co-planar arrays of IC packages provide especially good edge-on protection for each other.

17.7.5. Add-on shielding

(a) The minimum weight of add-on shielding is obtained by small dense local shields (i.e. large solid angle subtended by small mass). For trade-off purposes, a figure of merit for shielding in units such as "rads per gram" should be utilised.

(b) Even small solid angles can admit large amounts of radiation if the absorber in the path of that radiation is thin (say, less than 1 mm).

17.8. CONCLUSIONS

Cost-effectiveness in performance of satellites operating in a space radiation environment is achieved only if a coherent engineering approach to radiation effects is adopted. The approach summarised here requires some advanced physical techniques in device selection and the calculation of shielding. The use of these hardness engineering techniques in a space project should therefore be assigned a priority measured by both the orbital environment and the requirement of that project for MOS LSI devices and other radiation-sensitive technologies.

It should be emphasised that each part of a spacecraft acts as a radiation shield.

REFERENCES

Aerojet General Report 1242-CDR-1 (Dec. 1975)

E.J. Daly, H.D.R. Evans and C. Tranquille, 'The XMM Radiation Environment and its Effect on Payloads', ESTEC Working Paper EWP 1643, ESTEC/WM 1992.

E.J. Daly, L. Adams, A. Zehnder and S. Ljungfelt, 'ESA's Radiation Environment Monitor and its Technological Role', Paper IAF-92-0779 at 43 rd. IAF, Washington D.C. (1992)

D.R. Hollars, J.F. Janni and H.F. Schneider, "Degradation of Satellite Electronics Produced by Energetic Electrons", Paper present at AIAA 15th Aerospace Sciences Meeting, Los Angeles (24th Jan. 1977)

A.G. Holmes-Siedle, Nucl.Instr.Meth. 121, pp. 169-179 (1974)

A.G. Holmes-Siedle, ESTEC Contract AHS-EXO-77-1 (Feb. 1977)

A.G. Holmes-Siedle, L. Adams, B. Pauly and S. Marsden, "Calibration and Flight Testing of a Low Field PMOS Dosimeter", IEEE Trans.Nucl.Sci. NS-32 (6) (December 1985)

T.M. Jordan, "SIGMA, A Computer Programme for Space Radiation Dose Analysis within Complex Configurations", DAC-60878, McDonnell Douglas Astronautics Co. (1967)

G.F. Knoll, 'Radiation Detection and Measurement', Second edition, John Wiley and sons, New York, 1989

H.H. Sauer, 'SEL Monitoring of the Earth's Energetic Particle Radiation Environment', in: High-energy Radiation Background in Space, p. 216-221, American Institute of Physics, New York, 1989

A.P. Schmid et al, "Microcircuit Packages Incorporating Radiation Shields for Use in Spacecraft Electronics", Proc.Int.Soc. for Testing and Failure Analysis (ISTFA) (Oct. 1985)

Structural Mass Optimisation Programme, ESA SP-133 (July 1977)

V.A.J. van Lint, J.P. Raymond, A.R. Hart and M.L. Price, "Radiation Design Handbook for the Jupiter Probe", MRC/SD-R-14, Mission Research Corp., San Diego (May 1977)

PAGE INTENTIONALLY LEFT BLANK

SECTION 18. COMPUTER METHODS

18.1. INTRODUCTION

Earlier discussion indicates the complexity involved in estimating radiation effects within a spacecraft. Often, the designer will be provided with environment data in the form of orbit-averaged particle flux spectra for the project under consideration. However, such data can be generated by the use of the environment models described in Section 3 and their associated computer programs. The environment is also often specified in terms of the "dose-depth" curve giving the dose as a function of depth of shielding in a simple geometry (slab or sphere). The necessary end-point is most often the estimation of the radiation dose likely to be received by a particular device at a particular point within the spacecraft structure. "Manual" methods were described earlier, but powerful computer codes now serve as the main tools for the engineer. Some problems require an explicit computation of particle flux and this requires special computational techniques, in particular Monte-Carlo methods discussed in Section 18.3.2.

An overview of the radiation analysis problem is given in Figure 18.1. The steps necessary to provide the final dose can be summarised as:

(a) Prediction of orbital and mission particle fluxes,
(b) Generation of a spherical-geometry "dose-depth" curve from (a),
(c) Extrapolation of (b) to complex spacecraft geometries by means of sectoring, accounting for shielding afforded by various parts of the real spacecraft.

Simplifying assumptions are made in separating steps (b) and (c). A rigorous analysis would require that the geometry be explicitly considered as the dose is computed - such methods are usually of the "Monte Carlo" type described below.

Manual methods may be useful for a preliminary dose assessment, but the simplifications introduced may introduce undue error at the detailed design stage where highly detailed computer-based sector analysis of the spacecraft structure can be performed very efficiently.

A brief review is given here of the various computer programmes and their methods. Calculation of single-event upset rates is also described.

18.2. ENVIRONMENT CALCULATIONS

The environment models described in Section 3 are available on computer tape from the WDC-A-R&S (NSSDC) at NASA/GSFC and

can be used to produce the required particle flux spectra. To do this, they must be used in conjunction with an orbit generator, giving the spacecraft trajectory and a geomagnetic field program to provide the corresponding B-L coordinates of the trajectory. ESA/ESTEC have integrated these steps together in the UNIRAD system (Daly, 1988) which also includes programs for dose and equivalent fluence calculations. Recently a PC-based version has been marketed by Severn Communications Corporation in the U.S.

18.3. DOSE AND FLUX COMPUTATION

Over the last two decades, a number of computerised methods have been developed to handle the complete problem. Some of these are complex and require considerable computer capacity; some of them employ simplified approaches, making certain reasonable approximations. These methods are in wide use and are recommended especially when geometrical and material complexities of spacecraft are considered. Programs are available in Europe via the program library of the Nuclear Energy Agency (operated by the OECD). Some programs are also available from ESA and others from NASA via the COSMIC software agency. CERN have also developed the GEANT particle transport code.

It should be noted that many older programs are not designed for universal application, have poor documentation and/or are not clearly coded. These are important considerations when one is selecting codes, as the cost of circumventing such problems may be high.

18.3.1. Particle types to consider

18.3.1.1. Electrons

Problems to be dealt with in computing the transport of electrons through materials are electron scattering and the production of brehmsstrahlung (see below). Most interactions between energetic electrons and the electrons and atoms of the material through which they are moving involve small energy losses and trajectory deflections. This makes the computational treatment of electron transport difficult.

18.3.1.2. Protons

Because of their mass, protons do not undergo significant scattering in travelling through a medium. They slow down, losing energy quasi-continuously, in a straight line. Therefore, the well-known range-energy relation can be applied quite simply to their motion. Occasionally, protons produce secondary particles when they collide with atomic nuclei. Such "spallation products" are important in contributing to single-event-upset or radiobiological damage; computational treatment of these interactions is difficult.

18.3.1.3 Bremsstrahlung (photons)

As electrons slow down in material, they generate bremsstrahlung photons with a distribution of photon energies and directions. Photons subsequently interact through a number of processes (photoelectric, Compton, pair-production), resulting in loss or scattering. Photon transport calculations are therefore also difficult.

18.3.1.4 Other particles

The above three particle species are the main concern for total dose problems. A number of secondary particles can be produced in the interactions between protons or heavier ions and the spacecraft material, or in the residual atmosphere in low Earth orbit. These can include secondary protons, neutrons, spallation fragments and more exotic nuclear particles.

Continuous exposure to space radiation can also lead to "activation" of spacecraft material which then emits radiation.

Finally, on-board nuclear sources, e.g. thermoelectric generators, can be an important source of radiation.

These various "second-order" radiations must be considered in circumstances where there is a specific sensitivity to them, e.g. in manned flights and for interference with instrument detectors.

18.3.2. "Monte Carlo" techniques

Monte Carlo techniques numerically follow the trajectories of large numbers of particles and predict their interactions in the material through which they are travelling. Interactions usually have distributions of possible outcomes to which random sampling is applied. For electrons, successive individual interactions are too numerous to follow; instead, attention is given to a small section of the electron's path containing a large number of individual interactions. The net result of all the interactions can be expressed analytically and, at the end of each section, the electron energy loss is computed and its direction is altered by random sampling of a scattering distribution. The section length is chosen such that the energy loss in the section is a small fraction of the electron energy. This is the "condensed history" Monte Carlo technique (Berger, 1963).

Monte Carlo techniques can also be used to compute the transport and interactions of other particles and their secondaries, including bremsstrahlung, neutrons etc.

Some Monte Carlo programs include particle transport and interactions in complex geometries while others consider simple slab geometries. Some commonly used programs are:

GEANT3 (Brun et al., 1987, Alison et al., 1987).
GEANT has been developed at CERN for analysing problems in high-energy physics. Flexibility of problem definition is provided by the user writing a Fortran "main program" with calls to GEANT subroutines for geometry definition, initial particle properties and tracking and event data retention. The lower energy limit for most particles is 10 keV. GEANT is well supported by CERN, with many ancillary packages (graphics etc.) and network communications, and runs on a variety of computers.

ITS/Tiger (Halbleib et al., 1992)
The Integrated Tiger System, ITS provides three versions for analysing coupled electron-photon transport in 1, 2 and 3 dimensions and energies from 1 keV to 1 GeV. As a successor to the ETRAN codes, the electromagnetic shower physics is dealt with very rigorously.

HETC (Deitz, 1986)
The High-Energy Transport Code, HETC is a 3-dimensional code for full treatment of the transport of ions and associated secondaries (including protons, neutrons, pions and muons).

EGS4 (Neslon, Hirayama and Rogers, 1985, Nelson and Namito, 1990)
The Electron-Gamma Shower (EGS) code is a rigorous 3-dimensional code for simulating the electron-photon transport problem. Here again, the user writes elements of the analysis program, which call the EGS subroutines.

Typical outputs of the electron-bremsstrahlung codes are:

- Transmission and back-scatter of electrons and photons,
- Production of bremsstrahlung by electrons and its transport,
- Spectrum of energy deposition in a thick target by an electron beam,
- Flux spectra as a function of depth in the material and
- Deposition of dose as a function of depth of shielding (dose-depth).

18.3.3. Dose "look-up" table methods - SHIELDOSE

If one is always dealing with a simple (e.g. slab) geometry, then - for an incident particle of a single energy - the generated dose per unit fluence at a given depth of shielding will be the same. Seltzer (1979, 1980) has created a large data set containing the dose per unit of incident fluence as a function of depth of aluminium shielding and particle energy. The total dose at a given depth of shielding for a given incident particle spectrum is then found by summing the contributions from each particle energy, considering

the incident flux at that energy and the time duration. This method was presented in Section 16.6.

Seltzer's data set is created with the ETRAN Monte Carlo code (a forerunner of ITS) considering all the relevant physics, and his SHIELDOSE program can rapidly give the dose for any arbitrary input spectra. Protons are treated according to their range-energy relation with nuclear reactions neglected. Figure 18.2 shows the three simple geometries considered by SHIELDOSE. If one is not interested in performing a geometrical analysis, the appropriate geometry to choose will depend on the location of the particular dose point. However, the slab case may be too optimistic in practice since it represents a situation where there is relatively good shielding in most directions. The widespread use of the slab model stems from the fact that it is easier to compute doses with slabs than with spheres. The sphere case is more conservative because in a slab there are longer paths through the material in directions away from the normal. In subsequent sectoring, the sphere case should be used, since slant paths in a laterally infinite slab are meaningless when a small solid angle about a particular direction is considered.

This program is interfaced with the environment spectra and included in ESA's UNIRAD system.

18.3.4. Straight-ahead approximation methods

Simpler and shorter alternatives of full Monte Carlo codes exist where analytical methods have been developed for specific application to spacecraft. These include:

- CHARGE (Lilley and Yucker, 1969; available from NEA) and
- SHIELD (Davis and Jordan 1976; available from COSMIC).

These simpler codes assume in the first instance that particles travel in straight lines and, according to the basic range-energy relations, lose energy continuously. Corrections are applied to account for the angular effects and the "degraded" spectrum is computed at a number of depth intervals in the shielding. These methods have the advantage over SHIELDOSE that they can treat the effects due to material differences. They can consider laminations of materials in simple (slab, sphere) geometries. Differences between materials are not completely accounted for by normalising the thickness to density to give g/cm^2 (or by converting to the equivalent aluminium thickness).

18.3.5. The CHARGE program

In the case of electrons, an attempt is made to account for the effect of their angular scattering by applying "transmission coefficients" derived from Monte Carlo runs. For example, CHARGE uses the empirical relationships developed by Mar.

Bremsstrahlung is treated in CHARGE by using the Koch and Motz model for generation with transmission based on the exponential attenuation model of Goldstein. "Build-up" factors are applied to account for bremsstrahlung angular distribution effects.

As indicated above, proton-slowing can be treated well by straight-ahead methods.

The ability of CHARGE to treat laminations of different materials has been used in an ESTEC study (Daly and Adams, 1984), where the program was assessed and then applied to the problem of predicting the shielding efficiency of various laminations of high-Z and low-Z materials.

CHARGE can also optionally calculate the dose from secondary protons and neutrons. Typical dose-depth curves from CHARGE are shown in Figure 18.3. This shows the dose in water behind very large thicknesses of aluminium shielding (100 g/cm^2 is about 37 cm). At "normal" thicknesses (i.e. a few millimetres), the dose from secondary protons is almost two orders of magnitude lower than that due to primary protons. The incident proton spectrum in this example is "a typical trapped-proton spectrum". Other proton-

generated particles, e.g. muons, pions, electrons or positrons, are not treated by CHARGE owing to insufficiency of data. Alsmiller (1964) has shown that the doses due to muons and photons can be ignored if present understanding is reliable.

Given the appropriate fluence-to-response conversion functions, CHARGE can compute rad doses, rem doses for biological effects and activation response.

SHIELD, developed particularly for the analysis of the VOYAGER spacecraft, overcomes some of the deficiencies of the CHARGE program with electrons of energies greater than 10 MeV encountered in the Jovian environment. The Mar formula used by CHARGE was based on the lower electron energies found in Earth orbit.

Recently, efficient deterministic one-dimensional alternatives to Monte Carlo analysis have been developed for space application. These are the CEPX/ONELD discrete ordinate code for electron-photon transport (Beulter et al., 1991), the BRYNTRN code for nucleon transport (Wilson et al., 1989) and the HZETRN code for heavy-ion transport (Shinn and Wilson, 1992).

18.3.6. Sectoring analyses

Application of one of the simple-geometry techniques can produce the dose-versus-depth relationship which can be combined with solid-angle sectoring to produce an approximate dose at a point in a representative model of the spacecraft geometry. Often, the engineer is provided with this dose-depth curve as a specification of the environment. Sectoring is only an approximation since the angular scattering of electrons and angular distributions of bremsstrahlung are not explicitly treated. Used independently of the dose-depth curve, sectoring is useful for computing the distribution of spacecraft shielding about a particular point.

Manual methods for sectoring calculations were described previously, but computer programmes are available for the task:

- ESABASE/Radiation, an ESABASE analysis module (Daly, 1988; available from ESA),
- SIGMA II, developed for JPL (Davis and Jordan, 1976; available from COSMIC) and developed from SIGMA I/B (Jordan and Yucker, available from NEA),
- MEVDP, AFWL (Lilley and Hamilton, available from NEA).

As an ESABASE module, ESABASE/Radiation has the advantage of the use of the ESABASE "pre- and post-processing" visualisation utilities for geometry checking and 3-D display of results. The spacecraft geometry is defined in terms of simple shapes and the dose-depth curve taken automatically from the SHIELDOSE

program in the UNIRAD system which is fully integrated into ESABASE. ESABASE/Radiation, in common with other sectoring methods, employs ray-tracing where a large number of rays are followed out through the geometry; intersections with structure materials are found and the total shielding thickness along each ray computed. The elemental solid angles around the rays are used to "weight" the interpolated dose values from the the (4.pi) dose-depth curve at the appropriate depth values and an integration performed over all rays and solid angles. Thus, a highly detailed sectoring of complex spacecraft geometries is possible. ESABASE/Radiation is well documented and is being continually developed. Figure 18.4 shows the constituent part of ESABASE/Radiation and the data-flow between them.

SIGMA operates on basically the same principle. Multiple attenuation curves can be input, for example individual radiation species doses and ion fluences. Dependence on material of the attenuation of the various input radiation species can be partially accounted for by specifying different thickness-normalising factors for each material and radiation type. The usual tracing of the rays, accounting for their slant paths through materials, is augmented by a "minimum path" estimation to give the minimum shielding a multiply scattered electron would encounter. Parametric shielding calculations are possible where the sensitivity of the dose to additional "spot" shielding is computed. The COSMIC package containing SIGMA II also contains the shield optimisation programme SOCODE and the SHIELD program described above.

However, in common with other older programs, SIGMA with its limited documentation is quite difficult to use. The original SIGMA, still available through the NEA, was extremely difficult to use for the definition of complex geometries since it was necessary to define the shield structure in terms of bounding surface quadratic equations, and voids also had to be explicitly defined. The SIGMA II program available through COSMIC, has improved geometry definition facilities and no longer requires void specification.

18.3.7. Comparisons

While it is not the objective of this brief review of computer methods to make rigorous comparisons between the various approaches, a number of specific instances where comparison has been possible are given.

18.3.7.1. Charge validation examples

The CHARGE documentation contains a number of comparisons made by way of validation of the code. Agreement with other calculations of primary proton dose is good. Secondary nucleon doses are reasonable when compared with Monte Carlo results. Electron doses computed by CHARGE were found to be higher

than with other Monte Carlo methods, the disagreement being within a factor of 2 at normal shield thicknesses.

18.3.7.2. Bremsstrahlung dose - CHARGE and "manual" methods

The CHARGE documentation includes tabulated data for dose in water behind aluminium shielding in an elliptical polar orbit for which a trapped-electron spectrum is given. The bremsstrahlung dose calculated by the manual approximation is 0.6 rad (H_2O)/ month. The dose calculated by CHARGE is between 0.4 and 0.5 rad (H_2O)/month, depending on shield thickness. This correlation is considered to be reasonable.

18.3.7.3. Electron dose - CHARGE, SHIELD and BETA

Davis and Jordan (1976) compared the two "simplified" programs and the BETA Monte Carlo program in the calculation of an electron depth-dose curve for the Jupiter environment. The flux is isotropic upon a spherical aluminium shield with the dose point at the centre. Excellent agreement is obtained for shield thicknesses of up to 4 g/cm^2 (15 mm). Divergence thereafter is probably due to the weakness in CHARGE with electrons greater than 10 MeV energy.

18.3.7.4. Electron transmission - BETA, ETRAN and experiment

The BETA documentation contains a number of comparisons between experimental electron and bremsstrahlung transmission data which show very good agreement. ETRAN results have also been reported (Berger, 1968) and these too agree very closely with experimental data.

18.3.7.5. Comparisons between CHARGE and SHIELDOSE

The results of the ESTEC study mentioned in Section 18.3.3.1 showed that:

- In spherical geometry, there is good agreement between proton and bremsstrahlung doses;
- In slab geometry, the CHARGE bremsstrahlung dose is 2 to 3 times higher;
- SHIELDOSE predicts electron doses 2 to 3 times higher than CHARGE in spherical geometry, but agrees well in slab geometry. This is probably due to the solid sphere geometry of SHIELDOSE with account taken of back-scattered electrons;
- SHIELDOSE should be used as a tool for routine analysis with CHARGE available for situations where materials are important.

18.3.7.6. Comparisons between ITS and related codes and experiment

Lockwood et al. (1976) found very good agreement between the energy deposit in various multilayer geometries computed by an

early version of the TIGER code and experimental measurements. Sanford et al. (1985) reported on comparisons of measured doses of bremsstrahlung produced by 0.75 MeV electrons incident on Ta/C targets with doses calculated with the CYLTRAN Monte Carlo code. Again, close agreement over a wide range of Ta target thicknesses and angles was found. Kensek (1992) reported several other comparisons between experiment and the predictions of ITS and CEPXS/ONELD codes wich resulted in very good agreement.

18.4. SINGLE-EVENT UPSET PREDICTION

18.4.1. Ion-induced SEU

Pickel and Blandford (1980) first reported the basic method for single-event-upset-rate computation ("CRIER" - Cosmic-Ray Induced Error Rate). Cosmic-ray environments have since been comprehensively modelled by Adams and co-workers at NRL (Adams et al., 1981), on the basis of satellite data for cosmic-ray and flare ion fluxes. They developed the CREME suite of programs (Adams, 1986) which include these models, together with upset-rate computation which is functionally equivalent to Pickel and Blandford's method. The environment available from CREME include solar-cycle modulated GCR fluxes for most ions, 10% worst-case GCR fluxes, anomalous component fluxes and anomalous, worst-case and ordinary flare fluxes including mean or worst-case composition. Earth shadowing and transport through shielding material are also considered. For treating geomagnetic shielding, CREME computes an orbital attenuation function on the basis of Shea and Smart's world map of vertical cut-off rigidities. Energy and LET spectra are produced, the latter being composites of the fluxes of all ions as functions of ion stopping-powers (dE/dx) in silicon. CREME has data files of stopping-powers and ranges of cosmic-ray ions in aluminium and silicon for computing shielding effects and particles LETs.

To compute an upset or hit rate for an electronic device or a detector from the predicted fluxes, device characteristics must be specified, particularly the size of the sensitive volume and the critical charge, or equivalent, critical energy E_C, in the volume which results in upset (bit-flip) or registers as a "count'. The rate is found by integrating over the composite differential LET spectrum, $\phi(L)$, and the path-length distribution for the sensitive volume, p(l):

$$U = S/4 \int_{E_c/L_{max}}^{l_{max}} p(l) \int_{E_c/l}^{L_{max}} \phi(L)\, dL\, dl$$

where S is the total surface area of the sensitive volume. Integration limits are set by the sensitive volume dimensions and the critical energy E_C; E_C/L_{max} is the shortest path capable of supporting

upset, l_{max} is the maximum path length, E_C/l is the minimum particle LET necessary to cause upset on a path length l and L_{max} is the maximum LET of the spectrum. Figure 18.5 shows an overview of CREME.

Ion-beam tests can establish the threshold LET, defining the critical charge ($E_C = L_C$ x depth), and saturation cross-section, giving information about the sensitive volume. However, all the upsetting "bits" may not be the same, and often no sharp threshold in LET is apparent. In these cases, an integral over the measured response curve may be performed (Harboe-Sorensen et al., 1986). The upset-rate computation is sensitive to the value chosen for this critical charge, and derived from the LET threshold, because whereas particle fluxes fall rapidly with increasing LET, the sensitivity increases rapidly. Sensitive volume dimensions may be deducible from device technology data which is best obtained from the manufacturer, since to obtain the necessary information by "reverse engineering" is quite an extensive task.

The CREME program is used by ESA for evaluations of critical devices in various environments (Daly, 1988).

18.4.2. Proton-induced upsets

In Section 16.11.1, the phenomenon of proton-induced single-event effects was described. As with the computation of ion-induced SEU described above, proton-induced SEU rate prediction depends heavily on testing. Bendel and Peterson (1983) have described a method for making predictions of in-orbit proton-induced error-rate which is simple, provided the upset cross-section of a device as a function of proton energy is available from ground-tests.

The CREME programs include the BENDEL program, which implements the above model. This program requires an input proton spectrum which must be derived either from the AP8 trapped proton models or a solar proton model. The test data are characterised by the 'A' parameter which is chosen so that the standard model cross-section versus proton energy upset curve follows the test results most closely. A is the "apparent threshold" of the device.

It is often difficult to fit a unique A parameter to the test results. Recently Shimano et al. (1989) reported a two parameter modification which performed better. Stapor et al. (1990) gave a slightly different variant of this model and reported on the importance of a two-parameter model for newer devices with small feature sizes.

18.5. CONCLUSIONS

This section has provided a brief review of the many computer methods which are now available for performing analyses of particle fluxes and radiation doses in simple and complex models of spacecraft structures.

When one is using simple geometries for routine dose computation, the sphere case is preferable to the slab case unless the use of the latter can be justified by the location of a specific component in the spacecraft. Shielding in a single slab model is relatively good in most directions.

The use of the programs described in this section enables one to assess the environment and doses in spacecraft, considering the mission and structural materials and geometry. Their use is recommended as an integral part of the detailed spacecraft design phase.

The ESABASE/RADIATION module is designed as an easy-to-use tool for calculating mission radiation environments. The sectoring method makes it possible to use the UNIRAD suite of programs and the resulting dose in a complex model of the spacecraft geometry. It is recommended that this be used when necessary and where possible.

Figure 18.4 shows the constituents and data flow in the ESABASE/RADIATION module.

Alternatively CHARGE or SHIELD can be combined with SIGMA to compute doses in complex geometries.

If a high degree of accuracy is required, especially for problems where particle fluxes and interactions need explicit analysis, the Monte Carlo methods of Section 18.3.2. should be employed.

Single-event upset sensitivity should be assessed with the CREME program together with device data.

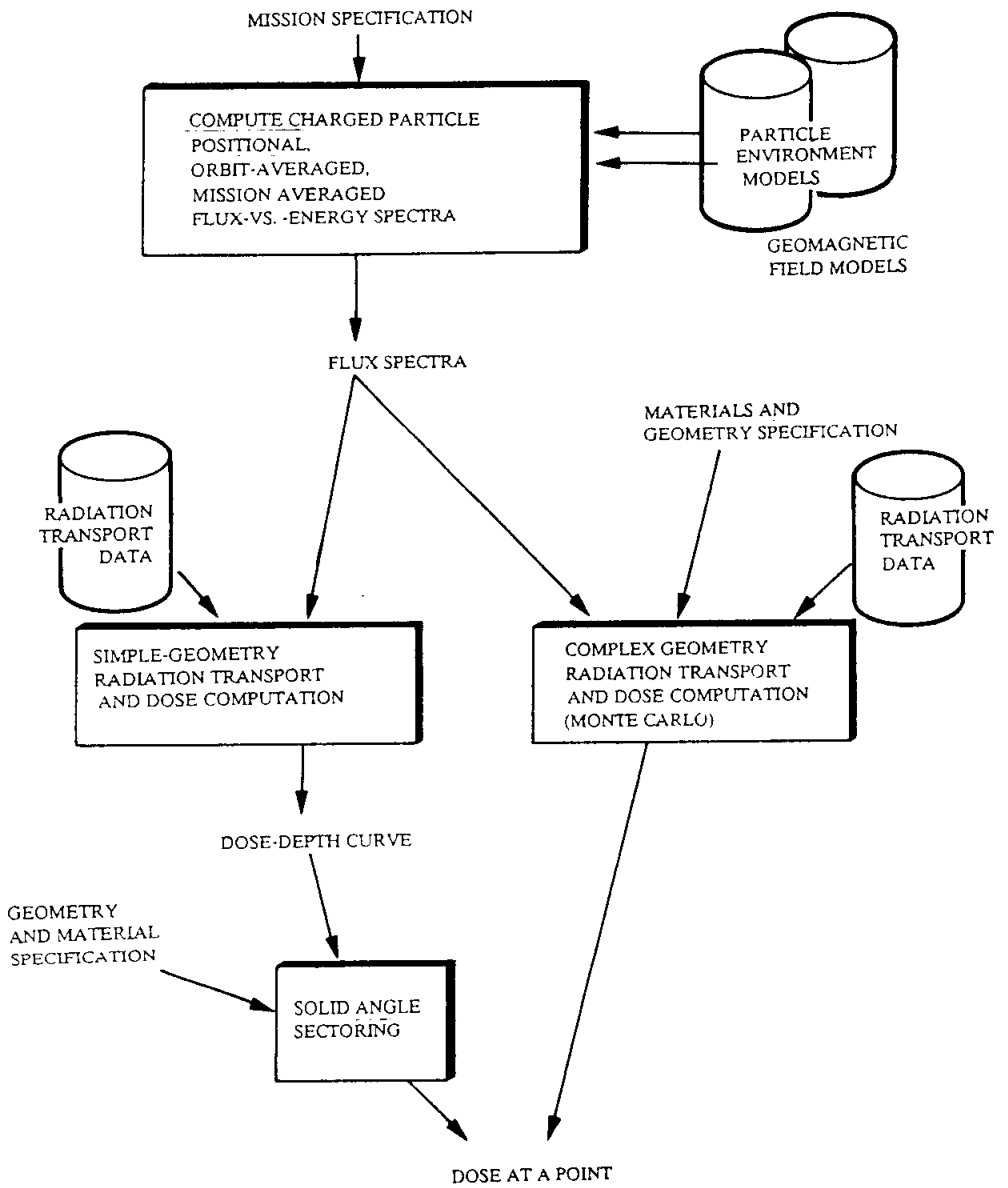

FIGURE 18.1 - RADIATION ANALYSIS OVERVIEW

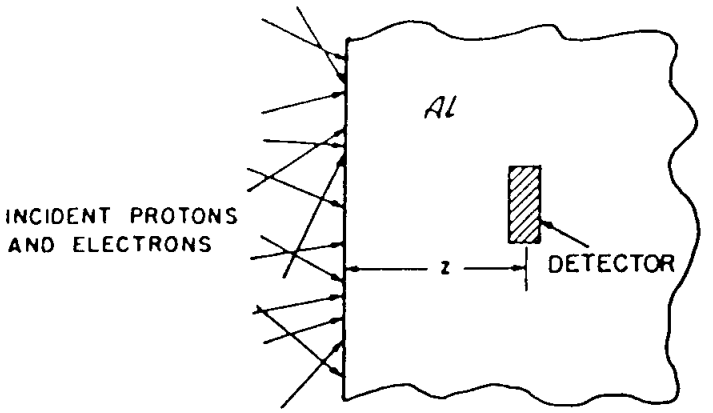

CASE 1. SEMI-INFINITE MEDIUM; ABSORBED DOSE IN DETECTOR DENOTED AS $\mathfrak{D}_{=}^{det}(z)$

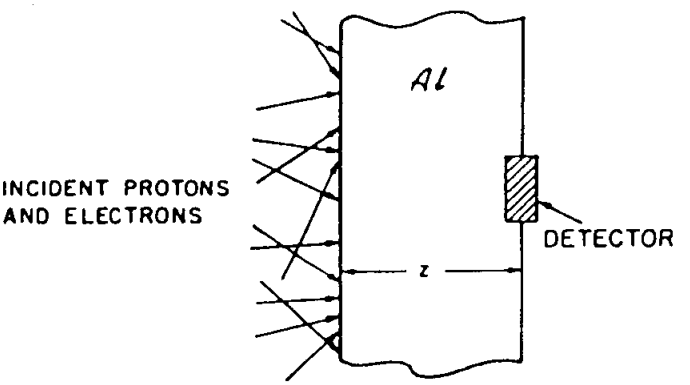

CASE 2. FINITE-THICKNESS SLAB; ABSORBED DOSE IN DETECTOR DENOTED AS $\mathfrak{D}_{-}^{det}(z)$

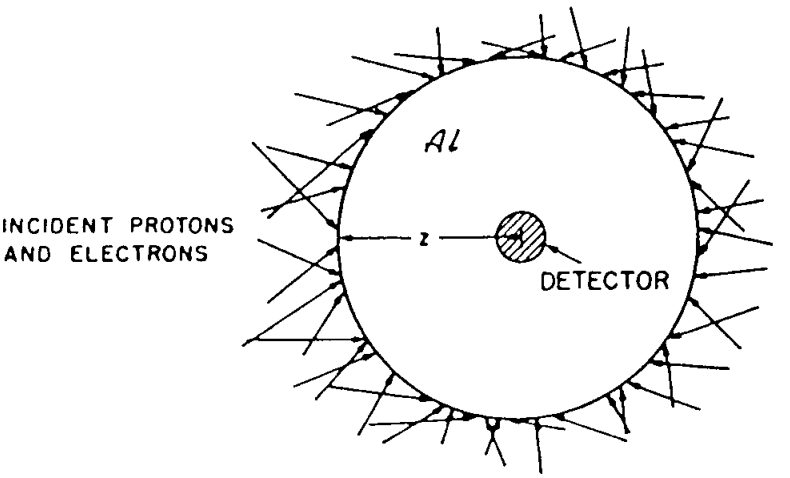

CASE 3. SOLID SPHERE; ABSORBED DOSE IN DETECTOR DENOTED AS $\mathfrak{D}_{\bullet}^{det}(z)$

Isotropic, broad-beam fluxes of protons and electrons are assumed incident on aluminium targets; absorbed dose is calculated for small volumes of detector materials Al, H_2O, Si and SiO^2.

FIGURE 18.2 - GEOMETRIES CONSIDERED IN "SHIELDOSE" CALCULATIONS

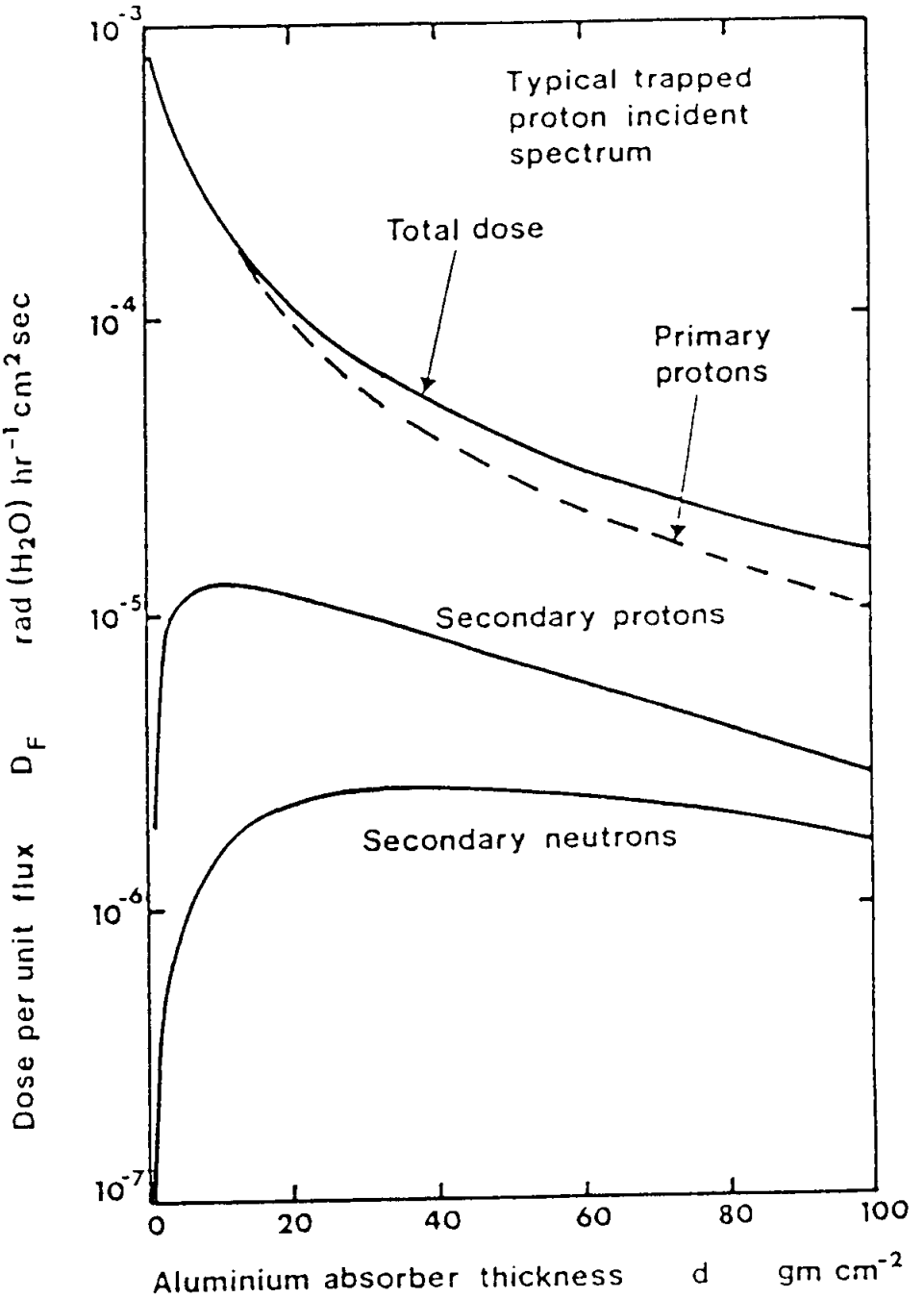

Dose-depth curves calculated by "CHARGE", showing effect of secondary particles generated by the passage of typical trapped protons through thick aluminium shielding.

FIGURE 18.3 - SECONDARY PARTICLE GENERATION

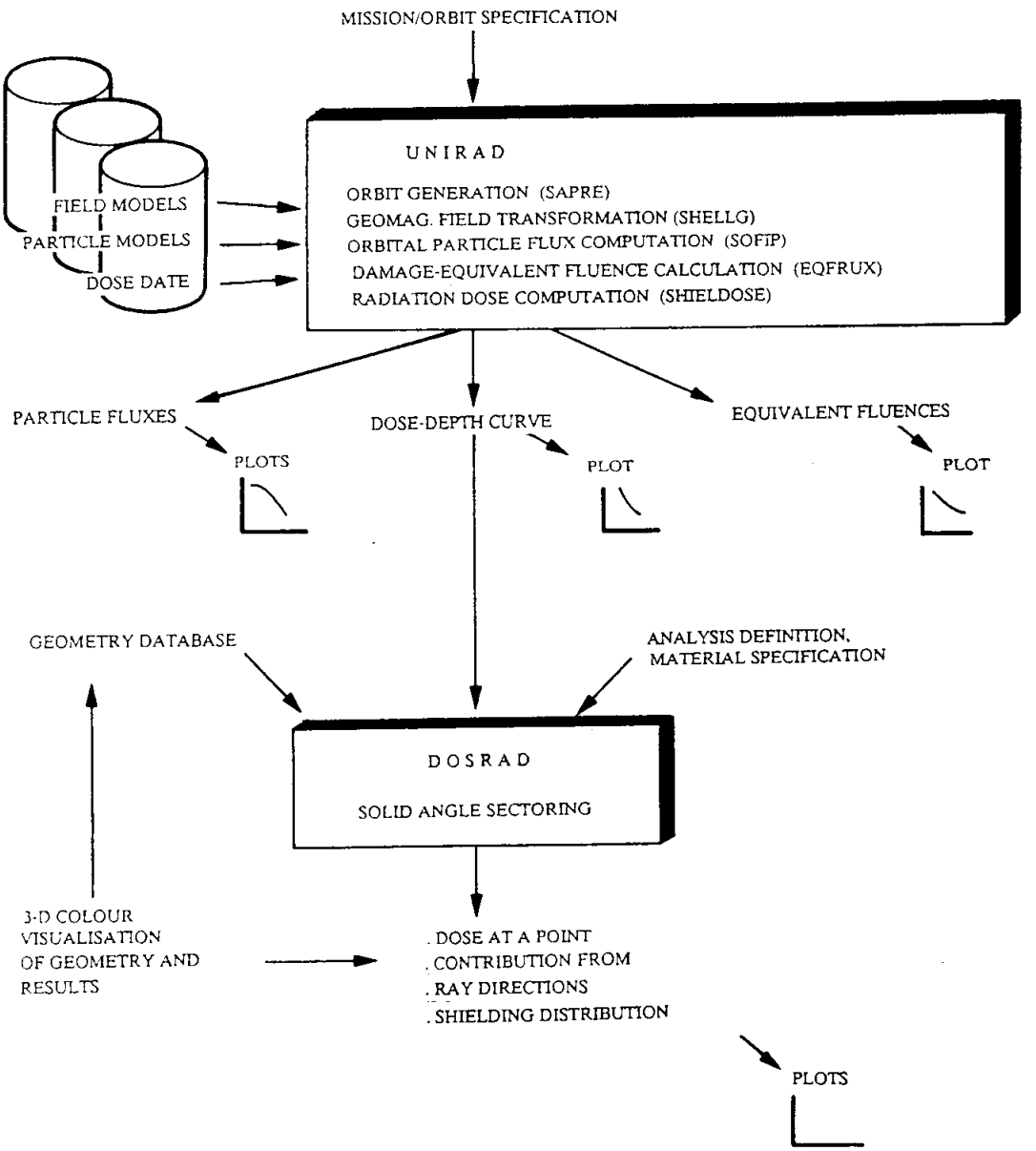

FIGURE 18.4 ARCHITECTURE OF THE ESABASE/RADIATION APPLICATION

REFERENCE

J.H. Adams, "Cosmic Ray Effects in Microelectronics Part IV", NRL Memorandum Report 5901 1986

J. Allison, R. Brun, F. Bruyant, F.W. Bullock, C.Y. Chang, J.J. Dumont, P. Hattersley, R.J. Hemingway, P.R. Hobson, et al., 'An Application of the GEANT-3 Geometry Package to the Description of the OPAL Detector', Comput. Phys. Commun. 47, 1, 55 (1987)

R.G. Alsmiller et al, ORNL-3714, Oak Ridge National Laboratory (1964)

R.G. Alsmiller, R.G., Nucl.Sci.Eng. 27, p. 158 (1967)

W.L. Bendel and E.L. Petersen, "Proton Upsets in Orbit", IEEE Trans. Nucl. Sci. NS-30, 6, 4481 (1983)

M.J. Berger, "Monte Carlo Calculation of the Penetration and Diffusion of Fast Charged Particles", Methods in Computational Physics, Vol. 1: Statistical Physics, p. 135 Academic Press (1963)

M.J. Berger & S.M. Seltzer, "Penetration of Electrons and Associated Bremsstrahlung through "Aluminium Targets", NASA SP-169 (1968)

D.E. Beulter, L.J. Lorence and D.B. Brown, " Dosimetry in Linac Electron-Beam Environments", IEEE Trans. Nucl. Sci., NS-38, 6, 1171 (1991)

R. Brun, F. Bruyant, M. Marie, A.C. McPherson and P. Zanarinin, 'GEANT3', CERN DD/EE/84-1, Revised 1987 and subsequently. To be revised CERN/CN-AS Group, 1993

E.J. Daly, "The Evaluation of Space Radiation Environments for ESA Projects", ESA Journal 12, 229 (1988)

E.J. Daly and L. Adams, "Radiation Doses in Spacecraft Assessment of Computer Programs", ESTEC EWP 1389 (May 1984)

H.S. Davis and T.M. Jordan, "Improved Space Radiation Shielding Methods", NASA-CR-146581 / JPL-TM-33-765 NASA/JPL (1976)

D. Dietz, 'The HETC/LHI/SGS Radiation Transport Code System', IEEE Trans. Nucl. Sci. NS-33, 5, 1131 (1986)

C.S. Dyer, P.R. Truscott, A.J. Sims, C. Comber and N.D.A. Hammond, "Particle Transport Simulation for Spaceborne, NaI Gamma-ray Spectrometers", IEEE Trans. Nucl. Sci. NS-35, 6, 1407 (1988)

J.G. Ferrante, P. Coffinier, B. Aube and J. de Kruyf, "Spacecraft Systems Engineering and Geometry Modelling: The ESABASE-MATVIEW Approach", ESA Journal 84/4, p. 381 (1984)

J.A. Halblieb, R.P. Kensek, T.A. Mehlhorn, G.D. Valdez, S.M. Seltzer and M.J. Berger, 'ITS Version 3.0: The Integrated TIGER Series of Coupled Electron/Photon Monte-Carlo Transport Codes', Report SAND91-1634 UC-405, March 1992. Code and documentation also available from NEA, Saclay, France.

R.P. Kensek, presentation on ITS at ESTEC, May 1992.
Comparison references included:
- G.J. Lockwood et al., Report SAND-79-0414, January 1980;
- J.R. Marbach, Ph.D. Diss., U. Texas Health Sci. Center, 1978;
- T.A. Mehlhorn and J.A. Halbleib, ISBN 0-89448-111-8, p. 608, (1983)
- A.R. Frederickson and S. Woolf, IEEE Trans. Nucl. Sci. 28, 6, 4186 1981.

H.W. Koch,and Motz, J.W., Rev.Mod.Phys. 31 920 (1959)

J.R. Lilley and W.R. Yucker, "CHARGE Code for Space Radiation Shielding Analysis", McDonnell-Douglas Report DAC-62231, McDonnell-Douglas Astronautics Co., Santa Monica, CA. USA (1969). Available as NEA package CC-0070/01, NEA, Gif-sur-Yvette, France.

G.J. Lockwood, G.H. Miller and J.A. Halbleib, "Electron Energy Deposition in Multilayer Geometries", IEEE Trans. Nucl. Sci. NS-23, 6, 1862 (1976)

W.R. Nelson, H. Hirayama and D.W.O. Rogers,'The EGS4 Code System', Report SLAC-265 UC-32 (E/I/A), Stanford Linear Accelerator, 1985

W.R. Nelson and Y. Namito, 'The EGS-4 Code System: Solution of Gamma-ray and Electron Transport Problems', Report SU-SLAC-PUB-5193, Stanford Linear Accelerator, 1990

J.C. Pickel, and Blandford, J.T., "Cosmic Ray Induced Errors in MOS Devices" IEEE Trans.Nucl.Sci. NS-27 (2), pp. 1006-1015 (April 1980)

T.W.L. Sanford, J.A. Halbleib and W. Beezhold,"Experimental Check of Bremsstrahlung Dosimetry Predictions for 0.75 MeV Electrons", IEEE Trans. Nucl. Sci. NS-32, 6, 4410 (1985)

S.M. Seltzer, "SHIELDOSE: A Computer Code for Space Shielding Radiation Dose Calculations" NBS Techn. Note 1116 (May 1980) (Also available through RSIC & NEA Library, CCC-379)

S.M. Seltzer, "Electron, Electron-Bremsstrahlung and Proton Depth-Dose Data for Space Shielding Applications" IEEE Trans.Nucl.Sci. NS-26, p. 4896 (Dec. 1979)

Y. Shimano, T. Goka, S. Kyboyama, K. Kawachi and T. Kanai, "The Measurement and Prediction of Proton Upset", IEEE Trans Nucl. Sci. NS-36, 6, 2344 (1989)

J.L. Shinn and J.W. Wilson, "An Efficient HZETRN (A Galactic Cosmic Ray Transport Code)", NASA-TP-3147 (1992)

W.J. Stapor, J.P. Meyers, J.B. Langworthy, E.L. Petersen, "Two Parameter Bendel Model Calculations for Predicting Proton Induced Upset", IEEE Trans. Nucl. Sci., NS-37, 6, 1966, (1990)

J.W. Wilson, L.W. Townsend, J.E. Nealy, S.Y. Chung, B.S. Hong, W.W. Buck, S.L. Lamkin, B.D. Ganapol, F. Khan and F.A. Cucinotta, "BRYNTRN: A Baryon Transport Model", NASA-TP-2887 (1989)

PAGE INTENTIONALLY LEFT BLANK

SECTION 19. RADIATION TESTING

19.1. INTRODUCTION

The sensitivity of semiconductor devices to radiation is often very variable and it is therefore impossible to use theory alone to predict the effect on a device of a given exposure to radiation. Actual irradiation tests must then be an integral part of the evaluation of a device and, sometimes, tests must be performed on each batch of devices. A large number of device radiation test programmes has been performed in Europe and an even larger number in the USA. The simulation of space radiation effects in the laboratory is quite difficult to achieve and the results thereof are often not those expected during planning.

This section is aimed at providing support in the design of adequate test programmes. It reviews:

- the main radiation sources which may be used together with their advantages and disadvantages and
- the main types of measurement which can be made, together with suitable implementation methods.

Reference is also made to the standard test procedures developed in the USA and Europe.

19.2. RADIATION SOURCES

19.2.1. Simulation of space radiation

The differences between radiation conditions in space and their simulation in the laboratory are frequently quite large. The incident space irradiation consists of a complex, mixed particle environment which, as discussed earlier, is altered and made even more complex by passage through spacecraft enclosures. The dose is delivered steadily over a long period of time - often, several years. Short-term variations in dose rate by up to 1 1/2 orders of magnitude may be experienced, depending on the orbit. Most of the time, one can only obtain radiation beams at a number of discrete energies and often it is also difficult to modify the rate at which the machine will deliver the radiation. Bearing these facts in mind, one must therefore modify the raw short-term results of "simulation" tests when converting them into predictions of space radiation conditions. One may also wish to monitor the irradiated device at intervals of minutes, days and months and introduce factors to allow for qualitative differences in space and laboratory radiation as well as the "dose rate effects" discussed in earlier sections.

Despite the above mentioned problems, a surprisingly wide range of devices can be tested suitably by the use of high-activity gamma-ray-emitting isotopes, e.g. the well-known cobalt-60 hot cell or

"irradiator". However, one must always classify carefully the physics of the effect one is aiming to simulate - whether it is classed as a total-dose ionisation effect, permanent bulk damage effect single-event upset or a transient effect of some other kind.

19.2.2. Gamma-rays

The source most commonly used for simulation of ionisation effects on silicon components or materials is Co-60 which emits photons of energy 1.173226 and 1.332483 MeV and has a half-life of 5.27 years. It is utilised for industrial irradiation, sterilisation, radiotherapy and biological research; well-designed irradiators are therefore widely distributed geographically. Several standard commercial irradiation cells are on the market and contract irradiation facilities are often available. It has been amply proven that ionisation due to gamma rays provides a useful simulation of the penetrating electrons and protons in the space radiation spectrum. For all practical purposes, a rad(Si) deposited by gamma-rays produces the same quantitative response in SiO_2 films with respect to charge-trapping and interface state creation as do space protons, electrons and bremsstrahlung.

Cobalt-60 is produced from inactive Co-59 by heavy neutron irradiation in a reactor. In a typical irradiator, a cylinder of cobalt-60 is sealed in a steel jacket and placed in a thick lead shield or concrete cell. A large number of electronic samples, arrayed in sockets in circuit boards, can be placed near the source and their response to the radiation can be monitored continuously by means of wires leading out of the cell. In some commercial irradiators, designed for the irradiation of chemicals or animals, the whole exposure takes place in an enclosed structure which can thus stand freely in the corner of the laboratory. Because gamma rays are so penetrating, circuit boards can be stacked. A source of medium strength will have an activity of about 1 000 curies (3.7×10^{13} becquerel).

Some typical configurations and dose rates are shown in Figures 19.1 and 19.2. Given a cell several metres in length, it can be seen that dose rates can be varied from over 10^5 rads.hr^{-1} (allowing the accumulation of mission doses in under an hour) to, say, 100 rad.hr^{-1}. The latter rate is only about 30 times a typical space dose rate (a high-radiation orbit may average 2×10^5 rad per 10 years or about 3.rad hr^{-1}) and, if real-time conditions are desired, shielding by a few centimetres of lead can produce a further reduction. Alternatively, a source of lower activity can be used at a closer distance. ESA has supported the development of one such low-rate irradiation facility - named LORAD - at Harwell, U.K. (see Hardman et al, 1985).

The medium-strength sources described above will cost about 20000 U.S. Dollars for the free-standing cell structure with automatic positioning of the isotope for timed exposures. The purchaser then has freedom to instal the optimum amount of isotope at a price of a few U.S. Dollars per curie.

Another isotope source which has been adopted widely as a practical irradiator is caesium-137. This emits 0.6 MeV gamma rays and has a half life of about 30 years.

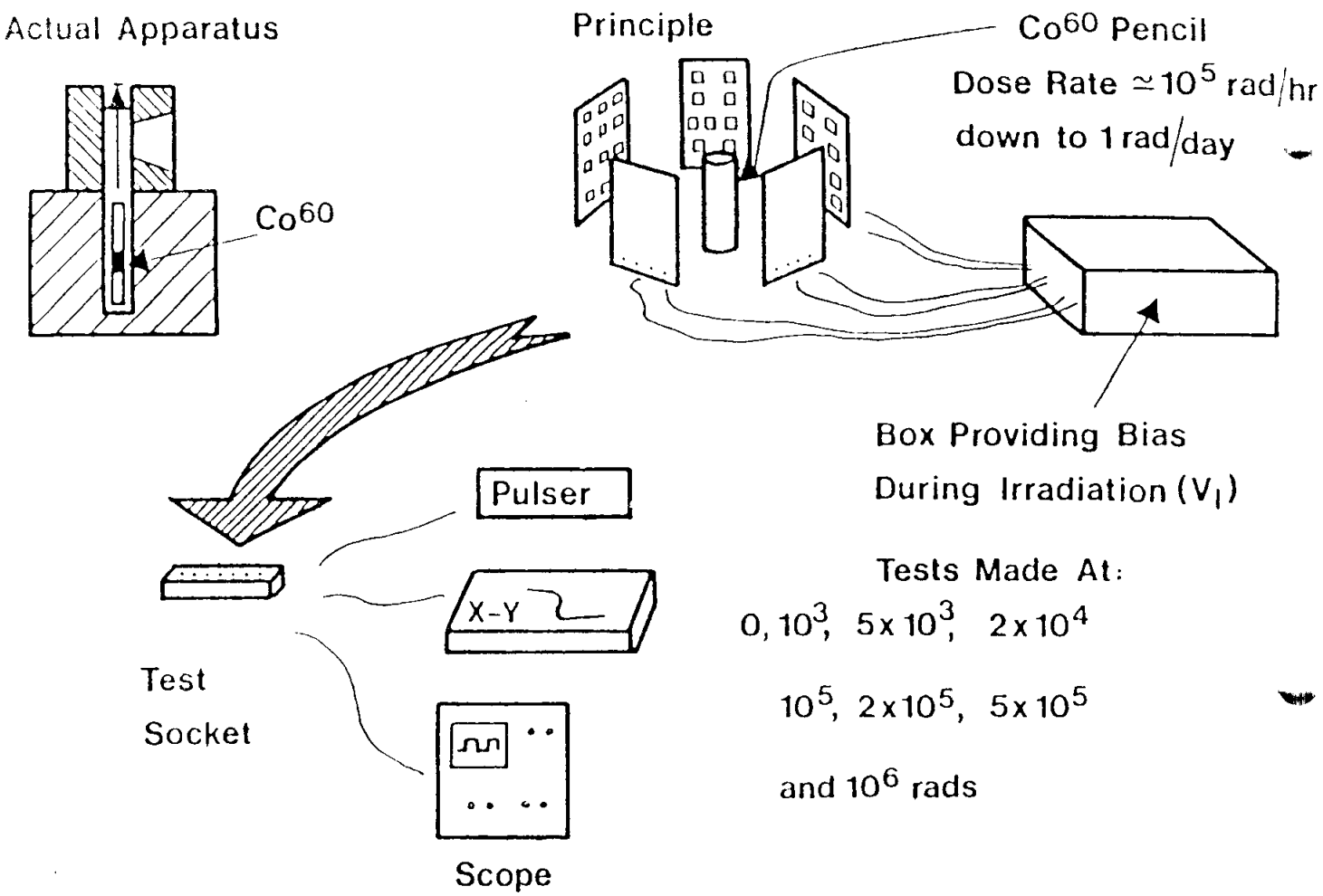

Typical arrangement for testing with Co-60 gamma rays.

FIGURE 19.1 - GAMMA-RAY TESTING

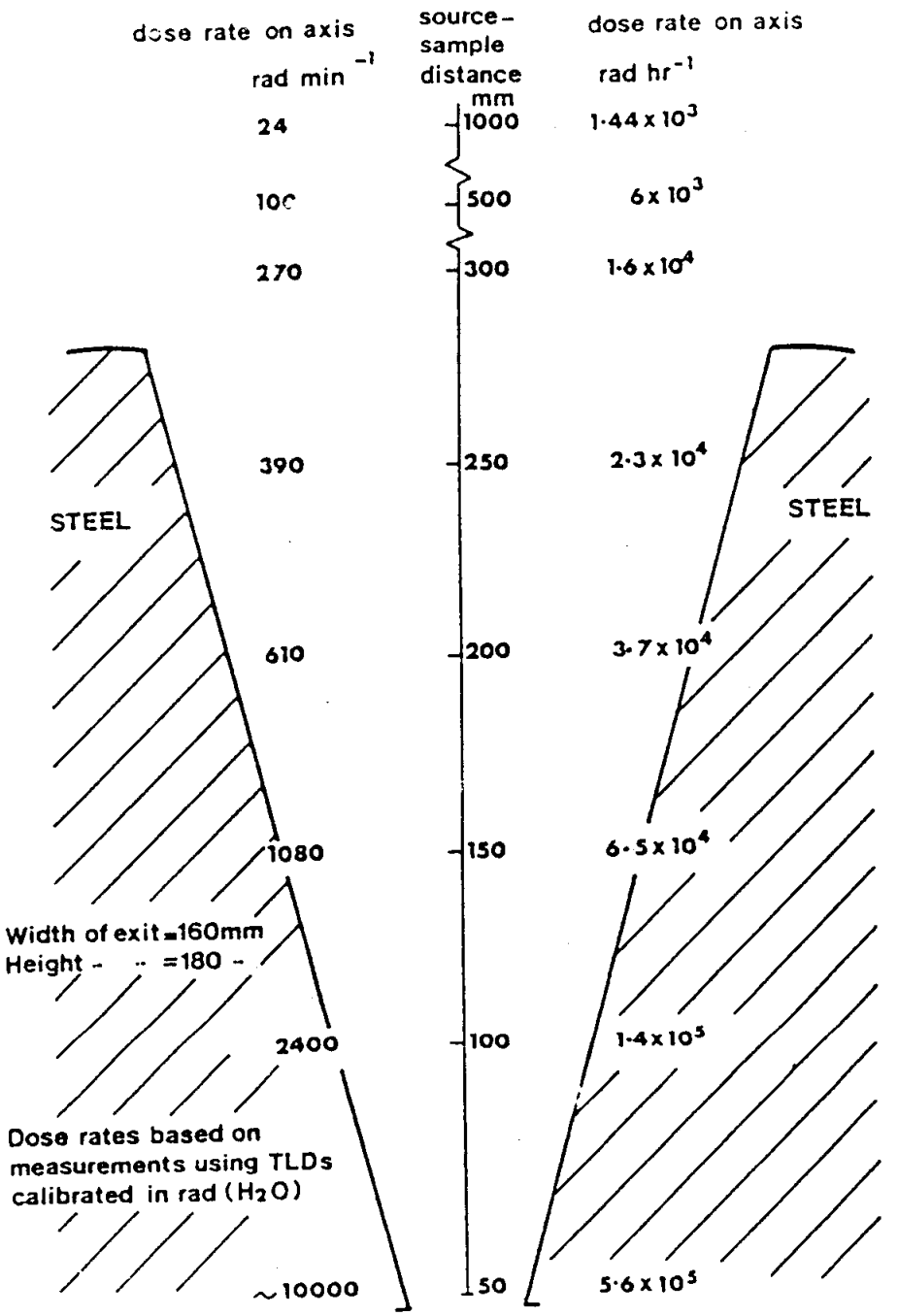

Cross-section of steel jaws of Co-60 Cave, with dose rates corresponding to position on axis. Doses are in rad (water). Activity approx. 1000 curies

FIGURE 19.2 - GAMMA-RAY TESTING

19.2.3. X-rays

Like gamma-rays, X-rays will simulate the space environment by inducing ionisation. Even low-energy X-rays, provided they can be introduced into the active region of the device and the doses correctly estimated, can be effective. They were first used on oxide-passivated devices by the staff of Bendix and RCA. The tube voltages were 150 and 250 keV respectively. The response of devices was found to be identical to that given by 1 MeV and 125 keV electrons as long as the base widths of the transistors were low enough to prevent interference from bulk damage. The same conclusion was reached with respect to an 85 keV radiographic X-ray set (23) over a wide range of bipolar and CMOS devices. ESTEC has routinely measured device responses in a 150 kV radiographic set (Adams et al). Careful dosimetry of a 320 kV X-ray set has been performed, using actual CMOS circuits as a cross-reference (Kelliher et al, 1985).

X-rays are generated when a beam of electrons bombards a target, usually of a high-Z metal such as tungsten or copper. For high beam currents, the target must be cooled; the power supply is large in size if high beam currents are desired. The electron beam, colliding with the target, excites a "white spectrum" of bremsstrahlung X-rays (actually peaked broadly at about half the beam energy), upon which the K and L peak emissions of the target metal are superimposed. For tungsten, the main peak is 59.3 keV (K_α) and for copper 8.04 keV (K_α). The L_α peak for tungsten is 8.396 keV. It is normally desirable to filter out these and also the lower-energy white radiation so as to avoid too much influence of the encapsulation on the dose penetrating to the active silicon device. However, one specialised wafer irradiator uses unfiltered tungsten radiation (Fleetwood et al, 1985). Dose rates at 10 mA in the 150 kV ESTEC source (tungsten X-rays) are approximately 10^3 rad.min^{-1} at a distance of 330 mm and about 10^2 rad.min^{-1} at 860 mm. The attenuation of this beam by a 0.3 mm Kovar lid is about threefold.

The use of X-rays requires care, but can be recommended for identification of sensitive technologies and the irradiation of limited numbers of devices. The main advantages are the low cost and wide distribution of X-ray equipment and the high safety standards available in X-ray equipment. The care required concerns the accurate administration of dose. In order to produce repeatable penetration power in an X-ray beam, the power-supply voltage and tube current must be stable. The ESTEC facility has line-voltage compensation of ~40V. The degree of filtration must be kept constant because this controls the X-ray photon energy spectrum. Both the degree of package penetration and the response of dosimetry are very sensitive to changes in energy spectrum.

Unlike gamma isotope facilities, X-irradiation methods have not yet been standardised. In view of the limited cone angle and relatively high absorption coefficient of kilovolt X-rays, isotope sources are preferred for bulky equipment, large part throughput and high-accuracy experiments.

TABLE 19(1) - TYPICAL FACTORS FOR CONVERTING ELECTRON FLUX TO DOSE

CGS units	Beam diameter 1.13 cm Area 1 cm^2	Beam diameter 2 cm Area 3.14 cm^2	Beam current
Flux ($cm^{-2}s^{-1}$)	6.2×10^{10}	1.97×10^{10}	10 nA
Dose rate (rad(Si) s^{-1})	2.07×10^{3}	6.57×10^{2}	
Flux ($cm^{-2}s^{-1}$)	6.2×10^{13}	1.97×10^{13}	10 A
Dose rate (rad(Si) s^{-1})	2.07×10^{6}	6.57×10^{5}	
MKS units	Beam diameter 0.013 m Area $10^{-4}m^2$	Beam diameter 0.02 m Area $3.14 \times 10^{-4}m^2$	Beam current
Flux ($cm^{-2}s^{-1}$)	6.2×10^{14}	1.97×10^{14}	10 nA
Dose rate (gray(Si) s^{-1})	20.7	6.57	
Flux ($cm^{-2}s^{-1}$)	6.2×10^{17}	1.97×10^{17}	10 A
Dose rate (gray(Si) s^{-1})	2.07×10^{4}	6.57×10^{3}	

For 1 MeV electrons incident normally, and with no cover on device (3×10^7 cm^2 = 1 rad(Si))

19.2.4. Electrons

All electron beams act as a source of ionisation, but only the high-energy machines (particles of energy considerably greater than 0.1 MeV) will produce displacement damage in semiconductors.

Consequently, one of the most generally useful sources is the Van de Graaff generator, especially because this machine can be designed to operate at any particle energy between 0.1 and 5 MeV.

An electron beam is accelerated by the field between earth (the target) and an electrode charged to a very high static potential. The charging is accomplished by means of a moving belt which carries charge from a d.c. generator to the insulated "head" electrode. Potentials of 5 million volts can be produced, but with the more common machines, 1 million volts is the limit. Electrons released in the head are accelerated away from it down an evacuated column and emerge through a titanium vacuum window as a beam of about 2 cm diameter. Devices can be placed in this beam. At 1 MeV, the electrons can travel several centimetres in air without great loss in energy, so that irradiation can be performed in air. Typical device encapsulation (e.g. 0.3 mm Kovar IC lids) extracts energy and scatters 1 MeV electrons heavily. Consequently, there is always uncertainty about the dose received at the chip of an encapsulated device. Some engineers object to removing the encapsulation for the purposes of testing. The dose rate can be varied by altering beam current and beam focus or sweeping the beam. Beam current can often be varied from 10 nA to 10 μA which, in a 20 mm diameter beam, yields particle fluxes from about 2×10^{10} $cm^{-2} .s^{-1}$ to 2×10^{13} $cm^{-2} .s^{-1}$. These fluxes correspond to dose rates from about 600 to 600 000 $rad.s^{-1}$.

Table 19(1) gives the conversion factors. Since the dose rates in space are in the range 10^{-5} to 10^{-3} $rad.s^{-1}$, the acceleration of test rate here is over 10^6 times. In many cases, this is acceptable, but it is inconvenient that, because beam currents cannot be controlled below a few nanoamperes, the dose rate cannot be lowered further.

Resonant-transformer accelerators yield electron-beam currents up to 1 mA in the 1 to 3 MeV range. Since the peak annual fluences encountered in space with $E > 0.5$ MeV are 3×10^{14} cm^{-2}, it can be seen that test runs need only a few minutes for actual irradiation.

A linear accelerator (LINAC) provides electrons of higher energies, typically 4 to 40 MeV in rapid, square pulses. Electrons fired from an electron gun in a waveguide can pick up RF energy and be accelerated from a few keV to several MeV. Average currents are again the microampere range, but instantaneous dose rates can be as high as 10^{10} $rad.s^{-1}$.

A typical experimental arrangement such as would be used for any high-energy electron (or proton) beam exposure is shown in Figure 19.3. It was developed at RCA for solar cells; using a 1 MeV Van de Graaff generator, it gives very high dose uniformity. Scanning of an array of samples can be achieved magnetically, thus avoiding movement of the samples, and it has been shown that doses can

be administered in this way with suitable accuracy. However, owing to the pulsed nature of the irradiation, other workers prefer to use a scattering foil to spread the beam.

In view of the price of an electron accelerator in the 0.5 to 3 MeV range (between 100 000 and 300 000 U.S. Dollars), the need to maintain a vacuum system, a large power supply and control circuits and the cost involved in servicing the pressurised insulated column, it would be impracticable to dedicate such a machine to space radiation testing use.

Another source of electrons of interest for special experiments on low dose rates is the isotope Sr-90/Y-90. It emits beta rays over a spectrum not dissimilar to that encounted in near-Earth space. Rates can be achieved such that a typical 1-year dose can be accumulated in several months, i.e. the acceleration factor is less than 10. Such a source is used at DERTS, Toulouse (F), for low-dose rate experiments on MOS devices.

Unfocussed beams of electrons in the kV range are easy to form with a kV power supply and a simple electron gun (television tube or "home-made" gun). Such beams can be used to irradiate thin films and beam currents of milliamperes can be obtained. One type of kV beam, which is of lower current but of much higher precision, is that used in the Scanning Electron Microscope (SEM) (see Galloway). Typical energy is 35 keV and the beam can be precisely aimed and scanned over a selected microscopic area of a semiconductor device (uncapped, of course). Currents are usually in the nanoampere range, but the irradiated area can be as small as a tenth of a micrometre square. Thus, the local dose can be made very high (many megarads per second). If the beam is rastered over the whole of the chip, dose rates as low as a few kilorads per second may be achieved.

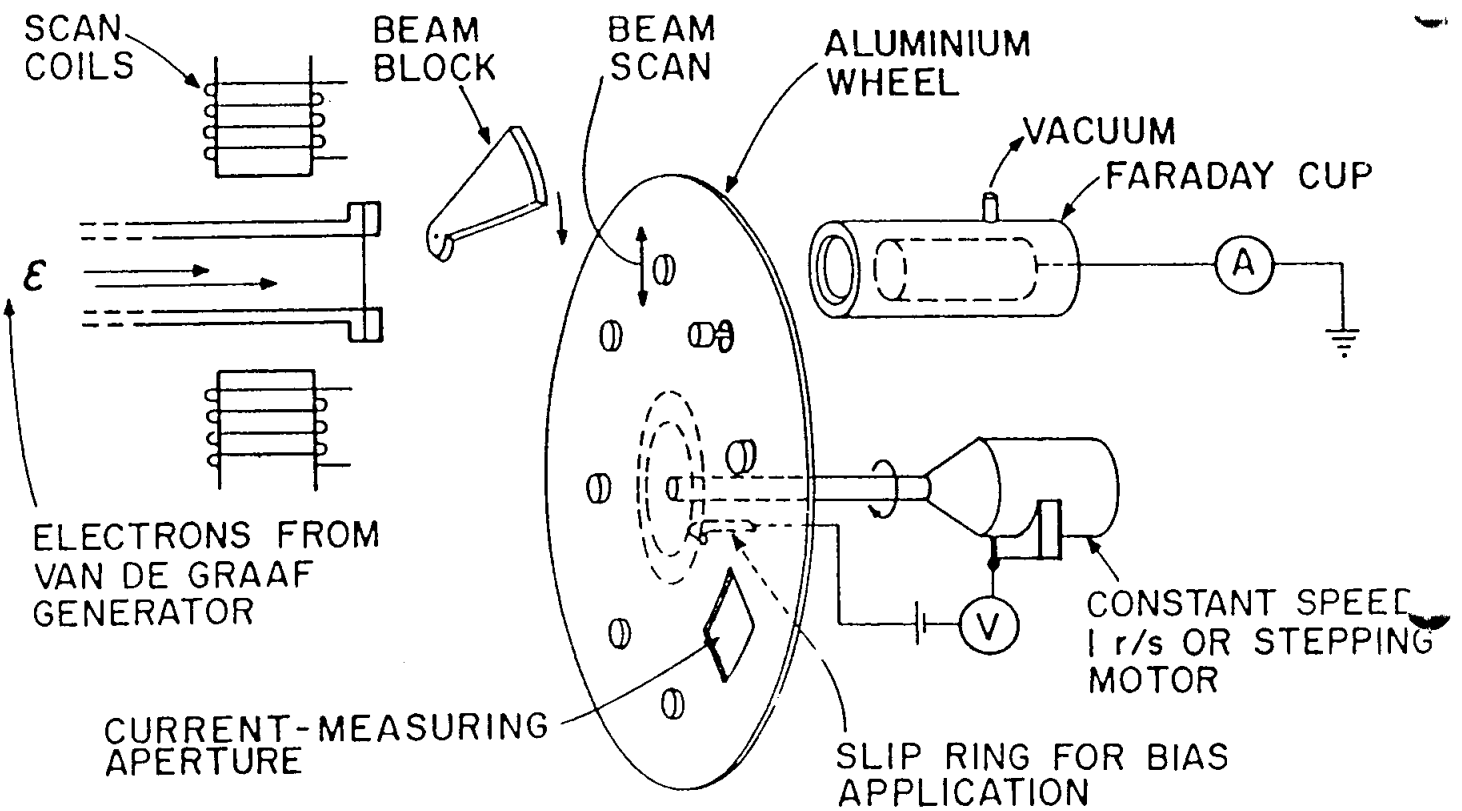

Typical arrangement for 1 MeV electron radiation testing

FIGURE 19.3 - ELECTRON BEAM TESTING

The SEM method is worthy of consideration because the beam is already used in the imaging mode for quality control inspection of semiconductor chips at low dose levels. The opportunity of adding a "sacrificial" high-dose irradiation on a selected area of the chip is therefore an economical complement to the usual inspection. The problem is dosimetry because the precise thickness of the "passivation" on wafers is not always known.

19.2.5. Protons

This section deals mainly with the displacement damage induced by protons in encapsulated silicon components. Only proton energies above 15 MeV, for which the range is 0.060" or 1.524 mm Al, need concern us. For surface coatings, energies down to 1 keV are vital and special facilities are available at ESTEC for their exposure . Recent work of imaging CCD's has shown that these are sensitive to low energy proton displacement damage requiring irradiation facilities between 0.5 MeV and 200 MeV.

For acceleration of protons to energies above 15 MeV, the most common machine is the cyclotron. In this instrument, high-frequency currents applied to two D-shaped electromagnets, supply energy to a beam of hydrogen ions injected into a circular "race track". The trajectory of the particles is an outward spiral and particles can be picked off at an exit tube. A typical maximum energy for a nuclear research cyclotron would be 20 MeV and fluxes of the order of 10^{13} cm^{-2} .hr^{-1} are achieved. As the damage efficiency of protons in silicon falls off sharply with energy, 20 MeV is very suitable for devices. The spectrum in space penetrating a compartment will be richest in this energy range, lower energies being attenuated greatly by the intervening absorber.

Useful work has been done with protons at 10 MeV (Boeing), 100 MeV (McGill University), 16.8 MeV (Princeton University) and at 22 and 40 MeV (NASA Langley). In Europe, some work has been done in the 7 to 50 and 200 to 3000 MeV ranges. Experiments on solar cells and bulk silicon have been used to construct the "BGR" curves mentioned earlier.

Since the annual proton fluences (E > 15 MeV) for the reference missions discussed previously are, at most, 10^{11} cm^{-2} (EXOSAT received 1.11 x 10^{10} cm^{-2} in 2 years), the fluences required for testing can be built up on a cyclotron in a fraction of an hour. Even at the peak of the proton belt, annual fluences (E > 10 MeV) are about 10^{13} cm^{-2}.

Most Van de Graaff machines can be converted for accelerating protons by reversing polarity and supplying a source of ionised hydrogen at the head. On some modern machines in the 0.5 to 3 MeV range, this conversion is effected with ease.

Other sources of high-energy protons occasionally available for irradiation are proton linear accelerators operating in the 10 to 100 MeV range and cyclotrons operating up to 800 MeV.

Very recently proton nuclear interactions have become important for single event upset and latchup in complex devices. Some modern integrated-circuit technologies are sensitive to the ionisation from nuclear reaction products. Significant risk exists for low Earth-orbiting satellites passing through the South Atlantic Anomaly (see Section 3). In order to study these, and other, proton effects ESA has sponsored the development of a Space Proton Irradiation Facility at the Paul Scherrer Institute, Villigen, Switzerland. This facility can be used to simulate continuous spectra (e.g. South Atlantic anomaly or Solar Flare) from 10 to 300 MeV. This is achieved by moving degraders in and out of the beam under computer control. An X-Y scanning system, also computer controlled, allows irradiation of an area 10 x 10 cm with high uniformity. Mono-energetic irradiations may also be carried out up to 590 MeV.

19.2.6. Neutrons

Although neutrons are not found in significant numbers in space, their bulk defect structures have a family resemblance to those produced by higher-energy protons and electrons. Also, a very large amount of nuclear-reactor testing has been performed in military programmes. Materials test reactors, which possess beam tubes or hydraulic tubes ("rabbits") or have a swimming-pool design, can be used for the exposure of samples to fast neutrons.

Neutrons are generated by the fission of uranium-235 and have energies spread over the range 0.1 to 3 MeV ("fission spectrum"). However, if the flux of neutrons is allowed to collide with the moderator material or coolant, the neutron energies are reduced to thermal energy of the order of 0.025 eV). This is undesirable for device irradiation because neutrons of energy below 10 keV yield few displacements. Moreover, they can be captured by the device materials, particularly gold and silicon, and produce radioactivity (the devices emerge "hot") and an inappropriate type of damage. Omnidirectional fast-neutron fluxes in reactor cores are usually well above 10^{15} cm^{-2} $.hr^{-1}$. They are accompanied by isotope gamma ray doses of the order of 10^{6} $rad.hr^{-1}$, which complicates the interpretation of responses.

Beams of 14 MeV neutrons from the fusion of deuterium and tritium ions, colliding at a few keV, can be produced in either electrostatic machines, which accelerate deuteron beams at 200 keV, or in various experimental plasma generators.

19.2.7. UV photon beams and other advanced oxide injection methods

Vacuum Ultraviolet (VUV) light gives, qualitatively, exactly the same type of charge build-up as high-energy radiation. However, the method at present is a research technique suitable mainly for characterising oxide film technology at the wafer stage. The same comments apply to avalanche injection techniques in which a controlled avalanche breakdown in the semiconductor injects hot electrons or holes into the oxide film. The difficulty is in control, dosimetry and interpretation. A third advanced method, not so well characterised, is the application of corona discharge to a bare oxide.

19.3. COSMIC RAY UPSET SIMULATION - HEAVY IONS

Single-Event Upset (SEU) simulation requires a source of energetic heavy ions with Linear Energy Transfer (LET) values ranging from about 1 MeV/mg/cm^2 to about 45 MeV/mg/cm^2. While the lower LET values are used to investigate the behaviour of a device around threshold LET, the higher values are used to establish the limiting cross-section or saturated error rate (see later). Table 19(2) gives a range of commonly used ions and their LET in silicon.

The machine used most frequently for SEU testing is the cyclotron, at accelerating potentials of up to 300 MeV, and with a range of gaseous ion sources such as krypton, argon, oxygen and neon. The device to be tested is mounted in an evacuated target chamber which contains silicon detectors and a Faraday cup for beam-monitoring and has feed-throughs for electrical connection. In general, provision is made for the device to be tilted with respect to the beam so as to allow the path-length of the ion through the device to be varied.

Cyclotrons for SEU testing include the 88-inch machine of the University of California at Berkeley (used by JPL and Aerospace groups) and the "ALICE" at IPN, Orsay (used by CNES, ESA and Harwell groups).

Although somewhat limited with respect to the maximum LET achievable, the Tandem Electrostatic Generator is also a suitable source of heavy ions. This generator is a special form of the Van de Graaff design. The accelerating electrode within the Tandem is half-way down the column and charged to a positive potential.

TABLE 19(2) - LINEAR ENERGY TRANSFER OF IONS COMMMONLY USED FOR SINGLE-EVENT-UPSET TESTING

NUCLIDE	ENERGY (MeV)	ENERGY/ NUCLEON (MeV/μm)	LET (SI) (MeV/mg/cm^2)
7 Li	15	2.10	0.6
12 C	35	2.92	1.0
20 Ne	150	7.50	2.9
16 O	21	1.31	4.0
20 Ne	46	2.30	6.4
40 Ar	300	7.50	7.5
40 Ar	150	3.75	11.0
35 Cl	35	1.00	15.0
56 Fe	400	7.14	18.0
56 Fe	300	5.36	20.0
56 Fe	150	2.68	23.0
84 Kr	60	0.71	27.0
84 Kr	150	1.79	35.0
129 Xe	81	0.63	40.0
241 A (alpha source)		-	0.6
252 Cf (fission frag ment source)		-	43.0

The ion source produces negative ions which are attracted by and accelerated towards the electrode. On nearing the electrode, they are stripped of their charge by foils to a positive charge stage and accelerated away from it towards the mass analyser and the target beam line. The Tandem produces two stages of acceleration and because the positive charge state can be quite high (e.g. Oxygen: +5), the overall acceleration energy may be several times the terminal voltage of the machine. The Tandem Generator at AERE, Harwell, has an LET range of about 0.5 to 37 MeV/mg/cm^2 and has been used successfully by the ESA/Harwell group for its investigation into threshold response.

A development in SEU testing by AERE and ESA is the use of fission products from a small radioactive source (1 microcurie of californium 252) for the production of upsets. The mean LET of the fission products is 43 MeV/mg/cm^2 which, in general, is sufficiently high to enable the limiting cross-section to be established. The LET can be degraded by the use of foils or atmospheric gases, but only to about 15 to 20 MeV/mg/cm^2; this is not low enough to permit the threshold of most of the modern technologies to be determined. The range of the fission particles is 15 μm in silicon and this should be taken into account, particularly for latchup testing.

The main advantages of the "CASE" system (Californium Assessment of Single-Event Effects) are its low cost, simplicity and flexibility. The entire test facility is contained within a simple bell jar and, provided the normal precautions for the handling of radioactive sources are taken, may be used in any laboratory. The system may be interfaced with any test equipment and used for extended periods to accumulate good SEU statistics. Figures 19.4 and 19.5 show schematics of cyclotron/Tandem and "CASE" test configurations and Table 19(3) gives the nuclear characteristics of the Californium 252 source.

TABLE 19(3) - NUCLEAR CHARACTERISTICS OF A CALIFORNIUM 252 SOURCE

Californium 252	: 1 microcurie source
Half-life	: 2.65 years
Neutron emission	: 4×10^3 n/s (average energy 2 MeV)
Neutron dose rate	: 0.023 mrem/hr at 1 m
Alpha particle emission	: 3.1×10^4 particles/s
Energy range	: 5.975 - 6.119 Mev
Fission fragment emission	: 10^3 particles/s (energy distribution peaks at 80 and 104 MeV)
Gamma exposure rate	: 0.002 mR/hr at 1 m

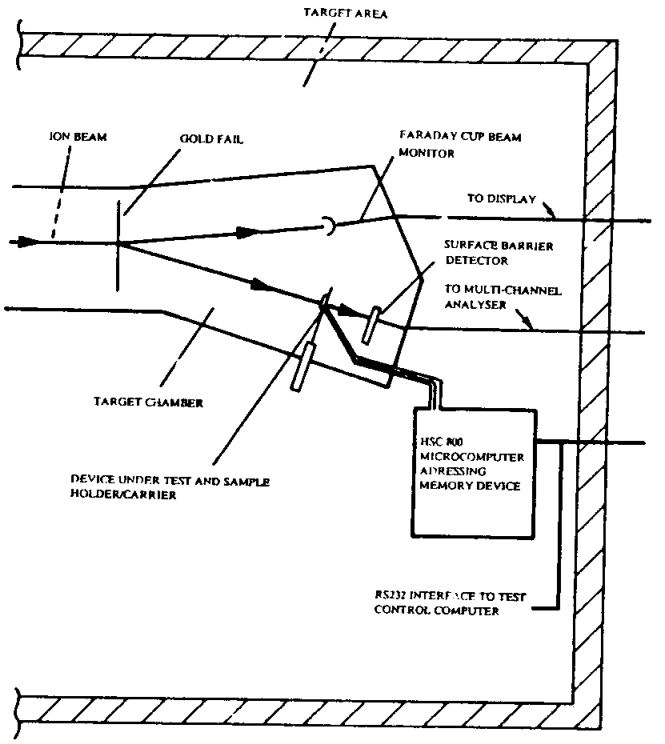

FIGURE 19.4 - CYCLOTRON ACCELERATOR TEST CONFIGURATION

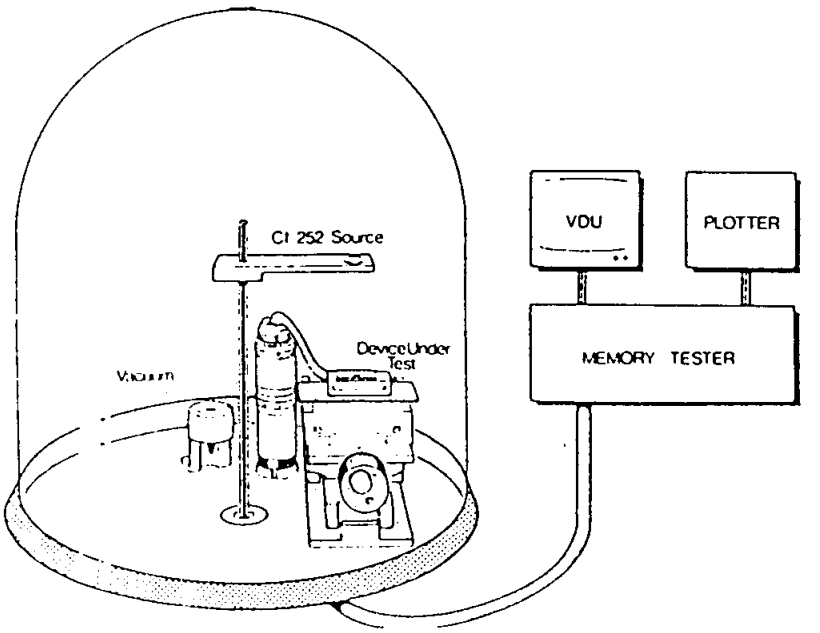

FIGURE 19.5 - "CASE" TEST CONFIGURATION

19.4. SUMMARY OF RADIATION SOURCES

In summary, the desirable features of radiation test sources for semiconductor devices are:

- Easy access (for "in situ" access and rapid sample change),
- Large area of beam (for large sample throughput),
- Highly penetrating radiation (avoids encapsulation problem)
- Unambiguous dosimetry,
- High stability (reduces dosimetry),
- Safety in operation,
- Low capital cost,
- Repeatability of doses from one facility to another,
- Flexibility in dose rate.

As isotope sources rate highly in all of the above criteria and cover a very wide range of the space radiation tests required for electronic and optical devices, their universal acceptance as standard radiation sources for total-dose ionisation effects is envisaged. In a number of cases, bulk displacement damage may be important (e.g. solar cells, thyristors) and here particle irradiation is essential. Single event upsets constitute another special group which requires particles to have the correct LET value and adequate range.

19.5. DOSIMETRY

19.5.1. General

Dosimetry is the process of measuring the amount of radiation to which a sample is exposed in a given radiation beam. It is also taken here to cover the measurement of particle or photon fluxes and of the absorption or deposition of energy in the radiation-sensitive sample of interest, usually silicon or silicon dioxide, but possibly plastic or optical material. Dosimetry grew up in the fields of radiobiology and medicine, where only energy deposition in the form of ionisation is of interest and takes place primarily in the aqueous or organic media of living tissue.

Thus, dosimetry methods and concepts have been developed mainly for the calculation of ionisation in carbon (organic materials), water and air (the medium used in ionisation gauges). We, on the other hand, are involved in the field of semiconductor components and are interested mainly in the deposition of ionisation energy in silicon oxide and silicon as well as the deposition of energy in the form of atomic displacements in lattices. Thus, space radiation covers certain fields not found in the dosimetry textbooks.

19.5.2. Definition and use of radiation units

Until recently, the gas ionisation chamber was the only means to measure electrically the dose derived from a radiation beam. This chamber is merely a pair of electrodes arranged to collect the air ions created in a certain volume, but the values thus measured still serve as a standard to which to relate other units and form the basis on which the Roentgen unit has been defined. The latter is that unit of exposure to radiation which creates air ions to the level of 2.58 x 10^{-4} coulombs per kg (previously defined as 1 esu.cm^{-3} in air of density 0.001293 at STP). This corresponds to the deposition of energy in air at the rate of 87 erg per gram.

The rad and gray (Gy) are units of energy deposition; a rad (100 grays) has been absorbed by the sample of interest when 100 erg per gram (1 joule per kg) has been deposited. One rad thus equals 10^{-2} Gy or 1 centigray (cGy). We can calculate the dose in any material from the exposure in roentgens if we know the relative absorption coefficients for the radiation in air and the material in question.

For 1 MeV photons, the factor for converting roentgens to rads in water is 0.965 rads.roentgen^{-1}, i.e. the flux of 1 MeV photons which yields 0.87 rads in air, yields 0.965 rads in water. Some other useful figures on relative photon energy absorption coefficients ((water)/ (material)) are given in Table 19(4).

The figures for glass and Al are very similar at 1 MeV (from which one may reasonably assume that the figures for SiO_2 and Si would be only marginally different, say 1.12 and 1.15 respectively). These figures are useful for calculating relative doses for radiation testing and in-orbit bremsstrahlung. Similar figures can be derived for electrons. The large differences at 100 keV are discussed later.

Even though the gray is the SI unit, the rad is used in this report because this is still the working unit for most published papers on radiation effects and also for current medical practice. Some workers continue to work in "rads", but write "cGy" instead.

TABLE 19(4) - RELATIVE PHOTON ENERGY ABSORPTION COEFFICIENTS ((WATER)/ (MATERIAL)) FOR VARIOUS MATERIALS

	1 MeV	100 keV
H	0.557	0.631
C	1.11	1.19
O	1.11	1.08
Al	1.15	0.663
Fe	1.18	0.117
Cu	1.20	0.0848
Pb	0.82	0.0112
Perspex (PMMA)	1.03	1.08
Polyethylene	0.970	1.05
LiF	1.20	1.14
Glass	1.12	0.788

Measurements of X-rays, gamma rays and electrons with the standard Farmer Dosimeter, which uses air, are performed in a surrounding of material of atomic weight precisely equivalent to water (water-equivalent phantom) under such conditions that the secondary-electron equilibrium setup is that which would be present in water. Doses measured in this way are expressed in rads (H_2O), i.e. rads calculated for water, derived from Farmer air ionisation current measurements. Other secondary dosimeters such as lithium fluoride dosimeters, exposed at the same time, can also be calibrated to read in the same units. In publications on semiconductor radiation effects, the dose scale is commonly given in rad(Si).

19.5.3. Dosimetry used in space simulation testing

19.5.3.1. Farmer air dosimeter

This is a small ionisation chamber dosimeter having thin graphite walls and containing dry air. When placed within a water phantom, it will read effectively the exposure expected in water itself.

19.5.3.2. Thermoluminescent dosimeter

Hot-pressed polycrystalline lithium fluoride chips or powder will absorb a proportion of radiation energy in the form of electrons which remain held in stable traps in the LiF lattice for a very long time at room temperature. On heating to about 150°C, the electron energy is released as light. This thermoluminescence is measured by a cooled photomultiplier and the signal emitted over a given swept temperature range is integrated. The integrated charge from

the tube is roughly in linear proportion to the radiation exposure over several decades and thus, with calibration, the value of the charge indicates the dose received. The main advantages of thermoluminescent chips are:

(a) their small size in comparison with the smallest ionisation gauge and
(b) the fact that the dose information can be read later.

Calcium sulphate and $MgSiO_4$ have also been used.

19.5.3.3. Other conventional dosimeters

For doses in the kilorad-megarad range, several other secondary dosimetric media have been used effectively. Photoluminescent silver doped glass and dye-containing plastics have been widely used. Optical colorations in dyed paper, soda glass or alkali halide crystals are also useful for mapping and rough quantitative estimates of dose.

19.5.3.4. Silicon devices as dosimeters

In theory, the effect of radiation on the threshold voltage of a MOS device - given strong oxide fields - should be near-linear over several decades. Early work with discrete MOS transistors demonstrated linearity of ΔV_T versus dose and showed that a 2-wire connection to the MOS device was all that was necessary. More recently, an improved response has been obtained with specially processed MOS devices. A Radiation Measurement Unit designed around these devices by ESTEC staff has been operated on two ESA spacecraft. MOS devices built for dosimetry are called "Space-charge Dosimeters" or "RADFETS" (Holmes-Siedle and Adams, 1986).

Silicon photodiodes are becoming quite commonly used in medical dosimetry and solar cells have been used to measure dose rate.

19.5.3.5. Faraday Cup

For beams of charged particles, a block of metal of the appropriate thickness will stop all the particles and the flow of the resultant charge can, of course, be measured. This arrangement is known as a Faraday Cup and refined forms are used for controlling many electron and proton machines in conjunction with single-particle counters collecting scattered radiation. The main refinements are the evacuation of air around the cup electrode and shaping of the cup so that secondary electrons do not escape.

19.5.3.6. Energy-dependence of dosimetric materials

The problem of dosimetry for encapsulated silicon devices is a particularly complex one, especially when low-energy beams are being used. However, the problems are not insoluble as the energy-absorption physics is well understood and good local dose estimates can be made.

The main problems fall into two fields:

(a) Widely differing photon absorption coefficients for Si, Fe, LiF and H_2O in the otherwise useful low energy region of 30 to 300 keV;
(b) The lack of secondary-electron equilibrium in typical device packages under test.

Owing to the strong dependence of the photoelectric absorption effect upon photon energy and atomic weight (e.g. see Table 10(2) and Johns & Cunningham, 1971), small variations in photon beam energy and the composition of a sample can affect both the attenuation of radiation in the device package and the amount absorbed in the active region. These considerations apply particularly to kilovolt X-ray machines. For X-rays in the 30 to 300 keV range, the dosimeter method used must simulate closely the device packaging and structure while close control must be kept on the penetrating power of the beam.

The energy-dependence problem in LiF dosimetry is adequately explained by reference to the well-known case of "tissue versus bone"; these materials have energy responses not too different from LiF and Si respectively. Energy absorption coefficient changes vary rapidly with photon energy for silicon and bone, and much more slowly for LiF, water and tissue. Thus, a shift of a few percent in photon energy can produce a large disparity in energy absorption between the two groups of materials. This is why control of accelerating voltage is of a high standard in many X-ray sets and must be checked with care in radiation testing. The energy dependence effect is further complicated by an additional dependence of thermoluminescent output per unit dose in LiF, which varies by a factor of 1.27 between 300 and 50 keV.

It will be clear then that potential problems associated with the control and measurement of X-ray dose have received much attention in the field of medical radiology, and methods have been developed to deal with them. The equilibrium question will not be described in detail here. The Bragg-Gray cavity theory concerned is well described in dosimetry manuals. Briefly, at the discontinuity between two dissimilar materials under irradiation, the secondary-electron spectrum and flux characteristic of the first persists for some distance until a new equilibrium ("Compton equilibrium" in

the megavolt range) is established. Thus, for example, if a small sample such as a silicon chip is irradiated by Co-60 gamma rays in a steel can (gases being ignored), the silicon receives much of its dose from the Compton electrons generated in the steel.

19.6. TEST PROCEDURES

19.6.1. Introduction

Having described radiation test facilities, we must now discuss how they should be used for irradiating semiconductor devices. The design of a valid space radiation simulation test is not easy. As many ESA contractors may attempt radiation tests, it is important that guidelines for testing be agreed and promulgated, so that these tests are both valid and amenable to comparison. This section does not attempt to present finished guidelines, but discusses recent draft procedures and makes comments on them.

19.6.2. The objectives of procedures

The objectives of a radiation qualification and test procedure are:

(a) To ensure that the long-lived degradation produced by space radiation lies within an acceptable range and
(b) To produce data which will be of further aid to the electronics designer in estimating the degraded "end-of-life" characteristics of the piece part.

It should be noted that these data enable equipment designers to introduce radiation tolerance into their designs in two different ways, namely:

(i) By an "accept/reject" approach, where only the more tolerant devices are accepted for the equipment and
(ii) By a "predict and derate approach", where sensitive devices are accepted and the circuit design allows for quite strongly degraded performance at end-of-life.

The combination of a standard procedure and data processing method should be such that a test procedure and format are achieved which present the information to advantage and enhance design optimisation. An ideal format is the "growth curve" in which the change of a parameter is plotted versus dose (or time in flight at a given spacecraft location). On these curves may be noted the "Fixed Failure Criteria" and the "Stated Dose or Fluence Values" suggested by some authors. The information contained in the full growth curve is more useful than either of the pieces of information mentioned above.

19.6.3. Comparison with military requirements

It will be noted that not all of the above objectives coincide with those of the test for military environments. In the latter, a single total-dose level is often set (e.g. either the "Tactical Environment" with doses in the kilorad range or the "Strategic Environment" with doses in the megarad range). In this case, the doses are in reality received in a few short pulses, so that intermediate points on the growth curve are of no interest. As explained elsewhere, the space designer will be considering components which degrade gradually. Also, of course, the space radiation test can ignore the transient effects of pulsed doses and there is no associated neutron damage. On the other hand, the range of semiconductor components used in the two fields are virtually identical and there is also some overlap with respect to the effects which occur in the two cases. Table 19.5 shows some of the organisations interested in standardising the radiation testing of electronic components. The document numbers of proposed radiation test methods are shown.

19.6.4. SEU procedure

Although two draft documents are known to exist (D. Nichols et al, 1984; E. Petersen and E. Wolicki, 1983), there is no standard SEU testing procedure at the present time. A MIL test method may be expected in the near future. For the correct interpretation of results, the radiation effects community therefore relies, for the time being, on publication of experimental tests. For exposure conditions, the information required is: type of machine, ion species, energy, LET and flux. Details of beam diagnostic techniques should be provided and accuracies quoted.

The techniques employed for monitoring of the device under test are extremely important and should be fully described, software flow charts being used as appropriate. In the testing of complex devices, a number of software and hardware precautions need to be taken, including latchup detection and protection as well as watchdog timers (C. Sansoe and R. Harboe-Sorensen, 1985).

TABLE 19(5) - STANDARDS ORGANISATIONS CONCERNED WITH RADIATION TEST PROCEDURES

Name	Specification number
International	
– ICE	See DIN specifications
– CIFAS	
European	
– SCCG	22900
– EUROSPACE	E-6733
National	
– KMT	KMT 0001/4 and
– DIN	53750 and 53751
– BSI	BS 9000
– CERT	
U.S.	
– ASTM	D 1672, D 2953
– ANSI	–
– MIL	MIL-STD-883, Methods 1018 - 1022
– ANS	–

19.7. RADIATION RESPONSE SPECIFICATION

19.7.1. General

In the many cases where neither time nor funds are available for the radiation hardening of devices, some hardening of a piece of equipment may be achieved by a rigorous selection of commercially available components. Once a specific device type has been chosen, there is still the serious question of assuring that all units in the batches used perform acceptably under radiation. This field, called "Hardness Assurance", has received much attention in military and space work and is a mixture of well-established Product Assurance techniques and special radiation assessment (Wolicki et al, 1985).

19.7.2. Product assurance techniques and special radiation assessment

Institutes in the USA and Europe have developed national and international standards for the assessment of devices under radiation. In Europe, for example, the ESA Space Components Coordination Group (SCCG) has issued a specification. In the U.K., a method for qualifying a series of "Radiation-Assessed Devices", has been circulated by BSI. This was issued by the Ministry of Defence as a draft for the British Standard Institute's BS 9000 series of electronics assessment methods. In the USA, a similar scheme exists under the ASTM and MIL specification systems. Some references to documents are given in the following sections.

19.7.3. ESA/SCC specification (Europe)

The ESA Space Components Coordination Group has developed a draft specification of radiation test procedures (ESA/SCC Basic Specification No. 22900, Draft B, dated 1988). The purpose of this specification is to define the testing of semiconductor devices for the effects of total dose ionising radiation relevant to the space environment. Cobalt-60 gamma rays or electron accelerators may be used.

19.7.4. BS 9000 specification and CECC (Europe)

A draft specification entitled "Specification of Basic Requirements for the Assessment of Semiconductor Components for Tolerance to High- Energy Radiation" has been submitted for a place in the BS 9000 series (BS 900X, Draft J, Sept. 1988). This is a comprehensive specification of radiation test and device assessment procedures, marking methods for BS 9000 device packages, amendments to BS 9000 data sheets and manufacturers' quality assessment. The effects considered include those connected with pulsed radiation, total dose and neutrons. The devices produced to this specification are entitled to the name "Radiation Assessed Devices". Note that this does not imply "radiation-hardened".

19.7.5. MIL specifications (USA)

Radiation standards adopted by the U.S. Department of Defense include the following parts of the MIL-STD System.

- Method 1015 (MIL-STD-750): Steady state primary photocurrent irradiation procedure (electron beam),
- Method 1017 (MIL-STD-883B): Neutron irradiation,
- Method 1019 (MIL-STD-883B): Steady state total dose irradiation procedure,
- Method 1020 (MIL-STD-883B): Radiation-induced latchup test procedure,

- Method 1021 (MIL-STD-883B): Dose rate threshold for upset of digital microcircuits,
- Method 1022 (MIL-STD-883B): MOSFET threshold voltage,
- Method 1023 (MIL-STD-883B): Dose rate response of linear microcircuits.

19.7.6. ASTM specifications (USA)

Radiation Standards adopted by ASTM, a civil body, include the following:

- E 721-85: Standard method for determining neutron energy spectra with neutron-activation foils for radiation-hardness testing of electronics.
- E 820-81: Standard practice for determining absolute absorbed dose rates for electron beams.
- F 448-80: Method for measuring steady-state primary photocurrent.
- F 526-81: Methods for dose measurement for use in linear accelerator pulsed radiation effects tests.
- E 668-78: Standard practice for the application of TLD systems for determining absorbed dose in radiation hardness testing of electronic devices.
- E722-85: Characterising energy fluence aspects in terms of an equivalent mono-energetic fluence for radiation hardness testing of electronics.
- E1249-88: Practice for minimising dosimetry errors in radiation hardness testing of silicon devices using Co-60 sources.
- E763-85: Method for calculation of absorbed dose from neutron irradiation by application of threshold foil data.
- E1250-88: Methods for application of ionsation chambers to assess low energy gamma component of Co-60 irradiators used in radiation hardness testing of silicon electronic devices.
- F1192-90: Standard guide for the measurement of single event phenomena (SEP) induced by heavy ion irradiation of semiconductors.

19.8. DEVICE PARAMETER MEASUREMENTS

This section describes briefly the parameters which are often degraded in silicon devices used in data-handling and also notes some features of their behaviour under irradiation which may require special procedures during testing. Three different desirable sorts of testing are defined: d.c. and a.c. parametric testing and functional testing. The first group discussed here, the d.c. tests, may form a large proportion of those performed for radiation effects.

19.8.1. MOS threshold voltage

The MOS threshold voltage (V_T) has been defined in Section 4. Briefly, it is that voltage at which a certain, practically measurable,

channel current (commonly 10 μA) flows after turn-on by inversion. The inversion point in an n-channel device is about 3V more positive than the flatband voltage. Some special problems in V_T ("hysteresis", distortion annealing) are covered by the discussion of C-V plots. V_T may be measured during irradiation, but it must be noted that:

(a) this disturbs the desired stable oxide field condition and

(b) even at a dose rate of 1 $rad.s^{-1}$, photovoltaic effects may interfere.

19.8.2. MOS flatband voltage (V_{FB}) and C-V plot

In an MOS capacitor, threshold channel currents do not exist. However, the whole capacitance-voltage curve contains even more information on the state of the semiconductor and interface. The flatband condition (at which surface potential is zero; hence, no bending of the silicon conduction band) lies on the C-V curve at a point where C/C_O has a value commonly about 0.8, on the depletion side of the minimum of the plot. Unfortunately, the capacitance of an LSI transistor gate is usually so small that most C-V sensing circuits cannot measure it. Special field plates or specially large transistors have to be fabricated; these are not normally provided on commercial integrated circuit chips. Such plates are provided, however, on some Process Validation Modules. Irradiation-induced interface states produce distortions in the C-V curve from which quantitative information can be obtained. One special experimental difficulty caused by irradiation is the production of "hysteresis" in the C-V plot due to the generation of "slow" states.

19.8.3. Quiescent current (I_{SS}) in CMOS logic

The "VTNZ" effect in CMOS logic leads to a drastic increase in current in the power supply circuit. This is usually measured in the V_{SS} circuit or earth leg of the devices concerned, using a nanoammeter. In LSI circuits, where V_T cannot be measured, the measurement of I_{SS} may be the only method available for detecting the onset of the VTNZ effect.

19.8.4. Leakage currents

The reverse leakage of p-n junctions is usually greatly increased by irradiation, especially when the junction is under bias; the field encourages charge build-up on the surface. Current may rise from picoamperes to milliamperes, thus upsetting the impedance matching of the test circuit. These currents will be temperature-sensitive, thus standard temperatures are important. Meters with a wide dynamic range should be used. Dose rates down to 1 $rad.s^{-1}$

can give detectable photocurrents; measurements during irradiation therefore require care.

19.8.5. Current gain

The conventional instrument used for measurement of the current gain of polar transistors is the oscilloscope curve tracer. This displays base current and collector current at several different values and the gain (i.e. the ratio) can be calculated. However, current steps are usually over less than a decade while, as indicated earlier, it is vital to measure radiation-induced degradation of gain over about four decades of collector current.

This illustrates two special features of radiation testing:

(a) Measurements of parameters at values far outside those to be used in flight may provide important diagnostic information on which the expert can base a more confident prediction of degradation in flight.
(b) The routine test instruments may not provide the best form of display or readings for our purpose. For example, the usual set of photographs from the curve tracer is a wholly inappropriate form; much more suitable would be a computer plot of the change in base current I_B versus dose, given for a range of values of I_C or I_E, spread over four orders of magnitude, followed by measurements gained by periodic tracking of the same parameters over several days after irradiation. The complete plotting format as derived by Brown and Horne (1967) is a suitable model to follow.

As explained elsewhere, the surface effect on gain behaves similarly to MOS effects, e.g. it can anneal slowly at room temperature and can often be reduced by heating.

19.8.6. Input offset in analogue ICs

In integrated analogue circuits, only the input and output points are accessible for measurement. The input offset voltage and current are two important parameters in operational amplifiers which degrade very seriously under ionising radiation.

19.8.7. Noise immunity and d.c. switching of logic gates

The switching characteristics of a bipolar or MOS logic gate can be plotted by stepping the input voltage and plotting the output currents or voltages. It is then simple to determine from these curves the loss in noise immunity.

19.9. AC AND FUNCTIONAL TESTING

With large-scale integrated circuits, such as memories and microprocessors, it is essential to test the circuits at the required switching rates and over the full voltage range because, when a number of integrated circuits operate together, the first functional degradation may be the inability of some section to transmit signals rapidly enough.

The same argument, of course, applies to high-frequency communications circuits, where devices may be working near their frequency cut-off or where the tuning of circuits may drift.

19.10. QUALIFICATION OF ENGINEERING MATERIALS

The procedure for testing and qualifying materials other than semiconductors will, in general, be simpler. The demands made on engineering materials are usually less severe, although thermal control and optical materials also require careful testing. ESA has a standard procedure for qualifying materials (J. Dauphin, 1980), but this only requires testing in special cases. Three qualification levels, A, B and C are set, depending on the severity of the intended use of the material. Three forms of sunlight environment are distinguished as shown in columns 1 and 2 (column 3 is our comment) of Table 19(6), and these can apply to qualification level A, B or C. No codes are given for the severity of the ionising radiation environment.

TABLE 19(6) - SUNLIGHT ENVIRONMENT CODES FOR ESA MATERIALS QUALIFICATION

Environment code	Code	Main contribution to damage
R	Outside in sunlight	UV, VUV and kilovolt particles
R	Outside in shadow	Kilovolt particles
R	Inside spacecraft	Mainly megavolt particles and brehmsstrahlung

Of course, packaged electronic devices and their circuit boards will always be "inside the spacecraft".

19.11. CONCLUSIONS

Radiation testing is not a simple art and should be approached by the use of exploratory experiments which will be useful in uncovering any pitfalls. Test design is best assigned to an expert

since test facilities are expensive, dosimetry is complex, unusual parasitics are often produced by radiation and statistics may be difficult. Extracting the correct prediction from a small sample of commercial devices requires considerable skill. This section has not attempted to describe a perfect set of facilities or a standard form of test. The problems mentioned prevent rigid standardisation at the moment. The descriptions given are intended to record the current state of the art, with some recommendations and warnings.

It is unfortunate that many of the tests performed never reach publication and are lost to general use. ESTEC is attempting to rectify this by placing some test reports in a data bank, using a standard format for reporting. Additionally, both DFVLR and CNES are building up compendia of test data.

REFERENCES

L. Adams, "Laboratory Simulation of the Space Radiation Environment for Electronic Components", Radiat.Phys.Chem.(15), pp. 525-535 (1979)

L. Adams and A.G. Holmes-Siedle, "Radiation Hardness Assurance of Space Electronics", Nuclear instruments and methods 314 (2), 355-344.

L. Adams and I. Thompson, "The Use of an Industrial X-ray Source for Electronic Components Radiation Effects Work", IEEE Trans.CHMT (3) 1, pp. 144-149 (March 1980)

J.M. Aitken and D.R. Young, IEEE Trans.Nucl.Sci. NS-24(6), pp. 2128-2135 (Dec. 1977)

D. Bielle-Daspet in J.E. Whitehouse (Ed) "Radiation Damage and Defects in Semi- conductors", IOP Conference Series No. 16, pp. 129-139, Institute of Physics (1973)

R.R. Brown, "Proton and Electron Permanent Damage in Silicon Semiconductor Devices", Boeing Report D2-90570 (1964)

R.R. Brown and W.E. Horne, "Space Radiation Equivalence for Effects on Transistors", NASA CR-814, U.S. Dept. of Commerce, Washington DC (July 1967)

G.J. Brucker, W.J. Dennehy and A.G. Holmes-Siedle, IEEE Trans.Nucl.Sci. NS-12(5), pp. 69-71 (Oct. 1965)

G.J. Brucker, E.G. Stassinopoulos, O. van Gunten, L.S. August and T.M. Jordan, "The Damage Equivalence of Electrons, Proton and Gamma Rays in MOS Devices", IEEE Trans.Nucl.Sci. NS-29(6), pp. 1966-1969 (1982)

G.J. Brucker, E.G. Stassinopoulos, P. Shapiro, L.S. August and T.M. Jordan, "Recovery of Damage in Rad-hard Devices During and After Irradiation by Electrons, Protons, Alphas and Gamma Rays", IEEE Trans.Nucl.Sci. NS-30(6), pp. 4157-4161 (1983)

G.J. Brucker, W.J. Dennehy and A.G. Holmes-Siedle, Proc. IEEE (Corresp.) 53, p. 1800 (Nov. 1965)

J.R. Cameron, N. Suntheralingam and J.N. Kenney, "Thermoluminescence Dosimetry", Madison, Univ. of Wisconsin Press (1968)

Product Assurance Division, ESTEC, ESA PSS-01-706, Issue 1 (1983)

W. Dennehy, A.G. Holmes-Siedle, IEEE Trans.Nucl.Sci. NS-17(6), p. 33 (Dec. 1970)

DERTS, Toulouse, 'Evaluation de la dégradation des dispositifs MOS, CMOS et LDCMOS et des composants optoélectroniques sousmis à irradiation dans un environment spatial', ESA CR(X)-1516 (Sept. 1977)

C.G. Emms, A.G. Holmes-Siedle, I. Groombridge and J.R. Bosnell, IEEE Trans.Nucl.Sci. NS-21(6), p. 159 (Dec. 1974)

Product Assurance Division, ESTEC, 'The Listing and Approval Procedure for Materials and Processes', ESA PSS-01-716 (Issue 1) October 1982

EUROSPACE Draft Specification E 6733, Paris (Febr. 1977)

D.M. Fleetwood et al, "Accounting for Dose Enhancement Effects with CMOS Transistors", To be published, IEEE Trans.Nucl.Sci. NS32(6) (Dec. 1985)

K. Galloway, "Important Considerations for SEM Total Dose Testing", IEEE Trans.Nucl.Sci. NS-24(6), pp. 2066-2070 (Dec. 1977)

A.S. Grove, "Physics and Technology of Semiconductor Devices", New York, Wiley (1967)

C.L. Hanks and D.J. Hamman, "Radiation Effects Design Handbook", NASA CR-1787, Battelle Memorial Inst., Columbus, Ohio (1971)

M. Hardman, J. Farren, D. Mapper and J.H. Stephen, "Low Level Radiation Testing of Microelectronic Components", Part 1 (1984); Part 2 (1985), AERE, Harwell, England

N.W. Holm and R.J. Berry (Eds), "Manual on Radiation Dosimetry", New York, Dekker (1970)

A.G. Holmes-Siedle and I. Groombridge, Thin Solid Films, 27, pp. 165-170 (1975)

A.G. Holmes-Siedle and L. Adams, "RADFETS: A review of the Use of MOS Devices as Integrating Dosi meters", Radiation Physics & Chemistry, 28(2) (1986)

A.G. Holmes-Siedle and K.H. Zaininger, IEEE Trans. Reliability R-17(1), pp. 34-44 (Mrch 1968)

G.W. Hughes and R.J. Powell, IEEE Trans.Nucl.Sci. NS-23(6), pp. 1569-1572 (Dec. 1976)

H.L. Hughes, IEEE Trans.Nucl.Sci. NS-16(6), pp. 195-202 (Dec. 1969)

ICRU Report on Clinical Dosimetry No. 10d, ICRU Publications, Washington DC (1963)

H.E. Johns and J.R. Cunningham, "The Physics of Radiology", Thomas (1971)

K. Kelliher, "Calibration of an On-site keV X-ray Equipment as a Total-Dose Simulator", British Aerospace Internal Reports (1985)

N.C. McDonald and T.E. Everhart, J. Appl. Phys. 39, pp. 2433-2447 (1968)

W.L. McLaughlin, Radiation Phys.Chem. 9, pp. 147-181 (1977)

NASA CR-61267, "Investigation of Spacecraft Coatings", U.S. Dept. of Commerce, Washington DC (1969)

G.P. Nelson and E.E. King, IEEE Trans.Nucl.Sci. NS-24(6), pp. 2341-2347 (Dec. 1977)

D.K. Nichols et al, "A Guideline for Heavy Ion Radiation Testing for Single Event Upset" (SEU), JPL-D-1412 (Jan. 1984)

E. Petersen and E. Wolicki, "Draft Procedure for VHSIC Single Event Upset Tests", NRL (March 1983)

W.J. Poch and A.G. Holmes-Siedle, RCA Eng. 16(3), p. 56 (1970)

W.J. Poch and A.G. Holmes-Siedle, IEEE Trans.Nucl.Sci. NS-17(6), p. 33 (Dec. 1970)

W.E. Price, "Steady State Total Dose Procedure", Method 1018 (Proposed) of MIL-STD-883A (1977)

L. Ricketts, "Fundamentals of Nuclear Hardening of Electronic Equipment", New York, Wiley (1972)

C. Sansoe and R. Harboe-Sorensen, "Single Event CASE Testing of SGS Z80A CPU, PIO and DMA for ERS-1 Using a LABEN and an ESTEC Microcomputer System", ESTEC Internal Working Paper EWP 1442 (Jan. 1986)

J.R. Srour, O.L. Curtis and K.Y. Chiu IEEE Nucl.Sci. NS-21(6), p. 73 (Dec. 1974)

A.G. Stanley, K.E. Martin and S. Douglas, "Radiation Design Criteria Handbook", JPL Tech.Mem. 33-763 (Aug. 1976)

E.G. Stassinopoulos, G.J. Brucker, O. van Gunten, A.R. Knudson and T.J. Jordan, "Radiation Effects in MOS Devices; Dosimetry, Annealing, Irradiation Sequence and Sources", IEEE Trans.Nucl.Sci. NS-30(3), pp. 1880-1884 (1983)

E.G. Stassinopoulos, O. van Gunten, G.J. Brucker, A.R. Knudson and T.M. Jordan, "The Damage Equivalence of Electrons, Protons, Alphas and Gamma Rays in Rad-hard MOS Devices", IEEE Trans.Nucl.Sci. NS-30(6), pp. 4363-4367 (1983)

E.G. Stassinopoulos, G.J. Brucker and O. van Gunten, "Total Dose and Dose-rate Dependence of Proton Damage in MOS Devices During and After Irradiation", IEEE Trans.Nucl.Sci. NS-31(6), pp. 1444-1447 (1984)

C.D. Taulbee, D.C. Nelson and B.G. Southward, ANS-ASTM STP 384, pp. 121-148 (May 1965)

I. Thomson, M.B. Christensen and G. Hanssens, ESTEC Internal Reports MISC-061 and MISC-066 (1977)

TOS Radiation Programme Report (RCA Corp., Princeton N.J.), NAS 5-9034, NASA Goddard SFC (Sept. 1965)

U.K. Ministry of Defence, Report SSWL 1291 (1976) "Transient Radiation Effects on Electronics; Semiconductors; Data Summary"

P. Vail and T. Stanley, IEEE Trans.Nucl.Sci. NS-24(6), pp. 2147-2153 (Dec. 1977)

E.A. Wolicki, I. Arimura, Carlon Eisen and H. Halpin, "Radiation Hardness Assurance for Electronic Parts: Accomplishments and Plans", IEEE Trans.Nucl.Sci. NS-32(6), pp. 4230-4236 (Dec. 1985)

J. Wysocki, IEEE Trans.Nucl.Sci. NS-13(6), p. 168 (Dec. 1966)

K.H. Zaininger and A.G. Holmes-Siedle, RCA Review 28, pp. 208-240 (1967)

COMPILATION OF RADIATION TEST DATA

Among the data banks established for the collection and dissemination of radiation test data of electronic components are the following:-

ESTEC, Noordwijk. "Radiation effects data base (RADFX) total dose and single event upset data (ions and protons)". Distributed on 'floppy discs' for PC's by Spur Electronics, U.K.

HAHN-MEITNER INSTITUT, Berlin (D) "Data Compilation of Irradiation-tested Electronic Components", HMI-B353 (loose-leaf computer-printed data sheets)

KAMAN-TEMPO, Santa Barbara (USA), Incorporates the data bank initiated by U.S. Army (HDL), Adelphi, MD, USA

NASA (USA), Available through P.A. Group, Goddard Space Flight Center, Greenbelt, MD, USA

SPACERAD (USA), Compilation; available through Jet Propulsion Lab., Pasadena, CA, USA and accessible via DARPANET electronic mail system

SPIRE (U.K.), Compilation; available through U.K. Ministry of Defence (AWD), London.

PAGE INTENTIONALLY LEFT BLANK

SECTION 20. PROCUREMENT OF PARTS

20.1. INTRODUCTION

In the section on equipment practice, a description was given of the engineering principles on which a system could be designed to give the best possible level of radiation tolerance within given mass and cost constraints. However, one problem which requires administrative intervention is the variability of the response to radiation of certain commercially procured components. Commercial semiconductor technology has developed without reference to radiation-induced responses. Earlier sections describe in detail how some electrically similar commercial parts may have very large, uncontrolled variability. The life-time of one sample in a given radiation environment may differ from that of another, electrically identical sample by a factor of 1000. Although some of the requirements for the control of radiation response in device manufacture are now understood, it still remains a challenge to exercise such control of both technical and administrative aspects in spacecraft parts. In this section, the administrative aspects are addressed and recommendations are made for the inclusion of radiation parameters in procurement specifications and device selection procedures.

20.2. SPECIFICATIONS

This section includes a number of comments on Table 20(1). This table contains the recommendations for different types of radiation specification which should form part of the procurement procedures. The word "risk" implies that the margin of safety required will be determined by the seriousness of a given failure. For example, an operational satellite will be assigned larger safety margins than an experimental one. Also, if the spacecraft is earning revenue, then weight-saving assumes major importance. Extra weight which can be devoted to payload (say, communication channels) may yield extra revenue, possibly up to 500,000 U.S. dollars over a 7-year mission. Thus, the item "Spacecraft Mass vs Usable Payload" in column 2 of Table 20(1) is an important factor. In this case, "add-on shielding" must be replaced as far as possible by solutions without weight penalty such as the procurement of hardened parts or the use of built-in shielding. The penalty of procuring hardened devices may be cost rather than weight but, if the facts are known soon enough, a calculation may show that the revenue gained is higher than the cost of hardened devices.

Further consideration of Table 20(1), shows that listed as a factor in making specifications at "Equipment Level" is "total circuit response"; it may or may not be necessary to verify the analysis by irradiation of a whole circuit. In Table 20(1), under "Piece Parts Level", it is implied that many designers may not be aware of the existence of hardened parts which may only be available by special

arrangement. There is also a possibility of confusion as to whether a given part is hardened against pulsed nuclear weapon effects or to space electron and proton effects ("Total dose"). Specifications should therefore give guidance on supply sources and the type of hardness required.

20.3. PARTS PROCUREMENT

20.3.1. Introduction

As the preceding sections will have made clear, silicon devices - especially the forms which carry thermally grown silicon dioxide layers - are subject to a variety of serious permanent degradation effects when irradiated. Two very different forms of "damage" are involved: one being true lattice damage in the silicon crystal; the other being the reversible, but long-lived build-up of charge in the oxide (ionisation effect). Most commercial manufacturers do not control the tendency of these oxide films to trap charge. This tendency is strongly influenced by process parameters such as the annealing temperature, growth ambient and growth time. While attempting to improve process yield, the manufacturer may change these frequently. Consequently, the sensitivity of devices to radiation often varies strongly from year to year. Radiation sensitivity must be monitored on a lot-to-lot basis, otherwise the prediction of spacecraft survival time becomes impossible. No well-tried system for the procurement of devices which are radiation tolerant to the standard required for space vehicles has yet been developed. We can therefore only state some principles. Some progress has been made by the U.S. Military who are implementing "Hardness Assurance" procedures. While the neutron requirements are not relevant, it should be noted that the military specifications also include a relevant gamma ray "total dose". In the U.K., the British Standards Institution (1983) is developing a "Radiation-Assessed Device" specification as part of the BS 9000 Series.

TABLE 20(1) - RECOMMENDATIONS AND FACTORS OF IMPORTANCE IN SPACE RADIATION SPECIFICATIONS

"Space radiation" sections of spec's at the following levels should include:	Important factors
SYSTEM LEVEL External environment for given duration Internal environment for given duration and several absorber materials: - Dose versus depth curves - Silicon damage versus depth curves - Degraded spectra for various depths - LET spectra for different shielding Rationale for use of built-in mass (i.e. lay-out) for protecting sensitive boxes Requirements for telemetry of degradation in orbit	- Risk - Mission duration - S/C mass versus usable payload - Specific cost - Siting of sensitive boxes - Tolerable upset rates
SUBSYSTEM LEVEL Mass budget, incl. shielding allowance Rules for worst-case analysis of degradation Latchup and single event upset tolerance Requirements for telemetry of degradation in orbit	- Mass distribution - Siting of sensitive piece parts - Circuit design - IC technology - Add-on mass
EQUIPMENT LEVEL Tolerable degree of degradation in output versus time Equipment level testing (if necessary) Latchup protection and single event upset tolerance Requirements for telemetry of degradation in orbit	- Board mass distribution - IC technology - Piece part test data base - Total circuit response
PIECE PART LEVEL Data base Total dose degradation and single event upset prediction method Detailed derating specifications Indication of hardened component availability Testing method	- Derating - Hardened series - Lot variation - Lot acceptance
MATERIALS LEVEL Lists of especially sensitive materials Testing methods	- Lot variation - External parts

20.3.2. Preliminary evaluation

Unless suitable recent data have been published, all investigations into a particular product will begin with an exploratory radiation test of a small number of parts, probably less than 10 units each, if possible from several batches of variants of the relevant production line. This exploratory test is essential because, in the field of ionisation effects, there are as yet no electrical tests which can give an indication of the sensitivity of oxide layers to ionisation. Despite the existence of prediction models, even the prediction of sensitivity to bulk damage effects may be subject to error. The test results must then be interpreted as far as possible in terms of a physical model which distinguishes between bulk damage and ionisation effects.

The variability of the response from device to device must be characterised by statistical methods to permit determination of the subsequent course of action. Of course, a high absolute level of sensitivity may immediately eliminate consideration of the device for certain applications where degradation cannot be tolerated. Note, however, that many circuit designers leave very large margins of safety in parameters such as h_{FE} (gain) and sometimes use a device with a rated gain of 100 in a function which only requires a gain of 10 or less. Thus, the radiation requirement does not inevitably place severe restrictions on the choice of devices. On the contrary, the test requirement serves mainly to identify a few catastrophically serious cases, the knowledge of which could be obtained in no other way. This statement applies strongly to discrete bipolar circuits and other analogue circuits. A rather special case are the MOS logic circuits, as the safety margins allowed by the IC designer may, for commercial reasons, have been made very small indeed.

20.3.3. Acceptance of supplier

Following the preliminary evaluation of a range of devices, it must be decided whether the variability of radiation sensitivity of products from otherwise acceptable manufacturers is tolerable for a given electrical type. Unlike many other decisions in procurement, this question depends on both the project concerned (i.e. general mission radiation level) and the circuit concerned (i.e. protection provided by box and spacecraft and the margin of degradation which can be tolerated by the designer).

This situation stems from the magnitude of the degradation which radiation can produce in electrical parameters (over 10 times those which are ever produced by normal life tests under electrical or mechanical stress) and the very large difference between radiation dose in "exposed" and protected locations (this is why it was stated recently - and confirmed by several experts - that it is unlikely that any rigid system of agency-wide "approval for radiation" will be

instituted for some time). If degradation of a particular supplier's product is tolerable for the project in question, then procurement can - in principle - proceed. If, however, the degradation is no smaller than the available margin of safety, then the batches intended for use in flight equipment are best subjected to sampling.

20.3.4. Truncation of spread

If the variability of degradation is not tolerable for the project in question and no alternative device is available, then some form of preselection of devices must be developed to permit an effective truncation of the distribution in sensitivity. As a rule, one has to choose between two expensive alternatives: either to place further controls on the manufacturer or to adopt an "Irradiate-Anneal" (IRAN) approach. A third alternative is to procure a hardened device, but this applies only to a small proportion of the bipolar and MOS devices which designers are likely to use in space equipment. Provided the "hardening" processes prove compatible with normal commercial practice and contractors press suppliers to adopt this approach, they may grow in number.

20.3.5. Some procedures for device selection

Van Lint and colleagues at Mission Research Corporation (1977) have proposed a rational series of selection steps. Essentially, one establishes a failure budget for each transistor in the system. This is a probability of failure factored by the number of transistors in the whole system and by a design margin, namely a figure near unity which determines whether the degradation is tolerable or not. Test or prediction data are then assumed to have a log-normal probability distribution. One can then determine whether the probability of going outside the design margin (DM 1) falls within the allowed "failure budget". The options are then:

(a) To reject the device in question,
(b) To change the "failure budget", i.e. to shift the "design burden" to another device,
(c) To relocate or shield (but this brings in mechanical designers) in order "to force DM to acceptance condition",
(d) To apply controls to truncate the distribution of sensitivity (as discussed above).

Approach (c) involves, of course, weight budgets and mechanical designers, while (d) will consume time.

20.4. MOS INTEGRATED CIRCUITS - SPECIAL CONSIDERATIONS

Attempts to truncate distributions in MOS structures are unlikely to be successful. Devices from one manufacturer in a given era are either "all bad" or "all good", i.e. the distribution is already a narrow

one. With increasing understanding of the underlying effects, it seems clear that any manufacturer should be capable of producing radiation-tolerant MOS devices, using "controlled SiO_2", provided a corporate decision to do so were made. The component specialist of a project must work with a manufacturer who has made this decision. He may also attempt to place a "radiation effects control" specification upon other manufacturers.

20.5. BIPOLAR DEVICES - SPECIAL CONSIDERATIONS

The spread in the radiation response of bipolar transistors is generally broader than for MOS technology. The oxides concerned are not so critical to good performance and hence, compared with MOS technology, less control of oxide growth is exercised. Another complication is that the degradation of gain, produced by the accumulated oxide effects, is strongly dependent upon the collector current or emitter injection level used. While most bipolar digital circuit varieties are fairly insensitive to radiation, problems can still arise; particularly where a mix of processes or lay-out rules are employed within a product family (as recently experienced with ALS devices).

Bipolar Analogue ICs show wide variability depending on the design techniques employed; "super beta" transistors and lateral NPN transistors can give rise to high radiation sensitivity.

20.6. U.S. PROCUREMENT PRACTICES

U.S. spacecraft procurement takes to some extent advantage of the system of military specifications and thus it is significant that there is now a Military Specification (MIL-SPEC) Radiation Requirements Committee as well as hardness assurance work funded by the Defense Nuclear Agency (see, for example, Van Lint and Smyth, 1977). Radiation test procedures now form part of MIL-STD-883 and parts are classified according to the following test levels:-

M: 3 kilorads,

D: 10 kilorads,

R: 100 kilorads,

H: 1 megarad.

These classifications will be included in the part number for JAN 38510 microcircuits and JAN TX/TXV discrete semiconductors.

Although more and more radiation-hardened "standard products" are becoming available as a result of development programmes at the Center for Radiation-Hardened Microelectronics at Sandia Laboratories, the problem of the procurement of radiation-sensitive

devices for both military and civil space programmes, is still treated on a case-by-case basis.

20.7. CONCLUSIONS

The procurement of radiation-tolerant systems is strongly affected by parts procurement factors. However, the impact of the radiation environment and the raw environment figures must be defined as appropriate in all levels of engineering and procurement specification. This is not done sufficiently at the moment and leads to a lack of awareness of latent problems until many of the effective options are closed. The response of parts to radiation is much more variable than might be expected from experience of other changes with time in space and, therefore, some unconventional (and often costly) procurement measures have to be considered from time to time.

REFERENCES

V.A.J. van Lint, J.P. Raymond, A.R. Hart and M.L. Price, "Radiation Design Handbook for the Jupiter Probe", MRC/SD-R-14, Mission Research Corp. (1977)

J.B. Smyth and V.A.J. van Lint, IEEE Trans.Nucl.Sci. NS-24 (6), pp. 2093-2097 (Dec. 1977)

A. Wolicki et al, "Hardness Assurance for Electronic Parts: Accomplishments and Plans"; Invited talk IEEE NSREC 85, Monterey, CA (July 1985)

British Standards Institution, "British Standard 900X: Specification of the Basic Requirements for the Assessment of Semiconductor Components for Tolerance to High Energy Radiation", Draft Issue J (Sept. 1983)

SECTION 21. PROJECT MANAGEMENT

21.1. INTRODUCTION

This chapter surveys some of the issues raised when projects have to perform, or commission, radiation effects work. Timing is one of the most important and controllable factors and some time-tables are given. Usually, specialist assistance is necessary; therefore, attention is given both to which experts are most needed and, perhaps most important, to the means of ensuring that their advice is sought at the right time; the latter issue is called "Maintaining Project Awareness". The practices followed in the U.S., where much larger groups of radiation effects workers exist, are also briefly discussed.

Most engineers and managers, although highly skilled, are not familiar with many of the phenomena which are important in the radiation-induced degradation of components. Only in the fields of nuclear power, military operations and space is equipment likely to be exposed to significant doses of radiation. Thus, "Radiation Hardness Engineering" has not yet been introduced as a routine part of the discipline of Engineering. Management must be aware that their staff will need education as well as technical support from experts and therefore plan to start such procedures in the conceptual stages of a project.

An indication of this necessity is that one of the earliest choices made by a spacecraft project are the orbital parameters. While the objective of the mission may be feasible only in a limited range of orbits, systems engineers may well be able to increase spacecraft life greatly by careful orbit adjustment to minimise radiation damage. Therefore, radiation may be a significant design parameter from the earliest stage of a project. An early knowledge of the "no go" areas of space could thus save considerable effort or cost penalty.

Device technology is another issue which, normally, is decided in good time. The importance of the question may be made clearer by one example. Inappropriate decisions by device manufacturers on the choice of gate dielectric for MOS devices held back the use of MOS technology in space for several years and probably cost many millions of dollars in remedial research.

21.2. FLOW CHARTS

Figures 21.1 and 21.2 show a version of the flow and interrelation of tasks in the radiation-hardening of space equipment. It will be seen that there are roughly six major steps:

- Development of an environmental specification,
- Development of a suitable model of structure and materials used,
- Study of the interaction of equipment and environment,
- Prediction of degradation with or without testing,
- Development of a balanced plan of corrective actions from a wider number of options,
- Refinement of those options.

Normally, it is necessary to repeat these steps several times, starting from approximate solutions and refining them as the project proceeds. Timing is dealt with in a later section.

21.3. MAINTAINING PROJECT AWARENESS

This phrase is used here in the sense that "awareness" can be said to be maintained if design and systems engineers neither over- nor underreact to the threat of radiation-induced changes and introduce these considerations into their work just as they would for any other environment such as vacuum or vibration. Eventually, it may be that engineers will be equipped to handle this environment similarly to any other but, in the present era, the assistance of an expert is still required. Awareness is formally maintained in the form of written specifications. Some suggestions for the form in which radiation should be included in specifications have been given earlier.

In addition to the consideration of radiation in the design phase, methods for telemetering "housekeeping" data of radiation-induced effects in space are being developed. This is done by arranging electrical in-flight monitoring at known "weak spots" in existing flight circuitry and by the use of dosimetric devices. These methods are being developed as part of ESA's In-orbit Technology Demonstration Project.

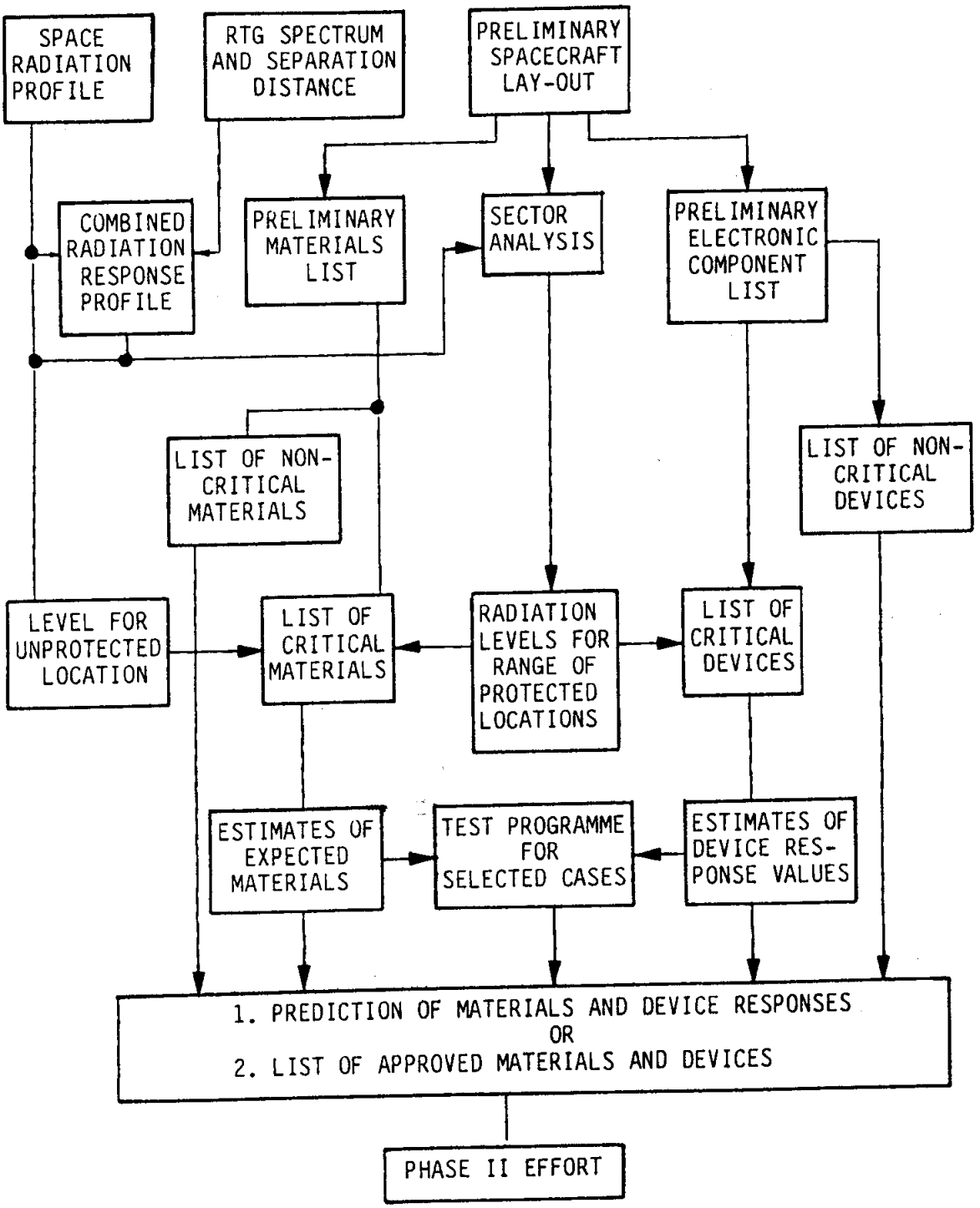

FIGURE 21.1 - PROJECT MANAGEMENT FLOW CHART: RADIATION ASSESSMENT OF SPACECRAFT - PHASE 1

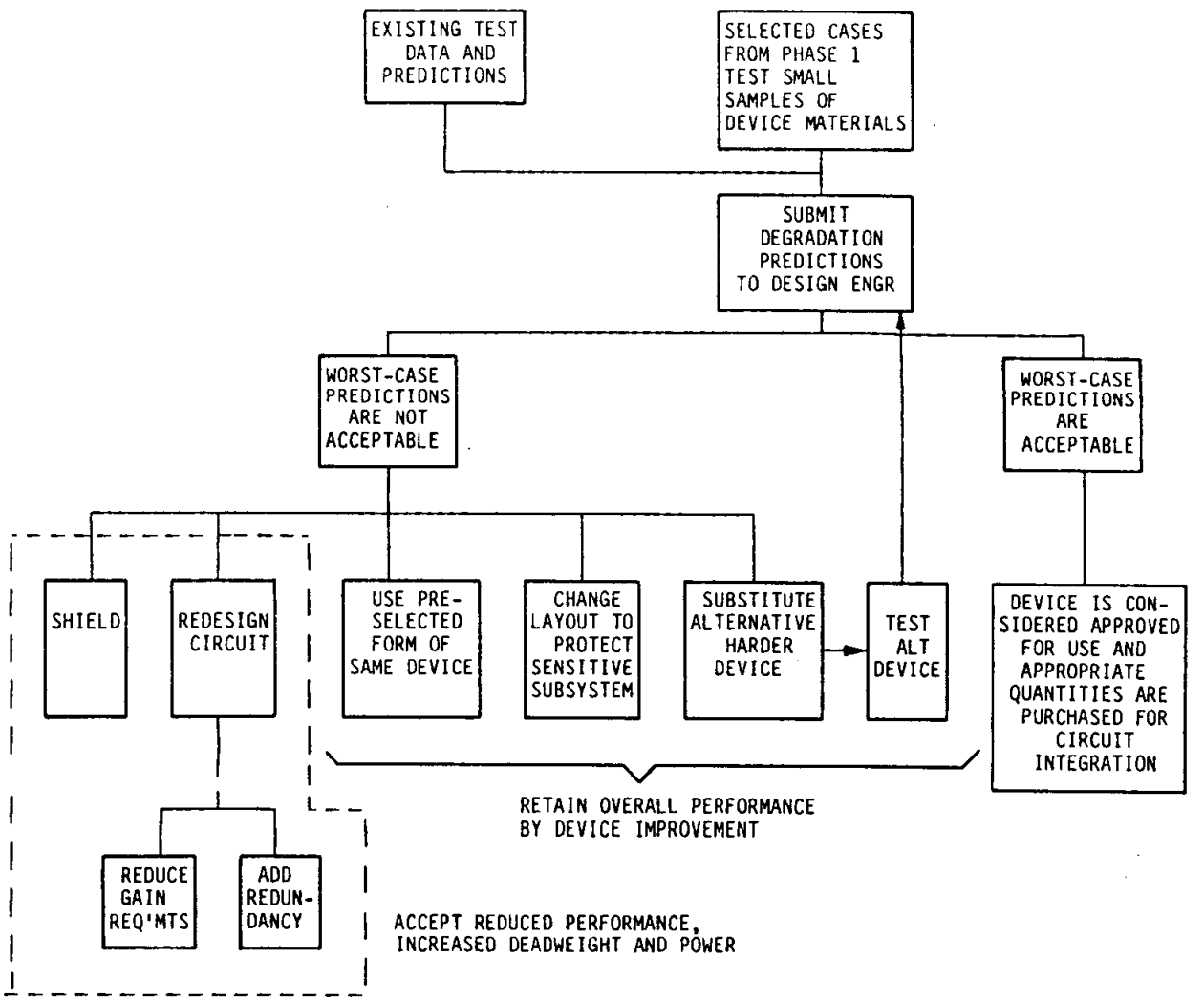

FIGURE 21.2 - PROJECT MANAGEMENT FLOW CHART: RADIATION ASSESSMENT OF SPACECRAFT - PHASE II

21.4. TIME SCHEDULE

The time schedule shown in Figure 21.3 was prepared in consultation with an ESA communications project. The "Simple Environment Assessment", "Sector Analysis" and "Detailed Sector Analysis" may require the tasks shown in Figure 21.1 to be repeated several times. Estimates are improved as design information is developed. Knowledge of device degradation will be accumulated together with data from "Forward Looking Research". Unexpected effects often occur in devices originally thought to be tolerant of radiation. The tasks shown in the prototype stage include the addition of last moment shielding to correct newly discovered problems of degradation ("band-aids") and "Lot Tests" to verify that purchased materials conform to the responses observed in trial samples.

Figure 21.4 shows a flow chart for investigations of piece-parts only, the interaction between a number of different engineering departments and appropriate sources of funding.

21.5. INFORMATION FLOW

The organisation of a Radiation Effects Engineering Group must ensure proper feedback of information between experimenters performing detailed applied physics work and engineers and physicists directly supporting the project. Preferably, all experts should have direct experience in project support and test work.

21.6. ROLES OF CONTRACTOR AND CONTRACTING AGENCIES

21.6.1. General

Like other engineering skills, "Radiation Effects Engineering" must be supplied by spacecraft development contractors. A contracting agency, for its part, needs to retain full cognizance of technical practices, promote new techniques, install some specialised test facilities and provide all contractors with environmental data in standard form.

It is the contractor's responsibility to understand the impact of the environment on his equipment and to design and test it accordingly.

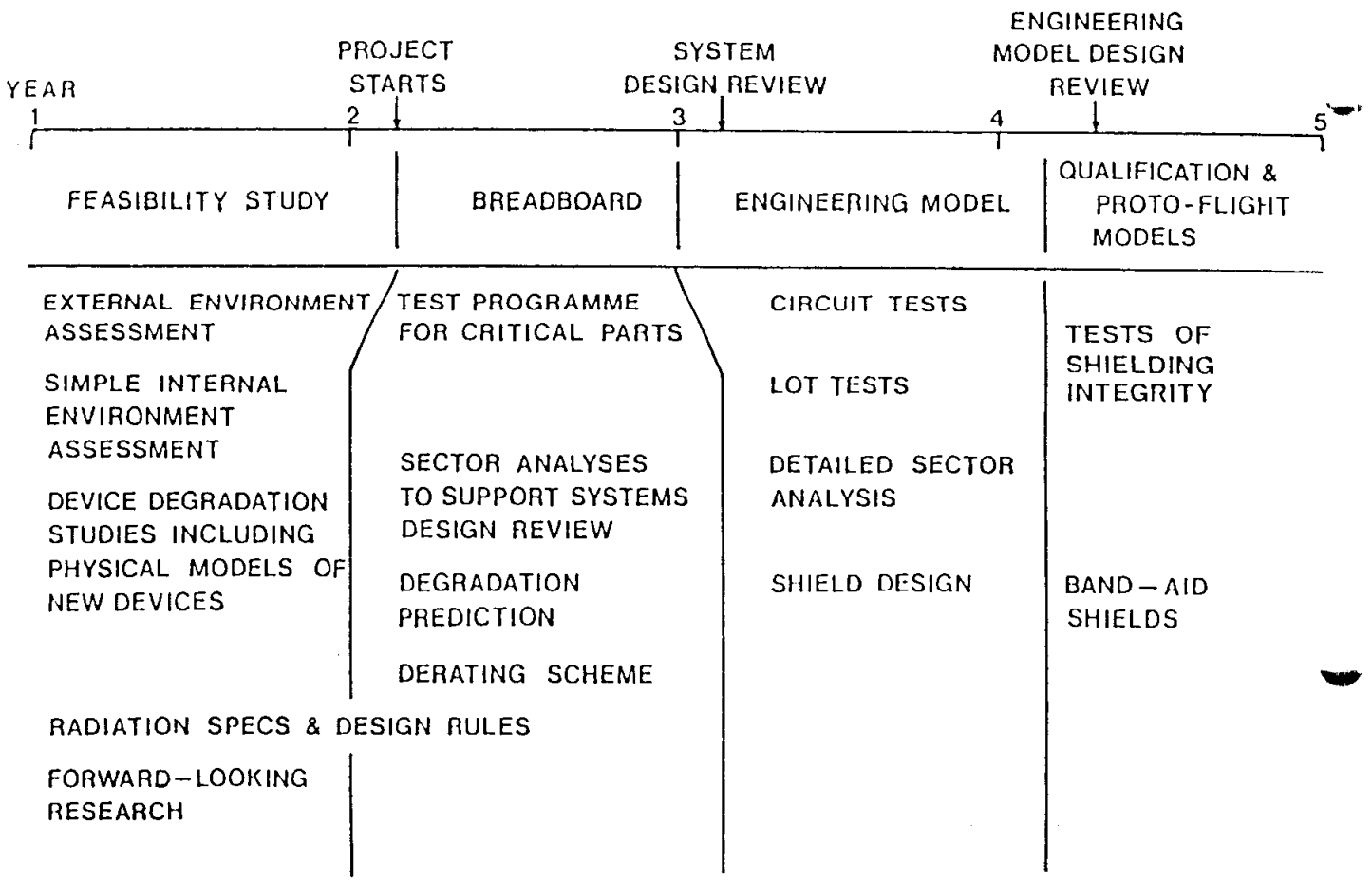

FIGURE 21.3 - PROJECT MANAGEMENT - TIMING

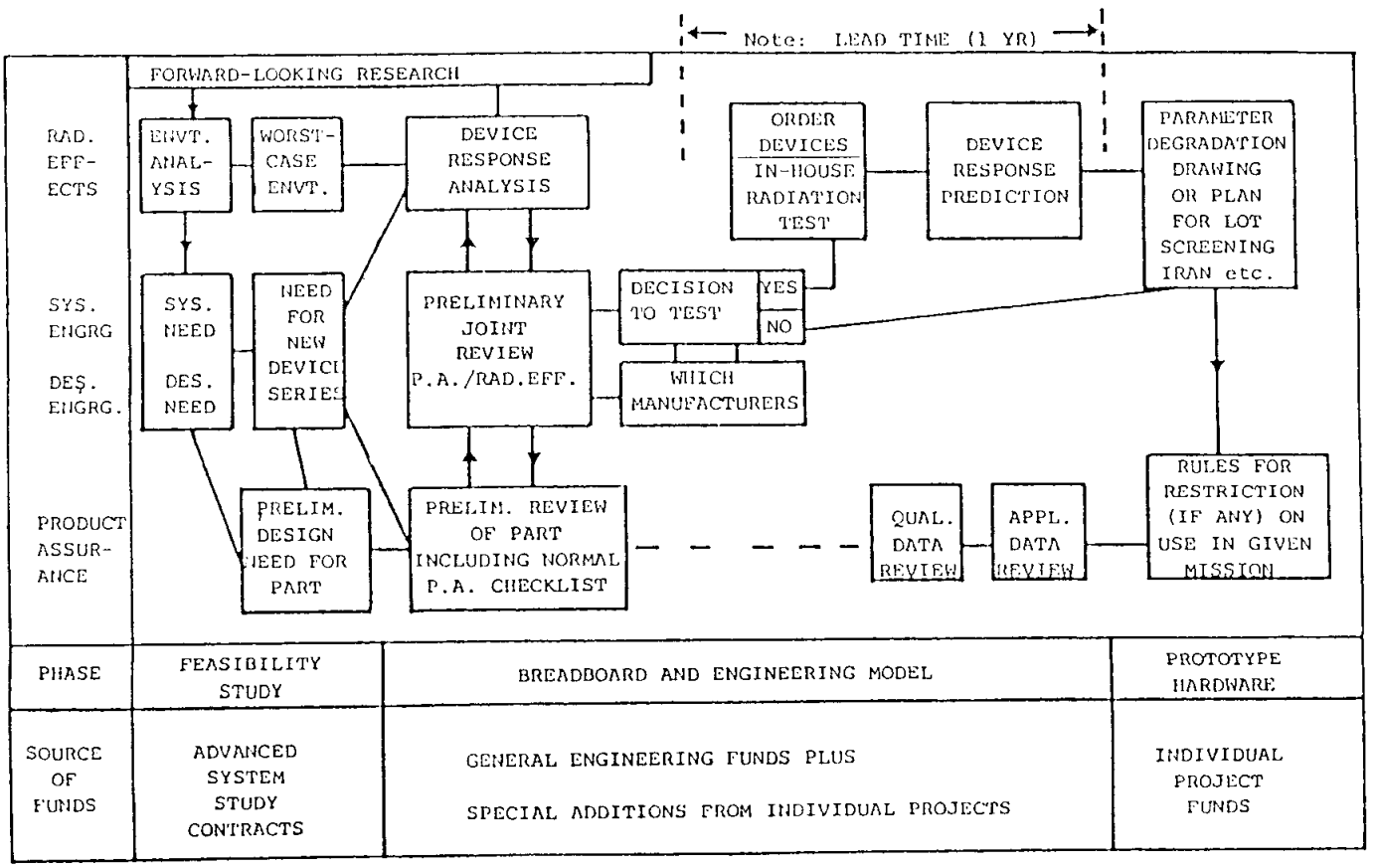

KEY: IRAN = Irradiate - anneal cycle
QUAL = Qualification, i.e. test and acceptance
P.A. = Product Assurance

FIGURE 21.4 - PROJECT MANAGEMENT - INTERACTION

TABLE 21(1) - U.S. PRACTICES IN RADIATION HARDNESS MANAGEMENT

1. Definition of environment		
For COMSAT	-	Contractor/COMSAT
For NASA	-	Customer
For Military	-	Customer
2. Identification of sensitive components		
For COMSAT	-	Contractor
For NASA	-	Joint endeavour
For Military	-	Contractor
3. Radiation analysis requirement		
For COMSAT	-	Completely in Contractor's hand. Approach is scrutinised and forms one of the criteria in contract award. COMSAT provides technical support.
For NASA	-	Varies according to Centre. GSFC: Contractor has overall responsibility, but analysis items are identified and deliverable for review and approval; GSFC has high degree of technical participation. JPS: Agency performs system circuit and parts analysis and selection.
For Military	-	Comprehensive analyses at all equipment levels required from Contractor. "Hardening", including extensive R & D, forms subprogramme.

21.6.2. Practices in the USA

Table 21(1) describes U.S. practices in the management of radiation effects. As implied by the term "management", most contractors in the USA have a Radiation Effects Group consisting of several workers.

The work is supported by:

(a) Pre-proposal or general engineering funds, the purpose of which is to improve the technical depth of proposals for large space systems contracts;

(b) Independent research and development funds, generally for the same purpose as (a), but emanating from the Government and loosely controlled by the latter;

(c) Technique contracts placed by agencies, which may or may not be directly connected with an individual space project;

(d) Direct funding by individual project offices to support the design of equipment.

To give an idea of the size of the "Radiation Effects Community" in the USA, the annual IEEE Conference on the subject is attended by over 1000 persons, possibly one third of whom are involved in space programmes.

21.7. GUIDELINES FOR DEVELOPMENT IN RADIATION EFFECTS

Some recommendations for future actions in the field of Radiation Effects Engineering are made later. At the present time, the most urgent needs are:

1. The establishment of a database on which predictions can be made,
2. Physical models permitting engineering predictions (still incomplete),
3. Formal guidelines for radiation effects control,
4. Development of testing techniques and facilities.

21.8. CONCLUSIONS

From the foregoing discussion, it will be clear that the management of radiation effects may create problems not encountered in other engineering fields. If penalties incurred by late reaction to such problems are to be avoided, then the organisation, timing and staffing to deal with them must be planned from phase A onwards.

REFERENCES

N.J. Rudie, "System Invisibility in the Nuclear Age", Defence Science and Electronics, pp. 16-26 (July 1985)

W.S. West, W. Poch, A.G. Holmes-Siedle, H.W. Bilsky and D. Carrol: "Subsystem Radiation Susceptibility Analysis for Deep Space Missions", NASA TR R-371, NASA Goddard SFC (Nov. 1971)

SECTION 22. A COMPLETE ANALYSIS

22.1. INTRODUCTION

In this document, a large number of methods have been presented for the calculation of local environments and the degree of device degradation in a form more convenient and detailed than was available hitherto. The following is an attempt to show how these techniques can be fitted together to solve a typical spacecraft equipment problem. This exercise will demonstrate that the techniques which have been described provide the basis of a procedure which can be used by engineering design staff.

22.2. SPACECRAFT MISSION AND GEOMETRY ASSUMPTIONS

The problem chosen is that of a small-scale integrated CMOS logic gate in a piece of equipment to be used in a 3-axis stabilised communications satellite with a required lifetime of seven years in geostationary orbit. The device is part of a circuit board contained - as is normal - in a stack of similar boards within an aluminium box, 1 to 2 mm thick. The box lies on a honeycomb platform of mass equivalent to less than 1 mm aluminium and is shadowed from some directions by other boxes which have masses equivalent to more than 7 mm of aluminium.

22.3. OTHER STARTING DATA REQUIRED

- External particle environment
- Electrical circuit criteria for determination of the maximum acceptable performance degradation
- Simplified model of CMOS response to radiation
- Test data

22.4. MISSION DOSE (D_M) CALCULATIONS

The dose reaching the CMOS device is determined by a dose-depth calculation for which a spherical shell is assumed, followed by a sector analysis of the spacecraft parts surrounding the device, as described in Sections 7 and 8. The external particle environment can be obtained by computerised integration of radiation fluxes around the orbit, for example with the UNIRAD program (see Section 2). The dose-depth calculations are best made by computer, e.g. the SHIELDOSE program (see Section 18).

A simplified example of a sector analysis is illustrated in Figure 22.1 which, for simplicity, shows only two dimensions. In this figure:

- The device package and the box cover have been merged and are represented as two 1 mm layers of aluminium;

- Various components above the device are represented as a 2 mm Al slab;
- Local components are represented as two overlapping Al slabs of 2 mm each and
- Two distant boxes are represented as Al blocks of 7 mm each.

Thus, over the angles shown, sectors A to K can each be regarded as filled by a uniform slab of thickness d as listed in the table in Figure 22.1. The 7-year dose for that value of d can be read from the dose- depth curve (inset) and then multiplied by the appropriate "fraction of 4 π". The sum is the Mission Dose, D_M shown here as 13.6 krad (Si) over 7 years.

The sector analysis will have to be repeated for other dose points (device locations) in question because the angles subtended at the dose point will, of course, change as the point moves. In view of this need for repetition and the fact that serious errors may be made in manual estimates such as the above, the use of computer calculations is recommended. ESA and many European companies and institutes use the ESABASE system (see Section 18). This allows a detailed geometry database to be maintained for a spacecraft and to be used by contractors, ESA and payload engineers for individual detailed analyses. This procedure has been adopted for the Cluster programme. An example of ESABASE use for sector analysis and radiation assessment may be found in Daly et al (1992).

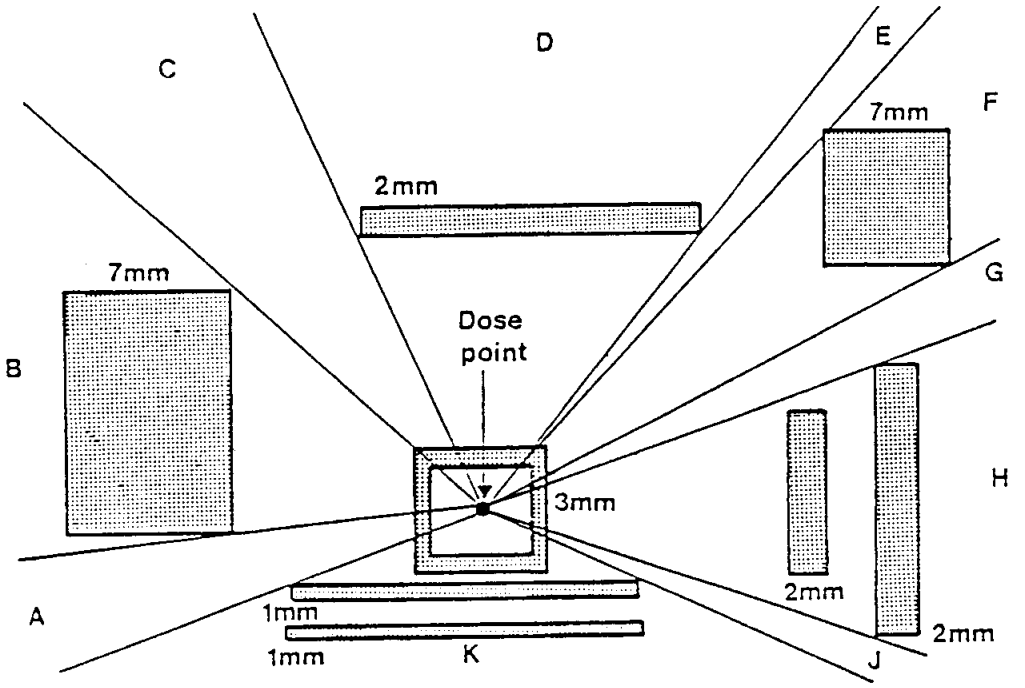

	d mm Al	fraction of 4π (approx)	7-year dose krad(Si)
A	3	·04	2·4
B	10	·12	·24
C	3	·08	4·8
D	5	·15	·9
E	3	·01	·6

	d mm Al	fraction of 4π (approx)	7-year dose krad(Si)
F	10	·07	·14
G	3	·02	1·2
H	7	·10	·3
J	3	·01	·6
K	5	·40	2·4

Total dose: 13·6 krad(Si) in 7 years

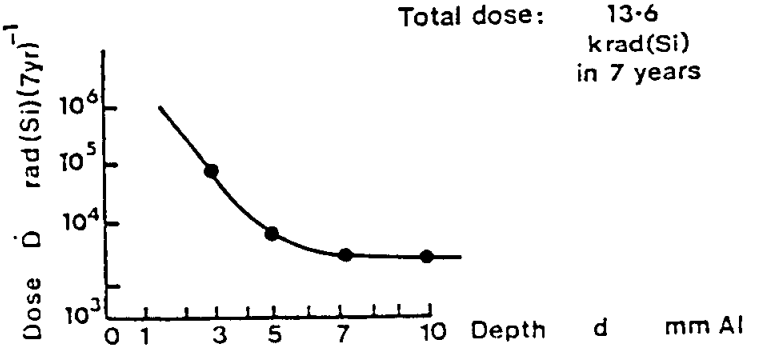

A simplified example of sector analysis for determination of dose deposited at a point within a spacecraft structure.

FIGURE 22.1 - SECTOR ANALYSIS

22.5. MAXIMUM ACCEPTABLE DOSE, D_A (MAX)

The preferable form of test data for a CMOS integrated circuit is the change of V_T as a function of dose for a well-defined d.c. value of V_I higher than 5V. The test doses covered should be as wide as possible but, with the model developed here, even one data point can be used (although, naturally, this gives reduced confidence). Data on the change of quiescent current versus dose can also be used, but are less amenable to analysis and more limited in use. The test data should be for a device which is closely related to the flight unit (of the same "vintage" and make). A value for the initial threshold voltage of the n-channel device is also required.

The following is a suitable procedure for applying the test data to determining D_A (max):

1. Plot ΔV_T versus dose and complete the response curve, if necessary by reference to the simple growth curve models. This can be done by assigning an 'A' value and constructing a simple model response curve for the device. This should be set to yield the best fit to the test data points.

2. If the value of V_I used during the test is not the same as that planned during flight, the model can be used to adjust the prediction curve.

3. If all gates of the logic device will be under cycled bias, some relief can be given.

4. On the adjusted model growth curve, note the dose at which $-\Delta V_{TN}$ approaches the original value of V_{TN}. This is the dose at which the VTNZ condition will cause an increase in I_{SS} (I_{SS} will, of course, begin to increase before the VTNZ condition is reached because a finite current, say 10μA, is used to define V_T). Electrical circuit analysis and a similar analysis of ΔV_{TP} will also indicate doses at which NIR, SSR and LF modes will occur.

5. D_A (max) is the radiation dose (rad (Si)) at which the critical performance parameters, as determined by electrical analysis, reach the "maximum tolerable" level of degradation. If test measurements of the critical performance parameters versus dose are available (e.g. I_{SS} , noise immunity, etc.), then these should be verified by means of the above ΔV_T analysis to ensure that they indicate the same magnitude for D_A (max). A higher dose value for the latter is likely because the simple ΔV_T analysis ignores interface states.

6. Compare D and D_A (max)

   If D_A (max) exceeds the mission dose, D_M, by an order of magnitude or more, use of the device at the dose point concerned can be approved. If the two dose figures lie closer together, more detailed analysis is warranted, including the following approaches, as the situation demands:

   (a) Refined calculation of DM,

   (b) Redesign of layout, thereby increasing built-in protection,

   (c) Redesign of circuit,

   (d) Device technology study,

   (e) Trade-off of life versus shield weight.

7. Corrective actions and follow-up

   As a result of the above analyses, corrective design changes and procurement action may be decided. The efficacy of these must be verified at the equipment acceptance stage. Checks for integrity of protection will be easier if the spacecraft layout has been computerised, as in the ESABASE system.

22.6. SUMMARY

Figure 22.2 summarises the procedures described above and also includes the other parts of Radiation Effects activity such as test development and research which go to support the analysis. Where appropriate, the computer program names are shown in brackets; blanks between brackets indicate that the required programs are not yet available.

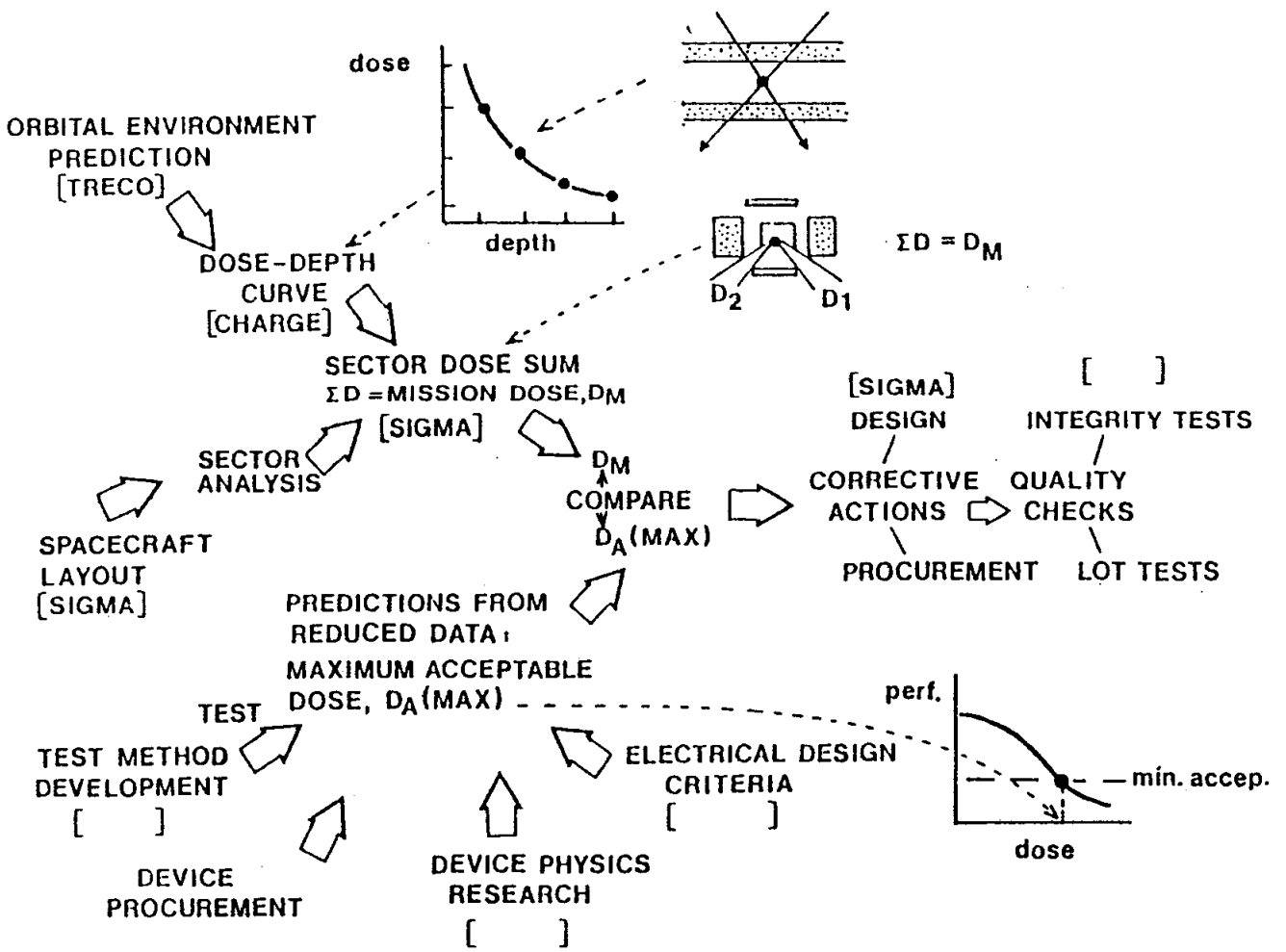

The interaction of the various stages in the analysis of radiation effects.

FIGURE 22.2 - COMPLETE ANALYSIS - FLOW CHART

REFERENCES

Daly E., H. Evans and C. Tranquille, "The XMM Radiation Environment and its Effects on Payloads", Estec Working Paper EWP 1643 (1992).

PAGE INTENTIONALLY LEFT BLANK

SECTION 23. RECOMMENDATIONS AND FUTURE DEVELOPMENTS

23.1. GENERAL

In the use of this document, one is made aware of the presence of gaps in the techniques necessary to improve the radiation tolerance of a spacecraft system. Further R&D work is needed before a coherent discipline for radiation tolerance engineering is available to European Design groups. Some of the fields needing more work are listed below:

System level engineering

- Orbital radiation analysis,
- Trade-offs for mission orbit selection,
- Orbit/weight/life/cost trade-offs,
- Written equipment procurement specifications, including improved environment specifications and radiation-effect control procedures,
- Detailed comparison of radiation transport and shielding computer programs.

Layout

- Radiation protection analysis of whole spacecraft,
- Computer-aided design of local spacecraft protection,
- Testing procedures for the integrity of protection after assembly,
- Written design rules for layout of:
  (a) Spacecraft,
  (b) Electronic boxes.

Electrical effects

- Scheme for predicting degradation of:
  (a) Bipolar,
  (b) MOS and
  (c) Optoelectronic devices,
- Scheme for predicting orbital upset rates from SEU,
- In-flight monitoring:
  - Telemetry of selected circuit points,
  - Distributed Radiation Monitoring Units (RMU),
  - Design rules for radiation tolerance of circuits.

Radiation test techniques

- Low-cost bench-top tests,
- Test guidelines (see MIL standards and ESA/SCC procedures),
- Standard methods of test interpretation,
- Dosimetry standardisation,
- Device Response Data Bank,

- Research into radiation effects on new devices.

Worthy of comment in the "lost opportunities" department are:

- The present lack of unambiguous monitoring of spacecraft circuits for signs of radiation-induced degradation and single-event upsets,
- The probability that, from time to time, unnecessary shield weight has been launched owing to imperfect knowledge of the existing built-in protection given by spacecraft structure and
- Lack of routine radiation environment monitoring.

Indeed, the relative cost-effectiveness of alternative methods of hardening has never been rationalised.

23.2. FUTURE DEVELOPMENTS IN RADIATION HARDNESS ENGINEERING

Changes in electronic and aerospace technology can affect the approach adopted to radiation-hardening of both manned and unmanned space vehicles. Although we recommend that "Radiation Hardness Engineering" should become a distinct and recognized part of space systems engineering and configuration control, it is not yet a discipline. Some of the influences causing change in spacecraft design are:-

A. In aerospace technology

- Lighter spacecraft structures can be assembled and launched from earth-orbiting bases,
- Satellites are now being serviced in orbit,
- Increased use of modular designs requires increased standardisation of all spacecraft equipment, but especially of MOS devices, shielding and dosimetry,
- Jupiter fly-by's incur high radiation environments,
- Use of space nuclear power systems (RTGs and reactors) will increase, especially if Lunar and Martian bases are developed,
- Spiral transfer to geosynchronous altitude from low earth orbit will be used; prolonged transit through the radiation belts imposes serious constraints on electronic and optical designs and
- Increasing popularity of eliptical orbits for science and communications.

B. In electronic technology

- New MOS fabrication methods (e.g. use of Si gate implantation, e-beams, dry plasma etching) will make control of hole-trapping in semiconductor/insulator structures more challenging,
- The expected scaling-down of MOS device geometry (including thinning of the gate oxide), although reducing the effectiveness

of charge build-up in the thinner oxides used, also confers added chances of new "electrical noise" phenomena, including single-event upsets, high-field electron avalanche effects and trapping.

The increasing use of optoelectronic devices will increase the impact of radiation-induced coloration in optical materials, of radiation-induced "optical noise" in optical signal-processing and of bulk-damage to CCD's.

To summarise the trends in aerospace technology: on the bad side, it appears that - in general - environments will become more severe and devices more sensitive to radiation; on the good side, it is likely that space vehicle degradation problems will be slightly relieved by the falling cost of launches, allowing replacement of modules in orbit and sometimes extra shielding. Radiation hardness engineering will still be needed in order to supply the rationale for choice between these two alleviating measures in payloads of ever-increasing complexity. It should not be assumed that the coming of the shuttle era will remove the need to limit the quantity of shielding.

For electronic technology, the good news is that empirical methods for controlling hole-trap densities in oxides are now offered commercially in some "radiation-hardened" device series. Moreover, now that oxides are more likely to be exposed to various avalanche injection processes, including hole injection, because of reduced device dimensions, more attention is paid to oxide-charging. The bad news is that the increasing use of dry technology for processing and the constraints of VLSI densities make the control of MOS device-charging more difficult, the use of small dimensions has already brought in two new effects: single-event upsets and electron-trapping.

In brief, it is not likely that the need for radiation hardness engineering will disappear and it is likely that research and development in this field will be required for some time, especially in the areas of device physics, testing, shielding and instrumentation.

PAGE INTENTIONALLY LEFT BLANK

SECTION 24. CONCLUSIONS

The effects of space radiation on electronic devices, especially those on LSI devices and optics, provide the engineer with a complex problem. This document is a manual which specifically addresses the engineering problem and some of its management aspects. Summary graphs, tables and calculation methods are presented which are intended to help spacecraft designers to gauge the significance of the space radiation problem from their particular point of view and then to communicate this problem to management.

Descriptions of the environment, effects and possible solutions have been couched, as far as possible, in simple language. Much of the graphical material is original to ESA and gives comparisons of data from several publications or unpublished data. In all areas, improvements in analytical methods have been sought. Some difficult questions of transmission of electrons and protons into electronic boxes have been clarified and approximate methods for calculating dose-depth curves are given. The method is useful for preliminary investigations, but computer approaches are recommended for detailed equipment design.

"Dose-depth" curves for orbits of importance ("reference missions") are compared. A simple example of a geometrical sector analysis for one mission is given. In view of the importance of its use in telecommunications, the geostationary Earth orbit (GEO), is given special attention. Because of the development of manned space stations, low Earth orbits (LEO) are also of increasing interest.

The problem of predicting the responses of advanced electronic devices to radiation is a challenging one because the device physics involved is complex and the field is in continual development. During the preparation of this handbook, existing methods have been reviewed and new ones developed, e.g. the Simple Engineering Model for MOS devices. The designer must have the design tools that allow him the choice of circuit alteration, added shielding or the premium cost on hardened devices. By force of circumstances, designers will have to use many devices that are probably only available in "unhardened form". Thus, the sections on procurement, radiation test procedures and project aspects will be useful to system engineers and management.

Looking forward, a more formal interaction with projects is sought. Considering the rapid developments in aerospace and semiconductor technology, ESA is encouraging forward-looking research in this field.

New trends in space include the use of space stations, increased use of on-board data processing and sensors and the great increase in complexity of integrated circuits. It is hoped that by outlining the present state of radiation effects analysis techniques and the provision of guidelines, this handbook will lead to enhancement of the efficiency of European and international space project systems.

PAGE INTENTIONALLY LEFT BLANK

ANNEX A
GLOSSARY OF TERMS

ABSORBER
Any matter intervening in the path of a radiation beam which thus absorbs energy from that beam.

ABSORPTION COEFFICIENT (μ)
Electromagnetic radiation penetrating a material is absorbed according to Lambert's Law: $I = I_0 e^{-\mu t}$.

ACCELERATION FACTOR
The ratio between the dose rate of radiation used in simulation and the dose of the same type of radiation expected in the actual environment. When a radiation beam is scanned across a sample surface, a distinction must be made between the instantaneous and time-averaged dose rate.

ADD-ON ABSORBER
A material added to equipment for the specific purpose of stopping radiation (in contrast to "built-in" absorber).

APOGEE BOOST MOTOR
Solid fuel rocket often forming the central core of spacecraft, especially geostationary vehicles.

BAND-BENDING (ψ_S)
A uniform electric field in a material is associated with a linear variation of potential with distance. If, however, the material responds to the applied potential by producing a space charge, the field will not be uniform and the potential-versus-distance plot will be curved. This often occurs near the surface of silicon (as in a MOS device) and is called "band-bending". (According to this system, band-bending at zero applied potential results from work function differences between the silicon and gate electrodes.)
In terms of surface potential, the degree of bending can be expressed as $\psi_S = E_C$ (bulk) - E_C (surface).
The conductivity of the silicon at the interface is a function of ψ_S. The condition of zero band-bending ($\psi_S = 0$) is called the "flat band" condition.

BAND-EDGE
See BAND GAP.

BAND-GAP
In perfectly crystalline inorganic insulators and semiconductors, there are well-defined regions of the energy-state diagram which are "forbidden bands". In these regions, there are no quantum energy states which can accommodate electrons or holes. The lowest of these bands

is often referred to as the band-gap. The lower edge is defined by electron potential energy 'E_V' (the top edge of the valence band); the upper edge is defined by 'E_C' (the bottom edge of the lowest conduction band).
The band-gap energy 'E_G ' is equal to E_C - E_V. Conduction in any inorganic solid involves the excitation of electrons from energy levels below 'E_V' to levels above 'E_C' and subsequent motion of the electron or the resulting hole.
The bands have a continuous overlap of quantum states which allow this. Very similar conditions occur even in non-crystalline but continuous networks such as the Si-O-Si-O network of an oxide thermally grown on silicon (see also CARRIER, FERMI LEVEL, TRAPPING and MOBILITY).

BGR CURVES
See DOSE TRANSMISSION.

BREMSSTRAHLUNG (BRAKE RADIATION)
X-rays produced when particles (mainly electrons, but also protons) are slowed down by interaction with matter. Sometimes also called "White Radiation" to distinguish it from the characteristic line spectra produced by each element.

BUILT-IN ABSORBER
Material forming part of the normal fabric of an equipment box or structure (in contrast with ADD-ON ABSORBER).

BULK DAMAGE
The disturbance of the lattice structure of matter by the displacement of atoms as frequently produced by energetic particles (term often used to distinguish between this type of damage and IONISATION EFFECTS or surface damage).

BULK DAMAGE FIGURE ($\Delta (1/\beta)_b$
Change in the reciprocal of the gain (β, h_{FE}) of a bipolar transistor under irradiation, as caused by the reduction of a minority carrier's lifetime (in contrast with SURFACE DAMAGE FIGURE).

CARRIERS
When electrons are excited across the BAND-GAP, both they and the resulting holes are mobile and will move if an electric field is applied (see MOBILITY). In inorganic oxides and semiconductors, electrons and holes are the main "carriers" of current. Ions usually contribute only to a very minor extent.
In n-type silicon, electrons are in the majority and holes in the minority (and vice versa in p-type silicon). Radiation or forward junction bias can produce "excess minority carriers". When the source of these is cut off, the excess will decay by recombination with majority carriers via DEEP

TRAPS. The time constant for this process, which is known as the minority carrier lifetime τ, is controlled by Shockley Hall-Read statistics.

CONDUCTION BAND
See BAND-GAP.

DAMAGE-EQUIVALENT FLUENCE
Bulk damage expressed in units of fluence of some standard energy of particle. The first unit developed was the Damage-Equivalent, Normally-Incident 1 MeV Electron cm^{-2}, sometimes abbreviated to "DENI". Other common unit: 1 MeV neutron cm^{-2}.

DEEP TRAP
A CHARGE TRAP is considered "deep" when it lies well away from the band-edges so that thermal excitation cannot depopulate it. In silicon, traps due to radiation-induced displacement damage lie deeper than 0.1 eV from the band-edges. Traps lying at the centre of the band-gap are the most efficient as recombination centres for minority carriers in semiconductors (see CARRIERS). Hole traps in silicon dioxide lie at depths greater than 2 eV. Thermal depopulation at room temperature is not significant for any trap lying deeper than 0.025 eV.

DEFECT
See TRAPPING.

DEPTH DOSE
Term used in medicine to indicate the total dose expected within a mass of tissue at a specified depth (see DOSE-DEPTH CURVE).

DOSE ('D')
Used broadly for any accumulated energy value, but strictly in dosimetry for the energy absorbed in a unit mass of material, usually by ionisation processes. Units are the "rad" and "gray" which are equivalent to respectively 100 $ergs.g^{-1}$ and 1 $J.kg^{-1}$ (1 Gy = 100 rad).

DOSE-DEPTH CURVE
Term used extensively in space engineering for a curve indicating the dose deposited in a given material behind various thicknesses of a separate absorber or array of absorbers.

DOSE RATE
The rate at which energy is transferred to a material by a radiation beam, e.g. $rad.s^{-1}$ (or $Gy.s^{-1}$).

DOSE TRANSMISSION CURVES
Term used for curves which indicate the effect of the thickness of a given slab of absorber on particles of a given energy, yielding the dose at a given depth in rads per unit fluence. An early set of these curves is referred to in this document as "BGR Curves", after the authors Brown, Gabbe and Rosenzweig.

ENERGY FLUX
The passage of energy in the form of penetrating particles, not necessarily stopped. Typical units: $erg.cm^{-2}$ and $W.m^{-2}$.

ENERGY TRANSMISSION COEFFICIENT (ETC)
The fraction of incident energy flux that emerges from an absorber slab.

EXPOSURE
An important term in dosimetry which expresses fluence in terms of its effect on a dosimetric medium (nearly always air at STP) and the number of air ions produced per unit mass. An exposure of 1 röntgen = exposure to that fluence of a given radiation which, in air, would generate 2.58×10^{-4} coulombs of ionic charge per kilogramme (term used in contrast with DOSE which varies from absorber to absorber).

FAST STATES
See INTERFACE STATES.

FERMI LEVEL (E_F)
An important mathematical concept of Fermi statistics which defines the electron population of the conduction band, whether populated by thermal or radiation-induced excitations. In the latter case, the term quasi-Fermi level is used. In undoped (intrinsic) silicon, E_F lies at the centre of the band-gap E_i.
In n- and p-type silicon, it lies respectively above and below E_i. Temperature and high doping move E_F towards the band-edges. BAND BENDING at the $Si\text{-}SiO_2$ interface changes the relation between E_F and E_C, hence the alterations of conductivity which accompany band bending (for E_C, see BAND GAP).

FLAT-BAND VOLTAGE (V_{FB})
In MOS devices, an important parameter which indicates the amount of charge in oxide. Gate voltage at which no surface band-bending is present. V_{FB} shifts under irradiation.

FLUENCE
Time-integrated flux. Unit: $e.cm^{-2}$. It is useful to add the symbol for the particle, e.g. "$e.cm^{-2}$ " or even "1 MeV $e.cm^{-2}$" (the unit "m^{-2}" is not often used in relation to radiation).

FLUX
Number of particles passing through a specific zone per unit time. For parallel beams, this will be a unit area; for omnidirectional radiation, the zone chosen is usually a sphere with cross-section 1 cm . In both cases, the unit is $cm^{-2} .s^{-1}$ (the unit $m^{-2} .s^{-1}$ is not often used in relation to radiation).

GRAY (Gy)
New radiation dose unit of the Système Internationale. Its value is $1\ J.kg^{-1} = 100$ rad.

GROWTH CURVE
Plot of change in threshold voltage or flat-band voltage (ΔV_T or ΔV_{FB}) against radiation dose 'D'. Important analytical tool in MOS testing and circuit design.

HARDENING, HARDENED
Terms used to describe improvement in the tolerance of a device or system to a radiation environment. Originally used by the military for sites invulnerable to attack.

HARDNESS ENGINEERING
A new term proposed here to describe briefly the whole process of introducing tolerance to radiation into a system, involving interaction with the design process at many points.

INITIAL TRAPPING PROBABILITY (A)
See TRAPPING.

INTERFACE INSTABILITY
See INTERFACE STATE.

INTERFACE STATE
At the interface between two dissimilar media, wave functions in any periodic solids must be disturbed. The quantum states at an Si-vacuum interface are called "surface states" or "Tamm states". At the interface between silicon and an oxide film thermally grown upon it, the opportunities for unique quantum states are numerous owing to the presence of lattice mismatch, non-stoichiometric conditions and impurities, especially hydrogen.
Those states which are observed in electrical measurements of MOS systems to accept or donate charge to the silicon are lumped under the operational term "interface states". If the exchange of charge is rapid (1 microsecond), the states are termed "fast".
In other quantum states, "slow" charge exchange may occur over many hours, leading to an INTERFACE INSTABILITY. Concentration of interface states may be plotted versus potential at the silicon surface. Local concentration D_{it} is usually expressed in units $cm^{-2}.eV^{-1}$.
Charge in these states in a given equilibrium condition Q_{it} is usually expressed in units of cm^{-2}.

IONISATION EFFECTS
A large class of radiation effects which involve the removal of an electron from a valence level, or below, in an atom and its escape beyond the excitation levels of that atom (for semiconductors, used in contrast with "bulk damage").

IRRADIATION BIAS
The electrical stress voltage placed on a device during irradiation. Some authors use the term "bombardment bias".

LARGE-SCALE INTEGRATION (LSI)
The integration of several hundred or more device elements on a single semiconductor chip.

LATCHUP
The onset of a self-sustaining conduction mechanism in a junction structure with four regions such as p-n-p-n in series and closely spaced. The mechanism is otherwise known as being of the SCR or thyristor type. Latchup can be triggered in certain complementary MOS integrated circuit designs and also in many junction-isolated bipolar integrated circuits by a pulse of radiation of dose rate greater than about 10^6 rad.s^{-1}.

LOGIC UPSET
Pulses of radiation of dose rate higher than about 10^6 rad s^{-1} generate photocurrents of significant magnitude in semiconductor junctions. They can so alter the voltages at circuit nodes that logic circuits can interpret the disturbance as a logic signal and change state. The proper signals passing through are thus "corrupted" by spurious data.

MAJORITY CARRIER
See CARRIERS.

MAXIMUM ACCEPTABLE DOSE D_A (MAX)
Term proposed here for the dose at which some specified degradation phenomenon reaches intolerable proportions for a given purpose of the device.

MODIFIED PROCESS (M1, M2)
Terms proposed here for a MOS ranking scheme. Used to describe only minor process modifications of MOS processing, e.g. modification of oxide growth temperatures or ambients, but not including the modification of layout, gate electrodes or any property.

MEDIUM-SCALE INTEGRATION (MSI)
The integration of 10 to 100 device elements in a single semiconductor chip.

MeV
Mega-electronvolt. Value: 1.6018×10^{-13} joules.

MISSION DOSE
The radiation dose acquired by a given component behind a given amount of absorber over the time specified for survival in orbit of a space vehicle.

MINORITY CARRIER
See CARRIERS.

MINORITY CARRIER LIFETIME ( )
The decay time constant for excess minority carriers (see CARRIERS).

MIS
Metal-Insulator-Semiconductor device of which MOS is an example.

MOBILITY (μ)
The velocity achieved by MAJORITY CARRIERS in a medium under unit electric field. Units: $cm^2\ V^{-1}\ s^{-1}$. In solids, mobility is controlled by TRAPPING and the scattering of carriers from charged DEFECTS.

MONTO CARLO TECHNIQUE
Calculation method involving the insertion of random numbers to simulate a phenomenon such as the random scattering experienced by electrons passing through an absorber.

NIR
See NOISE IMMUNITY.

NOISE IMMUNITY (V_{NIL} OR V_{NIH})
That voltage which, when applied to the input node of a logic device in either the high 'H' or low 'L' condition, will cause a spurious change of logic state. "Noise Immunity Reduction (NIR) is the term used for a degradation mode in logic circuits.

NUMBER TRANSMISSION COEFFICIENT (NTC)
The number fraction of incident particle flux that emerges from an absorber slab. The equivalent term for energy flux is the ENERGY TRANSMISSION COEFFICIENT.

PROTECTION
Collective term used to indicate a piece or whole arrays of absorbers without specifying whether they are "add-on" or "built-in".

RAD
Most commonly used unit of dose; equal to 100 erg g^{-1}.

RANGE
The depth to which a particle is likely to penetrate an absorber. Since stopping is a statistical process, several ranges ("practicable", maximum", "extrapolated", etc.) have to be defined.

RECIPROCITY
The condition which obtains when, irrespective of the dose rate, the damage or other effect produced depends on the total dose.

RÖNTGEN
Unit of EXPOSURE equivalent to the generation of 2.68×10^{-4} coulombs of air ion per kilogramme.

SECTOR ANALYSIS
Analytical process required for assessment of total protection of a given point within a spacecraft ("dose point"). Involves dividing the spacecraft

into sectors of roughly uniform thickness and calculating the dose transmission through each.

SHIELD
General term; as for PROTECTION.

SURFACE EFFECT
In MOS devices and bipolar transistors, the various effects which occur in the passivating layer at the top surface of the active chip.

SWITCHING SPEED
In a logic circuit, the time taken for a logic swing at an input node to be registered as a voltage swing at the output node of a logic gate is termed the "delay time" of that gate. Within that delay, we can consider the shape of the output voltage waveform and define a "rise time" for that wave-form. Both times may be altered by irradiation.
"Switching Speed Reduction" (SSR) is the term used for a degradation mode which can define the MAXIMUM ACCEPTABLE DOSE, D_A (max) of a logic circuit.

SWITCHING SPEED REDUCTION (SSR)
See SWITCHING SPEED.

SURFACE DAMAGE FIGURE ($\Delta(1/\beta)_S$
Change in the reciprocal of the gain (β, h_{FE}) of a bipolar transistor under irradiation, as caused by one of the "surface effects" (in contrast to BULK DAMAGE FIGURE).

SURFACE STATES
See INTERFACE STATES.

THRESHOLD VOLTAGE (V_T)
In MOS devices, the gate voltage at which the source-drain current reaches a specified value, commonly 10 μA.
"V_{TN}" is often used to denote V_T of the n-channel element of a CMOS device.
"V_{TP} " is often used to denote V_T of the p-channel element of a CMOS device.

THRESHOLD VOLTAGE SHIFT (ΔV_T)
One of the most important parameters in the analysis of radiation-induced degradation of CMOS devices. The difference in V_T values before and after irradiation or other treatment.

TRANSCONDUCTANCE (g_m)
The term for "gain" of a MOS device, i.e. the slope of the I_D -VG curve at a particular V_G and supply voltage.

TRAPPING

A local disturbance of the atomic network in a semiconductor or insulator; e.g. an impurity atom or the absence of an atom (vacancy) is termed a DEFECT and produces a local disturbance in the BAND-GAP. A quantum level of potential energy 'E_T' is found in the normally forbidden gap region.
Trapping occurs when a hole or electron falls into this potential well and is held there. If 'E_T' lies near 'E_C' or 'E_V', then the trap can be emptied by thermal excitation and be termed "shallow".
If 'E_T' is far from 'E_C' or 'E_V' (DEEP TRAPPING), then only recombination effects or high-energy excitation can empty the trap. Holes are very deeply trapped in SiO_2 near the interface (E_T-E_V> 2eV).

TRAPPING PROBABILITY (A)

The probability that a trap will capture an electron or hole for unit flux of holes is equal to N_TS, where 'N_T' is the density of empty traps per unit area and 'S' is the trapping cross-section. The term INITIAL TRAPPING PROBABILITY is used to express the probability of capture of holes in a MOS device early in the charge build-up process, i.e. when most of the existing traps are unfilled. This 'A' value is in the form of a fraction and used operationally to define the performance in space of a MOS device.

VACANCY

See TRAP.

VTNZ

Term proposed here to describe a form of degradation in an MOS device when radiation-induced shift brings 'V_{TN}' to zero.

VALANCE BAND

See BAND GAP.

WATER PHANTOM

A mass of absorber used to surround a detector for measuring radiation dose. Used, during calibration of a radiation beam, to establish a state of secondary electron equilibrium almost similar to that found in tissue or water under the same radiation. Certain plastics ("water- equivalent phantoms") can be used in place of a tank of water.

PAGE INTENTIONALLY LEFT BLANK

ANNEX B.
RADIATION HANDBOOKS, TEXTBOOKS AND REVIEWS

The publications in this section either give a comprehensive treatment of the engineering problems of radiation effects or contain extensive compilations of radiation test data. A list is given below in chronological order.

1963

- W.C. Cooley and R.J. Janda, "Handbook of Space Radiation Effects on Solar-Cell Power Systems". NASA SP-3003, U.S. Dept. of Commerce, Washington DC (1963).

1964

- J. Kircher and R. Bowman, "Effects of Radiation on Materials and Components", Reinhold (1964).

1965

- C.J. Goetzel, J.B. Rittenhouse and J.B. Singletary, "Space Materials Handbook", Pt. I, Addison-Wesley, Reading, Mass., USA (1965).

1966

- H. Oleson, "Radiation Effects on Electronic Systems", Plenum Press (1966).

1970

- N.W. Holm and R.J. Berry, "Manual on Radiation Dosimetry", Dekker, USA (1970).

1972

- L.W. Ricketts, "Fundamentals of Nuclear Hardening of Electronic Equipment", New York, Wiley (1972).

- M.H. Van de Voorde and C. Restat, "Selection Guide to Organic Materials for Nuclear Engineering" (July 1972).

1977

- N.J. Rudie, "Principles and Technique of Radiation Hardening", 3 Volumes, Western Periodicals Co., 13000 Raymer St., N. Hollywood, Cal. 91605 (1977).

- H.Y. Tada and J.R. Carter, "Solar Cell Radiation Handbook", 2nd Edition, JPL Publication 77-56, Jet Propulsion Laboratory, Pasadena, Cal. (Nov. 1977).

- D. Bräunig, W. Gaebler, W.R. Fahrner and H.G. Wagemann, "GfW Handbook for Data Compilation of Irradiation Tested Electronic Components", 1st Edition,

Report No. HMI-B248 (TN 53/08), DFVLR/BPT and Hahn-Meitner Institut für Kernforschung, Berlin, W.Germany (Nov. 1977). (Note: 2nd Edition 1981).

1978

- G. Holmes-Siedle and R.F.A. Freeman, "Radiation Effects Engineering Handbook (Methods of Improving the Radiation Tolerance of Electronics in Space Vehicles)", European Space Agency Report No. CR(P)-1067, (Fulmer Research Institute, Stoke Poges, Slough, England, Report No. R730/8, April 1978).

1979

- H. Schonbacher and A. Stolarz-Izycka, "Compilation of Radiation Damage Test Data, Part I: Cable Insulating Materials" (April 1979).

1980

- V.A.J. van Lint, T.M. Flanagan, R.E. Leadon, J.A. Naber and V.C. Rogers, "Mechanisms of Radiation Effects in Electronic Materials", Vol. I, Wiley, New York (1980).

1983

- The European Space Agency, "The particle and ultraviolet (UV) radiation testing of space materials". ESA PSS-01-706 Issue 1 (March 1983).

1989

- T.P. Ma, P.V. Dressendorfer, "Ionizing Radiation Effects in MOS Devices and Circuits". Wiley Interscience (1989).
- G.F. Knoll, "Radiation Detection and Measurement". Second edition. Wiley International (1989).

1991

- G.C. Messenger, M.S. Ash,"The Effects of Radiation on Electronic Systems". Second edition. Van Nostrand Reinhold (1991).

1992

- A.G. Holmes-Siedle, L. Adams, "Handbook of Radiation Effects". Oxford University Press. (1992).

ANNEX C
USEFUL DATA ON MATERIALS

C.1 DENSITIES AND CHEMICAL FORMULAS OF COMMERCIAL PLASTICS (IN ORDER OF INCREASING DENSITY)

Name	Density (*) (g/cm^{-3})	Typical formula	Example of trade name and properties
POLYPROPYLENE	0.90	$(CH_2)n$	Grace
POLYETHYLENE		$(CH_2)n$	Xylonite H.F.D.4201
- High density	0.941-0.965		
- Medium density	0.926-0.941		
- Low density	0.910-0.925		
POLYSTYRENE	1.04-1.08	$(C_7H_8)n$	Grace
POLYURETHANE	1.088	$(C_{10}H_{10}N_2O_4)n$	Thiokol Solithane 113 (d = 1.073)
ACRYLONITRILE-BUTADIENE-STYRENE (ABS)	1.06-1.08	$(C_{15}H_{19}N)n$	Genco
EPOXY	1.12	$(C_{18}H_{24}O_3N_2)n$	Shell Epikote 828 (d = 1.165)
NYLON	1.13-1.15	$(C_{12}H_{24}O_3H_2)n$	Nylon 6.6 (d = 1.13)
POLYVINYLIDENE CHLORIDE	1.15-1.80	$(C_2H_3Cl)n$	3M
POLYMETHYL METHACRYLATE (PMMA)	1.18-1.20	$(C_5H_8O_22)n$	Perspex, Lucite
PHENOL-FORMALDEHYDE	1.3-1.6	$(C_7H_7O)n$	Bakelite
POLYSULPHONE	1.41	$(C_{27}H_{22}SO_4)n$	Union Carbide P1700
POLYESTER	1.5-2.1	$(C_{24}H_{12}O_{12})n$	Mylar
SILICON	1.08-2.8	$(C_2H_6SiO)n$	Dow corning 93-500 (d = 1.08)
POLYTETRAFLUOROETHYLENE (PTFE)	2.1-2.3	$(CF_2)n$	Teflon
EPOXY-GLASS-FIBRE COMPOSITE	2.2	Composite	Fortin FR4

See next page.

(*) Tabulated densities from:

R.C. Weast, 'CRC Handbook of Chemistry and Physics' (1972-3), pp. C 764-774;
J. Brandrup and E.H. Immergut (Eds.), 'Polymer Handbook', Interscience 1966, tables IX-5;
N.A. Waterman (Ed.), 'Fulmer Materials Optimiser', Fulmer Research Institute, 1977.
(1 g/cm^{-3} = 1000 kg/m^{-3})

C.2 PROPERTIES OF SEMICONDUCTORS AND OXIDES (a)

Name	Band-gap E_G(300K) (eV)	Density (kg m^{-3}) (d)	Dielectric constant (k)	Carrier mobility electrons ($m^2V^{-1}s^{-1}$) (μ)	holes ($m^2V^{-1}s^{-1}$) (μ)
Si	1.12	2330	11.8	0.15	0.06
Ge	0.80	5330	16	0.39	0.19
GaAs	1.43	5320	10.9	0.85	0.04
CdS	2.42	2530	10.0	0.03	0.005
SiO_2					
- quartz	8.9(c)	2660	4.5	10^{-5}	-
- amorphous (Suprasil)	8.9	2200	3.8	0.002	-
- thermally grown on Si				0.017(b) -0.0034	$2x10^{-9}$
$A_{12}O_3$					
- sapphire	9.8	3870	9.4	-	-
- ceramic	9.8	3500	8.5	-	-

(a) Mainly from:
- A. Grove, 'Physics and Technology of Semiconductor Devices', (Wiley 1967.
- T.H. Laby, 'Tables of Physical and Chemical Constants', (Longmans 1973).

(b) SiO_2 Mobility data (see later table).

(c) H. Ibach and J.E. Rowe, Phys. Rev. 10, pp. 710-718 (1974)

C. 3 SILICON DIOXIDE IN VARIOUS FORMS: DRIFT MOBILITIES OF CARRIERS (*) AT ROOM TEMPERATURE (300K)

Name	Type	Electron mobility		Hole mobility		Ref.
		($cm^2V^{-1}s^{-1}$)	($m^2V^{-1}s^{-1}$)	($cm^2V^{-1}s^{-1}$)	($m^2V^{-1}s^{-1}$)	
Amersil Suprasil (2)						
- Fused Silica 200 m foil		20 ± 3	$2x10^{-3}$	-	-	1
Valpey natural	Natural x-cut Synthetic	10^{-1}	10^{-5}	-	-	2
Thermal oxide on silicon, 0.370 m	Dry O_2 (1000°C)	-	-	$2x10^{-5}$	$2x10^{-9}$	3
Thermal oxide on silicon, 0.862 m	Steam (1100°C)	-	-	$1x10^{-8}$	$1x10^{-12}$	4
Thermal oxide on silicon	Steam/air (1050°C)	17-34	-	-	-	5

1. R.C. Hughes, Physical Review Letter 30, pp. 1333-1336 (1973).
2. R.C. Hughes, Sandia Internal Report SC-RR 1720863 (Dec. 1972).
3. R.C. Hughes, Physical Review B15 2012 (1977) and private communication.
4. R.C. Hughes, Applied Physics Letter 26, pp. 436-438 (1975)
5. R. Williams, Physical Review 140, A 569-575 (1965)

(*) Ionic mobility in all forms is approximately $10^{-7}cm^2.V^{-1}.s^{-1}$ ($10^{-11}m^2.V^{-1}.s^{-1}$)

$1\ m^2.V^{-1}.s^{-1} = 10^{-4}cm^2.V^{-1}.s^{-1}$.

C. 4 RADIATION ABSORPTION EFFECTIVENESS OF VARIOUS MATERIALS USED IN SPACE VEHICLE EQUIPMENT BOXES

Material	Commercial name or Type number	Function	Typical thickness (mm)	Typical density (g cm^{-3})
ORGANIC				
Polyurethane	Thiokol solithane 113	Coating	0.1 - 1.0	1.073
Silicone	Dow Corning 93-500	Encapsulant gasketing	0.1 - 5	1.08
Epoxy	Shell Epon 828	Adhesive, coating or PCB	0.1 - 5	1.1
PTFE	BS 2848	Cable sleeving	0.1 - 5	2.1
Nylon	Nylon 6, 6	Bushings, spacers	0.5 - 5	1.13
Polysulfone	Union Carbide P1700	Connector mouldings	0.5 - 5	1.24
PVC	3M	Adhesive tape, cable sleeving	0.1 - 5	1.4
PVF	Kedlar	Cable sleeving	0.1 - 5	-
Polyester	Du Pont Mylar	Dielectric	0.025-0.1	-
Phenolic	Bakelite	Connector	0.5 - 5	1.6
DAP	Type 10256	Transistor pads	1 - 2	-
Neoprene	Neoprene	Gasketing	0.1 - 5	1.25
INORGANIC NON-METAL				
Beryllia	Nat. Beryllia Corp.	Heat-sink	0.1 - 3	3
Fibreglass	Fortin FR4 epoxy-glass laminate	PC board		2.1 - 2.5
Borosilicate glass	Corning 7740	Encapsulant	0.1 - 5	2.23
Mica	EAC 699	Isolation shim	0.1 - 1	2.6 - 3.2

C. 4 RADIATION ABSORPTION EFFECTIVENESS OF VARIOUS MATERIALS USED IN SPACE VEHICLE EQUIPMENT BOXES (CONTINUED)

Material	Commercial name or Type number	Function	Typical thickness (mm)	Typical density (g cm^{-3})
INORGANIC (Continued)				
Alumina	Various ceramics, Linde Sapphire	IC Header and Lid, epitaxial substrate	0.1 - 1 0.1 - 1	3.9 to 3.97
Silicon	Monsanto	Electronic chip	0.2 - 2.0	2.33
Silica	GEC crystal or Spectrosil B	Electronic crystal substrate, optical window	0.1 - 5	2.65
Gallium arsenide	Monsanto or Metals research	Electronic chip	0.1 - 1	5.32
Molybdenum disulphide	Moly-ITC-Bond	Lubricant	0.01 - 0.1	4.80
Zinc oxide		Pigment	0.01 - 0.1	5.6
ELEMENTAL METALS				
Beryllium		Structure	1 - 10	1.848
Magnesium		,,	1 - 10	1.738
Aluminium		,,	1 - 10	2.699
Iron		Bolts, sheets	0.1 - 5	7.87
Chromium		Plating	1.01 - 0.1	7.20
Tin		,,	-	7.31
Nickel		Structure	1 - 10	8.90
Copper		Cladding, cable, structure,heat-sink	0.01 - 10	8.93
Silver		Plating	.001 - .05	10.50
Lead		Solder	0.1 - 1	11.34
Gold		Plating, wire, thick film	.001 - 5	19.32
Tantalum		Shield	0.1 - 5	16.65
Platinum		Plating, wire	.001 - .01	21.45

C. 4 RADIATION ABSORPTION EFFECTIVENESS OF VARIOUS MATERIALS USED IN SPACE VEHICLE EQUIPMENT BOXES (CONTINUED)

Material	Commercial name or Type number	Function	Typical thickness (mm)	Typical density (g cm^{-3})
ALLOYS				
Brass	Cu70 Zn30	Structures	1 - 10	8.5
Kovar	Fe54 Ni29 Co17	IC Lids, connectors, wires	0.25 - 1.0	8.2
Solder	Pb64 Sn36	Solder joints	0.1 - 2.0	9.43
Stainless st.	Fe63 Cr25 Ni12(e.g.)	Bolts, vessels	1 - 10	7.5
Monel	Ni67 Cu28 Fe (etc.)	RF gaskets	0.1 - 1	8.8
Mu-metal	Fe18 Ni75 Cu5 Cr2	Magnetic shields, coil cores	0.1 - 5	8.58
COMPOSITES				
Fibre-board	Micaply 3M Cu-clad	PCB, box wall	0.1 - 5	2.2 (not incl. Cu)

PAGE INTENTIONALLY LEFT BLANK

ANNEX D.
USEFUL RADIATION DATA

D.1 RADIATION UNITS

ABSORBED DOSE

1 rad	= 100 erg g	= 6.25×10^{13} eV g^{-1} = 10^{-2} Gy
1 Mrad	=	6.25×10^{19} eV g^{-1} = 10 kGy
1 Gy	= 1 J.kg	= 100 rad
10^{20} eV g		= 1.6 Mrad = 16 kGy

1 röntgen (R) = 86.9 erg.g (air) = 2.58×10^{-4} C.kg^{-1} (air)
1 röntgen of 1 MeV photons = 1.95 x 10 photons.cm^{-2}

This fluence deposits: 0.869 rads in air,
0.965 rads in water,
0.865 rads in silicon,
0.995 rads in polyethylene,
0.804 rads in LiF,
0.862 rads in Pyrex glass (80% SiO).

DOSE EQUIVALENT:

1 rem = rad x quality factor
1 sievert = gray x quality factor

QUALITY FACTOR:

X Ray, Gamma, Beta	1
Fast neutrons	10 upwards
Alpha particles	20

RADIOACTIVITY

1 Curie (Ci) of radioactive material produces: 3.700×10^{10} disintegrations per second (or becquerels).

A 1 Ci point source emitting one 1MeV photon per disintegration gives an exposure of ..... 0.54 $R.hr^{-1}$ at 1 metre;

A 1 Ci ^{60}Co source gives ..... 1.29 $R.hr^{-1}$ at 1 metre.

Photon fluence at 1 metre from a 1 Ci point source = 1.059×10^{9} cm^{-2} (assuming 1 gamma ray per disintegration).

SI Units recommended by the International Commission on Radiation Units and Measurements (ICRU) (Brit. J. Radiology No. 49, p.476 (1976):

- Absorbed dose: the gray (Gy) = 100 rad = 1 J/kg,
- Exposure: the coulomb per kg (no name given) = 1 C/kg,
- Quantity activity: the Becquerel (Bq) = 1 s^{-1} = 2.703 x 10^{-11} Ci.

Old units to be abandoned over ten years.

D. 2 ENERGY ABSORPTION VERSUS PHOTON ENERGY FOR AIR

Energy (MeV)	Mass energy absorption coefficient (μ en/ρ) air ($cm^2. g^{-1}$)	Photon fluence per röntgen ($cm^{-2}. R^{-1}$)
0.01	4.61	11.8×10^{-8}
0.05	0.0406	267×10^{-8}
0.10	0.0234	232×10^{-8}
0.50	0.0296	36.7×10^{-8}
1.0	0.0278	19.5×10^{-8}
5.0	0.0174	6.24×10^{-8}
8.0	0.0152	4.47×10^{-8}
10.0	0.0145	3.75×10^{-8}

From H.E. Johns and J.R. Cunningham, 'The Physics of Radiology', Table A3 (C.C. Thomas, Illinois 1969)

D. 3 TYPICAL PERFORMANCE FIGURES FOR HIGH ENERGY RADIATION SOURCES

Source	Beam current	Typical energy deposition
ULTRAVIOLET 250 W mercury arc	-	10^7erg. cm^2. s^{-1} over 2 cm spot (5.2 $h\upsilon$ 3.4 eV)
100 W hydrogen arc	-	10^4erg. cm^{-2}. s^{-1} over 2 cm spot (12 $h\upsilon$ eV)
X-RAY 40 keV	20 mA	10^6 rads. hr^{-1} over 1 cm spot
GAMMA RAYS Cobalt 60 cells	-	10^5 rads. hr^{-1} over 10^3 cm^3
Spent fuel rig	-	10^6 rads. hr^{-1} over 10^3 cm^3
ELECTRONICS 4 MeV Linac 0.5 MeV VdG	 20μA 10μA	 5 x 10^8 rads. hr^{-1} in 5 cm spot 5 x 10^9 rads. hr^{-1} in 2.5 cm spot
100 keV TEM	20μA	10^8 rads. s^{-1} over 2 cm spot or 10^{12} rads. s^{-1} over 20 μm spot
30 keV SEM	0.1nA	10^2 rads. s^{-1} over 10^{-1} cm^2 or 10^8 rads. s^{-1} over 10^{-6} cm^2
3-15 keV Betaprobe	0.5μA	10^9 rads. s^{-1} in 1 mm spot
FAST NEUTRONS Dido reactor	-	10^{14} cm^{-2}. s^{-1} over 100 cm^{-3}
IONS 3 MeV protons 0.4 MeV protons 0.005 - 3 MeV ions	 2μA	 10^{13} cm^{-2}. s^{-1} over 1 cm spot 10^{12} cm^{-2}. s^{-1} over 1 cm spot 10^{13} cm-2. s^{-1} over 1 cm spot

D. 4 TYPICAL PHOTON ENERGIES AND WAVELENGTHS

	Energy $h\upsilon$, (eV)	Wavelength, λ (nm)
GAMMA RAYS		
Co-60 gamma (average)	1.173×10^6 and 1.33×10^6	10^{-3} approx.
1 MeV photon	1.00×10^6	1.2398541×10^{-3}
X-RAYS		
100 keV photon	10^5	0.012398541
Tungsten K α_1, 59 keV	5.9312824×10^4	0.0209017 (*)
HYDROGEN LINES		
Lyman α line	10.198785	121.56681
H_2 160.8 nm line	7.7105	160.8
MERCURY LINES		
Hg 253.7 nm	4.8871	253.7
Hg 312 nm	3.9739	312
Hg 365 nm	3.3969	365
Hg 436 nm	2.8437	436
VISIBLE LIGHT		
Violet	3.10 - 2.92	400 - 424
Blue	2.92 - 2.52	424 - 491
Green	2.52 - 2.16	491 - 575
Yellow	2.16 - 2.12	575 - 585
Orange	2.12 - 1.92	585 - 647
Red	1.92 - 1.77	647 - 700
KRYPTON LINE (primary wavelength standard	2.046706	606.7802106
NEAR INFRARED		
1 eV photon	1.0	1 239.8591 (1.24μm)
1μm photon	1.2398541	1 000.00 (1μm)
CO_2 line	0.116967	10 600.00 (10.6μm)
Thermal energy	0.025	45 594.16 (49.6μm)
FAR INFRARED		
100 μm photon	0.012398541	100 000.00 (100μm)
HCN line (44.859 cm^{-1})	0.0055764	222 292.07 (222.292μm)

(*) Value given by American Institute of Physics Handbook (McGraw-Hill), 1972) is 0.02090100 nm.

D. 5 RADIO ISOTOPES USEFUL IN IRRADIATION EXPERIMENTS, LIST OF MAIN EMISSION ENERGIES

Nuclide	Half life (yrs.)	Type of decay	PHOTONS		PARTICLES	
			Energy (MeV)	Percent emitted (%)	Energy (MeV)	Transition probability (%)
Co-60	5.27		1.173 1.333 (av. 1.25)	99.86 99.98	0.318 1.491	99.9 0.1
Ir-192	0.526 (192 d)		0.296 0.308 0.316 0.468 0.604 0.612	29.6 30.7 82.7 47.0 8.2 5.3	0.530 0.670	42.6 47.2
Cs-137	30		0.662 0.032 -0.038	85.1 8	0.512 1.174	94.6 5.4
Sr-90 + daughter Y-90	28 0.176		0.54 2.27	100 100	- -	- -
Kr-85	10.6		0.15 0.67	0.7 99.3	0.51 -	0.7 -
Cf-252	2.65	Spontaneous fission			Neutrons: 2 MeV Alphas: 5.9-6.1 MeV Fission: 80 and 104 MeV fragments	

(*) The Radiochemical Centre, Amersham, U.K. (1977)

D. 6 PRACTICAL RANGES (R_p) OF ELECTRONS IN ALUMINIUM

Particle energy (MeV)	Practical range		Particle energy (MeV)	Practical range	
	($g.cm^{-2}$)	(mm)		($g.cm^{-2}$)	(mm)
0.001	0.000012	4.446×10^{-5}	1.0	0.42	1.56
0.003	0.000038	1.408×10^{-4}	1.25	0.52	1.92
0.005	0.000080	2.964×10^{-4}	1.40	0.60	2.22
0.010	0.00017	6.299×10^{-4}	1.50	0.65	2.41
0.030	0.0015	0.0056	1.75	0.80	2.96
0.050	0.0041	0.015	2.0	0.95	3.52
0.100	0.0135	0.050	2.15	1.00	3.705
0.125	0.020	0.074	2.5	1.20	4.45
0.250	0.058	0.214	3.0	1.45	5.37
0.300	0.078	0.289	3.5	1.75	6.48
0.375	0.110	0.408	4.0	1.9	7.04
0.500	0.165	0.611	4.5	2.3	8.52
0.540	0.20	0.741	5.0	2.6	9.63
0.625	0.22	0.815	5.5	2.8	10.37
0.750	0.25	0.926	6.0	3.2	11.86
0.78	0.2969	1.000	7.0	3.7	13.70
0.97	0.40	1.48	8.0	4.2	15.56
1.0	0.42	1.56	9.0	4.7	17.41
			10.0	5.2	19.27

D. 7 SOME SELECTED VALUES OF THE RANGE OF PROTONS IN ALUMINIUM

Energy		Range	Energy		Range
(MeV)	(g. cm)	(mm)	(MeV)	(g. cm)	(mm)
0.1	0.00019	0.0007	4	0.034	0.126
0.3	0.00073	0.0027	10	0.163	0.604
0.5	0.00143	0.0053	13.1	0.270	1.00
			15	0.340	1.26
1	0.0039	0.0145	19.3	0.539	2.00
3	0.021	0.078	25	0.809	3.00
5	0.049	0.0182	29	1.080	4.00
10	0.163	0.604	30	1.130	4.2
30	1.13	4.187	37	1.619	6
50	2.80	10.37			
100	9.20	34.09	40	1.888	7
			43	2.159	8
			46	2.429	9
			48	2.699	10
			65	4.048	15
			74	5.397	20
			100	9.200	34.1

Collected from curves by:

- V. Linnenbom, NRL Report 588 (1962) and
- C.J. Calbick, Phys. thin films 2, pp. 63-145 (1964).

D. 8 MASS ATTENUATION COEFFICIENTS (μ/ρ) OF SELECTED MATERIALS OF PHOTONS OF ENERGIES 0.01 TO 100 MeV SUITABLE FOR CALCULATIONS ACCORDING TO LAMBERT'S LAW FOR NARROW GEOMETRY

(coherent scattering included; density g cm^{-3} in brackets)
after Hubbell (*)

TOTAL MASS ATTENUATION COEFFICIENTS

μ/ρ (cm^2. g^{-1}); (g. cm^{-3}) in brackets

Photon energy (MeV)	H_2 (8.988 x10^{-5})	Be (1.85)	C (2.25)	N_2 (1.250 x10^{-3})	O_2 (1.429 x10^{-3})	Mg (1.74)	A1 (2.6989)
0.01	0.385	0.593	2,28	3.57	5.78	20.8	26.3
0.05	0.335	0.156	0.187	0.187	0.213	0.329	0.369
0.10	0.294	0.133	0.150	0.150	0.156	0.169	0.171
0.50	0.173	0.0773	0.0871	0.0871	0.0873	0.0864	0.0844
1.0	0.126	0.0565	0.0636	0.0636	0.0637	0.0628	0.0613
5.0	0.0505	0.0235	0.0274	0.0274	0.0278	0.0287	0.0284
0.10	0.0325	0.0163	0.0196	0.0292	0.0269	0.0231	0.0231
50.0	0.0141	0.0102	0.0156	0.0156	0.0169	0.0222	0.0231
100.0	0.0116	0.00992	0.0163	0.0163	0.0179	0.0241	0.0251
	Si (2.42)	Fe (7.86)	Cu (8.93)	Sn (-7.29)	W (17.1)	Pb (11.34)	U (18.7)
0.01	34.2	173.0	224.2	141.6	95.5	133.0	178.0
0.05	0.437	1.94	2.62	10.70	5.91	7.81	1.11
0.10	0.184	0.37	0.461	1.68	4.43	5.40	1.91
0.50	0.0875	0.084	0.0836	0.0946	0.136	0.161	0.193
1.0	0.635	0.0599	0.0589	0.0578	0.0654	0.0708	0.0776
5.0	0.0297	0.0314	0.0318	0.0354	0.0407	0.0424	0.0445
10.0	0.0246	0.0298	0.0308	0.0385	0.0464	0.0484	0.0506
50.0	0.0252	0.0382	0.0410	0.0588	0.0760	0.0804	0.0850
100.0	0.0275	0.0432	0.0465	0.0677	0.0881	0.0934	0.0984

D. 8 MASS ATTENUATION COEFFICIENTS (μ/ρ) OF SELECTED MATERIALS OF PHOTONS OF ENERGIES 0.01 TO 100 MeV SUITABLE FOR CALCULATIONS ACCORDING TO LAMBERT'S LAW FOR NARROW GEOMETRY

(coherent scattering included; density g cm^{-3} in brackets)
after Hubbell (*)

TOTAL MASS ATTENUATION COEFFICIENTS
μ/ρ (cm^2. g^{-1}); (g. cm^{-3}) in brackets

Photon energy (MeV)	Air (1.205 x10-3)	H_2O (1.00)	SiO_2 (2.20-2.32)	Perspex PMMA (1.19)	Poly-ethylene	Bakelite (2.23)	Pyrex glass (2.23)
0.01	4.99	5.18	1.90	3.25	2.01	2.76	1.71
0.05	0.208	0.227	0.318	0.208	0.209	0.200	0.302
0.10	0.154	0.171	0.169	0.164	0.172	0.161	0.166
0.50	0.0870	0.0968	0.0874	0.0941	0.0995	0.0921	0.0870
1.0	0.0636	0.0707	0.0636	0.0687	0.0727	0.0673	0.0633
5.0	0.0275	0.0303	0.0287	0.0292	0.0305	0.0286	0.0284
10.0	0.0204	0.0222	0.0226	0.0211	0.0215	0.0206	0.0222
50.0	0.0161	0.0167	0.02028	0.0151	0.0142	0.0147	0.0201
100.0	0.0168	0.0172	0.0224	0.0154	0.0142	0.0150	0.0215

(*) Adapted from J.H. Hubbell, U.S. Nat. Bureau of Standards, Report NSDR-NBS-29 (U.S. Dept. of commerce, Washington D.C., Aug. 1969), Tables 3-1 to 3-36, columns 9 and 10, and Table 1-1, column 5.

ANNEX E. USEFUL GENERAL AND GEOPHYSICAL DATA

E. 1 GENERAL CONSTANTS

7 years	= 3.682×10^6 minutes = 2.209032×10^8 seconds
1 year	= 5.25960×10^5 minutes = 3.155760×10^7 seconds
1 day	= 1.440×10^3 minutes = 8.6400×10^4 seconds
1000 Å	= 0.1 μm = 100 nm
1 mm	= 0.03937 inch ~ 40 thou.
0.001 inch	= 25.4 μm
1 m^3	= 10^6 cm^3
1000 cm^3	= 10^{-3} m^3
1 litre	= 1000.028 cm^3 = 0.219 976 gallon
1 gm cm^{-3}	= 1000 $kg.m^{-3}$
1 eV	= $1.602\ 192 \times 10^{-19}$ joules
1 MeV	= $1.602\ 192 \times 10^{-13}$ joules
1 joule	= 10^7 erg
1 calorie	= 4.187 joules
1 eV/molecule	= 23.1 kcal/molecule
Permittivity of free space (ε_o)	= 8.86×10^{-14} $F.cm^{-1}$
	= 8.86×10^{-12} $F.cm^{-1}$
	= 55.4 electronic charges $V.\mu^{-1}$
Permeability of free space (μ_o)	= 1.26×10^{-6} $H.m^{-1}$
Electronic charge (q)	= $1.602\ 192 \times 10^{-19}$ coulomb
1 coulomb/cm^{-2}	= $6.241\ 459 \times 10^{18}$ electrons/cm^{-2}
1 μA/cm^{-2}	= 6.24×10^{12} electrons/cm^{-2} $.s^{-1}$
Velocity of light (c)	= $2.997\ 925 \times 10^8$ m/s.
1 newton	= 10^5 dynes
1 mm Hg	= 133.3224 Nm^{-2}
Boltzmann's constant (k)	= 1.38062×10^{23} $J.K^{-1}$, 6.62×10^{-5} eV K^{-1}
kT at room temperature	= 0.0259 eV
Planck's constant (h)	= 6.63×10^{-34} J.s
Avogadro's number	= 6.022×10^{23} $mole^{-1}$
Electron Rest Mass (m_e)	= 9.11×10^{-31} kg
Proton Rest Mass (m_p)	= 1.67×10^{-27} kg

E. 2 FREQUENCY, WAVELENGTH AND ENERGY

Energy x wavelength ($E \lambda$) = 1.239854×10^{-6} eV.m

Energy Wave-number (E/υ) = 1.98648×10^{-25} J.m

Wave-number energy (υ/E) = 8.06546 x 10s $eV^{-1} .m^{-1}$

Frequency energy $\frac{(f)}{E}$ = 2.417966×10^{14} $Hz.eV^{-1}$

Wavelength of photon of energy:

- 1 eV (infrared) = 1.239854 nm;
- 10.2 eV (Lyman α) = 121.55431 nm.

Energy of photon of:

- wavelength 1 µm (infrared) = 1.239854 eV;
- wavenumber 50 000 cm^{-1} = 6.19927 eV.

Wavelength of photon of wave-number:

- 50 000 cm^{-1} = 200 nm;
- 10 000 cm^{-1} = 1 µm;
- 50 cm^{-1} = 200 µm.

Wavenumber of photon of energy 1 eV = 8065.46 cm^{-1};
= 806 546 m^{-1}

E. 3 USEFUL GEOPHYSICAL AND ORBITAL PARAMETERS

Average radius of the Earth = 6 371.315 ±0.437 km
3 959 statute miles
3.438 nautical miles

Altitude of geostationary orbit = 35 863 km
22 284 statute miles
19 360 nautical miles

Geocentric distance of geostationary orbit = 42 234.314 km
6.629 R_E

Being circular and equatorial, the geostationary orbit is a special case of the geosynchronous orbit (period 24 hours).

1 statute mile	= 1.609344 km = 0.869 n mile
1 nautical mile	= 1.852 km = 1.151 statute mile
1 astronomical unit	= 1.496×10^{11} m
Gravitational acceleration	= 0.980665 m s^{-2} = 32.1741 ft s^{-2}